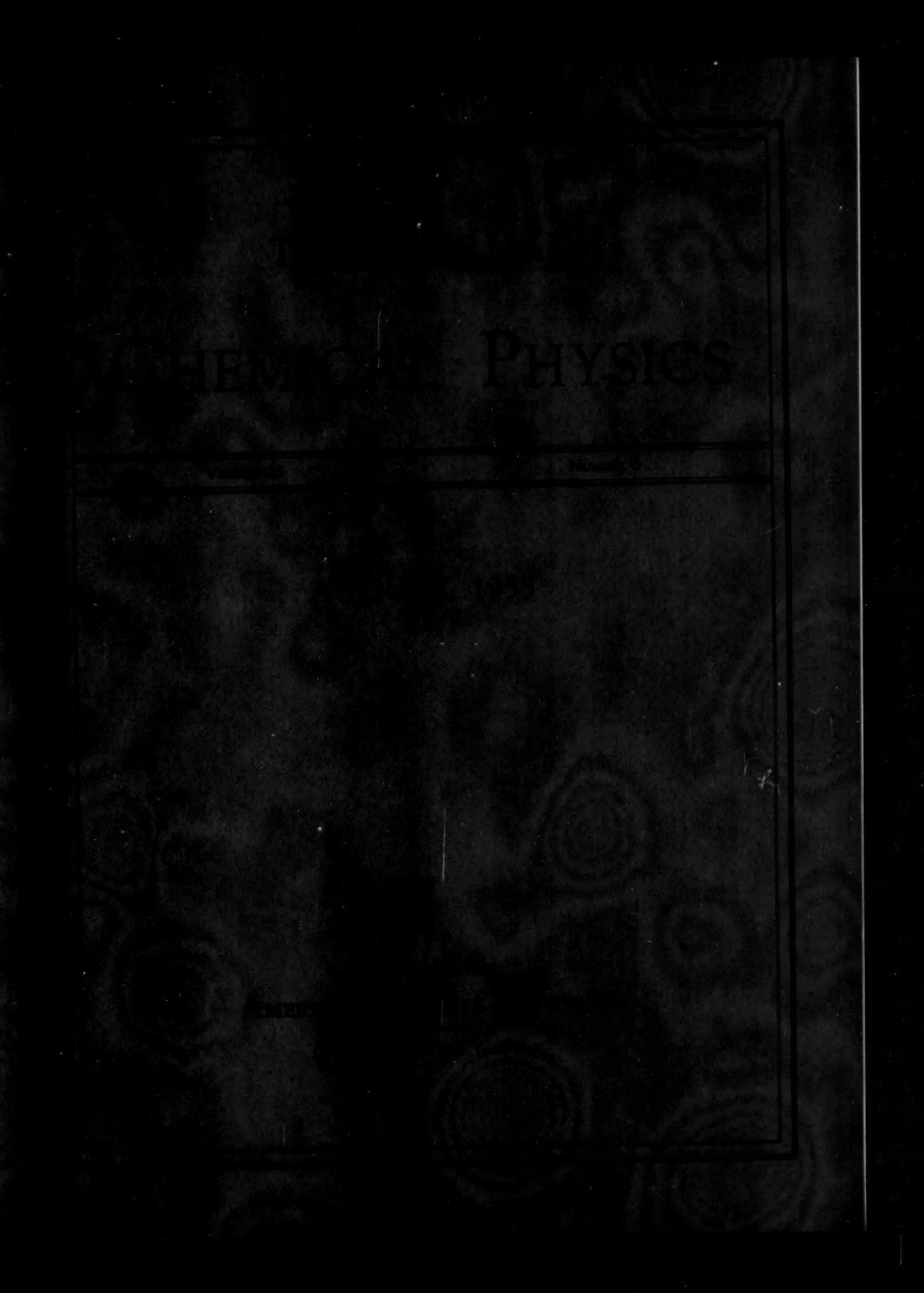

THE JOURNAL OF CHEMICAL PHYSICS

BOARD OF EDITORS

CLYDE A. HUTCHISON, JR., *Editor*

Associate Editors

Term ending December 31, 1956	Term ending December 31, 1956	Term ending December 31, 1957
RICHARD M. BADGER	BRYCE L. CRAWFORD, JR.	JAMES R. ARNOLD
DAVID M. DENNISON	H. S. GUTOWSKY	JACOB BIGELEISEN
JOHN G. KIRKWOOD	WILLIAM N. LIPSCOMB	WALTER GORDY
G. B. KISTIAKOWSKY	ELLIOTT W. MONTROLL	ALVIN H. NIELSEN
A. W. LAWSON	GEORGE SCATCHARD	EARLE K. PLYLER
S. S. PENNER	J. W. STOUT	WAVE H. SHAFFER
ROBERT L. SCOTT	GREGORY H. WANNIER	T. F. YOUNG

THE JOURNAL OF CHEMICAL PHYSICS is published monthly by the American Institute of Physics. Its purpose is to bridge a gap between journals of physics and journals of chemistry. The artificial boundary between physics and chemistry has now been in actual fact completely eliminated, and a large and active group is engaged in research which is as much the one as the other. It is to this group that the Journal is rendering its principal service and makes its greatest appeal, both as a prompt and efficient medium for publication of research and as a convenient and carefully edited assemblage of pertinent information.

Information for Contributors

Send manuscripts to Clyde A. Hutchison, Jr., Editor, *The Journal of Chemical Physics*, Institute for Nuclear Studies, University of Chicago, Chicago 37, Illinois. Unless otherwise stated submission of a manuscript is a representation that it has been neither copyrighted, published, nor submitted for publication elsewhere. Textual material (abstract, body of the paper, tabular material, references, and figure captions) must be in English, typewritten (except mathematical expressions) double spaced with wide margins on a durable, white paper, preferably letter size. The original copy, not the carbon, should be submitted. For general style, spellings, abbreviations, and form, consult recent issues of this journal. The authors' institutions are requested to pay a publication charge of $25.00 per page which, if honored, entitles them to 100 free reprints. Instructions will be sent with galley proofs.

An abstract must accompany each article. It should be adequate as an index and as a summary.

All but the simplest mathematical expressions should be carefully printed in by hand. Be sure to distinguish between capital and small letters. Indicate clearly superscripts and subscripts by inverted carets and carets, respectively. Avoid complicated superscripts and subscripts. Avoid repetition of a complicated expression by representing it by a symbol. Identify in the margin Greek letters and unusual symbols. Use fractional exponents instead of root signs. Use the solidus (/) for fractions wherever its use will save vertical space.

References should appear as footnotes, numbered consecutively. Literature citations of technical journals should be in the form indicated in the Style Manual of the American Institute of Physics and Chemical Abstracts (Chem. Abstracts 45, I-CCLV (1951)).

Tables may be typewritten on sheets separate from the running text. Each table must have a caption which will make the data in the table intelligible without reference to the text. Avoid complicated column headings.

Wherever possible **figures** should be planned for the width of a column (3 in.). A convenient reduction ratio is about 2:1 or 3:1. Lettering should be large enough on the original that when reduced it shall not be less than about $\frac{1}{16}$ in. (~1.5 mm). Line drawings must be in *india ink* on white paper or tracing cloth. Coordinate paper is not desirable but if used must be blue lined and the coordinate lines which are to show must be inked over. Pictures of apparatus, etc., should be glossy prints and should have maximum black and white contrast. Identify each original drawing or photograph on the back with the author's name and the figure number. Figures should be numbered consecutively. Captions should be typed on a separate sheet of paper.

A limited number of **alterations** in proof are unavoidable, but the cost of making extensive alterations after the article has been set in type will be charged to the author.

Proof and all correspondence concerning papers in the process of publication should be addressed to the Publication Manager, American Institute of Physics, 57 East 55 Street, New York 22, New York.

Subscription Price

	U. S. and Canada	Elsewhere
To members of the American Institute of Physics and Affiliated Societies	$12.00	$13.00
To all others	15.00	17.00

Back Number Prices

Yearly rate when complete year is available: $18.00.
Single copies: $1.75 each.

Subscriptions, renewals, and orders for single copies should be addressed to the American Institute of Physics, 57 East 55 Street, New York 22, New York.

Changes of address should be sent to the American Institute of Physics.

This Journal of Chemical Physics is published monthly at Prince and Lemon Streets, Lancaster, Pennsylvania.

Entered as second-class matter December 30, 1932, at the Post Office at Lancaster, Pa., under the Act of August 24, 1912. Acceptance for mailing at special rate of postage, provided for in paragraph (d-2), section 34.40, P. L. & R. of 1948, authorized February 3, 1933.

THE JOURNAL
OF
CHEMICAL PHYSICS

VOLUME 23, NUMBER 8 AUGUST, 1955

Reaction of Oxygen Atoms with Ethylene*

R. J. CVETANOVIĆ
Division of Applied Chemistry, National Research Council, Ottawa, Canada
(November 22, 1954)

Reaction of O-atoms, produced by mercury photosensitized decomposition of nitrous oxide, with ethylene has been studied at room temperature and 123°C. The primary step of the process appears to be a direct addition of the atom to the double bond to form an energy-rich intermediate which undergoes further reactions. The following products are formed: aldehydes (CH_3CHO, C_2H_5CHO, and C_3H_7CHO), CO, CH_4, C_2H_6, C_3H_8, C_4H_{10}, H_2, very small amounts of some other substances and traces of HCHO. At 24°C O-atoms react with ethylene 22 ± 5 times as readily as with *n*-butane. Assuming comparable pre-exponential factors for the two processes $\Delta E = -1.9$ kcal/mole, so that the activation energy of addition of oxygen atoms to the double bond in ethylene is estimated at close to 3 kcal/mole. In the presence of molecular oxygen the character of the reaction is profoundly changed.

INTRODUCTION

ONLY a relatively restricted amount of information on the oxygen atom reactions is available in the literature.[1] Although approximate estimates of collision efficiencies have been made for a number of organic compounds, there is considerable uncertainty with respect to the identity of the elementary reactions involved and the type of products formed. With the customary method of production of oxygen atoms by electrical discharge in molecular oxygen the process is obscured by the readily occurring reactions of any radicals produced with the molecular oxygen present in excess, leading to a complexity of products no longer characterizing the initial reaction of the atoms. This profound change in the character of the reaction is to be expected in view of the existing knowledge on oxidation processes and is also clearly demonstrated experimentally in the present work. It is, therefore, necessary to conduct experiments in the absence of molecular oxygen. This can be done conveniently by mercury photosensitized decomposition of nitrous oxide which, in contrast to molecular oxygen, reacts only extremely slowly with free radicals or atoms at not too elevated temperatures.

It has been shown[2] that the primary process in the quenching of Hg 6 ($^3P_1$) atoms by nitrous oxide is production of a molecule of nitrogen and an atom of oxygen. The rate of nitrogen formation serves, therefore, as an internal actinometer and is a measure of oxygen atoms participating in the process. It has also been shown[3] that the relative extents of the competing quenching processes in the mixtures of nitrous oxide with its reacting partners are amenable to quantitative treatment.

Reactions of oxygen atoms with a number of compounds have been studied in the indicated manner with the primary object of obtaining general information about the elementary processes involved and the type of products formed. In the present paper the investigation of the reaction of oxygen atoms with ethylene is reported.

EXPERIMENTAL

The experimental arrangement, the method of analysis of the noncondensable gases and the employed reagents have been described before.[2,3] Molecular oxygen was produced by heating reagent grade $KMnO_4$. Ethylene oxide was a Matheson Company product and was further purified by repeated bulb-to-bulb distillation *in vacuo*.

The products condensable in liquid nitrogen were separated into four fractions using a Le Roy still.[4] The

* Contribution No. 3693 from the National Research Council, Ottawa, Canada.

[1] E. W. R. Steacie, *Atomic and Free Radical Reactions*. (Reinhold Publishing Corporation, New York, 1954), second edition, pp. 599–605.

[2] R. J. Cvetanović, J. Chem. Phys. **23**, 1203 (1955).

[3] R. J. Cvetanović, J. Chem. Phys. **23**, 1208 (1955).

[4] D. J. Le Roy, Can. J. Research **B28**, 492 (1950).

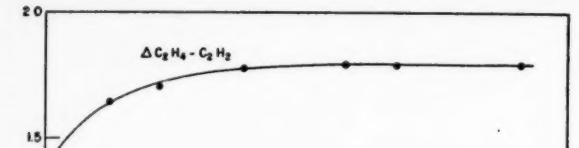

FIG. 1. Relative rates per O-atom consumed at 25°C with 10.5 mm N_2O and 8 mm C_2H_4 for varying extents of reaction.

"C_2" fraction was recovered at −182°C and the relative amounts of C_2H_4 and C_2H_6 ascertained by mass spectrometer. Analyses of this fraction were feasible only when smaller amounts of C_2H_4 were used initially. The second fraction was obtained at −152°C. It normally contained very large amounts of the unreacted N_2O and was further analyzed only in the experiments with 10 mm of N_2O taken initially. From an aliquot C_2H_2 was determined by mass spectrometer. Another aliquot was brought in contact with solid cuprous chloride-potassium hydroxide[5] to remove C_2H_2, and the remainder analyzed by mass spectrometer for C_3H_8 and N_2O. The amounts removed by Cu_2Cl_2−KOH solid absorbent, indicated in the tables and the graphs as "C_2H_2+X," were slightly greater than C_2H_2 determined by mass spectrometer. For reasons discussed below the compound X is tentatively identified with ketene. The third fraction from the Le Roy still was recovered at −82°C. It contained aldehydes, higher saturated hydrocarbons (mainly butane) and small amounts of ethylene oxide. A manometric method, combined with the use of solid absorbents, was developed for the analysis of these products. Aldehydes were polymerized on solid KOH at 100°C for 10 minutes and the remainder recovered at −78°C and measured. Under these conditions any ethylene oxide present was only slightly affected. Ethylene oxide was then removed on solid $CaCl_2$ at 100° for 40 minutes and the remaining hydrocarbons were recovered at −78°C. Synthetic mixtures of acetaldehyde, ethylene oxide, and *n*-butane gave an accuracy of a few percent. In several instances aldehydes were also determined polarographically and the values obtained by the two methods showed no inconsistency. It should be pointed out that the analytical method used for ethylene oxide is not necessarily specific and in the present work the values obtained are based on small differences in manometric measurements. It is certain, however, that at best very small amounts of this compound are formed. The last fraction was collected from the still at room temperature. It constituted a relatively very small part of the total product and contained mainly higher aldehydes (determined polarographically) and possibly some higher hydrocarbons, but little or no water. The combined "−82°" and "room temperature" fractions, as determined manometrically, are in the following referred to as "liquid products."

The individual aldehydes were identified by mass spectrometer after fractionation on a gas-liquid partition chromatograph.[6] Several determinations indicated that the aldehydes consisted of approximately 50% propionaldehyde, 35 to 40% acetaldehyde, and 10 to 15% butyraldehyde.

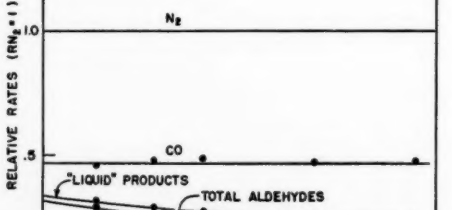

FIG. 2. Relative rates per O-atom consumed at 25°C with 100 mm N_2O and 8 mm C_2H_4 for varying extents of reaction.

RESULTS AND DISCUSSION

The Time Dependence and Stoichiometry of the Reaction

In order to arrive at the stoichiometry of the reaction, a number of experiments were carried out with 10 mm of nitrous oxide and 8 mm of ethylene, varying time of irradiation. With the relatively small initial quantities of the reactants most of the products could be determined with reasonable accuracy. The results are given in Table I. The rates of nitrogen formation exhibit a systematic scatter due to progressive decline in the amount of light absorbed. Using interpolated values of the light absorption, the quantum yield of nitrogen and of a number of other products is found to be independent of time up to quite large conversions, as shown in Table I.

[5] Blacet, MacDonald, and Leighton, Ind. Eng. Chem. Anal. Ed. 5, 272 (1933).

[6] A. B. Callear and R. J. Cvetanović, Can. J. Chem. 33, 1256 (1955).

TABLE I. Effect of irradiation time (at 25±1°C).

Run	Irradiation time (min)	R_{N_2} (molecule sec^{-1} ×10^{-15})	ϕ_{N_2}	Relative rates (R_{N_2}=1) ΔN_2O	ΔC_2H_4	CO	H_2	(C_2H_2+X)	CH_4	C_2H_6	C_3H_8	Higher RH	C_2H_4O	Total aldehydes	"Liquid products"
A. 10.5 mm N_2O+8 mm C_2H_4 (mean Ia≈3.3×10^{15} quanta sec^{-1})															
28	0	...	...	...	...	...	...	...	...	...	...	...	...	...	...
34	60	0.824	0.275	1.02	2.52	0.500	0.965	0.918	0.109	0.176	0.170	n.d.[a]	n.d.	0.344	0.440
23	90	0.967	0.276	1.00	2.53	0.502	0.929	0.874	0.106	0.197	0.175	0.088	0.022	n.d.	n.d.
32	180	0.837	0.270	1.01	2.55	0.499	0.851	0.807	0.106	0.169	0.170	0.121	0.031	0.280	0.452
29	250	0.919	0.270	0.987	2.47	0.501	0.763	0.721	0.101	0.160	0.164	0.131	0.026	0.226	0.414
31	310	0.864	0.270	1.00	2.42	0.505	0.713	0.677	0.098	0.145	0.170	0.162	0.032	0.216	0.450
30	400	0.901	0.273	0.964	2.30	0.503	0.603	0.545	0.091	0.158	0.174	0.134	0.033	0.185	0.376
B. 100 mm N_2O+8 mm C_2H_4 (mean Ia≈2.75×10^{15} quanta sec^{-1})															
43	45	1.82	0.663	n.d.	1.404	0.455	0.106	n.d.	0.115	0.164	n.d.	...	0.014	0.288	0.320
41	90	1.89	0.667	n.d.	1.402	0.472	0.105	n.d.	0.114	0.159	n.d.	0.002	0.016	0.264	0.290
40	135	1.81	0.668	n.d.	1.415	0.486	0.111	n.d.	0.113	0.151	n.d.	n.d.	0.014	0.240	0.278
42	225	1.85	0.663	n.d.	1.368	0.469	0.108	n.d.	0.110	0.153	n.d.	0.017	0.014	0.207	0.258
44	315	1.81	0.669	n.d.	1.310	0.474	0.099	n.d.	0.108	0.142	n.d.	0.024	0.016	0.170	0.240

[a] n.d. = not determined.

The ratios of the rates of formation of the products to the rate of nitrogen formation represent the relative rates per one oxygen atom entering into reaction. They are plotted in Fig. 1, taking the amount of nitrogen produced as a measure of the extent of reaction instead of irradiation time in order to eliminate drifts due to declining light absorption. For the primary process of interest are the values extrapolated to zero conversion. At very low conversions ethylene produces on quenching Hg $6(^3P_1)$ atoms only acetylene and an equal amount of hydrogen. Abstracting these quantities, the stoichiometry of the reaction between oxygen atoms and ethylene at negligible conversion and at the particular pressures of the reactants is approximately represented by the formula

$$0+1.38\ C_2H_4 \rightarrow 0.50\ CO+0.15\ CH_3CHO +0.20\ C_2H_5CHO+0.05\ C_3H_7CHO+0.03\ C_2H_4O +0.04\ CH_2CO+0.09\ H_2+0.11\ CH_4+0.17\ C_2H_6 +0.17\ C_3H_8+p(C_2H_4O)_s\ (p\times s=0.03),$$

where the amounts of products and the reactants are expressed as fractions relative to one oxygen atom consumed in the process.

Ketene has not been identified and is only very tentatively assumed to be produced, by analogy with mercury sensitized decomposition of ethylene oxide and in order to explain the difference in the amounts of acetylene determined by mass spectrometer and by direct gas analysis [the former values are shown only in Fig. 1, the latter are shown as (C_2H_2+X) in Fig. 1 and Table I]. Only extremely small quantities of formaldehyde have been found in the reaction products at 123°C. The small amount of polymer given has been derived from the material balance. There is indication that a polymer is formed, at least at finite conversions.

Extrapolation of the rates of ethylene consumption to zero conversion is somewhat uncertain. Combining information from Figs. 1 and 2, the latter for a similar set of experiments but with 100 mm of nitrous oxide, the value of 1.38 for ethylene consumption at zero conversion is obtained.

The results of the experiments with 100 mm of nitrous oxide and 8 mm of ethylene are given in Table I (B) and Fig. 2. With much decreased quenching by ethylene, both its consumption and hydrogen production were drastically reduced. The rate of CO formation was also slightly lowered, as well as the extrapolated value to zero conversion of aldehyde formation. In other respects, the main trends of products accessible for analysis remained essentially the same as in the experiments with 10 mm of nitrous oxide.

Dependence on the Ratio of the Reactants, Pressure, and Temperature

The results of a series of experiments at 25°C in which the ratio of ethylene to nitrous oxide was varied are

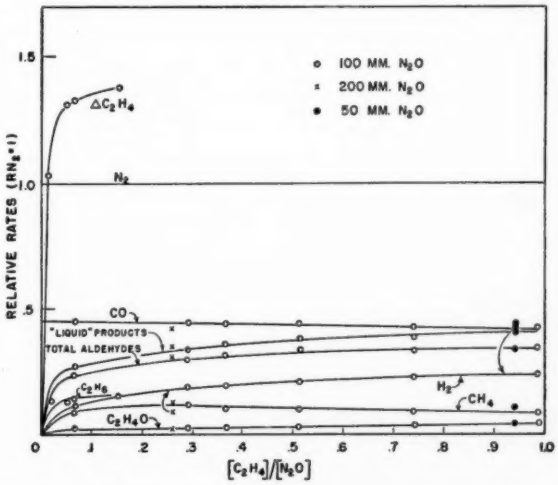

FIG. 3. Relative rates per O-atom consumed at 25°C for varying ratio of the reactants and the total pressure.

TABLE II. Effect of the ratio of reactants, pressure, and temperature.

Run	$\frac{(C_2H_4)}{(N_2O)}$ (mean)	Initial pressure (mm) N_2O	C_2H_4	Irradiation (min)	R_{N_2} (molecule sec^{-1} $\times 10^{-15}$)	ϕN_2	Relative rates ($R_{N_2}=1$) ΔC_2H_4	CO	H_2	CH_4	C_2H_6	C_2H_4O	Total aldehydes	"Liquid products"
					A. 25°C $pN_2O \approx 100$ mm									
12	0.018	98.9	3.11	90	4.14	0.757	1.029	n.d.[a]	n.d.	0.092	0.134	n.d.	n.d.	0.123
10	0.052	100.9	6.69	90	3.85	0.704	1.311	n.d.	n.d.	0.108	0.125	n.d.	n.d.	0.233
55	0.067	101.3	8.3	200	1.67	0.683	1.329	0.447	0.118	0.093	0.141	0.023	0.218	0.272
8	0.154	99.2	16.5	90	3.22	0.589	1.378	n.d.	n.d.	0.116	0.152	n.d.	n.d.	0.303
53	0.291	99.8	29.0	200	1.22	0.487	n.d.	0.443	0.186	0.117	n.d.	0.020	0.299	0.338
51	0.366	99.4	36.4	200	1.10	0.445	n.d.	0.437	0.197	0.102	n.d.	0.024	0.313	0.355
60	0.515	101.1	52.0	200	0.889	0.378	n.d.	0.432	0.208	0.108	n.d.	0.030	0.339	0.385
52	0.743	101.7	75.6	200	0.777	0.306	n.d.	0.423	0.229	0.088	n.d.	0.033	0.322	0.382
54	0.987	100.9	99.6	200	0.632	0.255	n.d.	0.419	0.237	0.082	n.d.	0.046	0.341	0.409
					B. 25°C $pC_2H_4 \approx 52$ mm									
57	0.258	202.6	52.3	200	1.24	0.514	n.d.	0.426	0.117	0.114	n.d.	0.021	0.303	0.343
60	0.515	101.1	52.0	200	0.889	0.378	n.d.	0.432	0.208	0.108	n.d.	0.030	0.339	0.385
58	0.943	56.0	52.8	200	0.624	0.262	n.d.	0.440	0.417	0.105	n.d.	0.040	0.340	0.406
					C. 123°C $pN_2O \approx 100$ mm									
189	0.147	100.1	14.7	90	2.16	0.617	n.d.	0.493	0.150	0.094	n.d.	n.d.	0.248	0.383
185	0.243	100.7	24.5	90	1.96	0.542	n.d.	0.487	0.195	0.086	n.d.	n.d.	0.269	0.428
187	0.398	99.9	39.7	105	1.56	0.436	n.d.	0.514	0.241	0.079	n.d.	n.d.	n.d.	n.d.
184	0.510	100.0	51.0	90	1.44	0.392	n.d.	0.522	0.278	0.068	n.d.	n.d.	0.235	0.487
188	0.768	99.8	76.6	90	1.10	0.312	n.d.	0.551	0.291	0.060	n.d.	n.d.	0.205	0.528
186	1.00	99.4	99.4	90	0.945	0.263	n.d.	0.575	0.328	0.054	n.d.	n.d.	0.190	0.514

[a] n.d. = not determined.

given in Table II (A, B) and in Fig. 3. The general decline in the rates with increasing ethylene to nitrous oxide ratio has been shown previously[3] to be due to the mutually competing quenching of Hg $6(^3P_1)$ atoms by the two reactants. More informative for the present study are the relative rates per oxygen atom consumed, plotted in Fig. 3. There is a small decrease in the rates of carbon monoxide and methane formation with increasing pressure and an opposite trend is shown by ethylene oxide and aldehyde with increasing ethylene to nitrous oxide ratio. A much larger pressure dependence is exhibited by the rates of hydrogen formation, in agreement with the postulated[7] formation of an excited ethylene molecule in the reaction with Hg $6(^3P_1)$ atoms.

The results of a similar series of experiments conducted at 123°C are given in Table II (C). Noteworthy is the reversal in the trends of CO and aldehyde formations in comparison with the reaction at 25°C. The "liquid" products other than the aldehydes appear to be mainly higher saturated hydrocarbons.

Reaction in the Presence of Molecular Oxygen

Several experiments were conducted with 100 mm of N_2O, 2 mm of O_2, and 3 to 85 mm of C_2H_4. Under those conditions only very little direct quenching by oxygen occurred. The results are given in Table III. The small amounts of molecular oxygen added brought about a very pronounced change in the amounts and the nature of the reaction products. There was a large increase in the rate of CO formation while ethane and hydrogen (the latter within a fairly large analytical uncertainty) were completely suppressed and methane and aldehydes drastically reduced. The most characteristic change, however, was in the amount and the composition of liquid products. While no attempt was made at an extensive and systematic quantitative investigation, sufficient information is available in Table III to indicate formation in important quantities of the products normally encountered in the reactions of free alkyl radicals with molecular oxygen, such as HCHO, HCOOH, alcohols, and water. The relatively small increase in ethylene consumption, the independence of the rates on the amount of ethylene, and the suppression of saturated hydrocarbons, suggest strongly that the primary reaction of oxygen atoms with ethylene is not affected by the presence of molecular oxygen and that the pronounced change in the over-all course of the reaction is due to the interaction of oxygen with free radicals formed in the primary process.

Estimate of the Activation Energy of the Reaction

The results of a number of experiments with 100 to 200 mm of N_2O and mixtures of varying amounts of C_2H_4 and $n-C_4H_{10}$ are given in Table IV. In the reaction of O-atoms with $n-C_4H_{10}$[8] very small amounts of CO and almost negligible amounts of CH_4 are formed, while in the case of C_2H_4 they are produced in relatively large quantities. From a comparison of these products in the ternary mixtures with the respective binary mixtures it is possible to obtain two independent values for $k_{C_2H_4}/k_{n-C_4H_{10}}$, the ratio of the respective rate constants

[7] D. J. Le Roy and E. W. R. Steacie, J. Chem. Phys. **9**, 829 (1941).

[8] R. J. Cvetanović (to be published).

TABLE III. Effect of addition of molecular oxygen.

Run	Initial pressures (mm) O_2	N_2O	C_2H_4	Irradiation time (min)	R_{N_2} (molecule sec^{-1} $\times 10^{-15}$)	ϕN_2	Relative rates ($R_{N_2}=1$) CO	CH_4	C_2H_6	ΔC_2H_4	ΔO_2	"$-82°$"	"Room temp."	Special tests	
							A. 23±1°C								
41	···	100.6	8.02	90	1.89	0.667	0.472	0.114	0.159	1.40	···	0.26[a]	0.03[a]		
101	2.2	102.0	8.24	60	3.05	0.663	0.780	0.036	<0.006	1.63	1.24	0.06[a]	0.75[b]		
103	1.87	103.0	8.29	60	3.07	0.669	0.775	0.037	none	1.59	1.10	n.d.[c]	n.d.	RCHO[d]	0.07
104	1.86	102.4	20.0	65	2.39	0.522	0.795	0.040	none	1.57	1.13	0.07[a]	n.d.		
105	1.87	102.2	86.8	105	1.28	0.280	0.811	0.039	none	n.d.	1.10	n.d.	n.d.	acid[e]	0.16
106	1.93	103.5	3.95	50	3.25	0.713	0.780	0.037	none	1.50	1.10	n.d.	n.d.	acid[e]	0.10
							B. 123±1°C								
199	···	91.3	14.9	120	1.28	0.582	0.491	0.095	n.d.	n.d.	n.d.	n.d.	n.d.	HCHO[f]	0.006
200	5.1	91.5	13.5	120	1.24	0.564	1.06	0.037	n.d.	n.d.	n.d.	n.d.	n.d.	HCHO[f]	0.47

[a] Mainly aldehydes.
[b] Manometric value; infrared and mass spectrometer analysis indicated alcohols (CH_3OH, possibly also C_2H_5OH), acid (probably HCOOH), water, and some heavier oxygen-containing compounds.
[c] n.d. =not determined.
[d] Determined polarographically in combined "$-82°$" and "room temperature" fractions.
[e] Titrated with 0.01N NaOH.
[f] Spectrophotometric determinations after absorption in water and treatment with chromotropic acid [C. E. Bricker and H. R. Johnson, Ind. Eng. Chem. Anal. Ed. **17**, 400 (1945)].

of the reactions of O-atoms with C_2H_4 and $n-C_4H_{10}$. Allowance for the slight pressure dependence of R_{CO} and R_{CH_4} can be made on the basis of trends in Fig. 3 and a similar graph for $N_2O-n-C_4H_{10}$ mixtures.[8] The values of $k_{C_2H_4}/k_{n-C_4H_{10}}$ obtained in this manner are given in the last two columns of Table IV, where the bracketed values are in the region of almost complete reaction with ethylene and are, therefore, subject to large error. The same value of 22±5 is obtained both from the rates of CO and of CH_4 formation. Inasmuch as the frequency factors for the two reactions can be assumed to be comparable, it is found that $\Delta E=-1.9\pm0.2$ kcal/mole. The activation energies for the reaction of O-atoms with pentane and hexane have been estimated[1] at about 5 kcal. The value for n-butane should be about the same, in which case the activation energy of the reaction of O-atoms with ethylene is close to 3 kcal/mole.

With the high pressures of the reactants used in these experiments very little hydrogen is produced from direct quenching by ethylene. On the basis of the relationships established before[3] it is possible to calculate the amount of hydrogen that would be produced provided no H-atoms are lost through addition to ethylene. When this is done, it is found that an appreciable fraction of H-atoms add to ethylene and thus increase its consumption, as well as, to a somewhat smaller extent, the formation of ethane. For this reason, the values of $k_{C_2H_4}/k_{n-C_4H_{10}}$ calculated from the rates of these two compounds in the ternary mixtures are too large, especially in the two runs (66 and 68) with larger amount of $n-C_4H_{10}$. However, even without any correction these values lead to an upper limit of ΔE which is only slightly larger than the above estimate. When corrections are made (which can be done only approximately) and the possible experimental errors are taken into account, the discrepancy seems to disappear altogether.

The Mechanism of the Reaction

Formation of acetaldehyde and ethylene oxide among other products in the reaction of O-atoms with ethylene indicates at least a partial addition of the atom to the molecule. At the same time the results indicate also quite a pronounced fragmentation. Experiments with added oxygen show that free radicals are involved in the process. In view of this and of the complexity of products formed, it is necessary to ascertain whether the reaction

$$C_2H_4+O\rightarrow C_2H_4O^*, \qquad (1)$$

addition of the atom to the double bond, which is the most logical possibility, is acceptable as the sole primary process. Such an addition would be highly exothermic and would result in the formation of an energy-rich molecule (indicated symbolically by $C_2H_4O^*$). The further fate of this intermediate would be expected to be somewhat similar but not necessarily identical to that of a normal ethylene oxide molecule after it absorbs a large amount of energy, for example, by a transfer from an excited mercury atom or by direct light absorption.

Photolysis of ethylene oxide has been investigated by Gomer and Noyes[9] who find as the principal products CH_4, C_2H_6, H_2, and CO with smaller amounts of CH_3CHO and HCHO. The authors postulate a primary splitting of ethylene oxide into CH_3 and HCO, followed by or simultaneous with decomposition of the latter into H and CO. It can be readily seen that a partial fragmentation of this kind of the $C_2H_4O^*$ could, at least qualitatively, explain the products formed in the reaction of O-atoms with ethylene.

In the mercury sensitized reactions of ethylene oxide[10] the main products were H_2, CO, CH_3CHO, and a polymer, with smaller amounts of CH_4, HCHO, and

[9] R. Gomer and W. A. Noyes, Jr., J. Am. Chem. Soc. **72**, 101 (1950).
[10] Phibbs, Darwent, and Steacie, J. Chem. Phys. **16**, 39 (1948).

TABLE IV. Reactions in mixtures of N_2O, C_2H_4, and $n-C_4H_{10}$ (24±1°C).

Run	Initial pressures (mm) N_2O	C_2H_4	$n-C_4H_{10}$	Irrad. (min)	R_{N_2} (molecule sec^{-1} $\times10^{-15}$)	ϕ_{N_2}	Relative rates ($R_{N_2}=1$) CO	H_2	CH_4	C_2H_6	ΔC_2H_4	$kC_2H_4/kn-C_4H_{10}$ from R_{CO}	from R_{CH_4}
65	101.5	7.90	...	130	1.52	0.68	0.453	0.108	0.108	0.151	1.40	...	...
61	100.9	24.9	24.7	200	1.16	0.50	0.399	0.125	0.104	n.d.[a]	n.d.	(8)[b]	(25)[b]
62	201.3	40.1	98.6	200	1.14	0.51	0.354	0.077	0.097	n.d.	n.d.	(40)[b]	(32)[b]
63	151.9	49.0	146.9	200	0.900	0.40	0.333	0.089	0.090	n.d.	n.d.	23	26
64	100.8	7.54	203.9	170	1.05	0.47	0.189	0.093	0.047	n.d.	n.d.	21	21
66	100.6	7.55	202.5	160	1.03	0.47	0.194	0.088	0.047	0.097	0.98	22	21
68	100.7	7.64	201.6	170	1.01	0.48	0.194	0.092	0.047	0.087	1.05	22	21
70	101.7	7.85	104.3	160	1.19	0.55	0.264	0.076	0.066	0.090	1.01	19	24

[a] n.d. = not determined.
[b] The bracketed values are subject to large experimental error.

"C_2 hydrocarbons" (a fraction recovered from a trap at −126°C). The ratio of CO to CH_3CHO, as well as the effect of pressure on the former and of the time of irradiation on the latter, was comparable with the observations made in the present work. It was thought, however, that predominantly a primary splitting into CH_2, CO, and H_2 occurred, a process not readily adaptable to explain formation of saturated hydrocarbons in the reaction of O-atoms and ethylene. In view of this, it was considered of interest to carry out some additional experiments in order to ascertain the nature of the "C_2 hydrocarbon" fraction and to follow the trends of the products in the presence of ethylene. It was found that considerable amounts of C_2H_6 and C_3H_8 as well as very small quantities of C_4H_{10} and possibly of ketene were among the products.

The same type of products is, therefore, formed in the mercury sensitized decomposition of ethylene oxide and in the reaction of oxygen atoms with ethylene. With ethylene added to ethylene oxide, the relative amounts of different products become roughly comparable in the two processes. In view of this, there seems to be sufficient justification for the postulate that in the reaction of O-atoms with ethylene the primary process is reaction (1). As can be expected, however, it is a matter of considerable difficulty to establish with certainty the subsequent steps, i.e., those leading from the $C_2H_4O^*$ intermediate to the final products observed. While for a more detailed discussion additional experimental information on ethylene oxide and its mixtures with ethylene is required, it seems reasonably certain that free radicals and atoms, probably at least partly of the type suggested by Gomer and Noyes,[9] play an important role. The reversals of the trends in the rates of CO and aldehyde formation at 23 and 123°C, pointed out above, are then readily explainable by abstraction of hydrogen from aldehyde at the higher temperature with subsequent decomposition of the free radical formed.

It should be pointed out that it is not certain *a priori* whether the oxygen atoms produced in mercury photosensitized decomposition of N_2O are in the normal (^3P) state or in the excited (^1D) state. It is also uncertain whether these two forms exhibit different reactivities. Kistiakowsky[11] came to the conclusion that the excited $O(^1D)$ atoms behaved in very much the same manner as the normal $O(^3P)$ atoms. The collision yield of the reaction of $O(^1D)$ or $O(^3P)$ atoms with hydrogen was found not to be larger than 10^{-4}, and with methane to be below 10^{-5} and probably smaller than 10^{-6}. On the other hand, Neujmin and Popov[12] reported very rapid reactions of the $O(^1D)$ atoms with hydrogen and with adsorbed carbon monoxide. For the reaction of the atoms with hydrogen a collision yield not smaller than about 10^{-1} and an activation energy of less than 1.4 kcal were indicated. The reason for the apparent controversy seems to be the difficulty of unambiguous interpretation of experimental observations. Harris and Siegel[13] have reported some preliminary experiments indicating a difference in behavior of $O(^3P)$ and $O(^1D)$ atoms in the presence of ethylene. However, little experimental detail was given and it is impossible to assess to what extent secondary phenomena might have played a role. In the present work, and in similar studies with other compounds,[8] the observed large variation in reaction rates is clearly incompatible with high reactivities of the order found by Neujmin and Popov. It can be concluded, therefore, that the excited $O(^1D)$ atoms, inasmuch as they do react more readily than the normal atoms, are of no importance in the experiments in which oxygen atoms are produced by mercury photosensitized decomposition of nitrous oxide.

ACKNOWLEDGMENTS

The author is indebted to Dr. F. P. Lossing and Miss Frances Gauthier for the mass spectrometer analyses, and to Dr. A. B. Callear and Mr. L. Doyle for gas chromatographic fractionation of "liquid products."

[11] G. B. Kistiakowsky, J. Am. Chem. Soc. **52**, 1868 (1930); G. B. Kistiakowsky and P. E. Millington, Z. physik. Chem. **B13**, 155 (1931).
[12] H. Neujmin and B. Popov, Z. physik. Chem. **B27**, 15 (1934); B. Popov, Acta Physicochim. U.R.S.S. **3**, 223 (1935).
[13] L. Harris and B. M. Siegel, J. Am. Chem. Soc. **63**, 2520 (1941).

Use of Molecular Quantum-Mechanical Approximations Exemplified in the Energy Calculation of the H_3^- System*

ROLAND S. BARKER, HENRY EYRING, DON A. BAKER, AND CHARLES J. THORNE
Departments of Chemistry and Mathematics, University of Utah, Salt Lake City, Utah

(Received November 12, 1954)

Certain approximations of molecular quantum mechanics are examined. The size of the resultant error due to approximate methods for specific multicenter integral evaluations are cited. Examination of the Sklar approximate multicenter electron repulsion formula together with the generalizations and extensions of Vroeland and Löwdin allow application of the underlying approximation principle to three center nuclear attraction integrals. Specific approximate formulation of these integrals is given.

The accumulation of computational errors arising from the many individual integral approximations in the energy evaluation of the linear H_3^- system is specifically examined. The ground state energy of this system found from the Heitler-London and Wang-like treatments were -70 kcal/mole and -84 kcal/mole for the Sklar type approximations, -1 kcal/mole and -19 kcal/mole for the Mulliken type approximations, and -26 kcal/mole and -41 kcal/mole for exact integral evaluations.

It is concluded that the Sklar type approximations, while preferable to the Mulliken type in a few specific evaluations lead like that formulation to considerable discrepancy between the over-all energy obtained for a polyatomic system. The Sklar approximations have the further disadvantage of requiring two-center integral evaluations not needed in the over-all energy calculations. However, both the Sklar and the Mulliken approximations do give a rapid method for evaluating "best" distance and effective charge parameters for use with more extensive exact integral variational method calculations.

1. INTRODUCTION

THE continual appearance of papers treating various theoretical approaches to molecular quantum mechanics based implicitly on neglect of interaction terms warrants examination of the errors thus introduced. Recognition of such a needed examination is made in Mulligan's work[1] relating to the ground state of carbon dioxide. In this work on CO_2 "all interactions are considered" and "every effort made to use as good approximations as possible." However, the question still remains as to the size error caused by the individual approximations. Others have considered facets of the over-all problem of justifying many of the approximations commonly used.[2–5]

References for detailed consideration of fundamental assumptions may be found in Slater's[6] original formulation and subsequent generalization by Eyring and associates[7] for higher electronic systems.

By use of the variational principle, one may calculate an energy for a molecular system, as

$$E \leq \frac{\int \psi H \psi^* d\tau}{\int \psi \psi^* d\tau}. \tag{1.1}$$

The integrations, $\int \cdots d\tau$ imply an integration over all the coordinates represented in the integrand. We have previously discussed in detail[8–10] some of the individual integral approximations. Approximation of the difficult three- and four-center integrals by the usual Mulliken and Rudenberg-Mulliken formulas in the energy calculations for the neutral H_3 metastable molecule and the H_3^+ ion were examined before. The conclusions of the earlier results that the Mulliken formulas are easier to apply and often give the best results are substantiated in the present work. The use and the degree of accuracy of other specific integral approximations is the purpose of the present communication. In the next section Sklar's approximate formulation for multicenter integrals is examined. The integral approximations could be applied to the H_3 and H_3^+ systems. However the H_3^- system selected for the present formulation has a greater number of electrons and thus more dependence on the multicenter approximate integrals. Examination of such dependence for multi-electron systems is the present objective.

2. SKLAR TYPE INTEGRAL APPROXIMATIONS

Sklar's approximate formula[11] for electron repulsion integrals indicates that for spherically symmetrical electron orbitals the product of two such orbitals centered at points A and B may be approximately expressed as the product of the overlap integral, $I_{AB}=\int x_A(1)x_B(1)d\tau_1$, and of a double orbital, $x_F^2(1)$,

* Sponsored by the Office of Ordnance Research, U. S. Army.

[1] J. F. Mulligan, J. Chem. Phys. **19**, 347 (1951).
[2] K. Rudenberg, J. Chem. Phys. **19**, 1433 (1951).
[3] P. O. Löwdin, J. Chem. Phys. **21**, 374 (1953).
[4] C. Vroelant, J. chim. phys. **49**, 141 (1952).
[5] H. Pelzer and E. Wigner, Z. physik. chem. **B15**, 445 (1932).
[6] J. C. Slater, Phys. Rev. **38**, 1109 (1931).
[7] Eyring, Walter, and Kimball, *Quantum Chemistry* (John Wiley and Sons, Inc., New York, 1944), p. 233.
[8] R. S. Barker and H. Eyring, J. Chem. Phys. **22**, 1182 (1954).
[9] Barker, Eyring, Thorne, and Baker, J. Chem. Phys. **22**, 699 (1954).
[10] R. S. Barker and H. Eyring (to be published).
[11] A. L. Sklar, J. Chem. Phys. **7**, 984 (1939).

centered at a point F between A and B. Thus,

$$x_A(1)x_B(1)\approx I_{AB}\cdot x_F^2(1). \tag{2.1}$$

The point F is located at the midpoint of A and B if orbitals x_A and x_B are of the same type and have the same effective charge Z. If the effective charges Z_A and Z_B of the orbitals associated with nuclei A and B are different, the point F may be located[4] between the nuclei at a position a distance R_{AF} from nucleus A and a distance R_{FB} from nucleus B, such that

$$\frac{R_{AF}}{R_{FB}}\approx\frac{Z_B^2}{Z_A^2} \quad \text{and} \quad R_{AB}\approx R_{AF}+R_{FB}. \tag{2.2}$$

The effective charge associated with the orbitals centered at F then is taken as

$$Z_F\approx[\tfrac{1}{2}(Z_A^2+Z_B^2)]^{\frac{1}{2}}. \tag{2.3}$$

Vroelant's recommended distance ratio (1.3) is seen to be that for which

$$R_{AF}Z_A^2-R_{FB}Z_B^2\approx 0. \tag{2.4}$$

More elaborate suggestions for the location of point F have also been made.[3]

Similar expressions may be written for two orbitals centered at C and D. That is,

$$x_C(2)x_D(2)\approx I_{CD}\cdot x_G^2(2). \tag{2.1'}$$

The point G is located between C and D in an analogous manner to that described, so that

$$\frac{R_{CG}}{R_{GD}}\approx\frac{Z_D^2}{Z_C^2}, \quad R_{CG}+R_{GD}\approx R_{CD},$$

and

$$Z_G=[\tfrac{1}{2}(Z_C^2+Z_D^2)]^{\frac{1}{2}}. \tag{2.2'}$$

Substitution of (2.1) and (2.1′) into the general electron repulsion integral definition gives the Sklar approximation. Thus,

$$L_{AB,CD}=\int\frac{1}{r_{12}}x_A(1)x_B(1)x_C(2)x_D(2)d\tau_1 d\tau_2$$

$$\approx I_{AB}\cdot I_{CD}\cdot L_{FF,GG}. \tag{2.5}$$

Exact evaluation formulas for needed overlap and Coulombic integrals with different effective orbital charges,

$$I_{AB}(R_{AB},Z_A,Z_B)=\int x_A(1)x_B(1)d\tau_1 \tag{2.6}$$

$$L_{FF,GG}(R_{FG},Z_F,Z_G)=\int\frac{1}{r_{12}}x_F^2(1)x_G^2(2)d\tau_1 d\tau_2, \tag{2.7}$$

have been studied by Roothaan.[12] Such integrals have been tabulated for a considerable range of internuclear distances and for many effective charges.[13,14]

Substitution of Eq. (2.1) into the general three center nuclear attraction integral leads to a Sklar type approximation for such integrals. Thus,

$$K_{C,AB}=\int\frac{1}{r_{C1}}x_A(1)x_B(1)d\tau_1$$

$$\approx I_{AB}\cdot G_{C,F^2} \tag{2.8}$$

G_{C,F^2} is the two center Coulombic attraction integral

$$\int\frac{1}{r_{C1}}x_F^2(1)d\tau_1.$$

These two-center integrals are generally available.[12,13] Modification and extension of the above formulation by use of Vroelant's[4] approximate product expressions for higher s and p orbitals is possible at once.

TABLE I. The linear three-center attraction integral $K_{a,bc}(R)$.

$R=R_{ab}=R_{bc}$	Actual value[a] (a.u.)	Sklar approx.[b] (a.u.)	R-M approx.[c] (a.u.)
1.00	0.501	0.501	0.516
1.50	0.313	0.311	0.331
2.00	0.197	0.194	0.212
2.50	0.124	0.122	0.135
3.00	0.0791	0.0774	0.0866
4.00	0.0323	0.0315	0.0354
6.00	0.00536	0.00523	0.00589

[a] Calculated from the exact formula of Hirschfelder, Eyring, and Rosen.
[b] $K_{a,bc}\approx I_{bc}\cdot G_{a,f^2}(R_{af})$.
[c] $K_{a,bc}\approx\frac{1}{2}I_{bc}\{G_{a,b^2}+G_{a,c^2}\}$.

TABLE II. The linear three-center attraction integral $K_{b,ac}(R)$.

$R=R_{ab}=R_{bc}$	Actual value[a] (a.u.)	Sklar approx.[b] (a.u.)	R-M approx.[c] (a.u.)
1.00	0.465	0.586	0.428
1.50	0.242	0.349	0.203
2.00	0.117	0.189	0.0894
2.50	0.0539	0.0966	0.0377
3.00	0.0240	0.0471	0.0155
4.00	0.00443	0.0102	0.00254
6.00	0.000128	0.000375	0.000062

[a] Calculated from the exact formula of Hirschfelder, Eyring, and Rosen.
[b] $K_{b,ac}\approx I_{ac}\cdot G_{b,f^2}(R_{bf}=0)=I_{ac}(R_{ac})$.
[c] $K_{b,ac}\approx\frac{1}{2}I_{ac}\cdot\{G_{b,a^2}+G_{b,c^2}\}=I_{ac}\cdot G_{a,b^2}$.

3. COMPARATIVE VALUES OF NUCLEAR ATTRACTION INTEGRAL APPROXIMATIONS

The effect of varying internuclear distances on the accuracy of the Sklar type and of the Rudenberg-Mulliken type[10] approximations is examined in Tables I and II. For 1s hydrogen-like orbitals

$$G_{a,f^2}(R_{af},Z_f)=\frac{1}{R_{af}}[1-e^{-2Z_fR_{af}}(Z_fR_{af}+1)].$$

[12] C. C. J. Roothaan, J. Chem. Phys. **19**, 1445 (1951).
[13] Thorne, Barker, and Eyring, *Tables of Quantum Mechanical Integrals. 1 and 111* (Nos. 10 and 14, Studies in Applied Mathematics, University of Utah, Salt Lake City, Utah, 1953 and 1954).
[14] Baker, Thorne, Barker, and Eyring, *Tables of Quantum Mechanical Integrals. 11* (No. 16 Studies in Applied Mathematics, University of Utah, Salt Lake City, Utah, 1954).

The numerical calculations of all tables are given in a.u. (atomic units), that is in units of the first Bohr radius $a_0=0.5292$ A, and energies in units of e^2/a_0. The integral notation is that used in our previous papers. "Actual" integral computations are defined as those obtained from closed form integration formulas or from evaluations by other means which yield values believed accurate to the stated number of places.

Several "actual values" for the three center attraction integral, $K_{C,AB}(D,Z_A,Z_B)$, with unequal orbital charges have recently been computed by Streetman and Matsen.[15] Comparative values from extensions of the original Sklar and of the Mulliken approximate formulations described before are given in Table III.

The series formulation[15,16] used to obtain the actual values of the unequal charge three-center nuclear attraction integral is

$$K_{c,ab}(D,Z_a,Z_b)=\{\tfrac{1}{2}D^2(Z_a^3Z_b^3)^{\frac{1}{2}}\}$$
$$\times\{\sum_{\tau=0}^{\infty}(2\tau+1)P_\tau(\nu_\theta)[M_\tau(\mu_\theta,2,\alpha)\cdot G_\tau(0,\beta)$$
$$-M_\tau(\mu_\theta,0,\alpha)\cdot G_\tau(2,\beta)]\}. \quad (3.1)$$

The notation is that used before.[16] Particular note should be made of the definitions of $\alpha=(D/2)(Z_b+Z_a)$ and $\beta=(D/2)(Z_b-Z_a)$. For a linear symmetrical system such as that of H_3^- to be discussed where $R=R_{ab}=R_{bc}$, the foregoing expression has the form,

$$K_{c,ab}\left\{(D=R,\ Z_b=\frac{1}{R}(\alpha+\beta),\ Z_a=\frac{1}{R}(\alpha-\beta)\right\}$$
$$=\{\tfrac{1}{4}R^2(Z_a^3Z_b^3)^{\frac{1}{2}}\}\{\sum f(\alpha,\beta)\}$$
$$=\frac{1}{R}[\{(\alpha+\beta)^{\frac{1}{2}}(\alpha-\beta)^{\frac{1}{2}}\}\{\sum f(\alpha,\beta)\}]. \quad (3.2)$$

The second factor (in brackets) does not involve R, Z_a, or Z_b, except as these quantities implicitly enter the parameters α and β. It may further be noted that a particular choice of α and β allows multiple selection of the implicit quantities R, Z_a, and Z_b. That is, several sets of these quantities will have the same Z and R values. Streetman and Matsen[15] have computed a few actual values of the integral, $K_{c,ab}\{R=1,\ Z_b=(\alpha+\beta),\ Z_a=(\alpha-\beta)\}$. This integral having $R=1$ is equivalent to the expression in brackets of Eq. (3.2) and thus allows ready evaluation of $K_{c,ab}$ for several other internuclear distances and orbital charge values. The "actual values" of Table III were thus adapted from Streetman and Matsen's computations.

TABLE III. The linear three-center unequal charge attraction integral $K_{c,ab}(R,Z_m,Z_0)$.

(R,Z_m,Z_0) $Z_b=Z_m$ $Z_0=Z_a=Z_c$	Actual[a] value	Vroelant-Sklar type[b] approx.	Rudenberg-Mulliken[c] approx.
(2,1.00,1.00)	0.1967	0.1936	0.2117
(2,1.25,0.75)	0.2035	0.2140	0.2031
(2,1.125,0.875)	0.2095	0.2068	0.2112
(2,1.25,0.50)	0.2274	0.2458	0.2236
(2,0.875,0.625)	0.2398	0.2487	0.2465

[a] Adapted from Streetman and Matsen.
[b] $K_{c,ab}\approx I_{ab}(R,Z_0,Z_m)\cdot G_{c,f^2}(R_{cf},Z_f)$.
[c] $K_{c,ab}\approx\frac{1}{2}I_{ab}\cdot\{G_{c,a^2}+G_{c,b^2}\}$.

TABLE IV. Angular depencence of $K_{a,bc}(\theta,R)$.

$R=R_{ab}$ $=R_{bc}$	$\angle ABC$	Actual value[a]	Sklar approx.[b]	R-M approx.[c]
2	0° ($J_{a,ab}$)	0.406	0.428	0.432
2	20°	0.381	0.403	0.382
2	60° (Eq. Δ)	0.294	0.310	0.277
2	100°	0.236	0.239	0.233
2	140°	0.206	0.196	0.213
2	180° (linear)	0.196	0.194	0.212

[a] Calculated from the series method of Coulson and Barnett.
[b] $K_{a,bc}\approx I_{bc}\cdot G_{a,f^2}$.
[c] $K_{a,bc}\approx\frac{1}{2}I_{bc}\{G_{a,b^2}+G_{a,c^2}\}$.

The described unequal charge approximations may be easily applied to the two-center attraction integrals $J_{a,ab}$ and $J_{b,ab}$. Thus, for example,

$$J_{a,ab}(R,Z_a,Z_b)=\int_{r_a}^{1}\frac{x_a x_b d\tau}{}$$
$$\approx I_{ab}\cdot G_{a,f^2} \qquad \text{(Sklar type approx.)}$$
$$J_{a,ab}(R,Z_a,Z_b)\approx\tfrac{1}{2}I_{ab}\{Z_a+G_{a,b^2}\}.$$
(Mulliken type approx.)

The two-center formulations allow numerical comparison, over a wide range of the parameters, of the various types of approximate values and of values from simple closed form actual integral expressions.[10]

The accuracy of the three-center attraction integral approximations for various internuclear angles is shown in Tables IV and V.

The actual values of Table IV were obtained using the first six terms of the infinite series of half-order Bessel functions advocated by Coulson[17] and Barnett and Coulson.[18] Helpful discussions and calculational aid with the actual value angular integral $K_{a,bc}$ have been received from M. Krauss (Chemistry Department, University of Utah) and are gratefully acknowledged.

The special case when $\angle ABC=0$ reduces the integral $K_{a,bc}$ to the two-center integral $J_{a,ab}$ For comparative purposes the value as calculated from the appropriate approximation is given.

[15] J. R. Streetman and F. A. Matsen, J. Chem. Phys. **22**, 1366 (1954).
[16] R. S. Barker and Henry Eyring, J. Chem. Phys. **21**, 912 (1953).
[17] C. A. Coulson, Proc. Cambridge Phil. Soc. **33**, 104 (1937).
[18] M. P. Barnett and C. A. Coulson, Trans. Roy. Soc. (London) **A243**, 489 (1951).

TABLE V. Angular dependence of $K_{b,ac}(\theta,R)$.

$R=R_{ab}=R_{bc}$	R_{ac}	$\angle ABC$	Actual value[a]	Sklar approx.[b]	R-M approx.[c]
2	0	0° (G_{b,a^2})	0.4725	0.4725	0.4725
2	2	60° (Eq. Δ)	0.2946	0.3096	0.2771
2	4	180° (linear)	0.1171	0.1183	0.0894
2.5	0	0° (G_{b,a^2})	0.3906	0.3906	0.03906
2.5	2.5	60° (Eq. Δ)	0.1936	0.2029	0.1790
2.5	5	180° (linear)	0.0539	0.0966	0.0377
3	0	0° (G_{b,a^2})	0.3300	0.3300	0.3300
3	3	60° (Eq. Δ)	0.1260	0.1315	0.1150
3	6	180° (linear)	0.0240	0.0471	0.0155

[a] From Hirschfelder and Weygandt, J. Chem. Phys. **6**, 806 (1938).
[b] $K_{b,ac}\approx I_{ac}\cdot G_{b,f^2}=I_{ac}$.
[c] $K_{b,ac}\approx I_{ac}\cdot G_{a,b^2}$.

4. COMPARATIVE VALUES OF MULTICENTER ELECTRON REPULSION INTEGRAL APPROXIMATIONS

The usual Sklar approximation as used, generalized, and extended by Sklar, Sklar-Lyddane, Parr-Crawford, Vroelant, Löwdin, and others[3,4,11] is applicable to multicenter repulsion integrals. For the type orbitals here considered the approximation may be formulated as Eq. (2.1). The various special cases may then be obtained by substitution of the appropriate orbitals of the particular desired integral in the general expression. Thus when the orbitals of A, B, and C are alike and the associated orbital centers are allowed to coincide, one obtains the ionic integral

$$L_{aa,\,ab}\approx I_{ab}\cdot L_{aa,\,ff}\ \{\text{Sklar ionic integral approx.}\}. \quad (4.1)$$

The point f about which the double orbital replacing the product of the orbitals associated with nuclei a and b centers is located as before described in Eq. (2.2). The two-center exchange integral is similarly obtained by substitution of a for A and C, and b for B and D in the general formulation (2.5). Thus,

$$L_{ab,\,ab}\approx I_{ab}{}^2\cdot L_{f^2,\,f^2}=(5/8)Z_f\cdot I_{ab}{}^2,$$
$$\{\text{Sklar exchange integ. approx.}\} \quad (4.2)$$

where $Z_f=\frac{1}{2}(Z_a{}^2+Z_b{}^2)^{\frac{1}{2}}$, and point f is as before cited. Special three-center integrals occurring in the linear symmetrical H_3^- system here considered are likewise easily obtained. For example the integral,

$$L_{b^2,\,ac}\approx I_{ac}\cdot L_{b^2,\,g^2}$$
$$\{\text{Sklar multicenter repulsion integ. approx.}\}. \quad (4.3)$$

When $Z_a=Z_b$ the point g in the needed coulombic integral of the foregoing formula coincides with B and this integral becomes

$$L_{bb,\,b'b'}(Z_f,Z_g)=\int\frac{1}{r_{12}}[x_b(1)]^2[x_{b'}(2)]^2d\tau. \quad (4.4)$$

If the charges Z_f and Z_g associated with 1s hydrogen like orbitals x_b and $x_{b'}$ are different, the foregoing one-center integral has the closed form expression

$$L_{bb,\,b'b'}(Z_f,Z_g)=\frac{Z_fZ_g(Z_f{}^2+3Z_fZ_g+Z_g{}^2)}{(Z_f+Z_g)^3}. \quad (4.5)$$

The above formula may be obtained by expanding the $(1/r_{12})$ term of Eq. (4.4) by the Neumann expansion in terms of associated Legendre polynomials, and carrying through the integration much as is done for the Coulombic integral occurring in the helium atom calculations.[19] The Sklar approximations of Table VI are then readily evaluated.

Few "actual values" of electron repulsion integrals with unequal orbital charges are available for integrals other than coulombic. The availability of unequal orbital charge Coulombic integrals[14,12] is fortunate as the exchange and multicenter integrals of all the approximations cited are expressed in terms of these integrals. Actual values for the unequal orbital charge exchange integrals may be computed by the infinite series formulation used by Zener, Rosen, Coolidge-James, Hirschfelder-Linnett, Kotani, and others.[20] For

TABLE VI. Internuclear distance dependence of some linear repulsion integrals.

Integral ($R=R_{ab}=R_{bc}$)	Actual value[a] (a.u.)	Sklar approx.[b] (a.u.)	Mulliken approx.[c] (a.u.)
$L_{a^2,\,ab}$(1.0)	0.5070	0.5194	0.5062
(2.0)	0.3080	0.3252	0.3082
(4.0)	0.07698	0.08062	0.08257
(6.0)	0.01531	0.01506	0.01864
$L_{ab,\,ab}$(1.0)	0.4367	0.4605	0.4346
(2.0)	0.1841	0.2150	0.1807
(4.0)	0.01563	0.02239	0.01563
(6.0)	0.0008140	0.001386	0.0008779
$L_{a^2,\,bc}$(1.0)	0.4171	0.4209	0.4208
(2.0)	0.1884	0.1875	0.1975
(4.0)	0.03222	0.0315	0.03525
(6.0)	0.005355	0.005233	0.005885
$L_{b^2,\,ac}$(1.0)	0.3358	0.3665	0.3252
(2.0)	0.09421	0.1183	0.08062
(4.0)	0.003923	0.006360	0.002519
(6.0)	0.0001178	0.0002342	0.00006244
$L_{ab,\,ac}$(1.0)	0.2788	0.3046	0.2718
(2.0)	0.05121	0.06155	0.04785
(4.0)	0.0006539	0.00082037	0.0005873
(6.0)	0.000004769	0.000005645	0.00004596
$L_{ab,\,bc}$(1.0)	0.3995	0.4085	0.3979
(2.0)	0.1412	0.1465	0.1483
(4.0)	0.009128	0.008867	0.01115
(6.0)	0.004364	0.0003695	0.005775

[a] Values from Hirschfelder (see reference 10).
[b] $L_{aa,ab}\approx I_{ab}\cdot L_{aa,ff}$; $L_{ab,ab}\approx I_{ab}{}^2\cdot L_{ff,ff}$; $L_{a^2,bc}\approx I_{bc}\cdot L_{a^2,ff}$; $L_{b^2,ac}\approx I_{ac}\cdot L_{bb,b'b'}$; $L_{ab,ac}\approx I_{ab}\cdot I_{ac}\cdot L_{ff,gg}$; $L_{ab,bc}\approx I_{ab}{}^2\cdot L_{ff,gg}$.
[c] $L_{aa,ab}\approx\frac{1}{2}I_{ab}\{L_{aa,aa}+L_{aa,bb}\}$; $L_{ab,ab}\approx\frac{1}{2}I_{ab}{}^2\{L_{aa,aa}+L_{aa,bb}\}$; $L_{a^2,bc}\approx\frac{1}{2}I_{ab}\times\{L_{aa,bb}+L_{aa,cc}\}$; $L_{bb,ac}\approx\frac{1}{2}I_{ab}\cdot L_{aa,bb}$; $L_{ab,ac}\approx\frac{1}{2}I_{ab}\cdot I_{ac}\{L_{aa,aa}+L_{aa,cc}+2L_{aa,bb}\}$; $L_{ab,bc}\approx\frac{1}{2}I_{ab}{}^2\{L_{aa,aa}+L_{aa,cc}+{}^2L_{aa,bb}\}$.

[19] See reference 7, p. 103.
[20] C. Zener and V. Guillemin, Phys. Rev. **34**, 999 (1929); N. Rosen, Phys. Rev. **38**, 255 (1931); A. S. Coolidge and H. M. James, J. Chem. Phys. **2**, 816 (1934). J. O. Hirschfelder and J. W. Linnett,

the 1*s* orbital integrals considered here, the integral may be written

$$L_{ab,\,ab}=\left\{\frac{R^5(Z_0Z_m)^3}{8}\right\}\{\sum_{\tau=0}^{\infty}(2\tau+1)[G_\tau(0,\beta)\times\{W_\tau(2,2,\alpha)G_\tau(0,\beta)-W_\tau(2,0,\alpha)G_\tau(2,\beta)\}+G_\tau(2,\beta)\{W_\tau(0,2,\alpha)G_\tau(0,\beta)-W_\tau(0,0,\alpha)G_\tau(2,\beta)\}]. \quad (4.6)$$

The integral may then be expressed as $(1/R)$ times a factor involving only α and β parameters in a manner similar to Eq. (3.2). The definitions of α and β are the same as given before. Thus,

$$L_{ab,\,ab}=\frac{1}{R}[\{(\alpha+\beta)^3(\alpha-\beta)^3\}\{\sum_{\tau}E_\tau(\alpha,\beta)\}]. \quad (4.7)$$

Using the foregoing formula and the tables of auxiliary functions of Kotani, Amemiya, and Simose,[20] the actual value computations for $L_{ab,\,ab}$ given in Table VII were made. Actual values of the integral for other R, Z_a, Z_b for which $\alpha=(R/2)(Z_b+Z_b)$ and $\beta=(R/2)(Z_b-Z_a)$ may be found at once by consideration of Eq. (4.7).

"Actual value" calculations for the unequal orbital charge ionic integral $L_{aa,\,ab}$ of Table VII were obtained by use of Barnett and Coulson's exact value formula.[18] Thus,

$$L_{aa,\,ab}(R,Z_a,Z_b)=\int\frac{1}{r_{12}}[a(1)]^2a(2)b(2)d\tau_1d\tau_2=J_{a,\,ab}(R,Z_0,Z_m)-J_{a,\,ab}{}'(R,\gamma,\delta)-I_{ab}{}'(R,\gamma,\delta) \quad (4.8)$$

TABLE VII. Effect of unequal charges on the electron repulsion integrals $L_{aa,\,ab}$ and $L_{ab,\,ab}$ ($Z_a=Z_c=Z_0$ and $Z_b=Z_m$).

Integral (R,Z_m,Z_0)	Actual value[a]	Sklar approx.[b]	Mulliken approx.[c]
$L_{aa,\,ab}$(1,1,1)	0.507045	0.5194	0.5062
(1,1.1,0.95)	0.473424	0.5058	0.4969
(1,1.3,0.70)	0.366558	0.3839	0.4232
(2,1,1)	0.308036	0.3252	0.3082
(2,1.1,0.95)	0.291638	0.3130	0.3005
(2,1.3,0.70)	0.229513	0.2556	0.2753
(4,1,1)	0.076982	0.08062	0.083
(4,1.1,0.95)	0.068274	0.07542	0.07761
(4,1.3,0.70)	0.060960	0.07682	0.08593
$L_{ab,\,ab}$(2.5,1.4,1)	0.184156	0.2150	0.181

[a] $L_{aa,ab}$ calculated from Eq. (4.8); $L_{ab,ab}$ calculated from Eq. (4.6).
[b] $L_{aa,ab}\approx I_{ab}\cdot L_{aa,ff}$; $L_{ab,ab}\approx I_{ab}{}^2\cdot L_{aa,a'a'}$.
[c] $L_{aa,ab}\approx\frac{1}{2}I_{ab}\cdot(L_{aa,aa}+L_{aa,bb})$; $L_{ab,ab}\approx I_{ab}{}^2(L_{aa,aa}+L_{aa,bb})$.

TABLE VIII. Angular dependence of electron repulsion integrals ($R=R_{ab}=R_{bc}$ and $Z_a=Z_b=Z_c=Z$).

Integral (R,θ)	Actual[a] value	Sklar[b] approx.	Mulliken[c] approx.
$L_{ab,\,bc}$(2.0,0°)	0.184156	0.2150	0.1807
(2.0,60°)	0.169845	0.2035	0.1636
(2.0,180°)	0.141207	0.1465	0.1483
(2.5,0°)	0.106622	0.1313	0.1043
(2.5,60°)	0.095383	0.1115	0.0909
(2.5,180°)	0.075091	0.0774	0.0820
(3.0,0°)	0.058506	0.0759	0.0574
(3.0,60°)	0.050862	0.0596	0.0481
(3.0,180°)	0.039101	0.0388	0.0435
$L_{aa,\,bc}$(2.0,0°)	0.308036	0.3470	0.3082
(2.0,60°)	0.258356	0.2699	0.2498
(2.0,180°)	0.188392	0.1875	0.1975
$L_{ab,\,ac}$(2.0,0°)	0.308036	0.3470	0.3082
(2.0,60°)	0.169844	0.2035	0.1636
(2.0,180°)	0.051214	0.06568	0.0479
$L_{bb,\,ac}$(2.0,0°)	0.425974	0.425974	0.425974
(2.0,60°)	0.258356	0.2699	0.2498
(2.0,180°)	0.094214	0.1183	0.08866

[a] See Barker and Eyring, (to be published).
[b] $L_{ab,bc}\approx I_{ab}{}^2\cdot L_{ff,ff}$; $L_{aa,bc}\approx I_{ab}\cdot L_{aa,ff}$; $L_{ab,ac}\approx I_{ab}\cdot I_{ac}\cdot L_{ff,bb}$; $L_{bb,ac}\approx I_{ac}\cdot L_{bb,ff}$.
[c] $L_{ab,bc}\approx\frac{1}{4}I_{ab}{}^2\{2L_{aa,bb}+L_{aa,cc}+L_{bb,bb}\}$; $L_{aa,bc}\approx L_{bc}\{L_{aa,bb}+L_{aa,cc}\}$; $L_{ab,ac}\approx\frac{1}{2}I_{ab}\cdot I_{ac}\{L_{aa,aa}+L_{aa,cc}+2L_{bb,aa}\}$; $L_{bb,ac}\approx I_{ac}\{L_{bb,aa}+L_{bb,cc}\}$.

where $\gamma=3Z_0$ and $\delta=Z_m$

$$J'_{a,\,ab}(R,\gamma,\delta)=4(Z_0{}^3Z_m{}^3)^{\frac{1}{2}}(RX^2)^{-1}\times[2\delta e^{-\gamma R}-(2\delta+RX)e^{-\delta R}]$$

$$I'_{ab}(R,\gamma,\delta)=8(Z_0{}^3Z_m{}^3)^{\frac{1}{2}}(RX^3)^{-1}\times[\delta(RX-4\gamma)e^{-\gamma R}+\gamma(RX+4\delta)e^{-\delta R}]$$

and $X=\delta^2-\gamma^2$.

The accuracy of the approximations for various internuclear angles is shown in Table VIII. When $\angle ABC=0$, the points A and C coincide and $L_{ab,\,bc}=L_{ab,\,ba}$, $L_{aa,\,bc}=L_{aa,\,ba}$, $L_{ab,\,ac}=L_{ab,\,aa}$, and $L_{bb,\,ac}=L_{bb,\,aa}$.

5. TRIAL FUNCTION FOR THE H_3^- SYSTEM

The electronic structures one may write for the H_3^- system are[f]

(covalent structure 1): $\overset{(-)}{A}\quad B-C\leftrightarrow A-B\quad\overset{(-)}{C}$,

(covalent structure 2): $\overset{(-)}{A-B}\quad C\leftrightarrow A-\overset{(-)}{B}\quad C$,

(ionic structure 1): $\overset{(+)}{A}\overset{(-)}{B}\overset{(-)}{C}\leftrightarrow\overset{(-)}{A}\overset{(-)}{B}\overset{(+)}{C}$,

(ionic structure 2): $\overset{(-)}{A}\overset{(+)}{B}\overset{(-)}{C}$.

[f] J. Chem. Phys. **18**, 130 (1950); Kotani, Amemiya, and Simose, Proc. Phys. Math. Soc. Japan **20**, Extra No. 1 (1938); **22**, Extra No. 1 (1940).

The trial function used in most approximate treatments is taken to be some linear combination of products of atomic orbitals. The 1s functions used in the system under discussion have the usual form. That is $a(n)=(Z_a/\pi)^{\frac{1}{2}}e^{-Z_a r_{an}}$, $b(n)=(Z_b/\pi)e^{-Z_b r_{bn}}$, and so forth. The electrons are denoted by $n=1$, 2, 3, or 4. The distance between the lth nucleus and the nth electron is r_{ln}. Letters represent single electron orbital functions (here 1s hydrogen-like orbitals) associated with nuclei of the same alphabetical designations, while the numbers following in parentheses specify the electron occupying the particular orbital. Z is the "effective nuclear charge" of the orbital.

Assignment of spin eigenfunctions to the electronic orbitals associated with the individual atoms of an electronic structure of the molecular system may be achieved by representing the corresponding structural eigenfunction by the linear combination

$$\phi=\frac{1}{\sqrt{4!}}\sum_{p}(-1)^{p}P_{p}(a\alpha)_1(a\beta)_2(b\alpha)_3(c\beta)_4, \quad (5.1)$$

where $(a\alpha)_1$ expresses the orbit-spin electronic wave function occupied by electron 1, $(a\beta)_2$ that of electron 2 and so on. P is the permutation operator, representing the operation of permuting the subscripts (interchanging the orbitals occupied by any pair of electrons). The coefficient $(-1)^p$ gives the proper sign for the term (of the linear combination function) in order to satisfy Pauli's principle. The function, φ, [Eq. (5.1)] may also be written as the Slater determinant,

$$\varphi=\frac{1}{\sqrt{4!}}\begin{vmatrix}(a\alpha)_1 & (a\beta)_1 & (b\alpha)_1 & (c\beta)_1\\ (a\alpha)_2 & (a\beta)_2 & (b\alpha)_2 & (c\beta)_2\\ (a\alpha)_3 & (a\beta)_3 & (b\alpha)_3 & (c\beta)_3\\ (a\alpha)_4 & (a\beta)_4 & (b\alpha)_4 & (c\beta)_4\end{vmatrix}. \quad (5.2)$$

It may also be denoted as

$$\varphi=\begin{pmatrix}a & a & b & c\\ \alpha & \beta & \alpha & \beta\end{pmatrix}. \quad (5.3)$$

The linear combination functions of the type of Eqs. (5.1), (5.2), or (5.3) adequately deal with electron exchange degeneracy. The electronic structural eigenfunction should contain, however, terms from other possible arrangements of spins representing the same structure, that is, from the spin degeneracy. This consideration allows one to write the possible electronic structural eigenfunctions in the usual manner. Thus,

$$\psi_{\text{cov. }1}=\psi A^-, BC+\psi C^-, AB=\begin{pmatrix}a & a & b & c\\ \alpha & \beta & \alpha & \beta\end{pmatrix}$$

$$-\begin{pmatrix}a & a & b & c\\ \alpha & \beta & \beta & \alpha\end{pmatrix}+\begin{pmatrix}c & c & a & b\\ \alpha & \beta & \alpha & \beta\end{pmatrix}-\begin{pmatrix}c & c & a & b\\ \alpha & \beta & \beta & \alpha\end{pmatrix}$$

$$\psi_{\text{cov. }2}=\psi B^-, AC=\begin{pmatrix}b & b & a & c\\ \alpha & \beta & \alpha & \beta\end{pmatrix}-\begin{pmatrix}b & b & a & c\\ \alpha & \beta & \beta & \alpha\end{pmatrix} \quad (5.4)$$

$$\psi_{\text{ion. }1}=\psi A^-B^-+\psi C^-B^-=\begin{pmatrix}a & a & b & b\\ \alpha & \beta & \alpha & \beta\end{pmatrix}+\begin{pmatrix}c & c & b & b\\ \alpha & \beta & \alpha & \beta\end{pmatrix}$$

$$\psi_{\text{ion. }2}=\psi A^-C^-=\begin{pmatrix}a & a & c & c\\ \alpha & \beta & \alpha & \beta\end{pmatrix}.$$

The above functions are independent as may be shown by Rumer's[21] vectorial method and must therefore all be retained in a complete treatment. Such a valence-bond-plus-ionic-terms treatment, then, as the trial function,

$$\psi=C_1\psi_{\text{cov. }1}+C_2\psi_{\text{cov. }2}+C_3\psi_{\text{ion. }1}+C_4\psi_{\text{ion. }2},$$

where the C's are compositional parameters. The simple covalent trial function (Heitler-London treatment) is

$$\psi_{\text{cov.}}=K_1\psi_{\text{cov. }1}+K_2\psi_{\text{cov. }2}. \quad (5.5)$$

The Hamiltonian operator for the H_3^- system may be written,

$$H=-\tfrac{1}{2}\sum_{n=1}^{4}\nabla_i^2+\sum_{l>p=a}^{c}R_{1p}^{-1}$$

$$-\sum_{l=a,n=1}^{c,4}r_{1n}^{-1}+\sum_{n>m=1}^{4}r_{nm}^{-1}, \quad (5.6)$$

where ∇_n^2 is the Laplacian operator for electron n, r_{1n} is the distance of electron n from nucleus 1, R_{1p} is the distance between nuclei 1 and p, r_{nm} the distance between electrons n and m. Energy minimization of the structural compositional constants C_i, when H is used as given in Eq. (5.6), leads to the usual secular determinant, $|H_{st}-ES_{st}|=0$. The matrix elements are defined as $H_{st}=\int\psi_s H\psi_t d\tau$, and $S_{st}=\int\psi_s\psi_t d\tau$, where ψ_s and ψ_t represent the sth and tth component structural eigen-

[21] G. Rumer, Ges. Wiss. Nachr. Göttingen, 377 (1932).

functions (5.4) of the trial function (5.5). Thus,

$$H_{22}=\int\psi_2 H\psi_2 d\tau$$

$$=\int\left\{\begin{pmatrix} b & b & a & c\\ \alpha & \beta & \alpha & \beta\end{pmatrix}-\begin{pmatrix} b & b & a & c\\ \alpha & \beta & \beta & \alpha\end{pmatrix}\right\}$$

$$\times H\left\{\begin{pmatrix} b & b & a & c\\ \alpha & \beta & \alpha & \beta\end{pmatrix}-\begin{pmatrix} b & b & a & c\\ \alpha & \beta & \beta & \alpha\end{pmatrix}\right\}d\tau$$

$$=\int\begin{pmatrix} b & b & a & c\\ \alpha & \beta & \alpha & \beta\end{pmatrix}H\begin{pmatrix} b & b & a & c\\ \alpha & \beta & \alpha & \beta\end{pmatrix}d\tau$$

$$-\int\begin{pmatrix} b & b & a & c\\ \alpha & \beta & \alpha & \beta\end{pmatrix}H\begin{pmatrix} b & b & a & c\\ \alpha & \beta & \beta & \alpha\end{pmatrix}d\tau$$

$$-\int\begin{pmatrix} b & b & a & c\\ \alpha & \beta & \beta & \alpha\end{pmatrix}H\begin{pmatrix} b & b & a & c\\ \alpha & \beta & \alpha & \beta\end{pmatrix}d\tau$$

$$+\int\begin{pmatrix} b & b & a & c\\ \alpha & \beta & \beta & \alpha\end{pmatrix}H\begin{pmatrix} b & b & a & c\\ \alpha & \beta & \beta & \alpha\end{pmatrix}d\tau. \quad (5.7)$$

Examination of

$$\int\begin{pmatrix} b & b & a & c\\ \alpha & \beta & \alpha & \beta\end{pmatrix}H\begin{pmatrix} b & b & a & c\\ \alpha & \beta & \beta & \alpha\end{pmatrix}d\tau,$$

a typical integral in the matrix element (5.7) shows the reduction to the simpler orbital integral form. The functional parts may be written as

$$\begin{pmatrix} b & b & a & c\\ \alpha & \beta & \alpha & \beta\end{pmatrix}=(1/4!)^{\frac{1}{2}}\sum_{\nu}(-1)^{\nu}P_{\nu}\{(b\alpha)_1(b\beta)_2(a\alpha)_3(c\beta)_4\}$$

and

$$\begin{pmatrix} b & b & a & c\\ \alpha & \beta & \beta & \alpha\end{pmatrix}=(1/4!)^{\frac{1}{2}}\sum_{\nu'}(-1)^{\nu'}P'_{\nu'}\{(b\alpha)_1(b\beta)_2(a\beta)_3(c\alpha)_4\}.$$

The integral may then be written,

$$\begin{pmatrix} b & b & a & c\\ \alpha & \beta & \beta & \alpha\end{pmatrix}H\begin{pmatrix} b & b & a & c\\ \alpha & \beta & \beta & \alpha\end{pmatrix}d\tau$$

$$=1/4!\int\sum_{\nu}(-1)^{\nu}P_{\nu}(d\alpha)_1(b\beta)_2(a\alpha)_3(c\beta)_4$$

$$\times H[\sum_{\nu'}(-1)^{\nu'}P'_{\nu'}(b\alpha)_1(b\beta)_2(a\beta)_3(c\alpha)_4]. \quad (5.8)$$

P and P' are, of course, the usual permutation operators. Since such permutations include all possible exchanges of pairs of electrons one may multiply [Eq. (5.8)] by any other permutation operator.[22] Thus one may multiply by the inverse operator, $(-1)^{\nu}(P_{\nu})^{-1}$, obtaining

$$\sum_{\nu}P_{\nu}(P_{\nu})^{-1}\{(b\alpha)_1(b\beta)_2(a\alpha)_3(c\beta)_4\}$$
$$=4!\{(b\alpha)_1(b\beta)_2(a\alpha)_3(c\beta)_4\}.$$

The integral (5.8) thus reduces to,

$$\int(b\alpha)_1(b\beta)_2(a\alpha)_3(c\beta)_4$$
$$\times H[\sum_{\nu''}(-1)^{\nu''}P'_{\nu''}\{(b\alpha)_1(b\beta)_2(a\alpha)_3(c\beta)_4 d\tau\}]. \quad (5.9)$$

Because of the orthogonality of the spin functions, all the terms in Eq. (5.9) will vanish except those for which the spins match identically.[23] Thus one has

$$\int\begin{pmatrix} b & b & a & c\\ \alpha & \beta & \alpha & \beta\end{pmatrix}H\begin{pmatrix} b & b & a & c\\ \alpha & \beta & \alpha & \beta\end{pmatrix}d\tau$$

$$=(b\,b\,a\,c|H|b\,b\,a\,c)-(b\,b\,a\,c|H|a\,b\,b\,c)$$
$$-(b\,b\,a\,c|H|b\,c\,a\,b)+(b\,b\,a\,c|H|a\,c\,b\,b)$$

$$=b^2\,b^2\,a^2\,c^2-ba\,b^2\,ab\,c^2-b^2\,bc\,a^2\,cb+ba\,bc\,ab\,cb. \quad (5.10)$$

The orbital integral notation, $\int b(1)b(2)a(3)c(4)|H|\times b(1)c(2)a(3)b(4)d\tau=(b\;b\;a\;c|H|b\;c\;a\;b)=b^2\;bc\;a^2\;cb$, is used in the foregoing. The Hamiltonian operator expression (5.6) allows one to write out the orbital integrals in terms of products of elemental integrals. The kinetic energy part of the operator, for example, will give terms such as,

$$ba\;b^2\;ab\;c^2=(b|\tfrac{1}{2}\nabla_1^2|a)\cdot I_{b^2}\cdot I_{ab}\cdot I_{c^2}$$
$$+I_{ba}\cdot(b-\tfrac{1}{2}\nabla_2^2 b)\cdot I_{ab}\cdot I_{c^2}+\cdots$$
$$=T_{ba}\cdot I_{ba}+T_{b^2}\cdot I_{ab}+\cdots$$

One may expand Eq. (5.7) and obtain,

$$H_{22}=b^2\,b^2\,a^2\,c^2-ba\,b^2\,ab\,c^2-b^2\,bc\,a^2\,cb+ba\,bc\,ab\,cb$$
$$+b^2\,b^2\,ac\,ca-bc\,b^2\,ab\,ca-b^2\,ba\,ac\,cb+bc\,ba\,ab\,cb$$
$$+b^2\,b^2\,ac\,ca-bc\,b^2\,ab\,ca-b^2\,ba\,ac\,cb+bc\,ba\,ab\,cb$$
$$+b^2\,b^2\,a^2\,c^2-b^2\,ba\,ab\,c^2-bc\,b^2\,a^2\,cb+bc\,ba\,ab\,cb$$
$$=2\{a^2b^2b^2c^2+b^2b^2ac\;ac\}$$
$$-4\{a^2b^2bc\;cb+b^2ab\;bc\;ac-ab\;babc\;cb\}.$$

Similarly,

$$H_{11}=4\{2(a^2c^2\;ab\;bc-a^2bc\;cb\;ac+ab\;ba\;ac\;ca)$$
$$+a^2a^2b^2c^2-a^2b^2c^2\;ac+a^2a^2bc\;cb-a^2b^2ac\;ca$$
$$-a^2c^2ab\;ba-a^2bc\;ab\;ca-a^2cbba\;ac$$
$$+b^2ac\;ac\;ca\}. \quad (5.11)$$
$$H_{12}=4\{2(a^2b^2cb\;ac)-a^2b^2c^2ab-a^2ab\;bc\;cb$$
$$+c^2ab\;ab\;ba-b^2ab\;ac\;ca$$
$$+ab\;ab\;bc\;ac-ab\;ba\;cb\;ac\}.$$
$$H_{21}=4\{2(a^2b^2bc\;ca)-a^2b^2c^2ba-a^2ba\;cb\;bc$$
$$+c^2ba\;ba\;ab-b^2\;ba\;ca\;ac+ba\;ba\;cb\;ca$$
$$-ba\;ab\;bc\;ca\}.$$

The above matrix elements H_{st} given in terms of orbital integrals have been shortened by reduction and collec-

[22] See reference 7, pp. 240–241.

[23] W. Heitler and F. London, Z. Physik 44, 455 (1927).

TABLE IX. Single structural energy calculations for linear symmetrical H_3^-.

Type calculation	ψ	R	Z	Binding energy (kcal/mole)
Actual integ. values	$\psi_{cov.1}$	2.0	1.00	20
	$\psi_{cov.1}$	2.25	0.89	35
Sklar integ. values	$\psi_{cov.1}$	2.0	1.00	46
	$\psi_{cov.1}$	2.22	0.90	58
Mulliken integ. values	$\psi_{cov.1}$	2.0	1.00	−3
	$\psi_{cov.1}$	2.27	0.88	14

tion of equivalent expressions in accord with the following principles. In the abbreviated notation for orbital integrals such as $a^2\ bc\ cb\ cb$ [Eq. (4.3)] the alphabetical symbolism pairs the orbitals of each electron and denotes the specified numerical electron by the position of such orbital pair. Consideration of the Hamiltonian operator H, the constituent atomic orbitals of the trial function ψ, and of the molecular geometry of the system under discussion then justifies the following operational rules and conventions.

Rule 1

The order of orbital pairs in an orbital integral term has no effect on its numerical value. (All the electrons in the Hamiltonian operator for the system are symmetrical and their numerical designations are thus interchangeable.) For the linear symmetrical H_3^- system, for example, $a^2\ bc\ cb\ cb \Rightarrow bc\ a^2\ cb\ cb$.

Rule 2

All the alphabetical designations of equivalent electronic orbitals centered at geometrically equivalent positions may be interchanged. Thus for the linear symmetrical H_3^- system "a" and "c" may be interchanged in the orbital expressions. For example, $c^2\ c^2\ ab\ bc \Rightarrow a^2\ a^2\ cb\ ba$. However, for the linear unsymmetrical H_3^- system $c^2\ c^2\ abbc \neq a^2\ a^2\ cb\ ba$.

Rule 3

The orbitals of an electron pair may be interchanged if the atomic orbital forms are equivalent. Thus for the linear symmetrical H_3^- system with the trial function composed of $1s$ orbitals of the form, $a(n)=(Z_a^3/\pi)^{\frac{1}{2}}e^{-Z_a r_{an}}$, $b(n)=(Z_b^3/\pi)^{\frac{1}{2}}e^{-Z_b r_{bn}}$, $ba=ab$ if $Z_a=Z_b$. If $Z_a \neq Z_b$, $ba \neq ab$ because the Laplacian part of the operator will then lead to nonequivalent expressions when acting on $a(n)$ and $b(n)$.

Use of the foregoing rules and the conventions that follow enable one to reduce and collect the matrix elements H_{st} into the simple expressions (5.11).

Convention 1

Reletter the electron orbitals of an orbital integral in conformity with the molecular geometry (rule 2) to secure as far as possible the greatest number of orbitals of lowest alphabetical designation. Thus, for example, for the linear symmetrical H_3^- system, $c^2\ cb\ ac\ b^2$ is to be written as $a^2\ ab\ ca\ b^2$.

Convention 2

Write the orbital pairs of the integral in order of increasing geometrical distance between the centers of the constituent orbitals. This may be accomplished by renumbering the electrons (rule 1). Thus $a^2\ ab\ ca\ b^2$ is to be written as $a^2\ b^2\ ab\ ca$.

Convention 3

Arrange the orbitals of the electrons, if possible, (rule 3) so the pair designation will appear in alphabetical order. Thus for the equal charge linear symmetrical H_3^- system, $a^2\ ba\ cb\ ca = a^2\ ab\ cb\ ac$ but if $Z_b \neq Z_a \neq Z_c$ the orbital integral must be written $a^2\ ba\ cb\ ca$.

Somewhat similar rules and conventions may be readily formulated for reducing and collecting equivalent elemental integral expressions. One may write, $K_{c,\,ab} \Rightarrow K_{a,\,bc}$, $L_{c^2,\,ab} \Rightarrow L_{a^2,\,bc}$, and so forth.

6. COMPARATIVE "ACTUAL VALUE" AND APPROXIMATE VALUE INTEGRAL ENERGY EVALUATIONS

The over-all comparative results of the use of "actual value" and of the various type "approximate value" integrals for a full scale molecular system calculation using the simple covalent (Heitler-London and Wang-type) formulations are given in Tables IX and X.

In the Wang-like treatment the trial functions (5.4) are modified by the use of orbitals containing the charge parameter Z. The orbital integral and elemental integral expressions are similar to those already employed except for this modification of the composite orbitals to let Z be other than unity. If one makes the substitution of variable $\rho=RZ$, it may be seen that the composite two-parameter (R,Z) integrals, except for the overlap and kinetic energy integrals I and T, may be written as the orbital charge Z times the formerly employed one-parameter (R) type integrals.[24] All terms derived from the orbitals that arise from parts of the Hamiltonian operator other than the kinetic energy terms have expressions unaltered except for the common factor Z and the substitution of ρ for R. The kinetic energy terms, contain a common factor of Z^2. Thus, for example,

$$T_{ab}(Z,R)=\int a(1)\,|-\tfrac{1}{2}\nabla_1^2|\,b(1)\,d\tau_1$$
$$=\tfrac{1}{2}Z^2-ZJ_{a,\,ab}(Z,R)=Z^2\{\tfrac{1}{2}-J_{a,\,ab}(\rho)\}.$$

This enables one to write the energy expression for a

[24] Giddings, Barker, and Eyring, J. Chem. Phys. 23, 344 (1955).

single structure, for example, as

$$E_{11}(Z)=Z(E_{11})+(Z^2-Z)\left(\frac{U_{11}}{S_{11}}\right), \qquad (6.1)$$

where

E_{11}=energy expression when $Z=1$, and

$$U_{11}=\int\psi_1|\sum_{n=1}^{4}-\tfrac{1}{2}\nabla_n^2|\psi_1 d\tau_1 \quad \text{with} \quad Z=1.$$

S_{11}, U_{11}, and E_{11} are independent of Z, at constant ρ, therefore Eq. (6.6) may be differentiated with respect to Z to give the single structural expressions,

$$Z_{\min}=\tfrac{1}{2}-\tfrac{1}{2}E_{11}\left(\frac{S_{11}}{U_{11}}\right) \quad \rho=\text{constant} \qquad (6.2)$$

and

$$E_{11}(Z)=-\tfrac{1}{4}\left(\frac{S_{11}}{U_{11}}\right)\left[E_{11}-\frac{U_{11}}{S_{11}}\right]^2 \quad \rho=\text{constant}. \qquad (6.3)$$

The results of a single structural treatment are given in Table IX. The energies of Tables IX and X are given with reference to three hydrogen atoms and an electron all infinitely far apart. The numerical values were obtained using $e^2/a_0=627.23$ kcal/mole.

When both covalent structures are used, the Wang-like procedure becomes somewhat more complicated. Approximate expressions similar to Eqs. (6.2) and (6.3) may be derived. Thus,

$$Z_{\text{cov.}}\approx\tfrac{1}{2}-\tfrac{1}{2}\left(\frac{E_{\text{cov.}}}{U_{\text{cov.}}}\right) \quad \rho=\text{constant} \qquad (6.2')$$

and

$$E_{\text{cov.}}(Z)\approx Z_{\text{cov.}}E_{\text{cov.}}+(Z_{\text{cov.}}^2-Z_{\text{cov.}})U_{\text{cov.}} \qquad (6.3')$$

where $U_{\text{cov.}}=K_1^2U_{11}+2K_1K_2U_{12}+K_2^2U_{22}$. The K's are found as before. These expressions are only approximate ones because the K's are somewhat dependent on $E_{\text{cov.}}$ and therefore on Z. One may use the $Z_{\text{cov.}}$, obtained from Eq. (6.7) in the exact energy expression for that particular Z, in which

$$H_{11}(Z)=ZH_{11}+(Z^2-Z)U_{11};$$

$$H_{12}(Z)=ZH_{12}+(Z^2-Z)U_{12};$$

and

$$H_{22}(Z)=ZH_{22}+(Z^2-Z)U_{22}.$$

The new value for $E_{\text{cov.}}$ found may then be used to re-evaluate the K's and a better U and Z found. By such iteration the "best" $Z_{\text{cov.}}$ and $E_{\text{cov.}}$ may be obtained. The results of various treatments are given in Table X. Exact values may be compared with those obtained by Stevenson and Hirschfelder.[25] The calculated binding energy of the system as computed from the approximate integrals does not alter significantly the conclusions as to the small quantities of ion to be expected, even at low pressures, made in the cited work of Stevenson and Hirschfelder.

TABLE X. Energy calculations for the H_3^- linear symmetrical system.

Type calculation	R	Z	K_1	K_2	Binding energy (kcal/mole)
Heitler-London treatment					
Actual integ. values	2.0	1.00	0.387	−0.191	26
Sklar integ. values	2.0	1.00	0.305	−0.412	70
Mulliken integ. values	2.0	1.00	0.398	−0.160	1
Wang-like treatment					
Actual integ. values	2.25	0.89			41
Sklar integ. values	2.22	0.90			84
Mulliken integ. values	2.27	0.88			19

7. LIMITATIONS AND USE OF INTEGRAL APPROXIMATIONS

Our present and previous investigations have led us to prefer the simple Mulliken-type approximation to others examined because of its ease of application. The use of only composite integrals whose evaluation is needed in any case in the over-all energy calculation is thus deemed a definite advantage. However such preference does not mean that better results may not be secured for particular integrals by the other approximations. Further it should be recognized that application of "corrections" or "normalization like procedures" previously described,[8] to the simple approximation methods lead to better results.

At first glance, the energy errors of the two approximations examined here might lead one to conclude that the energy of a system might well be taken as an average of that found using the two approximations. While this gives a good value for the H_3^- system, the success of the procedure appears fortuitous in the light of an examination of the individual integral evaluations.

The tables for the individual integral values indicate that generalizations as to the direction or magnitude of errors caused by the approximations examined are dubious if not dangerous. For $K_{a,\,bc}$ the Sklar approximation is smaller than the "actual" evaluation, while the Mulliken approximation gives larger values. For $K_{b,\,ac}$ the reverse is true. The angular dependence of the "actual" and approximate evaluations is also complex, as may be seen from an examination of Table IV.

[25] D. Stevenson and J. O. Hirschfelder, J. Chem. Phys. **5**, 933 (1937).

Anomalous Light Emission of Azulene

MICHAEL BEER* AND H. C. LONGUET-HIGGINS†
Department of Chemistry, University of Manchester, Manchester, England

Azulene was found to fluoresce with a frequency corresponding to transition from the second excited singlet level to the ground state. No phosphorescence was observed. No emission corresponding to transition from the lowest excited singlet to the ground state was observed. These phenomena are discussed.

THE light emission properties of azulene, the deep blue hydrocarbon, have been studied in solution.

EXPERIMENT

The following experiments were carried out:

(1) *Determination of total luminescence under excitation with ultraviolet light.* The exciting source was a 125-watt medium pressure mercury arc in a quartz envelope. Its output was passed through a 2-mm Corning 9863 filter and a 5-cm filter cell containing one molar aqueous solution of nickel sulfate. A quartz lens focused the beam on the sample. This was a solution of azulene in EPA (5 parts by volume of isopentane, 5 parts of ether, 2 parts of ethanol) in a quartz test tube. Low-temperature studies were made in a quartz Dewar flask that had a belt left unsilvered for observation. The coolant was liquid nitrogen. The reemitted radiation was photographed with a Hilger medium spectrograph on Kodak IIN plates using a $\frac{1}{2}$-mm slit and two hour exposures.

(2) *Separation of phosphorescence from fluorescence.* This experiment was carried out in the manner of Lewis and Kasha.[1] The exciting source was the same mercury arc as above. No filters were used. The phosphoroscope, of the rotating blade type, had a resolving time of 0.004 sec. IIN plates were exposed for two hours in the Hilger medium spectrograph with a $\frac{1}{2}$-mm slit width.

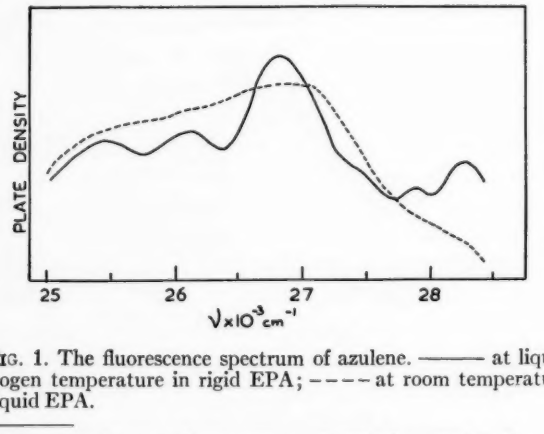

FIG. 1. The fluorescence spectrum of azulene. ——— at liquid nitrogen temperature in rigid EPA; – – – – at room temperature in liquid EPA.

(3) *Determination of total luminescence under excitation with sodium yellow light.* The exciting source was a 45-watt sodium lamp with a 1-cm filter cell containing a 5 percent aqueous solution of copper sulfate. All experiments were done at liquid nitrogen temperature as in experiment (1).

OBSERVATIONS AND DISCUSSION

(1) An emission was found in the rigid medium at liquid nitrogen temperature (Fig. 1). Its decay lifetime was too short to be observed with the phosphoroscope. At room temperature in fluid medium this emission persisted (Fig. 1) but the spectrum was more diffuse and the relative intensity of the O—O band was decreased. The most obvious vibrational spacing was 1420 cm^{-1}, a strongly infrared active frequency. The short decay lifetime and the persistence in liquid solution indicated that the emission was a fluorescence corresponding to a transition from an excited singlet level to the ground singlet.

However, while for all other organic substances so far reported the fluorescence spectrum was approximately the mirror image of the absorption system at *longest* wavelengths,[2] for azulene the fluorescence spectrum was the mirror image of the *second* system with the O—O band at 28 400 cm^{-1}. Thus in terms of the assignments of Mann, Platt, and Klevens,[3] the fluorescent state is not the low-lying ^1L_b state but the higher ^1L_a level.

This phenomenon implies that the probability of radiationless transitions from the second to the first excited level is small compared with the probability of radiative transition from the second excited level to the ground level. The explanation is probably to be found in the large energy difference between the two lowest excited levels. Their separation is 14 300 cm^{-1} which is greater than for any two adjacent singlet levels in any of the cata-condensed hydrocarbons.[4] Great separation disfavors intersection of potential energy surfaces, rendering radiationless transitions from the upper to the lower state improbable.

The weakening of the O—O emission band at room temperature is probably due to the broadening of the overlapping O—O absorption band of molecules in the ground state.

* Present address, Department of Physics, University of Michigan, Ann Arbor, Michigan.
† Present address, The University Chemical Laboratory, Cambridge, England.

[1] G. N. Lewis and M. Kasha, J. Am. Chem. Soc. **66**, 2100 (1944).

[2] M. Kasha, Discussions Faraday Soc. **9**, 14 (1950).

[3] Mann, Platt, and Klevens, J. Chem. Phys. **17**, 481 (1949).

[4] H. B. Klevens and J. R. Platt, J. Chem. Phys. **17**, 470 (1949).

(2) No slowly decaying phosphorescence could be separated by the phosphoroscope.

Most organic substances which fluoresce also emit phosphorescence when in a rigid medium. This phosphorescence is always at longer wavelengths. It is, however, not surprising that such a phosphorescence was not found for azulene, because assuming a fluorescence-phosphorescence frequency difference[5] of 2000–10 000 cm^{-1}, we find that the phosphorescent level of azulene would be above the lowest excited singlet level at 14 000 cm^{-1}.[3] A radiationless transition to the latter level could occur and, even if relatively slow, would compete against the highly forbidden triplet-singlet transition which gives rise to the phosphorescence.

(3) No infrared emission was found when exciting with sodium yellow radiation.

Absence of infrared radiation corresponding to emission from the lowest excited singlet level suggests that the potential energy surfaces of the ground and the lowest excited singlet states intersect. It seems worth mentioning that all attempts to eke luminescence out of dimethyl fulvene were fruitless.

[5] M. Kasha, Chem. Revs. **41**, 401 (1947).

ACKNOWLEDGMENTS

The authors wish to thank Professor M. Kasha for helpful discussions and Professor P. A. Plattner for a gift of azulene.

THE JOURNAL OF CHEMICAL PHYSICS VOLUME 23, NUMBER 8 AUGUST, 1955

Quenching of NaI Fluorescence by H_2, HCl, CO_2, and H_2O†

HOWARD G. HANSON
University of Minnesota, Duluth Branch, Duluth, Minnesota

(Received November 1, 1954)

The experimental quenching cross sections of H_2, HCl, CO_2, and H_2O for the sodium D lines arising from the optical dissociation of the sodium iodide molecule have been determined by measurements with a photomultiplier tube. The velocities of the excited sodium atoms after dissociation of the sodium iodide molecules by ultraviolet light of different wavelengths have been determined by using an approximation for the repulsive potential curve of an excited sodium atom and normal iodine atom obtained from a measurement of the excitation of the sodium D lines as a function of exciting ultraviolet wavelength. The variation of quenching cross section for HCl and CO_2 with relative velocities of excited sodium atom and quenching molecules shows a decrease of cross section with increase in relative velocity. The cross section for H_2 shows little change with relative velocity in the range of velocities used. H_2O shows little quenching action. The source of ultraviolet light was a hydrogen discharge lamp and the wavelength of the exciting ultraviolet light in the 2100 A–2500 A range was controlled by a reflection grating monochromator.

I. INTRODUCTION

TERENIN[1] observed the optical dissociation of sodium iodide by ultraviolet light in 1926. The dissociation products[2] are normal or excited sodium and iodine atoms. The dissociation products to be considered are a sodium atom in the 3^2P state and a normal iodine atom. In returning to the ground state, the sodium atoms emit D light. Any excess energy that the ultraviolet photon possessed over that necessary to dissociate the sodium iodide molecule and excite the sodium atom goes into kinetic energy of the dissociation products.[3] If an excited sodium atom engages in a collision of the second kind with a foreign molecule, it will not emit a D photon, and hence one might expect a quenching of the D lines fluorescence in the presence of foreign gases. The quenching cross section for this process has been measured for various gases and vapors by several investigators.[4–7] Quenching of the D lines in resonance radiation experiments has also been studied.[8–10] The source of ultraviolet light in past studies has been the spark lines of various metals. Little has been known about the relative efficiencies at different wavelengths in producing the D lines fluorescence from sodium iodide. The present study uses the continuous molecular spectrum of hydrogen as ultraviolet source and a monochromator to isolate narrow spectral regions. The relative intensities of D lines fluorescence have been measured as a function of exciting ultraviolet wavelength. From the data on the relative intensity distribution as a function of exciting wavelength, an experi-

† Supported in part by the Office of Ordnance Research.

[1] A. Terenin, Z. Physik **37**, 98 (1926).
[2] H. D. Schmitt-Ott, Z. Physik **69**, 724 (1931).
[3] T. R. Hogness and J. Franck, Z. Physik **44**, 26 (1927).
[4] J. G. Winans, Z. Physik **60**, 631 (1930).
[5] A. Terenin and N. Prileshajewa, Z. physik. Chem. **B13**, 72 (1931).
[6] Kisilbasch, Kondratjew, and Leipunsky, Physik. Z. Sowjetunion **2**, 201 (1932).
[7] H. G. Hanson, Ph.D. thesis, University of Wisconsin, 1948 (unpublished).
[8] R. G. W. Norrish and MacF. W. Smith, Proc. Roy. Soc. (London) **A176**, 295 (1940).
[9] L. V. Hamos, Z. Physik **74**, 379 (1932).
[10] R. Mannkopff, Z. Physik **36**, 315 (1926).

mental plot of the potential curve for sodium in the 3^2P state together with an iodine atom in the ground state has been constructed. With a knowledge of the upper repulsive state for the excited sodium atom together with an iodine atom, one can ascertain for all wavelengths of exciting ultraviolet light the relative kinetic energy of separation of the dissociation products due to the excess ultraviolet photon energy. Thus, it is possible to determine the dependence of quenching cross section on the relative speeds of excited sodium atoms with respect to quenching molecules.

II. EXPERIMENTAL

The experimental arrangement is shown in Fig. 1. The sodium iodide salt is placed in a 15 mm diameter Vycor tube which has a fused quartz side window. The tube is approximately 15 cm long with the side window equidistant from the ends. The tube is mounted vertically inside an electric furnace and attached to the vacuum system by a quartz to Pyrex glass seal. Figure 1 shows the top view of furnace and tube. The Nichrome wound furnace is cylindrical in shape and furnished with four viewing windows as shown. The furnace is closed at top and bottom. The windings are so arranged that the central portion of the furnace is at the highest temperature even if the four central windows allow considerable radiation cooling.

When the salt is heated under vacuum, some of it sublimes from the position in the Vycor tube below the windows to a cooler portion of the furnace above the windows, forming a porous plug of condensed salt in the upper portion of the tube. This porous salt plug prevents further rapid loss of salt from the tube. After long heating, an equilibrium arrangement of the two salt surfaces is attained, both surfaces being at the same temperature. This method dispenses with the necessity of using ground quartz stops as were found necessary by previous investigators.[4,5,7]

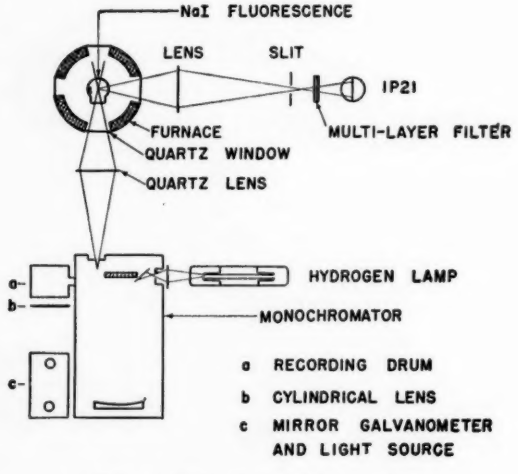

FIG. 1. Arrangement of apparatus.

The temperature of the furnace is held constant by a modified Wheelco temperature control to within $\pm 1°C$. The temperature is measured with a Chromel *P*-alumel thermocouple and a potentiometer.

The ultraviolet light source is a water-cooled hydrogen discharge lamp obtained from the Hanovia Chemical and Manufacturing Company. The lamp operates on a 5000 volt ac source at approximately $\frac{1}{2}$ amp. The lamp was monitored by a Photronic cell arrangement. The ratio of visible light output of the lamp as measured by the Photronic cell and the *D* line fluorescence intensity produced by the ultraviolet output of the lamp always remained constant even though the lamp's total intensity decreased with time as it heated when put in operation.

The monochromator is a Bausch and Lomb 500 mm focal length reflection grating instrument with a 100 mm$\times$100 mm grating area and a dispersion of 16.5 A per mm in the first order. The grating is blazed for ultraviolet in the first order. The slit width used is 3.0 mm, corresponding to a 50 A spread in exciting wavelength at any setting.

The ultraviolet light was brought to a focus in the sodium iodide fluorescence tube by a quartz lens, as shown in Fig. 1. An image of the cone of fluorescent light in the tube is imaged on a slit by a glass lens. Behind the slit is a multi-layer filter with peak transmittance for the *D* lines. The fluorescent light then falls on the 1P21 photomultiplier tube of a Photovolt Corporation photometer. The amplified current output of the photometer operates a G.E. reflecting galvanometer attached to the monochromator. The light beam from the reflecting galvanometer falls on photographic paper wound on an extension to the wavelength drum of the monochromator. The trace on the photographic paper then corresponds to the intensity of fluorescence as a function of exciting ultraviolet wavelength. Reference marks are put on the photographic paper for various wavelength settings of the drum before a trace is recorded. The wavelength drum is turned by a synchronous motor during the recording of the trace.

Measurements were made by drawing a base line and a smooth curve through the trace by eye and measuring the amplitude of the trace with a rule for a series of equispaced wavelengths. The average of measurements on 5 or 10 traces was used to determine the intensity of fluorescence at any exciting wavelength.

Quenching gas pressures were measured by a mercury manometer. A McLeod gauge and a Pirani gauge were used at low pressures. The gases used were of reagent quality obtained from the Air Reduction Sales Company.

III. RESULTS AND INTERPRETATION

The quenching cross section calculations are similar to those of Terenin and Prileshajewa.[5,11] If one assumes

[11] N. Prileshajewa, Physik. Z. Sowjetunion **2**, 351 (1932); **2** 367 (1932).

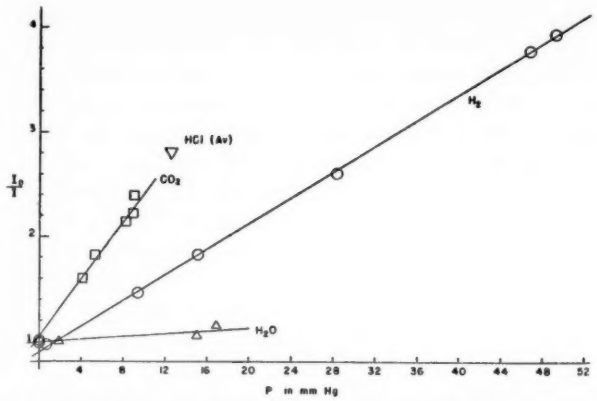

FIG. 2. I_0/I is the ratio of unquenched to quenched fluorescence. The data for H_2 and H_2O shown here was taken without the monochromator but using the total ultraviolet output of the hydrogen discharge lamp. The data for CO_2 and HCl is the average of I_0/I for all exciting wavelengths selected by the use of the monochromator.

that every collision between an excited sodium atom and a quenching molecule is a quenching collision, the Stern-Volmer relation can be stated

$$I/I_0=1/(1+z\tau) \tag{1}$$

where I/I_0 is the ratio of quenched to unquenched fluorescence, τ is the mean life time of the excited state of the atom and z is the expected number of collisions per second for the excited atom. Let the gas kinetic expression[12] for z be:

$$z=\pi^{\frac{1}{2}}n\sigma^2\alpha\psi(x)/x, \tag{2}$$

where n is the number of quenching molecules per cm³; $\pi\sigma^2$ is the quenching cross section; $\alpha=(2RT/M_Q)^{\frac{1}{2}}$, the most probable speed of quenching molecules (M_Q is the molecular weight of the quenching gas molecules); $v_{Na'}$ is the most probable speed of the excited sodium atoms; $x=v_{Na'}/\alpha$; and

$$\psi(x)=x\exp[-x^2]+(2x^2+1)\int_0^x \exp[-y^2]dy.$$

The most probable speed of the excited sodium atom, $v_{Na'}$, is calculated by the relationship

$$v_{Na'}=v_1+\tfrac{1}{3}v_{NaI}^2/v_1 \quad \text{for} \quad v_1>v_{NaI}$$

$$v_{Na'}=v_{NaI}+\tfrac{1}{3}v_1^2/v_{NaI} \quad \text{for} \quad v_{NaI}>v_1$$

where v_1 is the speed of the excited sodium atom relative to the sodium iodide molecule from which it came, and $v_{NaI}=(2RT/M_{NaI})^{\frac{1}{2}}$. From elementary considerations

$$v_1=[2wm_Im_{Na}^{-1}(m_I+m_{Na})^{-1}]^{\frac{1}{2}}, \tag{3}$$

where w is the excess energy of the exciting ultraviolet photon over the energy needed to dissociate the sodium iodide molecule and excite the sodium atom. Eliminating z between Eq. (1) and Eq. (2) and accounting for the number of quenching molecules per cm³ at different pressures and temperatures one obtains

$$\sigma^2=\left[\frac{1.04\times10^{-19}T}{\pi^{\frac{1}{2}}\tau\alpha}\cdot\frac{x}{\psi(x)}\right]\frac{(I_0/I-1)}{P_{MM}}, \tag{4}$$

where P_{MM} is the pressure of the quenching gas in mm Hg. Denoting the quantity in brackets in Eq. (4) by $1/K$, one obtains

$$I_0/I=K\sigma^2P_{MM}+1. \tag{5}$$

The value of K is fixed by choice of quenching gas, operating temperature, exciting ultraviolet wavelength and knowledge of the mean life of the excited state of the sodium atom. The value of τ was taken as 1.61×10^{-8} sec.[13]

From Eq. (5), it can be seen that if the Stern-Volmer relation holds a plot of I_0/I *vs* P_{MM} should yield a straight line with intercept of unity. Figure 2 shows the average values of I_0/I for all wavelengths of exciting ultraviolet light *vs* P_{MM} for the quenching agents used. It is to be noted that not all curves pass through 1.00 at zero pressure. The curves drawn are the best curves in the sense of "least squares." The failure to pass through 1.00 is apparently the result of an uncertainty in the observed value of I_0.

The uncertainty in I_0 was investigated. Figure 3 shows a curve of I/I_0 for small pressures of hydrogen which is a moderate quenching agent. An enhancement of fluorescence is observed during the increase of hydrogen pressure from zero to approximately 2 mm Hg. This enhancement was also observed for water vapor as quenching agent. The assumed explanation of this enhancement is that the distribution of the sodium

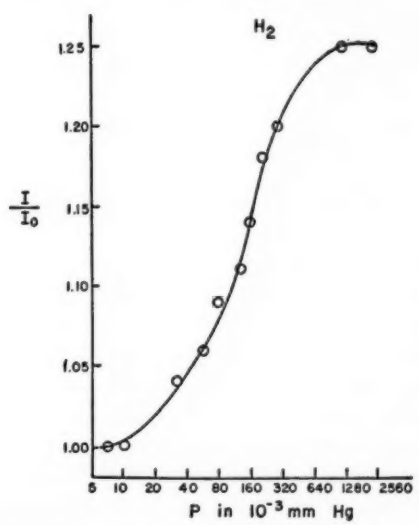

FIG. 3. The enhancement of NaI fluorescence by the addition of small pressures of a weakly quenching gas. A similar result was observed for H_2O as a quenching agent.

[12] L. B. Leob, *The Kinetic Theory of Gases* (McGraw-Hill Book Company, Inc., New York, 1934), 2nd edition, p. 102.

[13] G. Stephenson, Proc. Phys. Soc. (London) **A64**, 458 (1951).

FIG. 4. The intensity of D line emission following the optical dissociation of the NaI molecule by ultraviolet light as it depends on the wavelength of the exciting light for two different temperatures of NaI salt vapor.

iodide salt vapor density in the fluorescence tube changes during the transition from pressures where the mean free path is of the order of magnitude of the dimensions of the fluorescence tube to mean free paths that are small compared to the dimensions of the fluorescence tube. The vacuum attained during the measurement of I_0 was about 10^{-5} mm. Hg under optimum conditions. However, a certain amount of free iodine was always observed in the traps of the system after the salt had been heated for some time. The exact residual pressure due to this iodine vapor as well as the vapor pressure of the sodium iodine itself at various operating temperatures was unknown. Since the measured value of I_0 is subject to uncertainty, it was considered that the trend of the I_0/I curves for quenching pressures larger than 2 mm Hg would determine the experimental slope to be used together with Eqs. (4) and (5) to determine the value of σ^2. A "least squares" determination of the best straight line representation of I_0/I *vs* P_{MM} was made for every exciting ultraviolet wavelength. The value of P_{MM} corresponding to $I_0/I=2$ (irrespective of whether the curve passes through 1.00 at $P_{MM}=0$) was used to calculate σ^2 from Eq. (4), While this method is not exact, it minimizes the effects of errors in measurement of intensity of fluorescence at very low or very high quenching pressures and gave the most consistent results over different runs on the same quenching agents. Attempts to determine the "correct" value of I_0 by extrapolating to zero quenching pressure, using only data from higher quenching pressures, gave results which were less consistent between successive runs. This was probably due to the sensitivity of such a procedure to errors in measurement of the low values of I corresponding to high quenching pressures. A consideration of the error introduced by the method of treating the data will show that the values of σ^2 calculated may tend to be somewhat lower than their true values.

The measurement of intensity of unquenched fluorescence as a function of exciting wavelength necessitated a measurement of the intensity distribution of the source as a function of wavelength. The calibration of the hydrogen lamp together with the monochromator was accomplished by placing a sodium salicylate coated plate at the exit slit of the monochromator. The fluorescent response of the sodium salicylate was measured with the photometer. The response of a 1P21 photomultiplier tube to the fluorescence of sodium salicylate excited by ultraviolet light has been shown to be proportional to the number of exciting ultraviolet photons.[14] A thickness of quartz, approximately the same as that involved in the quenching apparatus, was placed between the sodium salicylate coated plate and the photomultiplier tube to equalize the optical paths during the calibration and the fluorescence measurements.

Figure 4 shows the relative intensity of sodium D lines fluorescence as it depends on exciting ultraviolet wavelength. The curves have been corrected for the characteristics of the source and, therefore, their shape should depend only on the properties of the sodium iodide molecules at the temperatures of measurement. Four experimental runs at intermediate temperatures gave curves which were intermediate between the extremes shown. The curves are normalized at their maxima. Since the slit width used corresponded to 50 A, it is not considered that the shift in maximum at the two temperatures is real. However, the onset of fluorescence approaching from the long wavelength side depends markedly on the temperature. A greater change in onset wavelength with temperature was observed by Visser[15] in the case of thallium iodide. A measurement on sodium iodide under unknown conditions by Prileshajewa[16] shows an onset wavelength of 2500 A and a maximum at 2380 A. Terenin and Prileshajewa[5] give 2430 A as the onset wavelength.

The upper repulsive state, as shown in Fig. 5 for sodium in the 3^2P state together with iodine in the ground state, was approximated in the following way: The lower potential curve for the sodium iodide molecule in the ground state is a Morse curve calculated from constants for sodium iodide listed by Herzberg.[17] The first eight vibrational levels are shown. The 3 mm slit on the monochromator corresponds to approximately 1000 cm^{-1} spread in the energy of the ultraviolet beam for any setting of the monochromator in the range used. This corresponds to the spacing of three or four vibrational levels so it is not possible to resolve

[14] K. Watanabe and Edward C. Y. Inn, J. Opt. Soc. Am. **43**, 32 (1953).

[15] G. H. Visser, thesis, Delft, 1932 Table 43 in P. Pringsheim, *Fluorescence and Phosphorescence* (Interscience Publishers, Inc., New York, 1949), p. 212.

[16] Presented in Fig. 8, p. 335 [J. M. Frank, Physik. Z. Sowjetunion **2**, 319 (1932)].

[17] G. Herzberg, *Spectra of Diatomic Molecules* (D. Van Nostrand Company, Inc., New York, 1950), 2nd edition, p. 555.

the contributions to the fluorescent intensity from individual vibrational levels. At the temperatures used, only the first seven or eight levels contribute significantly to the fluorescent intensity. The Franck-Condon principle in its simplest form was used together with the Boltzmann temperature distribution to calculate an approximation for the upper repulsive curves shown in Fig. 5. It was assumed that transitions directly upward occurred only at the turning points of vibrational states and were equally likely from either end of a vibrational state. Also that the number of upward transitions from any vibrational state was proportional to the population of that state. In Fig. 5, the relative Boltzmann populations of the vibrational states for two different temperatures are shown each individually referred to 100 percent for the zeroth level. The two upper repulsive curves calculated from the data taken at the two temperatures were obtained by plotting points directly above the ends of each vibrational level. The distance above the end points of the vibrational levels was obtained by noting the wavelength of exciting light in Fig. 4 corresponding to the percent of intensity expected from each level in terms of its relative population. (It was assumed that transitions upward from the *center* of the zeroth vibrational state were responsible for the maximum intensity of fluorescence and that the upper curve was a repulsive curve with no minima.) The fact that the curves for the two temperatures do not coincide indicates to some degree the error in the measurements and in the assumptions themselves. The maximum separation of the two curves is approximately one-half the energy interval corresponding to the slit width used in the experiment.

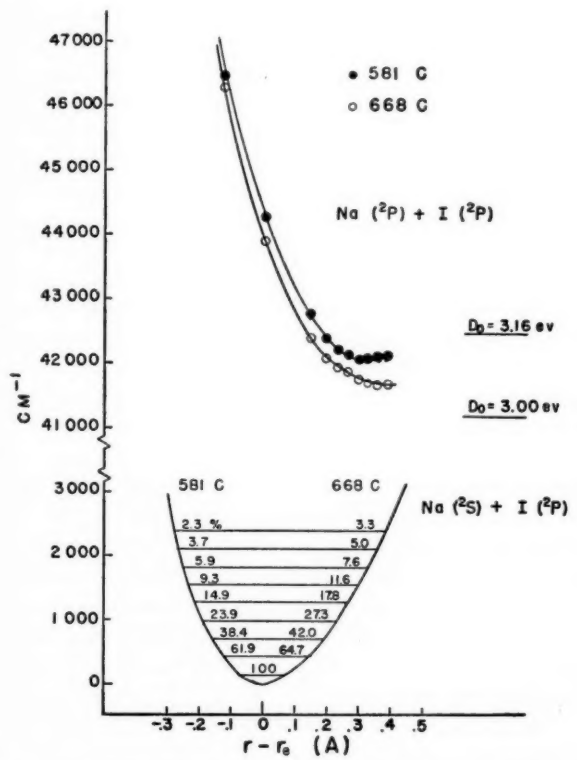

FIG. 5. The repulsive potential curve for the excited sodium atom together with a normal iodine atom as deduced from the data in Fig. 4. The lower potential curve is a Morse curve constructed from known constants of the NaI molecule.

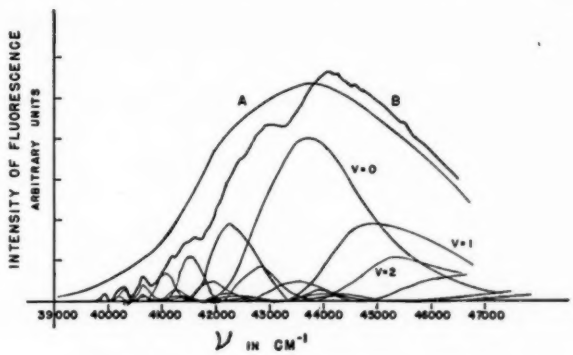

FIG. 6. Curve *A* is the observed intensity. Curve *B* is the calculated intensity which is the sum of the intensities obtained from considering the probability density functions of the first seven vibrational states of the sodium iodide molecule.

The potential curve obtained by the foregoing severely simplifying assumptions was investigated by the application of more conventional methods. Using the upper potential curve of Fig. 5 and the vibrational eigenfunctions of the first seven vibrational states of the sodium iodide molecule, a calculation of the expected distribution of intensity of fluorescence was made. The method used is similar to the methods discussed.[18]

The probability density distribution functions used were those of a harmonic oscillator calculated from the constants given for sodium iodide.[17] The probability density distribution curves were drawn to scale so that the classical turning points for each vibrational level coincided with the intersection of that vibrational level with the lower potential curve in Fig. 5. The difference between the Morse curve used and the true parabola one would have for a harmonic oscillator was small enough for the first seven vibrational states so that the same scale factor could be used for all seven probability density functions.

The contribution of each vibrational level to the total expected intensity was obtained by a "reflection" of the probability density function for each level from the upper curve.[17] The ν factor,[19] was omitted because the intensity of fluorescence observed depends only on the number of photons involved in transitions and not on the energy of each exciting ultraviolet photon. The contribution of each vibrational level to the intensity of fluorescence is shown in Fig. 6. Each level's contribution has been adjusted by the appropriate Boltzmann temperature factor. The calculations of

[18] See reference 17, p. 391.
[19] See reference 17, p. 393.

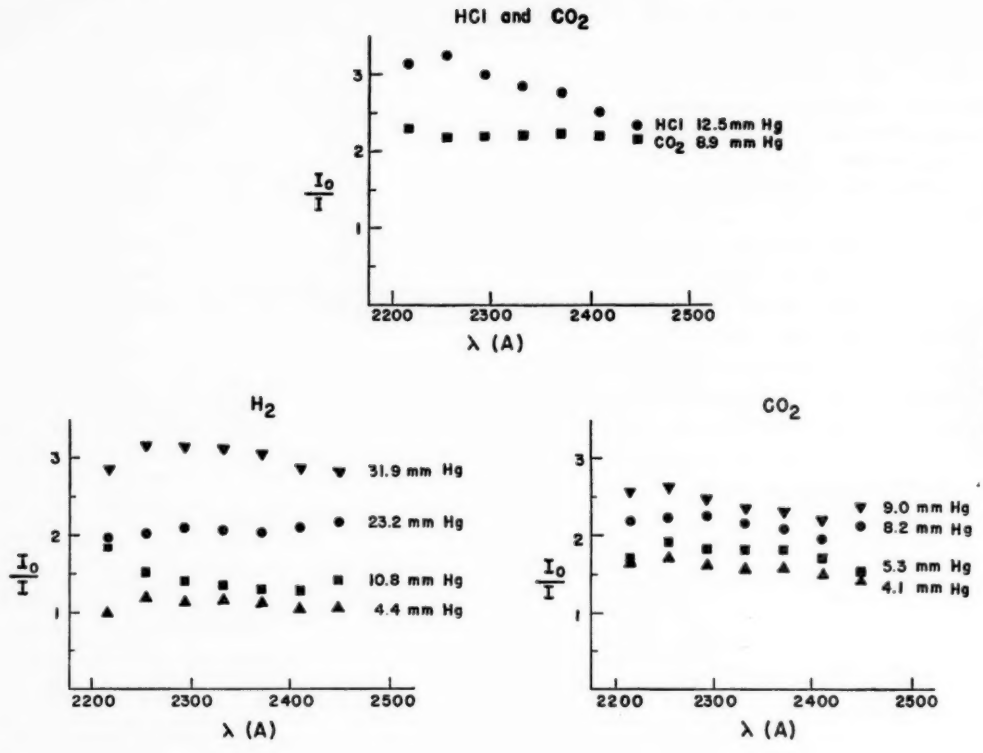

FIG. 7. The ratio of quenched to unquenched NaI fluorescence intensity for different wavelengths of exciting ultraviolet light for different quenching agents.

the "reflected" curves were done graphically. The calculations were made for the 668°C data only.

Curve B in Fig. 6 is the total intensity from the zeroth through the sixth vibrational level obtained by summing up the contributions from the individual states. Curve A is the observed fluorescent intensity distribution from Fig. 4 plotted against exciting ultraviolet energy expressed in cm^{-1}. It will be noted that a much better apparent agreement between curves B and A could be achieved by moving B about 500 cm^{-1} toward lower wave numbers (i.e., lower every point on the upper potential curve in Fig. 5 by 500 cm^{-1}). However, if one considers that, had the true (anharmonic) probability density functions for the sodium iodide molecule been used, curve B would be relatively higher at lower wave numbers and lower at higher wave numbers. This would be so because the loops in the anharmonic probability density functions would be larger on the side of r_e corresponding to larger internuclear distances. This modification of curve B by using the anharmonic probability density functions would probably give a fair agreement with the observed intensity curve A. For the determination of w [Eq. (3)] the potential curve in Fig. 5 was taken as an approximation to the upper potential curve for the sodium iodide molecule.

Two possible asymptote levels for large internuclear separation of the sodium iodide molecule for the upper state are shown in Fig. 5. The two levels are calculated from dissociation energies for the ground state of sodium iodide of 3.16 ev and 3.00 ev taken from spectroscopic data listed by Herzberg[17] and Terenin's[1,5,20] work on the optical dissociation of sodium iodide, respectively. Thermochemical data gives 3.07 ev. If the correct value is 3.16 ev, the possibility of a slight minimum in the upper potential curve exists. An asymptote at 42 100 cm^{-1} was assumed in the calculation of w, the excess energy of the dissociation partner.

The minimum value of w [Eq. (3)] for each exciting wavelength was determined from Fig. 5 in the following way. A vertical distance in cm^{-1} corresponding to an exciting wavelength was moved with its lower end on the lower potential curve until the upper end was on the upper repulsive curve. This point on the upper repulsive curve, together with the assumed asymptote for the repulsive curve for large internuclear distance of 42 100 cm^{-1}, determines w. The vertical distance between this point for each exciting wavelength and 42 100 cm^{-1} is a measure of w, the minimum excess kinetic energy shared by the dissociation partners for that particular exciting wavelength. The value is a minimum because upward transitions for the same wavelength originating in a point between the classical turning points for each vibrational level (corresponding to loops in the probability density functions between the classical turning points) could end further up on the upper repulsive curve yielding a larger value for w.

Figure 7 shows the quenching data on the quenching agents used, as a function of wavelength of excitation of fluorescence. The only agent to show a definite dependence on exciting wavelength is HCl.

[20] K. Butkow and A. Terenin, Z. Physik **49**, 865 (1928).

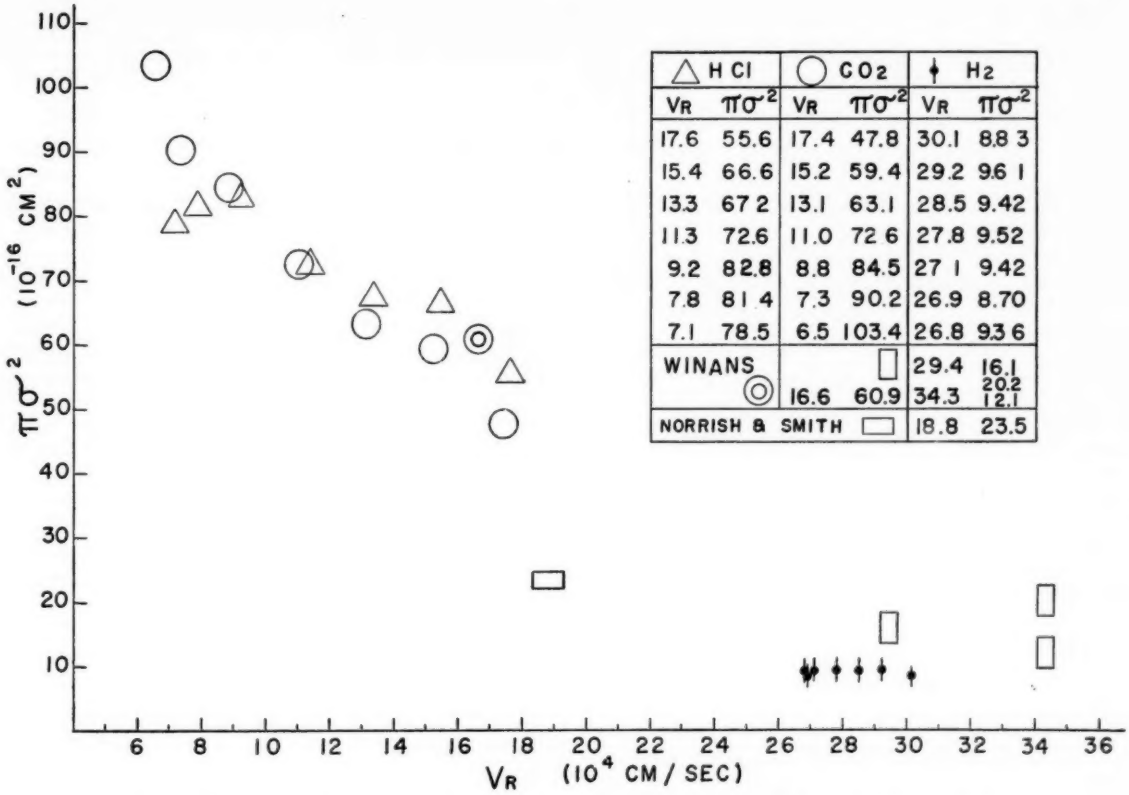

FIG. 8. The quenching cross sections are plotted against the most probable relative velocities between excited sodium atoms and quenching molecules.

Figure 8 shows the quenching cross section $\pi\sigma^2$ for the various quenching agents as calculated from Eq. (4) plotted against V_R, the average relative velocity of approach between excited sodium atoms and quenching molecules.

V_R is calculated from $V_R = v_{Na'} + \frac{1}{3}\alpha^2/v_{Na'}$ for $v_{Na'} > \alpha$ and $V_R = \alpha + \frac{1}{3}v_{Na'}^2/\alpha$ for $\alpha > v_{Na'}$. Since the light hydrogen molecules have average thermal velocities which are greater than the excited sodium atom velocities and since hydrogen is a relatively poor quencher, it is not surprising to see little dependence of the quenching cross section for hydrogen on V_R over the small range of V_R covered. It should be kept in mind also that the actual relative velocities involved in individual collisions vary from zero to several times V_R due to the Maxwellian distribution of speeds of the quenching molecules. The calculated cross sections for HCl and CO_2 show about the same relative decrease with increasing V_R in spite of the fact that HCl was the only one of the two to show a dependence of the measured I_0/I on the wavelength of the exciting ultraviolet light.

The quenching cross sections for H_2 and CO_2 from Winans[4] data and for H_2 from the resonance D line quenching experiments of Norrish and Smith[8] have been recalculated by the above method and are shown in Fig. 8.

In conclusion, it appears that for HCl and CO_2 and also for H_2 (considering the value of cross section at low relative velocities obtained by Norrish and Smith[8]) that the efficiency of quenching of the sodium D lines decreases with increasing of average relative velocity of approach between excited sodium atoms and quenching molecule. Since water vapor shows little quenching action, it can be classed with the weakly quenching gases listed by Norrish and Smith.[8]

Discussions of previous quenching experiments on sodium and other atoms can be found in the books by Mitchell and Zemansky,[21] and Pringsheim.[22]

The author wishes to thank Professor J. G. Winans for his helpful interest in this work, and the Graduate School of the University of Minnesota for furnishing the monochromator.

[21] A. C. G. Mitchell and M. W. Zemansky, *Resonance Radiation and Excited Atoms* (Cambridge University Press, Cambridge, England, 1934), first edition, p. 204.

[22] P. Pringsheim, *Fluorescence and Phosphorescence* (Interscience Publishers, Inc., New York, 1949), p. 108.

Shape of the Consolute Curve and its Consequences for the Theory of Binary Liquid Mixtures of Nonelectrolytes

F. KOHLER*
Department of Chemistry, University of North Carolina, Chapel Hill, North Carolina
(Received November 12, 1954)

The experimental results on the shape of the consolute curve of binary liquid mixtures with components A and B, especially the cubic dependence of the concentration on temperature, imply certain peculiarities in the behavior of the excess free energy of mixing ΔG_{exc}. The term ΔG_{exc} is expressed as $W \cdot x(1-x) \cdot \psi(x)$. Here $2W$ can be considered as the change in free energy, times Avogadro's number, when z contacts A–A and z contacts B–B are changed into $2z$ contacts A–B; x is the molefraction of one component, and z the coordination number. Moreover, $\psi(x)$ is much more sensitive than ΔG_{exc}, and has a theoretical significance, being proportional to the ratio of the number of A–B contacts in the system investigated to their number in a perfect solution if the assumptions of the strictly regular model are regarded as valid.

With the assumption that the system is symmetrical, the consolute curve consists of the points at which the first derivative of ΔG_m with respect to x vanishes. If the function ψ is expressed as a power series in $s=2x-1$, one also obtains T_c-T, T_c being the critical temperature, as a power series in s. The experimental results on the consolute curves serve now to determine the coefficients of the power series, by which ψ is given. Two additional assumptions are needed: (1) The coefficients of the high powers vanish in order to make use of the relation $\psi(1)=1$ and (2) the value of ΔG_{exc} for $T=T_c$ and $x=0.5$ is known approximately. With these assumptions the experimentally established flatness of the consolute curves leads to a curve for ψ *vs* x having a double-maximum ψ being greater than unity for high values of s, i.e., for great dilution of one component. This confirms earlier conclusions drawn from vapor pressure measurements and investigations of the volume change on mixing.

From a molecular point of view one can express this result by saying that the solvation of the diluted component is increased as compared to a perfect solution, even if the mixture is so strongly endothermic as to separate into two phases. The theoretical interpretation is not yet clear.

INTRODUCTION

PREVIOUS work on vapor pressures[1] has shown that the partial excess free energy becomes less concentration dependent when the component is highly diluted. Later it was pointed out[2] that the best way to discuss this unexpected behavior would be to consider a plot of the excess free energy of mixing ΔG_{exc}, divided by the product of both the molefractions, against the molefraction. In case of a regular solution such a plot would yield a horizontal line [Fig. 1(a)] whose ordinate is proportional to the change in energy $2w$ when a molecule of the one component, say A, in contact with another A-molecule, changes places with a B-molecule which had another B-molecule as neighbor, creating two $A-B$ pairs. Then ΔG_{exc} is given by one-half of this energy effect (w) times the number of $A-B$ pairs per mole mixture. This number is given by Nzx_Ax_B (x being the molefraction, z the coordination number, and N Avogadro's number) in both the perfect and the regular solution, so that for these cases $\Delta G_{exc}=wNzx_Ax_B = W \cdot x_Ax_B$ (in the case of the perfect solution W and therefore ΔG_{exc} are equal to zero). On the other hand, the strictly regular model[3] takes the fact into account that in an endothermic mixture there is less, and in an exothermic mixture there is more, chance for the formation of $A-B$ pairs [Fig. 1(a)]. Thus the plot of $\Delta G_{exc}/x(1-x)$ is a measure of the deviation of the number of $A-B$ contacts from the number in a perfect solution of the same concentration.

The experimental result of a low-concentration dependence of the partial excess free energy for small concentrations of one component corresponds to a positive deviation of the number of $A-B$ pairs from their value in a perfect mixture [solid portion of line in Fig. 1(b)]. To make this correspondence clear, let us consider the case of a zero-concentration dependence of the partial excess free energy for very small concentrations of the component A. Then ΔG_{exc} would be proportional only to the molefraction x_A, and $\Delta G_{exc}/x_A(1-x_A)$ would become $W/(1-x_A)$, a hyperbola with the limiting slope $+W$ at $x_A=0$. [In this case, of course, W may have a more complex meaning than wNz.] Therefore, if the limiting concentration dependence of the partial excess free energy has a value between zero and the parabola characteristic of the regular solution, the limiting slope of the function $\Delta G_{exc}/x(1-x)$ must have a value between $+W$ and zero.

As our previously investigated mixtures were all endothermic, one expects fewer $A-B$ contacts than in a perfect solution for approximately equimolar mixtures for the same reason that causes the negative deviations of the endothermic strictly-regular mixtures [this effect, predominating in the region where neither x_A nor x_B are very small, gives the dotted portion of the line in Fig. 1(b)]. Recently refined experiments[4] on vapor pressures of endothermic mixtures have given, indeed, support to this double-maximum shape of the function $\Delta G_{exc}/x(1-x)$, and experiments on volume changes[5] revealed similar double maxima of the function $\Delta V/x(1-x)$.

* On leave of absence from the University of Vienna, Austria.
[1] Ebert, Tschamler, and Kohler, Monatsh. Chem. **82**, 63 (1951).
[2] F. Kohler, in a report presented at a meeting of the Verein Österr. Chemiker, which took place at Graz, Austria, October, 1952. See also reference 4.
[3] E. A. Guggenheim, *Mixtures* (Oxford University Press, London, 1952).
[4] F. Kohler and A. Neckel, Monatsh. Chem. (to be published); see also A. Neckel, Dissertation, University of Vienna, 1954.
[5] F. Kohler and E. Rott, Monatsh. Chem. **85**, 703 (1954).

Since such behavior has not previously been described in the literature, it seems highly desirable to connect our results with other experimental findings. As the cubic connection between concentration and temperature along a consolute curve is one of the most striking facts[6] which cannot be explained by theory, the connection between this behavior and the free energy of mixing is very interesting.

GENERAL FORMULAS

For the sake of simplicity let us consider only the case of symmetrical systems; as only these are covered also by the theory of strictly regular solutions, this restriction does not seem to be too drastic. With this limitation the consolute curve is given by the points where the value of the first derivative of the free energy of mixing is zero. Putting

$$\Delta G_m = RT[x \ln x + (1-x)\ln(1-x)] + x(1-x)W\psi(x) \quad (1)$$

and substituting

$$s = 2x - 1$$

we get

$$d\Delta G_m/dx = RT \ln\frac{1+s}{1-s} - \left[s\psi(s) - \frac{1-s^2}{2}\frac{d\psi}{ds}\right]W. \quad (2)$$

Setting this expression equal to zero and writing $W/RT_c = \gamma$, we obtain the condition

$$\ln\frac{1+s}{1-s} = \gamma(T_c/T)\left(s\psi - \frac{1-s^2}{2}\frac{d\psi}{ds}\right) \quad (3)$$

for the value of s along the consolute curve. Now we can express ψ as a power series in s. As we assumed the system to be symmetrical, we should retain only the even powers of s. But remembering that the cubic relation describing the consolute curve implies a singularity at the critical mixing concentration, we consider the ψ function also to have two branches, which may be connected by a singular point at $s=0$. We write therefore,

$$\psi = c_0 + c_1 s + c_2 s^2 + c_3 s^3 + c_4 s^4 + \cdots \quad (4)$$

but we have to remember that we have to take the absolute values of the odd powers. In order that $s=0$ should be a solution of Eq. (3), however, we must set $c_1=0$. Then developing the logarithm in Eq. (3) as a power series and making some obvious rearrangements we obtain finally

$$\begin{aligned}\frac{T_c-T}{T}\frac{\gamma}{2}(c_0-c_2) &= 1-\frac{\gamma}{2}(c_0-c_2)+\frac{3}{4}\gamma c_3\frac{T_c}{T}s \\ &+\left[\frac{1}{3}-\gamma(c_2-c_4)\frac{T_c}{T}\right]s^2-\frac{5}{4}\gamma(c_3-c_5)\frac{T_c}{T}s^3 \\ &+\left[\frac{1}{5}-\frac{3}{2}\gamma(c_4-c_6)\frac{T_c}{T}\right]s^4-\frac{7}{4}\gamma(c_5-c_7)\frac{T_c}{T}s^5 \\ &+\left[\frac{1}{7}-2\gamma(c_6-c_8)\frac{T_c}{T}\right]s^6+\cdots.\end{aligned} \quad (5)$$

From the experimentally established cubic relation, which makes T_c-T proportional to s^3, we have the following consequences from (5):

$$c_0 - c_2 = 2/\gamma, \quad (6)$$

$$c_3 = 0, \quad (7)$$

$$c_2 - c_4 = 1/3\gamma. \quad (8)$$

It should be noted that the relations (6) to (8) correspond to a zero value of the second, third, and fourth derivative of ΔG_m at the point $s=0$. The coefficient of s^3 in (5) has been also determined experimentally,[7] and it has been recalculated here for the systems we refer to later. For a considerable variety of systems it has a value consistent with the relation

$$\gamma c_5 = 4/5(0.55 \pm 0.10)^3. \quad (9)$$

Equation (9) implies a nonzero value of the fifth derivative of ΔG_m at $s=0$. With the relations (6) to (9) the power series (4) can be expressed up to the fifth power of s in terms of c_0 and γ.

The next step is to get a connection between c_0 and γ. Therefore we make the somewhat drastic assumption that the higher coefficients in the power series (4) are negligible; then the relation $\psi(1)=1$ gives us the relation required.

Now the question remains, what value should be assigned to c_0 or γ. We shall compare our results to the theory of strictly regular solutions, which leads to the values

$$c_0 = 0.9276 \quad \text{and} \quad \gamma = 2.301$$

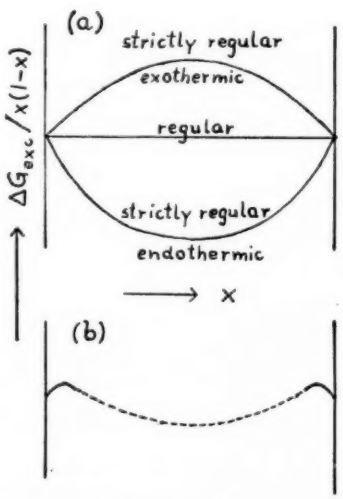

FIG. 1. The function $\Delta G_{exc}/x(1-x)$ as given by theory (a), and previous experiments (b).

[6] See, e.g., R. L. Scott, J. Chem. Educ. **30**, 542 (1953).

[7] B. H. Zimm, J. Chem. Phys. **20**, 538 (1952).

for the coordination number 8, and

$$c_0=0.9460 \quad \text{and} \quad \gamma=2.188$$

for the coordination number 12.[8] In our case there is a different relation between c_0 and γ, of course, but we shall consider the extremes given by $c_0=0.9276$ and $\gamma=2.188$ respectively, expecting that some value between should correspond to reality.

REFINED TREATMENT OF EXPERIMENTAL DATA

Before we proceed to numerical calculations it seems necessary to rexamine the assumption about the higher coefficients of the power series (4). Any assumption of this kind of course influences the power series (5) giving T_c-T, and we must be careful that we do not come too far from the experimental results.

First we rewrite (5) substituting the relations (6) to (8), and multiplying by T/T_c:

$$\frac{T_c-T}{T_c}\left(1+\frac{s^2}{3}\right)=\frac{5}{4}\gamma c_5 s^3+\left[\frac{T}{5T_c}-\frac{3}{2}\gamma(c_4-c_6)\right]s^4$$
$$-\frac{7}{4}\gamma(c_5-c_7)s^5+\left[\frac{T}{7T_c}-2\gamma(c_6-c_8)\right]s^6-\frac{9}{4}\gamma(c_7-c_9)s^7$$
$$+\left[\frac{T}{9T_c}-\frac{5}{2}\gamma(c_8-c_{10})\right]s^8+\cdots.$$

We shall refer mainly to the results of Zimm[9] on the perfluoromethylcyclohexane carbon-tetrachloride system, as these experiments seem to be the most precise over a sufficient temperature interval; also this system has the advantage that it consists of nonpolar components. The only disadvantage of this system is that it is rather unsymmetrical because of the high molar volume of perfluoromethylcyclohexane, while our considerations assume symmetrical systems. We can overcome this difficulty by using the volume fraction φ instead of the molefraction, as this has been frequently done in the literature.[10] Therefore we have put $s=2|\varphi_c-\varphi|$ in making use of the experimental data. Best fit to the experimental data was obtained with $\gamma\cdot c_5=0.172$, which is a little less than the number given by Zimm.[9] To make the possible influence of the higher powers in (10) better visible, we plot in Fig. 2 the expression

$$A=\left(\frac{T_c-T}{T_c}\frac{4}{5\gamma c_5 s^3}\right)^{\frac{1}{3}} \tag{11}$$

against s.

To complete the curve for higher values of s we use the data obtained by Hildebrand and Cochran.[11] These data can be compared to those[11] for other perfluoromethylcyclohexane systems. This comparison is made in Table I. As the last value for the carbon tetrachloride system seems to be very low, we also used $T_c-T=50.1$ to calculate the last point in Fig. 2. In Fig. 3 we show the results of the same treatment for the system methanol-cyclohexane from the work of Eckfeldt and Lucasse[12]; here $s=2|x_c-x|$, but as the two branches of the consolute curve, on the methanol-rich side and on the cyclohexane-rich side, show some differences, we have plotted the branches separated; in calculating A from the experimental points, we have assumed γc_5 to be 0.125; details of the treatment of these data are given below.

If we simply applied Eqs. (6) to (9), putting c_6 and all higher coefficients zero, c_4 would turn out to be of the order of magnitude -0.09. Therefore the coefficient of s^4 in the power series (10) would be approximately

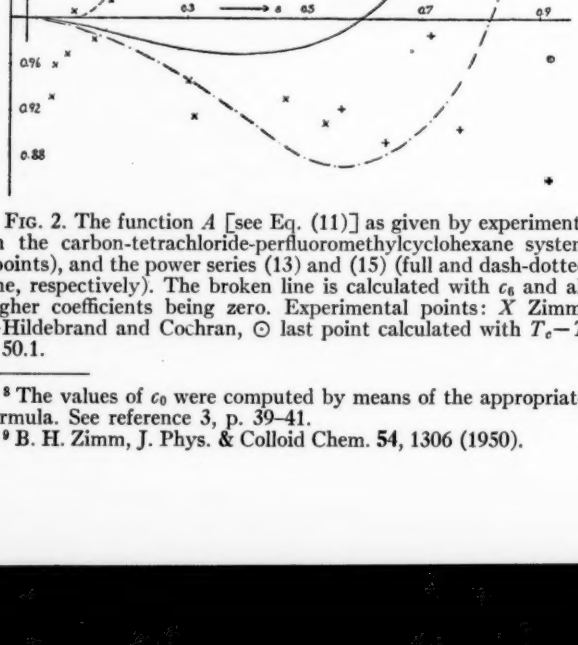

FIG. 2. The function A [see Eq. (11)] as given by experiments on the carbon-tetrachloride-perfluoromethylcyclohexane system (points), and the power series (13) and (15) (full and dash-dotted line, respectively). The broken line is calculated with c_6 and all higher coefficients being zero. Experimental points: X Zimm, +Hildebrand and Cochran, ⊙ last point calculated with $T_c-T=50.1$.

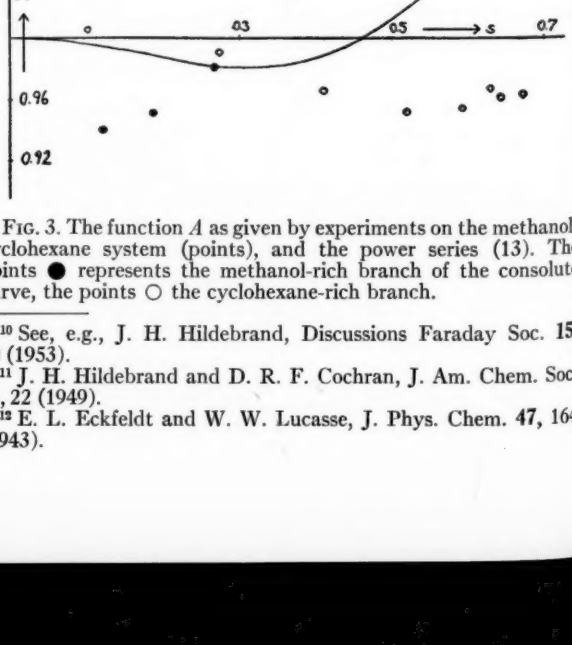

FIG. 3. The function A as given by experiments on the methanol-cyclohexane system (points), and the power series (13). The points ● represents the methanol-rich branch of the consolute curve, the points ○ the cyclohexane-rich branch.

[8] The values of c_0 were computed by means of the appropriate formula. See reference 3, p. 39–41.

[9] B. H. Zimm, J. Phys. & Colloid Chem. **54**, 1306 (1950).

[10] See, e.g., J. H. Hildebrand, Discussions Faraday Soc. **15**, 10 (1953).

[11] J. H. Hildebrand and D. R. F. Cochran, J. Am. Chem. Soc. **71**, 22 (1949).

[12] E. L. Eckfeldt and W. W. Lucasse, J. Phys. Chem. **47**, 164 (1943).

TABLE I. Comparison of the data obtained by Hildebrand and Cochran.

		T_c-T of perfluoromethylcyclohexane systems, component 2 being		
φ_2	s	CCl_4	$CHCl_3$	C_6H_6
0.833	0.564	9.3	9.2	9.2
0.231	0.640	12.4	11.6	15.8
0.909	0.716	23.8	23.9	24.2
0.167	0.768	22.8	21.3	26.4
0.091	0.920	34.8	43.0	50.1

$+0.50$. The value of A calculated with this coefficient is represented by the dotted line in Fig. 2. From this it is seen that the cubic relation between temperature and concentration would hold only over a range of about 0.2 in s, which corresponds to a range of about 0.2 degree, while this relation is well established over a range of about 5 degrees. To account for this it is necessary to put the coefficient of s^4 approximately zero, as can be seen also immediately from Fig. 2. The same can be seen from Fig. 3 and Fig. 4, which is an extension of a plot of the data of Atack and Rice on the cyclohexane-aniline system.[13,14] (Figure 4 is drawn with the assumption $\gamma c_5=0.072$.) Assuming an exactly zero value for the coefficient of s^4, which is equivalent to setting the sixth derivative of ΔG_m equal to zero for $s=0$, we obtain a value of c_6 which is different from zero and given by

$$c_4-c_6=2/15\gamma. \tag{12}$$

If we then put all higher coefficients beyond c_6 in the power series (4) equal to zero, we get

$$A^3=\frac{1-\frac{7}{5}s^2-\frac{8c_6\gamma}{5c_5\gamma}s^3+\frac{4}{5c_5\gamma}\frac{T}{T_c}\left(\frac{s^3}{7}+\frac{s^5}{9}+\frac{s^7}{11}+\cdots\right)}{1+s^2/3+s^4/5}. \tag{13}$$

This expression is plotted as a full line in Figs. 2, 3, and 4. The experimental results on the carbon-tetrachloride-perfluoromethylcyclohexane and on the cyclohexane-aniline system seem to indicate that we need here still further coefficients in the power expression (4), satisfying the relation $c_n<c_{n-2}$. For the sake of simplicity in the numerical calculations, we put tentatively

$$c_6-c_8=1/14\gamma \tag{14}$$

which corresponds to a zero value of the coefficients of s^6 in (10) and also a zero value of the eighth derivative

[13] O. K. Rice, J. Chem. Phys. (to be published). It should be noted that we are not concerned in this work with the possibility of a small flat portion of the consolute curve in the immediate neighborhood of the critical concentration. As we are interested in the concentration dependence of the excess free energy over the whole concentration range, we treat the experimental data as if the cubic relation persisted even in the immediate neighborhood of the critical concentration.

[14] The plot was extended by making use of the data of D. Atack and O. K. Rice, Discussions Faraday Soc. **15**, 210 (1953), and Ebert, Tschamler, and Wächter, Monatsh. Chem. **80**, 732 (1949).

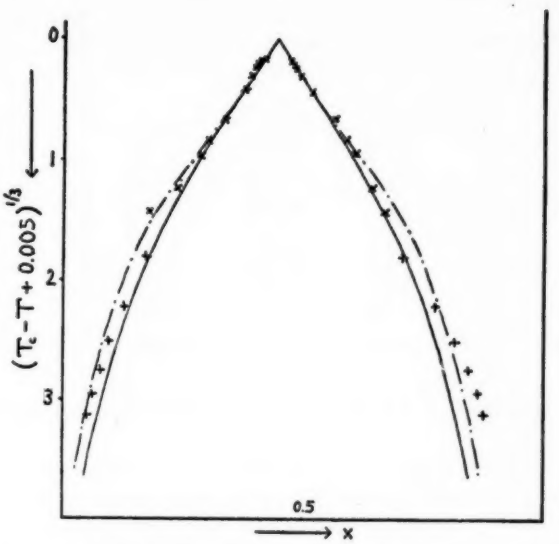

FIG. 4. $(T_c-T+0.005)^{\frac{1}{3}}$ of the system cyclohexane-aniline. The full and dash-dotted line correspond to the power series (13) and (15), respectively. Experimental points: X Atack and Rice, $+$Ebert, Tschamler, and Wächter.

of ΔG_m (for $s=0$). From (14), together with $c_7=c_9=c_{10}=\cdots=0$, we obtain

$$A^3=\frac{1-\frac{7}{5}s^2-\frac{2c_8\gamma}{c_5\gamma}+\frac{4}{5c_5\gamma}\frac{T}{T_c}\left(\frac{s^5}{9}+\frac{s^7}{11}+\cdots\right)}{1+s^2/3+s^4/5+s^6/7}. \tag{15}$$

This expression is plotted as a dotted line in Figs. 2 and 4. It corresponds to a still flatter consolute curve than does (13). The experimental points in Figs. 2 and 4 lie between Eqs. (13) and (15). It seems useless at this time, precise experimental data over the whole range of concentrations being lacking, to seek for a better adjustment of the coefficients of the power series. We shall try both sets of coefficients, corresponding to Eqs. (13) and (15), noting that Figs. 2 and 4 indicate that some expression in between should correspond to reality.

NUMERICAL CALCULATIONS

The coefficients of the power series (4) corresponding to Eqs. (13) and (15), respectively, are collected in Table II. In this table two rows always belong together, their only difference being the choice of c_0 or γ, respectively. The chosen value is italicized. The first four rows are calculated with $\gamma c_5=0.172$, as deduced from the carbon tetrachloride-perfluoromethylcyclohexane system. The ψ functions calculated with these sets of coefficients are shown in Fig. 5. The fifth and the sixth row in Table II are calculated with $\gamma c_5=0.125$, corresponding to the methanol-cyclohexane system, whereas in the last four rows $\gamma c_5=0.0724$, which fits the experimental data of the cyclohexane-aniline system. The

TABLE II. Sets of coefficients of the power series (4).

The set corresponds to Eq.	γ	c_0	c_2	c_4	c_5	c_6	c_8	$c_0\gamma$	$c_5\gamma$
(13)	2.449	*0.9276*	0.1113	−0.0248	0.0702	−0.0793	0	2.272	0.172
(13)	*2.188*	1.0073	0.0932	−0.0591	0.0786	−0.1201	0	2.204	0.172
(15)	2.520	*0.9276*	0.1338	+0.0015	0.0683	−0.0514	−0.0798	2.338	0.172
(15)	*2.188*	1.0378	0.1238	−0.0285	0.0786	−0.0895	−0.1221	2.271	0.172
(13)	2.462	*0.9276*	0.1155	−0.0199	0.0508	−0.0740	0	2.283	0.125
(13)	*2.188*	1.0133	0.0985	−0.0540	0.0572	−0.1150	0	2.220	0.125
(13)	2.482	*0.9276*	0.1217	−0.0127	0.0299	−0.0663	0	2.302	0.0724
(13)	*2.188*	1.0191	0.1043	−0.0482	0.0340	−0.1093	0	2.228	0.0724
(15)	2.550	*0.9276*	0.1422	+0.0113	0.0292	−0.0411	−0.0691	2.363	0.0724
(15)	*2.188*	1.0475	0.1327	−0.0198	0.0340	−0.0808	−0.1134	2.294	0.0724

ψ functions of the last six sets of coefficients are shown in Fig. 6.[15]

The existence of the double maximum seems to be beyond doubt. Considering the sets of coefficients in Table II, one realizes that the flatter the consolute curve is around the top (that means, the smaller the value of γc_5 within the same conditions for coefficients, and especially when (15) is applied instead of (13)), the greater is the curvature of the ψ curve around $s=0$ ($x=0.5$). This curvature is given primarily by c_2. To satisfy the boundary condition $\psi(1)=1$, the large positive value of c_2 must be balanced by negative coefficients of the high powers of (4), and this produces the double maximum. This double maximum is therefore the more pronounced the flatter the consolute curve; and the maxima shift simultaneously to higher values of s, that is to more dilute concentrations. From this point of view it is clear too, that the steep rise of the ψ curve around $s=0$, which is connected with the experimentally established flatness of the consolute curve, calls for greater negative coefficients of the higher powers of (4), if c_0 is high. Then the double maximum is more pronounced. One can suppose that the double maximum would disappear, if the value of c_0 became very low; such low c_0-values are, however, very unlikely.

It seems noteworthy, that the shape of the ψ curves is much more sensitive to the conditions for coefficients, corresponding to (13) or (15), respectively, than to the different values of γc_5. That means that the shape of the consolute curve at a few degrees below the critical temperature is more significant to the shape of the ψ curve than the exact value of the coefficient of the cubic power. Therefore it is very important that for all three systems considered, Eq. (12) seems to be necessary to fit the experimental data on the consolute curves.

There remains the necessity of making some remarks concerning the details of the numerical calculation.

[15] It is not permissible to say, of course, that the ψ functions themselves correspond to the carbon tetrachloride-perfluoromethylcyclohexane or any other particular system. The ψ functions do correspond to the hypothetical systems, which exhibit similar consolute curves to the investigated real systems, but with a critical concentration of $x_c=0.500$ and with perfect symmetry in the molefractions.

First, it is necessary to make an assumption about the dependence of γ on temperature. In the crude approximation of the regular solution theory we have $d\gamma/dT=0$, while Tschamler *et al.*[16,17] found a value of the heat of mixture at equimolal concentration $\Delta H_{x=0.5} \cong 500$ cal/mole for several systems in the neighborhood of the critical temperature, which would correspond to $d\gamma/dT=-0.004$. In our calculations we have used $d\gamma/dT=-0.002\gamma$ (note that γ is approximately 2), but only a slight difference would result from the use of another value for $d\gamma/dT$. As γ enters the theoretical expression for A [Eqs. (13) and (15) respectively] only in the last term, a greater negative value of $d\gamma/dT$ would lower the "experimental" points, which are obtained from Eq. (11) more than the theoretical curves in Fig. 2, obtained from Eqs. (13) and (15). We can certainly assume that the ψ function is independent of temperature in the temperature intervals with which we are concerned.

Since, in Eqs. (13) and (15) the right-hand side also varies with temperature, although very slowly because of the factors T/T_c and γ, it was necessary in performing the calculations to make a plot of T_c-T *vs* s from the experimental results. Errors in this plot would influence the calculations only in the interval $0.9<s<1$.

Calculating A from Eq. (13) a certain value must be assigned to the product $c_6\gamma$, and the use of Eq. (15) requires the knowledge of the value $c_8\gamma$. With the values listed in Table II, the product was formed and a mean value used for the calculations.

The data of Eckfeldt and Lucasse[12] were treated in the following manner: A plot was made of $(T_c-T+0.005)^{\frac{1}{3}}$ *vs* x, similar to Fig. 4; the addition of 0.005 to T_c was necessary to yield straight lines through the experimental points beneath the critical composition, when treated in this way. As critical composition we assumed $x_c=0.495$, when x is the molefraction of cyclohexane. The best straight lines which could be drawn in the described diagram determined the value of $\gamma c_5=0.125$.

[16] H. Tschamler, Monatsh. Chem. **79**, 223 (1948).

[17] Tschamler, Wettig, and Richter, Monatsh. Chem. **80**, 572 (1949).

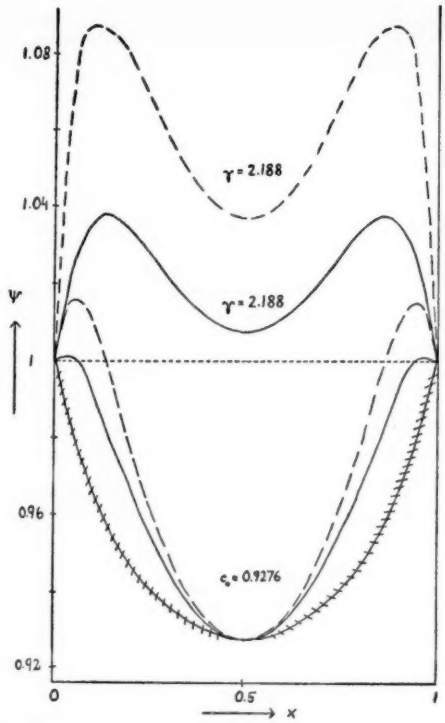

FIG. 5. The function ψ as given by the sets of coefficients of the first four rows of Table II. The full lines correspond to Eq. (13), the broken lines to (15). The function ψ as given by the strictly regular solution theory for the case of $z=8$ is included (-/-/-/-/-/-).

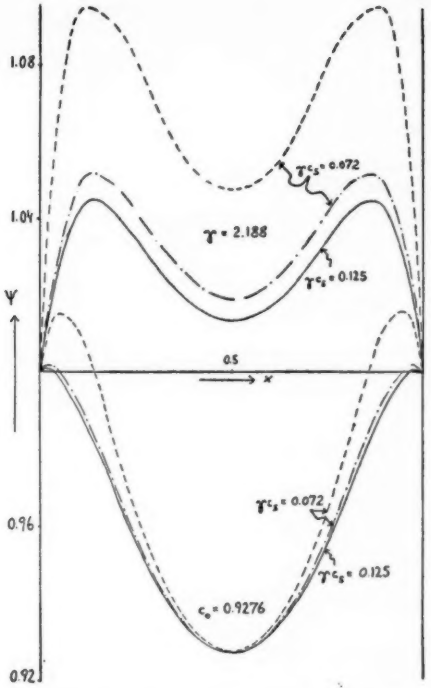

FIG. 6. The function ψ as given by the sets of coefficients of the last six rows of Table II. The full and dash-dotted lines correspond to Eq. (13), the broken lines to (15).

THE VALUE OF ΔG_{exc} at T_c

As the value of $\Delta G_{exc}/RT_cx(1-x)$ for $x=0.5$ is equal to $c_0\gamma$, which is given in the ninth column of Table II, an independent check of our assumptions is possible.

First let us consider the theoretical predictions. In the case of the simple regular mixtures $c_0\gamma=2$, whereas in the case of the strictly regular mixtures we get $c_0\gamma=2.07$ and 2.13 for a coordination number of 12 and 8, respectively. Our values for $c_0\gamma$ are significantly higher. On the other hand it is impossible for thermodynamical reasons[18] for $c_0\gamma$ to exceed the value 2.77.

The scarcity of experiments dealing with this question is deplorable, as can be seen best from a recent paper of Copp and Everett.[19] It should be noted that the values quoted by Copp and Everett for the mixtures of hexane with aniline and cyclohexane with methanol are open to question, as these values were calculated[20,21] from the consolute curve by means of an equation with two parameters for the partial free energies. Our own experience[22] with such equations indicates that the calculated free energies are too low.

But it is possible at least to estimate the $c_0\gamma$ values of real systems. Full use is made of two previous investigations[1,22] and some material is added (Table III), which shows $\Delta G_{exc}/RTx(1-x)$ at the point $x=0.5$ for systems where no phase separation occurs near the temperature of investigation. Therefore these values represent a rough lower limit of $c_0\gamma$.[23]

The partial pressures or the activity coefficients of the volatile component of the cyclohexane-aniline system at 40°C and of the β,β'dichlorodiethylether-methylcylohexane system at 0°C are given by the investigations cited. The activity coefficient of the non-volatile component was calculated from a numerical integration by means of the Simpson formula. Then the value of ΔG_{exc} was extrapolated over *ca.* 10° to T_c, which was possible, as the heats of mixture were known approximately.[16,22]

The system triethylamine-water is quoted here only for the sake of completeness. It is clear, however, that for a system with a lower critical temperature c_5 must be negative, which may also cause a change of the other coefficients in (4).

As the value 2.56 of the methanol-hexane system

[18] D. H. Everett, Discussions Faraday Soc. **15**, 267 (1953).
[19] J. L. Copp and D. H. Everett, Discussions Faraday Soc. **15**, 174 (1953).
[20] F. Scatchard and W. J. Hamer, J. Am. Chem. Soc. **57**, 1805 (1935).
[21] S. E. Wood, J. Am. Chem. Soc. **68**, 1963 (1946).
[22] Ebert, Tschamler, Fischer, and Kohler, Monatsh. Chem. **81**, 551 (1950).

[23] The fact that some systems without phase separation have even higher values of $c_0\gamma$ than other systems at T_c must not be taken too seriously. First, the experimental data are not very precise, and secondly, there is some difficulty in comparing alcoholic systems with systems in which such a strong hydrogen bond effect does not occur. Furthermore, according to our assumption, the c_0-values would have a precise meaning only in the case of symmetrical systems. The unsymmetry of most of the real systems may cause an additional error in those values.

TABLE III. The values of $\Delta G_{exc}/RTx(1-x)$ of real systems at equimolar concentration.

Systems with phase separation	Temperature of critical mixing (°C)	$\Delta G_{exc}/RTx(1-x)=c_0\gamma$	Reference
cyclohexane-aniline	+29.5	2.37	17
methylcyclohexane-β,β'dichlorodiethylether	− 9.0	2.22	1
triethylamine-water	+18.4	2.31	F. Kohler, Monatsh. Chem. **82**, 913 (1951).
n-hexane-methanol	+42.5	2.56	J. B. Ferguson, J. Phys. Chem. **36**, 1123 (1932)
Homogeneous systems	**Temperature of investigation (°C)**	$\Delta G_{exc}/RTx(1-x)<c_0\gamma$	**Reference**
n-heptane-ethanol	+30.0	2.33	Ferguson, Freed, and Morris, J. Phys. Chem. **37**, 87 (1933)
iso-octane-ethanol	+25.0	2.31	Kretschmer, Nowakowska, and Wiebe, J. Am. Chem. Soc. **70**, 1785 (1948).
methylcyclohexane-ethanol	+35.0	2.18	C. B. Kretschmer and R. Wiebe, J. Am. Chem. Soc. **71**, 3176 (1949).
cyclohexane-ethanol	+25.0	2.29	E. R. Washburn and B. H. Handorf. J. Am. Chem. Soc. **57**, 441 (1935).

seems to be exceptionally high, we can conclude that our values for $c_0\gamma$ of Table II are of the right order of magnitude.

CONCLUSIONS

The strange double-maximum shape of the ψ function may be an explanation for the circumstance that the simple regular model is sometimes more successful in giving the excess free energy of real systems than the theoretically founded strictly regular model. For the horizontal line can be a better approximation to the ψ curve than the flattened parabola of the strictly regular model, all points of which lie below the most likely ψ curve.

It may be repeated here that the ψ curve can be interpreted as proportional to the deviation of the number of $A-B$ contacts from their number in a perfect mixture, provided the assumptions of the strictly regular model are valid.[24] This interpretation may be extended even to systems separating into two phases, if these systems consist of molecules with no specific intermolecular forces such as strong dipoles or hydrogen bonds. Then one can express our result by saying that in dilute solutions the number of $A-B$ contacts is greater than expected for a perfect solution, or one can say that the solvation is enhanced in diluted solutions, in spite of the strongly endothermic energy-interaction.

These conclusions, which are in agreement with interpretations of our previous work on vapor pressures and volume changes,[4,5] are certainly puzzling and cannot give a definite answer, but they may open another point of view to further theoretical work.

[24] In fact in the strictly regular model the ψ curve, which is given in the notation of Guggenheim (reference 3) by $\overline{\overline{X}}/x(1-x)$, lies about halfway between unity and the ratio of the number of $A-B$ contacts in the mixture investigated to their number in a perfect mixture, which ratio is given by $\overline{X}/x(1-x)$. See reference 3, Eq. (4.04.8).

ACKNOWLEDGMENTS

The author is very much indebted to the Foreign Operations Administration for the grant of a two-year fellowship [Ta 01–101–3006 (OEEC–151), Scientists Research Project]. He has been deeply impressed by the hospitality and helpful attitude of faculty and staff of the chemistry department of the University of North Carolina. Special thanks are due to Professor Oscar K. Rice for valuable suggestions in writing this paper.

Solution of the Wave Equation for Internal Rotation of Two Completely Asymmetric Molecules*

DONALD G. BURKHARD AND JOHN C. IRVIN
Department of Physics, University of Colorado, Boulder, Colorado

(Received November 2, 1954)

The wave equation is derived from two completely asymmetric molecules undergoing mutual rotation about a common axis and subject to an arbitrary hindering potential. Matrix elements of the Hamiltonian are evaluated using the wave functions which describe the mutual rotation of two symmetric groups.

IN the present paper the wave equation is derived and solved for two completely asymmetric rigid molecules rotating about a common axis. The mutual rotation may be hindered by an arbitrary potential.

The wave mechanical description of internal rotation was first treated by H. H. Nielsen[1] who solved the problem for two rigid symmetric groups rotating about a common axis. This work was later amplified by Koehler and Dennison[2] who employed a model consisting of two rigid symmetric tops to account qualitatively for the infrared spectrum associated with the torsional motion of the hydroxyl and methyl groups in methyl alcohol. Since methyl alcohol is only slightly asymmetric, this model gives the essential features of the infrared spectrum but is not accurate enough to enable one to assign individual absorption lines. A more accurate model for methyl alcohol consisting of an asymmetric (hydroxyl) group and a symmetric (methyl) group undergoing hindered rotation was later employed by Burkhard and Dennison[3] to account for the complex microwave spectrum of methyl alcohol as measured with high precision by Coles.[4] The more general problem where both groups are partially asymmetric but where the center of mass of one of the groups must lie on the axis of mutual rotation was next treated by Burkhard.[5] In the present paper the hindered rotation problem for two rigid asymmetric groups has been completely generalized. The center-of-mass of both groups may lie off the axis of mutual rotation. All of the preceding results will appear as special cases.

There are a large number of molecules to which the results will be applicable. A few of the more obvious molecules in which torsional motion is important are the substituted ethanes and ethylenes, substituted hydrazine, hydrogen peroxide, and hydroxyl amine. The torsional motion will be infrared active only if the molecule has a dipole moment perpendicular to the axis of mutual rotation.

The potential energy will have a form appropriate to the model. In general, it may be written as a Fourier series in the angle of mutual rotation x. In the case of methyl alcohol, with a threefold potential associated with the hydrogens of the methyl group, it has been found that the potential is well represented by the expression $V=(H/2)(1-\cos 3x)$. H is the barrier height or the difference between a maximum and minimum of the potential.

DERIVATION OF THE KINETIC ENERGY

In Fig. 1, 0 is the center of mass of the total molecule. A and B are the centers of mass of the respective asymmetric groups which undergo hindered rotation about the axis PL as the net molecule rotates about 0. $\boldsymbol{\varrho}_1$ is a vector from 0 to A. $\mathbf{r}_i$ is a vector measured from A to a mass m_i in the group whose center of mass is A. $\boldsymbol{\varrho}_2$, $\mathbf{R}_i$, and M_i are similar quantities in group B. We see from the figure that when both A and B lie off the axis PL the vectors $\boldsymbol{\varrho}_1$ and $\boldsymbol{\varrho}_2$ change in magnitude as the two groups undergo mutual rotation. If A and/or B lie on PL, then $\boldsymbol{\varrho}_1$ and $\boldsymbol{\varrho}_2$ do not change in magnitude with mutual rotation. The case where A and B lie off the axis PL is analytically more complex than when one or both centers of mass lie on the axis PL. This is because the centers of gravity, A and B, "oscillate" with

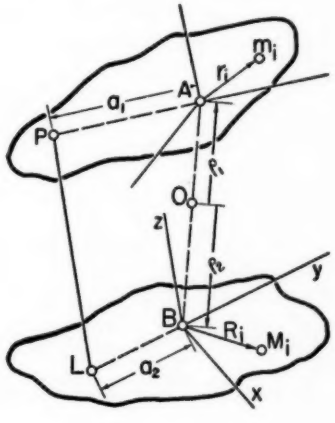

FIG. 1.

* This work was supported by the Office of Army Ordnance Research under contract No. DA-23-072-ORD-645.

[1] H. H. Nielsen, Phys. Rev. **40**, 445 (1932).

[2] J. S. Koehler and D. M. Dennison, Phys. Rev. **57**, 1006 (1940).

[3] D. G. Burkhard and D. M. Dennison, Phys. Rev. **84**, 408 (1951).

[4] D. K. Coles, Phys. Rev. **74**, 1194 (1948).

[5] D. G. Burkhard, J. Chem. Phys. **21**, 1541 (1953). In the matrix elements of this paper on p. 1544 the 2 in the term $K^2/2(C_1+C_2)$ should be deleted; and p. 1545, 7th line down, the first term under the integral sign should read $\sin^2 x$ rather than $\sin x$. Also on p. 1546 the 2 in the result seven lines up from the bottom of column one should be deleted. The term

$$\frac{\hbar^2}{2}\frac{C\delta}{C_1C_2}\int_0^{2\pi}\frac{(P^{k\tau n})^*\sin^2 x(ikC_1/C-d/dx)^2P^{k\tau' n'}}{1+\delta\sin^2 x}\,dx$$

should be added to the matrix elements on p. 1544.

respect to one another as the two groups rotate about PL, giving rise to additional terms in the kinetic energy.

For twice the kinetic energy one has

$$2T=\Sigma m_i\left[\frac{d}{dt}(\boldsymbol{\varrho}_1+\mathbf{r}_i)\right]^2+\Sigma M_i\left[\frac{d}{dt}(\boldsymbol{\varrho}_2+\mathbf{R}_i)\right]^2.$$

In order to calculate the time derivative of $\boldsymbol{\varrho}_1+\mathbf{r}_i$ we regard $\mathbf{r}_i$ as referred to a coordinate system located at the center of gravity of group A and rotating with the angular velocity $\boldsymbol{\omega}$. Similarly $\mathbf{R}_i$ will be referred to a coordinate system at B and will rotate with angular velocity $\boldsymbol{\Omega}$. It is convenient to leave the axes to which $\boldsymbol{\varrho}_1$ and $\boldsymbol{\varrho}_2$ are referred unspecified at present.

The term

$$\Sigma m_i\left[\frac{d}{dt}(\boldsymbol{\varrho}_1+\mathbf{r}_i)\right]^2$$

may be written

$$\Sigma m_i\left[\frac{d}{dt}(\boldsymbol{\varrho}_1+\mathbf{r}_i)\right]^2=\Sigma m_i\left[\frac{d\boldsymbol{\varrho}_1}{dt}+\dot{\mathbf{r}}_i+\boldsymbol{\omega}\times\mathbf{r}_i\right]^2$$

$$=\Sigma m_i\left(\frac{d\boldsymbol{\varrho}_1}{dt}\right)^2+\Sigma m_i\dot{\mathbf{r}}_i^2+\Sigma m_i(\boldsymbol{\omega}\times\mathbf{r}_i)^2$$

$$+\frac{2d\boldsymbol{\varrho}_1}{dt}\cdot\Sigma m_i\dot{\mathbf{r}}_i+\frac{2d\boldsymbol{\varrho}_1}{dt}\cdot\Sigma m_i(\boldsymbol{\omega}\times\mathbf{r}_i)+2\Sigma m_i\dot{\mathbf{r}}_i\cdot(\boldsymbol{\omega}\times\mathbf{r}_i).$$

$\dot{\mathbf{r}}_i$ represents the time rate of change of $\mathbf{r}_i$ with respect to the body-fixed coordinate system at A rotating with angular velocity $\boldsymbol{\omega}$. In the present treatment groups A and B are regarded as rigid so that $\dot{\mathbf{r}}_i$ is identically zero. Thus,

$$\Sigma m_i\left[\frac{d}{dt}(\boldsymbol{\varrho}_1+\mathbf{r}_i)\right]^2=m_1\left(\frac{d\boldsymbol{\varrho}_1}{dt}\right)^2+\Sigma m_i(\boldsymbol{\omega}\times\mathbf{r}_i)^2$$

where $m_1=\Sigma m_i$.

Similarly one has

$$\Sigma M_i\left[\frac{d}{dt}(\boldsymbol{\varrho}_2+\mathbf{R}_i)\right]^2=m_2\left(\frac{d\boldsymbol{\varrho}_2}{dt}\right)^2+\Sigma M_i(\boldsymbol{\Omega}\times\mathbf{R}_i)^2$$

where $m_2=\Sigma M_i$. $\boldsymbol{\Omega}$ is the over-all angular velocity of group B and will be different from the angular velocity of group A.

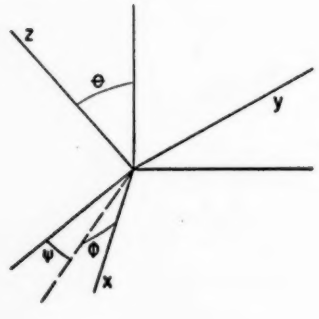

FIG. 2. $\theta=\theta_1$ for group A; $\theta=\theta_2$ for group B.

Thus twice the kinetic energy takes the form

$$2T=m_1\left(\frac{d\boldsymbol{\varrho}_1}{dt}\right)^2+m_2\left(\frac{d\boldsymbol{\varrho}_2}{dt}\right)^2$$
$$+\Sigma m_i(\boldsymbol{\omega}\times\mathbf{r}_i)^2+\Sigma M_i(\boldsymbol{\Omega}\times\mathbf{R}_i)^2.$$

Since $m_1\boldsymbol{\varrho}_1=-m_2\boldsymbol{\varrho}_2$, one can write

$$m_1\left(\frac{d\boldsymbol{\varrho}_1}{dt}\right)^2+m_2\left(\frac{d\boldsymbol{\varrho}_2}{dt}\right)^2=\frac{m_1m_2}{m_1+m_2}\left(\frac{d\boldsymbol{\varrho}}{dt}\right)^2,$$

where $\boldsymbol{\varrho}=\boldsymbol{\varrho}_1-\boldsymbol{\varrho}_2$.

Before proceeding with the calculation of $d\boldsymbol{\varrho}/dt$, one should observe that the remaining terms in the kinetic energy take the forms

$$\Sigma m_i(\boldsymbol{\omega}\times\mathbf{r}_i)^2=A_1'\omega_x^2+B_1'\omega_y^2+C_1'\omega_z^2$$
$$-2D_1'\omega_y\omega_z-2E_1'\omega_x\omega_z-2F_1'\omega_x\omega_y$$

and

$$\Sigma M_i(\boldsymbol{\Omega}\times\mathbf{R}_i)^2=A_2'\Omega_x^2+B_2'\Omega_y^2+C_2'\Omega_z^2$$
$$-2D_2'\Omega_y\Omega_z-2E_2'\Omega_x\Omega_z-2F_2'\Omega_x\Omega_y,$$

where the moments and products of inertia are calculated with respect to axes located at the centers of mass, A and B, of the respective groups. In setting up the actual metric it is convenient to describe the orientation of the coordinate systems introduced at A, B, and L in terms of Eulerian angles. We shall take the z axes of the coordinate systems at A, B, and L parallel to the axis of mutual rotation PL of the two groups. The angle which PL makes with a fixed orientation in space will be designated by the Eulerian polar angle θ. Rotations of groups A and B will be characterized by nodal angles φ_1 and φ_2, respectively. Both groups will have the same line of nodes and, therefore, the same azimuthal angle ψ. The Eulerian angles used are shown in Fig. 2.

Since the z axes of the coordinate systems at A and B are parallel to PL, it is not possible to eliminate all products of inertia from $\Sigma m_i(\boldsymbol{\omega}\times\mathbf{r}_i)^2$ and $\Sigma M_i(\boldsymbol{\Omega}\times\mathbf{R}_i)^2$. It is possible, however, to orient the axes so that the terms $-2F_1'\omega_x\omega_y$ and $-2F_2'\Omega_x\Omega_y$ are zero. On the other hand it may be desirable to retain these terms and choose the xy axes for other reasons. In order to leave this choice open we shall allow the xy axes in both group A and group B to have an arbitrary orientation and retain the xy products of inertia in the energy.

We now calculate $d\boldsymbol{\varrho}/dt$. One may refer the time derivative of $\boldsymbol{\varrho}$ to axes which follow group A or group B. If we refer $\boldsymbol{\varrho}$ to axes which follow group A, we have

$$\frac{d\boldsymbol{\varrho}}{dt}=\dot{\boldsymbol{\varrho}}+(\boldsymbol{\omega}\times\boldsymbol{\varrho}).$$

$\boldsymbol{\omega}$ is the rate of rotation of the axes fixed with respect to group A, and $\dot{\boldsymbol{\varrho}}$ is the time rate of change of $\boldsymbol{\varrho}$ as seen

from these axes. It is convenient to locate the origin of these axes at L. The fact that $\boldsymbol{\varrho}$ is referred to axes at L which remain parallel to previously defined Eulerian axes fixed at A is arbitrary and simply proves to be a convenient choice. The axes to which the components of $d\boldsymbol{\varrho}/dt$ are referred could equally well be fixed with respect to group B. The components of $\boldsymbol{\varrho}$ must now be obtained along the same axes to which the components $\omega_x, \omega_y, \omega_z$ of $\boldsymbol{\omega}$ are referred.

In terms of the preceding expression for $d\boldsymbol{\varrho}/dt$, twice the kinetic energy is

$$2T=\mu\dot{\boldsymbol{\varrho}}^2+2\mu\dot{\boldsymbol{\varrho}}\cdot(\boldsymbol{\omega}\times\boldsymbol{\varrho})+\mu(\boldsymbol{\omega}\times\boldsymbol{\varrho})^2 +\Sigma m_i(\boldsymbol{\omega}\times\mathbf{r}_i)^2+\Sigma M_i(\boldsymbol{\Omega}\times\mathbf{R}_i)^2$$

where

$$\mu=\frac{m_1m_2}{m_1+m_2}.$$

From Fig. 1,

$$\boldsymbol{\varrho}=\mathbf{LA}-\mathbf{LB},$$

$$\mathbf{LA}=h\mathbf{k}+\mathbf{PA}.$$

Thus for $\boldsymbol{\varrho}$ we have

$$\boldsymbol{\varrho}=\mathbf{PA}-\mathbf{LB}+h\mathbf{k}.$$

h is the distance between the point of intersection of a perpendicular from A with the axis of mutual rotation and the intersection of a perpendicular from B with the axis of mutual rotation. This is the distance PL shown in Fig. 1; $\mathbf{k}$ is a unit vector along the same axis. In order to find expressions for $\mathbf{PA}$ and $\mathbf{LB}$, we refer to Fig. 3 which shows these vectors in the xy plane looking down along the axis PL. ϵ_1 is the angle in the xy plane between $\mathbf{PA}$ and the ω_x component of $\boldsymbol{\omega}$. ϵ_2 is the angle which the Ω_x component of $\boldsymbol{\Omega}$ makes with $\mathbf{LB}$ in the xy plane.

a_1 and a_2 are the perpendicular distances from A and B to the axis of mutual rotation of the two groups. The orientation of the axes in the two groups is given by the Eulerian angles previously defined. φ_1 and φ_2 are the nodal angles of groups A and B, respectively. The angle of mutual rotation x is, then, given by $x=\varphi_1-\varphi_2$.

$\mathbf{PA}$ referred to axes along the direction of ω_x, ω_y is given by

$$\mathbf{PA}=\mathbf{i}a_1\cos\epsilon_1+\mathbf{j}a_2\sin\epsilon_1.$$

$\mathbf{i}$ and $\mathbf{j}$ are unit vectors in the direction of ω_x and ω_y. LB is given by

$$\mathbf{LB}=\mathbf{i}a_2\cos(x-\epsilon_2)-\mathbf{j}a_2\sin(x-\epsilon_2).$$

Thus for $\boldsymbol{\varrho}$ one has

$$\boldsymbol{\varrho}=\mathbf{i}[a_1\cos\epsilon_1-a_2\cos(x-\epsilon_2)] +\mathbf{j}[a_1\sin\epsilon_1+a_2\sin(x-\epsilon_2)]+h\mathbf{k}.$$

Thus,

$$(\partial\boldsymbol{\varrho}/\partial t)=\mathbf{i}a_2\dot{x}\sin(x-\epsilon_2)+\mathbf{j}a_2\dot{x}\cos(x-\epsilon_2).$$

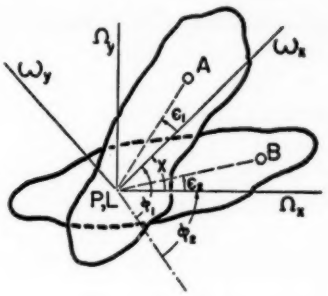

FIG. 3.

In order to obtain the kinetic energy in terms of $\theta, \psi, \varphi_1, \varphi_2$ and their time derivatives, we use the preceding expressions for $\boldsymbol{\varrho}$ and $\partial\boldsymbol{\varrho}/\partial t$, and express the components of the angular velocities in terms of the Eulerian angles. Thus,

$$\omega_x=\dot{\theta}\cos\varphi_1+\dot{\psi}\sin\theta\sin\varphi_1,$$

$$\omega_y=-\dot{\theta}\sin\varphi_1+\dot{\psi}\sin\theta\cos\varphi_1,$$

and

$$\omega_z=\dot{\varphi}_1+\dot{\psi}\cos\theta.$$

Expressions for $\Omega_x, \Omega_y, \Omega_z$ are obtained from $\omega_x, \omega_y, \omega_z$ by introducing φ_2 instead of φ_1. Making use of the above expressions, we find that twice the kinetic energy then becomes

$$\begin{aligned}2T=&\dot{\theta}^2[A_1\cos^2\varphi_1+B_1\sin^2\varphi_1+F_1\sin2\varphi_1\\
&+A_2\cos^2\varphi_2+B_2\sin^2\varphi_2+F_2\sin2\varphi_2\\
&-2a\sin\varphi_1'\sin\varphi_2']+\dot{\psi}^2[A_1\sin^2\varphi_1\sin^2\theta\\
&+B_1\cos^2\varphi_1\sin^2\theta+C_1\cos^2\theta-F_1\sin2\varphi_1\sin^2\theta\\
&-2E_1\sin\varphi_1\cos\theta\sin\theta-2D_1\cos\varphi_1\cos\theta\sin\theta\\
&+A_2\sin^2\varphi_2\sin^2\theta+B_2\cos^2\varphi_2\sin^2\theta+C_2\cos^2\theta\\
&-F_2\sin2\varphi_2\sin^2\theta-2E_2\sin\varphi_2\cos\theta\sin\theta\\
&-2D_2\cos\varphi_2\cos\theta\sin\theta-2a(\sin\varphi_1'\sin\varphi_2'\cos^2\theta\\
&+\cos\varphi_1'\cos\varphi_2')]+\dot{\varphi}_1^2[C_1]+\dot{\varphi}_2^2[C_2]\\
&+\dot{\theta}\dot{\psi}[A_1\sin2\varphi_1\sin\theta-B_1\sin2\varphi_1\sin\theta\\
&-2F_1\cos2\varphi_1\sin\theta-2E_1\cos\varphi_1\cos\theta\\
&+2D_1\sin\varphi_1\cos\theta+A_2\sin2\varphi_2\sin\theta\\
&-B_2\sin2\varphi_2\sin\theta-2F_2\cos2\varphi_2\sin\theta\\
&-2E_2\cos\varphi_2\cos\theta+2D_2\sin\varphi_2\cos\theta\\
&+2a\sin(\varphi_1'+\varphi_2')\sin\theta]+\dot{\theta}\dot{\varphi}_1 2[D_1\sin\varphi_1\\
&-E_1\cos\varphi_1]+\dot{\theta}\dot{\varphi}_2 2[D_2\sin\varphi_2-E_2\cos\varphi_2]\\
&+\dot{\psi}\dot{\varphi}_1 2[C_1\cos\theta-E_1\sin\varphi_1\sin\theta-D_1\cos\varphi_1\sin\theta\\
&-a\cos x'\cos\theta]+\dot{\psi}\dot{\varphi}_2 2[C_2\cos\theta-E_2\sin\varphi_2\sin\theta\\
&-D_2\cos\varphi_2\sin\theta-a\cos x'\cos\theta]+\dot{\varphi}_1\dot{\varphi}_2 2[-a\cos x'],\end{aligned}$$

where the following abbreviations have been introduced:

$$\varphi_1'=\varphi_1+\epsilon_1;\quad \varphi_2'=\varphi_2+\epsilon_2;\quad x'=x+\delta=\varphi_1'-\varphi_2';$$

$$\delta=\epsilon_1-\epsilon_2;\quad a=\mu a_1a_2;\quad b_1=\mu a_1^2;\quad b_2=\mu a_2^2;$$

$$f_1=\mu a_1h;\quad f_2=\mu a_2h;\quad g=\mu h^2;$$

$$A_1=A_1'+\tfrac{1}{2}g+b_1\sin^2\epsilon_1;\quad A_2=A_2'+\tfrac{1}{2}g+b_2\sin^2\epsilon_2;$$

$$B_1=B_1'+\tfrac{1}{2}g+b_1\cos^2\epsilon_1;\quad B_2=B_2'+\tfrac{1}{2}g+b_2\cos^2\epsilon_2;$$

$$C_1=C_1'+b_1;\qquad C_2=C_2'+b_2;$$

$$D_1=D_1'+f_1\sin\epsilon_1;\qquad D_2=D_2'-f_2\sin\epsilon_2;$$

$$E_1=E_1'+f_1\cos\epsilon_1;\qquad E_2=E_2'-f_2\cos\epsilon_2;$$

$$F_1=F_1'+b_1\sin\epsilon_1\cos\epsilon_1;\quad F_2=F_2'+b_2\sin\epsilon_2\cos\epsilon_2.$$

In the preceding expression the kinetic energy is expressed as a function of θ, ψ, φ_1, φ_2 and their time derivatives. The wave equation may now be obtained by expressing the Laplacian in curvilinear coordinates for which the metric is given by $2T$. The metric in this case has the value

$$g=N(1+L)\sin^2\theta,$$

where

$$L=(1/N)[M\sin^2x+P\cos^2x+Q\sin 2x+f(a)].$$

N, M, P, Q, and $f(a)$ are defined below:

$$\begin{aligned}N=&[(C_1C_2-a^2)(A_1B_1+A_2B_2-F_1^2-F_2^2)\\&-C_2(A_1D_1^2+B_1E_1^2+2D_1E_1F_1)\\&-C_1(A_2D_2^2+B_2E_2^2+2D_2E_2F_2)]\end{aligned}$$

$$\begin{aligned}M=&[(C_1C_2-a^2)(A_1A_2+B_1B_2)-C_2(A_2E_1^2+B_2D_1^2)\\&-C_1(A_1E_2^2+B_1D_2^2)+E_1^2E_2^2+D_1^2D_2^2\\&+2(E_1D_1E_2D_2+E_1D_1C_2F_2+E_2D_2C_1F_1)\\&+2(C_1C_2-a^2)F_1F_2]\end{aligned}$$

$$\begin{aligned}P=&[(C_1C_2-a^2)(A_1B_2+B_1A_2)-C_2(A_2D_1^2+B_2E_1^2)\\&-C_1(A_1D_2^2+B_1E_2^2)+E_1^2D_2^2+D_1^2E_2^2\\&-2(E_1D_1E_2D_2+E_1D_1C_2F_2+E_2D_2C_1F_1)\\&-2(C_1C_2-a^2)F_1F_2]\end{aligned}$$

$$\begin{aligned}Q=&[(D_1^2-E_1^2)(E_2D_2+C_2F_2)\\&+E_2D_2C_1(A_1-B_1)+(C_1C_2-a^2)F_2(A_1-B_1)\\&-(D_2^2-E_2^2)(E_1D_1+C_1F_1)-E_1D_1C_2(A_2-B_2)\\&-(C_1C_2-a^2)F_1(A_2-B_2)]\end{aligned}$$

$$\begin{aligned}f(a)=&\sin^2(x+\delta)[-a^2(C_1C_2-a^2)]\\&+\cos(x+\epsilon_1)[2a(C_1C_2-a^2)F_2\sin\epsilon_2\\&+2a(C_1D_2E_2\sin\epsilon_2+C_1E_2^2\cos\epsilon_2)]\\&+\cos(x-\epsilon_2)[2a(C_1C_2-a^2)F_1\sin\epsilon_1\\&+2a(C_2D_1E_1\sin\epsilon_1+C_2E_1^2\cos\epsilon_1)]\\&+\cos(x+\delta)[-2a(C_1C_2-a^2)(A_1+A_2)\\&+2a^2(D_1D_2\sin\epsilon_1\sin\epsilon_2+E_1D_2\cos\epsilon_1\sin\epsilon_2\\&+D_1E_2\sin\epsilon_1\cos\epsilon_2+E_1E_2\cos\epsilon_1\cos\epsilon_2)]\\&+\sin(x+\epsilon_1)[2a(C_1C_2-a^2)(A_2\sin\epsilon_2-B_2\sin\epsilon_2\\&+F_2\cos\epsilon_2)+2aC_1(D_2^2\sin\epsilon_2+D_2E_2\cos\epsilon_2)]\\&+\sin(x-\epsilon_2)[-2a(C_1C_2-a^2)(A_1\sin\epsilon_1\\&-B_1\sin\epsilon_1+F_1\cos\epsilon_1)-2aC_2(D_1^2\sin\epsilon_1\\&+D_1E_1\cos\epsilon_1)]+\cos(x+\delta)\sin x[-2a(D_2E_1B_1\\&-D_1E_2A_1-D_1E_2B_2+D_2E_1A_2+F_1D_1D_2\\&-F_2D_1D_2-F_1E_1E_2+F_2E_1E_2)]\\&+\cos(x+\delta)\cos x[-2a(D_1D_2A_1\\&+D_1D_2A_2+E_1E_2B_1+E_1E_2B_2\\&+F_1D_1E_2+F_2D_1E_2+F_1E_1D_2+F_2E_1D_2)]\\&+\cos(x+\delta)\cos(x+\epsilon_1)\cos(x-\epsilon_2)[2a^2E_1E_2]\\&+\cos(x+\delta)\cos(x+\epsilon_1)\sin(x-\epsilon_2)[-2a^2D_1E_2]\\&+\cos(x+\delta)\sin(x+\epsilon_1)\cos(x-\epsilon_2)[2a^2E_1D_2]\\&+\cos(x+\delta)\sin(x+\epsilon_1)\sin(x-\epsilon_2)[-2a^2D_1D_2]\\&+\sin^2(x+\delta)[a^2(A_1+A_2)(B_1+B_2)-a^2(F_1^2+F_2^2)]\\&+\sin^2(x+\delta)\sin 2x[-a^2(F_1A_2-F_1B_2\\&-F_2A_1+F_2B_1)]+\sin^2(x+\delta)\sin^2x[a^2(A_1-B_1)\\&\times(A_2-B_2)]+\sin^2(x+\delta)\cos 2x[-2a^2F_1F_2]\\&+\sin^2(x+\delta)\cos(x-\epsilon_2)[2a^3F_1\sin\epsilon_1]\\&+\sin^2(x+\delta)\cos(x+\epsilon_1)[2a^3F_2\sin\epsilon_2]\\&+\sin^2(x+\delta)\sin(x+\epsilon_1)[2a^3(A_2\sin\epsilon_2\\&-B_2\sin\epsilon_2+F_2\cos\epsilon_2)]+\sin^2(x+\delta)\sin(x-\epsilon_2)\\&\times[-2a^3(A_1\sin\epsilon_1-B_1\sin\epsilon_1+F_1\cos\epsilon_1)]\\&+\sin^2(x+\delta)\cos(x+\delta)[-2a^3(A_1+A_2)]\\&+\sin^4(x+\delta)[-a^4].\end{aligned}$$

Note that the long group of terms in "a" goes to zero when "a" goes to zero. These terms arise solely from the fact that the centers of mass of both groups lie off the axis of mutual rotation. We recall that "a" is

given by $a=\mu a_1 a_2$. After writing out the Laplacian, making the substitutions, $\varphi=C_1\varphi_1/C+C_2\varphi_2/C$, $x=\varphi_1-\varphi_2$, and introducing the abbreviations,

$R_1=(1/2g)(\partial g/\partial\varphi_1)=-R_2=-(1/2g)(\partial g/\partial\varphi_2)$,
$\mathfrak{L}=(1/\sin\theta)(\partial/\partial\psi)-\cot\theta\partial/\partial\varphi$,
$Q_1=(C_1/C)(\partial/\partial\varphi)+\partial/\partial x$,
$Q_2=(C_2/C)(\partial/\partial\varphi)-\partial/\partial x$, $\alpha_1=A_1-B_1$, $\alpha_2=A_2-B_2$,
$\beta_1=E_1D_1+C_1F_1$, $\beta_2=E_2D_2+C_2F_2$,
$\gamma_1=D_1^2+C_1\alpha_1$, $\gamma_2=D_2^2+C_2\alpha_2$,

and inserting the hindering potential, the wave equation takes the form shown below. Because of the symmetry of the wave equation with respect to the indices 1 and 2, only half the terms are presented. The remaining terms may be obtained by interchanging the subscripts 1 and 2 throughout. The terms so obtained should be added to those shown in order to display the complete wave equation. This interchange applies to all quantities: moments of inertia, angles, operators, etc. Note that under the interchange $1\rightleftarrows2$, $N\rightleftarrows N$, $L\rightleftarrows L$, $x\rightleftarrows-x$. For brevity we have retained in the trigonometric functions φ_1 and φ_2, where it is understood that they are to be replaced by $\varphi_1=\varphi+C_2x/C$, $\varphi_2=\varphi-C_1x/C$. Also note $\varphi_1'=\varphi_1+\epsilon_1$, $\varphi_2'=\varphi_2+\epsilon_2$, $x'=\varphi_1'-\varphi_2'$, $\delta=\epsilon_1-\epsilon_2$.

Group I(a) $+\frac{2}{\hbar^2}(1+L)[V(x)-E]u$:

$$-\frac{1}{N}\Big\{\tfrac{1}{2}[(C_1C_2-a^2)(A_1+B_1)-C_1(D_2^2+E_2^2)]\times\Big[\frac{1}{\sin\theta}\frac{\partial}{\partial\theta}\Big(\sin\theta\frac{\partial u}{\partial\theta}\Big)+\cot^2\theta\frac{\partial^2u}{\partial\varphi^2}-\frac{2\cot\theta}{\sin\theta}\frac{\partial^2u}{\partial\psi\partial\varphi}+\frac{1}{\sin^2\theta}\frac{\partial^2u}{\partial\psi^2}\Big]\Big\}-\frac{1}{2C}\frac{\partial^2u}{\partial\varphi^2}-\frac{C}{2C_1C_2}\frac{\partial^2u}{\partial x^2}+\frac{2}{\hbar^2}(1+L)[V(x)-E]^{\dagger}u.$$

Group I(b):

$$+\frac{1}{N}\{a[\tfrac{1}{2}(C_1C_2-a^2)+\tfrac{1}{2}(E_1E_2+D_1D_2)\cos x-D_1E_2\sin x]\cos x'-a^2[\tfrac{1}{2}(A_1+B_1)-\tfrac{1}{2}a\cos x']\sin^2x'\}\times\Big\{\frac{1}{\sin\theta}\frac{\partial}{\partial\theta}\Big(\sin\theta\frac{\partial u}{\partial\theta}\Big)+\cot^2\theta\frac{\partial^2u}{\partial\varphi^2}-\frac{2\cot\theta}{\sin\theta}\frac{\partial^2u}{\partial\psi\partial\varphi}+\frac{1}{\sin^2\theta}\frac{\partial^2u}{\partial\psi^2}\Big\}.$$

Group II:

$$-\frac{1}{N}[\{(C_2/C_1)(A_1D_1^2+B_1E_1^2+2D_1E_1F_1)-\tfrac{1}{2}(A_1+B_1)[D_2^2+E_2^2-C_2(A_2+B_2)]$$
$$+(a^2/C_1)(A_1B_1+A_2B_2-F_1^2-F_2^2)\}Q_1^2u+\{[-\alpha_1\beta_2+F_1(-E_2^2+\gamma_2)]\sin2x+\tfrac{1}{2}[\alpha_1(-E_2^2+\gamma_2)+4F_1\beta_2]\cos2x$$
$$-2a[-\alpha_1C_2\sin\epsilon_1\sin(x-\epsilon_2)-C_2F_1\sin(x-\epsilon_1-\epsilon_2)+\gamma_2\sin\epsilon_2\sin(x+\epsilon_1)+\beta_2\sin(x+\epsilon_1+\epsilon_2)$$
$$+E_2^2\cos\epsilon_2\cos(x+\epsilon_1)-C_2(A_1+A_2)\cos x']+a^2C_2\sin^2x'\}(R_1Q_1-Q_1^2)u$$
$$+\{-2[-\alpha_1\beta_2+F_1(-E_2^2+\gamma_2)]\cos2x+[\alpha_1(-E_2^2+\gamma_2)+4F_1\beta_2]\sin2x$$
$$+2a[-\alpha_1C_2\sin\epsilon_1\cos(x-\epsilon_2)-C_2F_1\cos(x-\epsilon_1-\epsilon_2)+\gamma_2\sin\epsilon_2\cos(x+\epsilon_1)+\beta_2\cos(x+\epsilon_1+\epsilon_2)$$
$$-E_2^2\cos\epsilon_2\sin(x+\epsilon_1)+C_2(A_1+A_2)\sin x']-a^2C_2\sin2x'\}Q_1u$$
$$+\{[A_1D_1D_2+B_1E_1E_2+F_1(D_1E_2+E_1D_2)]\cos x+[-(A_1+B_2)D_1E_2-F_1(E_1E_2-D_1D_2)]\sin x$$
$$+a[A_1(B_1+B_2)-F_1^2+\tfrac{1}{2}\alpha_1\alpha_2\sin^2x-F_1F_2\cos2x+\alpha_1F_2\sin2x-\tfrac{1}{2}(E_1E_2+D_1D_2)\cos x+E_2D_1\sin x]\cos x'$$
$$-\tfrac{1}{2}a[(E_1E_2-D_1D_2)\cos(\epsilon_1+\epsilon_2)-E_2D_1\sin(\epsilon_1+\epsilon_2)]+2a^2[-F_1\cos(\epsilon_1+\epsilon_2)\sin x$$
$$+F_1\sin(\epsilon_1+\epsilon_2)\cos x-\alpha_1\sin\epsilon_1\sin(x-\epsilon_2)-A_1\cos x']\cos x'-\tfrac{1}{2}a^3\sin^2x'\cos x'\}\{R_1(Q_1-Q_2)+2Q_1Q_2\}u$$
$$+\{[A_1D_1D_2+B_1E_1E_2+F_1(D_1E_2+E_1D_2)]\sin x-[-(A_1+B_2)D_1E_2-F_1(E_1E_2-D_1D_2)]\cos x$$
$$+a[A_1(B_1+B_2)\sin x'-F_1^2\sin x'+\tfrac{1}{2}\alpha_1\alpha_2(\sin^2x\sin x'-\sin2x\cos x')$$
$$-F_1F_2(2\sin2x\cos x'+\cos2x\sin x')-E_2D_1\cos(x+x')]+\alpha_1F_2(-2\cos2x\cos x'+\sin2x\sin x')$$
$$-\tfrac{1}{2}(E_1E_2+D_1D_2)\sin(x+x')]+2a^2[-A_1\sin2x'+F_1\cos(\epsilon_1+\epsilon_2)\cos(2x+\delta)+F_1\sin(\epsilon_1+\epsilon_2)\sin(2x+\delta)$$
$$+\alpha_1\sin\epsilon_1\cos(x+x'-\epsilon_2)]+\tfrac{1}{2}a^3(\sin2x'\cos x'-\sin^3x')\}(Q_1-Q_2)u$$
$$+(R_1/2)[(A_1+B_1+2B_2)E_2^2+(A_1+B_1+2A_2)D_2^2$$
$$-C_2(A_1A_2+B_1B_2+A_1B_2+A_2B_1+2A_1B_1+2A_2B_2-2F_1^2-2F_2^2)+4D_2E_2F_2]Q_1u].$$

† The "interchange" does not apply to the quantity $2(1+L)[V(x)-E]$. It takes its present form in the completed equation.

Group III:

$$-\frac{1}{N}[\{-C_2[(A_1+A_2)D_1+E_1F_1]-R_1C_2[(A_2+B_1)E_1+D_1F_1]+(D_2\beta_1-E_2\gamma_1)(\sin x+R_1\cos x)$$
$$+(E_2\beta_1+D_2\gamma_1)(\cos x-R_1\sin x)+a[(\alpha_1E_2-D_2F_1)\sin(2x+\delta)-(\alpha_1D_2+E_2F_1)\cos(2x+\delta)$$
$$-(D_2F_1\sin x+E_2F_1\cos x)\cos x'+[(A_2+B_1)E_1+D_1F_1]\sin x']+aR_1\cos x'[(A_2+B_1)E_1+D_1F_1$$
$$+(\alpha_1E_2-D_2F_1)\cos x+(\alpha_1D_2+E_2F_1)\sin x]\}\{\sin\varphi_1(\pounds u)+\cos\varphi_1\partial u/\partial\theta\}$$
$$+\{-C_2[(A_2+B_1)E_1+D_1F_1]+R_1C_2[(A_1+A_2)D_1+E_1F_1]+(E_1^2D_2-E_2\beta_1)(\sin x+R_1\cos x)$$
$$+(E_1^2E_2+D_2\beta_1)(\cos x-R_1\sin x)+a[(\alpha_1E_2-D_2F_1)\cos x\cos x'+(\alpha_1D_2+E_2F_1)\sin x\cos x'$$
$$-D_2F_1\cos(2x+\delta)+E_2F_1\sin(2x+\delta)-[(A_1+A_2)D_1+E_1F_1]\sin x']$$
$$+aR_1\cos x'[-(A_1+A_2)D_1-E_1F_1+D_2F_1\sin x+E_2F_1\cos x]\}\{-\cos\varphi_1(\pounds u)+\sin\varphi_1\partial u/\partial\theta\}$$
$$+\{aC_2[E_1\sin(x-\epsilon_2)+D_1\cos(x-\epsilon_2)]-a^2[-(E_2\cos\epsilon_2+D_2\sin\epsilon_2)\sin x'+D_1\cos(x+x'-\epsilon_2)$$
$$+E_1\sin(x+x'-\epsilon_2)]-aR_1[C_1(E_2\cos\epsilon_2+D_2\sin\epsilon_2)-C_2E_1\cos(x-\epsilon_2)+C_2D_1\sin(x-\epsilon_2)]$$
$$-a^2R_1\cos x'[-D_1\sin(x-\epsilon_2)+E_1\cos(x-\epsilon_2)-D_2\sin\epsilon_2-E_2\cos\epsilon_2]\}\{\sin\varphi_1'(\pounds u)+\cos\varphi_1'\partial u/\partial\theta\}$$
$$+\{aC_2[E_1\cos(x-\epsilon_2)-D_1\sin(x-\epsilon_2)]+a^2(E_2\cos\epsilon_2+D_2\sin\epsilon_2)\cos x'\}\{-\cos\varphi_1'(\pounds u)+\sin\varphi_1'\partial u/\partial\theta\}$$
$$+\{2C_2[(A_2+B_1)E_1+D_1F_1]+2a[(-\alpha_1E_2+D_2F_1)\cos x-(\alpha_1D_2+E_2F_1)\sin x]\cos x'\}\{\sin\varphi_1(\pounds)+\cos\varphi_1\partial/\partial\theta\}Q_1u$$
$$+\{-2C_2[(A_1+A_2)D_1+E_1F_1]-2a(D_2F_1\sin x+E_2F_1\cos x)\cos x'\}\{-\cos\varphi_1(\pounds)+\sin\varphi_1\partial/\partial\theta\}Q_1u$$
$$+\{2[(D_1\gamma_2+E_1\beta_2)\sin x-(E_1\gamma_2-D_1\beta_2)\cos x]+2a[(A_1+B_2)E_2+D_2F_2\cos x']\{\sin\varphi_2(\pounds)+\cos\varphi_2\partial/\partial\theta\}Q_1u$$
$$+\{2[(D_1\beta_2+E_1E_2^2)\sin x-(E_1\beta_2-D_1E_2^2)\cos x]-2a[(A_1+A_2)D_2+E_2F_2]\cos x'\}\{-\cos\varphi_2(\pounds)+\sin\varphi_2\partial/\partial\theta\}Q_1u$$
$$+\{-2aC_2[E_1\cos(x-\epsilon_2)-D_1\sin(x-\epsilon_2)]-2a^2(E_2\cos\epsilon_2+D_2\sin\epsilon_2)\cos x'\}\{\sin\varphi_1'(\pounds)+\cos\varphi_1'\partial/\partial\theta\}Q_1u$$
$$+\{-2aC_2(E_1\cos\epsilon_1+D_1\sin\epsilon_1)-2a^2\cos x'[E_2\cos(x+\epsilon_1)+D_2\sin(x+\epsilon_1)]\}\{\sin\varphi_2'(\pounds)+\cos\varphi_2'\partial/\partial\theta\}Q_1u].$$

Group IV:

$$-\frac{1}{N}\Big[\{[\tfrac{1}{2}\alpha_1(C_1C_2-a^2)+\tfrac{1}{2}C_2(D_1^2-E_1^2)]\cos2\varphi_1+[(C_1C_2-a^2)F_1+C_2E_1D_1]\sin2\varphi_1$$
$$+\tfrac{1}{2}a(C_1C_2-a^2)\cos(\varphi_1'+\varphi_2')+a[E_2D_1\sin(\varphi_1+\varphi_2)-\tfrac{1}{2}(E_1E_2-D_1D_2)\cos(\varphi_1+\varphi_2)]\cos x'$$
$$+a^2[\tfrac{1}{2}\alpha_1\cos2\varphi_1+F_1\sin2\varphi_1+\tfrac{1}{2}a\cos(\varphi_1'+\varphi_2')]\sin^2x'\Big\{\frac{1}{\sin^2\theta}\frac{\partial^2u}{\partial\psi^2}-\frac{\partial^2u}{\partial\theta^2}+\cot^2\theta\frac{\partial^2u}{\partial\varphi^2}-\frac{2\cot\theta}{\sin\theta}\frac{\partial^2u}{\partial\psi\partial\varphi}+\cot\theta\frac{\partial u}{\partial\theta}\Big\}$$
$$+\{\tfrac{1}{2}[\alpha_1(C_1C_2-a^2)+C_2(D_1^2-E_1^2)]\sin2\varphi_1-[(C_1C_2F-a^2)_1+C_2E_1D_1]\cos2\varphi_1+\tfrac{1}{2}a(C_1C_2-a^2)\sin(\varphi_1'+\varphi_2')$$
$$-a[E_2D_1\cos(\varphi_1+\varphi_2)+\tfrac{1}{2}(E_1E_2-D_1D_2)\sin(\varphi_1+\varphi_2)]\cos x'+a^2[\tfrac{1}{2}\alpha_1\sin2\varphi_1-F_1\cos2\varphi_1$$
$$+\tfrac{1}{2}a\sin(\varphi_1'+\varphi_2')]\sin^2x'\Big\{2\cot\theta\frac{\partial^2u}{\partial\theta\partial\varphi}-\frac{2}{\sin\theta}\frac{\partial^2u}{\partial\psi\partial\theta}+\frac{2\cot\theta}{\sin\theta}\frac{\partial u}{\partial\psi}-(1+2\cot^2\theta)\frac{\partial u}{\partial\varphi}\Big\}\Big]=0.$$

The boundary conditions governing the solutions of the wave equation are the same as those applying to two symmetric groups undergoing hindered rotation.[2] The functions must remain finite at the poles $\theta=0$, π, and they must be periodic with period 2π in the angles ψ, φ_1, and φ_2.

We note that the wave equation has the following form:

$$[\text{Group I(a)}]+[\text{Groups I(b) to IV}]+(2/\hbar^2)(1+L)[V(x)-E]u=0$$

which may be written

$$[\text{Group I(a)}]+(2/\hbar^2)[V-E]u-\frac{L}{1+L}[\text{Group I(a)}]+\frac{[\text{Groups I(b) to IV}]}{1+L}=0.$$

Note that $[\text{Group I(a)}]+(2/\hbar^2)[V-E]$ (we shall hereafter refer to these terms as Group I′) when set equal to zero is identical to the wave equation of Koehler and Dennison, provided that the reciprocal of their

moment of inertia $1/A$ is replaced by

$$2N/[(C_1C_2-a^2)(A_1+A_2+B_1+B_2) -C_1(D_2^2+E_2^2)-C_2(D_1^2+E_1^2)].$$

The solution to this part of the equation, subject to the boundary conditions, may be written

$$u=\frac{1}{2\pi}e^{iK\varphi}\exp(iM\psi)\exp(-iC_1Kx/C)P(x)^{K\tau n}\Theta_{JKM}.$$

The quantity $e^{iK\varphi}\exp(iM\psi)\Theta_{JKM}$ is the usual rigid symmetric top wave function.

$$M(x)=\exp(-iC_1Kx/C)P(x)^{K\tau n}$$

for a potential of periodicity n satisfies the equation

$$d^2M/dx^2+(R'+S\cos nx)M=0,$$

where

$$R'=(2C_1C_2/C\hbar^2)(E^{K\tau n}-H/2),\quad S=C_1C_2H/C\hbar^2.$$

The n in the function $P(x)^{K\tau n}$ is not related to the periodicity of the barrier, but is a quantum number classifying the internal rotational states. In the limit of an infinitely high barrier (parabolic potential) n goes over to the simple harmonic oscillator vibrational quantum number. The quantum number τ depends on the multiplicity of the potential function. J, K, and M are the usual symmetric top quantum numbers. The energy is equal to the sum of $E^{K\tau n}$ and E^{JK} where the latter is the symmetric top energy. The $E^{K\tau n}$ arise from the internal motion and are the eigenvalues of the equation in $M(x)$.

$$E^{JK}=\frac{\hbar^2}{2}\left\{\frac{1}{2N}[(C_1C_2-a^2)(A_1+A_2+B_1+B_2) -C_1(D_2^2+E_2^2)-C_2(D_1^2+E_1^2)] \times(J^2+J-K^2)+\frac{K^2}{C}\right\}.$$

The boundary conditions require $P(x)^{K\tau n}$ to be periodic in x with period 2π, and it is customary to express it as

$$P(x)^{K\tau n}=\Sigma a_m e^{imx}.$$

MATRIX ELEMENTS

The matrix elements of the Hamiltonian corresponding to the complete wave equation may now be evaluated using the wave functions for the group I′ terms. Group I′ terms, from the above discussion, yield elements of the Hamiltonian which are diagonal in all four quantum numbers. Terms of Group II do not contain θ nor φ and are, therefore, diagonal in J and K. Some of the integrals in x will vanish for certain symmetries. Each term of Group III contains the sine or cosine of $\varphi+(C_2x/C)$ or $\varphi-(C_1x/C)$ and therefore will connect states where $K\rightarrow K\pm1$. When the sine and cosine functions in φ and x in Group III are replaced by exponentials, and the elementary integrals in ψ and φ evaluated, one is left with the following integral in θ common to the whole group:

$$\int_0^\pi \Theta^*_{JKM}\left[-\frac{M}{\sin\theta}+(K+1)\cot\theta+\frac{d}{d\theta}\right]\Theta_{J'K+1M}\sin\theta d\theta.$$

This integral has been evaluated[5] and has the value $[(J-K)(J+K+1)]^{\frac{1}{2}}$ where $J'=J$. As previously mentioned all integrals in x can only be carried out when the nature of the hindering potential is specified.

Group IV terms all contain terms in the sine and cosine of 2φ and, therefore, will have nonvanishing integrals in φ for $K\rightarrow K\pm2$. When these terms are put in exponential form and the integrals in ψ and φ evaluated, one is left with the following integral in θ common to the whole group:

$$\int_0^\pi \Theta^*_{JKM}\left[\frac{M^2}{\sin^2\theta}+K(K+2)\cot^2\theta-2M(K+1)\frac{\cot\theta}{\sin\theta} -(K+2)+\left(3\cot\theta+2K\cot\theta-\frac{2M}{\sin\theta}\right)\frac{d}{d\theta}+\frac{d^2}{d\theta^2}\right] \times\Theta_{J'K+2M}\sin\theta d\theta.$$

This integral has been evaluated[5] and has the value[6]

$$[(J-K)(J-K-1)(J+K+1)(J+K+2)]^{\frac{1}{2}}$$

where

$$J'=J.$$

We are led, then, to the following matrix elements. Some additional abbreviations have been introduced: $\mathfrak{A}_1=-iK+2d/dx$, $\mathfrak{A}_2=-\mathfrak{A}_1$, $\mathfrak{B}_1=d/dx$, $\mathfrak{B}_2=iK-d/dx$, $\mathfrak{D}_1=R_1\mathfrak{A}_1+2\mathfrak{B}_1\mathfrak{B}_2$, $\mathfrak{D}_2=\mathfrak{D}_1$, $\mathfrak{E}_1=\mathfrak{B}_2^2-R_2\mathfrak{B}_2$, $\mathfrak{E}_2=\mathfrak{B}_1^2-R_1\mathfrak{B}_2$, $\mathfrak{F}_1=R_1+2[i(K+1)-d/dx]$, $\mathfrak{F}_2=R_2+2d/dx$, $\xi_1=e^{-ix}$, $\xi_2=1$, $\eta_1=e^{-i2x}$, $\eta_2=e^{ix}$, $P=(P^{K\tau n})^*/(1+L)$. All integrals in x are from 0 to 2π. Again the symmetry of the terms with respect to the interchange $1\rightleftarrows2$ of the subscripts is utilized to save space. About half the matrix elements are shown. The remainder may be obtained from those presented by interchanging the subscripts 1 and 2 in all terms, with the exception of a few terms noted. They are the first few $K\rightarrow K$ elements and all of the $K\rightarrow K+2$ matrix elements. In terms written in the form $\sin2xO_i$ $(i=1,2)$, the operator O_i is not part of the argument of the trigonometric function. The result of the operation O_i is multiplied by the trigonometric function. Brackets separating these terms are

[6] The symmetric top wave function implicit in the present paper differs from that of both Dennison [Revs. Modern Phys. **3**, 2, 280 (1931)] and King, Hainer, and Cross [J. Chem. Phys. **11**, 27 (1943)]. The representation of the latter becomes equivalent to the present one if one substitutes $(-1)^K\Theta_{JKM}$ for our Θ_{JKM}. Thus all our $K\rightarrow K\pm1$ matrix elements in θ differ in sign from those of K.H.C. It should also be mentioned that the wave function in the present paper differs from that of reference 3 by the phase factor $(-1)^K$.

omitted for brevity. The matrix elements are extremely lengthy and algebraically complex. It should be kept in mind, however, that the results apply to the general case of two completely asymmetric molecules undergoing mutual rotation about a common axis. A considerable reduction in the amount and complexity of calculation may be effected in those cases where some degree of symmetry is present in the molecule.

$$H_{JK\tau n}{}^{JK\tau n}=(\hbar^2/2N)\{\tfrac{1}{2}[(C_1C_2-a^2)(A_1+B_1+A_2+B_2)-C_1(D_2^2+E_2^2)-C_2(D_1^2+E_1^2)]$$
$$\times(J^2+J-K^2)+K^2N/C\}+E^{K\tau n}.$$

$$H_{JK\tau' n'}{}^{JK\tau n}=(-\hbar^2/2N)\Big[\{\tfrac{1}{2}[(C_1C_2-a^2)(A_1+B_1+A_2+B_2)-C_1(D_2^2+E_2^2)-C_2(D_1^2+E_1^2)]$$
$$\times(J^2+J-K^2)+K^2N/C\}\int PLP^{K\tau' n'}dx-(NC/C_1C_2)\int PL[(iC_1K/C)-d/dx]^2P^{K\tau' n'}dx\Big].$$

The above terms are complete as shown and are not to be subjected to an interchange $1\rightleftarrows 2$ of subscripts. In the following matrix elements indices 1 and 2 should be interchanged and the result added to the terms displayed:

$$H_{JK\tau' n'}{}^{JK\tau n}=-\frac{\hbar^2}{2N}\Big[\Big\{\frac{C_2}{C_1}(A_1D_1^2+B_1E_1^2+2D_1E_1F_1)-\tfrac{1}{2}(A_1+B_1)[D_2^2+E_2^2-C_2(A_2+B_2)]$$
$$+\frac{a^2}{C_1}(A_1B_1+A_2B_2-F_1^2-F_2^2)\Big\}\int P\mathfrak{B}_1{}^2P^{K\tau' n'}dx+\{A_1D_1D_2+B_1E_1E_2+F_1(D_1E_2+E_1D_2)\}$$
$$\times\int P(\sin x\mathfrak{A}_1+\cos x\mathfrak{D}_1)P^{K\tau' n'}dx-\{(A_2+B_1)E_1D_2-F_1(E_1E_2-D_1D_2)\}$$
$$\times\int P(\cos x\mathfrak{A}_1-\sin x\mathfrak{D}_1)P^{K\tau' n'}dx-\{\alpha_2\beta_1+F_2(E_1^2-D_1^2)-\alpha_1F_2C_1\}$$
$$\times\int P(\sin 2x\mathcal{E}_1-2\cos 2x\mathfrak{B}_2)P^{K\tau' n'}dx$$
$$-\tfrac{1}{2}\{\alpha_2(\gamma_1-E_1^2)+4F_2\beta_1\}\int P(\cos 2x\mathcal{E}_1+2\sin 2x\mathfrak{B}_2)P^{K\tau' n'}dx$$
$$+\tfrac{1}{2}\{(A_1+B_1+2B_2)E_2^2+(A_1+B_1+2A_2)D_2^2+4D_2E_2F_2-C_2[(A_1+B_1)(A_2+B_2)$$
$$+2(A_1B_1+A_2B_2-F_1^2-F_2^2)]\}\int PR_1\mathfrak{B}_1P^{K\tau' n'}dx\Big]$$
$$+\frac{\hbar^2}{2N}(J^2+J-K^2)a\Big[\tfrac{1}{2}(a^2-C_1C_2)\int P\cos x'P^{K\tau' n'}dx-\tfrac{1}{2}(E_1E_2+D_1D_2)\int P\cos x\cos x'P^{K\tau' n'}dx$$
$$+D_1E_2\int P\sin x\cos x'P^{K\tau' n'}dx+\tfrac{1}{2}a(A_1+B_1)\int P\sin^2x'P^{K\tau' n'}dx-\tfrac{1}{2}a^2\int P\cos x'\sin^2x'P^{K\tau' n'}dx\Big]$$
$$-\frac{\hbar^2a}{2N}\Big[\{A_1(B_1+B_2)-F_1^2\}\int P(\sin x'\mathfrak{A}_1+\cos x'\mathfrak{D}_1)P^{K\tau' n'}dx$$
$$+\tfrac{1}{2}\alpha_1\alpha_2\int P[(\sin^2x\sin x'-\sin 2x\cos x')\mathfrak{A}_1+\sin^2x\cos x'\mathfrak{D}_1]P^{K\tau' n'}dx$$
$$+\alpha_1F_2\int P[(-2\cos 2x\cos x'+\sin 2x\sin x')\mathfrak{A}_1+\sin 2x\cos x'\mathfrak{D}_1]P^{K\tau' n'}dx$$
$$+\{\tfrac{1}{2}(E_1E_2+D_1D_2)-2aF_1\sin(\epsilon_1+\epsilon_2)\}\int P[-\sin(2x+\delta)\mathfrak{A}_1-\cos x\cos x'\mathfrak{D}_1]P^{K\tau' n'}dx$$

$$-\{E_2D_1-2aF_1\cos(\epsilon_1+\epsilon_2)\}\int P[\cos(2x+\delta)\mathfrak{A}_1-\sin x\cos x'\mathfrak{D}_1]P^{K\tau'n'}dx$$

$$-F_1F_2\int P[(2\sin 2x\cos x'+\cos 2x\sin x')\mathfrak{A}_1+\cos 2x\cos x'\mathfrak{D}_1]P^{K\tau'n'}dx$$

$$-2aA_1\int P(\sin 2x'\mathfrak{A}_1+\cos^2 x'\mathfrak{D}_1)P^{K\tau'n'}dx$$

$$+2a\alpha_1\sin\epsilon_1\int P[\cos(2x-2\epsilon_2+\epsilon_1)\mathfrak{A}_1-\sin(x-\epsilon_2)\cos x'\mathfrak{D}_1]P^{K\tau'n'}dx$$

$$+\tfrac{1}{2}a^2\int P[(\sin 2x'\cos x'-\sin^3 x')\mathfrak{A}_1-\sin^2 x'\cos x'\mathfrak{D}_1]P^{K\tau'n'}dx$$

$$-\{\tfrac{1}{2}(E_1E_2-D_1D_2)\cos(\epsilon_1+\epsilon_2)+E_2D_1\sin(\epsilon_1+\epsilon_2)\}\int P\mathfrak{D}_1P^{K\tau'n'}dx$$

$$+2C_1\alpha_2\sin\epsilon_2\int P[\sin(x+\epsilon_1)\mathfrak{E}_1-\cos(x+\epsilon_1)\mathfrak{B}_2]P^{K\tau'n'}dx$$

$$+2C_1F_2\int P[\sin(x+\epsilon_1+\epsilon_2)\mathfrak{E}_1-\cos(x+\epsilon_1+\epsilon_2)\mathfrak{B}_2]P^{K\tau'n'}dx$$

$$-2\gamma_1\sin\epsilon_1\int P[\sin(x-\epsilon_2)\mathfrak{E}_1-\cos(x-\epsilon_2)\mathfrak{B}_2]P^{K\tau'n'}dx$$

$$-2\beta_1\int P[\sin(x-\epsilon_1-\epsilon_2)\mathfrak{E}_1-\cos(x-\epsilon_1-\epsilon_2)\mathfrak{B}_2]P^{K\tau'n'}dx$$

$$+2E_1^2\cos\epsilon_1\int P[\cos(x-\epsilon_2)\mathfrak{E}_1+\sin(x-\epsilon_2)\mathfrak{B}_2]P^{K\tau'n'}dx$$

$$-2C_1(A_1+A_2)\int P(\cos x'\mathfrak{E}_1+\sin x'\mathfrak{B}_2)P^{K\tau'n'}dx$$

$$-aC_1\int P(\sin^2 x'\mathfrak{E}_1-\sin 2x'\mathfrak{B}_2)P^{K\tau'n'}dx\Big].$$

$$H_{JK+1\tau'n'}{}^{JK\tau n}=-\frac{\hbar^2}{4N}[(J-K)(J+K+1)]^{\frac{1}{2}}\Big[\{-[(A_1+B_2)E_2+D_2F_2]+i[(A_1+A_2)D_2+E_2F_2]\}$$

$$\times\int P\xi_2[-C_1(\mathfrak{F}_1-i)+a\sin x'-a\cos x'\mathfrak{F}_2]P^{K+1\tau'n'}dx$$

$$+\{\alpha_1E_2-D_2F_1+iE_2F_1\}$$

$$\times\int P\xi_1\{-C_1(\sin x+\cos x\mathfrak{F}_1)+a[\sin(2x+\delta)+\cos x\cos x'(i-\mathfrak{F}_2)]\}P^{K+1\tau'n'}dx$$

$$+\{\alpha_1D_2+E_2F_1+iD_2F_1\}$$

$$\times\int P\xi_1\{-C_1[-\cos x+\sin x\mathfrak{F}_1]+a[-\cos(2x+\delta)+\sin x\cos x'(i-\mathfrak{F}_2)]\}P^{K+1\tau'n'}dx$$

$$+E_1D_1(D_2-iE_2)\int P\eta_1(i+\mathfrak{F}_1)P^{K+1\tau'n'}dx$$

$$-(E_2D_1^2-iD_2E_1^2)\int P\xi_1(\sin x+\cos x\mathfrak{F}_1)P^{K+1\tau'n'}dx$$

$$+(D_2D_1^2+iE_2E_1^2)\int P\xi_1(\cos x-\sin x\mathfrak{F}_1)P^{K+1\tau'n'}dx$$

$$+aC_2E_1e^{-i\epsilon_1}\int P\xi_1[\sin(x-\epsilon_2)+\cos(x-\epsilon_2)(i-\mathfrak{F}_2)]P^{K+1\tau'n'}dx$$

$$+aC_2D_1e^{-i\epsilon_1}\int P\xi_1[\cos(x-\epsilon_2)-\sin(x-\epsilon_2)(i-\mathfrak{F}_2)]P^{K+1\tau'n'}dx$$

$$-aC_2(E_1\cos\epsilon_1+D_1\sin\epsilon_1)e^{-i\epsilon_2}\int P\xi_2\mathfrak{F}_2P^{K+1\tau'n'}dx$$

$$+a^2E_2e^{-i\epsilon_2}\int P\xi_2[\cos x'\sin(x+\epsilon_1)+\cos(x+\epsilon_1)(\sin x'-\cos x'\mathfrak{F}_2)]P^{K+1\tau'n'}dx$$

$$-a^2D_2e^{-i\epsilon_2}\int P\xi_2[\cos x'\cos(x+\epsilon_1)-\sin(x+\epsilon_1)(\sin x'-\cos x'\mathfrak{F}_2)]P^{K+1\tau'n'}dx$$

$$+a^2(E_2\cos\epsilon_2+D_2\sin\epsilon_2)e^{-i\epsilon_1}\int P\xi_1[\sin x'+\cos x'(i-\mathfrak{F}_2)]P^{K+1\tau'n'}dx\Big].$$

The following $K\rightarrow K+2$ matrix elements are complete as shown and no additional ones are to be added by interchanging indices.

$$H_{JK+2\tau'n'^{JK\tau n}}=\frac{\hbar^2}{8N}[(J-K)(J-K-1)(J+K+1)(J+K+2)]^{\frac{1}{2}}$$

$$\times\Big[\{(C_1C_2-a^2)(\alpha_1+i2F_1)+C_2(D_1+iE_1)^2\}\int Pe^{-i2x}P^{K+2\tau'n'}dx$$

$$+\{(C_1C_2-a^2)(\alpha_2+i2F_2)+C_1(D_2+iE_2)^2\}\int PP^{K+2\tau'n'}dx$$

$$+2a(C_1C_2-a^2)e^{-i(\epsilon_1+\epsilon_2)}\int Pe^{-ix}P^{K+2\tau'n'}dx$$

$$+2a\{i(E_2D_1+D_2E_1)-(E_1E_2-D_1D_2)\}\int Pe^{-ix}\cos x'P^{K+2\tau'n'}dx$$

$$+a^2(\alpha_1+i2F_1)\int Pe^{-i2x}\sin^2x'P^{K+2\tau'n'}dx$$

$$+a^2(\alpha_2+i2F_2)\int P\sin^2x'P^{K+2\tau'n'}dx$$

$$+2a^3e^{-i(\epsilon_1+\epsilon_2)}\int Pe^{-ix}\sin^2x'P^{K+2\tau'n'}dx\Big].$$

ACKNOWLEDGMENTS

The authors are grateful to Mr. Neil Ashby, Mr. Carlos Varsavsky, and Mr. John Hutcherson for their assistance in checking various phases of the algebraic work.

Inertial Effects and Dielectric Relaxation*

E. P. Gross
Physics Department, Syracuse University, Syracuse, New York
(Received November 2, 1954)

The study of dielectric relaxation in compressed gases requires an extension of existing theory. As the gas pressure is lowered below several hundred atmospheres, the inertial response of the dipoles gives rise to large deviations from the Debye equations. The absorption and dispersion depend on collision time and frequency of applied field in a manner which is sensitive to the molecular constants and to the state of dynamical order of the compressed gas.

These phenomena are investigated by studying the response to an alternating electric field of a dilute solution of dipolar molecules in a nonpolar compressed gas. The dipoles are described by a classical distribution function which is a function of angular velocity, orientation, and time. We assume that the duration of collision may be neglected compared to the time between collisions, the period of the applied field, and the mean thermal period. The distribution function satisfies a kinetic equation; the effects of collisions are described by a collision kernel. One kernel yields a soft impact theory which is a generalization of Debye's Brownian motion treatment to include inertial effects. The complex polarization is given in the form of a convergent infinite continued fraction. Other models studied involve strong collisions and partial specular reflection.

A common feature of all models is that the Debye relaxation shape is found at high pressures. Inertial corrections are important in the region between one and a few hundred atmospheres; the corrections depend on the model. Another common feature is the way in which the discrete rotational lines are linked with the Debye spectrum. The collision frequency $1/\tau$ increases with increasing gas pressure; at low pressures it is proportional to the width of a rotation line. At high pressures when the Debye shape is found, the relaxation time t^* is given by $t^*=1/\tau(I/kT)$. Here I is the moment of inertia of the dipole, k is Boltzmann's constant, and T is the temperature of the reservoir. Thus the relaxation time varies inversely with time between collisions. The physical reason is that collisions hinder the drift motion of the dipoles which is the cause of the relaxation of the polarization.

At lower pressures the main contribution to the polarization arises from dipoles rotating with an angular frequency close to that of the applied field. This is related to the known result that the main contribution to the static polarization is from librating dipoles.

I. INTRODUCTION

THE present communication deals with some aspects of the dielectric relaxation process which are particularly significant for compressed gases. The effects which concern us are usually classed as "inertial corrections." For the most studied case of dielectric absorption and dispersion in liquids, the corrections are negligible, except at frequencies much greater than the relaxation frequency. These high frequencies are in the far infrared for most systems and are relatively inaccessible; in addition overlapping vibrational lines greatly complicate analysis in any concrete case. Inertial corrections are of greater interest for the subject of dielectric absorption in compressed gases. For, as the gas pressure is lowered, the time between collisions increases, and there is time for the inertial response of the dipoles to come into play. We shall find that the inertial contributions are very large and striking in the pressure region from a few atmospheres to a few hundred atmospheres.

One of the treatments given is a generalization of the Brownian motion approach of Debye.[1,2] Debye works with a distribution function which specifies the number of dipoles of a given orientation at a given time; this function satisfies the Smoluchowski equation. We employ a more general distribution function which contains additional information concerning the number of dipoles of a given angular velocity. The general distribution function yields a superior understanding of the physical nature of the relaxation process, and an insight into the transition from the low-pressure rotational line structure to the high-pressure relaxation spectrum. In this connection, an interesting result is the following. Consider a dilute solution of polar molecules in a nonpolar gas. Let β be the collision frequency, a quantity which determines the width of individual rotational lines of the polar molecule, and which increases monotonically with pressure. Let I be the moment of inertia of the dipole, k Boltzmann's constant, and T the temperature of the nonpolar gas. Then the Debye relaxation time t^*, (at high pressures, when the Debye equations hold), is given by $t^*=\beta(I/kT)$. t^* increases with increasing pressure, which is the correct trend. Thus both the line breadth and the Debye relaxation time are proportional to the collision frequency. Physically the Debye time is the time for an initial polarization to decay in absence of a field. This time should increase with collision frequency, since collisions hinder the drift motion of the dipoles, which is the agency causing changes in the polarization.

Of course, the Brownian motion model of small velocity and energy changes is likely to be satisfied in a gas only if the mass and moment of inertia of the dipole molecule are large compared to these characteristics of the nonpolar gas. For dipoles with characteristics comparable to those of the nonpolar constituent, collisions are likely to involve large exchanges of energy (of the order of kT). To obtain insight into this case, other models are discussed in Secs. IV and V. At high pressures, a dipole perhaps satisfies the conditions of the Brownian motion treatment more closely, although violent collisions are still present. A dipole comes into

* Work sponsored by Office of Scientific Research.
[1] P. Debye, Ber. deut. physik. Ges. **15**, 777 (1913).
[2] P. Debye, *Polar Molecules* (Dover Publications, New York, 1945).

the range of force of several nonpolar molecules at once, and is continually altering its state. In any case we obtain the Debye spectrum at high pressures even for models involving energetic collisions. Thus the universality of the Debye spectrum becomes partly understandable.

The discussion of an adequate physical model raises the following important question: Are the characteristics of the interactions of a dipolar molecule reflected in a sensitive dependence of the shape of the absorption and dispersion spectrum? If this were the case, one would be equipped with a tool for investigating the nature of the dynamical ordering in compressed gases. To see this, consider a gas mixture consisting of a nonpolar gas and of a polar gas of much smaller concentration. The extent of coupling between nonpolar molecules while one of them (or all) are colliding with a dipole affects the collision. Closely related are the fluctuations in local density, energy, and momentum in the nonpolar system. One can measure the response (absorption and dispersion) of the dipoles to an alternating electric field as a function of angular frequency; they serve as probes of the dynamical behavior of the nonpolar gas. The dielectric tool is practically unique in this respect, since one can employ fields whose period is comparable to the duration of a fluctuation of the nonpolar system.

For the case of normal liquids our question has been answered basically in the negative. The omnipresence of the Debye relaxation shape precludes more detailed analysis of the microscopic processes by means of dielectric research. There is perhaps more hope for the compressed gas where inertial effects enter, and where a wide range of densities and temperatures is at one's disposal. We make a first attempt to investigate the question by comparing the predicted absorption and response for several different collision models. The results are not entirely conclusive. It is found that the relaxation spectrum does depend (in magnitude and shape) sensitively on the collision model. The effect, however, is mostly due to the disparity of masses and moments of inertia of the polar and nonpolar molecules. It may be difficult to go beyond this to conclusions about the state of order. One may not be able to say much more than "The nonpolar molecules appear to be coupled, since the effective mass in a collision with a polar molecule is greater than that of a single nonpolar molecule." As another aspect of the problem, consider a system in which polar and nonpolar molecules have comparable characteristics. At low pressures collisions then involve strong energy interchanges. At high pressures one expects a model with more gradual interchanges to be better. However, dielectric measurements do not appear capable of ruling out a model in which strong interchanges remained predominant at high pressures. The sensitivity to a model is greatest at lower pressures and it is there that measurements will be most useful. We leave these questions to the future, pending experimental investigation of the inertial effects themselves.

Our treatment will be schematic, i.e., not derived from the fundamental Hamiltonian of the system. This is the case with all existing theories of dielectric relaxation. The following points give an idea of the type of abstraction made, and of the more general type of theory needed:

1. We deal with two-dimensional linear dipoles. This simplification is no restriction conceptually and permits expression of the results in easily surveyable mathematical form.

2. The rotational degrees of freedom of the polar molecules are the only ones considered. Actual interactions involve changes of the translational motions as well. Failure to consider these changes is perhaps not serious from the point of view of examining different models, since we use a schematic representation of the over-all effects of collisions on the rotational coordinates. However, this point would have to be considered more carefully in the interpretation of experimental measurements.

3. The duration of collision is assumed to be negligible compared to the characteristic times for the polar molecule. These are (a) the mean thermal angular period $(I/kT)^{\frac{1}{2}}$ and (b) the mean time between collisions, τ. τ is assumed independent of the angular velocity of the polar molecule. The duration of the collision is also taken as small compared to the period $2\pi/w$ of the applied field (where w is the angular frequency). As has been discussed in an earlier paper dealing with spectral line broadening,[3] these assumptions imply that the angular position is unchanged as a result of collision, but the angular velocity may change abruptly. The models are perhaps valid for inert nonpolar gases with short-range force fields. It would be more realistic to treat cases where the duration of collision is comparable to other frequencies, i.e., quasiadiabatic collisions; however, we do not treat these here. The Brownian motion model is considered here from the impulse point of view, i.e., as a succession of small frequent instantaneous collisions; it may be considerably more general, though. It is important to note that the duration of collision need not be short compared to the characteristic fluctuation times of the nonpolar gas. During a collision there may be strong couplings between the nonpolar molecules or these couplings may be negligible. These effects are expressed in the over-all schematic "kernel" describing the results of a collision in altering the state of the dipoles.

The reasons for choosing "impulsive" models where the duration of collision is negligible are (a) mathematical simplicity, (b) a wide variety of cases is compatible with the impulsive assumption, and (c) at high pressures where the assumption breaks down seriously, the results indicate insensitivity to models not involving adiabatic shifts.

[3] E. P. Gross, Phys. Rev. **97**, 395 (1955), henceforth referred to as I.

4. The treatment is based on classical mechanics. The actual absorption spectrum of the gas as a function of foreign gas pressure, (nonpolar gas density), can be understood as follows: Low foreign gas pressures imply collision frequencies $1/\tau$ small compared to the resonant frequency $h/8\pi I$ and to the angular frequency w. Then the absorption spectrum consists of a series of well-defined rotational lines with breadths proportional to the gas pressure. The existence of these lines is a consequence of the nonzero value of Planck's constant h. For collision frequencies larger than the lowest resonant frequencies, strong overlapping occurs and the absorption in the microwave region is a monotonically increasing function of frequency. However, the situation is still not classical, since many of the rotational lines corresponding to high quantum numbers, remain resolved. Only when the collision frequency is comparable to $(kT/I)^{\frac{1}{2}}$ is the entire structure lost. Then, the contributions to the absorption at any frequency come from many lines; this is the condition for the applicability of the classical picture. However, a quantum treatment shows that the classical results for the low frequency absorption are accurate at collision frequencies less than $(kT/I)^{\frac{1}{2}}$. The sharp rotational structure of the low frequency lines is lost at foreign gas pressures of the order of 50 atmospheres. The absorption and dispersion spectrum at pressures between 50 and a few hundred atmospheres may be treated classically; one expects it to be sensitive to inertial effects. It is important to realize that the process of absorption in compressed gases provides us with a situation unusual in the theory of dielectrics. We have a case in which the finite moment of inertia of the dipole and the nonzero value of Planck's constant are expected to lead to important deviations from the Debye spectrum. A discussion of quantum-mechanical effects will be given elsewhere. This treatment is necessary since the conditions of validity of a strictly classical approach and of the impulsive approximation are not simultaneously satisfied in a real system, i.e., the duration of collision is $\approx (I/kT)^{\frac{1}{2}}$.

II. MODELS OF THE DIELECTRIC RESPONSE OF THE TWO DIMENSIONAL ROTATOR

The two-dimensional rotator is characterized by a permanent dipole moment m, and a moment of inertia I. The relevant quantities with the dimensions of a frequency are: the angular frequency w of the applied field, the collision frequency $1/\tau$, and the mean thermal angular frequency $(kT/I)^{\frac{1}{2}}$. The state of a rotator at time t is described by the angle ϑ between the dipole axis and the electric field E, and by the angular velocity v.

We work with a distribution function[3] $f(v,\vartheta,t)$, defined so that $fdvd\vartheta$ represents the number of dipoles with state variables in the ranges v, $v+dv$ and ϑ, $\vartheta+d\vartheta$. The total number of molecules per unit volume is N, and is independent of time. The number of dipoles per unit volume and per unit angle with axis at angle ϑ is

$$n(\vartheta,t)=\int f(v,\vartheta,t)dv.$$

The electric polarization, $P(t)$, is given by

$$P(t)=m\int\int \cos\vartheta\, f dv d\vartheta.$$

In accordance with the assumption of instantaneous collisions, we divide the changes in f into a kinematic part and a part arising from collisions. We write

$$\frac{\partial f}{\partial t}+v\frac{\partial f}{\partial \vartheta}-\frac{mE\sin\vartheta}{I}\frac{\partial f}{\partial v}=\frac{\delta f}{\delta t}. \tag{1}$$

The term $v\partial f/\partial\vartheta$ represents the drift in ϑ space, while $-mE\sin\vartheta/I(\partial f/\partial v)$ accounts for the drift in velocity space as a result of the angular acceleration. Before discussing the collision term $\delta f/\delta t$, let us examine the case of thermal equilibrium in a static field. Since we are neglecting adiabatic shifts, the form of the collision term must be such that collisions maintain the distribution function $f_{eq}(v,\vartheta)$, appropriate to the static field.

$$f_{eq}=C\exp\left\{-\frac{Iv^2}{2kT}+\frac{mE_0\cos\vartheta}{kT}\right\}, \tag{2}$$

where C is a field strength dependent constant. The first approximation, valid for small field strengths, is $C\approx(I/2\pi kT)^{\frac{1}{2}}N/2\pi$. The mean angular velocity at any point is zero, the total kinetic energy per unit volume is $NkT/2$. The polarization is

$$P_{eq}=\frac{\partial}{\partial\alpha}[\ln J_0(-i\alpha)]\approx\frac{Nm^2E_0}{2kT}, \tag{3}$$

where J_0 is the Bessel function of order zero and $\alpha=mE_0/kT$. The factor $\frac{1}{2}$ enters rather than the usual factor $\frac{1}{3}$, and is a characteristic feature of the two dimensional model.

We now turn our attention to the collision term $\delta f/\delta t$. A variety of collision models will be examined. These are

$$\frac{\delta f}{\delta t}=-\frac{f(v)}{\tau}+\frac{(1-A)}{\tau}f(-v)+\frac{An(\vartheta,t)}{\tau}(I/2\pi kT)^{\frac{1}{2}}\exp\left(-\frac{Iv^2}{2kT}\right), \tag{4a}$$

$$\frac{\delta f}{\delta t}=-\frac{f}{\tau}+\frac{C(t)}{\tau}\exp\left\{\frac{mE(t)\cos\vartheta-Iv^2/2}{kT}\right\}, \tag{4b}$$

$$\frac{\delta f}{\delta t}=\beta\left\{\frac{\partial}{\partial v}(vf)+\frac{kT}{I}\frac{\partial^2 f}{\partial v^2}\right\}, \tag{4c}$$

$$\frac{\delta f}{\delta t}=-\frac{f(v)}{\tau}+\frac{1}{\tau}\left(\frac{\delta}{\pi}\right)^{\frac{1}{2}} \times\int_{-\infty}^{+\infty} f(v')\exp\{-\delta(v-\gamma v')^2\}dv', \tag{4d}$$

with $\delta(1-\gamma^2)=I/2kT$.

These collision expressions have been discussed in reference 3. All incorporate the assumption of instantaneous collisions; (t is the only time appearing).

Assumption (4a) states that a fraction $(1-A)$ of colliding molecules are specularly reflected. The remainder, a fraction A, is re-emitted with a Maxwellian distribution of velocities at the temperature of the foreign gas. We note that $A=1$ gives a purely Maxwellian reemission; this assumption may be approximately appropriate when the nonpolar gas and polar gas consist of molecules of comparable mass and moment of inertia. It may happen that the nonpolar gas (or liquid) consists of strongly coupled molecules, so that there are appreciable interchanges of energy and momentum among these molecules during the time of collision of one molecule with a dipole. From the point of view of assumption (1), this possibility can only be crudely taken into account by the admixture of a specularly reflected portion. The case of almost pure specular reflection ($A\approx 0$) becomes a valid approximation when the dipoles are much lighter than the reservoir molecules. For pure specular reflection ($A=0$) there is, of course, no energy dissipation due to collisions, hence no dielectric absorption.

The second assumption was introduced in differing forms by Kronig,[4] Van Vleck and Weisskopf,[5] and Frohlich.[6] It has been criticized in reference 3 as being inappropriate for collisions of gas molecules, on the grounds that it implies discontinuous changes of position (or angular orientation) upon collision. Collisions induce changes of position which depend on the applied field at a given time. Assumptions (4a), (4c), and (4d) differ from (4b) in that encounters leave the position unaltered.

Assumption (4c) is the collision rate of change of the distribution function for a model of dipoles undergoing rotatory Brownian motion. The present treatment [assumption (4c)] is a generalization of Debye's work,[1,2] because of the inclusion of inertial terms.

Assumption (4d) contains a variety of interesting special cases. In particular, one obtains assumption (4a) (with the special value $A=1$), by choosing $\gamma=0$. The Fokker-Planck assumption (4c) results when $\gamma\to 1$, $\delta\to\infty$ in an appropriate manner. We work out the dielectric response in this paper only for the high pressure region. In assumption (4d) the relationship $\delta(1-\gamma^2)=I/2kT$ is necessary to obtain correct equilibrium. Thus as $\gamma\to 1$, $1/\tau$ must $\to\infty$. The connection with assumption (4c) is then $(\gamma-1)/\tau\to\beta$. This means that the collision rate $1/\tau$ must tend to infinity. However, $\gamma\to 1$ implies infinitely weak collisions; β is thus the "effective collision frequency."[7]

Our present object is to derive absorption and dispersion spectra on the basis of the models proposed in order to see if noticeable differences result. The models discussed do not even roughly cover the range of types one might expect. In particular, failure to include adiabatic shifts excludes an important class of systems.

We shall investigate small amplitude disturbances of the system of dipoles, i.e., processes linear in the applied electric field. We introduce the notation

$$f_0=C\exp(-Iv^2/2kT); \tag{5}$$

f_0 is the equilibrium distribution in absence of fields. The distribution function f is written as

$$f=f_0(1+\phi),\quad n(\vartheta,t)=\frac{N}{2\pi}(1+\rho); \tag{6}$$

$\phi(v,\vartheta,t)$ is a dimensionless quantity which measures the deviation of the distribution function from equilibrium. It will be found to be proportional to the magnitude of the applied electric field. We also have introduced $\rho(\vartheta,t)$, a dimensionless measure of density variation.

On physical grounds the solutions $\phi(v,\vartheta,t)$, $\rho(\vartheta,t)$ must be periodic in ϑ with the period 2π. ϕ and ρ are therefore expanded in Fourier series, e.g.,

$$\phi=\sum_{n=-\infty}^{+\infty}\phi_n(v,t)\exp[in\vartheta]. \tag{7}$$

The equations satisfied by the Fourier coefficients ϕ_n are

$$\frac{\partial\phi_n}{\partial t}+\left(\frac{1}{\tau}+inv\right)\phi_n+\frac{mvE}{2kTi}[\delta(n,1)-\delta(n,-1)]=\Delta_{jn},\quad j=1,\cdots 4; \tag{8}$$

where

$$\delta(n,l)=0\ \text{for}\ n\neq 1,\qquad =1\ \text{for}\ n\neq 1:$$

$$\Delta_{1n}=\frac{P_nA}{\tau}+\frac{(1-A)}{\tau}\phi_n(-v,t), \tag{9a}$$

$$\Delta_{2n}=-\frac{1}{\tau}\frac{mE}{2kT}[\delta(n,1)+\delta(n,-1)], \tag{9b}$$

$$\Delta_{3n}=\beta\left\{\frac{kT}{I}\frac{\partial^2\phi_n}{\partial v^2}-v\frac{\partial\phi_n}{\partial v}\right\}, \tag{9c}$$

[4] R. Kronig, Physica **5**, 65 (1938).

[5] J. H. Van Vleck and V. Weisskopf, Revs. Modern Phys. **17**, 227 (1945).

[6] H. Frohlich, Nature **157**, 478 (1946); *Theory of Dielectrics* (Oxford University Press, New York, 1949).

[7] τ, β, γ are assumed independent of velocity.

and

$$\Delta_{4n}=\frac{1}{\tau}\left(\frac{\delta}{\pi}\right)^{\frac{1}{2}}\int_{-\infty}^{+\infty}dv'\phi_n(v')$$
$$\times\exp\left\{-\frac{I}{2kT}(v'^2-v^2)-\delta(v-\gamma v')^2\right\}, \quad (9d)$$

where $\delta(1-\gamma^2)=I/2kT$.

III. GENERALIZED BROWNIAN MOTION TREATMENT

In this section we discuss the generalization of Debye's theory to include inertial contributions, that is, assumption (3). Attempts to guess at a generalization were made earlier,[8-10] the results are only partially correct. A systematic approach to the problem must be based on the Fokker-Planck equation.† To an approximation linear in the field strength, this is Eq. (8) together with Eq. (9c). We introduce the dimensionless variables

$$z=v(I/2kT)^{\frac{1}{2}},\quad w'=w(I/kT)^{\frac{1}{2}},\quad t'=t(kT/I)^{\frac{1}{2}},$$
$$E'=mE/kT,\qquad \beta'=\beta(I/kT)^{\frac{1}{2}},$$
$$f_0=N(I/2\pi kT)^{\frac{1}{2}}\exp[-z^2].$$

In the following discussion, we suppress the primes, understanding that all quantities are in the dimensionless form. We obtain solutions by expanding $\phi_n(z)$ in Hermite polynomials of z:

$$\phi_n=\sum_{k=0}^{\infty}\sigma_{nk}H_k(z). \quad (10)$$

The σ_{nk} will satisfy simple difference equations. Once they have been determined, the polarization is given by

$$P=\frac{Nm}{2}(\sigma_{10}+\sigma_{-10}). \quad (11)$$

Using the recurrence formulas for Hermite polynomials Eq. (8) becomes an inhomogeneous, three-term differential-difference equation for σ_{nk}. We first study the solutions of the homogeneous equation. Thus we imagine a situation in which the distribution function differs from equilibrium at $t=0$, and study the relaxation to equilibrium. An example is the case where there was a static electric field E_0 when $t<0$, and at $t=0$ this field is turned off. The general solution of the homogeneous equation is the sum of exponentials e^{pit}. These equations may be solved by successive approximations. In first approximation we put σ_{n2} and higher σ_{nk} equal to zero. The two roots are

$$2p=-\beta\pm(\beta^2-4n^2)^{\frac{1}{2}}.$$

The case $n=1$ determines the decay of the polarization. For $\beta\gg2$ the positive sign yields a root $p\approx-(1/\beta)$; there is a very slow decay of the polarization. The other root represents a more rapid decay. The slowly decaying term is also found when one proceeds to higher approximations. Physically, the explanation is clear. Large β means high friction or collision frequency; this hinders the molecules in their kinematic motions and prevents a new polarization from being established. Since β is in dimensionless units we expect a relaxation time $t^*=\beta(I/kT)$, proportional to β and to the moment of inertia. We shall find this to be the case in the theory of the response to an alternating field. Our first approximation then corresponds to the Debye approximation.

Let us now obtain the solution of the inhomogeneous Eq. (8). We assume ϕ, $E\sim\exp(iwt)$ and solve the difference equation by continued fraction methods. The polarization is given by the formula (using dimensionless units):

$$P=\frac{NmE}{2}\cfrac{1}{1+iw(\beta+iw)+\cfrac{2iw}{iw+2\beta+\cfrac{3}{iw+3\beta+\cdots}}}. \quad (12)$$

For the static case ($w=0$), formula (12) yields Eq. (3). The expression for the polarization is simple if

$$\left|\cfrac{2w}{iw+2\beta+\cfrac{3}{\cdots}}\right|\ll|1+iw(\beta+iw)|. \quad (13)$$

Then

$$P=NmE/(1-w^2+iw\beta). \quad (14)$$

Except for the presence of w^2, this is the Debye relaxation formula. From our results, sufficient conditions for the validity of the Debye formula are

$$\beta\gg(kT/I)^{\frac{1}{2}},\quad w\ll(kT/I)^{\frac{1}{2}}, \quad (15)$$

where we have reverted to customary units.

A case which differs greatly from the Debye approximation is $\beta\gg1$ and $w\gg1$. Then the lowest approximation to the continued fraction is adequate. [See the criterion (13).] The polarization is given by Eq. (14), where, however, w^2 cannot be neglected. One finds a negative real part for the polarization, which is of the same type as in the response of free electrons to an alternating field. In fact, if $w\gg1$ the polarization is in ordinary units

$$P=\frac{Nm^2E}{2I}\frac{1}{-w^2+iw\beta}.$$

[8] I. Rocard, J. phys. radium **4**, 247 (1933).
[9] V. A. Dimetrief and S. Gurevich, Zhur. Eksptl. i Theoret. Fiz. **16**, 937 (1946).
[10] J. G. Powles, Trans. Faraday Soc. **44**, 802 (1948).
† *Note added in proof.*—Professor H. Fröhlich has kindly pointed out that a treatment similar to this section has been sketched by Dr. H. Sack [Kolloidzeitschrift **134**, 75 (1953)].

TABLE I. ($w=0.1$) Comparison of $P/(NmE)/2$ for Debye and inertial formulas.

β	Debye	Inertial
10	$0.50-i\,0.50$	$0.50-i\,0.50$
5	$0.80-i\,0.40$	$0.80-i\,0.40$
2	$0.96-i\,0.19$	$0.95-i\,0.24$
1	$0.99-i\,0.10$	$0.98-i\,0.17$
0.7	$1.00-i\,0.07$	$0.99-i\,0.14$
0.5	$1.00-i\,0.05$	$0.99-i\,0.14$
0.3	$1.00-i\,0.03$	
0.1	$1.00-i\,0.01$	

This is the electron gas polarization with m replacing the charge e and I the mass m_0 of the electrons. With $m=ea$ and $I=m_0a^2$, where a is the distance between the charges making up a dipole, one finds exactly the electron gas polarization. The ends of the dipole behave effectively as linear charges.

The continued fraction converges rapidly for $\beta\gg1$ and for β smaller than or comparable to unity, provided that $w\gg1$. Application of well-known convergence criteria in the theory of continued fractions,[11] shows that the fraction of Eq. (12) converges for all values of β. The speed of convergence, however, decreases as β decreases. The limit $\beta\ll1$ is not important, since quantum effects, which give rise to the rotational line structure, are then dominant.

In Tables I and II we compare the values of complex polarization according to the Debye formula with the values given by the complete formula (12), (called the inertial formula). The polarization is given for several values of β and for two typical values of w, $w=0.1$, and $w=1$. It is seen that for $w=0.1$, the real parts of the absorption differ little, but that the predicted absorptions differ appreciably for $\beta<2$, i.e., at foreign gas pressures below a few hundred atmospheres. For the case $w=1$, the differences are appreciable for both the dispersion and the absorption.

Let us now examine the Debye formula which has been obtained. In the remainder of this section we use customary units. From Eq. (14) one has at the high pressure limit (provided $w<(kT/I)^{\frac{1}{2}}$),

$$P=\frac{Nm^2}{2kT}\frac{1}{1+iw\beta(I/kT)}. \tag{16}$$

The Debye relaxation time t^* is given by

$$t^*=\beta(I/kT). \tag{17}$$

Now β is a measure of the dissipative action of the nonpolar gas, since it is the proportionality constant of the Fokker-Planck equation. Thus t^* increases with pressure, as is found experimentally. We see that β has the dimensions of a collision rate, so that $1/\beta$ is a "time between collisions." One may apply the Fokker-Planck assumption to treat the broadening of a spectral line. This has been done classically for the harmonic oscillator in I; it is found that $1/\beta$ is in fact a time between collisions and that the width of the line increases with increasing β. Thus the connection between the rotational lines and the relaxation spectrum can be expressed as follows. The frictional collision rate β determines the width of the lines at low pressures ($\beta\ll(kT/I)^{\frac{1}{2}}$). When individual line structure is lost, inertial corrections to the shape of the absorption are important and the dependence on pressure and frequency differs from that given by the Debye theory. At high pressures one arrives at the Debye line shape, with a relaxation time $t^*=\beta I/kT$, i.e., inversely proportional to the collision time.

The reversal of the effects of the parameter β has its source in the general connection between the Smoluchowski and the Fokker-Planck equations.[12] The Smoluchowski equation was used by Debye in his theory of dielectric relaxation.[2] For the three-dimensional dipole he took $\beta=\delta\pi\eta a^3$, where η is the macroscopic viscosity of the surrounding medium and a is a length of the order of the dimensions of the dipole. With the models of this and later sections one obtains Debye's result, where, however, β is given the more microscopic significance of a collision frequency. However, no literal significance should be attributed to the concept of a collision frequency for a liquid.

Let us consider, briefly, some numerical examples in order to assess the regions where inertial corrections are important. The linear molecule COS has a moment of inertia $I=(1.37)\cdot10^{-38}$ g-cm^2. It will satisfy the assumptions of a Brownian motion treatment only with a very light foreign gas such as helium. However, the results of Secs. IV and V show that the expected qualitative behavior is similar when one uses other models. At 300°K one has $(kT/I)^{\frac{1}{2}}=1.73\cdot10^{12}$/sec. This is the classical mean thermal angular frequency, and lies near the frequency of the most populated rotational lines. The second rotational line is near 1.25 cm, or $w=1.51\cdot10^{11}$ sec^{-1}, a convenient experimental wavelength. For this line $w(I/kT)^{\frac{1}{2}}\approx8.7\cdot10^{-2}$. At pressures of the foreign gas of the order of one atmosphere, the rotational lines are still separable,[13] so that $\beta(I/kT)^{\frac{1}{2}}\approx10^{-2}$. If the collision frequency is roughly proportional to foreign gas density, $\beta(I/kT)^{\frac{1}{2}}$ will be unity at a pressure of the order of 100 atmospheres. At 200 atmospheres the Debye relaxation time $t^*\approx10^{-12}$ sec, which is very short; t^* decreases as the pressure increases and reaches the value expected for the liquid. Thus COS is a typical case of a dipole for which Table I may apply. However, careful assessment must be made of the contribution to the dispersion and absorption of the vibrational lines which start at about 1 mm.[14]

[11] O. Perron, *Kettenbruchen* (Chelsea Publishing Company, New York, 1950), Chap. 7.

[12] S. Chandrasekhar, Revs. Modern Phys. **15**, 40 (1943); R. W. Davies, Phys. Rev. **93**, 1169 (1954).

[13] W. D. Hershberger, J. Appl. Phys. **17**, 495 (1946); J. E. Walter, J. Appl. Phys. **17**, 814 (1946).

[14] W. C. King and W. Gordy, Phys. Rev. **90**, 319 (1953).

If one considers a molecule with a moment of inertia about a hundred times that of COS, $w\approx(kT/I)^{\frac{1}{2}}$ is in the K band region and $t^*\approx10^{-10}$ second at 200 atmospheres. One is then in a position to carry out measurements near the peak of the absorption line and perhaps even on the high-frequency tail. It would be important to examine the dispersion for this case, in view of Table II.

The detailed interpretation of the experimental data requires knowledge of the equation of state of the foreign gas at high pressures. A naive kinetic theory interpretation of β as proportional to the foreign gas density may well break down. The difference between the inertial and the Debye formulas is, however, very sizable in the regions discussed, so that experimental data should be amenable to conclusive qualitative interpretation.

IV. COMPARISON OF MODELS

Let us now discuss the other models characterized by assumptions (4a), (4b), and (4d). For assumption (4d) the polarization is

$$P=\frac{NmE}{2}\frac{1}{1+iw\left\{\dfrac{1-\gamma}{\tau}+iw+\dfrac{2}{\dfrac{1-\gamma^2}{\tau}+iw+\dfrac{3}{\cdots}}\right\}}. \tag{18}$$

This expression reduces to our previous formula (12) for the Brownian motion limit. One lets γ approach unity, as $1/\tau$ lends to infinity in such a way that $\beta=(1-\gamma)/\tau$. Then $(1-\gamma^2)/\tau=[(1-\gamma)(1+\gamma)]/\tau\to[2(1-\gamma)]/\tau=2\beta$ and $(1-\gamma^k)/\tau=k\beta$. Another limiting case is $\gamma=0$, corresponding to Maxwellian reemission [$A=1$ of assumption (4a)].

It will be noticed that formula (18) reduces to Debye's equation in the high-pressure limit, i.e., when $(1-\gamma)/\tau$ and $w<1$. This gives some insight into the onmipresence of the Debye formula. In agreement with the discussion in the introduction, we see that differences in the models (aside from the proper definition of the collision frequency), are first encountered when one examines inertial effects. These differences become more significant as the pressure is lowered.

For assumption (4a)

$$P=\frac{NmE}{2}\times\frac{1}{1+iw\left\{\dfrac{2-A}{\tau}+iw+\dfrac{2}{\dfrac{A}{\tau}+iw+\dfrac{3}{\dfrac{2-A}{\tau}+iw+\cdots}}\right\}}. \tag{19}$$

TABLE II. ($w=1$) Comparison of $P/(NmE)/2$ for Debye and inertial formulas.

β	Debye	Inertial
10	$0.01-i\,0.10$	$0.00-i\,0.10$
5	$0.04-i\,0.19$	$0.00-i\,0.19$
2	$0.20-i\,0.40$	$0.01-i\,0.40$
1	$0.50-i\,0.50$	$0.07-i\,0.60$
0.7	$0.67-i\,0.47$	$0.11-i\,0.65$
0.5	$0.80-i\,0.40$	$0.15-i\,0.70$
0.3	$0.92-i\,0.28$	$0.20-i\,0.73$
0.1	$0.99-i\,0.10$	$0.25-i\,0.77$

Formula (19) requires a finite value of A/τ for convergence of the fraction, so that one is not permitted to pass to the limit of perfect specular reflection.

It is seen from Eq. (18) that the fastest convergence is obtained as $\gamma\to1$. As mentioned in Sec. III, for the Brownian motion case the continued fraction converges at all pressures. For $\gamma\neq1$ the simplest criteria fail to indicate the region of convergence in the complex plane. As will be seen in the following section, the polarization for the Maxwellian emission limit ($\gamma=0$), is also expressible in terms of the error function of complex argument. While this function has been studied and tabulated in some detail,[15] precise criteria of convergence of its continued fraction representation are not known. The discussion of Sec. V indicates that the possible failure of convergence for $|(1/\tau)+iw|<\sqrt{2}$, and thus the breakdown of the development of the solution in Hermite polynomials, is not merely a formal question. The rigorous discussion within the framework of the linear approximation given in Sec. V yields a contribution from a pole in the complex velocity plane. This is the mathematical reason for the difficulties the Hermite development encounters in the low-pressure region (for $\gamma\neq1$).

For assumption (4b) the polarization is

$$P=\frac{NmE}{2}\left(1+\frac{B}{\tau}\right)\Big/\left[1+\left(\frac{1}{\tau}+iw\right)B\right], \tag{20}$$

where

$$B=\frac{1}{\tau}+iw+\cfrac{2}{\dfrac{1}{\tau}+iw+\cfrac{3}{\dfrac{1}{\tau}+iw+\cdots}}. \tag{21}$$

In the limit $1/\tau\gg1$ the expression for the polarization takes the Debye form. This result for the transition from low to high pressures is, however, very different from that of assumptions (4a), (4c), and (4d). For the Debye relaxation time t^* is equal to the time between collisions τ. As pressure increases, one expects this τ to decrease, giving a relaxation frequency which moves in the high-

[15] J. B. Rosser, *Theory and Applications of* $\exp[x^2]\int_0^x\exp[-x^2]dx$ (Mapleton House, Brooklyn, New York, 1948).

frequency direction. This is an effect opposite in direction from experiment. Experiments on effects of pressure on liquids show that the relaxation time moves to lower frequencies. For normal liquids it may be pushed into the centimeter region. Furthermore, for any reasonable estimate of the collision rate at high pressures, the relaxation time $t^*=\tau$ is too small.

Assumption (4b) is at variance with the physical picture that collisions hinder molecules from carrying out their kinematic (inertial) motions and thus increase the time for a given polarization to decay. This picture depends crucially on the inertial properties of an electric dipole. Assumption (4b) may be more appropriate for magnetic dipoles for which the basic equation of motion is first order in time.

V. COMPLETE SOLUTION FOR ABRUPT COLLISIONS

The discussion of Sect. IV is not complete for assumption (4a), (4c), and (4d). The continued fractions (20) and (21) probably fail to converge in the region of low pressures. In this section we investigate a method of solution which gives more complete information.

We first carry out the analysis on the basis of assumption (4b), since it leads to equations of the simplest mathematical form. For steady-state processes it suffices to consider the inhomogeneous solution. The solution is

$$\phi_{\pm 1}=\frac{mE_0}{2kT}\frac{\left(\frac{1}{\tau}\pm iv\right)e^{iwt}}{\left(\frac{1}{\tau}\pm iv+iw\right)}. \tag{22}$$

It will be noticed that as $1/\tau\to 0$, the perturbation $\phi_{\pm 1}$ becomes very large for $v=\pm w$. Such angular velocities correspond to dipoles which rotate at a frequency equal to the frequency of the applied field. The varying electric field, which has a constant direction, can be decomposed into two rotating "traveling wave" fields. The dipoles in question stay in phase with the one or the other of the rotating components for a long time. There is thus a large energy and momentum exchange between these dipoles and the electric field. This situation is encountered in other problems involving microwave devices,[16] linear accelerators,[16] and plasma oscillations.[17] The discussion is clarified by going to a coordinate system which rotates with one of the field components. There are two types of dipoles. One type continuously gains or loses phase with respect to the field as does a rotating pendulum. The other type carries out oscillatory motion about a point of lowest potential energy in the rotating system. In the linear approximation one incorrectly makes no distinction between these physically different types. In fact in linear approximation a dipole moving at exactly the angular frequency of the applied field receives the same torque indefinitely (or until it changes its velocity abruptly by collision). In reality these particles speed up or slow down so that the direction of the torque is reversed.

In dimensionless units the polarization is

$$P=\frac{NmE_0}{2}e^{iwt}\left\{1-\frac{iw}{(2\pi)^{\frac{1}{2}}}\int_{-\infty}^{+\infty}\frac{\exp[-\zeta^2]}{\frac{1}{\tau}-i\zeta+iw}\right\}. \tag{23}$$

The polarization can be evaluated by contour integration

$$P=\frac{NmE_0}{2}e^{iwt}\{1-iw\sqrt{2}F(\Omega)\}, \tag{24}$$

where we have introduced the error function of complex argument

$$F(\Omega)=\exp[\Omega^2]\left\{\frac{\sqrt{\pi}}{2}-\sum_{n=0}^{\infty}(-1)^n\frac{\Omega^{2n+1}}{(2n+1)n!}\right\}. \tag{25}$$

The error function can be expanded as a continued fraction

$$F(\Omega)=\cfrac{1}{2\Omega+\cfrac{2}{2\Omega+\cfrac{4}{2\Omega+\cdots}}}. \tag{26}$$

The first few terms give a good representation for $|\Omega|>1$, although the exact domain of convergence is not known.[15]

It is easily verified that formula (25), together with Eq. (27), yields the expression (20) of Sec. IV. The important point now is to examine the solution at low pressures. Equation (25) yields for $1/\tau\to 0$

$$P=\frac{NmE}{2}\left\{1-iw\sqrt{2}\exp\left(-\frac{w^2}{2}\right)\times\left[\frac{\sqrt{\pi}}{2}-\frac{i}{\sqrt{2}}\int_0^w\exp\left[\frac{w^2}{2}\right]dw\right]\right\}. \tag{27}$$

Thus the result is that there is a nonzero absorption as $1/\tau\to 0$. This conclusion at first sight appears strange, since collisions with the nonpolar molecules are necessary if the dipoles are to dissipate the energy acquired from the electric field. Otherwise these dipoles will "heat up" so that saturation effects occur and energy will be delivered back to the electric field; after a short time there would be no absorption per cycle. The absorption of Eq. (27) has a definite meaning, however. One fixes the collision frequency $1/\tau$ at any finite value, arbitrarily small. Then the field strength E_0 can be chosen small enough so that the linear approximation is valid

[16] J. C. Slater, *Microwave Electronics* (D. Van Nostrand Company, Inc., New York, 1950), Chaps. 11 and 12.
[17] D. Bohm and E. P. Gross, Phys. Rev. **75**, 1864 (1949).

for all dipoles (including the trapped ones). In Eq. (22) this means that $|\phi_{\pm 1}| \ll 1$ for all dipoles. The energy input per unit time from the field is proportional to E_0^2. This power can then be dissipated to the reservoir without saturating the dipole system. Thus, Eq. (27) for the limit $1/\tau \to 0$ must be understood as applying when the electric field simultaneously decreases to zero.

The absorption predicted by Eq. (27) can be understood directly. We shall show that the energy is taken from the electric field mainly by the trapped dipoles. Energy is given to dipoles moving more slowly than the field and taken from dipoles moving more rapidly. The excess number of slow dipoles, when one considers a region dv about $v=w$, is $-(\partial f_0/\partial v)_{v=w}dv$. The energy delivered per unit time to a dipole is the torque acting times the angular velocity. In linear approximation this is of the order of mE_0w. The range dv which is pertinent, i.e., the trapping range, is given by $I/2(v+dv)^2 - Iv^2/2 \approx mE$ or $dv \approx mE/Iw$. Multiplying the three quantities we find $m^2E_0^2/I(\partial f_0/\partial v)_{v=w}$. This is the absorption, which within a numerical factor, is associated with the imaginary part of the polarization in Eq. (27). The privileged role of the trapped dipoles may be seen in a more precise way by noting that the imaginary part of (27) comes entirely from the poles at $v=\pm w$.

The foregoing picture of the absorption process is closely related to the physical analysis of the static polarization of linear dipoles. It is known[18,19] that the calculation of the static polarization may be arranged so that the integration in phase space is performed as an integration over the phases and over the energy of the dipoles. The only contributions to the polarization are seen to come from the low-energy dipoles which oscillate about the point of lowest potential energy.

[18] W. Alexandrow, Physik Z. **22**, 258 (1921).
[19] P. Debye, *Polar Molecules* (Dover Publications, New York, 1945), p. 151.

We complete the discussion by stating the results of the complete analysis of assumption (4a).[20] It may be verified by direct substitution that for $A=0$ the solution is

$$\phi_{\pm 1} = \frac{E}{2} \frac{iz\sqrt{2} + \lambda_{\pm 1}/\tau}{\frac{1}{\tau} + iw \pm iz\sqrt{2}}, \tag{28}$$

$$P_{\pm 1} = \lambda_{\pm 1} \frac{E}{2}, \quad \lambda_{\pm 1} = \frac{1 - 2\Omega F(\Omega)}{1 - \frac{1}{\tau}\sqrt{2}F(\Omega)},$$

$$P = \frac{NmE}{2} \left\{ \frac{1 - 2\Omega F(\Omega)}{1 - \frac{1}{\tau}\sqrt{2}F(\Omega)} \right\}.$$

For $0 \leq A \leq 1$ we define

$$\Omega_A = \frac{1}{\sqrt{2}} \left[\left(\frac{1}{\tau} + iw \right)^2 - \frac{(1-A)^2}{\tau^2} \right]^{\frac{1}{2}}. \tag{29}$$

The polarization is

$$P = \frac{NmE}{2} \frac{\{1 - 2\Omega_A F(\Omega_A)\}}{1 - \frac{A}{\tau}\left(\frac{2-A}{\tau} + iw \right) \frac{F(\Omega_A)}{\Omega_A}}. \tag{30}$$

Numerical study of the polarization reveals significant differences from the Fokker-Planck assumption for low pressures (β or $1/\tau < 1$). The discussion of these differences will be carried out in connection with a quantum-mechanical treatment.

[20] The mathematical details are carried out in a technical report available from the author: Technical Note P-1, AF 18(600)-1124, Syracuse University.

Absorption Spectra of Iodine and Bromine in the Gas Phase and "Inert" Solvents. I. Iodine*

DENNIS F. EVANS†
Laboratory of Molecular Structure and Spectra, Department of Physics, University of Chicago, Chicago 37, Illinois
(Received November 11, 1955)

The strong absorption of iodine dissolved in paraffin hydrocarbons in the region of 2200 A–2600 A is not shown either by gaseous iodine or by iodine dissolved in perfluoroheptane (PFH) or di-perfluorohexyl ether, and is present only to a much smaller extent for iodine dissolved in chloroform.

The interaction of iodine with *n*-heptane has been studied quantitatively in PFH solution. It is concluded that the above absorption is a charge transfer transition due to a very weak, or possibly collisional type, complex, and is not a solvent shift of the $N-V$ transition of the iodine molecule.

GENERAL INTRODUCTION

IT is now generally recognized that iodine and bromine (in common with many other substances) form a series of molecular complexes of the "donor-acceptor" type with a wide variety of organic compounds.[1] These complexes can, in general, be recognized by the presence of a characteristic and very strong absorption band, which does not seem to be due to either of the components individually and which has been interpreted by Mulliken[2] as a "charge transfer" transition.

The main aim of the present investigation, and that described in the succeeding paper, has been to obtain reliable results for the true absorption spectra of iodine and bromine, and also to study spectro-photometrically very weak interactions which may or may not be examples of complex formation.

ULTRAVIOLET ABSORPTION OF IODINE

Introduction

It was shown by Freed and Sancier[3] that cyclopropane forms a well-defined complex with iodine. More recently, the ultraviolet absorption spectra of iodine in paraffin hydrocarbons have been measured by Hastings *et al.*[1] They observed that the absorption in the region 2200 A to about 2600 A was greater in cyclohexane and 2,3-dimethylbutane than in *n*-hexane and *n*-heptane, and concluded that this was due to complex formation. By assuming that the spectrum of iodine dissolved in *n*-hexane was characteristic of the iodine itself, they were able to derive the spectra of the assumed very weak cyclohexane and dimethylbutane complexes.

In order to obtain further information, measurements have been made on the ultraviolet absorption of iodine in the gas phase and in several inert solvents.

Experimental

Cp iodine was sublimed from potassium iodide and kept in a desiccator. The solvents, with the exception of chloroform, were purified by passage through a tube packed with silica gel. Cp chloroform was shaken with concentrated sulfuric acid to remove alcohol, washed with water, dried over calcium chloride, and fractionally distilled.

All measurements were made at room temperature ($23\pm2°C$) on a Beckman DU spectrophotometer, using cells varying in length from 0.011 cm to 10 cm.

Results

The results obtained are shown in Fig. 1. It can be seen that the strong absorption of iodine dissolved in *n*-heptane in the region 2200–2600 A is not shown either by gaseous iodine or by iodine dissolved in perfluoroheptane (PFH) or di-perfluorohexyl ether, and is present only to a much smaller extent for iodine dissolved in chloroform. The transparency of iodine dissolved in PFH was first noted qualitatively by J. S. Ham.[4]

Accordingly, it seems likely that this absorption (and that shown by iodine dissolved in *n*-hexane) is not characteristic of the iodine itself, but is due to some form of interaction with the paraffin hydrocarbons. It is noteworthy that although ethers form quite strong complexes with iodine,[5] with charge transfer bands in the region of 2500 A, the substitution of fluorine for hydrogen in di-perfluorohexyl ether results in the complete absence of a charge transfer band with iodine down to at least 2100 A. The visible band of iodine dissolved in di-perfluorohexyl ether is also at about 5200 A (as for iodine in the gas phase) instead of at approximately 4700 A as is found for iodine dissolved in normal ethers.

Since PFH seems to behave as an inert solvent towards iodine, the interaction of *n*-heptane with

* This work was assisted by the Office of Ordnance Research under Project TB2-0001 (505) of Contract DA-11-022-ORD-1002 with the University of Chicago.

† Permanent address (after October 1, 1954): Lincoln College, Oxford University, Oxford, England.

[1] McConnell, Ham, and Platt, J. Chem. Phys. **21**, 66 (1953); Hastings, Franklin, Schiller, and Matsen, J. Am. Chem. Soc. **75**, 2900 (1953), and references given in these papers.

[2] R. S. Mulliken, J. Am. Chem. Soc. **74**, 811 (1952).

[3] S. Freed and K. M. Sancier, J. Am. Chem. Soc. **71**, 2703 (1949).

[4] J. S. Ham, J. Am. Chem. Soc. **76**, 3881 (1954).

[5] J. S. Ham, J. Chem. Phys. **20**, 1170 (1952).

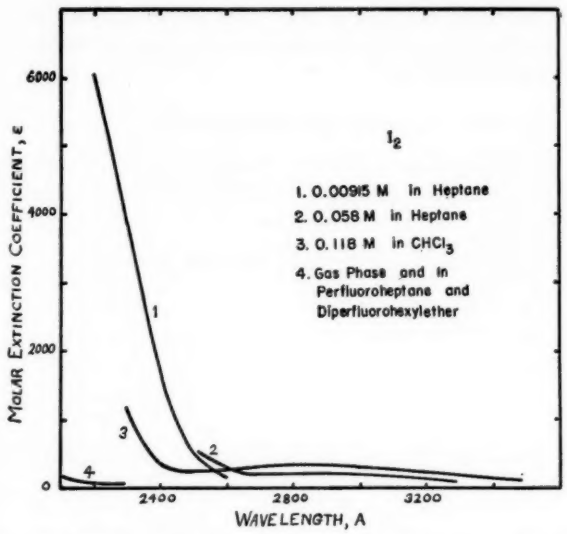
I_2
1. 0.00915 M in Heptane
2. 0.058 M in Heptane
3. 0.118 M in $CHCl_3$
4. Gas Phase and in Perfluoroheptane and Diperfluorohexylether
MOLAR EXTINCTION COEFFICIENT, ε
WAVELENGTH, A

FIG. 1. The absorption of iodine in the gas phase is slightly different from its absorption in the two fluorinated solvents but, because of the large scale of graph, it has not been attempted to show this difference.

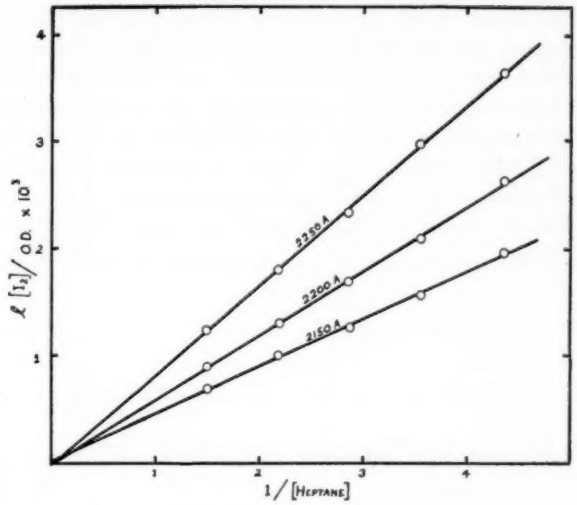

FIG. 2. Concentrations are in moles/liter.

iodine in PFH solution has been studied quantitatively, using the method described by Benesi and Hildebrand.[6] If a complex BI_2 is formed in solution, and if the concentration of B is much greater than that of the iodine, then a plot of $1/[B]$ against $[I_2]l/o.d.$ should give a straight line, slope $1/\epsilon K$ and intercept on the y axis $1/\epsilon$ where l is the length of the cell used. The optical density of the charge transfer band is o.d., and ϵ and K are, respectively, the molar extinction coefficient and equilibrium constant of the complex. Very accurate results cannot be expected in the present case, since it was impossible to work on the peak of the absorption band, and it is well known that slight solvent shifts of charge transfer bands occur when the medium is altered, almost certainly due to changes in refractive index.[4] These shifts will naturally cause larger errors if the tail of an absorption band is studied. However, since only relatively dilute solutions of *n*-heptane in PFH were used, such errors should not be too serious.

The results obtained at various wavelengths are shown in Fig. 2. Good straight lines are obtained, which, however, pass almost exactly through the origin. This is consistent with either a very weak complex having a high extinction coefficient or alternatively with the occurrence of a charge transfer transition during a collision between an iodine molecule and a hydrocarbon molecule. It is possible that low temperature measurements might be able to decide between the two alternatives since, if an exothermic complex is formed, the absorption should increase considerably on decreasing the temperature (as was, in fact, found for cyclopropane[3]).

The possibility that the ultraviolet absorption of iodine dissolved in paraffin hydrocarbons is due to a solvent shift of the strong $N-V$ transition of the iodine molecule (with a maximum at about 1750 A[7]) seems definitely excluded by the above measurements. Thus, the addition of small amounts of *n*-heptane to a solution of iodine in PFH causes a large shift of the absorption tail towards longer wavelengths whereas this would not be expected for a solvent shift, and was not, in fact, found in one genuine example which has been studied (see following paper). Furthermore, since chloroform has a much higher refractive index around 2300 A than *n*-heptane, on the basis of a solvent shift the absorption of iodine should be at longer wavelengths when dissolved in chloroform than when dissolved in *n*-heptane, whereas the converse is the case (Fig. 1).

Accordingly, it seems probable that the absorption spectra derived by Hastings *et al.* for the 2, 3-dimethylbutane- and cyclohexane-iodine complexes are erroneous, and that the charge transfer bands lie at considerably shorter wavelengths than reported by these authors. In order to obtain further information on this point, it is hoped to extend the curves given in Fig. 1 into the vacuum ultraviolet. Photographic measurements down to 1820 A on iodine dissolved in *n*-heptane by Ham, Platt, and McConnell[8] show a very broad band with a maximum at 1880 A.

The absorption below about 2500 A shown by oxygen dissolved in paraffin hydrocarbons[9] (but not in PFH), which was formerly interpreted as an enhancement of the $^3\Sigma_u^+ - {}^3\Sigma_g^-$ transition of the oxygen molecule, is probably exactly analogous to that shown by iodine (and also bromine) in the same solvents.

The low absorption maximum at 2800 A found for iodine dissolved in chloroform (and, though less

[6] H. A. Benesi and J. H. Hildebrand, J. Am. Chem. Soc. **71**, 2703 (1949).

[7] H. Cordes, Z. Physik **97**, 603 (1935).

[8] Ham, Platt, and McConnell, J. Chem. Phys. **19**, 1301 (1951).

[9] D. F. Evans, J. Chem. Soc., 345 (1953).

evident, at about 2850 A for iodine dissolved in *n*-heptane) is probably due to I_4 or other iodine polymers since it does not obey Beer's law, and almost vanishes at high dilution. It is presumably the same band as that reported for iodine vapor at 2670 A by Friedheim and Kortüm,[10] who also found a shoulder at about 3100 A for iodine dissolved in cyclohexane.

Neither of these bands obeyed Beer's law. McConnell has recently suggested that the 2670 A band is an intermolecular charge transfer transition between two I_2 molecules in I_4.[11]

ACKNOWLEDGMENTS

I should like to thank Professor R. S. Mulliken for many helpful discussions, and the hospitality shown during my stay in Chicago.

[10] G. Kortüm and G. Friedheim, Z. Naturforsch **2a**, 20 (1947).

[11] Harden McConnell, J. Chem. Phys. **22**, 760 (1954).

THE JOURNAL OF CHEMICAL PHYSICS VOLUME 23, NUMBER 8 AUGUST, 1955

Absorption Spectra of Iodine and Bromine in the Gas Phase and "Inert" Solvents.* II. Bromine

DENNIS F. EVANS†
Laboratory of Molecular Structure and Spectra, Department of Physics, University of Chicago, Chicago 37, Illinois
(Received November 7, 1954)

The effect of foreign gases on the continuous absorption of bromine in the region 2200 A–5100 A has been studied. Contrary to the results of Bayliss and Rees, no increases in intensity were observed. The absorption of bromine in various inert solvents has also been measured. The results are similar to those obtained with iodine and have been interpreted in an analogous manner. No maxima were found at 2725 A and 2500 A for bromine dissolved in chloroform and cyclohexane, respectively, in disagreement with Aikin, Bayliss, and Rees.

INTRODUCTION

THE absorption spectra of bromine in the gas phase and in solution have been the subject of many previous investigations. However, the results obtained have not always been in agreement, and in particular there has been considerable controversy as to the effects of foreign gases on the continuous absorption of gaseous bromine. Both the present measurements, and those made previously, are in agreement in showing the presence of a peak at 4150 A, interpreted as due to $a'\Sigma^+_g - {}'\Pi_u$ transition, and a shoulder at about 4900 A, probably due mainly to a $\Sigma_g^+ - {}^3\Pi_{0+u}$ transition. At shorter wavelengths the absorption drops to a very low value around 3000 A, and then commences to rise again. Beyond 5100 A in the direction of long wavelengths, the continuum is overlaid with band structure due to transition to the ${}^3\Pi_{0+u}$ state,[1] and at longer wavelengths to the ${}^3\Pi_{1+u}$ state, of the bromine molecule.[2]

The latest and most complete investigation of the effect of foreign gases on the spectrum described above was by Bayliss and Rees[3] who give references to previous work on the subject. Using oxygen, nitrogen, carbon dioxide, hydrogen chloride, hydrogen bromide, helium, and neon at about 60 cm pressure as inert gases, they reported; (1) increases in intensity of the two visible continua by amounts ranging from 8 to 30% (with an error of about ±5%), (2) very large increases in intensity of the weak ultra-violet continuum (as much as a hundred fold around 3000 A), with absorption maxima at 2700 A and 2900 A (the latter only with oxygen). This work has been carefully repeated, using both carbon dioxide and nitrogen for the ultraviolet and carbon dioxide for the visible continua, since these gases showed among the largest effects according to Bayliss and Rees.

Measurements have also been made of the absorption of bromine dissolved in various "inert" solvents.

EXPERIMENTAL

Cp bromine was shaken with sodium hydroxide solution to remove iodine and chlorine, dried with phosphorus pentoxide, and distilled. The solvents used were purified as described previously.[4] Oxygen-free nitrogen and carbon dioxide (for medical purposes) were obtained from cylinders and dried with phosphorus pentoxide. Blank tests showed no absorption down to 2200 A. All measurements were carried out at room temperature (23±2°C) on a Beckman DU spectrophotometer.

The absorption cell consisted of a 1 or 10 cm quartz cell fitted with a three-way tap lubricated with a meta-

* This work was assisted by the Office of Ordnance Research under contract with The University of Chicago, Chicago, Illinois.

† Permanent address (after October 1, 1954): Lincoln College, Oxford University, Oxford, England.

[1] W. G. Brown, Phys. Rev. **39**, 777 (1932).

[2] O. Darbyshire, Proc. Roy. Soc. (London) **159**, 93 (1937).

[3] N. S. Bayliss and A. L. G. Rees, Trans. Faraday Soc. **35**, 792 (1939).

[4] Dennis F. Evans, J. Chem. Phys. **23**, 1424 (1955), preceding paper.

phosphoric acid graphite mixture. It could be connected either to a tube containing bromine immersed in a constant temperature bath, or to a supply of nitrogen or carbon dioxide.

To carry out an experiment, the evacuated cell was first filled with bromine at a suitable pressure and the spectrum measured. The inert gas (at a partial pressure of about 70 cm) was then admitted into the cell, the three-way tap quickly closed, and the cell inverted until complete mixing had taken place as shown by constant optical densities. In this way there was no change in the concentration of bromine between the two measurements. The inward rush of gas assured that there was no loss of bromine by diffusion out of the cell.

RESULTS

Effect of Foreign Gases on the Continuous Absorption of Bromine

No effect whatsoever, within the experimental error, was observed in the regions studied by Bayliss and Rees (2200 A–5100 A), due to the presence of 60 cm pressure of nitrogen or carbon dioxide. The experimental precision was about 0.3% in the region of the main maximum, falling to about 10% at the "trough" around 3000 A. Hence any effect seems to be 100- to 1000-fold less than that reported by Bayliss and Rees. Furthermore, although not all the inert gases used by these authors have been studied, it seems very likely that there are no new transitions of the bromine molecule with maxima at 2700 A and 2900 A which are made allowed by the presence of foreign gases.

The effects observed by Bayliss and Rees for the visible continua may possibly be due to insufficient precision of the photographic method or to errors in analysis, since the same sample of bromine was not used for vacuum and inert gas studies. It may be noted that Vesper and Rollefson,[5] using a somewhat similar method to the present, found at 5020 A no effect greater than 0.5% due to air. The very large increases in intensity reported for the ultraviolet continuum are rather difficult to explain, but may possibly be due to impurities in the gas samples used by Bayliss and Rees.

In the region 5200–5900 A, where band structure occurs, a considerable increase in intensity (up to as much as 30%) was observed, using carbon dioxide as the inert gas, in agreement with the results of Kondratjev and Polak,[6] and of Jost,[7] for bromine, and similar to those of Rabinowitch and Wood[8] for iodine. This effect is clearly due to the broadening of the band lines by the inert gas.

[5] H. G. Vesper and G. K. Rollefson, J. Am. Chem. Soc. **57**, 620 (1934).
[6] V. Kondratjev and L. Polak, Z. Physik, **76**, 386 (1932).
[7] Jost, Z. Physik. Chem. B, **3**, 102 (1929).
[8] E. Rabinowitch and W. C. Wood, Trans. Faraday Soc. **32**, 540 (1936).

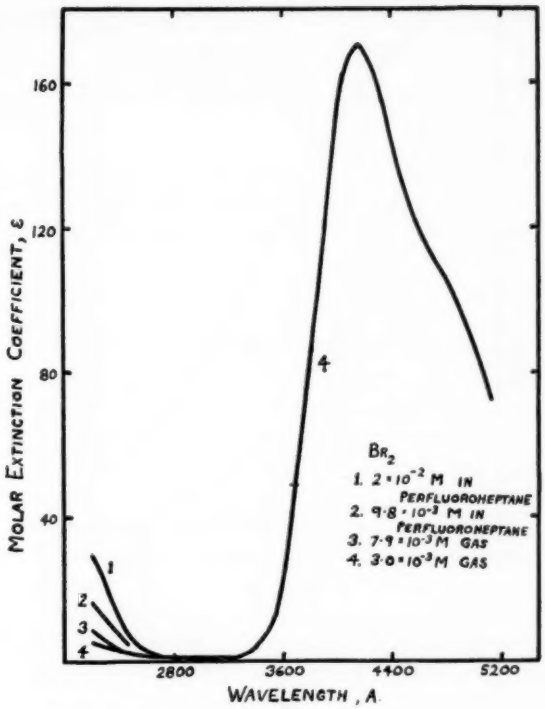

FIG. 1.

The absorption spectrum obtained for gaseous bromine from 2200 A to 5100 A is shown in Fig. 1. It is in fair agreement with those of Acton, Aikin, and Bayliss[9] and of Aikin and Bayliss,[10] measured in the absence of inert gases. However the maximum reported by the latter authors at 2250 A was not found, the absorption rising steadily down to 2150 A, the lowest wavelength at which measurements were made. Furthermore, since Beer's law is not obeyed in this region, it seems likely that no new band due to the Br_2 molecule is present. The absorption at short wavelengths is probably due partly to the tail of the strong N−V transition (with a maximum at 1600 A),[11] and partly to absorption by bromine polymers such as Br_4.

Ultraviolet Absorption of Bromine in Solution

The results obtained are shown in Figs. 1 and 2. It can be seen that, as in the case of iodine, the ultraviolet absorption of bromine dissolved in perfluoroheptane is very similar to that of gaseous bromine, although the deviations at short wavelengths from Beer's law seem to be more marked. The strong absorption shown by bromine in *n*-heptane and cyclohexane (and to a lesser extent in chloroform) is analogous to that found for iodine,[4] and is presumably due to charge transfer transitions.

The results obtained for cyclohexane and chloroform

[9] Acton, Aikin, and Bayliss, J. Chem. Phys. **4**, 474 (1936).
[10] R. G. Aikin and N. S. Bayliss, Trans. Faraday Soc. **34**, 1371 (1938).
[11] H. Cordes and H. Sponer, Z. Physik. **63**, 334 (1930).

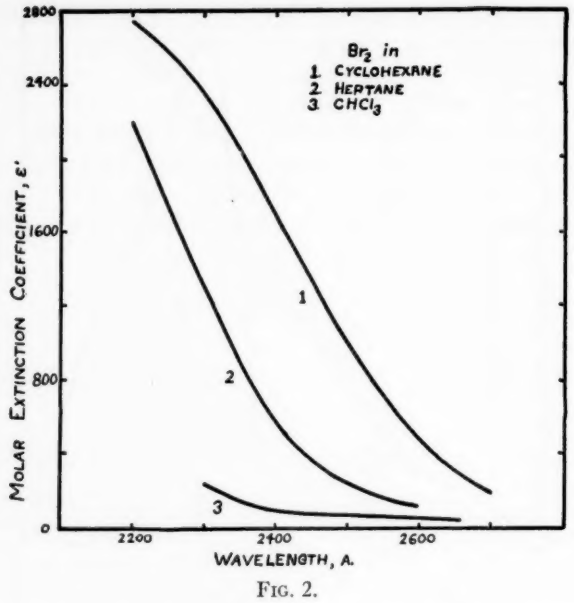

FIG. 2.

are in considerable disagreement with those of Aikin, Bayliss, and Rees.[12] No maxima were found at 2725 A and 2500 A respectively as reported by these authors, and in addition considerably lower extinction coefficients were obtained. However, the present absorption curve for bromine dissolved in cyclohexane is in good agreement with that of Pestemer and Treiber.[13] It may be noted that since bromine reacts with cyclohexane and *n*-heptane (after an appreciable induction period) it was necessary to make measurements within a few minutes of the preparation of the solutions. That the spectra obtained were characteristic of the bromine itself, and not due to reaction with the solvent or dissolved impurities was evident from the initial constancy of the absorption readings, and the fact that Beer's law was obeyed over a wide range of concentrations. It is possible that the differing results of Aikin, Bayliss, and Rees may have been due to impurities in the solvents used.

[12] Aikin, Bayliss, and Rees, Proc. Roy. Soc. (London) **169A**, 234 (1938).

[13] M. Pestemer and E. Treiber, Ber. Deut. Chem. Ges. **74**, 964 (1941).

POSTSCRIPT

After this paper and the preceding one had been written, a note appeared by Bayliss and Sullivan,[14] on the vacuum ultraviolet absorption spectra of iodine and bromine. For gaseous bromine at 48 000 cm^{-1} (~2100 A, the longest wavelength for which figures are given) they reported a molar extinction coefficient of 14 000, which is roughly a thousand fold greater than that found in the present work. As mentioned above at short wavelengths the molar extinction coefficient of bromine varies with concentration, so that a more exact comparison cannot be given. This enormous discrepancy is not due to scattered light in the Beckman spectrophotometer used in the present research (Bayliss and Sullivan used photographic photometry with a grating vacuum spectrograph), since for iodine in heptane the molar extinction coefficient at 2100 A as measured on the Beckman was found to agree very well with that obtained by Ham, Platt, and McConnell using a Cario-Schmitt-Ott fluorite vacuum spectrograph. A similar discrepancy seems to exist for gaseous iodine; thus at 2100 A a molar extinction coefficient of ~100 was obtained in the present work (see preceding paper), whereas, at 2040 A Bayliss and Sullivan quote a value of 29 000. Furthermore, unpublished measurements made here on gaseous iodine below 2000 A with a Cairo-Schmitt-Ott vacuum spectrograph indicate that the values obtained by these authors at shorter wavelengths are also much too high.

ACKNOWLEDGMENTS

I should like to thank Professor R. S. Mulliken for many helpful discussions, and the hospitality shown during my stay in Chicago.

[14] Noel S. Bayliss and John V. Sullivan, J. Chem. Phys. **22**, 1615 (1954).

Perfluoroheptane as a Spectroscopic Solvent*

DENNIS F. EVANS†
Laboratory of Molecular Structure and Spectra, Department of Physics, University of Chicago, Chicago 37, Illinois
(Received November 17, 1954)

Solvent shifts of ultraviolet absorption bands (relative to the gas phase) have been shown to be much less for perfluoroheptane than for *n*-heptane. The oscillator strength of the 2400 A band of styrene has been measured in the gas phase and in perfluoroheptane and *n*-heptane solution. Small increases were observed in solution, which are, however, less than those calculated theoretically.

INTRODUCTION

IT has been shown in the preceding papers that the absorption spectra of iodine and bromine in PFH are very similar to those of the gaseous halogens in the spectroscopic region studied. Although the ionization potential of PFH does not seem to be known, it would be expected to be very high from the great transparency of PFH in the vacuum ultraviolet. This would account fot the absence of any charge transfer bands down to at least 2100 A. PFH also has a much lower refractive index and dispersion than other nonfluorine containing organic compounds; at 2250 A and room temperature the refractive index of *n*-heptane is 1.46, while that of PFH is only 1.28. This value is extrapolated from the data given by Olives *et al.*[1] using Drude's formula. Since a similar extrapolation is satisfactory for the paraffin hydrocarbons, which are much less transparent in the vacuum ultraviolet, no serious error should be involved in the extrapolation. Accordingly, the properties of PFH as a spectroscopic solvent for nonpolar substanes other than iodine and bromine have been investigated. It was found by Ham[2] that the charge transfer bands of several aromatic-iodine complexes were at considerably shorter wavelengths in PFH than in heptane, and this was related to the differences in refractive index. Unfortunately no gas data are available.

The absorption spectra chosen were the "forbidden" 2600 A benzene bands and the strong bands in isoprene, napthalene, and styrene. Quantitative intensity measurements have been made for the latter compound.

EXPERIMENTAL

Commercial samples of styrene and isoprene were shaken with sodium hydroxide solution to remove any inhibitors, washed, dried, and fractionally distilled immediately before use (the former compound *in vacuo*). Cp benzene was shaken with concentrated sulfuric acid, washed, dried, and fractionally distilled. Cp naphthalene was twice recrystallized from alcohol.

The quantitative intensity measurements on gaseous styrene were carried out by a simple method which gives a direct comparison of the intensities in solution and in the gas phase (in the presence of an atmosphere of air). This comparison is of interest in connection with theoretical considerations.[3,4]

A suitable quantity of styrene vapor was introduced into a 1 cm stoppered quartz cell filled with air, and the spectrum recorded. The bottom of the cell was then cooled in liquid nitrogen until all the styrene vapor had condensed, and some *n*-heptane or PFH added. The cell was then allowed to attain room temperature, completely filled with the solvent, and the spectrum remeasured. Measurements were made on a Beckman DU spectrophotometer with calibrated wavelength scale.

RESULTS

The results obtained are shown in Table I and Fig. 1. In those cases where previous measurements have been made,[5] the agreement is, in general, very satisfactory.

DISCUSSION

The solvent shifts for PFH seem to be much less than for *n*-heptane. This is in qualitative agreement

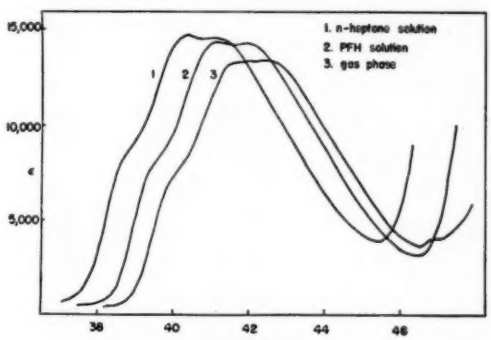

FIG. 1. The absorption of styrene in the gas phase and in solution.

* This work was assisted by the Office of Ordnance Research under Project TB2-0001 (505) of Contract DA-11-022-ORD-1002 with the University of Chicago.

† Permanent address (after October 1, 1954): Lincoln College, Oxford University, Oxford, England.

[1] Olives, Blumkin, and Cunningham, J. Am. Chem. Soc. **73**, 5722 (1951).

[2] J. S. Ham, J. Am. Chem. Soc. **76**, 3881 (1954).

[3] N. Q. Chako, J. Chem. Phys. **2**, 644, (1934); R. S. Mulliken and C. A. Rieke, Proc. Phys. Soc. (London); Repts. Progr. Phys. **8**, 231 (1941).

[4] J. Schuyer, Rec. trav. chim. **72**, 933 (1953).

[5] N. S. Bayliss and Lois Hulme, Australian J. Chem. **6**, 257 (1953); Am. Petroleum Inst. Res. Proj. 44, "Catalog of ultraviolet spectrograms."

TABLE I. Solvent shifts to longer wavelengths (cm^{-1}).

Benzene[a] Four strongest peaks of 2600 A band		Isoprene Main peak at 46 360 cm^{-1} in gas			Napthalene Main peak at 47 510 cm^{-1} in gas	
PFH	*n*-heptane	PFH	PFH+ *n*-heptane[b]	*n*-heptane	PFH	*n*-heptane
45	280	470	620	1560	1110	2220
55	290					
35	280					
20	275					
Av 40 cm^{-1}	av 280 cm^{-1}					

[a] Gas data from Sponer H. Sponer, Chem. Rev. **41**, 301 (1947).
[b] Mole fraction of *n*-heptane =0.143.

with Bayliss' theory,[6] but the magnitudes of the PFH shifts are in general smaller than those calculated from the formula derived by Bayliss, i.e., $\Delta\gamma = C(F/\gamma a^3) \times (n^2-1/2n^2+1)$ where F is the oscillator strength of the transition (given by $4.32\times10^{-9}\int \epsilon d\gamma$), γ is the frequency in cm^{-1}, a is the cavity radius, n is the refractive index of the solvent at the frequency γ, and C is a numerical factor. This is not surprising in view of the approximations involved in the derivation of this formula.

It can be seen from Table I that the addition of an appreciable quantity of *n*-heptane to a dilute solution of isoprene in PFH causes only a small shift of the absorption to longer wavelengths. This behavior is very different from that found previously for iodine.

The oscillator strengths f of the 2400 A styrene transition have been calculated from the data shown in Fig. 1 (two short extrapolations were necessary because of the appearance of other transitions). The results obtained for styrene in the gas phase and dissolved in PFH and *n*-heptane are, respectively, 0.293, 0.316, and 0.327. Although these figures may be in error by several percent, the relative values should be correct to about ±2 percent. Accordingly the increase in oscillator strength is approximately 8 percent for PFH, and 12 percent for *n*-heptane.

These increases are considerably smaller than those predicted by the theory of Chako,[3] according to which oscillator strengths in solution should be increased relative to the gas phase by the factor $(n+2)^2/9n$. For PFH and *n*-heptane the calculated values are 15 percent and 29 percent, respectively. Previous measurements[7] on strong absorption bands also show that Chako's theory is inadequate, but in these no definite increases in intensity were observed in going from gas to solution. However, in view of the limited accuracy of these measurements and also the fact that the compounds studied did not include styrene, there does not seem to be any real discrepancy. A modification of Chako's theory has recently been described by Schuyer[4] using the Onsager model instead of the simple Lorentz-Lorentz one. Unfortunately, it is not possible to test this theory adequately with the present results since not all the necessary data are known, but it seems likely that even the improved expression derived by Schuyer will give too high relative intensities for spectra in solution. The most likely explanation is that given by Jacobs and Platt[7] to explain the deviations from Chako's formula, namely, that even in the gas phase the transition takes place in an effective dielectric due to the periphery of the molecule itself.

ACKNOWLEDGMENTS

I should like to thank Professor R. S. Mulliken for many helpful discussions and the hospitality shown during my stay in Chicago.

[6] N. S. Bayliss, J. Chem. Phys. **18**, 292 (1950).

[7] L. E. Jacobs and J. R. Platt, J. Chem. Phys. **16**, 1137 (1948), and references given in this paper.

Magnetic Susceptibility and Free Energy of Graphite Bromide*

G. R. HENNIG, *Argonne National Laboratory, Lemont, Illinois*

AND

J. D. MCCLELLAND, *North American Aviation, Inc., Downey, California*

(Received November 7, 1954)

The magnetic susceptibility of graphite bromide residue compounds has been measured by a Faraday method. The addition of bromine decreased the diamagnetism of graphite. Fair agreement was obtained between the measured diamagnetism and values calculated by assuming an undistorted graphite band structure depleted in electrons due to the dissociation and ionization of two out of eleven bromine molecules. It has also been shown that the transfer of electrons from the graphite bands to bromine can account for the observed pressure dependence of the graphite bromine equilibrium.

ONE of the characteristic chemical properties of graphite is its ability to absorb a number of substances such as chlorine, bromine, or ferric chloride, between the carbon layers. The reaction products have been called lamellar compounds. On decomposition, they are usually converted to residue compounds,[1] in which the reactant is more randomly scattered through the carbon lattice, presumably at lattice imperfections.

When bromine reacts with graphite it ionizes partially and thereby removes electrons from the graphite lattice. Thus it lowers the Fermi level of the graphite electrons and alters those properties of graphite which are sensitive to the electron distribution. The magnetic susceptibility is a particularly interesting property to study under these conditions of gradual electron depletion.

The magnetic susceptibility of the lamellar compounds of graphite with bromine has been studied in detail,[2] while the residue compounds have been subjected to only a cursory investigation.[3]

EXPERIMENTS AND RESULTS

Measurements were performed on small cubic samples of graphite, 0.3 mm on edge. They were cut from adjacent positions of a bar of high purity Acheson graphite, the same bar as was used in previous studies.[1]

Bromination of weighed samples was carried on in the vapor above a solution of bromine in carbon tetrachloride. The reaction was allowed to proceed for 24 hours in a thermostat at 25.0°C after which the samples were left for 6 days in open containers in a fume hood to allow excess bromine to escape. The samples were then weighed to determine the amount of retained bromine. Subsequently, they were warmed for 24 hours at 50°C without any noticeable loss in weight.

The magnetic susceptibility was measured by means of a Faraday nonuniform field method.[4] The magnet pole pieces were contoured to provide a region in which the force exerted upon the sample was uniform. This region was several times the volume of the sample used, thus eliminating positioning errors. Forces of the order of 0.01 dyne could be measured using a small electrodynamic balance. The effect of ferromagnetic impurities was eliminated by a Honda-Owens plot using fields ranging from 8500 to 16 000 oersteds. The relative precision of the values reported is ½ percent, whereas the accuracy is about one percent.

The magnetic susceptibility is expressed in terms of the "total susceptibility," which is the sum of the susceptibilities measured in three orthogonal directions. This total susceptibility has been shown[4] to be related

TABLE I. Bromine content and magnetic susceptibility of graphite bromide residue compounds.

Bromine concentration 100 × mole fraction solution	Atom percent Br/C	Susceptibility $-\Sigma\chi \times 10^6$
3.62	0.0165	20.79
5.34	0.0541	20.63
6.99	0.2974	19.49
7.81	0.4386	18.38
8.59	0.5422	17.81
9.37	0.6549	17.19
10.13	0.7240	16.66
10.89	0.7690	16.71
11.66	0.8261	16.34
12.36	0.8952	15.86
6.01	0.0856	20.54
6.66	0.1938	19.69
7.48	0.4160	18.41
8.27	0.6504	17.03
9.06	0.6954	16.73
9.83	0.7180	16.48
13.0	0.9162	15.87
13.8	0.9598	15.33
14.4	0.9778	15.12
15.2	1.0033	15.44
control	0.0000	20.57

* Based on work performed under the auspices of the U. S. Atomic Energy Commission.

[1] G. R. Hennig, J. Chem. Phys. **19**, 922 (1951).

[2] Juza, Lubbe, and Heinlein, Z. anorg. Chem. **258**, 105 (1949).

[3] M. Goldsmith, J. Chem. Phys. **18**, 523 (1950). The limited data of this reference have been analyzed and the susceptibility changes interpreted along similar lines as in the present paper by R. Smoluchowski, Revs. Modern Phys. **25**, 178 (1953).

[4] W. P. Eatherly and J. D. McClelland, Phys. Rev. **89**, 661 (1953).

to the spur of the susceptibility tensor, and is a constant for any given type of graphite, regardless of the degree of orientation.

The results are shown in Table I. The first column of the table contains the concentration of bromine in mole fraction in the carbon tetrachloride solution. The second column gives the concentration of bromine as atom percent in the sample, determined from the weight increase. The third column contains the total gram susceptibility.

DISCUSSION

Pressure Dependence of Bromine Content and Free Energy of Graphite Bromide

The conditions of the bromination were more carefully controlled than in previous brominations,[5] and in consequence a number of observations on the dependence of the bromination on bromine pressure are possible.

In Fig. 1, the extent of bromination has been plotted against the mole fraction of bromine in the carbon tetrachloride solution. The values for the lamellar compounds have been obtained by combining the experimental results for residue compounds with the data of reference 5, Fig. 1. It is apparent that very little bromination occurs at bromine mole fractions less than 0.058 corresponding to bromine pressures lower than 20 mm Hg. Similarly, a threshold pressure of 4 mm Hg has been reported by Juza[2] for the bromination of natural graphite at 0°C. Beyond this threshold pressure, the bromine content of at least the residue compounds seems proportional to the square root of the additional bromine concentration. Such a square root dependence might be interpreted as evidence for bromine atom formation were it not for overwhelming evidence[3,6] from susceptibility and x-ray measurements against dissociation. In fact, the formation of lamellar graphite bromide is probably[7] correctly described by

$$C+3.5m\ Br_2(g)\rightarrow C^{m+}(3Br_2\cdot Br^-)_m. \quad (1)$$

To estimate the free energy change per gram atom of carbon, ΔF_m, of this reaction one rewrites it as the sum of the three hypothetical reactions (2) to (4). The first of these

$$3.5m\ Br_2(p_m)\rightarrow 3.5m\ Br_2(l);\qquad \Delta F_2=-3.5mRT\ln(p_m/p_e) \quad (2)$$

represents the condensation of bromine at pressure p_m different from the saturation pressure p_e. The second reaction

$$C+3.5m\ Br_2(l)\rightarrow C\cdot 3.5m\ Br_2 \quad (3)$$

represents the formation of layers of un-ionized bromine to contain $3.5m$ moles per gram atom of carbon. The free energy change of this reaction is $\Delta F_3=3.5m\,B$, where B is proportional to the work involved in wedging graphite layers apart and inserting layers of bromine molecules. This work term per molecule is presumably independent of the total number of such bromine molecules already present and is essentially the difference between a van der Waals carbon-carbon bond and carbon-bromine bond. The additional entropy term included in B is probably also independent of the bromine concentration because a rigid superlattice is formed and no real mixing occurs. The third reaction

$$C\cdot 3.5m\ Br_2\rightarrow C^{m+}(3Br_2\cdot Br^-)_m \quad (4)$$

is the transfer of m electrons from carbon to bromine. The free energy

$$\Delta F_4=-\sum_1^m \epsilon_i+mE,$$

where E is the free energy of partly dissociating and ionizing the bromine and ϵ_i, the energy of the ith electron in graphite. The work of ionizing the bromine consists of dissociation and electron affinity terms which are essentially independent of the concentration. The ionization of the graphite, however, results in a lowering of the Fermi energy, so that for each electron removed the energy ϵ_i decreases. An additional energy term has been neglected, namely the electrostatic interaction of the ions which will certainly become an important term at high bromine concentration. Furthermore, the introduction of bromine may progressively distort the electronic band structure of graphite; this effect has also been neglected. It is hoped that these terms are small for the rather dilute compounds described in this report.

The total free energy of reaction (1) is then

$$\Delta F_m=\sum_2^4 \Delta F_i=-\sum_1^m \epsilon_i$$

$$-3.5mRT\ln(p_m/p_e)+m(3.5B+E). \quad (5)$$

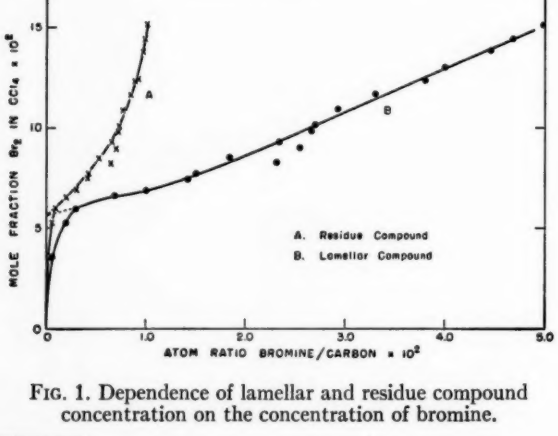

FIG. 1. Dependence of lamellar and residue compound concentration on the concentration of bromine.

[5] G. R. Hennig, J. Chem. Phys. **20**, 1438 (1952).
[6] W. Rudorff, Z. anorg. u. allgem. Chem. **245**, 383 (1941).
[7] G. R. Hennig, J. Chem. Phys. **20**, 1443 (1952).

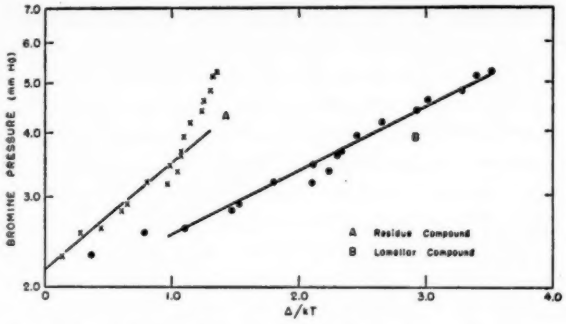

FIG. 2. Lowering of the Fermi level of graphite by bromine. [Eqs. (7) and (8).]

If p_0 is the bromine pressure in equilibrium with an infinitely dilute graphite bromide compound, for which $m=1$, ΔF_1 will be zero:

$$0=-\epsilon_1-3.5RT\ln(p_0/p_e)+3.5B+E. \quad (6a)$$

Similarly the free energy does not change if a mole of bromine at equilibrium is added to an infinite amount of the compound at any concentration:

$$0=-\epsilon_m-3.5RT\ln(p_m/p_e)+3.5B+E. \quad (6b)$$

Subtracting Eq. (6a) from Eq. (6b) we find

$$\epsilon_1-\epsilon_m=\Delta=3.5RT\ln(p_m/p_0). \quad (7)$$

The energy difference $\epsilon_1-\epsilon_m$ equals Δ, the lowering of the Fermi energy of graphite in the lamellar compounds.

It is not certain that a similar derivation is possible for the residue compounds, since they are not in equilibrium with bromine vapor at the time they are analyzed. The assumption can nevertheless be made that the residue compounds were originally in equilibrium with the same vapor pressure of bromine as their parent lamellar compounds. This assumption would be justified if it could be shown that the residue compounds are already formed within the lamellar compounds from which they are derived. If this assumption is made, relation (7) will also hold for residue compounds except for the numerical factor 3.5, which must be replaced by 2.75 in all equations [Eqs. (1) through (7)], since the residue compounds are $C_n^+(Br^-_{5.5})$.

In Fig. 2, Eq. (7) has been plotted for lamellar compounds and the modified Eq. (7) for residue compounds. The vapor pressure of bromine was calculated from the mole fraction of bromine by Henry's law which holds[8] to a mole fraction of 0.03. At larger concentrations the pressure was estimated from the distribution coefficient of bromine between carbon tetrachloride and water,[9] and the pressure above water solutions.[10] The value of m was calculated from the weight of bromine absorbed by the graphite. The value of m was used to calculate Δ from the relation

$$\alpha_m=\frac{\Delta^2}{4.4}+\frac{k^2T^2\pi^2}{13.2}-\frac{k^2T^2}{1.1}[e^{-\Delta/kT}-(\tfrac{1}{4})e^{-2\Delta/kT}+\cdots], \quad (8)$$

which is derived[1] from Wallace's calculation[11] of the energy spectrum of electrons in two-dimensional graphite. According to Wallace the energy ϵ near the band edge in two-dimensional graphite can be written as

$$|\epsilon|=1.2\times10^{-7}|\mathbf{k}|, \quad (9)$$

where the energy, ϵ, and wave vector $\mathbf{k}$ are measured from the zone boundary. The value of α in Eq. (8), calculated from Eq. (9), is unity. However, this value of unity would cause both curves in Fig. 2 to be far from linear, and would also cause poor agreement with some other experimental properties. Therefore, the constant in Eq. (9) was arbitrarily reduced from 1.2×10^{-7} to 0.6×10^{-7}, resulting in an α of 0.31. This value gave an approximately linear plot for lamellar compounds with a slope $(RT\ln p/p_0)/\Delta$ of 0.29, the value required by Eq. (7). This choice of α also yields a fairly linear plot for at least the dilute residue compounds with a slope of 0.42, which is close to the anticipated value of 0.36.

Magnetic Susceptibility

In Fig. 3, the susceptibility of graphite bromide residue compounds has been plotted against the acceptor concentration. Unfortunately, the values reported by Juza[2] for lamellar compounds scatter too much to be of use in the present discussion. Actually, all susceptibility values were first corrected for the diamagnetism of the

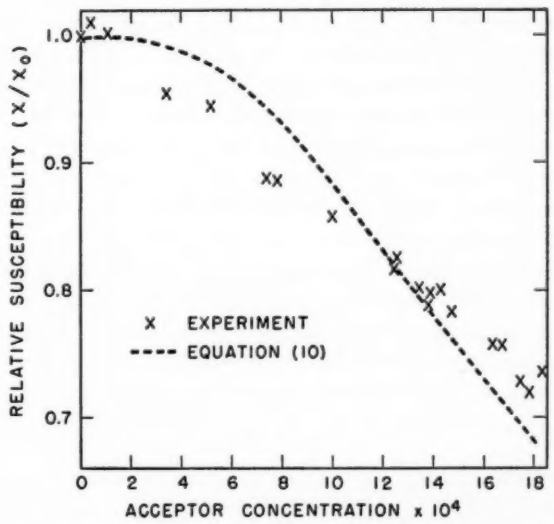

FIG. 3. The relative susceptibility of conduction electrons in graphite containing acceptors.

[8] G. N. Lewis and H. Storch, J. Am. Chem. Soc. **39**, 2544 (1917).
[9] A. A. Jakowkin, Z. physik. Chem. **18**, 588 (1895).
[10] A. Hantzsch and A. Vogt, Z. physik. Chem. **38**, 705 (1901).
[11] P. R. Wallace, Phys. Rev. **71**, 622 (1947).

atom cores[12] by subtracting -1.2×10^{-6}, so that the values plotted are the susceptibility contributions of the conduction electrons. The assumption has here been made that bromine itself does not contribute appreciably to the susceptibility. This assumption is probably valid as long as bromine atoms are not present. This absence of bromine atoms in graphite has been demonstrated by the temperature dependence of the susceptibility[3] and by paramagnetic resonance measurements.[13] The acceptor concentrations in Fig. 3 were obtained from experimental determinations of the acceptor concentrations of bromide residue compounds.[7] At bromine concentrations exceeding 8×10^{-3} atom percent, the empirical relation[7] was used that two out of every eleven bromine atoms are ionized in the residue compounds. It appears that the susceptibility decreases nearly linearly with the bromine content after an initial slight rise. This initial rise in the susceptbility is unfortunately within the magnitude of the precision of the measurements; however, the rise[14] appears to be confirmed by back-extrapolation of the linear portion of the curve.

It is of interest to attempt a comparison of the measured susceptibility with calculated values based on various models of graphite. According to Ganguli and Krishnan,[15] the large diamagnetism of graphite is caused by one quasi-free electron per atom. According to their Eqs. (17) and (18), the susceptibility would be proportional to the number n of free electrons at high temperatures and to $n^{\frac{1}{3}}$ at low temperatures. Since the brominations decreased n by at most 0.2 percent, the susceptibility should have decreased by less than 0.2 percent, which contrasts with the experimental 30 percent. It has been suggested by Mrozowski that in view of other shortcomings the Ganguli-Krishnan theory should be revised by attributing the susceptibility not to one electron per atom, but merely to all the electrons in the upper, normally empty, conduction band plus all the holes in the nearly full lower band. These n_{eff} number of holes and electrons are again supposed to occupy ellipsoidal energy surfaces of parameters $\alpha_1,\alpha_2,\alpha_3$. Instead of using the same ellipsoidal energy surfaces for which the susceptibility equations are derived, Mrozowski unfortunately utilizes entirely different energy contours to calculate n_{eff}, thus his relations are internally inconsistent. Furthermore, this model also predicts the wrong behavior with bromination. At, and particularly below, room temperature the diamagnetism should be proportional to n_{eff} and thus increase with bromination, yet it was found by experiment to decrease. Even the asymptotic high temperature equation could, as Mrozowski himself points out,[16] predict a decrease in diamagnetism with bromination only if an energy spectrum of the electrons is used for n_{eff} which does not satisfy other electrical properties.

The use of free or nearly free electron approximations is however an unjustifiable simplification. Instead, the actual energy surfaces calculated for graphite by Wallace should be used[3] in estimating the susceptibility. This has been done by Eatherly[12] who derived a relation between susceptibility and energy from the Peierls equation for susceptibility and Wallace's equation for two-dimensional graphite, including higher-order terms in γ_1, the exchange integral between next nearest neighbors. The resulting equation is

$$\chi/\chi_0=\operatorname{sech}^2\Delta/2kT, \tag{10}$$

where x_0 is the susceptibility for zero Δ, the difference in energy between the zone edge and the Fermi level. The value Δ was again calculated from Eq. (8) using as before the value of $\alpha=0.31$. Furthermore, both calculated curves were displaced by letting $m=(\text{Br}^-)-1.1\times10^{-4}$ to compensate for the initial rise in the experimental curve. This displacement amounts to the assumption that bromination initially removes 1.1×10^{-4} excess electrons in the upper band. The calculated susceptibility has been plotted in Fig. 3. It compares reasonably well with the experimental values.

For completeness one ought to compare other experimental properties with values calculated from Eq. (8) and the adjusted Eq. (9). The Hall coefficient agrees at best qualitatively, but could be brought into good agreement if an initial donor concentration of 4.6×10^{-4} were assumed instead of 1.1×10^{-4} which seemed indicated by the susceptibility values.

The resistivity calculated from the equations changes by a factor of 3 more slowly with acceptor concentration than the experimental values. Thus the electrical resistance is the only property of those determined which differs very seriously from the calculated values. This deviation may perhaps in part be attributed to several assumptions in the calculation. The assumption of a constant relaxation time $\tau(E)$ in graphite is uncertain although it has recently been partly justified by Robinson.[17] Since this assumption affects directly the resistance and, only to a lesser extent, the other properties, it may be responsible for the strong deviation of the calculated resistance. However, it is obviously an approximation to assume a two-dimensional model for graphite; the calculations should have been based on energy spectra derived by Wallace for three-dimensional graphite or, still better, on revised equations reported recently by Carter and Krumhansl.[18] Even if the correct energy spectrum of the electrons had been utilized, the

[12] W. Eatherly, North American Aviation, Inc., Downey, California, Report NAA-SR-146 (July 25, 1951).
[13] Hennig, Smaller, and Yasaitis, Phys. Rev. **95**, 1088 (1954).
[14] Such a rise has been observed at the North American Aviation Company during the graphitization of index rod.
[15] N. Ganguli and K. S. Krishnan, Proc. Roy. Soc. (London) **A177**, 168 (1941).
[16] S. Mrozowski, Phys. Rev. **85**, 609 (1952).
[17] J. E. Robinson, Phys. Rev. **98**, 227A (1955).
[18] J. L. Carter and J. A. Krumhansl. J. Chem. Phys. **21**, 2238 (1953).

methods used to derive some of the properties are still only approximate. It has, for example, been pointed out by Adams[19] that important contributions to the susceptibility are neglected if the susceptibility is calculated from the Peierls equation in problems like the present one where the Fermi surface lies close to electron states in two bands which are nearly degenerate.

[19] E. N. Adams II, Phys. Rev. **89**, 633 (1953).

ACKNOWLEDGMENTS

The authors are indebted to W. P. Eatherly for many helpful discussions and suggestions.

THE JOURNAL OF CHEMICAL PHYSICS VOLUME 23, NUMBER 8 AUGUST, 1955

Pulse Technique for Measurement of the Probability of Formation and Mobility of Negative Ions

K. B. McAfee, Jr.
Bell Telephone Laboratories, Inc., Murray Hill, New Jersey
(Received November 12, 1955)

A new technique for measurement of the attachment coefficient of electrons to molecules has been devised. The technique involves production of a beam of electrons in an attaching gas. The transient current flowing after the initiation and termination of the electron beam is interpreted as a flow of negative ions produced by electron-molecule collisions. Analysis of the transient current which may last several milliseconds yields a value for the mobility of the negative ions thus formed. The ratio of the magnitude of the electron beam current to the negative ion current yields a direct measure of the attachment coefficient.

Preliminary results obtained with SF_6 show a very large attachment coefficient. Values of α/p (the ratio of attachment coefficient to pressure) are considerably larger in SF_6 than those obtained for O_2 in studies elsewhere. As might be expected the mobility of negative ions formed in SF_6 is much lower than that observed for other gases. This is attributed to the very large collision cross section resulting from (1) the interaction between the negative ion and neutral gas molecules comprising polarization attraction and hard sphere repulsion and (2) resonance or exchange interaction.

INTRODUCTION

THE study of the formation of negative ions[1] in the gas phase has been undertaken in several ways. One method has been that of the mass spectrograph where negative ions are drawn out though small holes in the anode of a gas discharge or bombardment chamber and subsequently analyzed. Another basic technique involves the production of a swarm of electrons within the gas at pressures of the order of a millimeter. With the latter technique the quantity usually measured is α, defined as the number of attachments per electron per centimeter of travel parallel to the applied electric field. In the present paper a new technique of the swarm type will be described for the measurement of electron attachment in gases and preliminary results obtained with an attaching gas (SF_6) will be discussed.[2] The technique to be described differs from previous methods of measurement[3] in that separation of electron and ion components of current is accomplished by a study of the transient response of the system without the use of interposed electron filters. It permits measurement simultaneously of the attachment coefficient and the negative-ion mobility.

In order for attachment to take place yielding a stable negative-ion, it is necessary that electronic states of the atom or molecule exist in which there is a positive electron affinity. That is, E_0-E_- the energy difference between the normal states of the atom or molecule and the ion must be positive. In order to permit the formation of a stable negative ion, the energy of the electron affinity as well as the kinetic energy of the electron must be dissipated either by production of some vibrationally excited modes in the molecule, or by collision with another molecule or the wall, or by some other such process.

EXPERIMENTAL METHOD

The technique to be described employs a pair of plane parallel electrodes consisting of an anode A and a photoelectric cathode C mounted as shown in Fig. 1(a) so that it can be irradiated by ultraviolet light. This light is pulsed and the current due to the drift of the emitted electrons and the ions formed by their capture by the gas is observed.

A block diagram of the equipment is shown in Fig. 2. The source of ultraviolet radiation used has been an SC-2537 Hanovia source providing almost monochromatic radiation of the intense mercury line at 2537 A. The source is pulsed by driving a switching tube (807) which is in series with the quartz lamp

[1] H. S. W. Massey, *Negative Ions* (University Press, Cambridge, England, 1950).
[2] A somewhat similar method has been used by Hornbeck for the study of positive ions; see J. A. Hornbeck, Phys. Rev. **83**, 374 (1951).
[3] See however, A. Doehring, Z. Naturforsch. **7a**, 253 (1952) and P. Herreng, Cahiers phys. **38**, 1 (1952).

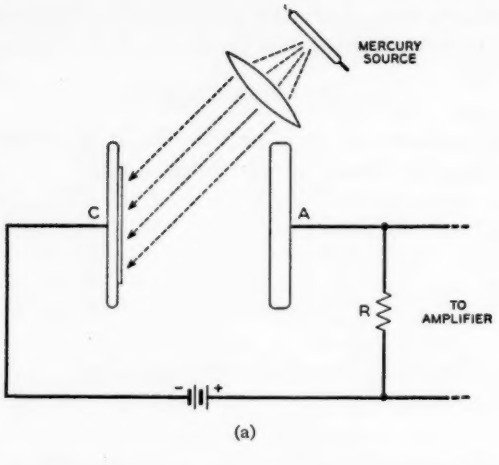

FIG. 1(a). Pulsed ultraviolet light from the mercury source impinges upon the cathode C. Electrons ejected from C as well as negative ions are collected at the anode A. (b). Oscillogram of current pulse.

and the high-voltage supply. Tubes have been constructed so that the uv radiation passes either directly through holes in the anode to the cathode, or enters from the side of the tube. Since electrons are ejected from the anode as well as the cathode a problem exists when the perforated anode is used in that these electrons may attach before they are returned to the plate by the field. The sluggish current of negative ions from the anode adds to that of the cathode giving rise to an unnecessarily complicated pattern to analyze. Unless it can be demonstrated that contributions to the current from the anode are very small, the superior technique appears to be side illumination. The cathode consists of a nickel disk upon which a mixture of the carbonates (Ca, Sr, Ba) has been deposited. The cathode is then activated by induction heating to 850°C. Activation of the cathode to yield copious emission of electrons was not difficult; however, the admission of gas to the tube, regardless of attempts to purify it, made repeated reactivation necessary. The output of the tube was amplified by a Tektronix wide-band preamplifier before being presented on an oscilloscope. Synchronization is provided from the pulse generator.

The amplifier and scope may be calibrated by introducing a voltage to the preamplifier through the attenuator shown. Time markers are utilized by modulation of the z-axis of the oscilloscope. With the separation of the plates of about two centimeters and the voltage about ten volts the ion collection time proves to be several hundred microseconds. For such measurements the ultraviolet pulse generator is set to give pulses of about 1 millisecond in length. Quite rectangular pulses may be obtained by adjusting the current and voltage across the SC–2537 tube.

The patterns observed on the scope may be interpreted in the following manner. In the case of an evacuated tube a rectangularly pulsed source of radiation yields a similarly shaped pulse of electrons crossing the interelectrode space, and consequently a rectangular wave shape is obtained for current in the external circuit. In the presence of a gas which attaches electrons, however, the current in the external circuit will consist of two components. One component will be a result of the electrons which cross the space without attachment. On the scale of time considered here the transit time of the unattached electrons is effectively zero. The other component results from the newly formed negative ions. It will increase for a period of time equal to the negative ion transit time after which a steady-state condition will exist. Figure 1(b) shows typical oscillograms obtained for the conditions just described. A light pulse of one millisecond length was applied to the tube and current flowing is shown in the upper oscillogram. Since the current is entirely electronic it rises to its full value in one electron transit time and remains so until the light pulse is switched off. The lower oscillogram shows the effect of attachment. A light pulse of length about two milliseconds is shown. Negative ions formed by attachment are collected in a time τ [shown between the arrows in Fig. 1(b)] a thousand or more times the electron transit time. Their mobility can be determined from τ and the spacing. The total current flowing is the sum of the electron and ion components. When the light pulse is turned off, the electron component is removed and consequently a sharp decrease in the height of the pulse is observed. The tail of the pulse consists entirely of negative ions. If, during the application of the light pulse, electrons exceed the ionization energy of the gas the total current will increase. As the voltage (or ratio of field strength to pressure) across the tube increases in experiments to be described, the total current flowing did not show a sizeable variation with (E/p) across the tube, although it was possible to obtain such a variation at very high and very low values of E/p.

Another effect upon pulse height is the dependence of the back diffusion rate of electrons leaving the cathode upon E/p. Since α is determined from a function of the ratio of electronic to ionic current, variation in back diffusion will not influence the results. Ionization in the tube, however, will produce positive ions strongly influencing the current ratio and must be

eliminated to obtain results interpretable by the theory of the next section.

Experimentally it has been observed that the transit time of negative ions in SF_6 can be made as long as several milliseconds although very short spacings and high fields permit measurement of the ion current with ions only a few hundred microseconds old. The next section will show how it is possible to determine the attachment coefficient of the gas by measurement of the ratio of the electron current, represented in Fig. 1(b) by the perpendicular portion of the curve, to the total emission current i_0.

THEORY

The differential equation governing the motion of the ionic charges in the tube is

$$\frac{\partial \rho}{\partial t} = -v\frac{\partial \rho}{\partial x} + \alpha i_0 e^{-\alpha x}, \tag{1}$$

where ρ = density of negative ions which in one dimension we may write as number of ions/cm, v = drift velocity of negative ions, α = number of attachments per cm per electron, i_0 = the cathode emission current, and x = distance from the cathode.

The dependence of the distribution of ion density upon space and time, a solution of (1) is

$$x<vt \qquad \rho(x) = \frac{i_0}{v}(1-e^{-\alpha x}), \tag{2}$$

$$x>vt \qquad \rho(x,t) = \frac{i_0}{v}e^{-\alpha x}(e^{\alpha vt}-1). \tag{3}$$

In these solutions we assume that a step function of light arrives at the plate at $t=0$. The significance of these solutions is the following. At a given time t_1 for distances $0<x<vt_1$ the distribution of negative ions is an increasing function of x approaching the value i_0/v in the limit for x and t approaching ∞. For $x>vt_1$ the negative ion density drops off exponentially. The two solutions join at $x=vt_1$. For a time Δt later the point of juncture of the two solutions has moved a distance Δtv. The point of discontinuity at t_1 moves with the drift velocity v until $vt=X$ where X is the interelectrode spacing. After this time the steady-state solution (2) obtains.

The negative-ion current, i_n, flowing after $t=0$ is given by

$$i_n(t) = \frac{v}{X}\int_0^X \rho(x,t)dx. \tag{4}$$

Now $\rho(x,t)$ may be taken from Eqs. (2) and (3). For $0<t<X/v$, $i_n(t)$ is given by the sum of two integrals and may be expressed as

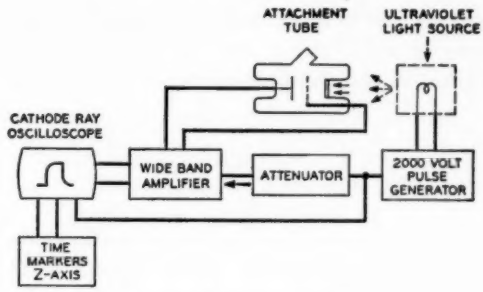

FIG. 2. Schematic diagram of apparatus.

$$i_n(t) = \frac{i_0}{X}\left[\int_0^{vt}(1-e^{-\alpha x})dx + \int_{vt}^X e^{-\alpha x}[e^{\alpha vt}-1]dx\right]. \tag{5}$$

The limits of integration are those over which the solutions (2) and (3) hold. Integrating we have, for the transient negative-ion current,

$$t<\frac{X}{v} \quad i_n(t) = i_0\left\{\frac{vt}{X} + \frac{e^{-\alpha X}}{\alpha X}[1-e^{\alpha vt}]\right\}. \tag{6}$$

For $t>X/v$ we have the steady-state solution

$$i_n(t) = i_0\left[1+\frac{1}{\alpha X}(e^{-\alpha X}-1)\right]. \tag{7}$$

If, after the steady-state solution has been established, the exciting light is cut off, collection of the ions present in the tube results in another transient negative-ion current. The transient current flowing is then given by a solution to the differential equation,

$$\frac{\partial \rho}{\partial t} = -v\frac{\partial \rho}{\partial x}, \tag{8}$$

where now for $t=0$, $\rho(x,0)$ is given by Eq. (2). Thus,

$$i_n = i_0\left[1-\frac{vt}{X}-\frac{1}{\alpha X}(1-e^{-\alpha(X-vt)})\right]. \tag{9}$$

Equation (9) is the form of the decaying negative-ion transient flowing after the light pulse has been switched off.

The initial and decaying transient negative-ion currents given by (6) and (9) are seen to differ in that 1 in Eq. (6) is replaced by $e^{\alpha X}$. Physically the reason for this difference is that during the initial transient the electron pulse which gives the second term in (1) is present while this term is absent in Eq. (8) for the decay pulse.

So far only the contribution of negative ions to the

current has been considered. The contribution of the electrons to the current carried in the tube may be determined in the steady state by the integral

$$i_e = i_0 \int_0^X \frac{x}{X}(+\alpha)e^{-\alpha x}dx + i_0 e^{-\alpha X}. \tag{10}$$

The first term represents the proportion of current carried by electrons which attach during their travel to gas molecules. The second term is the contribution to current of the electrons which cross the interelectrode space unattached.

The electron current is then given by

$$i_e = \frac{i_0}{\alpha X}(1-e^{-\alpha X}). \tag{11}$$

It is obvious that the sum of (11) and (7), the steady-state solution, is $i_T = i_e + i_n = i_0$. It is also observed that for values of E/p (the ratio of field strength to pressure) used in the measurements to be given that the total steady-state current i_T is not dependent in significant measure upon E/p as is expected for no ionization in the tube.[4] At high values of E/p the current i_T increases very sharply showing the presence of positive ions.

Figure 3 shows a composite plot of the expected shape of the current pulse flowing after the rectangular light pulse of length t_0 has been applied. The times τ are the equal transit times $\tau = X/v$ of the two negative ion transients. The current carried by the electrons is shown shaded in the plot.

Experimentally an easy ratio to measure is that of the electron current to the total current flowing. This is given by

$$\frac{i_e}{i_0} = \frac{1-e^{-\alpha X}}{\alpha X} = \frac{1-e^{-y}}{y}. \tag{12}$$

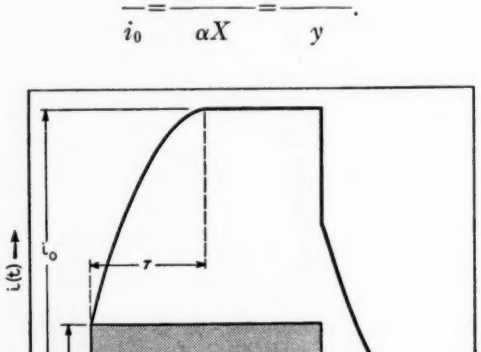

FIG. 3. Current passing through attachment tube. The total charge carried by electrons across the gap is shown shaded.

[4] It is also expected that the electron back diffusion is not dependent in significant amount upon the field strength to pressure ratio in the observed range.

Equation (12) is a unique relationship between the experimentally measured quantity i_e/i_0 and the attachment coefficient. This relationship from which the coefficient is determined is plotted in Fig. 4.

Further information may be sought from the shape of the transient negative-ion pulse given in Eq. (6).

In Eq. (6), if we set

$$\frac{vt}{X} = \eta \quad \alpha X = y$$

we have $i_n/i_0 = \eta + (e^{-y}/y)[1-e^{y\eta}]$.

A plot of the shape of the arrival pulse is shown in Fig. 5(a) for three different values of the quantity y. Some feeling for the form of the negative-ion current pulse may be gained from the figure. It is observed that a wider separation or larger attachment coefficient has then the effect of making the collection pulse more linear. This is a useful point in the design of tubes for measurement of attachment since a sharply discontinuous current trace is capable of better analysis.

Put in parametric form the negative-ion current flowing after the ultraviolet source has been shut off is given in Eq. (9). Thus,

$$i/i_0 = \left[1-\eta-\frac{1}{y}(1-e^{-y(1-\eta)})\right].$$

Curves for two values of the parameter y are shown in Fig. 5(b). This time the effect of increasing the separation of the plates is also to make the collection pulse more linear in time.

DETERMINATION OF THE PROBABILITY OF ATTACHMENT PER COLLISION

The method of pulsed light just described has a number of advantages over the older dc method. A direct measurement of the mobility of the ions whose ages are all less than a millisecond is provided. Although the attachment coefficient α is the experimentally observed parameter, it is believed that a refinement of the

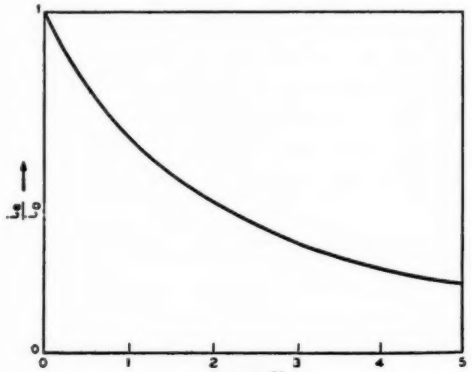

FIG. 4. Determination of attachment coefficient from measured parameters.

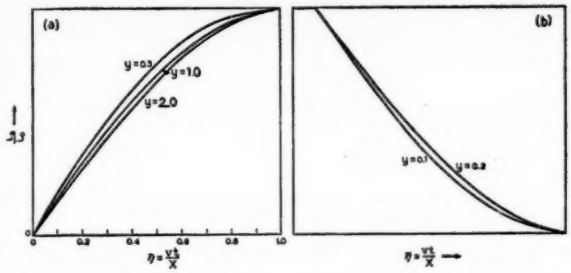

FIG. 5. Negative-ion current flowing. (a) Immediately subsequent to pulsed initiation. (b) After termination of pulse.

technique should permit the measurement of h, the probability of attachment per collision. This quantity may be evaluated provided a value for the drift velocity, w, has been measured. The determination of h proceeds from

$$h=\alpha w\left(\frac{u}{\lambda}\right)^{-1}. \tag{13}$$

Here u is the mean velocity of agitation of the electrons and λ is the mean free path where the ratio u/λ may be determined from the relationship[5]

$$\frac{u}{\lambda}=\frac{1}{Cw}\frac{e}{m}E, \tag{14}$$

so that

$$h=C\alpha w^2\frac{m}{eE}. \tag{15}$$

All quantities in (15) are known. While the value C requires some assumption as to the velocity distribution its numerical value is not thought to vary to a critical extent with the distribution chosen. The value[3] of C has been determined to be approximately 5/4.

RESULTS

Preliminary results have been obtained with the heavy molecule SF_6. The symmetrical structure in which the sulfur atom occupies the center of a regular octahedron whose corners are occupied by the fluorine atoms has been confirmed by electron diffraction,[6] infrared,[7] and Raman[8] measurements. A discussion of the chemical properties of the gas subject to high electric fields has recently been published.[9] Its chemical inertness and, as it turned out, its large attachment coefficient make it suitable for measurement by the pulsed-light method. Many vibrational degrees of freedom permit the energy of attachment to be transformed into excited vibrational states of the molecule.

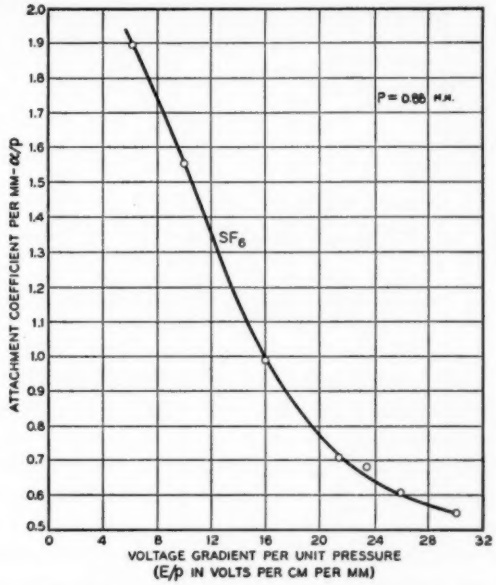

FIG. 6. Preliminary determination of α, the attachment coefficient in SF_6.

Previous attempts[10] have been made to measure the attachment coefficient of SF_6. The results reported suggest that SF_6 does not attach electrons at low field strengths—a finding which Goldstein attributes to the lack of permanent dipole moment in the molecule. Measurements of the attachment coefficient α by the pulse method just described, however, have shown the existence of a large probability of attachment of electrons to SF_6 at field strengths from 3 to 88 volts/cm and from values of E/p (the ratio of field strength to pressure) from 3 to about 30 volts/cm-mm. A comparison shows the attachment coefficient larger by a factor of ten than that of oxygen[11] over most of the range of E/p. Mass spectrographic[12] studies permit identifying the ions present in the gas at very low pressures (0.2 micron). Only the four ions SF_6^-, SF_5^-, F^-, and F_2^- are found to exist. A plot of the observed dependence of α/p upon E/p is shown in Fig. 6. It will be noted that only one pressure (0.88 mm Hg) is shown although an extension of the present measurements to determine the variation of α/p with pressure is in progress. The value of α/p obtained for the gas is very high in comparison with values found for other attaching gases. Its determination is independent of the attachment process (i.e., whether a resonant capture process or dissociative process is operating) so that it is not necessary to specify the exact nature of the electron-molecule interaction. All determinations shown in Fig.

[5] See L. B. Loeb, *Fundamental Processes of Electrical Discharge in Gases* (John Wiley and Sons, Inc., New York, 1939), pp. 178–179.

[6] Brockway and Pauling, Proc. Natl. Acad. Sci. U. S. **19**, 68 (1933).

[7] Eucken and Ahrens, Z. Physik, Chem. **B26**, 297 (1934).

[8] Yost, Steffens, and Gross, J. Chem. Phys. **2**, 311 (1934).

[9] Edelson, Bieling, and Kohman, Ind. Eng. Chem. (September, 1953).

[10] L. A. Goldstein, Ann. phys. **9**, 723–803 (1938).

[11] A recent compilation of experimental determinations of electron attachment in oxygen has been published. See M. A. Harrison and R. Geballe, Phys. Rev. **91**, 1 (1953).

[12] A. J. Ahearn and N. B. Hannay, J. Chem. Phys. **21**, 119 (1953). See also W. H. Hickam and R. E. Fox, Phys. Rev. **98**, 557(A) (1955).

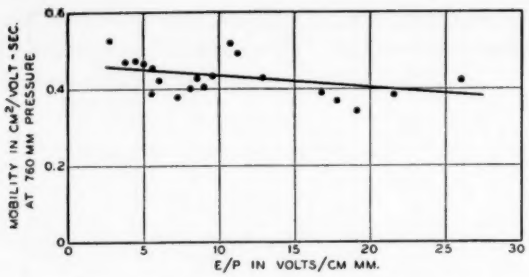

FIG. 7. Mobility of negative ions in SF_6 as a function of E/p.

6, are under conditions of no ionization in the gas. This fact is determined because the steady-state current i_0 has the same value for E/p up to 30 volts/cm-mm as under a condition where the total voltage across the tube is less than the ionization potential (15.9 volts) of SF_6.

For values of E/p of less than 20 volts/cm-mm the observed curves of $i(t)$ *versus* t visually approximated those predicted by the expressions derived earlier. Within the limits of the present resolution only one negative ion species has been observed in the gas below a field strength of the order of 20 volts/cm-mm. The mobility extrapolated to $E/p=0$ is about 0.45 ± 0.2 cm²/volt sec at 760 mm Hg. Figure 7 shows a plot of the mobility *versus* E/p. The scatter of the observed points from a straight line can probably be attributed to difficulty in locating the exact termination of the ion pulse which has become somewhat smeared out as a result of diffusion of the ions.

DISCUSSION

It has been determined by examination of the intensities of the four negative ions produced in the mass spectrograph with SF_6 at pressures up to 0.2 micron that SF_6^- and SF_5^- are more abundant by a factor of somewhat greater than 100. One means of identification of the ions produced is a comparison of their mobilities with those predicted from the classical ionic mobility theory of Langevin.[13,14] The assumptions of that theory are thought to be appropriate to negative ions in SF_6. These are that the negative ions are hard spheres which make elastic collisions with a gas composed of hard spheres. The field strengths used are such that the velocity distribution of both ions and gas atoms is close to Maxwellian. Molecules and ions are assumed to attract one another by a polarization force attributed to the negative charge on the ion. The van der Waals forces are not regarded to be significant. A calculation of the low field mobility is then possible if the following properties of the gas are known: hard-sphere cross section, polarizability, and gas temperature. Hard-sphere cross section can be taken with reasonable accuracy from viscosity measurements.[15] Polarizability of SF_6 is known from dielectric constant measurements.[16]

[13] Langevin, Ann. Chem. Phys. **8**, 239 (1905).
[14] Hassé and Cook, Phil. Mag. **12**, 554 (1931).

TABLE I. Ion mobility (cm²/volt sec) at 760 mm Hg.

Negative ion	Hard-sphere theory (Langevin)	Measured mobility	Hard-sphere theory corrected for exchange effect
SF_6^-	0.78	0.45	0.46–0.56
SF_5^-	0.80		

An interaction which has not been considered as yet is that which may be attributed to the exchange of the electron between an ion and molecule where the core of both particles is the same. As a result of the overlapping of the wave functions the electron is considered to oscillate back and forth between the two particles during a collision giving rise to resonance attraction and repulsion. In addition, the possibility that the electron may transfer from the ion to the neutral molecule after the collision has taken place must be included. An estimation of the exchange effect has been carried out and is shown in Table I. This estimate has been made by employing the viscosity cross section increased by an amount $\Delta\sigma$ which has been determined experimentally[17] for the rare gas atoms. Furthermore, $\Delta\sigma$ is the increase in viscosity cross section as a result of the exchange effect in the series He, Ne, A, Kr, and Xe. It has been determined that this increase does not vary markedly in the aforementioned series and thus it is thought to represent a fair approximation. The two values shown in the last column of Table I are calculated using the largest and smallest (Xe, He) exchange cross sections. No correction for the exchange effect need be applied in the case of SF_5^-, since the cores of the colliding negative ion and the molecule SF_6 are not identical. Thus theory and experiment differ by a factor two if the negative ion observed is SF_5^-. Although the agreement in observed and predicted mobility and mass spectrographic abundance evidence then strongly suggest the identification of the negative ion with SF_6^-, the role of clustering, the effects of pressure and temperature, as well as the possible importance of impurities are of significance and are under investigation.

ACKNOWLEDGMENTS

The author is greatly indebted to his colleagues, J. A. Hornbeck and G. T. Kohman for their advice and support during the course of this research. Solutions for the ion currents were pointed out by W. C. Herring, while discussions concerning the exchange interaction with G. H. Wannier were invaluable.

[15] R. E. Plump (private communication).
[16] Watson, Rao, and Ramaswamy, Proc. Roy. Soc. (London), **187**, 431, 558 (1934); Fuoss, J. Am. Chem. Soc. **60**, 1633 (1938).
[17] J. A. Hornbeck, Phys. Rev. **84**, 615 (1951); G. H. Wannier, Bull. Am. Phys. Soc. **29**, No. 5, 20 (1954).

Intramolecular Charge Transfer Spectra Observed with Some Compounds Containing the Nitro or the Carbonyl Group

SABURO NAGAKURA
Institute of Science and Technology, University of Tokyo, Tokyo, Japan
(Received November 18, 1954)

A new method, which proved to be useful for the theoretical study of electron migration for the monosubstituted benzene molecule, is employed to interpret strong absorption bands observed with various unsaturated compounds containing the nitro or the carbonyl group. Consequently, it is shown that these absorptions correspond to the transition between two energy levels produced by the interaction of the highest occupied level of the electron donating group with the lowest vacant one of the electron accepting group, and that theoretical values of transition energies and oscillator strengths evaluated by use of the present method are in very good agreement with the observed values. Furthermore, the present interpretation of these absorptions is discussed in comparison with the earlier resonance viewpoint.

INTRODUCTION

As is well known, nitro and carbonyl groups show a strong tendency to receive electrons from other π-electron systems. Namely, these two groups may be called typical electron accepting groups. In the previous paper,[1] electron migration from the benzene ring to these groups was discussed on the basis of the energy level diagram determined by the combination of the ionization potential and the near ultraviolet absorption spectrum. Moreover, it was also pointed out briefly that characteristic absorption bands which appear at 2510, 2370, and 2300 A for nitrobenzene, acetophenone, and benzoic acid, respectively, may be regarded as "intramolecular charge transfer absorption;" *viz.*, the absorption due to the transition between energy levels produced by the interaction of the highest occupied level of benzene with the lowest vacant one of the electron accepting group.

In the present paper, it will be shown that similar absorption also occurs with other compounds containing the nitro or the carbonyl group, such as nitramide (H_2NNO_2), nitropropene ($H_3CHC=CHNO_2$), crotonic acid ($H_3CHC=CHCOOH$), actophenone ($H_3COCC_6H_5$), nitrophenol ($HOC_6H_4NO_2$), etc., and that its wavelength and intensity can be explained reasonably by use of molecular energy level diagrams. Furthermore, the marked characteristic of the present method will be discussed in comparison with the earlier one from the resonance viewpoint in which absorption of this kind was explained by resonance between polar and nonpolar structures.[2,3]

ABSORPTION SPECTRA OF SOME UNSATURATED COMPOUNDS CONTAINING THE NITRO OR THE CARBONYL GROUP

First of all, an explanation will be made in detail considering the absorption spectrum of the nitro compound. Although simple nitro compounds, such as nitromethane, show a weak absorption band ($\epsilon=18$) at about 2800 A,[1] no strong band, whose molar extinction coefficient is larger than 1000, appears on the longer wavelength side of 2000 A. On the other hand, a characteristic absorption band with molar extinction coefficient larger than 4000, can be observed in this wavelength region with compounds where the nitro group conjugates with some electron donating groups (X), such as $-NH_2$, $-HC=CHCH_3$, $-HC=CHCH=CHCH_3$, 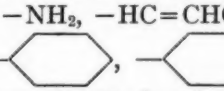 , 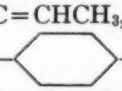 $-OH$, etc. (see Fig. 1). The wavelength (λ_{max}) and molar extinction coefficient (ϵ) of the absorption maximum observed with these nitro compounds (O_2N-X) are tabulated in Table I.[4-7]

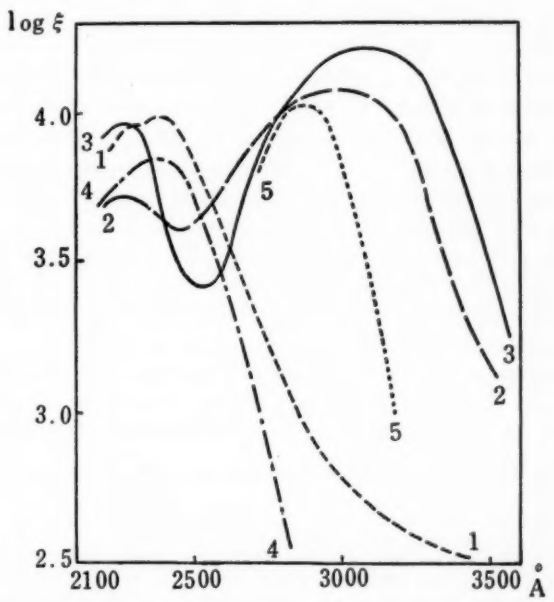

FIG. 1. Near ultraviolet absorption spectra observed with some unsaturated nitro compounds. 1. $MeCH:CHNO_2$ in ethanol. 2. $Me(CH:CH)_2NO_2$ in ethanol. 3. $PhCH:CHNO_2$ in ethanol. 4. $(CH_3)_2NNO_2$. 5. $HOPhNO_2$ in naphtha.

[1] S. Nagakura and J. Tanaka, J. Chem. Phys. **22**, 236 (1954).
[2] W. H. Rodebush, Chem. Revs. **41**, 317 (1947).
[3] Braude, Sondheimer, and Farbes, Nature **173**, 117 (1954).
[4] Braude, Jones, and Rose, J. Chem. Soc. 1104 (1947).
[5] R. N. Jones and G. D. Thorn, Can. J. Research **27B**, 828 (1949).
[6] S. Nagakura, unpublished work.
[7] G. Kortüm, Z. Elektrochem. **47**, 55 (1941).

TABLE I. Absorption spectra of unsaturated compounds containing the nitro and the carbonyl group and the ionization potential (I_p) of the electron donating group (HX).

X	XNO_2 λ_{max}	ϵ	Solvent	$XCOCH_3$ λ_{max}	ϵ	Solvent	XCOOH λ_{max}	ϵ	Solvent	I_p (ev)
$-NH_2$	225[a]	5900	water	171.7[d,e]		vacuum		...		10.52
$-N(CH_3)_2$	240[a]	6300	dioxane	197.4[d,e]		vacuum		...		9.21
$-CH=CHCH_3$	229[b]	8700	*n*-hexane	224[f]	9700	alcohol	208[j]	12 600	hexane	9.84
$-CH=CHCH=CHCH_3$	298[b]	12 000	alcohol	271[f]	22 500	alcohol	261[f]	25 600	hexane	8.81
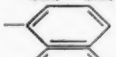	251[c]	9200	naphtha	237[g]	12 600	*n*-heptane	230[h]	29 000	ether	9.52
	286[c]	10 600	naphtha	267[h]	19 100	ether	251[h]	18 300	ether	9.03
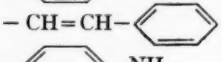	299[b]	17 800	*n*-hexane	286[i]	23 500	alcohol	278[k] (cis) 279 (trans)		hexane hexane	8.86
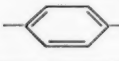	320[c]	14 600	naphtha	296[h]	21 400	ether	277[h]	20 600	ether	(8.6)[l]

[a] See reference 5.
[b] See reference 4.
[c] See reference 6.
[d] See reference 8.
[e] These two values are concerned with $HCONH_2$ and $HCON(CH_3)_2$. Therefore, they are probably somewhat different from values of H_3CCONH_2 and $H_3CCON(CH_3)$.
[f] See reference 9.
[g] See reference 1.
[h] See reference 10.
[i] See reference 11.
[j] See reference 12.
[k] See reference 13.
[l] This value was obtained from experimental values of λ_{max}.

Similar absorptions are also observed with unsaturated ketones and carboxylic acids as shown in Table I.[8–15] Hereupon it is to be noticed that absorption spectra of some carbonyl compounds are more complicated in their shapes compared with those of nitro compounds, because they show one or two other weak bands on the longer wavelength side of the strong band under consideration. For instance, in the case of mesityloxide $(H_3C)_2C=CHCOCH_3$, a weak band with molar extinction coefficient smaller than 100, occurs at about 3250 A.[6] This may be due to an $n\rightarrow\pi^*$ transition as the 2800 A band of acetone is [16–18]. Moreover, another kind of weak absorption band, whose molar extinction coefficient is about 1000, can be observed at about 2800 A with acetophenone and benzoic acid.[10] This conclusively corresponds to the 2600 A band of benzene. In the present paper, further mention will not be made of these weak bands because their origins have already been discussed by other authors.[19] At any rate, it will be shown below that the experimental results tabulated in Table I can be explained without contradiction on the basis of the molecular energy level diagram determined by use of the ionization potentia of HX, which is given in the last column of Table I.

THEORETICAL CONSIDERATION BY USE OF ENERGY LEVEL DIAGRAMS

By use of the same method as described in the previous paper,[1] the highest occupied level (H) and the lowest vacant one (V) can be determined with HX, CH_3NO_2, CH_3COOH, and CH_3COCH_3 by a combination of the experimental knowledge of the ionization potential and of the absorption spectrum. The results are shown in Fig. 2. In the present work, Morrison's data[20] are employed as the ionization potential value necessary for the determination of the H level except in cases of dimethylamine,[21] propene,[22] and 1-methylbutadiene.[23] Then the highest occupied level of benzene (H_B), which was estimated as -9.24 ev in the previous paper, is determined as -9.52 ev in Fig. 2. A similar discrepany is also seen for the highest occupied level of acetone.[24]

The lowest vacant level (V) was determined by adding the excitation energy, which was obtained from the

[8] H. D. Hunt and W. T. Simpson, J. Am. Chem. Soc. **75**, 4540 (1953).
[9] K. Bowden *et al.*, J. Chem. Soc. **39**, 45 (1946).
[10] H. Dannenberg, Z. Naturforsch. **4b**, 327 (1949).
[11] Wilds, Beck, Close, Djerassi, Johnson, Johnson, and Shunk, J. Am. Chem. Soc. **69**, 1985 (1947).
[12] Hausser, Kuhn, Smakula, and Hoffer, Z. physik. Chem. **B29**, 371 (1935).
[13] A. Smakula and A. Wassermann, Z. physik Chem. **A155**, 353 (1931).
[14] C. M. Moser and A. Kohlenberg, J. Chem. Soc. 804 (1951).
[15] H. Shüller, Z. Naturforsch. **3a**, 313 (1948).
[16] H. L. McMurry, J. Chem. Phys. **9**, 231 (1941).
[17] H. Baba, J. Chem. Soc. Japan **72**, 214 (1951).
[18] S. Nagakura, Bull. Chem. Soc. Japan **25**, 164 (1952).
[19] For instance, A. D. Walsh, Trans. Faraday Soc. **42**, 62 (1946). This paper is concerned with benzaldehyde.
[20] J. D. Morrison and A. J. C. Nicholson, J. Chem. Phys. **20**, 1021 (1952).
[21] The ionization potential of dimethylamine was obtained by subtracting 0.2 ev from that of methylamine determined by Morrison (reference 20). According to the measurement of Sugden, Walsh, and Price [Nature **148**, 272 (1941)], the difference in the ionization potential between methylamine and dimethylamine is 0.2 ev.
[22] R. E. Honig, J. Chem. Phys. **16**, 105 (1948).
[23] W. C. Price and A. D. Walsh, Proc. Roy. Soc. (London) **A147**, 220 (1940).
[24] The ionization potential value of nitromethane was determined as 11.32 ev by J. D. Morrison (private communication from Dr. Morrison). It was our careless mistake that the highest occupied level of nitromethane was estimated as -10.50 ev in the previous paper. See reference 1.

TABLE II. Calculated and observed values of the energy difference (ΔE) between W_n and W_e.

X	XNO_2 obs. (ev)	XNO_2 calc. (ev)	XNO_2 calc. (ev)[a]	$XCOCH_3$ obs. (ev)	$XCOCH_3$ calc. (ev)	XCOOH obs. (ev)	XCOOH calc. (ev)
$-NH_2$	5.49[b]	5.61	5.93	7.19	7.36	...	...
$-N(CH_3)_2$	5.14	4.86	4.87	6.52	6.53	...	...
$-CH=CHCH_3$	5.39	4.24	5.28	5.51	5.76	5.94	6.00
$-CH=CHCH=CHCH_3$	4.41	3.22	4.18	4.56	4.64	4.73	4.89
	4.92	3.62	4.71	5.21	5.09	5.37	5.45
	4.32	3.20	4.24	4.62	4.63	4.92	4.97
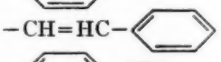	4.13	3.23	4.20	4.32	4.65	4.44 4.425	4.92
	3.86	...	...	4.17	...	4.46	...

[a] Values calculated by assuming V_{NO_2} as -5.5 ev.
[b] This value, observed with the aqueous solution, will become considerably larger in an inert solvent.

electronic absorption spectrum, to the highest occupied level (H).

It is seen from Fig. 2 and the reason described in the previous paper[1] that the interaction between the highest occupied level of the electron donating group (H_X) and the lowest vacant one of the electron accepting group (V_A) is important[25] and, as the result of it, two new levels W_n and W_e occur. Moreover, according to a simple quantum mechanical calculation, W_n, W_e and the difference between them (ΔE) can be represented approximately by the following equations:

$$W_n=\tfrac{1}{2}\{H_X+V_A-[(H_X-V_A)^2+4C_X^2C_A^2\beta^2]^{\frac{1}{2}}\}, \quad (1)$$

$$W_e=\tfrac{1}{2}\{H_X+V_A+[(H_X-V_A)^2+4C_X^2C_A^2\beta^2]^{\frac{1}{2}}\}, \quad (2)$$

$$\Delta E=[(H_X-V_A)^2+4C_X^2C_A^2\beta^2]^{\frac{1}{2}}, \quad (3)$$

where β is the resonance integral, and C_X and C_A are the coefficients of appropriate atomic orbitals in the highest occupied orbital of the electron donating group and in the lowest vacant one of the electron accepting group, respectively. In the present calculation, β is assumed to be 3 ev and C_X and C_A can be obtained by the simple LCAO method.[26] Furthermore, the oscillator strength f for the transition between W_n and W_e can be calculated by the following equation[1]:

$$f=(4.704\times10^{-7})\nu\left(e\int\psi_N r\psi_E d\tau\right)^2, \quad (4)$$

where ψ_N and ψ_E are the orbital wave functions for the levels W_n and W_e, respectively, which are represented by the linear combination of molecular orbital functions for levels, H_X and V_A, and ν is the energy difference between these two levels represented in units of cm^{-1}.

[25] The reason for this was explained in detail in the previous paper. For instance, the interaction between the highest occupied levels of electron donating and electron accepting groups may probably be negligibly small, because H_A is the level of the nonbonding electron in the oxygen atom.

[26] The author expresses his sincere thanks to Mr. H. Tsubomura and Mr. J. Tanaka for their kindness in giving information about their calculations for styrene and phenol.

The values of ΔE and f evaluated by the combination of Eqs. (3) and (4), and H_X and V_A given in Fig. 2 are tabulated in Tables II and III. In these tables, the observed values are also shown for the purpose of comparison.

Inspection of Table II shows that in the case of carbonyl and carboxyl compounds, there is good agreement between observed and theoretical values of ΔE but in the case of nitro compounds the theoretical values are generally smaller than the experimental ones. As a possible reason for this, the following two facts should be considered. One reason is that the absolute value of the resonance integral may be larger for the nitro compound than that for the other compounds, and another is that the level V_A may be too low for this compound. Generally speaking, it is sure that the present approximation in which V_A given in Fig. 2 is used instead of the Coulomb integral $\alpha_A=\int\varphi_A H\varphi_A d\tau$ (φ_A is the molecular orbital wave function for the level V_A) is not always right. In other words, it turns out that the value of V_A should become higher than that given in Fig. 2, because of the repulsion energy between

TABLE III. Calculated and observed values of the oscillator strength (f).[a, b]

Compound	Obs.	Calc.
$O_2N-CH=CHCH_3$	0.35	0.20
$O_2N-CH=CHCH=CHCH_3$	0.38	0.36 (*trans*) 0.25 (*cis*)
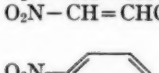	0.21	0.28
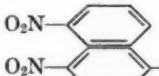	0.24	0.36
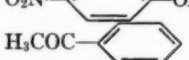	0.26	0.36
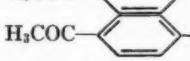	0.35	0.48

[a] The observed values of f were obtained from the absorption curve by use of the following equation: $f=4.32\times10^{-9}\epsilon\Delta\nu$.
[b] f values for nitro compounds were calculated by assuming V_{NO_2} as -5.50 ev.

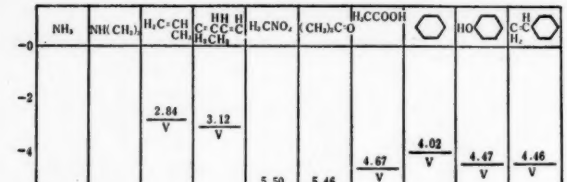

FIG. 2. Molecular energy level diagrams.

electrons.[27] In fact, we are led to good accordance between calculated and observed values of ΔE for the nitro compounds, too, by estimating the V_{NO_2} value at -5.5 ev[28] (see Table II).

DISCUSSION OF THE RESULT

It is seen from Tables II and III that the agreements between the observed and calculated values are sufficiently good for both the wavelength and the oscillator strength.[29] This seems to suggest that the present treatment on the basis of the energy level diagram is, in spite of its simplicity, very powerful for the interpretation of the absorption spectra of this kind. In addition to this, it can easily be shown that there is intimate relation between the present treatment and the earlier one from the resonance viewpoint. According to the latter, the above mentioned absorption spectra can be explained by resonance between the nonpolar and polar structures, such as HO—⟨⟩—NO_2 and HO^+=⟨⟩=NO_2^- for *p*-nitrophenol. In that case, it is well known that the normal and excited states are principally constructed from the nonpolar and the polar structures, respectively. According to the present method,[1] the change of the charge distribution in levels W_n and W_e caused by electron migration can be evaluated with nitramide and *p*-nitrophenol as shown in Fig. 3. The results apparently show that in the level W_e the electron migration is conspicuously larger than in the level W_n, and that the former corresponds to the polar structure and the latter to the nonpolar one. Therefore, it may be expected that both methods lead to similar conclusions qualitatively. Moreover, in my opinion, the present method seems to be superior in that absorption spectra of many compounds[30] can be explained systematically and quantitatively, or at least semiquantitatively, by such simple theoretical considerations.

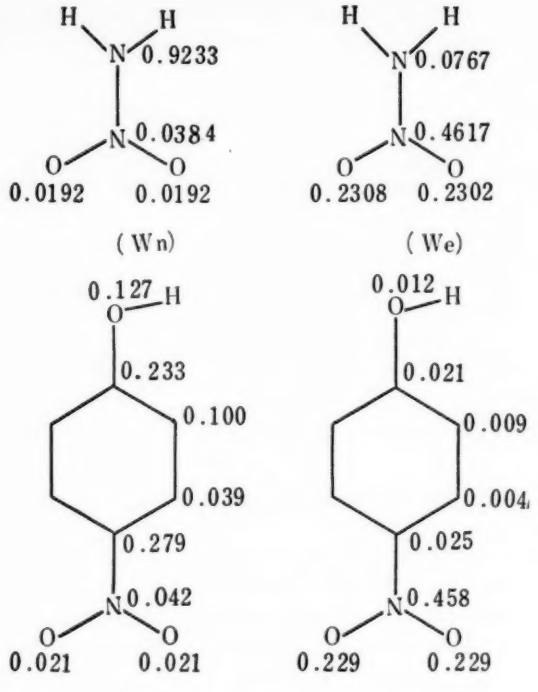

FIG. 3. Distributions of a migrating electron in levels W_n and W_e of nitramide and *p*-nitrophenol.

In this connection, one more point should be mentioned. As seen clearly from the distributions of a migrating electron given in Fig. 3, the transition from

[27] In the present approximation, the Coulomb integral α_A can be represented more exactly by the following equation:

$$\alpha_A=\int\varphi_A H\varphi_A d\tau=\int\varphi_A H_A{}^+\varphi_A d\tau+\int\varphi_A V_X{}^+\varphi_A d\tau+R.$$

The first term on the right-hand side of the above equation can be set equal to V_A, the second represents the attraction energy due to the X^+ group, and the third the increment of the interelectronic repulsion energy. The sum of the first and the third terms may be regarded as equal to the electron affinity (E_A). So α_A may be written as follows:

$$\alpha_A=V_A+\int\varphi_A V_X{}^+\varphi_A d\tau+R=E_A+\int\varphi_A V_X{}^+\varphi_A d\tau.$$

In some cases, it may be expected that both energy terms $\int\varphi_A V_X{}^+\varphi_A d\tau$ and R can compensate each other and α_A becomes almost equal to V_A. But in general α_A is probably higher than V_A and lower than E_A. The author wishes to express his sincere thanks to Professor Mulliken for his kindness in giving helpful advice about this subject.

[28] This value was determined in such a way as to explain the experimental values of ΔE for various nitro compounds as satisfactorily as possible.

[29] The wavelength of the absorption maximum under consideration is strongly dependent on the solvent. It shifts to long wavelengths in water and alcohol compared with *n*-hexane or other inert solvents. For instance, λ_{max} for nitrobenzene is 251, 259, and 268 mμ in naphtha, alcohol, and water, respectively. Therefore, it may be expected that experimental values of ΔE for H_2NNO_2, $H_2CCH=CHCH=CHNO_2$, etc. should be larger in the inert solvent than those given in Table II. Taking into consideration these ambiguities of experimental results, it seems to be of no significance to expect better accordance between theoretical and experimental values of ΔE.

[30] In the present paper, the treatment is restricted to *p*-derivatives alone and *o*- and *m*- derivatives are not taken into consideration. But it seems to be possible to explain similar absorptions observed with these two derivatives on the basis of the molecular energy level diagram. This problem will be discussed in detail in a later paper.

W_n to W_e should be accompanied by electron transfer from the electron donating group to the electron accepting one. Hence the absorption under consideration may be called an intramolecular charge transfer spectrum. The present method, which was applied to intramolecular charge transfer spectra with success, may also be useful for the interpretation of intermolecular charge transfer spectra developed by Mulliken.[31] In fact, the relation between the ionization potential of the electron donating molecule and the wavelength of the absorption characteristic for molecular compounds, which was pointed out by McConnell, Hastings, *et al.*,[32,33] is explained easily by the use of Eq. (3). For instance, the relationship between them, which was observed with molecular compounds involving iodine as the electron acceptor can be interpreted almost satisfactorily by assuming the lowest vacant level of iodine (V_{I_2}) as -6.0 ev. This value is only a little higher compared with that (-7.0 ev) determined by the present method, namely by the combination of the ionization potential and electronic absorption spectrum of the iodine molecule,[34] but very much lower than that (-1.8 ev) determined from the electron affinity.[31,32]

There is no ionization potential value observed with aniline. Therefore it is impossible to calculate ΔE values for *p*-nitroaniline, *p*-aminoacetophenone, and *p*-aminobenzoic acid. But, using the experimental values of ΔE and Eq. (3), the ionization potential of aniline can be predicted. Actually it is estimated as 8.76, 8.73, and 8.62 ev from ΔE values for *p*-nitroaniline, *p*-aminoacetophenone, and *p*-aminobenzoic acid, respectively. Whether these values are reasonable or not, cannot be determined conclusively till the experimental value is obtained by the electron impact method, but they seem to be considerably reasonable in comparison with ionization potential values of other monosubstituted benzene molecules.

[31] R. S. Mulliken, J. Am. Chem. Soc. **72**, 600 (1950); **74**, 811 (1952).
[32] McConnell, Ham, and Platt, J. Chem. Phys. **21**, 66 (1953).
[33] Hastings, Franklin, Shiller, and Matsen, J. Am. Chem. Soc. **75**, 2900 (1953).
[34] S. Nagakura and J. Tanaka, J. Chem. Soc. Japan **75**, 933 (1954).

THE JOURNAL OF CHEMICAL PHYSICS VOLUME 23, NUMBER 8 AUGUST, 1955

Ionic Conductance of Some Solid Metallic Azides

P. W. M. JACOBS AND F. C. TOMPKINS
Imperial College of Science and Technology, University of London, South Kensington, London, S.W.7, England
(Received November 8, 1954)

Measurements of the ionic conductance of several metallic azides have shown an unusually low activation energy for the structure sensitive conductance in potassium, calcium, and strontium azides. This is here associated with the mobility of surface lattice defects.

THE ionic conductance of solid Li, Na, K, Ca, Sr, and Ba azides has been measured over as wide a temperature range as possible and the activation energies for conductance obtained. These measurements were made in order to test Mott's theory[1] of the growth of nuclei during thermal decomposition and also as part of a general program concerned with relating the ease of thermal decomposition to physical properties (conductance, absorption spectra before and after coloration, etc.). Particular attention has been devoted to the potassium salt, since an abnormally low activation energy observed in the lower temperature region could not be interpreted on the basis of the Koch and Wagner mechanism[2] and has been ascribed to a migration energy for the surface conductance of defects. An approximate calculation of the migration energy supports this conclusion.

EXPERIMENTAL AND RESULTS

The details of the conductance apparatus and procedure and the methods of preparing the azides have been described in previous papers.[3,4] All the salts examined obeyed the general equation

$$\log\kappa = \log A - \frac{E}{2.303RT}, \qquad (1)$$

where κ is the specific conductance in ohm^{-1} cm^{-1}, A is a constant, and E the activation energy for the conductance process in kcal/mole. The results are summarized in Table I, where each value of E and $\log A$ represents the mean of at least three series of determinations. The maximum deviations from the mean values of E are ± 0.3 percent for Li, Na, and K azides and ± 1.2 percent for Ca, Sr, and Ba azides, the accuracy

[1] N. F. Mott, Proc. Roy. Soc. (London) **A172**, 325 (1939).
[2] E. Koch and C. Wagner, Z. physik. Chem. **B38**, 295 (1937).
[3] P. W. M. Jacobs and F. C. Tompkins, Proc. Roy. Soc. (London) **A215**, 254 (1952).
[4] P. W. M. Jacobs, J. Sci. Instr. **30**, 204 (1953).

being lower for the alkaline earths because of their lower specific conductance. The above values of A and E for potassium azide differ slightly from those given in a previous paper[3] which referred to three runs on a single preparation. The results given here represent the mean for eleven runs on four different preparations and are considered to be of greater accuracy. The results for potassium azide are shown separately in Fig. 1. The reproducibility is satisfactory for preparations precipitated from carefully neutralized solutions (phenol phthalein). Included in this plot are results obtained using KN_3 precipitated from solutions containing CO_3^{2-} ions. This has the effect of lowering the conductance, although the temperature coefficient remains unaltered. Many attempts to incorporate divalent cation impurities in KN_3 by co-precipitation were unsuccessful.

DISCUSSION

For many salts the plot of $\log\kappa$ against $1/T$ shows two linear sections associated with activation energies E_1 (for the low-temperature region) and E_2. These have been related to the energies for migration of the mobile species (E_0) and for creation of defects (W_0) by the equations

$$E_1=E_0, \quad E_2=E_0+\tfrac{1}{2}W_0. \tag{2}$$

As a provisional hypothesis, we assume that in our temperature range the alkali azides are predominantly catonic conductors and that the conducting species are

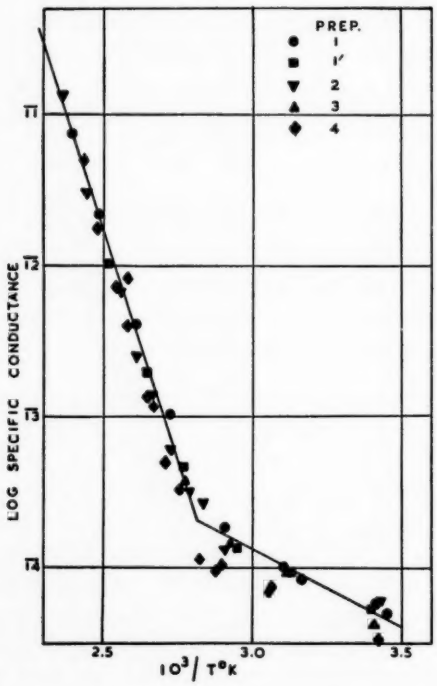

FIG. 1. Ionic conductance of various preparations of potassium azide as a function of temperature. Preparation 1, neutral solution; 1', same preparation as 1 but pre-irradiated with ultraviolet light; 2, excess acid; 3, neutral solution; 4, potassium carbonate added.

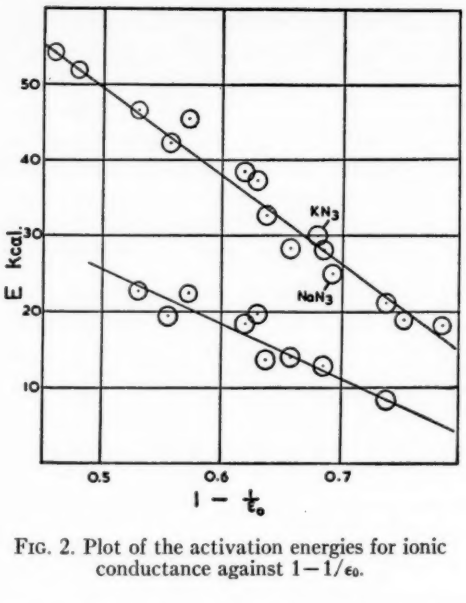

FIG. 2. Plot of the activation energies for ionic conductance against $1-1/\epsilon_0$.

cation vacancies rather than interstitial cations. By comparison with the values for the alkali halides, the experimental activation energies E of 19.1, 25.0, and 30.1 kcal/mole for the Li, Na, and K azides appear to be E_2-values and this is supported by the plots of E_2 and E_1 against $1-1/\epsilon_0$, where ϵ_0 is the high-frequency dielectric constant, shown in Fig. 2. The dielectric constants of KN_3 and NaN_3 are not given in the literature and were therefore interpolated from the smooth curve obtained by plotting the wavelength of the ultraviolet absorption edge against ϵ_0 (data for 11 salts being available). The points for KN_3 and NaN_3 lie quite definitely on the E_2-line. Unfortunately, we have no knowledge of ϵ_0 for LiN_3, but the value of E of 19.1 kcal is comparable with that of E_2 for LiI (21.2 kcal) but much larger than that of E_1 for this salt (8.4 kcal).

The experimental E-values found for the alkaline earth azides are of a lower order of magnitude and could refer to E_1. In the other salts containing divalent cations for which transport numbers have been determined,[5] the majority ($BaCl_2$, $BaBr_2$, BaI_2, $PbCl_2$, and $PbBr_2$) show an anion transport number of unity: E_1 may therefore be the activation energy for the mobility of anion vacancies in BaN_6 but the generally low values found for the divalent azides indicate that these are most probably for ions in special positions.

Since the corresponding values for KCl, KBr, and KI are 22.8, 22.4, and 19.6 kcal/mole, respectively, the low temperature value of 4.5 kcal/mole in KN_3 is unlikely to be that for the activation energy for the bulk migration of cation vacancies. This is supported by an independent estimate of E_1. The energy required to create a pair of vacancies is given by

$$W_0=W_L-W_P \tag{3}$$

[5] P. W. M. Jacobs and F. C. Tompkins, Quart. Rev. 6, 238 (1952).

where W_L is the lattice energy per ion pair and W_P the total polarization energy ($W_P^+ + W_P^-$). The lattice energy of potassium azide can be calculated from the following thermochemical data:

$$\Delta H°_f KN_3(c) = -1.4 \text{ kcal/mole}^{6}$$
$$\Delta H°_f N_3^-(g) = 31 \text{ kcal/mole}^{6}$$
$$\Delta H°_f K^+(g) = 120.9 \text{ kcal/mole.}^{7}$$

Using a Born-Haber cycle, we find $W_L = 153$ kcal/mole. The polarization energy W_P may be estimated only indirectly. In general, two methods exist for the calculation of W_P. In that due to Jost,[8] the creation of a vacant site is regarded as equivalent to scooping out a hole of radius R in a medium of uniform dielectric constant ϵ_0. The polarization energy resulting is

$$W_P = \left(1 - \frac{1}{\epsilon_0}\right)\frac{e^2}{2R}. \quad (4)$$

This method should be independent of the type of crystal lattice, but the difficulty lies in choosing values for R^+ and R^-. Mott and Littleton[9] have improved Jost's method by calculating the dipoles on the nearest and next-nearest neighbors directly in a NaCl-type lattice, and applying Jost's formula to the rest of the lattice. Their method involves a great deal of calculation not justified by our present needs and moreover can only be applied in its present form to f.c.c. lattices. Accordingly, we have estimated the polarization energy indirectly by plotting the experimental values for the alkali and silver halides given by $W_L - 2(E_2 - E_1)$ against $(1 - 1/\epsilon_0)1/a$, where a is the anion-cation distance. If $R^+ + R^-$ is proportional to a, these results should all lie on a straight line. As shown in Fig. 3, this is approximately true, particularly at the higher values of the dielectric constants, the maximum deviation being +5 percent for NaCl. The polarization energy in KN_3 obtained by interpolation from Fig. 3 is 134 kcal. Hence $W_0 = 19$ kcal and $E_1 = 20.5$ kcal,

TABLE I. Values of the constants in the conductance equation.

Salt	Temp. range °K	log$A$	E kcal/mole
LiN_3	300–370	0.840	19.1
NaN_3	375–490	0.490	25.0
KN_3	390–500	4.59	30.1
CaN_6	290–370	−9.56	5.3
SrN_6	300–380	−10.70	5.1
BaN_6	295–380	−5.99	11.6

[6] P. Gray and T. Waddington (private communication).
[7] R. R. Bichowsky and F. D. Rossini, *Thermochemistry of Chemical Substances* (Reinhold Publishing Corporation, New York, 1936).
[8] W. Jost, J. Chem. Phys. **1**, 466 (1953).
[9] N. F. Mott and M. J. Littleton, Trans. Faraday Soc. **34**, 385 (1938).

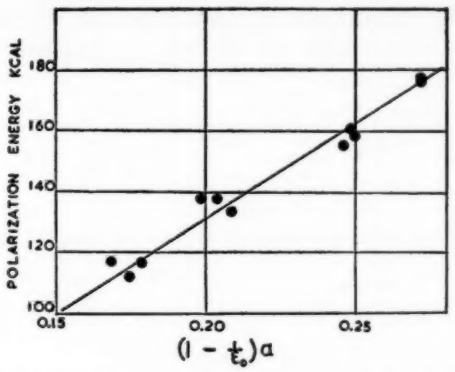

FIG. 3. Plot of the polarization energy, calculated from the lattice energies and activation energies for conductance, against $(1 - 1/\epsilon_0)a$.

which is of the order expected. It is therefore most unlikely that the experimental value of 4.5 kcal refers to E_1 and we conclude that this energy refers rather to the mobility of surface vacancies, as first suggested by Smekal.[10] The low values found in Ca, Sr, and Ba azides are also considered to refer to surface conductance.

On this basis, one would expect three regions corresponding to surface conductance, the usual bulk structure-sensitive conductance, and the characteristic conductance of the salt, with activation energies of 4.5 kcal, about 20 kcal and 30 kcal, respectively. In practice only the first and last of these two can be differentiated, although the transition region is somewhat diffuse (Fig. 1). It may be that the bulk structure-sensitive conductance is not differentiated because of a fortuitous combination of the values of the activation energies and the number of vacant sites. If we calculate the value of the activation energy necessary for bulk conductance such that this represents one percent of the surface conductance at the temperature at which the characteristic conductance begins to be appreciable then we find a value of 18 kcal in substantial agreement with the value estimated from the polarization energy. The hypothesis of surface conductance has received further confirmation from the agreement between the number of vacant sites in the surface layers calculated from the conductance data and from the rate of photolysis of potassium azide.[3]

The conditions of preparation of the azide would be expected to cause variation in surface conductance. In presence of CO_3^{2-}, or with excess OH^- in presence of air, leading to CO_3^{2-}, the divalent anion is preferentially attached to normal surface anion sites producing additional anion vacancies (to maintain electroneutrality) and reducing the number of cation vacancies by pair formation. The number of mobile charged carriers is thus reduced and consequently the conductance is smaller than in the "neutral" salt.

[10] A. Smekal, Z. physik. Chem. **B**, 442 (1931).

Perturbation Method for the Calculation of Molecular Vibration Frequencies. II. Generalization of the Theory

P. W. Higgs
Wheatstone Physics Laboratory, King's College, Strand, London, W. C. 2, England
(Received November 4, 1954)

The perturbation theory developed previously for calculating frequencies by Wilson's F and G matrix method is now generalized in two respects: the effects, on the one hand, of degeneracy amongst the approximate frequencies and, on the other, of interaction constants coupling the two classes of vibration are considered.

I. INTRODUCTION

IN a previous paper,[1] which will be referred to here as I, a method was described for obtaining the roots λ of the nth order determinantal equation

$$|\mathbf{GF}-\lambda\mathbf{I}|=0, \tag{1}$$

in which $\mathbf{F}$ and $\mathbf{G}$ are, respectively, the potential and inverse kinetic energy matrices for a molecule and $\lambda=4\pi^2\nu^2$ where ν is a vibration frequency, as an infinite series in the eigenvalues and eigenvectors of two secular equations of orders n_A and n_B, where $n_A+n_B=n$. These simpler equations were obtained by partitioning the vector $\mathbf{y}$ of internal coordinates describing the motion into two classes:

$$\mathbf{y}=\begin{pmatrix}\mathbf{y}_A\\ \mathbf{y}_B\end{pmatrix}, \tag{2}$$

in which the A and B coordinates are those involved mainly in high- and low-frequency modes, respectively. The equations which have to be solved are then

$$\mathbf{x}_A\mathbf{G}_{AA}\mathbf{F}_{AA}=\lambda^0{}_A\mathbf{x}_A, \tag{3a}$$

$$\mathbf{x}_B\mathbf{G}^*{}_{BB}\mathbf{F}_{BB}=\lambda^1{}_B\mathbf{x}_B, \tag{3b}$$

in which $\mathbf{x}_A$, $\mathbf{x}_B$ are row eigenvectors, the F and G matrices have been partitioned according to the scheme (2) and

$$\mathbf{G}^*{}_{BB}=\mathbf{G}_{BB}-\mathbf{G}_{BA}\mathbf{G}_{AA}{}^{-1}\mathbf{G}_{AB}; \tag{4}$$

the eigenvalues $\lambda^0{}_A$, $\lambda^1{}_B$ correspond to approximate values of the high and low frequencies (ν_A,ν_B), respectively. The actual method of performing the separation into A and B frequencies is to a large extent arbitrary; to lead to a rapidly convergent series for the exact eigenvalues, the sets $\lambda^0{}_A$, $\lambda^1{}_B$ must be well separated.

In I two assumptions were made: the first was that the solutions of Eq. (3) are nondegenerate; the second was that

$$\mathbf{F}_{AB}=\mathbf{0}. \tag{5}$$

The purpose of this paper is to remove these unnecessarily restrictive assumptions.

[1] P. W. Higgs, J. Chem. Phys. **21**, 1131 (1953).

II. REMOVAL OF DEGENERACIES

Let $\lambda^0{}_{Ai}$ be an eigenvalue of Eq. (3a) of degeneracy d_{Ai} $(\sum_i d_{Ai}=n_A)$ and let $\mathbf{x}_{Ai\alpha}$ $(\alpha=1$ to $d_{Ai})$ be one of the corresponding eigenvectors; similarly, let $\lambda^1{}_{Bj}$ be an eigenvalue of Eq. (3b) of degeneracy d_{Bj} $(\sum_j d_{Bj}=n_B)$ and let $\mathbf{x}_{Bj\beta}$ $(\beta=1$ to $d_{Bj})$ be one of the corresponding eigenvectors. Then, as in I, these vectors may be shown to be orthogonal in the sense that

$$\mathbf{x}_{Ai\alpha}\mathbf{G}_{AA}\mathbf{x}'_{Ah\gamma}=0 \quad (h\neq i),$$

$$\mathbf{x}_{Bj\beta}\mathbf{G}^*{}_{BB}\mathbf{x}'_{Bk\delta}=0 \quad (k\neq i).$$

Moreover, the eigenvectors of a degenerate set may be *made* orthogonal by the Schmidt process: if this is done, then

$$\mathbf{x}_{Ai\alpha}\mathbf{G}_{AA}\mathbf{x}'_{Ai\gamma}=0 \quad (\gamma\neq\alpha),$$

$$\mathbf{x}_{Bj\beta}\mathbf{G}^*{}_{BB}\mathbf{x}'_{Bj\delta}=0 \quad (\delta\neq\beta).$$

After normalization according to the convention

$$\mathbf{x}_{Ai\alpha}\mathbf{G}_{AA}\mathbf{x}'_{Ai\alpha}=1,$$

$$\mathbf{x}_{Bj\beta}\mathbf{G}^*{}_{BB}\mathbf{x}'_{Bj\beta}=1$$

all the vectors may be put together, as in I, to form regular square matrices $\mathbf{X}_A$, $\mathbf{X}_B$ which are solutions of the eigenvalue equations in the form

$$\left.\begin{aligned}\mathbf{X}_A\mathbf{G}_{AA}\mathbf{F}_{AA}&=\mathbf{\Lambda}^0{}_A\mathbf{X}_A,\\ \mathbf{X}_B\mathbf{G}^*{}_{BB}\mathbf{F}_{BB}&=\mathbf{\Lambda}^1{}_B\mathbf{X}_B,\end{aligned}\right\} \tag{6}$$

where

$$\mathbf{\Lambda}^0{}_A=\text{diag }(\lambda^0{}_{Ai};\ d_{Ai}\text{ times}),$$

$$\mathbf{\Lambda}^1{}_B=\text{diag }(\lambda^1{}_{Bj};\ d_{Bj}\text{ times}),$$

and which satisfy the conditions

$$\left.\begin{aligned}\mathbf{X}_A\mathbf{G}_{AA}\mathbf{X}'_A&=\mathbf{I}_A,\\ \mathbf{X}_B\mathbf{G}^*{}_{BB}\mathbf{X}'_B&=\mathbf{I}_B,\end{aligned}\right\} \tag{7}$$

where $\mathbf{I}_A$, $\mathbf{I}_B$ are unit matrices of orders n_A, n_B.

As before, we may transform Eq. (1) into the form

$$|\mathbf{H}-\lambda\mathbf{I}|=0 \tag{8}$$

by pre- and postmultiplying **GF** and **I** by the matrices **P** and **Q**, respectively, defined by the equations

$$\mathbf{P}=\begin{pmatrix}\mathbf{X}_A, & \mathbf{0}\\ -\mathbf{X}_B\mathbf{G}_{BA}\mathbf{G}^{-1}{}_{AA}, & \mathbf{X}_B\end{pmatrix},$$

$$\mathbf{Q}=\begin{pmatrix}\mathbf{G}_{AA}\mathbf{X}'_A, & \mathbf{0}\\ \mathbf{G}_{BA}\mathbf{X}'_A, & \mathbf{G}^*{}_{BB}\mathbf{X}'_B\end{pmatrix}.$$

If, for the present, we retain condition (5), then

$$\mathbf{GF}=\begin{pmatrix}\mathbf{G}_{AA}\mathbf{F}_{AA}, & \mathbf{G}_{AB}\mathbf{F}_{BB}\\ \mathbf{G}_{BA}\mathbf{F}_{AA}, & \mathbf{G}_{BB}\mathbf{F}_{BB}\end{pmatrix}, \tag{9}$$

and with the aid of Eq. (6) we obtain the transformed matrix in the form

$$\mathbf{H}=\mathbf{PGFQ}=\begin{pmatrix}\mathbf{\Lambda}^0{}_A+\mathbf{\Gamma}_{AB}\mathbf{\Lambda}^1{}_B\mathbf{\Gamma}_{BA}, & \mathbf{\Gamma}_{AB}\mathbf{\Lambda}^1{}_B\\ \mathbf{\Lambda}^1{}_B\mathbf{\Gamma}_{BA}, & \mathbf{\Lambda}^1{}_B\end{pmatrix}, \tag{10}$$

where

$$\left.\begin{aligned}\mathbf{\Gamma}_{AB}&=\mathbf{X}_A\mathbf{G}_{AB}\mathbf{X}'_B,\\ \mathbf{\Gamma}_{BA}&=\mathbf{\Gamma}'_{AB}.\end{aligned}\right\} \tag{11}$$

So far the analysis has not differed in any essential respect from that of Paper I. It is when we come to consider the perturbation series that differences arise, for now we have to remove the degeneracies. Let the series for the exact eigenvalues of Eq. (1) be

$$\lambda_{Ai\rho}=\lambda^0{}_{Ai}+\lambda^1{}_{Ai\rho}+\lambda^2{}_{Ai\rho}+\cdots\text{etc.},$$

$$\lambda_{Bj\sigma}=\lambda^1{}_{Bj}+\lambda^2{}_{Bj\sigma}+\lambda^3{}_{Bj\sigma}+\cdots\text{etc.}$$

Then by applying the ordinary matrix perturbation theory for degenerate eigenvalues to the problem we arrive at the following formulas for the first correction terms:

$\lambda^1{}_{Ai\rho}$ is one of the d_{Ai} roots of the equation

$$|H^1{}_{Ai\alpha,\,Ai\gamma}-\lambda^1{}_{Ai\rho}\delta_{\alpha\gamma}|=0,$$

that is,

$$|\mathbf{x}_{Ai\alpha}\mathbf{G}_{AB}\mathbf{F}_{BB}\mathbf{G}_{BA}\mathbf{x}'_{Ai\gamma}-\lambda^1{}_{Ai\rho}\delta_{\alpha\gamma}|=0 \tag{12a}$$

or

$$|\sum_{j,\beta}\{\Gamma_{Ai\alpha,\,Bj\beta}\lambda^1{}_{Bj}\Gamma_{Bj\beta,\,Ai\gamma}\}-\lambda^1{}_{Ai\rho}\delta_{\alpha\gamma}|=0. \tag{13a}$$

$\lambda^2{}_{Bj\sigma}$ is one of the d_{Bj} roots of the equation

$$|\sum_{i,\alpha}\{H^1{}_{Bj\beta,\,Ai\alpha}H^1{}_{Ai\alpha,\,Bj\delta}/(\lambda^0{}_{Bj}-\lambda^0{}_{Ai})\}-\lambda^2{}_{Bj\sigma}\delta_{\beta\delta}|=0,$$

that is,

$$|\{-\mathbf{x}_{Bj\beta}\mathbf{G}^*{}_{BB}\mathbf{F}_{BB}\mathbf{G}_{BA}\mathbf{G}^{-1}{}_{AA}\mathbf{F}^{-1}{}_{AA}\mathbf{G}^{-1}{}_{AA}\mathbf{G}_{AB}\mathbf{F}_{BB}\mathbf{G}^*{}_{BB}\mathbf{x}'{}_{Bj\delta}\}-\lambda^2{}_{Bj\sigma}\delta_{\beta\delta}|=0 \tag{12b}$$

or

$$|-(\lambda^1{}_{Bj})^2\sum_{i,\alpha}\{\Gamma_{Bj\beta,\,Ai\alpha}(\lambda^0{}_{Ai})^{-1}\Gamma_{Ai\alpha,\,Bj\delta}\}-\lambda^2{}_{Bj\sigma}\delta_{\beta\delta}|=0. \tag{13b}$$

More complicated expressions may be obtained for the second correction terms. The form of these depends upon whether the degeneracy has been entirely removed by the first correction.

III. INCLUSION OF INTERACTION CONSTANTS

The other restrictive assumption made thus far, which is also readily removed, is the condition (5), which states that all potential constants for interaction of the coordinates of class A with those of class B are to be neglected. It is often useful to consider the effect upon the frequencies of such interaction constants and, as they are usually small, they may be treated by perturbation theory as an additional means of coupling between the A and B systems.

If $\mathbf{F}_{AB}$ is retained in the F matrix, the product **GF** no longer has the simple form (9) but is now given by the expression

$$\mathbf{GF}=\begin{pmatrix}\mathbf{G}_{AA}\mathbf{F}_{AA}+\mathbf{G}_{AB}\mathbf{F}_{BA}, & \mathbf{G}_{AA}\mathbf{F}_{AB}+\mathbf{G}_{AB}\mathbf{F}_{BB}\\ \mathbf{G}_{BA}\mathbf{F}_{AA}+\mathbf{G}_{BB}\mathbf{F}_{BA}, & \mathbf{G}_{BA}\mathbf{F}_{AB}+\mathbf{G}_{BB}\mathbf{F}_{BB}\end{pmatrix}. \tag{14}$$

After transformation by **P** and **Q** this matrix becomes

$$\mathbf{H}=\begin{pmatrix}\mathbf{\Lambda}^0{}_A+\mathbf{\Gamma}_{AB}\mathbf{\Phi}_{BA} & \\ +\mathbf{\Phi}_{AB}\mathbf{\Gamma}_{BA}+\mathbf{\Gamma}_{AB}\mathbf{\Lambda}^1{}_B\mathbf{\Gamma}_{BA}, & \mathbf{\Phi}_{AB}+\mathbf{\Gamma}_{AB}\mathbf{\Lambda}^1{}_B,\\ \mathbf{\Phi}_{BA}+\mathbf{\Lambda}^1{}_B\mathbf{\Gamma}_{BA}, & \mathbf{\Lambda}^1{}_B\end{pmatrix} \tag{15}$$

in which

$$\left.\begin{aligned}\mathbf{\Phi}_{AB}&=\mathbf{X}_A\mathbf{G}_{AA}\mathbf{F}_{AB}\mathbf{G}^*{}_{BB}\mathbf{X}'_B,\\ \mathbf{\Phi}_{BA}&=\mathbf{\Phi}'_{AB}.\end{aligned}\right\} \tag{16}$$

The transformed secular equation is again Eq. (8), but with **H** now defined by Eq. (15).

In applying perturbation theory we now treat $\mathbf{\Phi}_{AB}$ as a first-order quantity in addition to $\mathbf{\Lambda}^1{}_B$. The first-order term in **H** is thus

$$\mathbf{H}^1=\begin{pmatrix}\mathbf{\Gamma}_{AB}\mathbf{\Phi}_{BA}+\mathbf{\Phi}_{AB}\mathbf{\Gamma}_{BA}+\mathbf{\Gamma}_{AB}\mathbf{\Lambda}^1{}_B\mathbf{\Gamma}_{BA}, & \mathbf{\Phi}_{AB}+\mathbf{\Gamma}_{AB}\mathbf{\Lambda}^1{}_B\\ \mathbf{\Phi}_{BA}+\mathbf{\Lambda}^1{}_B\mathbf{\Gamma}_{BA}, & \mathbf{\Lambda}^1{}_B\end{pmatrix}.$$

So in the case of nondegenerate approximate frequencies the first correction terms are as follows:

$$\lambda^1{}_{Ai}=\sum_{j=1}^{nB}\Gamma_{Ai,\,Bj}(2\Phi_{Bj,\,Ai}+\lambda^1{}_{Bj}\Gamma_{Bj,\,Ai}), \quad (17a)$$

$$\lambda^2{}_{Bj}=-\sum_{i=1}^{nA}(\Phi_{Bj,\,Ai}+\lambda^1{}_{Bj}\Gamma_{Bj,\,Ai})^2/\lambda^0{}_{Ai}. \quad (17b)$$

The corresponding second corrections may be derived from the general formulas given in I in terms of $\mathbf{H}^1$ by substituting the appropriate generalized expressions for the matrix elements.

It appears now that two distinct effects contribute to the frequency shifts: potential coupling, represented by the matrix $\mathbf{\Phi}_{AB}$; and kinetic coupling, represented by $\mathbf{\Gamma}_{AB}$.

IV. MOST GENERAL CASE

As will be obvious from the foregoing sections, in the most general case of all the following equations have to be solved for the first correction terms $\lambda^1{}_{Ai\rho}$ ($\rho=1$ to d_{Ai}), $\lambda^2{}_{Bj\sigma}$ ($\sigma=1$ to d_{Bj}):

$$\Big|\sum_{j,\beta}\{\Gamma_{Ai\alpha,\,Bj\beta}\Phi_{Bj\beta,\,Ai\gamma}+\Phi_{Ai\alpha,\,Bj\beta}\Gamma_{Bj\beta,\,Ai\gamma}+\Gamma_{Ai\alpha,\,Bj\beta}\lambda^1{}_{Bj}\Gamma_{Bj\beta,\,Ai\gamma}\}-\lambda^1{}_{Ai\rho}\delta_{\alpha\gamma}\Big|=0; \quad (18a)$$

$$\Big|-\sum_{i,\alpha}\{\Phi_{Bj\beta,\,Ai\alpha}+\lambda^1{}_{Bj}\Gamma_{Bj\beta,\,Ai\alpha}\}(\lambda^0{}_{Ai})^{-1}\times\{\Phi_{Ai\alpha,\,Bj\delta}+\Gamma_{Ai\alpha,\,Bj\delta}\lambda^1{}_{Bj}\}-\lambda^2{}_{Bj\sigma}\delta_{\beta\delta}\Big|=0. \quad (18b)$$

V. ACKNOWLEDGMENTS

I would like to thank Professor H. C. Longuet-Higgins for his helpful comments during the preparation of this paper and the Royal Commission for the Exhibition of 1851 for the award of a Senior Studentship, during the tenure of which this work was carried out.

THE JOURNAL OF CHEMICAL PHYSICS VOLUME 23, NUMBER 8 AUGUST, 1955

Perturbation Method for the Calculation of Molecular Vibration Frequencies. III. Skeletal Stretching Vibrations of Normal Paraffins

P. W. Higgs*
Wheatstone Physics Laboratory, King's College, Strand, London, W.C. 2, England
(Received November 15, 1954)

The perturbation theory developed in a previous paper is applied to the skeletal vibrations of the zigzag configuration of the *n*-paraffins. By treating the CCC bending force constant as small compared with the CC stretching force constant the first-order correction to the stretching frequencies is obtained in closed form. It is compared with the corresponding term in the Kirkwood-Pitzer formula for the frequencies of long-chain paraffins.

1. INTRODUCTION

THE most stable configuration of the *n*-paraffins $H(CH_2)_nH$, and that which is the only form found in the crystalline state,[1,2] consists of a planar zigzag arrangement of the carbon skeleton and terminal hydrogens with the CH_2 groups disposed symmetrically in planes normal to the zigzag axis, all the angles being approximately tetrahedral. Attempts have been made to account for the frequencies of those in-plane modes in which the carbon skeleton suffers most of the deformation by treating the skeleton as a zigzag chain of equal point masses. If a force field containing only a single stretching constant for the CC bonds is employed, the secular equations admit of an analytic solution,[3] but the frequency spectrum obtained does not agree well with the infrared and Raman data. If a bending constant for the CCC angle is now introduced, the solution is no longer explicitly analytic but approximate expressions may be derived for long chains, where end effects are comparatively unimportant, by imposing periodic boundary conditions.[4,5] By a suitable choice of the bending constant reasonable agreement with the general features of the observed spectra may be achieved.[6]

In this paper it is shown that a treatment of the bending constant as a perturbation by the method described in an earlier paper[7] (to be referred to henceforth as I) leads to a closed analytic expression for the first-order correction to the stretching frequencies for all chain lengths. For long chains it is found that this expression tends asymptotically to the first-order term in the Kirkwood-Pitzer formula.

In Sec. 2 the problem is formulated in the F and G matrix formalism and the approximate secular equations I(5a) for the stretching frequencies are solved. In

* Now at the Department of Mathematical Physics, The University, Drummond Street, Edinburgh 8, Scotland.
[1] A. Müller, Proc. Roy. Soc. (London) **A120**, 437 (1928).
[2] C. W. Bunn, Trans. Faraday Soc. **35**, 482 (1939).
[3] J. Barriol, J. phys. radium **10**, 215 (1939).
[4] J. G. Kirkwood, J. Chem. Phys. **7**, 506 (1939).
[5] K. S. Pitzer, J. Chem. Phys. **8**, 711 (1940).
[6] Brown, Sheppard, and Simpson, Disc. Faraday Soc. **9**, 261 (1950).
[7] P. W. Higgs, J. Chem. Phys. **21**, 1131 (1953).

Sec. 3 the first-order correction term is calculated. Section 4 consists of a resumé of the Kirkwood-Pitzer solution and a comparison of that solution with the present work. The results are discussed in Sec. 5.

2. SECULAR EQUATIONS

Let us consider a regular zigzag chain of N point masses m in the xy plane, the zigzag axis lying along the x axis (see Fig. 1). We define internal coordinates for stretching and bending as follows:

y_{Ar} = increment of $(r, r+1)$ bond length ($r=1$ to $N-1$);

y_{Bs} = equilibrium bond length × increment of $(s, s+1, s+2)$ bond angle ($s=1$ to $N-2$).

Inspecting Fig. 1 we see that for small displacements the equations relating y_{Ar}, y_{Bs} to the Cartesian displacements of the masses are

$$\left.\begin{aligned} y_{Ar} &= (-x_r+x_{r+1})\sin\tfrac{1}{2}\theta+(-1)^r(y_r-y_{r+1})\cos\tfrac{1}{2}\theta,\\ y_{Bs} &= (-x_s+x_{s+2})\cos\tfrac{1}{2}\theta\\ &\quad -(-1)^s(y_s-2y_{s+1}+y_{s+2})\sin\tfrac{1}{2}\theta, \end{aligned}\right\} \quad (1)$$

where θ is the equilibrium bond angle. If we write Eqs. (1) in matrix notation as

$$\mathbf{y}=\mathbf{B}\mathbf{r},$$

where $\mathbf{r}$ is the column vector of Cartesian displacements and $\mathbf{B}$ the rectangular matrix of coefficients, then the inverse kinetic energy matrix for internal vibrations[8,9] is given by the formula

$$\mathbf{G}=\mathbf{B}\mathbf{M}^{-1}\mathbf{B}',$$

in which $\mathbf{M}$ is the diagonal matrix of atomic masses (in this problem simply $m\mathbf{I}$, where $\mathbf{I}$ is the unit matrix). From the foregoing equations we obtain the following expressions for the nonzero elements of the G matrix:

$$\left.\begin{aligned} G_{Ar,Ar} &= 2m^{-1},\\ G_{Ar,Ar+1} &= m^{-1}\cos\theta = G_{Ar,Ar-1};\\ G_{Bs,Bs} &= 2m^{-1}(2-\cos\theta),\\ G_{Bs,Bs+1} &= 2m^{-1}(1-\cos\theta) = G_{Bs,Bs-1},\\ G_{Bs,Bs+2} &= -m^{-1}\cos\theta = G_{Bs,Bs-2};\\ G_{Ar,Bs} &= -m^{-1}\sin\theta = G_{Bs,Ar}\\ &\quad (s=r-2,\ r-1,\ r,\ r+1). \end{aligned}\right\} \quad (2)$$

These formulas are special cases of those tabulated by Decius.[10]

If we suppose that the bonds are identical and assume that the force field contains only force constants k_A, k_B for stretching and bending respectively, the potential energy matrix takes on a particularly simple

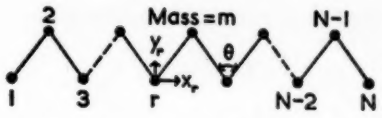

FIG. 1. Model of paraffin chain.

form in which the only nonzero elements are

$$\left.\begin{aligned} F_{Ar,Ar} &= k_A,\\ F_{Bs,Bs} &= k_B. \end{aligned}\right\} \quad (3)$$

We are interested in solving the secular equations for the row vector $\mathbf{x}$ which is related to $\mathbf{y}$ by the transformation

$$\mathbf{x}=\mathbf{y}'\mathbf{G}^{-1}.$$

Since, in a normal mode of frequency ν, $\mathbf{y}$ satisfies the relations

$$\mathbf{G}\mathbf{F}\mathbf{y}=\lambda\mathbf{y},$$

where $\lambda=4\pi^2\nu^2$, these equations are in general

$$\mathbf{x}\mathbf{G}\mathbf{F}=\lambda\mathbf{x},$$

and become in this particular problem

$$\left.\begin{aligned} \lambda x_{Ar} &= (k_A/m)\{(x_{Ar-1}\cos\theta+2x_{Ar}+x_{Ar+1}\cos\theta)\\ &\quad -\sin\theta(x_{Br-2}+x_{Br-1}+x_{Br}+x_{Br+1})\}\\ \lambda x_{Bs} &= (k_B/m)\{(-x_{Bs-2}\cos\theta+2x_{Bs-1}\sqrt{1-\cos\theta}\\ &\quad +2x_{Bs}\sqrt{2-\cos\theta}+2x_{Bs+1}\sqrt{1-\cos\theta}-x_{Bs+2}\cos\theta)\\ &\quad -\sin\theta(x_{As-1}+x_{As}+x_{As+1}+x_{As+2})\}. \end{aligned}\right\} \quad (4)$$

By setting $k_B=0$ in the first of Eqs. (4) we obtain for the approximate secular equations I(5a)

$$\lambda^0{}_A x_{Ar}=(k_A/m)\{2x_{Ar}+\cos\theta(x_{Ar-1}+x_{Ar+1})\}. \quad (5)$$

The standard method of dealing with such a linear second-order finite difference equation is to write as a trial solution

$$x_{Ar}=a\exp(ir\phi),$$

which satisfies (5) provided that

$$\lambda^0{}_A=(2k_A/m)(1+\cos\theta\cos\phi). \quad (6)$$

Obviously $\pm\phi$ give rise to the same $\lambda^0{}_A$, so the general solution for x_A is

$$x_{Ar}=a\exp(ir\phi)+b\exp(-ir\phi).$$

Now the boundary conditions which have to be imposed are

$$x_{A0}=0, \quad x_{AN}=0,$$

corresponding to the end equations $r=1$, $N-1$ of the set (5). Therefore the actual solution is

$$x_{Ar}=c\sin(r\phi) \quad (7)$$

[8] E. B. Wilson, Jr., J. Chem. Phys. **7**, 1047 (1939).
[9] E. B. Wilson, Jr., J. Chem. Phys. **9**, 76 (1941).
[10] J. C. Decius, J. Chem. Phys. **16**, 1025 (1948).

with ϕ limited to the roots of the equation

$$\sin(N\phi)=0. \tag{8}$$

The roots of (8) which give rise to distinct nontrivial solutions (7) are

$$\phi_j=j\pi/N, \quad j=1\cdots N-1. \tag{9}$$

So the approximate row vector in the jth normal mode has the form

$$x_{Ajr}=c_j\sin(jr\pi/N), \tag{10}$$

where c_j is so far arbitrary, and from (6) the jth approximate stretching frequency is given by

$$\lambda^0{}_{Aj}=(2k_A/m)\{1+\cos\theta\cos(j\pi/N)\}. \tag{11}$$

3. PERTURBATION THEORY

In order to apply the perturbation theory developed in I we must normalize our solution according to convention I (6a),

$$\mathbf{x}_{Aj}\mathbf{G}_{AA}\mathbf{x}'_{Aj}=1.$$

On substituting from Eqs. (2) and (10) we find this condition becomes

$$(2c_j^2/m)\{\sum_{r=1}^{N-1}\sin^2(jr\pi/N) + \cos\theta\sum_{r=1}^{N-2}\sin(jr\pi/N)\sin(\overline{jr+1}\pi/N)\}=1.$$

The trigonometric series are readily summed by converting them into sums of geometric progressions: the resulting expression for the normalizing factor is

$$c_j^{-2}=(2N/m)\{1+\cos\theta\cos(j\pi/N)\}. \tag{12}$$

We are now in a position to evaluate the first-order correction to the stretching frequencies arising from the nonzero bending force constant. The formula which we require is[11]

$$\lambda^1{}_{Aj}=\mathbf{x}_{Aj}\mathbf{G}_{AB}\mathbf{F}_{BB}\mathbf{G}_{BA}\mathbf{x}'_{Aj}. \tag{13}$$

By substituting matrix elements from (2), (3), (10), and (12) into (13), we obtain the expression

$$\lambda^1{}_{Aj}=\frac{k_B\sin^2\theta}{Nm\{1+\cos\theta\cos(j\pi/N)\}}\sum_{s=1}^{N-2}\{\sum_{r=s-1}^{s+2}\sin(jr\pi/N)\}^2.$$

On transforming and evaluating the trigonometric sums we eventually arrive at the formula

$$\lambda^1{}_{Aj}=\frac{4k_B\sin^2\theta\cos^2(j\pi/N)\{1+\cos(j\pi/N)\}}{m\{1+\cos\theta\cos(j\pi/N)\}} \times\{1-(2/N)[1-\cos(j\pi/N)]\}. \tag{14}$$

[11] Equation (13) is an alternative form of the expression for $\lambda^1{}_A$ given on p. 1133 of I, the original form of **H** being used in place of I (11).

The exact stretching frequencies are to be derived from the equation

$$\lambda_{Aj}=\lambda^0{}_{Aj}+\lambda^1{}_{Aj}+\lambda^2{}_{Aj}+O(k_B^3/k_A^2), \tag{15}$$

where $\lambda^0{}_{Aj}$, $\lambda^1{}_{Aj}$ are given by (11) and (14), respectively. To evaluate the second-order term $\lambda^2{}_{Aj}$ we should have to solve the approximate secular equations I(5b) for the bending modes, for the second-order perturbation term calculated in I cannot be transformed into a form containing explicitly only $\mathbf{x}_{Aj}$ and the F and G matrices. Unfortunately, the equations I(5b) are somewhat intractable when applied to this problem.

4. KIRKWOOD-PITZER FORMULA

The exact secular equations (4) may be partially solved by writing as a trial solution

$$\left.\begin{aligned} x_{Ar}&=a\exp(ir\phi),\\ x_{Bs}&=b\exp(is\phi).\end{aligned}\right\} \tag{16}$$

By the substitution (16) we get from Eqs. (4) the pair of simultaneous equations

$$\lambda a=(k_A/m)\{2a(1+\cos\theta\cos\phi) -4b\sin\theta e^{-\frac{1}{2}i\phi}\cos\tfrac{1}{2}\phi\cos\phi\},$$

$$\lambda b=(k_B/m)\{-4a\sin\theta e^{\frac{1}{2}i\phi}\cos\tfrac{1}{2}\phi\cos\phi +4b(1+\cos\phi)(1-\cos\theta\cos\phi)\}.$$

On eliminating a, b from these equations we obtain for λ the formula

$$\lambda=\alpha\pm\sqrt{(\alpha^2-\beta^2)}, \tag{17}$$

in which

$$\alpha=(k_A/m)(1+\cos\theta\cos\phi) +(2k_B/m)(1+\cos\phi)(1-\cos\theta\cos\phi),$$

$$\beta^2=(8k_Ak_B/m^2)(1+\cos\phi)\sin^2\phi.$$

The upper branch of Eq. (17) corresponds to stretching frequencies λ_A, the lower to bending frequencies λ_B.

We run into difficulty when we try to find the allowed values of the parameter ϕ. The boundary conditions to be fulfilled are now six in number, namely

$$\left.\begin{aligned} x_{A0}=x_{AN}=x_{B-1}=x_{B0}\\ =x_{BN-1}=x_{BN}=0.\end{aligned}\right\} \tag{18}$$

Consequently, the general solution has to contain besides term (16) not only a term corresponding to $-\phi$ but also four others, corresponding to parameters $\pm\phi'$, $\pm\phi''$ which yield the same value of λ when substituted into Eq. (17). The determinantal equation which determines the allowed values of ϕ, ϕ', ϕ'' has no simple analytic solution.

Kirkwood[4] suggested that for long chains, where presumably end effects are comparatively unimportant, this difficulty could be avoided by replacing the true boundary conditions (18) by the requirement that the solution should be periodic, with the period equal to

the chain length. That is to say, the condition to be imposed on the solution (16) is

$$x_{A0}=x_{AN}, \quad x_{B0}=x_{BN}. \tag{19}$$

The allowed values of ϕ then turn out to be

$$\phi_j=2j\pi/N. \tag{20}$$

This solution is unsatisfactory in two respects: it yields frequencies which are degenerate in pairs, contrary to observation, and it disagrees with the exact solution (9) for $k_B=0$.

Pitzer[5] pointed out that it would be more reasonable to impose the condition of periodicity in *twice* the chain length, that is, to allow the ends to vibrate either in phase or in opposition (phase difference$=\pi$). The allowed values of ϕ now turn out to be just those given by Eq. (9). This is much more satisfactory: the degeneracies disappear, the solution is correct for $k_B=0$, and there is a certain amount of agreement with the observed spectra.

Let us now expand the Pitzer formula in ascending powers of k_B/k_A. From Eqs. (17) and (9) we obtain for the stretching frequencies

$$\lambda_{Aj}=\lambda^0{}_{Aj}+\lambda^1{}_{Aj}+O(k^2{}_B/k_A),$$

where

$$\lambda^0{}_{Aj}=(2k_A/m)\{1+\cos\theta\cos(j\pi/N)\}$$

and

$$\lambda^1{}_{Aj}=\frac{4k_B\sin^2\theta\cos^2(j\pi/N)\{1+\cos(j\pi/N)\}}{m\{1+\cos\theta\cos(j\pi/N)\}}$$

$$(j=1\cdots N-1). \tag{21}$$

The expression (21) differs from (14), the correct first-order term, by the absence of the factor

$$f(N,j)=1-(2/N)\{1-\cos(j\pi/N)\}. \tag{22}$$

Evidently, as $N\to\infty$ the Pitzer formula becomes successively more accurate.

5. DISCUSSION

It is instructive, in order to estimate the relative usefulness of (14) and (17), to tabulate $f(N,j)$ for a number of values of N and j: this is done in Table I. It appears that even for quite small values of N (e.g., $N=5$) f is close to unity for $j=1$; more generally, it is for small values of j that the terms (14) and (21) agree best, and this agreement improves rapidly as N increases. So the Pitzer formula (17) is likely to be reliable for calculating the lower frequencies of the stretching spectrum; for these same frequencies the correct first-order term (14) is at its largest and therefore the perturbation series is likely to be insufficiently convergent. On the other hand, for large values of j, where the correct first-order term is small and the perturbation series probably converges rapidly, the Pitzer formula is likely to be inadequate.

TABLE I. Values of $f(N,j)$.

N	j	$f(N,j)$	N	j	$f(N,j)$
2	1	0.0	10	1	0.990
				2	0.962
3	1	0.667		3	0.918
	2	0.0		4	0.862
				5	0.8
4	1	0.854		6	0.738
	2	0.5		7	0.682
	3	0.146		8	0.638
				9	0.610
5	1	0.924			
	2	0.724	12	1	0.994
	3	0.476		2	0.978
	4	0.276		3	0.951
				4	0.917
6	1	0.955		5	0.876
	2	0.833		6	0.833
	3	0.667		7	0.790
	4	0.5		8	0.75
	5	0.378		9	0.715
				10	0.689
8	1	0.981		11	0.672
	2	0.927			
	3	0.846			
	4	0.75			
	5	0.654			
	6	0.573			
	7	0.519			

However, there is one major obstacle in the way of a satisfactory interpretation of the paraffin skeletal frequencies on the present model. The stretching frequencies are not entirely disentangled from those of all the other modes of vibration which are symmetric with respect to the zigzag plane. In particular, the wagging frequencies of the terminal methyl groups are believed to lie very close to the upper end of the stretching spectrum.[12] Thus distortion of this spectrum is likely to occur in the very region in which the perturbation formula calculated in this paper is expected to be most reliable. Evidently some method must be found of dealing with the interaction between the skeletal stretching and methyl wagging modes before an adequate interpretation can be given of the skeletal frequencies.[13]

VI. ACKNOWLEDGMENTS

The author is indebted to Professor H. C. Longuet-Higgins for helpful discussions of this problem and to the Royal Commission for the Exhibition of 1851 for the award of a Senior Studentship.

[12] See, for example, reference 6.

[13] A referee has pointed out that strong coupling is to be expected also between the methylene wagging modes and the skeletal stretching modes. It seems to the author that the effectiveness of this may be reduced by the relative remoteness of the methylene frequencies ($\sim$1300 cm^{-1}, whereas the methyl frequencies near 1000 cm^{-1} actually overlap the skeletal stretching band): for the theory presented in I indicates that the effectiveness of any coupling is greatly enhanced by the proximity of the frequency of the perturbing mode to that of the mode to be perturbed. Nevertheless, it may well be true that the methylene wagging will have to be taken into account.

Hydrodynamic Frictional and Diffusion Coefficients in Idealized Liquids. I.* The Collisional Contribution

F. C. COLLINS AND H. RAFFEL
Department of Chemistry, Polytechnic Institute of Brooklyn, Brooklyn 1, New York
(Received November 19, 1954)

The approximate method of calculation of the collisional contribution to transport properties in liquids presented in an earlier paper is now extended to the calculation of the similar contribution to the frictional and diffusion coefficients. For the special case where the diffusing molecule is large compared to its neighbors, the calculated collisional contribution to the frictional coefficient is in good agreement with Stokes' law and the Langevin equation of colloid statistics is valid. However, for small diffusing molecules, the calculated frictional coefficient is not independent of the velocity of the given molecule. Numerical diffusion coefficients using molecular parameters obtained from sonic velocity data are about three times the experimental values as might be expected from the corresponding behavior of the calculated viscosity coefficient contribution previously reported. In spite of the failure of the Stokes equation for the frictional coefficient of small molecules, the Stokes-Einstein equation represents fairly satisfactorily the case of self-diffusion. This is due to the averaging over all velocities of the diffusing molecule.

INTRODUCTION

IN an earlier paper[1] the collisional transport of momentum across the bodies of the molecules in an idealized liquid undergoing steady viscous shear was calculated and compared with the coefficients in the phenomenological pressure tensor in order to determine the collisional contribution to the shear viscosity. A similar treatment is here developed for the hydrodynamic frictional coefficient ζ_{12} and the diffusion coefficient D_{12} in the case of binary liquid solutions. The assumptions made concerning the nature of the microscopic processes in the liquid are similar to those in the previous paper and will not be repeated here. The same nomenclature will be used here except where otherwise specified.

THE HYDRODYNAMIC FRICTIONAL COEFFICIENT

The binary diffusion constant D_{12} is given by Einstein[2] in terms of a mean frictional coefficient $\langle\zeta_{12}\rangle$ as

$$D_{12}=kT/\langle\zeta_{12}\rangle \tag{1}$$

where the frictional coefficient is averaged over all values of the velocity of the molecule under consideration and those of the molecules with which it collides. Equation (1) should be valid for both colloid particles and small molecules. The frictional coefficient ζ_{12} also appears in the Langevin[3] equation well-known in colloid statistics:

$$m_1\frac{d\mathbf{c}_1}{dt}+\zeta_{12}\mathbf{c}_1=\mathbf{A}(t) \tag{2}$$

where c_1 is the velocity of the particle and m_1 its mass. The instantaneous force acting on the colloid particle is assumed to be divisible into two parts: (1) a systematic part proportional to the velocity of the given molecule and (2) a random part $\mathbf{A}(t)$, where t is the time. The random part is assumed to have the property

$$\int_{t_0}^{t_0+\tau}\mathbf{A}(t)dt=0 \tag{3}$$

where τ is a plateau time short compared to macroscopic observational times but long in comparison with molecular collisional processes. The frictional coefficient ζ_{12} for the particle among neighbors all of species 2 is a mean value averaged over an ensemble of all velocities $\mathbf{c}_2$ of the neighbors with which the particle collides. The frictional coefficient is tacitly assumed to be independent of the magnitude of the velocity $\mathbf{c}_1$. The validity of an extension of Eq. (2) to the case of small molecules is open to question with respect to the implied constancy of ζ_{12}.

In the molecular case, let us express the mean force exerted on a molecule having the known velocity $\mathbf{c}_1$ as

$$m_1\frac{d\mathbf{c}_1}{dt}=\langle\mathbf{F}\rangle=\zeta_{12}(c_1)\mathbf{c}_1 \tag{4}$$

where the force $\langle\mathbf{F}\rangle$ is the time average and not the instantaneous force appearing in Eq. (2) and $\zeta_{12}(\mathbf{c}_1)$ is explicitly a function of the velocity magnitude. We now wish to calculate ζ_{12} (c_1) from kinetic theory. We will assume that the time average force $\langle\mathbf{F}\rangle$ is equal to the ensemble average force exerted by neighbors having all possible values of the collision parameters. The quasi-equilibrium treatment of the earlier paper[1] will again be used wherein the neighbors are assumed to have a Maxwell-Boltzmann distribution of velocities independent of the velocity $\mathbf{c}_1$.

We wish to determine for a molecule having the velocity $\mathbf{c}_1(0)$ at $t=0$, the mean component of the velocity in the original direction after the lapse of the

* The material presented in this paper was taken from the dissertation submitted by Helen Raffel in partial fulfillment of the requirements for the degree of Doctor of Philosophy of the Polytechnic Institute of Brooklyn.

[1] F. C. Collins and H. Raffel, J. Chem. Phys. **22**, 1728 (1954).
[2] A. Einstein, Z. Elektrochem. **14**, 235 (1908).
[3] P. Langevin, Compt. rend. **146**, 530 (1908); S. Chandrasekhar, Revs. Modern Phys. **15**, 1 (1943).

short time t^*: $\langle \mathbf{c}_1(t^*)\cdot\mathbf{c}_1(0)/c_1(0)\rangle$. The limitations on t^* will be discussed presently.

The average rate of change of velocity in the original direction during the time t^* will be given by

$$m_1\frac{d\mathbf{c}_1}{dt}=\frac{1}{t^*}\left[\left\langle \mathbf{c}_1(t^*)\cdot\frac{\mathbf{c}_1(0)}{c_1(0)}\right\rangle\frac{\mathbf{c}_1(0)}{c_1(0)}-\mathbf{c}_1(0)\right] =\frac{1}{t^*}\left[\left\langle\frac{\mathbf{c}_1(t^*)\cdot\mathbf{c}_1(0)}{c_1^2(0)}\right\rangle-1\right]\mathbf{c}_1(0). \tag{5}$$

Combining Eqs. (4) and (5) leads to

$$\zeta_{12}(c_1)=\frac{m_1}{t^*}\left[1-\left\langle\frac{\mathbf{c}_1(t^*)\cdot\mathbf{c}_1(0)}{c_1^2(0)}\right\rangle\right]. \tag{6}$$

Let us now choose t^* small enough so that the probability that the given molecule experience more than one collision during t^* becomes negligible. Then

$$\mathbf{c}_1(t^*)=\mathbf{c}_1' \text{ if a collision has occurred}$$
$$=\mathbf{c}_1 \text{ if a collision has not occurred.}$$

Thus the average component of the velocity in the original direction at the time t^* will be

$$\left\langle\frac{\mathbf{c}_1(t^*)\cdot\mathbf{c}_1(0)}{c_1(0)}\right\rangle_{c_1}=\langle\mathbf{c}_1'\cdot\mathbf{c}_1\rangle\frac{\mathbf{c}_1}{c_1}P(t^*)+\frac{\mathbf{c}_1^2}{c_1}[1-P(t^*)] \tag{7}$$

where $P(t^*)$ is the probability that a collision occurs during the time t^* and the subscript c_1 indicates partial averaging over $\mathbf{c}_2$ and the collision parameters, but not over c_1.

If the molecules are taken to be perfectly elastic spheres, the laws of conservation of energy and momentum lead to the following relations[4]:

$$\mathbf{c}_1'-\mathbf{c}_1=2M_2(\mathbf{g}_{21}\cdot\mathbf{k})\mathbf{k}$$
$$\mathbf{c}_2'-\mathbf{c}_2=-2M_1(\mathbf{g}_{21}\cdot\mathbf{k})\mathbf{k} \tag{8}$$

where $\mathbf{k}$ is a unit vector along the line of centers of the colliding molecules, $\mathbf{g}_{21}=\mathbf{c}_2-\mathbf{c}_1$, the relative velocity, $M_2=m_2/(m_1+m_2)$, and $M_1=m_1/(m_1+m_2)$.

If we now assume molecular chaos with respect to the neighbors, the probability that a given sphere having the velocity $\mathbf{c}_1$ does not experience a collision within the distance s from an arbitrary starting point at $t=0$ is given by the well-known function

$$1-P(s)=\exp(-s/\langle s\rangle_{c_1})$$

or

$$1-P(t^*)=\exp(-c_1t^*/\langle s\rangle_{c_1}) \tag{9}$$

where $\langle s\rangle_{c_1}$ is the mean free path of a molecule with the velocity magnitude c_1.

Substitution of Eqs. (7), (8), and (9) into Eq (6) gives

$$\zeta_{12}(c_1)=\frac{m_1}{t^*c_1^2}[2M_2\langle(\mathbf{g}_{21}\cdot\mathbf{k})(\mathbf{c}_1\cdot\mathbf{k})\rangle_{c_1}P(t^*)]. \tag{10}$$

Now the assumptions already made concerning the magnitude of t^* enable us to expand the exponential of Eq. (9) and to discard terms of order higher than first. Equation (10) then reduces to

$$\zeta_{12}(c_1)=-\frac{2m_1M_2}{c_1\langle s\rangle_{c_1}}\langle(\mathbf{g}_{21}\cdot\mathbf{k})(\mathbf{c}_1\cdot\mathbf{k})\rangle_{c_1}. \tag{11}$$

If the averaging process is indicated explicitly, Eq. (11) becomes

$$\zeta_{12}(c_1)=-\frac{2m_1M_2}{c_1\langle s\rangle_{c_1}}\frac{\int\int(\mathbf{g}_{21}\cdot\mathbf{k})(\mathbf{c}_1\cdot\mathbf{k})Z_{12}d\mathbf{c}_2d\mathbf{k}}{\int\int Z_{12}d\mathbf{c}_2d\mathbf{k}} \tag{12}$$

where Z_{12} is the frequency with which a molecule of species 1 having the velocity $\mathbf{c}_1$ and surrounded by molecules of species 2 suffers collisions. We may also express the mean free path in terms of the collision frequency as follows:

$$\langle s\rangle_{c_1}=c_1\Big/\int\int Z_{12}d\mathbf{c}_2d\mathbf{k}. \tag{13}$$

By the use of Eq. (13), Eq. (12) may be expressed as

$$\zeta_{12}(c_1)=-\frac{2m_1M_2}{c_1^2}\int\int(\mathbf{g}_{12}\cdot\mathbf{k})(\mathbf{c}_1\cdot\mathbf{k})Z_{12}d\mathbf{c}_2d\mathbf{k}. \tag{14}$$

The collision frequency $Z_{12}(c_1)$ may be readily obtained by a derivation paralleling that presented in the earlier paper.[1] Here however the species of the molecule under consideration is different from the species of its neighbors. Further, in the present case, the distribution of velocities is independent of position. The resulting equation (paralleling Eq. (6) of the previous paper) is

$$dZ_{12}=\frac{\nu_1\sigma_{12}^2(1-\cos\Omega^*)}{2(v_f)_2}(\mathbf{g}_{12}\cdot\mathbf{k})f(\mathbf{c}_2)d\mathbf{c}_2d\mathbf{k} \tag{15}$$

where ν_1 is the average number of nearest neighbors surrounding a molecule of species 1, σ_{12} is the mean collision diameter of molecules of species 1 and 2, $(v_f)_2$ is the free volume accessible to a molecule of species 2 having one of its nearest neighbors of species 1, and $f(\mathbf{c})$ is the Maxwell-Boltzmann distribution.

$$f(\mathbf{c})=\left(\frac{m}{2\pi kT}\right)^{\frac{3}{2}}\exp\left(-\frac{mc^2}{2kT}\right). \tag{16}$$

The quantity $(1-\cos\Omega^*)$ is the fraction of the collision sphere of the given molecule which is available for a

[4] S. Chapman and T. G. Cowling, *Mathematical Theory of Non-Uniform Gases* (Cambridge University Press, London, 1939), pp. 54–58.

collision involving a single nearest neighbor. It is discussed in detail in the previous paper[1] to which reference may be made.

Upon introducing Eq. (15) into Eq. (14) we obtain

$$\zeta_{12}(c_1)=-\frac{m_1M_2\nu_1\sigma_{12}(1-\cos\Omega^*)}{(\nu_f)_2}\times\int\int c_1^{-2}(\mathbf{g}_{21}\cdot\mathbf{k})(\mathbf{c}_1\cdot\mathbf{k})f(\mathbf{c}_2)d\mathbf{c}_2d\mathbf{k}. \quad (17)$$

In the integration of Eq. (17), $\mathbf{c}_1$ is held fixed in direction and is used as the z-axis so that

$$d\mathbf{c}_2=\mathbf{c}_2^2\sin\psi d\epsilon d\psi dc_2$$
$$d\mathbf{k}=\sin\theta d\varphi d\theta.$$

We then have

$$\mathbf{c}_1\cdot\mathbf{k}=c_1\cos\theta$$
$$\mathbf{c}_2\cdot\mathbf{k}=c_2\cos\psi.$$

The integration over the orientations of $\mathbf{k}$ requires some care to be taken in the choice of limits for $\mathbf{c}_2$. It is necessary that $\mathbf{g}_{21}\cdot\mathbf{k}$ be greater than zero for a collision to occur. Hence we must have that $\mathbf{c}_2\cdot\mathbf{k}\geqslant\mathbf{c}_1\cdot\mathbf{k}$. In view of this, it is convenient to divide the integration into two cases:

(a) $0\leqslant c_2\leqslant c_1|\cos\theta|$. In this case, if $\theta<\pi/2$, there are no possible values of ψ and ϵ which will lead to a collision. For $\pi/2\leqslant\theta\leqslant\pi$, all values of ψ and ϵ are allowable, i.e., $0\leqslant\psi\leqslant\pi$, $0\leqslant\epsilon<2\pi$.

(b) $c_1|\cos\theta|\leqslant c_2\leqslant\infty$. Here it is required that $0\leqslant\psi\leqslant\cos^{-1}[(c_1/c_2)\cos\theta]$ in order that the requirements for a collision be satisfied. All possible values of ϵ are allowed: $0\leqslant\epsilon\leqslant2\pi$.

Upon expanding $(\mathbf{g}_{21}\cdot\mathbf{k})^2$ and introducing Eq. (16), Eq. (17) becomes

$$\zeta_{12}(c_1)=-\frac{m_1M_2\nu_1\sigma_{12}^2(1-\cos\Omega^*)}{(\nu_f)_2}\left(\frac{m_2}{2\pi kT}\right)^{\frac{3}{2}}\times\int\cdots\int(c_2^2\cos^2\psi+c_1^2\cos^2\theta-2c_1c_2\cos\psi\cos\theta)c_1\cos\theta c_1^{-2}\exp(-a_2c_2^2)\times c_2^2\sin\psi\sin\theta d\epsilon d\psi dc_2d\varphi d\theta \quad (18)$$

where $a_2=m_2/2kT$. As the integrations over ϵ and φ do not involve the remaining variables, these integrations can be carried out immediately

$$\int_0^{2\pi}\int_0^{2\pi}d\epsilon d\varphi=(2\pi)^2.$$

Equation (18) may then be written in the somewhat expanded form

$$\zeta_{12}(c_1)=-\frac{m_1M_2\nu_1\sigma_{12}^2(1-\cos\Omega^*)}{(\nu_f)_2}\left(\frac{m_2}{2\pi kT}\right)^{\frac{3}{2}}4\pi^2\times\int\cdots\int[\exp(-a_2c_2^2)c_2^4c_1^{-1}\cos^2\psi\times\sin\psi\cos\theta\sin\theta+\exp(-a_2c_2^2)c_2^2c_1\times\sin\psi\cos^3\theta\sin\theta-2\exp(-a_2c_2^2)c_2^3\times\cos\psi\sin\psi\cos^2\theta\sin\theta]d\psi dc_2d\theta. \quad (19)$$

Let us label the three integrals in Eq. (19) in order I, II, and III and integrate each separately under cases (a) and (b) discussed above.

$$\mathrm{I(a)}=\int_{\pi/2}^{\pi}\int_0^{c_1|\cos\theta|}\int_0^{\pi}\exp(-a_2c_2^2)c_2^4c_1^{-1}\times\cos^2\psi\sin\psi\cos\theta\sin\theta d\psi dc_2d\theta$$
$$=\frac{1}{3a_2}\int_{\pi/2}^{\pi}\exp(-a_2c_1^2\cos^2\theta)c_1^2\cos^4\theta\sin\theta d\theta+\frac{1}{2a_2^2}\int_{\pi/2}^{\pi}\exp(-a_2c_1^2\cos^2\theta)\cos^2\theta\sin\theta d\theta+\frac{1}{2a_2^2}\int_{\pi/2}^{\pi}\int_0^{c_1|\cos\theta|}\exp(-a_2c_2^2)c_1^{-1}\cos\theta\sin\theta dc_2d\theta$$

$$\mathrm{I(b)}=\int_0^{\pi}\int_{c_1|\cos\theta|}^{\infty}\int_0^{\cos^{-1}[(c_1/c_2)\cos\theta]}\exp(-a_2c_2^2)c_2^4c_1^{-1}\times\cos^2\psi\sin\psi\cos\theta\sin\theta d\psi dc_2d\theta$$
$$=-\frac{1}{3a_2}\int_{\pi/2}^{\pi}\exp(-a_2c_1^2\cos^2\theta)c_1^2\cos\theta\sin\theta d\theta+\frac{1}{4a_2^2}\int_0^{\pi}\int_{c_1|\cos\theta|}^{\infty}\exp(-a_2c_2^2)c_1^{-1}\cos\theta\times\sin\theta dc_2d\theta$$

$$\mathrm{II(a)}=\int_{\pi/2}^{\pi}\int_0^{c_1|\cos\theta|}\int_0^{\pi}\exp(-a_2c_2^2)c_2^2\sin\psi\times\cos^3\theta\sin\theta d\psi dc_2d\theta$$
$$=\frac{1}{a_2}\int_{\pi/2}^{\pi}\exp(-a_2c_1^2\cos^2\theta)c_1^2\cos^4\theta\sin\theta d\theta+\frac{1}{a_2}\int_{\pi/2}^{\pi}\int_0^{c_1|\cos\theta|}\exp(-a_2c_2^2)c_1\cos^3\theta\sin\theta dc_2d\theta$$

$$\mathrm{II(b)}=\int_0^{\pi}\int_{c_1|\cos\theta|}^{\infty}\int_0^{\cos^{-1}[(c_2/c_1)\cos\theta]}\exp(-a_2c_2^2)c_2^2c_1\times\sin\psi\cos^3\theta\sin\theta d\psi dc_2d\theta$$

$$=-\frac{1}{a_2}\int_{\pi/2}^{\pi}\exp(-a_2c_1^2\cos^2\theta)c_1^2\cos^4\theta\sin\theta d\theta+\frac{1}{2a_2}\int_0^{\pi}\int_{c_1|\cos\theta|}^{\infty}\exp(-a_2c_2^2)c_1\cos^3\theta\sin\theta dc_2d\theta$$

$$\mathrm{III}(a)=2\int_{\pi/2}^{\pi}\int_0^{c_1|\cos\theta|}\int_0^{\pi}\exp(-a_2c_2^2)c_2^3\times\cos\psi\sin\psi\cos^2\theta\sin\theta d\psi dc_2d\theta=0$$

$$\mathrm{III(b)}=2\int_0^{\pi}\int_{c_1|\cos\theta|}^{\infty}\int_0^{\cos^{-1}[(c_1/c_2)\cos\theta]}\exp(-a_2c_2^2)c_2^3\times\cos\psi\sin\psi\cos^2\theta\sin\theta d\psi dc_2d\theta$$

$$=-\frac{1}{2a_2^2}\int_0^{\pi}\exp(-a_2c_1^2\cos^2\theta)\cos^2\theta\sin\theta d\theta.$$

At this point, it is profitable to combine the several integrals and we have:

$$\mathrm{I(a+b)+II(a+b)+III(a+b)}$$

$$=\frac{1}{4a_2^2}\int_0^{\pi}\int_{c_1|\cos\theta|}^{\infty}\exp(-a_2c_2^2)c_1^{-1}\cos\theta\sin\theta dc_2d\theta \quad \text{(A)}$$

$$+\frac{1}{2a_2}\int_0^{\pi}\int_{c_1|\cos\theta|}^{\infty}\exp(-a_2c_1^2)c_1\cos^3\theta\sin\theta dc_2d\theta \quad \text{(B)}$$

$$+\frac{1}{2a_2^2}\int_{\pi/2}^{\pi}\int_0^{c_1|\cos\theta|}\exp(-a_2c_2^2)c_1^{-1}\times\cos\theta\sin\theta dc_2d\theta \quad \text{(C)}$$

$$+\frac{1}{a_2}\int_{\pi/2}^{\pi}\int_0^{c_1|\cos\theta|}\exp(-a_2c_2^2)c_1\cos^3\theta\sin\theta dc_2d\theta \quad \text{(D)}$$

$$-\frac{1}{4a_2^2}\int_0^{\pi}\exp(-a_2c_1^2\cos^2\theta)\cos^2\theta\sin\theta d\theta. \quad \text{(E)}$$

The terms in the foregoing equation are labeled (A) to (E) as indicated to facilitate bookkeeping.

In (A) and (B), we require integrations of the form:

$$\int_0^{\pi}\int_{c_1|\cos\theta|}^{\infty}\exp(-a_2c_2^2)\cos^n\theta\sin\theta dc_2d\theta \quad (20)$$

where n is an odd integer. Upon making the substitutions:

$$w=a_2^{\frac{1}{2}}c_2$$
$$z=\cos\theta$$

the integral (20) becomes

$$-\frac{1}{a_2^{\frac{1}{2}}}\int_1^{-1}\int_{a_2^{\frac{1}{2}}c_1|z|}^{\infty}\exp(-w^2)z^n dwdz.$$

The foregoing integral may be now decomposed into a sum of integrals and the order of integration reversed as follows:

$$-\frac{1}{a_2^{\frac{1}{2}}}\int_1^{-1}\int_0^{\infty}\exp(-w^2)z^n dwdz+\frac{1}{a_2^{\frac{1}{2}}}\int_1^{0}\int_0^{a_2^{\frac{1}{2}}c_1z}\exp(-w^2)z^n dwdz+\frac{1}{a_2^{\frac{1}{2}}}\int_0^{1}\int_0^{-a_2^{\frac{1}{2}}c_1z}\exp(-w^2)z^n dwdz$$

$$=-\frac{1}{a_2^{\frac{1}{2}}}\int_1^{-1}\frac{\pi^{\frac{1}{2}}}{2}z^n dz+\frac{1}{a_2^{\frac{1}{2}}}\int_0^{a_2^{\frac{1}{2}}c_1}\int_1^{w/a_2^{\frac{1}{2}}c_1}\exp(-w^2)z^n dzdw+\frac{1}{a_2^{\frac{1}{2}}}\int_0^{a_2^{\frac{1}{2}}c_1}\int_{-w/a_2^{\frac{1}{2}}c_1}^{-1}\exp(-w^2)z^n dzdw \quad (21)$$

as n is odd, the first integral in Eq. (21) is identically zero and the next two integrals cancel each other. Hence (A) and (B) are both equal to zero.

In (C) and (D), the integrals to be evaluated are of the form

$$\int_{\pi/2}^{\pi}\int_0^{c_1|\cos\theta|}\exp(-a_2c_2^2)\cos^n\theta\sin\theta dc_2d\theta$$

where n is again an odd number. Upon making the same substitutions as before, decomposing and reversing the order of integration, we obtain,

$$-\frac{1}{a_2^{\frac{1}{2}}}\int_0^{a_2^{\frac{1}{2}}c_1}\int_{-w/a_2^{\frac{1}{2}}c_1}^{-1}\exp(-w^2)z^n dzdw. \quad (22)$$

Using the form (22) and integrating by parts, the integrals (C) and (D) become:

$$\mathrm{(C)}=-\frac{\exp(-a_2c_1^2)}{8a_2^3c_1^2}+\left(\frac{1}{8a_2^{7/2}c_1^3}-\frac{1}{4a^{5/2}c_1}\right)\times\int_0^{a_2^{\frac{1}{2}}c_1}\exp(-w^2)dw$$

$$\mathrm{(D)}=-\left(\frac{1}{8a_2^2}+\frac{3}{16a_2^3c_1^2}\right)\exp(-a_2c_1^2)+\left(\frac{3}{16a_2^{7/2}c_1^3}-\frac{c_1}{4a_2^{\frac{1}{2}}}\right)\int_0^{a_2^{\frac{1}{2}}c_1}\exp(-w^2)dw.$$

The integral (E) is integrated by parts to yield

$$(\mathrm{E})=\frac{\exp(-a_2c_1^2)}{4a_2^3c_1^2}+\frac{1}{8a_2^3c_1^2}\int_1^{-1}\exp(-a_2c_1^2z^2)dz.$$

The last integral can be brought into a form paralleling that of the other integrals by making the substitution $w=a_2^{\frac{1}{2}}c_1z$. Then

$$(\mathrm{E})=\frac{\exp(-a_2c_1^2)}{4a_2^3c_1^2}-\frac{1}{4a_2^{7/2}c_1^3}\int_0^{a_2^{\frac{1}{2}}c_1}\exp(-w^2)dw.$$

Upon summing the several integrals and introducing the result into Eq. (19), we have

$$\zeta_{12}(c_1)=\frac{m_1M_2\nu_2\sigma_{12}^2(1-\cos\Omega^*)}{(v_f)_2}\left(\frac{m_2}{2\pi kT}\right)^{\frac{3}{2}}$$
$$\times4\pi^2\left[\left(\frac{1}{16a_2^3c_1^2}+\frac{1}{8a_2^2}\right)\exp(-a_2c_1^2)\right.$$
$$-\left(\frac{1}{16a_2^{7/2}c_1^3}-\frac{1}{4a_2^{5/2}c_1}-\frac{c_1}{4a_2^{\frac{3}{2}}}\right)$$
$$\left.\times\int_0^{a_2^{\frac{1}{2}}c_1}\exp(-w^2)dw\right]. \quad (23)$$

The behavior of the frictional coefficient $\zeta_{12}(c_1)$ as a function of the velocity magnitude is illustrated in Fig. 1. The region where $c_1\ll a_2$ corresponds to the case of a colloid particle in solution. Here the frictional coefficient is constant in agreement with the well-known assumptions of colloid statistics. In the molecular case, however, where $a_1^{\frac{1}{2}}\approx a_2^{\frac{1}{2}}$ and c_1 is of a corresponding order of magnitude, ζ_{12} increases with c_1 and finally becomes proportional to c_1. Thus the Langevin Eq. (2) cannot be extended to the molecular case.

It is now of interest to determine whether the limiting form of Eq. (23) for $c_1\geq0$ is consistent with

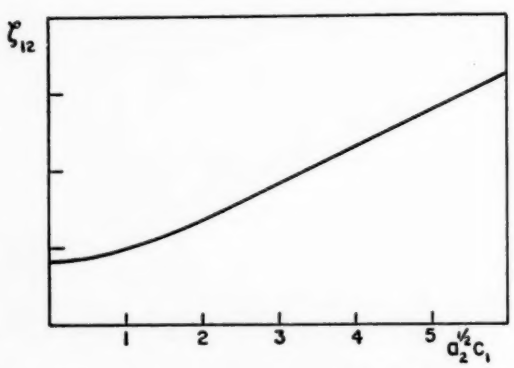

FIG. 1. The dependence of the hydrodynamic frictional coefficient $\zeta_{12}(c_1)$ upon the velocity magnitude c_1. (The frictional coefficient ζ_{12} is in arbitrary units while c_1 is given in units of $a_2^{-\frac{1}{2}}$.)

Stokes' law:

$$\zeta_{12}=6\pi r\eta$$
$$=6\pi\sigma_{12}\eta_e \quad (24)$$

where the particle radius r has been replaced by the collision diameter σ_{12}. As ζ_{12} here calculated represents only the collisional contribution to the frictional coefficient, the total viscosity coefficient η is replaced by the collisional contribution η_e to the viscosity.[1] By making use of the usual expansion of the error function for small values of the argument, it can be readily shown that

$$\lim_{c_1\to0}\zeta_{12}(c_1)=\frac{m_1M_2\nu_2\sigma_{12}^2(1-\cos\Omega^*)}{(v_f)_2}$$
$$\times\left(\frac{m_2}{2\pi kT}\right)^{\frac{3}{2}}4\pi^2\frac{3}{8a_2^2}. \quad (25)$$

In the earlier paper, the factor $\nu\sigma^2(1-\cos\Omega^*)/(v_f)_2$ was eliminated from the equation for the collisional contribution to the viscosity coefficient for a pure liquid by comparing the hydrostatic pressure calculated for the collisional process with that from the uniform potential free volume theory. In the present instance, the two forms of the equation for the pressure may be assumed to be as follows:

$$p=\frac{\pi kT\nu_2\sigma_{12}^3(1-\cos\Omega^*)}{3v_1(v_f)_2}$$
$$=\frac{kT}{v_1[1-(v_0/v)^{\frac{1}{3}}]}. \quad (26)$$

The pressure here is that transmitted across the body of the particle of species 1, v_1 is the partial molecular volume of this species and v_0/v is the ratio of the "incompressible" volume to the molecular volume of the solvent species 2. By analogous assumptions, Eq. (32) of the previous paper[1] can be put into the following form for the collisional contribution to the viscosity coefficient of the neighbors acting upon the particle 1:

$$\eta_e=\frac{2}{5}\frac{\sigma_{12}(m_2kT)^{\frac{1}{2}}}{\pi^{\frac{1}{2}}v_1[1-(v_0/v)^{\frac{1}{3}}]}. \quad (27)$$

By combining Eqs. (25) to (27), the frictional coefficient becomes

$$\lim_{c_1\to0}\zeta_{12}(c_1)=\frac{45\pi v_1\eta_e}{2^{\frac{3}{2}}\sigma_{12}^2}. \quad (28)$$

The partial molecular volume v_1 for a large spherical particle can be assumed to be $4\pi\sigma_{12}^3/3$ which, when substituted into Eq. (28), gives

$$\lim_{c_1\to0}\zeta_{12}(c_1)=6.74\pi\sigma_{12}\eta_e \quad (29)$$

which is in quite good agreement with Stokes' law, Eq. (24).

THE DIFFUSION COEFFICIENT

In order to calculate the binary diffusion coefficient D_{12} according to Eq. (1), we require to average Eq. (23) over all values of the velocity magnitude c_1 using the Maxwell-Boltzmann distribution Eq. (16). After integration over orientation of the velocity vector, the required remaining integration over Eq. (23) is as follows:

$$\langle\zeta_{12}\rangle=\frac{m_1M_2\nu_2\sigma_{12}^2(1-\cos\Omega^*)(m_1m_2)^{\frac{1}{2}}}{(v_f)_2(kT)^3}16\pi^3$$
$$\times\left\{\int_0^\infty\left(\frac{1}{16a_2^3c_1^2}+\frac{1}{8a_2^2}\right)\exp[-(a_1+a_2)c_1^2]\right.$$
$$\times c_1^2dc_1-\int_0^\infty\left(\frac{1}{16a_2^{7/2}c_1^3}-\frac{1}{4a_2^{5/2}c_1}-\frac{c_1^3}{4a_2^{\frac{1}{2}}}\right)$$
$$\left.\times\int_0^{a_2^{\frac{1}{2}}c_1}\exp(-a_1c_1^2-w^2)dwc_1^2dc_1\right\}. \quad (30)$$

The integration over w is readily effected by introducing the substitution, $w=\alpha c_1$: $dw=c_1d\alpha$ and reversing the order of the integration. We then obtain

$$\langle\zeta_{12}\rangle=\frac{m_1M_2\nu_2\sigma_{12}^2(1-\cos\Omega^*)(m_1m_2)^{\frac{1}{2}}}{(v_f)_2(kT)^3}8\pi^3\frac{\pi^{\frac{1}{2}}}{32}$$
$$\times\left(\frac{2kT}{m_1+m_2}\right)^{7/2}\left[\frac{1+M_2}{M_1^2M_2^2}-\frac{1}{M_2^{7/2}}\ln\frac{1+M_2^{\frac{1}{2}}}{M_1^{\frac{1}{2}}}\right]$$
$$=\sigma_{12}^2\nu_2(1-\cos\Omega^*)(\tfrac{1}{2}\pi\mu kT)^{\frac{1}{2}}\mathfrak{M}/(v_f)_2 \quad (31)$$

where $M_1=m_1/(m_1+m_2)$, $M_2=m_2/(m_1+m_2)$, $\mu=m_1m_2/(m_1+m_2)$, and

$$\mathfrak{M}=1+\frac{1}{M_2}-\frac{M_1^2}{M_2^{\frac{3}{2}}}\ln\frac{1+M_2^{\frac{1}{2}}}{M_1^{\frac{1}{2}}}.$$

Then, upon making use of Eq. (26), Eq. (31) assumes the simple form

$$\langle\zeta_{12}\rangle=\frac{3(\frac{1}{2}\pi\mu kT)^{\frac{1}{2}}\mathfrak{M}}{\pi\sigma_{12}[1-(v_0/v)^{\frac{1}{3}}]}. \quad (32)$$

The collisional contribution to the binary diffusion coefficient is then, from Eq. (1):

$$D_{12}=\frac{\sigma_{12}[1-(v_0/v)^{\frac{1}{3}}]}{3\mathfrak{M}}\left[\frac{2\pi kT}{\mu}\right]^{\frac{1}{2}}. \quad (33)$$

In an earlier communication,[5] it was pointed out that the ratio $(v_0/v)^{\frac{1}{3}}$ can be evaluated directly from sonic velocity measurements by the use of the free volume equation of state. The collisional diameter may be calculated from density and sonic velocity measurements on the basis of a reasonable assumption as to the molecular packing ratio in the liquid quasi-lattice. However, the constant so introduced varies but little with variation in the form assumed for the quasi-lattice.[5] Accordingly, Eq. (33) can be compared with experiment with but little ambiguity. As shown in Table I, the values so calculated are of the order of two times the experimental diffusion coefficients. This order of agreement follows the reciprocal order of agreement in the case of the collisional contribution to the shear viscosity coefficient.[1]

TABLE I. Comparison of binary diffusion coefficients calculated from Eq. (33) with experimental values for various liquid pairs.

Solute	Solvent	$D_{calc}\times10^5$ 7.3°	15°	25°	$D_{obs}\times10^5$ 7.3°	15°	25°	D_{calc}/D_{obs} 7.3°	15°	25°
C_6H_5Cl	C_6H_6		3.72	4.01		2.15[c]			1.73	
C_6H_5Br	C_6H_6	3.46	3.55	3.81	1.45[a]	1.86[c]		2.38	1.91	
C_6H_5I	C_6H_6	3.32	3.40	3.66	1.35[a]	1.50[c]		2.46	2.27	
CCl_4	C_6H_6	3.38	3.47	3.73	1.51[a]					
$CHCl_3$	C_6H_6		3.72	3.99		2.11[c]			2.24	1.76
C_6H_5Br	$C_6H_5CH_3$	3.01	3.18	3.41	1.59[a]					
$CHBr_3$	$CHCl_3$		2.95	3.16		1.54[b]	1.81[b]		1.92	1.72

[a] From Stearne, Irish, and Eyring, J. Phys. Chem. **44**, 981 (1940).
[b] From M. H. Navidi, thesis, Brooklyn Polytechnic Institute, 1953.
[c] From International Critical Tables.

It is now of interest to determine whether Eq. (33) agrees with the special form of the Stokes-Einstein equation obtained by combining Eqs. (1) and (24):

$$D_{12}=\frac{kT}{6\pi\sigma_{12}\eta_c}. \quad (34)$$

Introducing the collisional viscosity coefficient contribution from Eq. (27) into Eq. (33) leads to

$$D_{12}=\frac{2}{15}\left(\frac{2}{M_1}\right)^{\frac{1}{2}}\frac{kT}{\mathfrak{M}\eta_c}\frac{\sigma_{12}^2}{v_1}. \quad (35)$$

In the case of self-diffusion, $M_1=\frac{1}{2}$, $\mathfrak{M}=3.70$, and $\sigma_{12}=(v_0/v)^{\frac{1}{3}}v^{\frac{1}{3}}$. The ratio $(v_0/v)^{\frac{1}{3}}$ from sonic velocity measurements is ordinarily close to 0.9 while β is $2^{1/6}$ for a close packed cubic quasi-lattice. Then

$$D_{12}=\frac{kT}{2.77\pi\sigma_{12}\mathfrak{N}_c} \quad (36)$$

in fair agreement with Eq. (34).

The above calculations and their comparison with experiment indicate that the intermolecular collisional process in the case of the hydrodynamic frictional and diffusional coefficients parallels its contribution to the shear viscosity. The mechanism of transport of momen-

[5] F. C. Collins and M. H. Navidi, J. Chem. Phys. **22**, 1254 (1954).

tum across the bodies of molecules upon collision may be viewed as the idealized contribution of the pairwise intermolecular potential energy function to the transport process. The attractive part of the potential energy function also makes a significant contribution. This arises from the unbalanced intermolecular attractive force field resulting from the distribution of nearest neighbors by the velocity c_1 of the molecule under consideration. Calculated diffusion coefficients taking account of both contributions to the frictional coefficient are then correspondingly lower. These calculations will be the subject of a subsequent paper.

THE JOURNAL OF CHEMICAL PHYSICS VOLUME 23, NUMBER 8 AUGUST, 1955

Heat of Formation and Entropy of Titanium Tetrachloride from an Investigation of the Equilibrium: $TiO_2(s)+4HCl(g) = TiCl_4(g)+2H_3O(g)$*

MILTON FARBER† AND A. J. DARNELL‡
Jet Propulsion Laboratory, California Institute of Technology, Pasadena 3, California
(Received November 19, 1954)

The equilibrium, TiO_2(rutile)$+4HCl=TiCl_4(g)+2H_2O(g)$, was studied in the temperature range of 800–1400°K by means of a flow method in which HCl was passed over a sample of rutile. The heat of reaction was found to be 12.9 kcal/mole in this temperature range. This leads to a value of -182.9 ± 0.5 kcal/mole for ΔH_f of $TiCl_4(g)$ and -192.5 ± 0.5 kcal/mole for ΔH_f of $TiCl_4(l)$. The entropy of $TiCl_4(g)$ at 1100°K is found to be 124 cal/°/mole.

INTRODUCTION

A STUDY of the equilibrium,

$$TiO_2(\text{rutile})+4HCl(g)=TiCl_4(g)+2H_2O(g) \quad (1)$$

has been made in the temperature range 800°–1400°K by passing HCl at one atmosphere over a sample of powdered rutile.

Values for the heat of formation of $TiCl_4$, which have been cited in the literature, have been based on a single experimental measurement made by Thomsen[1] in 1870. Thomsen measured the heat of hydrolysis of $TiCl_4$. From the heat of reaction for Eq. (1), both the heat of formation and entropy of $TiCl_4(g)$ can be obtained since the thermodynamic quantities for TiO_2, HCl, and H_2O are now quite accurately known.

EXPERIMENTAL

A flow diagram of the apparatus, including the dimensions of the equipment, for studying the equilibria of Eq. (1) is shown in Fig. 1.

The TiO_2 was placed in the quartz reaction tube which was inserted in a tubular combustion furnace which was heated by means of globar elements. The HCl entered the quartz tube very close to barometric pressure and the flow rate was adjusted to a low enough value to insure equilibrium between HCl and TiO_2. The N_2 shown in Fig. 1 was used only for flushing out the system between tests. It was found that volume flow rates of less than 5 cc per minute or velocity of approximately 1 cm per minute of HCl were necessary to maintain equilibrium over a sample of TiO_2 with a surface area of approximately 15 square cm. Figure 2 shows the constancy of weight loss of rutile per unit volume *versus* flow rate in this low flow range. This would indicate that the atmosphere of HCl passing over the sample of TiO_2 is saturated with the gaseous products produced in the equilibrium. Furthermore a calculation of the diffusion rate of material in this apparatus shows that approximately 98% of the material has diffused into the volume of the apparatus within 30 seconds while approximately 10 minutes is the elapsed time for the HCl to pass over the sample in this flow range.

At this rate of flow, pressure drop through the tube was less than 0.5% of barometric pressure. Thus the pressure in the tube was essentially barometric. The flow rates were determined by measuring the change in pressure with time in the specially designed stainless steel HCl pressure chamber of known volume which contained the dry HCl. Constancy of flow rate was indicated by the Fisher-Porter Flowmeter. The pressure measurements were made with a precision of ±0.1 psi. The gas was preheated by means of the quartz beads and the temperature of the gas passing over the boat was kept constant to ±3°C. Rutile was prepared by heating anatase in a furnace at 1050°C for 3 hours. An x-ray diffraction analysis of the cooled sample showed complete conversion from anatase to rutile.

* This paper presents the results of one phase of research carried out at the Jet Propulsion Laboratory, California Institute of Technology, sponsored by the Department of Army, Ordnance Corps and the Department of Navy, Office of Naval Research, under Contract No. DA-04-495-ORD 18.

† Present address: Aerojet-General Corporation, Azusa, California.

‡ Present address: General Petroleum Corporation, Los Angeles, California.

[1] J. Thomsen and Ann Pogg, *Thermochemische Untersuchungen* (Leipzig, 1870), Bd 1, pp. 193–224, 227.

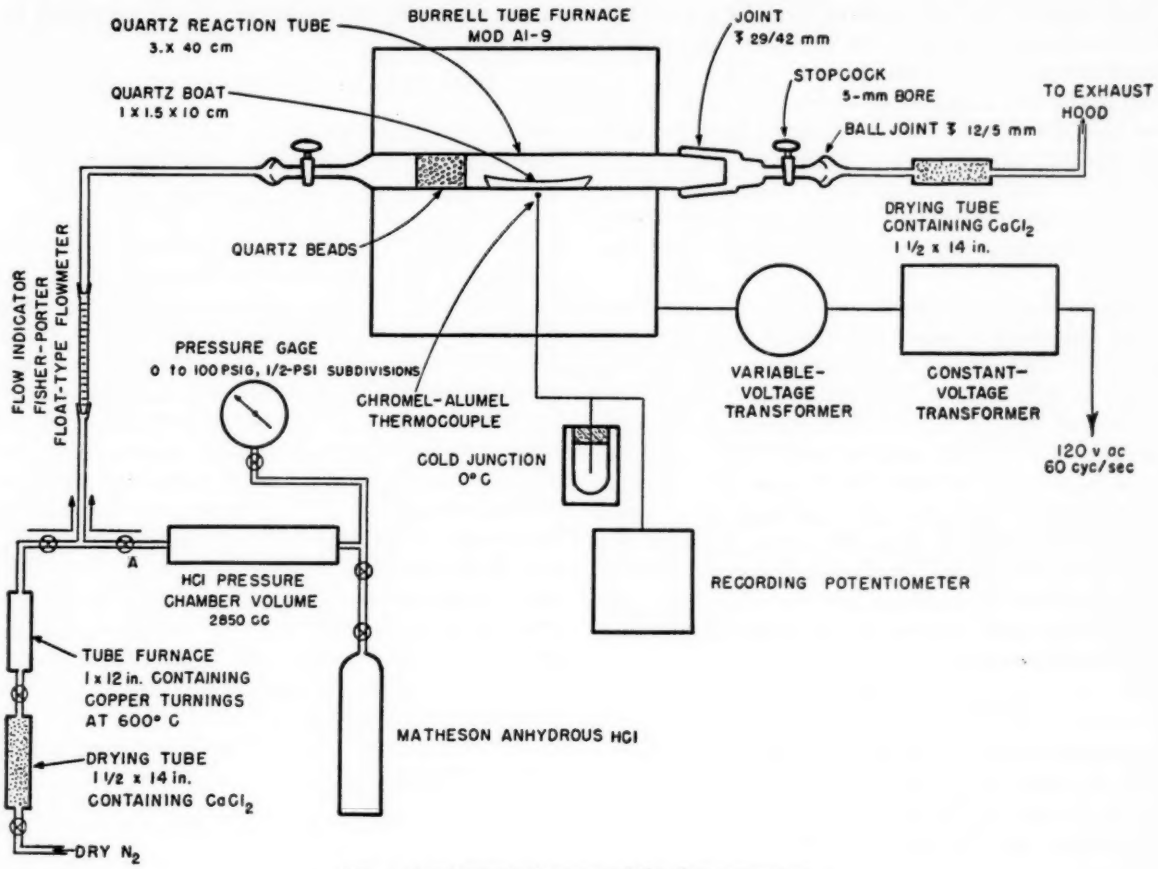

FIG. 1. A schematic diagram of the flow apparatus.

It was assumed that rutile was in the III form at room temperature. The total quantity of HCl passing at a constant flow-rate over the sample was measured and the amount of TiO_2 reacting was determined by measuring the difference in weight of the TiO_2 sample before and after each test.

It was assumed that gases leaving the TiO_2 boat shown in Fig. 2 are at equilibrium with respect to the reaction represented by Eq. (1). Then P_{TiCl_4}, the equilibrium partial pressure of $TiCl_4$ in the gases leaving the boat can be calculated, assuming the perfect gas law obtains, by the following relationship:

$$P_{TiCl_4}=\frac{\frac{m}{M}RT_h}{V_h}. \tag{2}$$

The quantity m/M represents the moles of TiO_2 reacted in time t which is equivalent to the moles of $TiCl_4$ formed. Furthermore, T_h is the temperature of the furnace of V_h which is the total volume of gases passing over the boat of TiO_2. If it is assumed that the number of moles of $TiCl_4$ and H_2O in the equilibrium mixture is negligibly small compared to the number of moles of HCl, Eq. (2) may be rewritten as

$$P_{TiCl_4}=\frac{m}{M}\frac{RT_0}{V_0}, \tag{3}$$

where T_0 is the ambient temperature and V_0 the total volume of HCl entering the system in time t at ambient temperature and at barometric pressure.

The partial pressure of H_2O was assumed to be twice that of $TiCl_4$ in accordance with the stochiometry of Eq. (1) and that of the HCl as one atmosphere less 4 times the partial pressure of $TiCl_4$ since the total pressure of the system was always maintained at barometric pressure. This correction to HCl pressure was very small, amounting to less than 2% of the total pressure which is in keeping with the assumptions made in arriving at Eq. (3).

In order to ascertain the fact that the reaction of HCl and TiO_2 proceeds according to Eq. (1) and that no oxychlorides are formed several experiments were performed.

In one experiment the deposit that collects in the cold end of the tube (the right side of the tube outside the furnace in Fig. 1) during the flow of HCl over the TiO_2 in the furnace has been analyzed and found to contain 2.2% Cl. This deposit is presumably formed when $TiCl_4$

and H_2O react in the cold zone to form TiO_2 and HCl. If $TiOCl_2$ were forming in the hot zone and were volatilized and deposited in the cold end, or if $TiCl_4$ and H_2O formed in the hot zone and recombined to give $TiOCl_2$ in the cold zone, it would be presumed that the solid would analyze approximately 50% Cl. The 2% Cl found in the residue could be due to absorbed HCl in the moist TiO_2 or due to a very small amount of $TiOCl_2$. No Cl was found in the residual TiO_2 in the boat after each test.

Another experiment was performed to determine whether any $TiOCl_2$ would be formed when Cl_2 was passed over TiO_2 at a high temperature. During the previous flow experiments in which HCl was passed over TiO_2, quantities in the neighborhood of 50 to 100 mg of TiO_2 per liter (at ambient conditions) of HCl in a temperature range of 900–1300°K were used in forming the reaction products. Two previous experiments cited in the literature[2,3] show that when Cl_2 is passed over TiO_2 in this same temperature range the loss of TiO_2 ranges from 0.1 to 10 mg per liter at ambient conditions of Cl_2. Both references cite $TiCl_4$ as being the reaction product according to

$$TiO_2+2Cl_2=TiCl_4+O_2. \quad (4)$$

This experiment was repeated at a single temperature, 1040°K. Six liters of Cl_2 were passed over the rutile in a period of 70 hours. The average loss in TiO_2 was approximately 1 mg/liter which checks with the data of Galmiche.[3]

In another experiment that was performed $TiCl_4(g)$ was passed over TiO_2 to determine whether any $TiOCl_2$ or other oxychloride forms. For example, if $TiOCl_2$ forms when HCl is passed over TiO_2, according to the following,

$$2TiO_2(s)+4HCl(g)=2TiOCl_2(g)+2H_2O(g), \quad (5)$$

then it would be expected that $TiCl_4$ would react with TiO_2 to give this oxychloride according to

$$TiO_2(s)+TiCl_4(g)=2TiOCl_2(g). \quad (6)$$

One atmosphere of He containing 30 mm of $TiCl_4$ was passed over rutile at a temperature of 1122°K for a period of 22 hours with no evidence of change of weight of the boat and contents during this time. The flow rates of the gas over the solid in all these experiments were of the order of 1 cm/min which should allow time for the reaction. The lack of reaction of TiO_2 with $TiCl_4$ establishes the preference of the formation of $TiCl_4$ over that of $TiOCl_2$ in the preceding experiments.

The assumption that the gaseous products are H_2O, HCl, and $TiCl_4$ seems valid if the dissociation of $TiCl_4$ into $TiCl_3$ and Cl_2 is assumed to be small. This dissociation is found to be less than 1% at 1100°K in the temperature range studied as calculated from the values of the heats of formation of $TiCl_3$ and $TiCl_4$.[4] Another indication that only negligible amounts of $TiCl_3$ were formed is that the quartz tube did not have any deposit on it in the region that was kept at or a little below the furnace temperature.

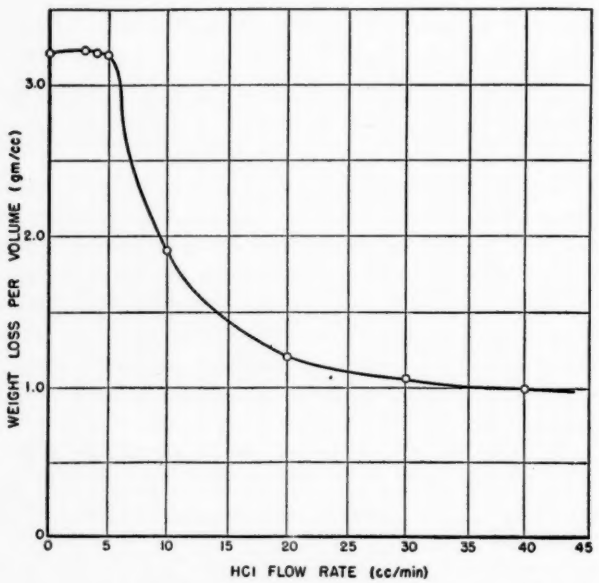

FIG. 2. Wt. loss of TiO_2 (rutile) per unit volume in a steady-state reaction with $HCl(g)$ at 1190°K.

DISCUSSION OF RESULTS

A plot for 1190°K of the wt loss of TiO_2 per unit volume *versus* the volumetric flow rate of HCl is shown in Fig. 2. Measurements were made at several temperatures over the range 800°–1400°K and experimental results including the calculated equilibrium constants K and free energies ΔF are given in Table I. Figure 3 shows a plot of the logarithm of K *vs* $1/T$. The ΔH_r of the reaction is given from the van't Hoff relationship as the slope of the line in this figure and is found to be 12.9 kcal/mole.

From the ΔH of the reaction, a value of ΔH_f for $TiCl_4$ can be calculated if the ΔH_f values of TiO_2 (rutile), $H_2O(g)$, and $HCl(g)$ are known. Values of

TABLE I. Experimental data and calculated free energies for the reaction TiO_2 (rutile)$+4HCl=TiCl_4(g)+2H_2O$.

T(°K)	Wt. loss of TiO_2 (g)	Flow rate of HCl (cc/min)	Wt. loss of TiO_2 per cc of HCl (g/cc)	p_{TiCl_4} (atmos)	$K=\frac{p_{TiCl_4}p^2_{H_2O}}{p^4_{HCl}}$	ΔF kcal/mole
876	0.1629	2.0	2.11×10^{-5}	0.00652	1.23×10^{-6}	23.6
878	0.0824	4.1	2.09×10^{-5}	0.00643	1.18×10^{-6}	23.7
977	0.1067	4.1	2.80×10^{-5}	0.00845	2.77×10^{-6}	24.8
977	0.1073	4.0	2.69×10^{-5}	0.00828	2.60×10^{-6}	25.0
1005	0.0767	2.1	2.85×10^{-5}	0.00871	3.05×10^{-6}	25.3
1088	0.1646	5.0	3.41×10^{-5}	0.0105	5.50×10^{-6}	26.2
1183	0.1832	4.6	4.11×10^{-5}	0.0124	9.39×10^{-6}	27.4
1296	0.1372	3.1	4.57×10^{-5}	0.0140	1.38×10^{-5}	28.6
1317	0.1508	3.6	4.56×10^{-5}	0.0140	1.38×10^{-5}	29.2

[2] W. Kongro and R. Jahn, Z. Anorg. Chem. **210**, 325–336 (1933).
[3] P. Galmiche, Ann. Chim. **3**, 243–270 (1948).
[4] Rossini, Wagman, Evans, Levine, and Jaffa, *Selected Values of Chemical Thermodynamic Properties* (National Bureau of Standards, Washington, D. C., February, 1952), Circular 500.

TABLE II. Thermodynamic data for the reaction TiO_2 (rutile)$+4HCL=TiC_4(g)+2H_2O(g)$.

ΔH_r at 1100°K	12.9 kcal/mole
ΔS_r at 1100°K	−12.3 cal/°/mole
ΔF_r at 1100°K	26.4 kcal/mole
ΔC_p at 1100°K	2.6 cal/°/mole
ΔH_r at 298°K	15.0 kcal/mole
ΔS_r at 298°K	−8.9 cal/°/mole
$\Delta F=-RT\ln K=15{,}775+2.6T\ln T-8.4T$ (cal)	
$\Delta H_{298°K}(TiCl_4g)=-182.9\pm0.5$ kcal/mole	
$\Delta H_{298°K}(TiCl_4l)=-192.5\pm0.5$ kcal/mole	
$S_{1100°K}(TiCl_4g)=124$ cal/°/mole	

−22.0 and −57.8 kcal/g mol were chosen for the standard heats of formation ΔH_f at 298°K for $HCl(g)$ and $H_2O(g)$, respectively.[4] The heat of formation of TiO_2 has been determined by a number of investigators,[5–13] with values ranging from −215 to −225.5 kcal/mole. The most recent determination made by Humphrey and listed in the literature[13] gives −225.5 kcal for the heat of formation of TiO_2 (rutile) by means of a constant volume combustion of Ti metal with oxygen. The value for ΔH_r of 12.9 kcal/g mol for the reaction represented by Eq. (1) as obtained from the slope of Fig. 3 can be assumed as the heat of reaction in the temperature range of the set of experiments, nominally from 850–1350°K with an average value at 1100°K. This value of ΔH_r at 1100°K can be used to obtain the heat of formation of $TiCl_4(g)$ at 1100°K as follows:

$$\Delta H_f^{1100}\ TiCl_4(g)=\Delta H_r^{1100}-2\Delta H_f^{1100}\ H_2O(g)+4\Delta H_f^{1100}\ HCl(g)+\Delta H_f^{1100}\ TiO_2. \quad (7)$$

Combining the known standard heats of formation with the enthalpy differences[14,15] between 298 and 1100°K for the substances, a value of -182.9 ± 0.5 kcal/mole is obtained for ΔH_f at 298°K for $TiCl_4(g)$. Employing the heat of vaporization of 9.6 kcal/mole[16] a value of 192.5 ± 0.5 kcal/mole is obtained for ΔH_f at 298°K for $TiCl_4(1)$.[17] Laschtschenko[14] has reported heats of transition amounting to 1.05 kcal/mole between the various forms of rutile. If these were taken into account the value obtained for ΔH_f of $TiCl_4$ would be lowered by 1 kcal. The thermodynamic quantities obtained are listed in Table II.

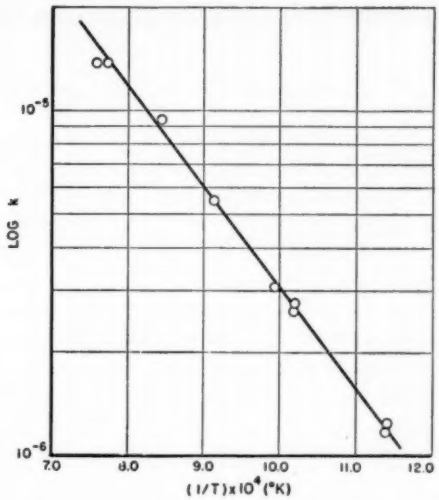

FIG. 3. The logarithm of the equilibrium, TiO_2 (rutile)$+4HCl=TiCl_4(g)+2H_2O(g)$ as a function of the reciprocal of the absolute temperature.

The entropy of the reaction is found to be −12.3 cal/°/mole in the temperature range investigated and leads to a value of 124 cal/°/mole for the entropy of $TiCl_4(g)$ at 1100°K. This value is higher than the 117 cal/°/mole calculated from spectroscopic[15] data based on the assumption that the $TiCl_4$ molecule is a rigid rotator and harmonic oscillator. The difference in entropy between the calculated and experimental value may be interpreted to be in part the anharmonic contribution to the entropy.

[5] W. A. Roth and U. Wolf, Rec. trav. chim. **59**, 511–515 (1940).
[6] W. H. Mixter, Am. J. Sci. **33**, 45–48 (1912).
[7] W. A. Roth and G. Becker, A. physik chem. **A159**, 1–26 (1932).
[8] Neumann, Kroger, and Kunz, Z. anorg. u. allgem. Chem. **218**, 379–401 (1934).
[9] W. A. Roth and G. Becker, Z. physik chem. Bodenstein-Festbund, 55–60 (1931).
[10] Sieverts, Gotta, and Halberstadt, Z. anorg. u. allgem. Chem. **187**, 155–64 (1930).
[11] A. Sieverts and A. Gotta, Z. anorg. u. allgem. Chem. **199**, 384–86 (1931).
[12] W. A. Roth, Naturwissenachaften **19**, 860 (1931).
[13] G. L. Humphrey, J. Am. Chem. Soc. **73**, 1590 (1951).
[14] F. R. Bichowsky and F. D. Rossini, *Thermochemistry of Chemical Substances* (Reinhold Publishing Corporation, New York, 1936).
[15] K. K. Kelley, "Contributions to the Data on Theoretical Metallurgy"—X. High-Temperature Heat-Content, Heat-Capacity, and Entropy Data for Inorganic Compounds," U. S. Bureau of Mines Bulletin No. 476 (1949).
[16] K. K. Kelley "Contributions to the Data on Theoretical Metallurgy, III. The Free Energies of Vaporization and Vapor Pressures of Inorganic Substances," U. S. Bureau of Mines, Bulletin No. 383, p. 106 (1935).
[17] While this paper was in process of publication two values for the heat of formation of $TiCl_4(l)$ have been reported: Skinner and Ruerwein have reported a value of -191 ± 1 kcal/mole [J. Phys. Chem. **59**, 113 (1955)], and Johnson, Nelson, and Prosen have reported a value of -192.9 ± 0.5 kcal/mole (private communication reported in NBS Report No. 3663).

Infrared Spectra of Oxonium Halides and the Structure of the Oxonium Ion

C. C. FERRISO AND D. F. HORNIG
Department of Chemistry, Metcalf Research Laboratory, Brown University, Providence 12, Rhode Island

The monohydrates of the hydrogen halides exist as ionic crystals. The infrared spectra of OH_3F, OH_3Cl, OH_3Br, OH_3I, and OD_3Cl at $-195°C$ showed the four fundamental frequencies expected for a symmetrical pyramid at about 1100 cm^{-1} (ν_2), 1700 cm^{-1} (ν_4), 2600 cm^{-1} (ν_1 or ν_3), and 3200 cm^{-1} (ν_1 or ν_3). The high-frequency bands, which are very broad at $-195°C$, did not sharpen on cooling to 8°K, indicating that their breadth is caused by some frozen-in disorder.

THE purpose of this investigation was to observe the infrared spectrum of the oxonium ion (OH_3^+) and to ascertain its structure. The monohydrates of the hydrogen halides were chosen for the study since if they are ionic the OH_3^+ ion is the only species in these systems which will have an infrared absorption spectrum.

The formation of oxonium ions in water has often been postulated[1] but little direct evidence of their existence has been obtained until recently. By comparing the powder x-ray diffraction patterns of perchloric acid monohydrate and ammonium perchlorate, Volmer[2] concluded that the monohydrate exists in the solid as $OH_3^+ClO_4^-$. On the other hand, Luizzati,[3] who studied single crystals of nitric acid monohydrate, found unequal N—O distances and concluded that the structure was not oxonium nitrate. More recently,[4,5] nuclear magnetic resonance spectra of the crystalline monohydrates of several inorganic acids have been studied and found to be characteristic of a set of three protons arranged in an equilateral triangle.

In a preliminary account of the present work[6] we have reported the infrared spectra of OH_3Cl and OH_3Br and concluded that the OH_3^+ ion existed in a symmetrical pyramidal configuration, similar to that of NH_3 with which it is isoelectronic, and is strongly hydrogen bonded. At about the same time Bethell and Sheppard[7] reported the spectrum of the OH_3^+ ion in crystalline nitric acid monohydrate, but their observations were complicated by the overlapping NO_3^- spectrum. The frequencies reported in the two investigations were in excellent agreement. We should now like to give a more detailed account of the observations on OH_3Cl and OH_3Br as well as to report the results of studies on the hydrates of HF and HI.

The monohydrates of the hydrogen halides, except HI, are well defined compounds of exact composition. Rupert[8] observed a tri-, di-, and monohydrate in the H_2O–HCl system. He reports the monohydrate to be a stable species melting at $-15.3°C$. Roozeboom[9] found four stable hydrates, mono through tetra, in the $HBr \cdot H_2O$ system, the compound $HBr \cdot H_2O$ melting at $-15.6°C$. A study of the HI–H_2O system by Pickering,[10] on the other hand, indicates that the monohydrate does not exist. A thermal study of the freezing points of the system HF–H_2O[11] shows the existence of three compounds: $H_2O \cdot HF$, m.p. $-35.5°C$; $H_2O \cdot 2HF$, incongruent melting; and $H_2O \cdot 4HF$, m.p. $-100.4°C$.

EXPERIMENTAL

The spectra were taken with a Perkin-Elmer Model 83 spectrometer modified for use as a ratio-recording double beam instrument.[12] CaF_2, NaCl, and KBr prisms, calibrated with absorption lines of H_2O, NH_3, CO_2, etc., were used. Nonscattering films of the samples were condensed on AgCl blanks which had previously been cooled to $-195°C$ and studied at the same temperature in a low temperature cell similar to that described previously.[13]

In order to prepare the samples of OH_3X, H_2O vapor at a pressure of 18 mm Hg was admitted to a two-liter flask and the sample subsequently condensed in a liquid nitrogen trap. The flask was then evacuated and an equal pressure of dry HX admitted. The sample in the trap was then warmed and the two gases mixed by diffusion. In the work described in our previous communication and in the preparation of the OH_3I here, the H_2O was admitted to the flask and HX was added until the pressure doubled. Presumably because of gas imperfections, the method led to a systematic excess of HX and was abandoned. The gaseous mixtures were then admitted into the cell in small bursts through a stopcock connecting the mixing system to the cell. Following this procedure any desired film thickness could be obtained. Samples of OH_3X were condensed on KBr, NaCl, AgCl, and KRS-5, and the same spectra were obtained in each case, indicating no orientation effects by the backing material.

[1] E. Hückel, Z. Electrochem. **34**, 536 (1918).
[2] M. Volmer, Ann. Chem. **440**, 200 (1924).
[3] V. Luizzati, Acta Cryst. **4**, 239 (1951).
[4] R. E. Richards and J. A. S. Smith, Trans. Faraday Soc. **48**, 1216 (1951).
[5] Y. Kaliuchi *et al.*, J. Phys. Soc. Japan **7**, 102 (1952).
[6] C. C. Ferriso and D. F. Hornig, J. Am. Chem. Soc. **75**, 4113 (1953).
[7] D. E. Bethell and N. Sheppard, J. Chem. Phys. **21**, 1421 (1953).
[8] F. F. Rupert, J. Am. Chem. Soc. **31**, 851 (1909).
[9] J. Roozeboom, Rec. Trav. Chem. Pays-Bas **5**, 328 (1886).
[10] U. S. Pickering, Ber. Deut. chem. Ges. **26**, 2307 (1893).
[11] G. H. Cady and J. H. Hildebrand, J. Am. Chem. Soc. **52**, 3843 (1930).
[12] Hornig, Hyde, and Adcock, J. Opt. Soc. Am. **40**, 497 (1950).
[13] E. L. Wagner and D. F. Hornig, J. Chem. Phys. **18**, 296 (1950).

Anhydrous commercial HCl* and HBr,* dried over P_2O_5, were used to prepare OH_3Cl and OH_3Br, respectively. The purity of these gases was 99.6%, and no evidence of impurities was found in the spectra.

Hydrogen iodide, not available commercially in anhydrous form, was prepared from the reaction of sodium iodide with phosphoric acid.[14]

The HI thus prepared was passed through a CO_2 trap to remove I_2, dried over P_2O_5, and distilled from a liquid nitrogen trap. Photodecomposition of HI was prevented by wrapping the entire mixing system with aluminum foil when preparing OH_3I.

The DCl used in preparing the samples of OD_3Cl was obtained by reacting NaCl with *d*-phosphoric acid. The *d*-phosphoric acid was prepared by adding 99.99% deuterium oxide† to P_2O_5 until all but a small amount of P_2O_5 had been used up in the reaction. From the relative integrated intensity of the OH and OD stretching bands it was estimated that the sample was 95% deuterated. Therefore it probably contained about 85% OD_3^+, 15% OD_2H^+, and less than 1% of other ions (ODH_2^+ and OH_3^+).

Commercial anhydrous HF‡ and distilled H_2O were used to prepare samples of OH_3F. The preparation of these samples was carried out in a copper system. The glass portions of the system and cell were protected from attack by HF by baking on a thin film of "Glyptal." It was observed that the HF "creeps" under the Glyptal coating and peels it off. However, if all the glass in the apparatus was first covered with a thin film of Apiezon "M" grease, the resulting coating remained impervious to HF attack.

EXPERIMENTAL RESULTS

The infrared absorption spectra obtained for OH_3Cl, OD_3Cl, OH_3Br, OH_3I, and OH_3F at $-195°C$, from 400 cm^{-1} to 4000 cm^{-1}, are reproduced in Fig. 1. The lower lines represent thick films while the upper lines indicate much thinner samples. Although the spectra reproduced are those obtained on a AgCl backing, spectra have been observed using KBr, NaCl, and CaF_2 backing material, and these indicate that there are no reactions occurring with the sample which might lead to spurious results. The infrared band center and a tentative assignment are given in Table I. Because of the broadness of the bands, an uncertainty of approximately ± 6 cm^{-1} is introduced in determining the band minima, well outside the accuracy with which frequencies can be determined on sharp peaks.

The general features of the spectra can be interpreted in terms of a pyramidal oxonium ion. We would expect four infrared active fundamentals consisting of two bending modes and two stretching modes.[15] All four fundamentals are present in the spectrum of each of the oxonium halides.

The lowest frequency peak near 1100 cm^{-1} in all of the OH_3^+ compounds must be ascribed to the symmetric bend, ν_2, and the peak near 1700 cm^{-1} to the doubly degenerate bend, ν_4. The corresponding frequencies in crystalline NH_3 are 1060 cm^{-1} and 1646 cm^{-1}.[16]

The two peaks in the OH stretching region are both exceedingly broad and it is not immediately obvious which corresponds to the symmetric stretching vibration ν_1 and which to the degenerate stretch, ν_3. In addition to the fundamental vibrations, all of the compounds show a peak near 2100 cm^{-1} which corresponds well with the expected position of $2\nu_2$.

There is no evidence in the present spectra of OH_3Cl, OH_3Br, or OH_3F of bands due to either HX or H_2O. Ice has intense bands at 812 cm^{-1} [17] and 3150 cm^{-1},[18] crystalline HCl at 2704 cm^{-1} and 2746 cm^{-1},[19,20] HBr at 2404 cm^{-1} and 2438 cm^{-1} [21] and HF, a broad band at *ca* 3500 cm^{-1},[22] none of which appear in the spectra of the equimolar compound. In the OH_3Cl and OH_3Br spectra published previously[6] a peak due to hydrogen halide molecules was observed. However, since great care was taken to make the present specimens with the correct composition, it must be presumed that the earlier specimens contained a slight excess of the hydrogen halide because of the method used in preparing them.

The OH_3I spectrum, on the other hand, shows an HI peak at 2120 cm^{-1},[21] so if the sample had the stoichiometric composition, it is possible that it also contains free H_2O. At first sight the great intensity of the peak at 3235 cm^{-1} also suggests that this is the case. However, the OH_3I sample was prepared by the same method as the OH_3Cl and OH_3Br whose spectra were published previously, so that it is likely that there actually was a slight genuine excess of HI. Certainly the general parallelism between the four spectra suggests that it contains OH_3I in large part.

The relative intensities of the two stretching bands vary considerably from one compound to another. Although it would be hard to prove that this may not be connected with the presence of free H_2O, no corresponding variations are observed in the vicinity of the H_2O bending vibration, 1620 cm^{-1}, except in OH_3I where the peak at this frequency is also more intense. Furthermore, we have condensed mixtures with compositions ranging from 90% HCl–10% H_2O to 10% HCl–90% H_2O. The peak at 3250 cm^{-1} was

* The Matheson Company, East Rutherford, New Jersey.

[14] N. L. Alpert, Phys. Rev. **75**, 398 (1949).

† Norsk Hydro-Elektrisk Kvaelstofaktieselskab, Oslo, Norway.

‡ The Matheson Company, East Rutherford, New Jersey.

[15] G. Herzberg, *Infrared and Raman Spectra of Polyatomic Molecules* (D. Van Nostrand Company, Inc., New York, 1945), p. 110.

[16] F. P. Reding and D. F. Hornig, J. Chem. Phys. **19**, 594 (1951).

[17] F. P. Reding, thesis, Brown University (1951).

[18] J. J. Fox and A. E. Martin, Proc. Roy. Soc. (London) **A174**, 234 (1940).

[19] G. H. Hettner, Z. Physik **78**, 141 (1932).

[20] Lee, Sutherland, and Wu, Proc. Roy. Soc. (London) **A176**, 493 (1940).

[21] W. E. Osberg, thesis, Brown University (1951).

[22] Private communication, Gordon L. Hiebert, Brown University.

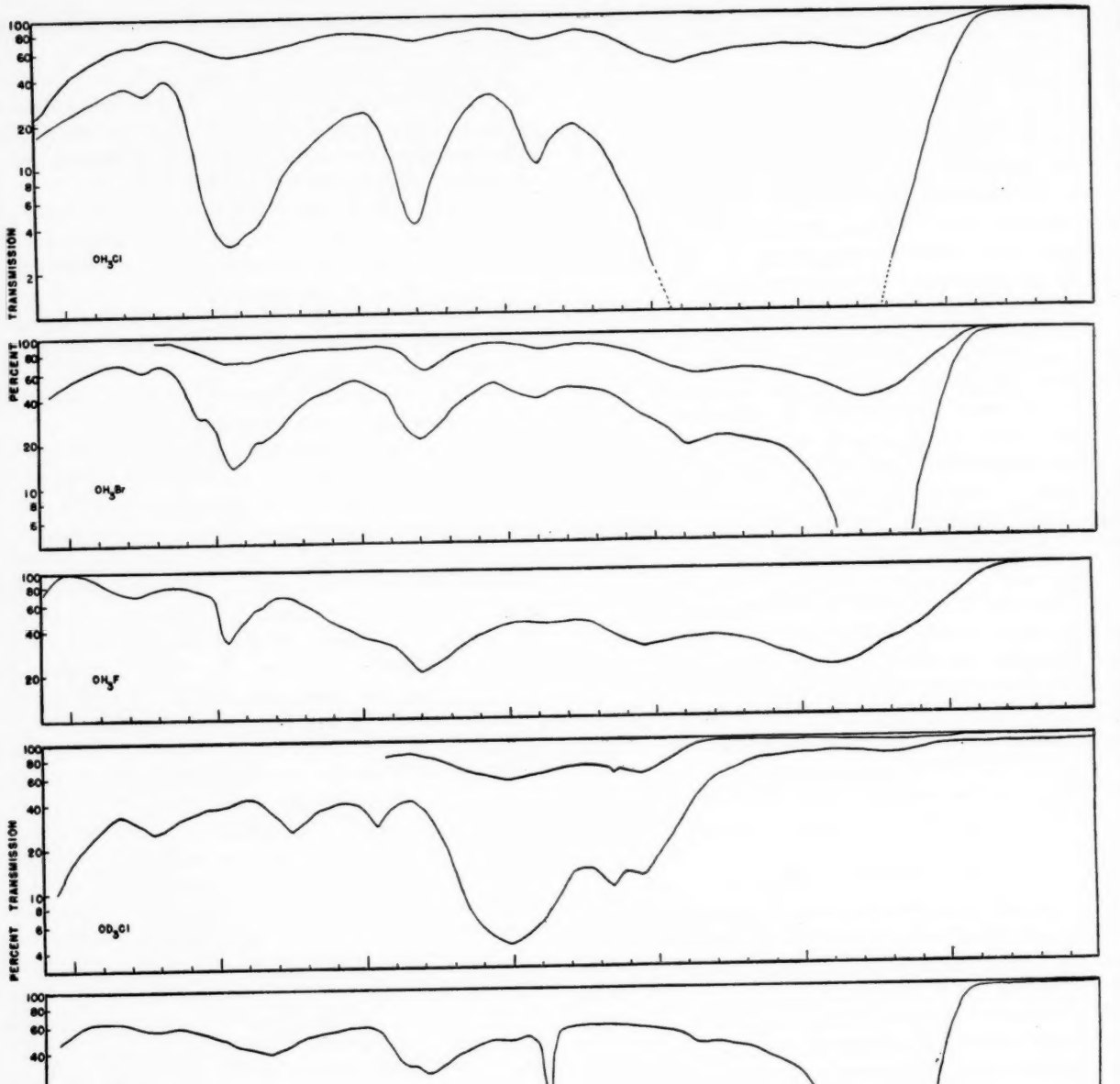

FIG. 1. Infrared spectrum of oxonium slats at −195°C.

present even when an enormous excess of HCl was present; the presence of excess H_2O produced spectra which were complicated by the diffuse ice spectrum.

The frequency of the parallel bending vibration, ν_2, is remarkably constant in all four OH_3X compounds. However, its intensity and appearance differ considerably from one to another, definite structure appearing in OH_3Cl and OH_3Br. Whether the structure results from having several molecules in a unit cell or from combinations with lattice frequencies is difficult to say. In OH_3Br at least, there is the suggestion that the peaks at 1150 cm^{-1} and 950 cm^{-1} are sum and difference bands involving a lattice frequency of about 100 cm^{-1}.

The perpendicular bending vibration, ν_4, appears to be split in OH_3I, and in addition to the possibilities mentioned in connection with ν_2 it is also possible here that the degeneracy is removed. However, since the peak at 1640 cm^{-1} may be caused by H_2O, speculation is fruitless.

The only low frequency bands observed were the weak bands near 750 cm^{-1} which appeared in the spectra of the thick films. An investigation of the lower frequency region with a KRS-5 prism showed no further

TABLE I. Vibrational frequencies in oxonium salts.

Assignment	OH_3Cl	OH_3Br	OH_3F	OH_3I	OD_3Cl	OH_2NO_3[a]
O-H stretch (OD_2H^+)	...	...	...	...	3260	...
ν_3 or ν_1	3235	3250	3150	3350[b]	2445	3380
O-D stretch (OD_2H^+)	...	...	...	...	2350	...
ν_3 or ν_1	2590	2610	2468	2635	2000	2650
$2\nu_2$	2109	2100	2120	2050	1545	...
ν_4	1700	1705	1705	1705 1640[b]	1255	1670
O-D bend (OD_2H^+)	...	...	...	...	1015	...
ν_2	1150	1150	1150	1160	785	1130
	1060	1060	1048			
		950				
ν_L	770	750	740	810	...	816 670

[a] See reference 7.
[b] May be due all or in part to free H_2O.

absorption down to 300 cm^{-1}. This poses an interesting problem since the torsional vibrations of the OH_3^+ ions (librations) perpendicular to the symmetry axis might have been expected to appear in this region. This frequency occurs at 362 cm^{-1} in the spectrum of crystalline ammonia[16] and is the most intense band in the entire spectrum. If the OH_3X crystals are strongly hydrogen bonded, as the great width and low frequencies of the stretching vibrations seem to indicate, this frequency ought to be higher in these compounds than in ammonia. Analogous frequencies occur at 812 cm^{-1} in ice,[16] 391 cm^{-1} in NH_4Cl[13] and 500 cm^{-1} in NH_4F.[23,24] This problem cannot be answered yet but one can say that *if* the bands at 770 cm^{-1} represent this frequency, the dipole moment of the OH_3^+ ion must be very small, at least ten times smaller than in ammonia.

FUNDAMENTAL STRETCHING VIBRATIONS

The only major question in the assignment concerns the hydrogen stretching vibrations, ν_1 and ν_3. The bands at 2635 cm^{-1} in OH_3I, 2610 cm^{-1} in OH_3Br, 2590 cm^{-1} in OH_3Cl and 2468 cm^{-1} in OH_3F must be fundamentals since no overtone or combination assignment fits them; the same applies to the bands at 3250 cm^{-1} in OH_3Br, 3235 cm^{-1} in OH_3Cl and 3150 cm^{-1} in OH_3F, which are in the more usual O—H stretching region as well. Some of the absorption in the region between 2500 cm^{-1} and 3500 cm^{-1} may well have its origin in the combination band, $\nu_2+\nu_4$, which is expected near 2750 cm^{-1}, and in $2\nu_4$, which should occur at about 3400 cm^{-1}, but these cannot account for the peaks.

In order to facilitate the assignment of the OH_3^+ spectrum, a sample of OD_3Cl was prepared. The thin film of OD_3Cl appears to mirror the OH_3Cl spectrum almost perfectly except for the appearance of OD_2H^+ peaks at 2350 cm^{-1} and 3260 cm^{-1}. Hence the OD_3^+ stretching frequencies are probably 2000 cm^{-1} and 2445 cm^{-1}. The question then is whether the high or low frequency should be assigned to ν_1 and vice versa for ν_3. The Teller-Redlich product ratios, if ν_1 is taken as the high frequency, are:

$$\text{Species } A \quad \frac{2590\times1060}{2000\times785}=1.75 \text{ (harmonic value}=1.86)$$

$$\text{Species } E \quad \frac{3235\times1700}{2445\times1255}=1.79 \text{ (harmonic value}=1.88).$$

If ν_1 is assumed to be the low frequency, one gets

$$\text{Species } A \quad \frac{3235\times1060}{2945\times785}=1.79 \text{ (harmonic value}=1.86)$$

$$\text{Species } B \quad \frac{2590\times1700}{2000\times1255}=1.75 \text{ (harmonic value}=1.88).$$

The harmonic values were calculated for C_3 symmetry, tetrahedral angles and an O—H distance of 0.98 A. It is apparent that the product ratios offer no basis for a choice between the two possibilities; they do demonstrate that in either case the O—H stretching vibrations are very anharmonic.

Nevertheless, we are inclined to the opinion that the lower frequency should be ascribed to the antisymmetric vibration, ν_3, and the higher frequency to ν_1. In NH_4F the antisymmetric stretching vibration of NH_4^+ is known to be lower in frequency than the breathing vibration[23,24] and from a comparison of heavy ice and ice, White[25] has come to the same conclusion for H_2O. Both of these compounds form moderately strong hydrogen bonds. In the case of NH_4F a qualitative explanation of this phenomenon has been given which would also apply here. Perhaps the strongest reason for believing that the high frequency is ν_1 is that in a study of the Raman spectrum of concentrated solutions of

[23] L. F. H. Bovey, J. Opt. Soc. Am. **41**, 836 (1951).
[24] R. C. Plumb and D. F. Hornig, J. Chem. Phys. **23**, 947 (1955).
[25] H. F. White, thesis, Brown University, 1953.

HCl in water, Busing[26] found no HCl band, but instead a very broad band extending from the vicinity of 2500 cm^{-1} to a center in the vicinity of 3200 cm^{-1}, in addition to the usual water bands. It seems likely that the band is caused by the OH_3^+ ions and, since the symmetric vibration can be expected to be much more intense in the Raman spectrum, it seems probable that it can be assigned to ν_1. Nevertheless, a final answer to the problem is not available.

LINE WIDTHS

All of the bands in the spectrum are wide but the O—H stretching bands are extraordinarily so. This behavior is common in strongly hydrogen bonded compounds[27] although in NH_4F, for example, all of the peaks are quite sharp. The question that can be asked is whether the widths arise from some sort of frozen-in disorder in the crystal or whether they are caused by combinations between the internal vibrations and the lattice frequencies of the crystal. In order to shed some light on this problem we cooled OH_3Cl to liquid helium temperature in a cell kindly loaned to us by G. L. Hiebert. A film was prepared at the liquid nitrogen temperature and cooled to 8°K; the spectrum was essentially unchanged. Hence it is safe to conclude that the width of the bands does not arise from dynamic effects but from some sort of disorder which was already "frozen in" at the temperature of liquid nitrogen.

[26] Private communication, W. R. Busing, Yale University.

[27] R. Rundle and M. Parasol, J. Chem. Phys. **20**, 1487 (1952); R. C. Lord and R. E. Merrifield, *ibid.*, **21**, 166 (1953).

THE JOURNAL OF CHEMICAL PHYSICS VOLUME 23, NUMBER 8 AUGUST, 1955

Modified Atomic Orbital Method. I. The Electronic Structure of the Ethylene Molecule*

KIMIO OHNO AND TAKASHI ITOH
Department of Physics, Faculty of Science, University of Tokyo, Tokyo, Japan
(Received November 19, 1954)

It is well known that the energy intervals separating ionic and covalent states, as given by the conventional ASMO method, are too large. In order to avoid this difficulty, a modification of the nonempirical atomic orbital method is proposed, and is applied to the ethylene molecule. The principal point of the modification is to use different atomic orbitals for covalent and ionic structures of the molecules in order to assess more correctly the energies of the ionic structures. The results of the calculation are fairly satisfactory in that they are as good as those of the semiempirical method by Moffitt. Some errors due to assumptions and approximations made in this calculation are discussed.

I. INTRODUCTION

IN describing electronic states of molecules by the atomic orbital method, we can generally obtain a comparatively accurate wave function by adding wave functions representing ionic structures to wave functions representing covalent structures. But up to the present, the same atomic orbitals have been used to describe both covalent and ionic structures. As atomic orbitals are usually determined by minimizing the energy of a neutral atom, the consequence is that ionic structures are treated by less accurate approximations as compared with covalent ones. Therefore, it has been impossible to assess properly the relative locations of some molecular levels or to predict the correct positions of some absorption bands.

There is a similar situation with regard to the molecular orbital method or the ASMO LCAO method which is now prevalent in quantitative molecular calculations. Some states turn out to be purely covalent and some others to be purely ionic and the ASMO theory predicts too high energies for the latter. For example, the theoretical value of the singlet-triplet separation of the excited B_{1u} states of the ethylene molecule is 8.6 ev while the observed value is 1.2 ev and, again, the theoretical prediction of the $^3\Sigma_u^- - ^3\Sigma_u^+$ interval of the oxygen molecule is 9.5 ev while the observed one is 1.4 ev.

Errors of 1∼2 ev seem to be inevitable in the present state of knowledge of molecular structures, but errors of 8 ev are too large to be permissible in some applications especially to the analysis of absorption bands.

Moffitt, who has carried out a series of detailed investigations[1–4] of this problem, has pointed out that the chief source of the error is our inability to describe correctly the term values of atomic states. So he has proposed a different quantitative theory called the method of atoms in molecules, in which he has separated

* A similar calculation has been made independently by Mr. Oohata and Mr. Aono.

[1] W. Moffitt, Proc. Roy. Soc. (London) **A210**, 224 (1951); **A210**, 245 (1951).
[2] W. Moffitt and J. Scanlan, Proc. Roy. Soc. (London) **A218**, 464 (1953).
[3] W. Moffitt, Proc. Roy. Soc. (London) **A218**, 486 (1953).
[4] W. Moffitt and J. Scanlan, Proc. Roy. Soc. (London) **A220**, 530 (1953).

the problem of atoms from that of molecules and has recommended the use of the experimental term values for the solution of the former problem and the treatment of the latter problem according to the perturbation technique using the usual atomic functions. This method was applied by him and Scanlan to π-electron states of oxygen,[1] ethylene,[2] cyclobutadiene, and benzene[4] and they succeeded in obtaining remarkably good agreement with experiment in the first two cases. In the case of the last two, the results were not so satisfactory as before but still compared favorably with the results by the ASMO method.

Pariser and Parr[5] proposed a simplified semiempirical ASMO theory in which the resonance integrals β and the Coulomb repulsion integral of the same atomic orbital $(qq; qq)$ are treated as empirical parameters and are determined in such a way as to fit some theoretical values to the corresponding experimental ones. Thus they succeeded in producing results in close agreement with observed values. The empirical parameter $(qq; qq)$ is equated to $I-A=E^{+}+E^{-}-2E$, where I is the ionization potential of the atom in its valence state, A is the electron affinity, and E^{+}, E^{-}, E are the energies of the positive ion, the negative ion, and the neutral atom, respectively. The quantity $I-A$ is related directly to the relative location of covalent and ionic states. So, although the method of Pariser and Parr appears to be different from that of Moffitt, they have much ground in common and are closely connected with each other.

Both of these two methods are semiempirical and it would be highly desirable to devise a nonempirical theory which can predict the observed values without resorting to any experimental data. In this paper, we should like to present a nonempirical calculation by which we can remove the difficulty mentioned above.

The essential point of the new method consists in the use of different atomic orbitals for covalent and ionic structures, namely we should determine the atomic orbitals by minimizing the energy of the structure of the molecule under consideration. An intuitive basis of this method is to be found in the following argument. In the negative ions, the charge clouds must presumably be more spread out than those of the neutral atoms owing to the larger inter-electronic repulsion, while conversely in the positive ions, the charge clouds must contract on account of the decrease in the repulsion. The simplest way of introducing this effect into the calculation is to adjust the screening constants in the exponents of the atomic orbitals separately for the positive and negative ions. Up to the present, the screening constant determined by minimizing the energy of the ground state of the neutral atom has also been used for the ions, and it is due to this fact that we have been misled in the estimation of the energy of the ions and accordingly in the treatment of the ionic structures of molecules. By our modification, we expect to remove this shortcoming, and in the following sections, the π-electron states of the ethylene molecule are calculated by this method.

[5] R. Pariser and R. G. Parr, J. Chem. Phys. **21**, 466 (1953); **21**, 767 (1953).

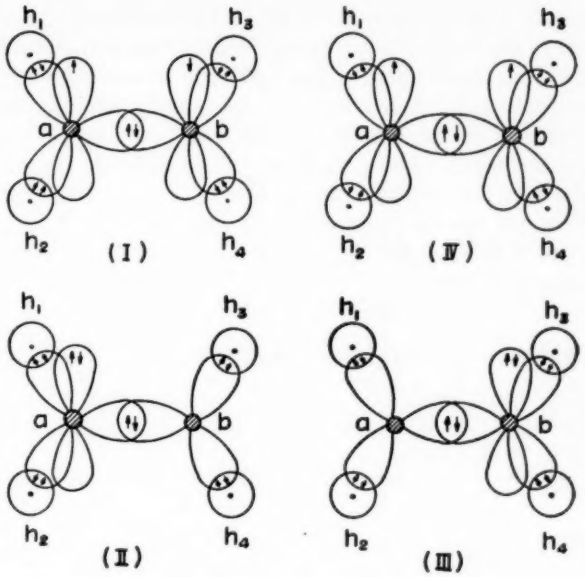

FIG. 1. The canonical structures of the ethylene molecule.

A number of studies were carried out on this simplest π-electron problem. Among others, Murai[6] performed the calculation, by taking different effective charges of the $2p\pi$ carbon atomic orbitals for the different molecular states but his result seems not to be so successful. One can see from the above discussions that the atomic orbital scheme is more adequate for adjusting the effective nuclear charges.

II. THE MODEL AND THE WAVE FUNCTION

We will treat the ethylene molecule in its stable form only, that is to say, assuming it to be planar and of symmetry D_{2h}. The four canonical structures given in Fig. 1 are considered. Structure (I) is a covalent structure with six sets of electron-pair bonds, four of which are formed between the σ orbitals of the carbon atoms and the $1s$ orbitals of the hydrogen atoms, and two between the σ and $2p\pi$ orbitals of the carbon atoms. Structure (II) is an ionic structure in which the carbon atom a has two $2p\pi$ electrons and the carbon atom b has none, thus leaving 5 sets of electron-pair bonds. The role of the atom a and b is reversed in structure (III). Structure (IV) is again a nonionic structure but there is no electron-pair bond between the two $2p\pi$ electrons, and their spins are parallel. The other five sets of electron-pair bonds remain unchanged.

If we take all the electrons into account, we are faced with a formidable sixteen electron problem. If we are to reduce the problem within practicable limits, we have to make these two drastic simplifying assumptions. First, the $1s$ electrons of both atoms are supposed to be

[6] T. Murai, Progr. Theoret. Phys. **7**, 345 (1952).

shrunk into the atomic nuclei, thus reducing the problem to one of twelve electrons. Secondly we do not treat the electrons in the attached hydrogen atoms explicitly, but only take their effect into account in keeping the electrons of the carbon atoms, which are bonded to the hydrogen atoms, in their sp^2 hybridized orbitals. The problem is now reduced to one of eight electrons. Then we can immediately write down the wave functions of these eight electrons for the above four structures as follows:

$$\Psi_{\rm I}=\frac{1}{\sqrt{8!}}\sum_P(-1)^P P\pi_a(1)\pi_b(2)\frac{\alpha_1\beta_2-\beta_1\alpha_2}{\sqrt{2}}$$
$$\times\sigma 1_a(3)\sigma 1_b(4)\frac{\alpha_3\beta_4-\beta_3\alpha_4}{\sqrt{2}}\sigma 2_a(5)\frac{\alpha_5\beta_9-\beta_5\alpha_9}{\sqrt{2}}$$
$$\times\sigma 3_a(6)\frac{\alpha_6\beta_{10}-\beta_6\alpha_{10}}{\sqrt{2}}\sigma 2_b(7)\frac{\alpha_7\beta_{11}-\beta_7\alpha_{11}}{\sqrt{2}}$$
$$\times\sigma 3_b(8)\frac{\alpha_8\beta_{12}-\beta_8\alpha_{12}}{\sqrt{2}},$$

$$\Psi_{\rm II}=\frac{1}{\sqrt{8!}}\sum_P(-1)^P P\pi_a^-(1)\alpha_1\pi_a^-(2)\beta_2$$
$$\times\sigma 1_a^-(3)\sigma 1_b^+(4)\frac{\alpha_3\beta_4-\beta_3\alpha_4}{\sqrt{2}}$$
$$\times\sigma 2_a^-(5)\frac{\alpha_5\beta_9-\beta_5\alpha_9}{\sqrt{2}}\sigma 3_a^-(6)\frac{\alpha_6\beta_{10}-\beta_6\alpha_{10}}{\sqrt{2}}$$
$$\times\sigma 2_b^+(7)\frac{\alpha_7\beta_{11}-\beta_7\alpha_{11}}{\sqrt{2}}\sigma 3_b^+(8)\frac{\alpha_8\beta_{12}-\beta_8\alpha_{12}}{\sqrt{2}},$$

$$\Psi_{\rm III}=\frac{1}{\sqrt{8!}}\sum_P(-1)^P P\pi_b^-(1)\alpha_1\pi_b^-(2)\beta_2$$
$$\times\sigma 1_a^+(3)\sigma 1_b^-(4)\frac{\alpha_3\beta_4-\beta_3\alpha_4}{\sqrt{2}}$$
$$\times\sigma 2_a^+(5)\frac{\alpha_5\beta_9-\beta_5\alpha_9}{\sqrt{2}}\sigma 3_a^+(6)\frac{\alpha_6\beta_{10}-\beta_6\alpha_{10}}{\sqrt{2}}$$
$$\times\sigma 2_b^-(7)\frac{\alpha_7\beta_{11}-\beta_7\alpha_{11}}{\sqrt{2}}\sigma 3_b^-(8)\frac{\alpha_8\beta_{12}-\beta_8\alpha_{12}}{\sqrt{2}},$$

$$\Psi_{\rm IV}=\frac{1}{\sqrt{8!}}\sum_P(-1)^P P\pi_a(1)\pi_b(2)\frac{\alpha_1\beta_2+\beta_1\alpha_2}{\sqrt{2}}$$
$$\times\sigma 1_a(3)\sigma 1_b(4)\frac{\alpha_3\beta_4-\beta_3\alpha_4}{\sqrt{2}}\sigma 2_a(5)\frac{\alpha_5\beta_9-\beta_5\alpha_9}{\sqrt{2}}$$
$$\times\sigma 3_a(6)\frac{\alpha_6\beta_{10}-\beta_6\alpha_{10}}{\sqrt{2}}\sigma 2_b(7)\frac{\alpha_7\beta_{11}-\beta_7\alpha_{11}}{\sqrt{2}}$$
$$\times\sigma 3_b(8)\frac{\alpha_8\beta_{12}-\beta_8\alpha_{12}}{\sqrt{2}},$$

where $\sigma 1_a$, $\sigma 2_a$, $\sigma 3_a$ are σ orbitals of the carbon atom a which are pointing out towards the other carbon atom b and the hydrogen atoms 1 and 2, respectively. Here we use spins of ghost-like electrons 9–12 to express the valence state wave function explicitly. It is to be understood that, in constructing the energy matrix, we carry out the summation over the spin variables of those electrons also.

Using these structural functions we can construct the state function with correct symmetries as follows:

$$\left.\begin{matrix}\Psi_N(^1A_g)\\ \Psi_Z(^1A_g)\end{matrix}\right\}=\Psi_{\rm I}+\left\{\begin{matrix}C\\ C'\end{matrix}\right\}(\Psi_{\rm II}+\Psi_{\rm III}),$$
$$\Psi_V(^1B_{1u})=\Psi_{\rm II}-\Psi_{\rm III},$$
$$\Psi_T(^3B_{1u})=\Psi_{\rm IV}.$$

In these functions we have assumed purely covalent electron-pair bond for all σ bonds. This assumption might be questioned with the light of the recent work of Mueller,[7] who seems to have shown that, in the case of the C—C σ bond of ethylene, the ionic structure contributed just as much as the covalent structure. This does not seem to conform with our usual physical concept and in this paper we have followed the old picture mainly because of its simplicity.

III. THE ENERGY MATRIX AND ITS EVALUATION

As we do not treat explicitly the attached hydrogen atoms and the 1s electrons of the carbon atoms, the Hamiltonian of the system becomes

$$\mathfrak{H}=\sum_{i=1}^{8}\left(-\tfrac{1}{2}\Delta_i-\frac{4}{r_{ai}}-\frac{4}{r_{bi}}\right)+\sum_{i<j}^{8}\frac{1}{r_{ij}}=\sum_{i=1}^{8}F_i+\sum_{i<j}^{8}\frac{1}{r_{ij}}.\dagger$$

Now we proceed to construct the energy matrix with respect to the four functions $\Psi_{\rm I}$, $\Psi_{\rm II}$, $\Psi_{\rm III}$, $\Psi_{\rm IV}$. Here we are forced to introduce a further approximation in order to avoid the complexity of higher-order permutations which is inherent in the atomic orbital method. Namely, we neglect all the overlap integrals between the σ orbitals. We can hardly justify this procedure straightforwardly, because the overlap integral between $\sigma 1_a$ and $\sigma 1_b$ at least cannot be small. However, as we are interested in π-electron states of the molecule, we may allow ourselves to hope that this assumption does not bring about great changes in the intervals of these states. Adopting this assumption and treating σ orbitals as sp^2 hybridized orbitals, the energy matrix and the overlap matrix are computed straightforwardly.

Then we can see that the energy matrix consists of three parts: (1) the π-electron part, (2) the σ-electron part and (3) the $\pi-\sigma$ interaction part. In part (2), terms involving orbitals of positive and negative ions

[7] C. R. Mueller, J. Chem. Phys. **22**, 120 (1954).

† The atomic unit is used throughout this paper.

TABLE I. Value of $I-A$.

Method	$I-A$
$Z=Z^+=Z^-=3.25$	17.2 ev
$Z=3.25$, $Z^+=3.60$, $Z^-=2.90$[a]	12.3 ev
semiempirical[b]	10.5 ev

[a] These values are determined by Slater rules.
[b] R. S. Mulliken, J. Chem. Phys. **2**, 782 (1934).

always appear in pairs. Let us approximate them by the sum of the corresponding neutral terms for example

$$(s_a^-|F|s_a^-)+(s_b^+|F|s_b^+)\doteqdot 2(s_a|F|s_a),$$

$$(\sigma 1_a^-\sigma 1_a^-;\sigma 2_a^-\sigma 2_a^-)+(\sigma 1_b^+\sigma 1_b^+;\sigma 2_b^+\sigma 2_b^+)\doteqdot 2(\sigma 1_a\sigma 1_a;\sigma 2_a\sigma 2_a),$$

$$(\sigma 1_a^-\sigma 1_a^-;\sigma 1_b^+\sigma 1_b^+)\doteqdot(\sigma 1_a\sigma 1_a;\sigma 1_b\sigma 1_b),$$

$$(\sigma 1_a^-\sigma 1_b^+;\sigma 1_b^+\sigma 1_a^-)\doteqdot(\sigma 1_a\sigma 1_b;\sigma 1_b\sigma 1_a),$$

$$(\sigma 1_a\sigma 1_a^-;\sigma 2_a\sigma 2_a^-)+(\sigma 1_b\sigma 1_b^+;\sigma 2_b\sigma 2_b^+)\doteqdot 2(\sigma 1_a\sigma 1_a;\sigma 2_a\sigma 2_a),$$

$$(\sigma 1_a\sigma 1_a^-;\sigma 1_b\sigma 1_b^+)\doteqdot(\sigma 1_a\sigma 1_a;\sigma 1_b\sigma 1_b).$$

Moreover, let us put the special intra-atomic overlap integrals

$$T_\sigma^+=\int\sigma_a^*(1)\sigma_a^+(1)d\tau_1,\quad T_\sigma^-=\int\sigma_a^*(1)\sigma_a^-(1)d\tau_1,$$

$$T_\sigma^{+-}=\int\sigma_a^{-*}(1)\sigma_a^+(1)d\tau_1$$

as equal to unity, then the part (2) of each energy matrix element becomes a product of a constant factor $E(\sigma)$ and the corresponding element of the overlap matrix. So we can drop out the part (2) in the calculation of the π-electron levels. This procedure corresponds to the usual π-electron approximation. The resulting simplified energy matrix and the overlap matrix are given in the appendix.

In performing the numerical calculations, we have used Slater type orbitals. The effective charges in the exponent of the atomic orbitals ought in principle to be determined by minimizing the energy of the structure as mentioned in the introduction but this is somewhat laborious. As we see in Table I, the value determined by Slater rules gives a fairly good value for the essential quantity $I-A$, and moreover, Slater rules are very simple and have far-reaching applicability. We have therefore determined to use the value given by Slater rules in this calculation. Accordingly we have used the nodeless $2s$ orbitals and have assumed the same effective charges for the $2s$ and the $2p$ orbitals.

As we have used different atomic orbitals for the ions and the neutral atoms, many heteropolar integrals appear in the energy matrix in addition to the usual homopolar integrals whose values are obtained by the interpolation from the table of Kotani and others.[8]

[8] Kotani, Ishiguro, Hijikata, Nakamura, and Amemiya, J. Phys. Soc. Japan **8**, 463 (1953).

Table II. Electronic states of ethylene.[a]

State	This paper I[b]	This paper II[c]	obs[d]	Moffitt[e]	Murai[f]	ASMO[d]
$Z(^1A_g)$	13.6	14.9	...	...	15.8	...
$V(^1B_{1u})$	7.7	8.6	7.6	7.3	11.2	11.4
$T(^3B_{1u})$	5.4	5.8	6.4	5.5	4.6	2.8
$N(^1A_g)$	0.0	0.0	0.0	0.0	0.0	0.0
$V-T$	2.3	2.8	1.2	1.8	6.6	8.6

[a] Equilibrium internuclear distance of 1.353 A is used.
[b] The result by the present method; the $\sigma-\pi$ exchange is neglected.
[c] The result by the present method; the $\sigma-\pi$ exchange is included.
[d] C. M. Moser, J. Chem. Phys. **21**, 2098 (1953).
[e] See reference 2.
[f] See reference 6.

The hetero-polar molecular integrals have been evaluated in the following way:

(a) one-center integrals have been computed exactly by the use of Roothaan's formula,[9]

(b) two center Coulomb integrals have been calculated by the geometric mean approximation, for example

$$(\pi_a^-\pi_a^-;s_b^+s_b^+)\doteqdot[(\pi_a^-\pi_a^-;s_b^-s_b^-)(\pi_a^+\pi_a^+;s_b^+s_b^+)]^{\frac{1}{2}},$$

(c) two center hybrid and exchange integrals have been evaluated by Mulligan's approximation,[10] for example

$$(\pi_a^-\pi_b^-;s_b^-s_b^+)\doteqdot T_\sigma^{+-}\frac{S^{--}}{S}(\pi_a\pi_b;s_bs_b),$$

(d) $\sigma-\pi$ exchange integrals have been equated with corresponding homopolar ones.

The inter-nuclear distance has been taken to be 1.353 A.[11]

IV. RESULTS AND DISCUSSION

In Table II our results are compared with experiment, with similar calculation excluding $\sigma-\pi$ exchange, and with other previous calculations. The agreement with experiment is very satisfactory although somewhat fortuitous. It appears that the errors arising from the simplifying assumptions made above tend to cancel out. For example, let us consider the error due to the assumption

$$(\sigma_a^+|F|\sigma_a^+)+(\sigma_a^-|F|\sigma_a^-)\doteqdot 2(\sigma_a|F|\sigma_a),$$

where

$$F=-\tfrac{1}{2}\Delta-\frac{4}{r_a}-\frac{4}{r_b}.$$

As the one-center nuclear attraction part arising from the second term of F is linear in the effective charge Z and as by Slater rules Z^++Z^- is equal to $2Z$, the above

[9] C. C. J. Roothaan, J. Chem. Phys. **19**, 1445 (1951).
[10] J. F. Mulligan, J. Chem. Phys. **19**, 347 (1951).
[11] G. Herzberg, *Infrared and Raman Spectra of Polyatomic Molecules* (D. Van Nostrand Company, Inc., New York, 1945), p. 439.

equation is exact so far as this part is concerned. Also the equality is satisfied fairly well concerning the third term. But the kinetic energy part is quadratic in Z, so the right side of the equation is smaller than the left side by $(\Delta Z/2)^2$ in the atomic units, where $\Delta Z=Z^+-Z=Z-Z^-$. As there are three such pairs of + and − terms, the estimate of the energy of the ionic structure is too low by about 2.4 ev. On the other hand, taking the values of effective charges as determined by Slater rules, $I-A$ is larger than the semi-empirical and more reliable value by 1.8 ev (see Table I). These two errors almost cancel each other out.

Nevertheless, it would seem clear that the present modification achieves a great improvement upon the conventional ASMO and probably upon the usual AO theory.

It is interesting to note that the effect of $\sigma-\pi$ exchange interaction has the same tendency as in the case of benzene.[12] In both cases $\sigma-\pi$ exchange gives larger intervals between almost all the excited states and the ground state and, generally speaking, the agreement with observed data is somewhat better if this effect is neglected.

There are several points which require further investigation, for example, the effect of overlap between σ orbitals, the determination of the optimum effective charges by a variational method, the accurate evaluation of the heteropolar integrals and so on. The authors hope to clarify these points in the future.

V. ACKNOWLEDGMENT

The authors would like to express their hearty thanks to Professor M. Kotani for his encouragement and discussions.

APPENDIX: THE ELEMENTS OF THE ENERGY AND OVERLAP MATRICES

$$\begin{aligned}H_{\mathrm{II}}=&2[(\pi_a|F|\pi_a)+S(\pi_a|F|\pi_b)]\\&+[(\pi_a\pi_a;\pi_b\pi_b)+(\pi_a\pi_b;\pi_b\pi_a)]\\&+2[\textstyle\sum(\pi_a\pi_a;\sigma\sigma)+S\sum(\pi_a\pi_b;\sigma\sigma)]\\&-[\textstyle\sum(\pi_a\sigma;\sigma\pi_a)+S\sum(\pi_a\sigma;\sigma\pi_b)]\\&+(1+S^2)E(\sigma),\end{aligned}$$

$$\begin{aligned}H_{\mathrm{II\,II}}=H_{\mathrm{III\,III}}=&2(\pi_a^-|F|\pi_a^-)+(\pi_a^-\pi_a^-;\pi_a^-\pi_a^-)\\&+2[\textstyle\sum(\pi_a^-\pi_a^-;\sigma_a^-\sigma_a^-)+\sum(\pi_a^-\pi_a^-;\sigma_b^+\sigma_b^+)]\\&-[\textstyle\sum(\pi_a^-\sigma_a^-;\sigma_a^-\pi_a^-)+\sum(\pi_a^-\sigma_b^+;\sigma_b^+\pi_a^-)]\\&+E(\sigma),\end{aligned}$$

$$\begin{aligned}H_{\mathrm{IV\,IV}}=&2[(\pi_a|F|\pi_a)-S(\pi_a|F|\pi_b)]\\&+[(\pi_a\pi_a;\pi_b\pi_b)-(\pi_a\pi_b;\pi_b\pi_a)]\\&+2[\textstyle\sum(\pi_a\pi_a;\sigma\sigma)-S\sum(\pi_a\pi_b;\sigma\sigma)]\\&-[\textstyle\sum(\pi_a\sigma;\sigma\pi_a)-S\sum(\pi_a\sigma;\sigma\pi_b)]\\&+(1-S^2)E(\sigma),\end{aligned}$$

$$\begin{aligned}H_{\mathrm{I\,II}}=H_{\mathrm{I\,III}}=&\sqrt{2}S^-(\pi_a|F|\pi_a^-)\\&+\sqrt{2}T_\pi^-(\pi_b|F|\pi_a^-)+\sqrt{2}(\pi_a\pi_a^-;\pi_b\pi_a^-)\\&+\sqrt{2}S^-[\textstyle\sum(\pi_a\pi_a^-;\sigma_a\sigma_a^-)+\sum(\pi_a\pi_a^-;\sigma_b\sigma_b^+)]\\&+\sqrt{2}T_\pi^-[\textstyle\sum(\pi_b\pi_a^-;\sigma_a\sigma_a^-)+\sum(\pi_b\pi_a^-;\sigma_b\sigma_b^+)]\\&-1/\sqrt{2}\cdot S^-[\textstyle\sum(\pi_a\sigma_a^-;\sigma_a\pi_a^-)+\sum(\pi_a\sigma_b^+;\sigma_b\pi_a^-)]\\&-1/\sqrt{2}\cdot T_\pi^-[\textstyle\sum(\pi_b\sigma_a^-;\sigma_a\pi_a^-)+\sum(\pi_b\sigma_b^+;\sigma_b\pi_a^-)]\\&+\sqrt{2}T_\pi^-S^-E(\sigma)\end{aligned}$$

$$\begin{aligned}H_{\mathrm{II\,III}}=&2S^{--}(\pi_a^-|F|\pi_b^-)+(\pi_a^-\pi_b^-;\pi_a^-\pi_b^-)\\&+2S^{--}\textstyle\sum(\pi_a^-\pi_b^-;\sigma^-\sigma^+)\\&-2S^{--}\textstyle\sum(\pi_a^-\sigma_b^-;\sigma_b^+\pi_b^-)+(S^{--})^2E(\sigma),\end{aligned}$$

$$H_{\mathrm{I\,IV}}=H_{\mathrm{II\,IV}}=H_{\mathrm{III\,IV}}=0,$$

$$\begin{aligned}E(\sigma)=&2(s_a|F|s_a)+4(\sigma_a|F|\sigma_a)\\&+6(\sigma1_a\sigma1_a;\sigma2_a\sigma2_a)-3(\sigma1_a\sigma2_a;\sigma2_a\sigma1_a)\\&+\textstyle\sum\sum(\sigma_a\sigma_a;\sigma_b\sigma_b)+(\sigma1_a\sigma1_b;\sigma1_b\sigma1_a)\\&-(\sigma1_a\sigma2_b;\sigma2_b\sigma1_a)-\textstyle\sum(\sigma2_a\sigma_b;\sigma_b\sigma2_a),\end{aligned}$$

$$O_{\mathrm{II}}=1+S^2,$$

$$O_{\mathrm{II\,II}}=O_{\mathrm{III\,III}}=1,$$

$$O_{\mathrm{IV\,IV}}=1-S^2,$$

$$O_{\mathrm{I\,II}}=O_{\mathrm{I\,III}}=\sqrt{2}T_\pi^-S^-,$$

$$O_{\mathrm{II\,III}}=(S^{--})^2,$$

$$O_{\mathrm{I\,IV}}=O_{\mathrm{II\,IV}}=O_{\mathrm{III\,IV}}=0,$$

where

$$S=\int\pi_a^*(1)\pi_b(1)d\tau_1,$$

$$S^-=\int\pi_a^*(1)\pi_b^-(1)d\tau_1,$$

$$S^{--}=\int\pi_a^{-*}(1)\pi_b^-(1)d\tau_1.$$

In these expressions, $\sum$ sign before integrals containing σ means the summation over $\sigma1_a$, $\sigma2_a$, $\sigma3_a$, $\sigma1_b$, $\sigma2_b$, $\sigma3_b$, while $\sum$ sign before integrals containing σ_a (or σ_b) means the summation over $\sigma1_a$, $\sigma2_a$, $\sigma3_a$ (or $\sigma1_b$, $\sigma2_b$,$\sigma3_b$).

[12] K. Niira, J. Phys. Soc. Japan 8, 630 (1953).

Magnetism on Optical Excitation of Manganese-Activated Zinc Sulfide Phosphors

KEICHI OSHIMA AND HIROSHI NAGANO
Institute of Science and Technology, University of Tokyo, Tokyo, Japan
(Received November 15, 1954)

Changes of magnetic susceptibility accompanying the optical excitation of manganese-activated zinc sulfide phosphors were measured. It was found that there was some change in susceptibility for phosphors containing manganese more than 9.0×10^{-4} g Mn/g ZnS. While there was concentration quenching for manganese emission intensity at high manganese concentration, the value of susceptibility change increased monotonically with concentration. From these results it is concluded that the nonradiative process in concentration quenching does not affect much the excitation probability and the lifetime of the excited state which is of the multiplicity giving rise to the susceptibility change.

I. INTRODUCTION

THE measurement of changes of magnetic susceptibility accompanying excitation of phosphors is an interesting technique to investigate the character of the excited states. As for inorganic phosphors, Johnson and Williams[1] measured the change in paramagnetic susceptibility with excitation of manganese-activated zinc fluoride phosphor, and concluded the nontemperature-dependent exponential after-glow of manganese-activated luminescent solids to result from a difference in multiplicities of the excited and the ground states of the divalent manganese ion.

In a research program on doubly activated phosphors we have attempted to investigate the character of the excited state in the manganese-activated zinc sulfide phosphor, which is considered to be doubly activated with zinc and manganese. This phosphor is photoconductive and exhibits temperature dependent bimolecular after-glow, which means that the migration of the electron through the conduction band is the rate-determining step in the luminescent process and the energy of excitation absorbed by zinc centers is transferred to emitting centers of manganese by some mechanism of sensitization. In this case, therefore, the excited state of manganese may not be identical with that in zinc fluoride. Actually, Dexter,[2] in his recent theoretical treatment of sensitized luminescence of solids, showed that there can be two kinds of mechanism of energy transfer for exciting the luminescence of manganese by sensitization. One is due to dipole-quadrupole interaction and the other to exchange interaction between the sensitizing and the sensitized activators. Of these two types of mechanism, in a first approximation, only the latter may excite manganese in a spin-flip transition, which gives rise to the change in multiplicity of the state of manganese.

The present work was undertaken to determine whether multiplicity changes are active in the excitation of manganese by measuring the change in magnetic susceptibility with excitation.

[1] P. D. Johnson and F. E. Williams, J. Chem. Phys. **17**, 435 (1949).
[2] D. L. Dexter, J. Chem. Phys. **21**, 836 (1953).

II. METHOD AND APPARATUS

The apparatus used for the measurement was similar to that of Jensen.[3] The sample is placed in an inhomogeneous magnetic field with its initial susceptibility nearly compensated with some substance of opposite sign, and the minute change of susceptibility due to photoexcitation is measured by the displacement of the torsion balance beam. In our apparatus, a quartz torsion beam 27 cm long with a sample holder at one end and a pointer at the other end, was suspended with a quartz torsion fiber about 5μ in diameter and 30 cm long. An inhomogeneous magnetic field of 4000 oersted and a field gradient of 2000 oersted per cm was produced by an electromagnet with one nontapered pole 10 cm in diameter, and the other pole tapered to 1 cm in diameter at the face.

The field strength of the magnet was kept constant by controlling the current through the coils. This was achieved by controlling the output voltage of the dc generator supplying the magnet, with a regulating circuit which changes the current through the field coils of the generator. The detail of this circuit will be published elsewhere. With this device, the fluctuation of the magnetic field was kept to less than one thousandth of the total field strength.

The displacement of the pointer at the end of the torsion beam was read with the ocular scale of a microscope.

The sample was irradiated vertically with the 3650 A line of a mercury discharge lamp filtered with Wratten 18 a.

In making the measurement, a known amount of phosphor was placed on the sample holder. To set the sample always at the same position, the weight of the sample was balanced by counterweight mounted on the other arm of the balance beam by bringing the pointer to a prescribed point.

The susceptibility of the sample and the holder, as a whole, changed from diamagnetic to paramagnetic, when the concentration of manganese in the sample was increased. This susceptibility was nearly balanced by placing pieces of platinum or bismuth on the sample holder.

[3] P. Jensen, Ann. Physik **34**, 161 (1939).

When the magnet was switched on, the torsion head was adjusted to place the sample to the same part in the field.

The sample was irradiated and the displacement of the pointer was read at its stationary value. Calibration of the change in susceptibility was made by a small amount of pure platinum ($\chi=0.982\times10^{-6}$) and bismuth ($\chi=-1.340\times10^{-6}$) metals. It was found that a force of 1.07×10^{-4} dyne gave one division displacement of the pointer at the scale.

III. EXPERIMENTAL RESULTS

The results obtained for phosphors of different manganese concentrations are given in Table I. The phosphors were prepared by heating 30 min at 950°C with NaCl flux of 0.02 g/g ZnS. The activator concentrations were determined by polarographic analysis.

The variation of susceptibility change and manganese luminescence intensity with increase in manganese content is given in Fig. 1. The susceptibility change was not detectable with the samples of manganese content less than 3.0×10^{-4} g Mn/g ZnS. From 9.0×10^{-4} to 8.2×10^{-3} g Mn/g ZnS manganese content, the change increased parallel to the emission intensity of the manganese luminescence of the sample. With more manganese content, the susceptibility change increased still, while the luminescence intensity dropped rapidly by concentration quenching.

IV. DISCUSSION

The excitation process of manganese in zinc sulfide is not so simple as that in zinc fluoride, and the magnetic susceptibility change might result from various causes. In our measurement, however, as we observed no change in susceptibility for zinc sulfide without manganese, it is evident that the measured susceptibility change is caused by the change of multiplicity in manganese activator. The change of susceptibility due to the temperature rise of the samples was evaluated to be less than 1 to 10 percent of the observed values.

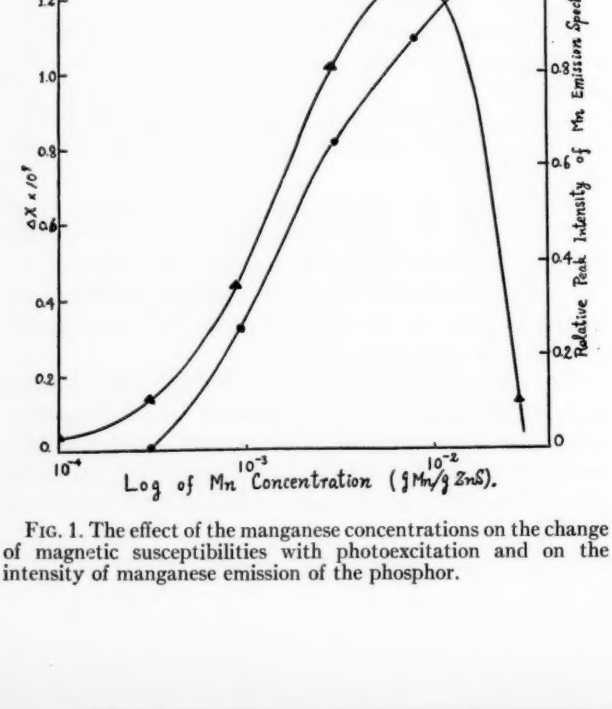

FIG. 1. The effect of the manganese concentrations on the change of magnetic susceptibilities with photoexcitation and on the intensity of manganese emission of the phosphor.

The paramagnetic susceptibility of an ion of transition group with multiplicity S is given by the following expression[4]:

$$\chi_M=\{N\beta^2/3k(T+\Delta)\}[4S(S+1)]$$

and, when we make quantitative considerations, the measured absolute value of the susceptibility change of manganese in zinc sulfide is found to be quite small, the order of magnitude of one thousandth, compared with that estimated from the number of manganese activator ions and the value observed by Johnson and Williams in zinc fluoride.

This discrepancy will be explained either from the smallness in number of the manganese activators excited to the state which changes multiplicity, or from the much shorter lifetime of the excited state of manganese in zinc sulfide.

As we could not estimate the number of excited manganese ions correct enough in our experiment, we did not try to carry our quantitative considerations further.

However, Shionoya[5] concluded, from the results of his measurements on intensities of zinc and manganese emissions of these phosphors, that the dipole-quadrupole process was likely to be predominant in the excitation of manganese. And then, we may explain our result by assuming that only a small fraction of the manganese centers are excited by exchange interaction to different multiplicity.

Yet, there is another attractive mechanism which shows the possibility of susceptibility change with dipole-quadrupole transfer process. If a series of excited states exists in manganese ion below that to which transfer occurs, some of which are of the multiplicity

TABLE I. The change of magnetic susceptibilities with photoexcitation.

g Mn/g ZnS	$\Delta\chi\times10^9$
1.0×10^{-4}	...
3.0×10^{-4}	...
9.0×10^{-4}	0.31
3.0×10^{-3}	0.81
8.2×10^{-3}	1.08
2.8×10^{-2}	1.36

[4] P. W. Selwood, *Magnetochemistry* (Interscience Publishers, Inc., New York, 1943).

[5] S. Shionoya, Bull. Fac. Eng. Yokohama Natl. Univ. 3, 97 (1954).

giving rise predominantly to the susceptibility change, and if the ion cascades down through these states, a susceptibility change will be observed.

The other result shown in Fig. 1 indicates some interesting features of the exciting mechanism. The curve of susceptibility change resembles that of emission intensity of manganese for low concentration of manganese, but with higher concentration, there is no concentration quenching in susceptibility change. It can be concluded from this result that the nonradiative process of concentration quenching does not affect much the excitation probability and the lifetime of the excited state which is of the multiplicity giving rise to the susceptibility change.

V. ACKNOWLEDGMENTS

The authors should like to thank Professor S. Makishima for his encouragement and comments on this work. They are also thankful to Mr. Yoshihide Kotera for the preparation and analysis of the samples, and Assistant Professor Shigeo Shionoya for supplying us with his data of the optical measurement on the phosphors used, as well as their many valuable discussions.

THE JOURNAL OF CHEMICAL PHYSICS VOLUME 23, NUMBER 8 AUGUST, 1955

Infrared Spectrum of Solid Ammonium Azide: A Vibrational Assignment

DAVID A. DOWS,* ERIC WHITTLE,† AND GEORGE C. PIMENTEL
Department of Chemistry and Chemical Engineering, University of California, Berkeley, California

(Received November 8, 1954)

Infrared spectra of solid ammonium azide at 68°K are presented. The solid, prepared by sublimation onto a cold salt window, seems to be a disordered crystal which becomes ordered on warming above 150°K. The annealed crystal displays spectral features with spacings of 10–20 cm^{-1} which can be attributed to crystal site perturbations. A band at 1830 cm^{-1} appears which is assigned as a combination involving a lattice torsional motion of the ammonium ion (420 ± 20 cm^{-1}). A vibrational assignment of solid ammonium azide is made. The vapor over ammonium azide at room temperature contains predominantly hydrazoic acid and ammonia.

SPECTRAL studies of ammonium halides have been directed at the investigation of rotation in the solid state. Wagner and Hornig[1] have examined the infrared spectra of solid ammonium chloride and of solid ammonium bromide and conclude that the ammonium ion does not undergo free rotation in the solid lattice. More recent neutron diffraction studies[2] and infrared spectral studies[3] have been interpreted to indicate that in the room temperature modification of ammonium iodide, one-dimensional free rotation occurs about a hydrogen bond between the ammonium ion and one iodide ion, whereas in the two known low-temperature modifications, this free rotation does not occur. Proton magnetic resonance studies of the ammonium halides[4] have been interpreted to indicate hindered rotation of the ammonium ions in the solids. Examination of the spectra of other ammonium salts may aid in corroborating these interpretations and in understanding the contrasting behaviors of the ammonium halides. Ammonium azide gives such an opportunity since the crystal structure of this compound has been determined by Frevel.[5] Accordingly, the infrared spectrum of solid ammonium azide at 68°K has been obtained and is presented here.

EXPERIMENTAL

Ammonium azide was prepared by mixing hydrazoic acid gas with an excess of ammonia gas. The excess ammonia was removed by evacuating the reaction vessel after cooling it to −78°C. The solid obtained had a vapor pressure of about 0.7 mm Hg, in agreement with the data of Frost, Cothran, and Browne.[6]

The infrared spectrum was obtained in the spectral region 600–4000 cm^{-1} with a Perkin-Elmer Model 21 spectrophotometer equipped with sodium chloride and calcium fluoride optics. Frequency accuracy is about 30, 10, and 4 cm^{-1} at 3000, 2000, and 1000 cm^{-1}, respectively, and spectral slit widths are shown in the figure.

The solid films were prepared by subliming ammonium azide onto the salt window of a conventional cold cell using liquid nitrogen or liquid nitrogen under vacuum as the coolant. The cell window was made of silver chloride and the temperature of the window was meas-

* Present address: Chemistry Department, Cornell University, Ithaca, New York.
† Present address: Chemistry Department, University College, Cardiff, Great Britain.

[1] E. L. Wagner and D. F. Hornig, J. Chem. Phys. **18**, 296 (1950); **18**, 305 (1950).
[2] H. A. Levy and S. W. Peterson, J. Chem. Phys. **21**, 366(L) (1953).
[3] R. C. Plumb and D. F. Hornig, J. Chem. Phys. **21**, 366(L) (1953).
[4] Gutowsky, Pake, and Bersohn, J. Chem. Phys. **22**, 643 (1954).
[5] L. K. Frevel, Z. Krist. **A94**, 197 (1936).
[6] Frost, Cothran, and Browne, J. Am. Chem. Soc. **55**, 3516 (1933).

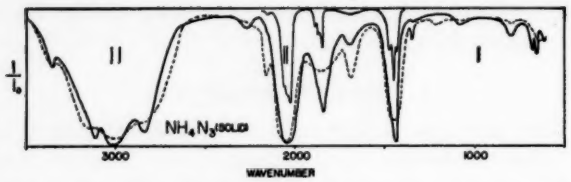

FIG. 1. Absorption spectrum of solid ammonium azide at 90°K; solid curve: phase *I*; dashed curve: phase *A*.

ured by means of a copper-constantan thermocouple imbedded in the center of the window.

SPECTRA

The spectrum of the solid obtained by subliming ammonium azide onto a AgCl window at either 68 or 90°K is shown by the dashed curve in Fig. 1. As this solid (hereafter called phase *A*) was warmed slowly a rather sudden change in the spectrum was noted at about 160°K. The spectrum did not change further upon recooling or upon warming to room temperature where ammonium azide slowly sublimes from the window. The spectrum of this solid material, phase *I*, is shown by the solid curve in Fig. 1.

Several spectral differences between phases *I* and *A* are evident. In the spectrum of phase *I*, most of the bands are narrower, several bands are of lower intensity or are not observed (notably, 2160, 1690, 1345, 1200, and 858 cm^{-1}), and several bands appear or increase in intensity (notably, 1830, 1088, 808, 664, and 652 cm^{-1}). The bands observed in the spectra of phases *I* and *A* are listed in Table I with relative intensities.

To clarify the nature of the transition, a solid film was prepared at 68°K and allowed to warm at a rate of about 20° per hour from 68°K to 190°K. The infrared spectrum between 2200 and 1600 cm^{-1} was examined at 3–5° intervals. Four spectral features in this region are noticeably altered during such a treatment. The band at 2160 cm^{-1} narrows in the temperature range 120–140°K and begins decreasing in intensity at about 150°K. The band was reduced in intensity by a factor of about three at 190°K. The band at 1690 cm^{-1} decreases in intensity or broadens as the solid is warmed above 150°K. The band at 1830 cm^{-1} becomes sharper and more intense in the temperature range 150–190°K. The absorbance ($\log I_0/I$) at the maximum of absorption of this band was about doubled as the temperature changed from 155 to 158°K, again doubled at 161°K, and doubled a third time at 190°K. The band at 2050 cm^{-1} becomes sharper over this same temperature interval and the maximum of absorbance increased by a factor between two and three.

After warming to 190°K, the sample received the following treatment: (a) recooled to 78°K and held at this temperature for $8\frac{1}{2}$ hours; (b) cooled to 68°K for $2\frac{1}{2}$ hours; (c) warmed to 78°K for $7\frac{1}{2}$ hours; (d) recooled to 68°K for 4 hours; and (e) warmed slowly till the sample distilled from the window. During this period of about 25 hours, the infrared spectrum between 3600 and 600 cm^{-1} was examined ten times and no spectral evidence of a return to the solid *A* form was detected. [The resolved details of the bands at 2050, 1675, 1430, and 664 cm^{-1} were observed during treatment (d).]

An attempt was made to examine the infrared spectrum of the vapor over solid ammonium azide at room temperature using a 50-cm multiple reflection cell. All of the observed spectral features were in accord with the infrared spectrum of hydrazoic acid.

TABLE I. Observed frequencies: solid ammonium azide.[a]

Phase *A* (cm^{-1})	Phase *I* (cm^{-1})	Assignment	Motion
3355(4)	3355(4)	$\nu_1'+\nu_2'$	
3160(8)	3160(6)	$\nu_3(B)$ or $\nu_2+\nu_4$	
3040(10)	3040(10)	$\nu_3(A)$	N–H *s*
2880(8)	2880(6)	$\nu_3(B)$ or $2\nu_4$	
...	2270(1)	$\nu_4+2\nu_6$	
2160(5)	...	HN_3(?)	
2050(10)	2030(10)	ν_2'	N–N–N asym. *s*
1830(2)	1851(2)		
...	1841(4)		
...	1830(6)	$\nu_4+\nu_6$	
1690(5)	1671(2)	ν_2	N–H *b*
1440(8)	1441(6)		
...	1428(8)	ν_4	N–H *b*
...	1420(6)		
1345(2)	1345($\frac{1}{2}$)	ν_1'	N–N–N sym. *s*
1200(1)	...	...	
1088(?)	1088(1)	$\nu_4-\nu_6$(?)	
808(?)	808(1)	$2\nu_6$	
...	664(2)		
...	652(2)	ν_9	N–N–N *b*
620(?)	611(?)		
...	(420±20)	ν_6	(NH_4^+ *t*)

[a] *s* = stretch, *b* = bend, and *t* = torsion.

DISCUSSION

Site Group Selection Rules

The crystal structure of ammonium azide at room temperature is of the space group D_{2h}^7 with four molecules per unit cell.[5] Each ammonium ion is surrounded by four azide ions at approximately tetrahedral angles, and there are two slightly different distances (2.94 and 2.99 *A*) between the nitrogen atom of each ammonium ion and the nearest nitrogen atoms of the neighboring four azide groups. The ammonium ions occupy sites of symmetry C_2 and hence have nine nondegenerate, infrared- and Raman-active vibrations in the site group approximation. The azide ions are linear and symmetric and are distributed equally between two sets of sites, both of which have symmetry C_{2h}. Although the site group analyses for both sets give equivalent results, the frequencies observed for the two kinds of azides are not necessarily identical. In the site group approximation, each azide ion has four nondegenerate vibrations, two of these derived from the degenerate bending motion of the hypothetical free azide ion. One vibration is Raman-active only and the others infrared-active only. Table II shows the

TABLE II. Site group analysis for ammonium azide.

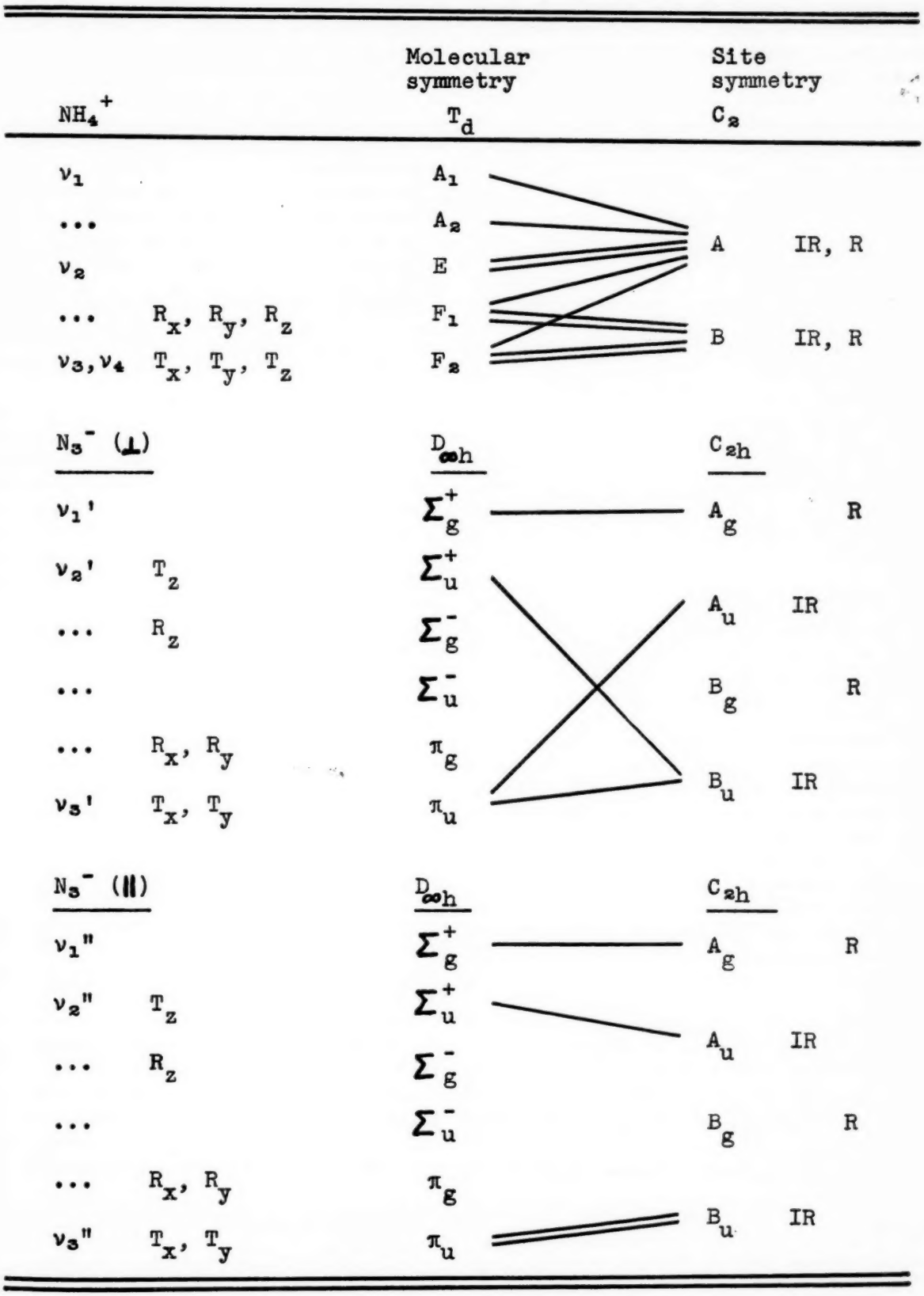

resolution of species of point groups T_d and $D_{\infty h}$ into those of point groups C_2 and C_{2h}, respectively. Each of the two types of azide ions is distinguished by a symbol, $\parallel$ or $\perp$, which indicates the angle between the axis of the linear N_3 group and the principal twofold axis of the C_{2h} site. The vibrations of the hypothetical free ammonium and azide ions are listed in the first column, and prime designations are used to distinguish the two types of azide ion.

Assignment

The assignment of ammonium azide is based upon the spectrum of solid phase *I* for reasons discussed later. The analyses of the infrared or Raman spectra of the ammonium halides,[1] several metal azides,[7,8] methyl azide,[9] and hydrazoic acid[9,10] are helpful in identifying fundamental vibrations.

The absorption between 2800 and 3200 cm^{-1} is attributed to the ammonium N—H stretching motions, ν_1 and ν_3, and is discussed in detail in the next section. The bands at 1430 and 1675 cm^{-1} are assigned as the N—H bending motions, $\nu_4(F_2)$ and $\nu_2(E)$, respectively. These frequencies can be compared to the corresponding assignments for ammonium chloride (1402 and 1712 cm^{-1}) and for ammonium bromide (1401 and 1686 cm^{-1}).[1]

The intense band at 2050 cm^{-1} is clearly associated with the asymmetrical stretching motions of the azide groups, ν_2' and ν_2''. The corresponding vibrations of HN_3 and CH_3N_3 absorb at 2140 and 2143 cm^{-1} respectively, whereas the metal azides absorb in the region 2040–2080 cm^{-1}.

The symmetrical stretching motions of the azide groups, ν_1' and ν_1'', are not infrared-active in the crystal environment under consideration. In the Raman spectra of the metal azides, this absorption is observed in the region 1330–1370 cm^{-1}, in HN_3 at 1274 cm^{-1}, and in CH_3N_3 at 1295 cm^{-1}. The band near 1345 cm^{-1} is tentatively assigned to ν_1' and ν_1''.

The azide bending motions of the metal azides are observed in the region 630–640 cm^{-1}. Ammonium azide has two sharp bands at 664 and 652 cm^{-1} and these are attributed to ν_3' and ν_3'' without more detailed interpretation.

With this selection of fundamental frequencies, the absorption at 3355 cm^{-1} can be designated $\nu_1'+\nu_2'$. The rather intense band at 1830 cm^{-1} has no obvious assignment on the basis of combinations of the assigned fundamental frequencies. In analogy to ammonium chloride and ammonium bromide, this band is assigned as a combination involving a torsional motion of the ammonium ion (henceforth identified as ν_6)‡ and the N—H bending mode, ν_4. Assuming a small amount of anharmonicity, ν_6 is assigned to be 420±20 cm^{-1}. This makes it possible to identify the absorption at 808 cm^{-1} as $2\nu_6$. The band observed at 2270 cm^{-1} may be the ternary combination, $\nu_4+2\nu_6$. The frequency of ν_6 can be compared to the corresponding frequencies for ammonium chloride, 390 cm^{-1}, and ammonium bromide, 319 cm^{-1}.[1]

The appearance of a torsional frequency involving the ammonium ion shows that this ion does not rotate freely in the crystal of ammonium azide. The relative magnitudes of the frequencies of these three alleged torsional modes of ammonium ion are qualitatively consistent with the hydrogen bond energies as inferred from the frequencies of the N—H stretching motions in NH_4N_3, NH_4Cl, and NH_4Br.

Phase *A*

The spectra of phases *I* and *A* and the thermal behavior (the failure to return to phase *A* on recooling phase *I*) are reminiscent of the similar behaviors of 1,2-dichloroethane as reported by Malherbe and Bernstein[11] (attributed to the presence of unstable rotational isomers), of hydroxylamine as reported by Nightingale and Wagner,[12] and of hydrazoic acid.[10] The transitions in NH_4Cl and NH_4Br are presumably not of this type, since Wagner and Hornig's discussion[1] implies that it is possible to obtain the low-temperature stable forms by cooling the solid from room temperature.

It is possible that phase *A* cannot be obtained from phase *I* because of supercooling of phase *I*, *i.e.*, phase *A* could be a stable crystal modification. However, the broadness of the bands indicates that phase *A* is more likely to be a glass, a disordered (unstable) crystal, or phase *I* with defects frozen in. Several features of the spectrum of phase *A* indicate that this phase is very similar to phase *I* (such as the diffuse structure near 3000 cm^{-1}). Furthermore, the spectral feature of phase *A* at 2160 cm^{-1} is quite close to the frequency of the most intense band of solid HN_3, while the feature at 1200 cm^{-1} is reasonably close to the second most intense band.

The evidence seems to favor strongly the interpretation of the phase *A* as a defective or disordered solid phase *I* including trapped hydrazoic acid (and, presumably, also ammonia). The appearance of hydrazoic acid in the gas phase above ammonium azide at room temperature tends to corroborate the identification of the 2150 cm^{-1} absorption as a band of HN_3. (This

[7] L. Kahovec and K. W. F. Kohlrausch, Monatsh. Chem. **77** 180 (1947).
[8] T. Y. Wu, "Vibration spectra and structure of polyatomic molecules[11] (National University of Peking, Kunming, China, 1939), see p. 341 of suppl.
[9] E. H. Eyster and R. H. Gillette, J. Chem. Phys. **8**, 369 (1940).
[10] D. A. Dows and G. C. Pimentel (to be published).

‡ The numbering of ν_6 is in accord with that of reference 1. The lattice vibration frequency, called ν_6 by Wagner and Hornig, was not identified.
[11] F. E. Malherbe and H. J. Bernstein, J. Chem. Phys. **19**, 1607 (1951).
[12] R. E. Nightingale and E. L. Wagner, J. Chem. Phys. **22**, 203 (1954).

vaporization of ammonium azide to ammonia and hydrazoic acid is in accord with the similar behavior of the ammonium halides.[13]) The absence of spectral features of ammonia (except possibly 1088 cm^{-1}) may be because of inherently lower intensities. The spectral properties, particularly the transition from phase *A* to *I* over a temperature range of at least 30°K and the reluctance of phase *I* to return to phase *A*, are indicative of an ordering transition.

Phase *I*

The spectrum of phase *I* was examined under optimum resolution in a search for spectral details associated with the lattice perturbations. Although the factor group analysis based upon a unit cell containing four molecules of NH_4N_3 predicts a complex spectrum, the interpretation of the spectrum on the basis of the site group analysis[14] seems to be adequate to explain most of the observed spectral features.

The triply degenerate ammonium ion bending motion at 1430 cm^{-1} is expected to produce a triplet with one *A* component and two *B* components. Since the *B* components should interact and split, these are identified as the features at 1441 and 1420 cm^{-1} and the central feature at 1428 cm^{-1} is assigned as the *A* component. The doubly degenerate azide bending motions, ν_3' and ν_3'', each should split into a doublet with both components infrared-active. Two sharp spectral features are assigned to this motion at 664 and 652 cm^{-1}. Poorly resolved structure of the band at 2050 cm^{-1} suggests features lie at about 2030, 2048, and 2059 cm^{-1}. This band should give only two vibrations in the site symmetry, one caused by each type of azide group. The suggested structure can be explained only with a more detailed analysis. The band at 1830 (assigned as $\nu_4+\nu_6$) displays features at 1830, 1841, 1851, and 1865 (?). The resolved features of the bands at 1430, 664, and 1830 cm^{-1} could be caused by site symmetry perturbations. The spacings observed are between 10 and 20 cm^{-1}.

The site group considerations applied to the N—H stretching vibrations permit a consistent interpretation. The splitting of ν_3 and ν_4 should be qualitatively similar but, since the stretching frequency is much more sensitive to hydrogen bonding, the splitting of ν_3 should be much larger. The frequency difference associated with the different hydrogen bond lengths (2.99 and 2.94 A) was guessed (with the aid of the oxygen-oxygen hydrogen bond plot given by Lord and Merrifield[15]) to be about 200 cm^{-1}. Assigning the features at 3160 and 2880 cm^{-1} as the two *B* components, the splitting is 280 cm^{-1}. Unfortunately, the interpretation of these features is complicated by the presence of an overtone near 2860 cm^{-1} ($2\nu_4$) and a combination near 3100 cm^{-1} ($\nu_2+\nu_4$). The intensity of the observed band at 2880 cm^{-1} suggests it is not caused solely by the overtone $2\nu_4$. The combination $\nu_2+\nu_4$ could, however, interact in Fermi resonance with ν_3 and account for the two features at 3160 and 3040 cm^{-1}. Such Fermi resonance has been observed in the spectra of NH_4Cl and NH_4Br,[1] producing splittings of 80 and 90 cm^{-1}, respectively.

In view of the observed splitting of ν_4, the former explanation seems preferable.

[13] F. Metzger, Helv. Phys. Acta **16**, 323 (1943).
[14] R. S. Halford, J. Chem. Phys. **14**, 8 (1946).
[15] R. C. Lord and R. E. Merrifield, J. Chem. Phys. **21**, 166 (1953).

Low Resolution Electronic Spectrum of Crystalline *para*-Dimethoxybenzene with Application to Benzene

ANDREAS C. ALBRECHT* AND WILLIAM T. SIMPSON†
Department of Chemistry, University of Washington, Seattle, Washington

The spectrum of a thin (0.37μ) crystal of *para*-dimethoxybenzene for light incident on the 001 plane and polarized along the *a* and *b* crystallographic axes is given. From this, approximate spectra are determined for the two in-plane directions of the molecule. Absorption at 2900 A is polarized predominately in a direction perpendicular to the line joining the substituents while absorption at 2350 A is parallel to this line. The 2600 and 2000 A absorptions in benzene are related respectively to the 2900 and 2350 A bands in dimethoxybenzene and consequently the benzene bands are found to arise from transition to upper states of species B_{2u} and B_{1u} respectively. The relation to conventional orbital theory is briefly discussed.

INTRODUCTION

THE electronic spectrum of crystalline *p*-dimethoxybenzene (DMB) has been studied in order to provide information about the electronic states of benzene itself. The principal direct experimental result of this paper is the determination of optical density in the quartz ultraviolet for light incident on the 001 plane of very thin crystals of DMB. The light was plane polarized along the *a* and *b* crystallographic axes in separate experiments. This gave information from which can be derived the directions of electron vibration in individual molecules. It is a short step further to deduce the nature of the benzene electronic states, because the bands of DMB are related to the two main bands of benzene in the quartz ultraviolet at 2000 (Angstrom units understood) and 2600.

Part of this work was briefly reported in a Letter to the Editor[1] in which it was shown that the 2600 band of benzene comes from an $A_{1g}\rightarrow B_{2u}$ transition. The present paper contains the details of that research and further, experimental proof that the 2000 band of benzene is $A_{1g}\rightarrow B_{1u}$. Unfortunately at the time the letter was submitted for publication the prior work of Broude *et al.* and Davydov had not been discovered. These workers obtained the B_{2u} assignment using solid benzene, and hence the necessary perturbation from the asymmetry of the crystal forces.[2] The B_{2u} assignment was obtained independently also by D. S. McClure.[3]

The program for solving the problem of the benzene assignment was begun by us with attempts to use as a tool the photo-oxidation of *p*-dimethylamino dimethylaniline to Wurster's Blue with polarized light.[4] This work has been completed with the determination of the crystal structure of Wurster's Blue perchlorate[5] and has led to the absolute determination of the direction of electronic oscillation in the bands of the radical and the parent amine. The results obtained in the photo-oxidation work[6] lead to conclusions in complete agreement with the main conclusions reached here.

The plan of the present paper is to give the experimental part first. There follows a section in which the polarization of the transitions of a single DMB molecule are obtained. In the succeeding sections, the relation to the electronic states of benzene itself is shown and in the final section it is pointed out that simple orbital theory gives the results found experimentally.

EXPERIMENTAL

The solution spectra of DMB in 95% ethanol and in methanol were observed using the Beckman Model DU spectrophotometer. Eastman Kodak white label (m.p. 55–57°) was used without further purification.

Crystals of DMB sufficiently thin for absorption studies were obtained by a sublimation procedure developed by Nelson.[7] Such crystals were conspicuous for their red and green interference colors in ordinary light and their extreme flexibility. Once a crystal had been selected it was mounted on a quartz plate, placed in a holder, and checked for the presence of holes, for uniformity of thickness, and for the extinction directions. The holder was a brass disk with an azimuth scale mounted at the perimeter and having a recess ($\frac{1}{2}$ in. diameter) in the center in which the quartz plate and crystal could be firmly fixed, and a smaller hole in the center (0.12 in. in diameter) through which the measuring beam could pass. The holder was machined so that it could be mounted on a drum and turned through any desired arc.

The spectrophotometer consisted of a Bausch and Lomb 250 mm focal length grating monochromator and a photovolt multiplier photometer series 520-M. The

* Shell Predoctoral Research Fellow 1952–1953. Present address: Department of Chemistry, Massachusetts Institute of Technology, Cambridge, Massachusetts. This paper is taken from the writer's Ph.D. thesis.

† This research was supported in part by the Air Research and Development Command, Contract No. AF 18(600)–375.

[1] A. C. Albrecht and W. T. Simpson, J. Chem. Phys. **5**, 940 (1953).

[2] Broude, Medevedev, and Prikhot'ko, Zhur. Eksptl. i Teort. Fiz. **21**, 665 (1951); and A. S. Davydov, Zhur. Eksptl. i Teort. Fiz. **21**, 673 (1951).

[3] Ohio State Spectroscopy Symposium, 1953.

[4] G. N. Lewis and D. Lipkin, J. Am. Chem. Soc. **64**, 2801 (1942).

[5] D. Turner and A. C. Albrecht (to be published).

[6] A. C. Albrecht and W. T. Simpson, J. Am. Chem. Soc. (to be published).

[7] R. C. Nelson and W. T. Simpson, J. Chem. Phys. **6**, 1146 (1955).

source was a Beckman No. 2230 hydrogen discharge lamp and the light was polarized by reflection from a stack of quartz plates. The drum carrying the brass crystal holder was attached to the monochromator directly in front of the entrance slit, while the photomultiplier research unit was mounted at the exit of the monochromator. By having the grating between the sample and the detector, any possible effects due to crystal fluorescence were eliminated. The source was focused onto the crystal using a modified form of the condensing system of the monochromator, the light being polarized just after having passed through the lenses. The system had an equivalent aperture ratio of about $f/8$ and the light passing through the sample was not strictly parallel. The slits of the monochromator were adjusted to give the desired resolution and at the same time the maximum ratio of the intensity of incident light, I_0, to the intensity of the apparent scattered light, I_s. The I_s was arbitrarily considered to equal the light recorded when the wavelength dial of the monochromator was set at 1600, where I_0 is zero. The evaluation of scattered light at other wavelengths using filters indicated that the value recorded at the 1600 setting was representative. Ratios of $I_0/I_s \sim 1000/1$ were obtained. With the crystal sample in position, I_s was considerably reduced and still greater ratios were obtained. Both the entrance slit and the exit slit were set at 0.65 mm. horizontally and 2.50 mm vertically for optimum conditions. The polarization of the incident light was for convenience determined at 4180 using Polaroid and was assumed to be constant throughout the ultraviolet region.[8]

In DMB, an orthorhombic crystal, the principal directions of electronic oscillation are coincident with the orthogonal crystallographic axes a, b, and c. By applying the optical data available[9] and observing the interference figure formed when viewing a crystal flake under the microscope using strongly convergent light it was possible to identify the face of the flake as the 001 face, the face normal to the c axis. The a and the b axes were distinguished both by the use of a quartz wedge and by a study of the interference figure.

When a crystal sample had been prepared and was found suitable for measurement, I_0 readings were taken at every 50 A from 2150 to 3150 with only the quartz plate in position. The crystal was then mounted on the quartz plate, the holder rotated so that the sample would be viewed along one of its axes and measurements were recorded of the transmitted intensity at every 50 A within the same region. The holder was then rotated so that the second axis could be observed and intensities were recorded again at 50 A but this time moving the wavelength dial in the reverse direction.

[8] The change in the Brewsterian angle with wavelength is at most 2° and this has a negligible effect on the determination of the degree of polarization.

[9] Goodwin, Przybylska, and Robertson, Acta Cryst. **3**, 279 (1950).

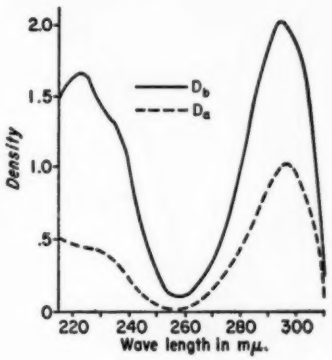

FIG. 1. Spectrum of *p*-dimethoxybenzene with light polarized along the a and b crystallographic axes.

The samples were finally checked for constant thickness over the area of illumination by observing transmitted intensities at 90° intervals in holder position. If alternate readings were not found to be equal within 5% the experimental results were discarded.

Because sublimation occurred during each single experiment, it was decided to run experiments in pairs. A second crystal was run just as described above, but viewing the axes in the reverse order. If the first run were in error because of a change in crystal thickness Δl between, say, first the a axis and second the b axis determinations, and if the thickness change were the same in the second run in which the b axis spectrum was read first, then the sum (or average) densities would be properly independent of errors caused by sublimation. Because of the measurement sequence described above, the scheme of running pairs of crystals will be seen actually to provide a detailed correction for sublimation at every wavelength, provided only that the thickness changes as the same linear function of time during each single experiment. A crystal spectrum determined from a pair of runs by averaging optical densities is really the spectrum of a hypothetical crystal having a constant effective thickness.

Two complete crystal spectrum determinations were carried out, as well as studies in limited wavelength ranges. All were in qualitative agreement, but one of the complete experiments was judged the better, mainly because the other appeared to have some systematic error in the measurements of I_0. The results of the poorer experiment were discarded. The final densities were corrected for the fact that the measuring light was incompletely polarized (96%).

In the next section we see how to translate the crystal spectrum data into a form which expresses the absorption characteristics of individual molecules.

RESULTS

The direct result of the experimentation is a record of the optical density of the crystal for light polarized along the a and b axes (which are also the principal directions). The two spectra are given in Fig. 1. We now show the connection with molecular adsorption. To this end a molecule fixed coordinate system is de-

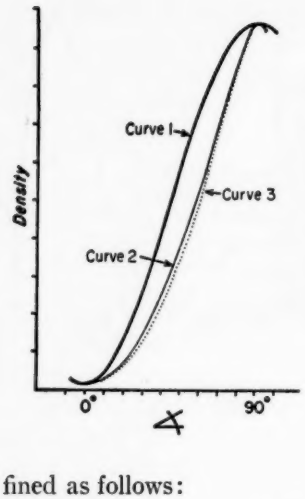

FIG. 2. Variation of extinction with angle between direction of polarization of light and a crystal axis. Curve 1 is constructed from the crystal geometry by projecting individual molecule extinction coefficients onto the polarization vector of the incident beam. Curve 2 is constructed by projecting molecular extinctions onto the principal axes, and considering the incident beam as divided into two independent beams along these axes. Curve 3 was obtained experimentally.

fined as follows:

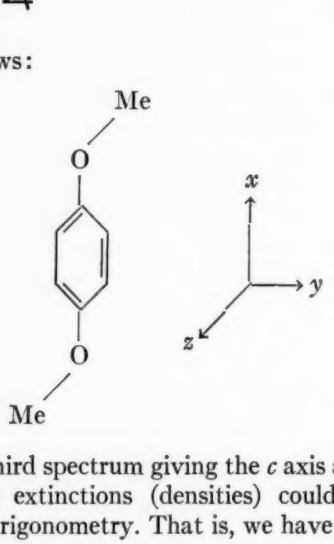

If we had a third spectrum giving the c axis absorption, then relative extinctions (densities) could be easily obtained by trigonometry. That is, we have

$$\begin{pmatrix} k_x \\ k_y \\ k_z \end{pmatrix} = \mathbf{M} \begin{pmatrix} k_a \\ k_b \\ k_c \end{pmatrix}$$

where the k's are molar extinction coefficients (these quantities are often symbolized as ϵ_x, etc.) and the matrix $\mathbf{M}$ embodies the appropriate trigonometric relationships. Now we use Beer's law, e.g.

$$k_a = D_a C l$$

where D_a is the a axis density, C the concentration, and l the actual thickness. This gives

$$\frac{1}{Cl}\begin{pmatrix} k_x \\ k_y \\ k_z \end{pmatrix} = \mathbf{M} \begin{pmatrix} D_a \\ D_b \\ D_c \end{pmatrix}$$

which can be written as

$$\begin{pmatrix} D_x \\ D_y \\ D_z \end{pmatrix} = \mathbf{M} \begin{pmatrix} D_a \\ D_b \\ D_c \end{pmatrix}.$$

This requires the definitions e.g.

$$D_x = k_x / Cl$$

and also some care in interpreting the meaning of l. The quantity D_c is not here determined experimentally, but is determined conceptually by measurements carried out on the 010 or 100 face of a crystal having the same thickness, l, occurring in the D_a and D_b determinations. The transformation matrix is

$$\mathbf{M} = \begin{pmatrix} -0.0313 & -0.1445 & 1.1756 \\ -0.7172 & 2.0238 & -0.3073 \\ 1.7466 & -0.8796 & 0.1321 \end{pmatrix}.$$

It is found in practice from its inverse. The matrix $\mathbf{M}^{-1}$ is easily obtained by making a $\cos^2$ projection of unit vectors of the molecule fixed coordinate system for each[10] differently oriented molecule in the unit cell onto the appropriate principal direction, and averaging. (The crystal structure determination of Goodwin, Przybylska, and Robertson[9] was used to give the individual positions.)

The theoretical and experimental variation of density with the angle between the polarization vector of the measuring light and one of the principal directions of the crystal is given respectively by curves 2 and 3 of Fig. 2. Here the extinction coefficients for the molecules are projected onto the principal axes in determining the theoretical curve. If on the other hand extinction coefficients for the molecules are projected onto the polarization vector of the incident light a theoretical density *vs* angle relationship like curve 1 is predicted. This treatment would lead to the erroneous prediction that in the solid Beer's law is obeyed for all angles. The former approach is the correct one as can be seen from the figure.[11]

The values D_x, D_y, and D_z cannot be obtained because D_c is not directly known. To avoid this difficulty we may appeal to other experiments. The two bands in DMB at 2350 and 2900 correspond to bands in, for example, hexamethylbenzene at 2200 and 2700. The amount of out-of-plane (z) absorption for the hexamethylbenzene bands has been determined to be respectively 2% and 3%.[7] Accordingly we make the approximate assumption

$$D_z = 0$$

and can then obtain a solution to the problem based on this approximation. ($D_z = 1.7466 D_a - 0.8796 D_b + 0.1321 D_c$, so that the assumption $D_z = 0$ and a knowledge of D_a and D_b allows an approximate D_c to be determined.) The approximate solution is given in Fig. 3, and the areas expressed as percentages in column one of Table I.

[10] The coupling between molecules in the crystal is assumed to result in an essentially negligible displacement of levels compared to the resolution employed. To the extent that this assumption is valid it is unnecessary to take account of the phase relations between electronic oscillations (speaking classically) in adjacent and neighboring molecules.

[11] We are indebted to Dr. R. C. Nelson for very materially helping to clarify this situation for us.

The curves in Fig. 3 are intuitively satisfactory. The 2900 band is y, with some x which, however, is not in the zero-zero region. Similarly, the 2350 band is x with some y in the high energy part. There is a region of negative density for D_x, but this need not be particularly disturbing considering the use made of $D_z=0$, and the possible experimental errors. Nevertheless various aspects of the experiment were considered in more detail.

Primarily, the assumption $D_z=0$ was given an independent test, as follows: The solution spectrum (the solvent is 95% ethanol, Fig. 4) can be considered as giving

$$D_a+D_b+D_c$$

providing the crystal thickness is known, because $k_{\text{soln}}=(1/3)(k_x+k_y+k_z)$ and hence $=(Cl/3)(D_x+D_y+D_z)$. But $D_x+D_y+D_z=D_a+D_b+D_c$. The $D_a+D_b+D_c$ value obtained from k_{soln} is sure to be inaccurate in its detailed dependence on wavelength because an individual molecule is in a different environment in solution than in the crystal. However, the integral over a band of the D_x, D_y or D_z curve should match fairly well between solution and crystal.[12]

The analysis was carried out using k_{soln} to determine $D_a+D_b+D_c$, D_a and D_b were taken from Fig. 1 as before, and D_c determined by subtraction. Then curves of D_x, D_y, and D_z were determined using the matrix **M**. The thickness, l, was determined to be $0.37\pm0.05\times10^{-4}$ cm (see Appendix). The D_x, D_y, and D_z curves obtained from this analysis were integrated and the percentages over the two bands found. They are given in column three of Table I. It will be seen that the integrated z absorption is zero within experimental error, which confirms the approach used in obtaining Fig. 3.

Several sources of error will be briefly discussed. The matrix **M** should be replaced by an effective **M** based on the fact that the light was not perfectly collimated. When this is done the amount of x in the y band (2950) and also the amount of y in the x band (2350) changes by $\sim3\%$. The orientation of the molecules is such that the y absorption is insensitive to errors in D_a and D_b but the x absorption recorded in Fig. 3 may be in error by $D_x=\pm0.4$. Nevertheless the shape of the D_x curve is in the broader details correct, and this is of first importance in the decision that the 2900 band is y (x absorption predominates only in the region corresponding to transition to highly excited vibrational levels of the upper electronic state).

TABLE I. Percentages of x, y, and z absorption in two absorption bands of p-dimethoxybenzene.

	From Fig. 3, i.e. for $Dz=0$			From Fig. 3, modified to give no $D_z<0$			Using solution data: Error from uncertainty in crystal thickness in parenthesis.		
	x	y	z	x	y	z	x	y	z
2900 Band	27	73	0	30	69	0.2	3 (±16)	100 (±17)	−4 (±6)
2350 Band	79	21	0	79	21	0	75 (±16)	25 (±11)	0 (±3)

[12] The 2350 band probably extends to shorter wavelengths out of the region of our measurements so that in this band we are unable to carry out a thorough match of areas.

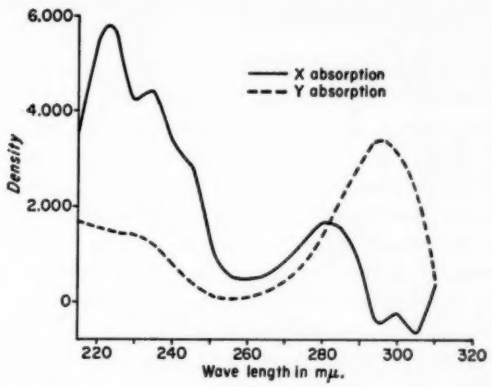

FIG. 3. Relative absorption for oscillations in the long direction (x) and short direction (y) of p-dimethoxygenzene computed from the data in Fig. 1 under the assumption that out-of-plant (z) absorption is zero.

There is very likely a small amount of z absorption in both bands, and unfortunately the orientation of the molecules is such that the curves in Fig. 3 are sensitive to variations in the amount of z and in the shape of any assumed D_z curve. For example, it is possible to eliminate the $D_x<0$ portion of Fig. 3 in the region around 3000 by assuming $D_z=0$ and $D_z=0.048$, 0.028, 0.079 at 2950, 3000, and 3050, respectively. The percentages in the 2900 band are changed as shown in the second column of Table I.

To summarize this section, interpretation of Fig. 3 shows that the 2900 and 2350 bands are respectively y and x.

CONCLUSIONS

We now examine the results to see what conclusions can be reached about benzene. The compound DMB is considered as a simply perturbed benzene molecule. It is believed that the extra electrons introduced by the substitution are in a low enough potential so as not to produce any new bands in the region studied.[13] There no doubt is some exchange interaction with the oxygen π electrons in the ground and excited states, but this does not invalidate any of the conclusions to be reached here. The main requirement is that the benzene bands may be thought of as going adiabatically into the DMB bands when some hypothetical perturbation is slowly turned on. There is a large amount of prior evidence to show that the requirement is fulfilled, but the most convincing evidence is obtained by examining the spectrum of DMB in the framework of the analysis

[13] This idea receives support from the fact that the solution spectrum of DMB undergoes no profound changes as the solution is made strongly acid enough to put a proton onto the methoxy group.

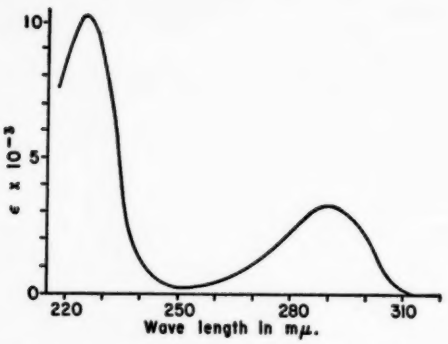

FIG. 4. Spectrum of *p*-dimethoxybenzene in 95% ethanol.

of the substituted benzene spectra made by Doub and Vandenbelt.[14]

Accordingly we shall adopt the correlation that the 2900 band of DMB has grown out of the 2600 band of benzene and the 2350 band of DMB out of the 2000 band of benzene. The correlation with the 2600 band is best because the extensive vibrational analyses of this band make it extremely likely that the band represents transition to just one upper state. In the region of the so-called 2000 band of benzene there is according to theoretical calculations the possibility of transition to two electronic states, B_{1u} and E_{2g},[15] though transition to the B_{1u} state should be far more intense.[16] To add to the uncertainty, two bands corresponding to the 2000 region of benzene have been found in the vapor spectrum of hexamethylbenzene.[7] Thus to be safe we should say that the 2350 band of DMB is correlated with the prominent band in the 2000 region of benzene. Even this conclusion requires that the Doub and Vandenbelt comparisons be made with careful attention to intensity.[17]

The next point is whether the crystal spectrum of DMB can be used without any more caution than has already been applied to give information about single molecule properties. The behavior of solid DMB (e.g., M.P.=55–57°C) suggests it is a Van der Waals solid. There is no opportunity for hydrogen bonding in the ordinary sense. Most particularly, a comparison of the solution and solid spectra (Figs. 4 and 1) shows that the peaks of the bands have undergone very little shift in going to the solid phase.

The crystal structure determination[9] turned up some anomalous bond lengths in the benzene ring. However, even if these can be verified it is not believed that the correlation with the benzene bands is vitiated because other benzene derivatives in the Doub and Vandenbelt scheme would be expected also to have similar irregularities.

Summarizing, the 2000 and 2600 bands of benzene become polarized x and y respectively on *para*-disubstitution. If it can be demonstrated that these bands are forbidden in benzene, becoming allowed on perturbation, the benzene upper states are then B_{1u} and B_{2u} respectively. This identification follows immediately from an examination of character tables for D_{6h} and the correlation with the group of lower symmetry (V_h) generated by paradisubstitution.[18]

The vibrational analysis of the 2600 band shows it to be forbidden. The intensity of the 2000 band on what might be called a "reduced basis" (that is, when account is taken of the closeness to the strong 1800 band) is the same as the 2600 band so the 2000 band in all probability also represents a forbidden transition.[19] It is concluded that the 2000 and 2600 bands of benzene are respectively B_{1u} and B_{2u}.

DISCUSSION

There is already known to be an E_{1u} upper level for benzene (1800 band). Now the identification of the B_{1u} and B_{2u} levels has been made definite so that altogether there is at hand a practical confirmation of conventional theory.

There are various forms that the theory of benzene electronic states has taken, most of which join in the prediction of low lying valence shell transitions taking place to E_{1u}, B_{1u}, and B_{2u} upper levels.[20] Let us enumerate the minimum assumptions involved. The assignments follow from a group theoretical direct product of the orbital species of the highest filled (degenerate) level and the lowest unfilled (degenerate) level. As a corollary it is only required to assume a single configuration approach with the π-electron approximation. Included in the π-electron approximation is the recognition that the azimuthal coordinate is the critical one in characterizing the changes in electronic motion.

In the free-electron treatment the hexagonal periodicity is missing, but still there is given an identification of upper levels equivalent to E_{1u}, B_{1u}, and B_{2u}. In addition, when interelectronic interaction is introduced in the free-electron approach the E_{1u} level is found to lie highest,[21] as is observed. The B_{1u} and B_{2u} levels still have the same energy, but they are different when ac-

[14] L. Doub and J. M. Vandenbelt, J. Am. Chem. Soc. **69**, 2714 (1947) and **71**, 2414 (1949).
[15] Parr, Craig, and Ross, J. Chem. Phys. **18**, 1561 (1950).
[16] J. R. Platt, J. Chem. Phys. **19**, 1418 (1951).
[17] The possibility can be ruled out that the 2350 band DMB might have grown from a weak transition in the 2000 region while the prominent benzene 2000 band has weakened and in a sense disappeared.
[18] Actually the symmetry for DMB is lower than V_h if account is taken of the methyl groups.
[19] Additional evidence has been obtained by R. S. McDonald (thesis, Massachusetts Institute of Technology, (1952)) who photographed the benzene 2000 band at liquid N_2 and He temperatures using vitreous samples. He obtained a vibrational structure which by its well resolved appearance suggests that the 2000 band is forbidden.
[20] M. Goeppert Mayer and A. L. Sklar, J. Chem. Phys. **6**, 645 (1938).
[21] W. T. Simpson, J. Chem. Phys. **17**, 1218 (1949). The material in the section on selection rules is directly applicable to benzene.

count is taken of the hexagonal periodicity.[15,20,22] Yet it is incorrect to interpret the B_{1u} and B_{2u} split as being introduced solely by the hexagonal periodicity. For example, in the application of the simple LCAO method (in which interelectronic interaction is in a sense neglected), the periodicity is incorporated but the split does not occur. Thus the B_{1u}, B_{2u} split comes from the combined effect of the periodicity and the interelectronic interaction.

The B_{1u}, B_{2u} split given by one configuration orbital theory is[20] $2(2\eta-\xi)>0$ where

$$\eta=\int \varphi_{+1}(\nu)\varphi_{+2}(\nu)\varphi_{+1}(\mu)\varphi_{+2}(\mu)\frac{1}{r_{\mu\nu}}d\tau$$

$$\xi=\int \varphi_{+1}(\nu)\varphi_{+1}(\nu)\varphi_{+2}(\mu)\varphi_{+2}(\mu)\frac{1}{r_{\mu\nu}}d\tau.$$

It is possible, after some rearrangement, and with the neglect of overlap, to write the first integral as

$$\eta=\sum_{k=0}^{5} e^{6i(2\pi k/6)} \sum_{\substack{n=k,\ k,\pm1,\\ k\pm2,\ k+3}} \cos 3[2\pi(n-k)/6]J_{nk}$$

where J_{nk} is the Coulomb repulsion of electrons in atomic orbitals on atoms n and k. The second integral is the same except that the cosine term is $\cos 2[2\pi(n-k)/6]$. The equivalent integrals in free electron approximation are obtained by summing over a fine dust of AO's (Dirac δ functions) so that the first sum in η becomes

$$\lim_{N\to\infty} \sum_{k=0}^{N} e^{6i(2\pi k/N)}=0.$$

This sum is actually zero for, say, $N=11$. It is just the hexagonal (and not higher) periodicity that makes the sum different from zero and allows the Coulomb repulsion given by the second part of the product of sums to be manifested.

[22] W. E. Moffitt and J. Scanlan, Proc. Roy. Soc. (London) **A220**, 530 (1953).

APPENDIX. DETERMINATION OF CRYSTAL THICKNESS

A sublimation flake of DMB was mounted on the quartz plate, and spectrophotometric measurements were made as described in the Experimental section, except that readings were taken only at 2500, 2550, 2600, 2650, and 2700. In this spectral range the absorption is weak so that having very thin crystals was not essential to the study. After readings had been made both along the *a* and the *b* axes, the area was measured.

The quartz plate containing the crystal was placed in a specially built cell with windows of Polaroid arranged perpendicularly. Because of the extinction phenomenon, light entering the cell and passing through the crystal could be transmitted with the crystal properly oriented. No other light, of course, could pass through the crossed Polaroids. An enlarged photographic print was made of the image formed by the transmitted light and a scale was photographed simultaneously to gauge the degree of magnification. From the print the crystal area was determined by planimeter.

Next the crystal was, in effect, weighed. It was dissolved in 5.00 ml of methanol and optical densities were recorded at 2800, 2850, 2900, 2950, and 3000. By using previously determined extinction coefficients in methanol a value of the concentration of DMB in the solution was obtained so that using Beer's law and the molecular weight, the weight of the crystal could be obtained. With the density known from the crystallographic studies and with the area and weight of the crystal determined as described above the thickness was thus established.

Three crystals were individually studied in this fashion and found to be 3.11, 1.43, and 0.72μ thick. Curves were plotted of optical density *vs* thickness for the measurements made at the five different wavelengths, and the optical density of the hypothetical crystal recorded in Fig. 1 was located on these curves. The thickness was determined to be $0.37\pm0.05\mu$. Errors considered included optical density errors for the calibrating crystals and the unknown crystal, sublimation, and the unevenness of crystal thickness for the calibrating crystals. The first-mentioned error appeared to be the most serious.

Effect of Crystal Orientation on the Activation Energy for the Catalytic Decomposition of Formic Acid on Silver

H. M. C. Sosnovsky
C.S.I.R.O., Division of Tribophysics, University of Melbourne, Australia
(Received November 16, 1954)

Single crystalline sheets of silver have been used as catalysts for the decomposition of formic acid. The activation energy for the zero-order reaction was found to vary from 16.0 kcal/mole with a crystal face close to {111} to 30.4 kcal/mole with a crystal face close to {110}.

INTRODUCTION

THE influence of the geometrical arrangement of the atoms in the surface of a metal on its catalytic activity has been the subject of investigation since the work of Balandin.[1] Studies of the effects of crystal structure[1] and lattice parameter[2] in a series of different metals do not necessarily give a clear indication of geometrical effects because of the effects due to simultaneous changes in the electronic configuration. However, the geometrical factor can be studied in isolation by investigating the catalytic properties of different crystal planes of the same metal and experiments of this kind have provided evidence that it may be of considerable importance. For example, Beeck and collaborators have shown that the hydrogenations of ethylene[3] and of ethane to methane[4] proceed respectively 5 and 6 times faster on nickel films oriented to present the {110} plane to the reagents than on films with random orientation. On the other hand, the dehydrogenation of cyclohexane on oriented platinum films is 10 times slower than on unoriented films.[5] According to Leidheiser and Gwathmey[6] the hydrogen-oxygen reaction is faster on the {111} faces of copper single crystals than on the {100} faces and the same is true for the decomposition of carbon monoxide on nickel crystals.[6] The hydrogenation of benzene, however, proceeds at equal speed on oriented and unoriented films of nickel.[5]

No general picture of the effect of crystal orientation on catalysis has emerged largely for lack of systematic investigation. An approach to the problem has been made in the work described in this paper. The zero-order vapor phase decomposition of formic acid to carbon dioxide and hydrogen on silver[7] has been studied with a series of single crystals of different orientations. The crystals were prepared in the form of thin sheets so that the surfaces of each one presented to the vapor were predominantly of the same type. Particular attention has been devoted to the influence of the crystal orientation on the activation energy since the latter is, in principle, independent of the surface area.

EXPERIMENTAL

Apparatus

Reaction rates were measured in the flow apparatus shown diagrammatically in Fig. 1. Formic acid was volatilized from the evaporation vessel E, a device designed to give a steady rate of evaporation.[8] At the beginning of an experiment dry air was admitted at F to the required pressure as indicated by the mercury manometer M_1. This caused the liquid to rise into the upper part of the right arm of the U tube which was heated by a nichrome wire winding. Evaporation then began and continued at a constant rate which could be varied by adjusting the air pressure on the left-hand side, and so altering the length of the heated column of formic acid. The lower part of the U tube was made from capillary tubing to minimize oscillation of the liquid and thereby diffusion of formic acid containing dissolved air into the right-hand side. The vapor passed via the capillary orifice O_A to the reaction vessel in which the catalyst crystal was suspended. The reaction products (CO_2+H_2) and excess formic acid passed through a second orifice O_B (of somewhat greater diameter than O_A) and entered a sequence of traps. Formic acid was removed at 0°C and −78°C and carbon dioxide at −187°C. The hydrogen passed to a previously evacuated 5-liter globe G. The pressure in G was measured at frequent intervals by a Pirani gauge previously calibrated against a McLeod gauge with pure hydrogen (admitted by the palladium tube P). The rate of pressure rise in G was thus a direct measure of the reaction rate.

The Pyrex reaction vessel was heated in a furnace provided with electronic temperature control. The crystal hung from the sealed-off hollow glass plug H within 1 mm of the thermocouple well and could be removed (together with the thermocouple) by withdrawing H. In order to minimize dead-space, H fitted closely in the neck of the reaction vessel which was sealed by a cone-and-socket joint as shown. The

[1] Reviewed by M. W. Trapnell, Advances in Catalysis **3**, 1 (1951).
[2] O. Beeck, Revs. Modern Phys. **17**, 61 (1945).
[3] Beeck, Smith, and Wheeler, Proc. Roy. Soc. (London) **A177**, 62 (1940).
[4] O. Beeck, Discussions Faraday Soc. **8**, 118 (1950).
[5] O. Beeck and A. W. Ritchie, Discussions Faraday Soc. **8**, 159 (1950).
[6] H. Leidheiser, Jr., and A. T. Gwathmey, J. Am. Chem. Soc. **70**, 1200, 1206 (1948).
[7] O. Rienäcker, Z. anorg. u. Allgem. Chem. **227**, 353 (1936).
[8] C. T. Zahn, Rev. Sci. Instr. **1**, 299 (1930).

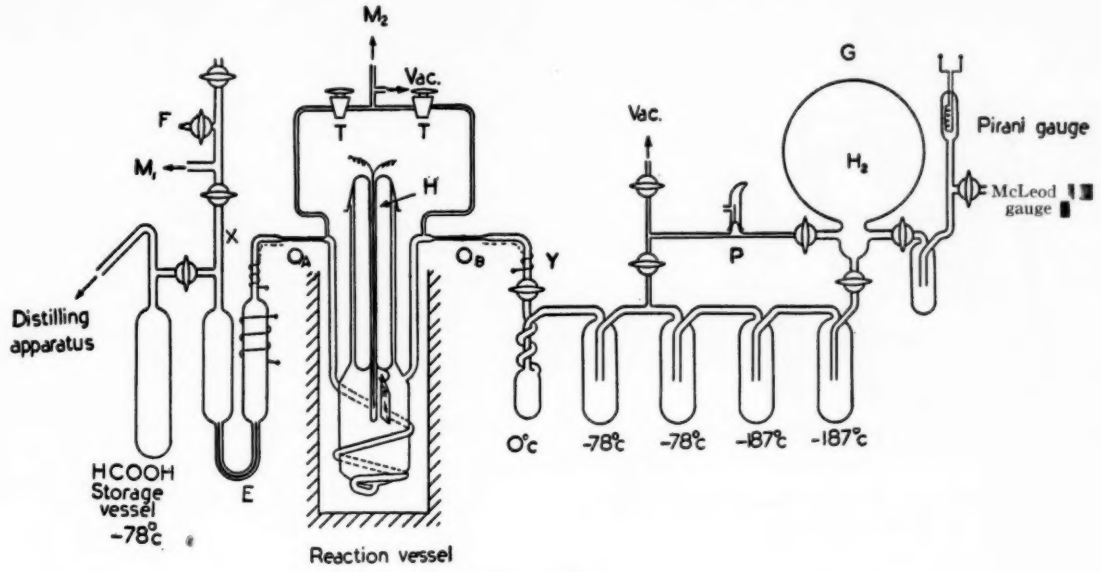

FIG. 1. Apparatus.

temperature of the catalyst was uniform over its length with ±0.1°C and remained constant within ±0.1°C during an experiment. The pressure in the reaction vessel and the pressure difference across it (always found to be ⩽1 mm) were measured by the mercury manometer M_2. The taps TT were kept closed during an experiment except when the manometer was being read. Connecting tubing from X to Y and the part of the reaction vessel exterior to the furnace were heated by a Nichrome winding to prevent condensation.

Materials

Analytical grade formic acid was dried over oxalic acid and anhydrous calcium sulphate and distilled. This was followed by several vacuum distillations. Dissolved gases were carefully removed by the usual freezing and melting technique. The silver was of ⩾99.995 percent purity obtained from the Royal Mint, Melbourne.

Preparation of Single Crystals

A piece of silver of the shape and thickness of the final crystal (6×2×0.025 cm) was cut from rolled sheet and a hole drilled in one end. After being washed with ether, it was melted in a graphite mould in a tube furnace with a longitudinal temperature gradient of 10°/cm and allowed to cool to room temperature; the crystal was then removed. The mould was made of graphite rendered sulfur-free by boiling in hydrochloric acid and baking *in vacuo* after unsuccessful attempts to use silica and several metals. The design finally adopted is shown in Fig. 2. The interior surfaces of the mould were polished with 6–15μ alundum powder. The crystal was macroscopically flat with a mirror finish. The orientation of its macroscopically flat surface was determined from an x-ray Laue back reflection diagram, care being taken to avoid contamination of the surface in handling. The crystals were introduced into the apparatus without any surface treatment in the condition they came from the mould.

Preliminary Experiments

The experiments were carried out between 155° and 200°C. With some catalysts (mainly oxides) the products of formic acid decomposition are H_2O and CO.[9] The occurrence of this reaction in our experiments would give rise to CO instead of, or in addition to, H_2 in the globe G. This was tested by comparing the pressure as recorded by the Pirani gauge with that as measured by the McLeod gauge. Several different crystals and the polycrystalline metal were used at a number of temperatures but in no case was an amount of CO detected beyond the experimental error (~1 percent) of the pressure measurements. With several crystals the rate of flow of formic acid at constant pressure was varied (in one experiment by a factor of ~50) by altering the diameters of the orifices 00. No change in reaction rate was observed. With the flow rate adopted for most of the experiments, comparison of the amount of H_2 produced with the amount of formic acid condensed in the traps (determined by titration) showed that less than 0.01 percent of the formic acid passing over the catalyst decomposed.

The catalytic effect of the walls of the reaction vessel and connecting tubing was determined over the complete temperature range. The corresponding correction to the rate obtained with the catalyst present was generally about 5 percent of the measured rate. The decomposition on Pyrex glass was found to yield

[9] C. N. Hinshelwood and B. Topley, J. Chem. Soc. **123**, 1014 (1923).

FIG. 2. Graphite mould for preparation of thin single crystals.

CO_2 and H_2 exclusively. It was of zero order with an activation energy of *ca* 23 kcal/mole.

Procedure

For each new crystal the procedure finally adopted was as follows: Formic acid was passed over the crystal until about 2×10^{-6} mole had been decomposed. This decomposition normally proceeded at a steady rate. The apparatus was then pumped out (to $10^{-5}-10^{-6}$ mm) for 3 hours and left overnight at the temperature of the experiment. After a further 3 hours' pumping another run was carried out. The new rate was found to be steady but usually higher than the previous one. This procedure was repeated until subsequent runs gave the same rate. The largest increase from initial to final rate observed was 70 percent. The increase in rate was always larger with crystals close to the {110} orientation than with those close to {100} and {111} orientations. With 3 of the 17 crystals studied the rate decreased (by ~10 percent) to its final value. In all cases the final rate remained constant even after the lapse of a week and could be reproduced after runs at other temperatures had been carried out (see Fig. 3).

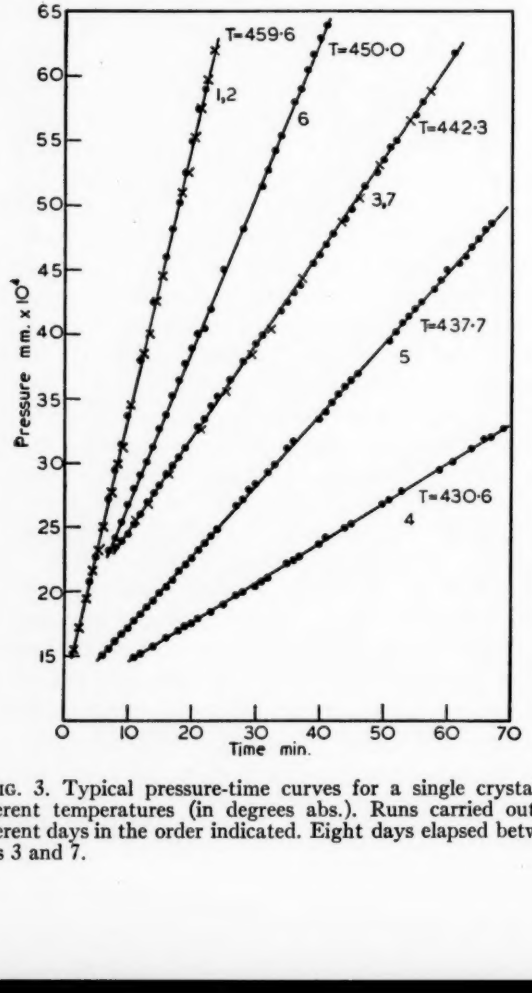

FIG. 3. Typical pressure-time curves for a single crystal at different temperatures (in degrees abs.). Runs carried out on different days in the order indicated. Eight days elapsed between runs 3 and 7.

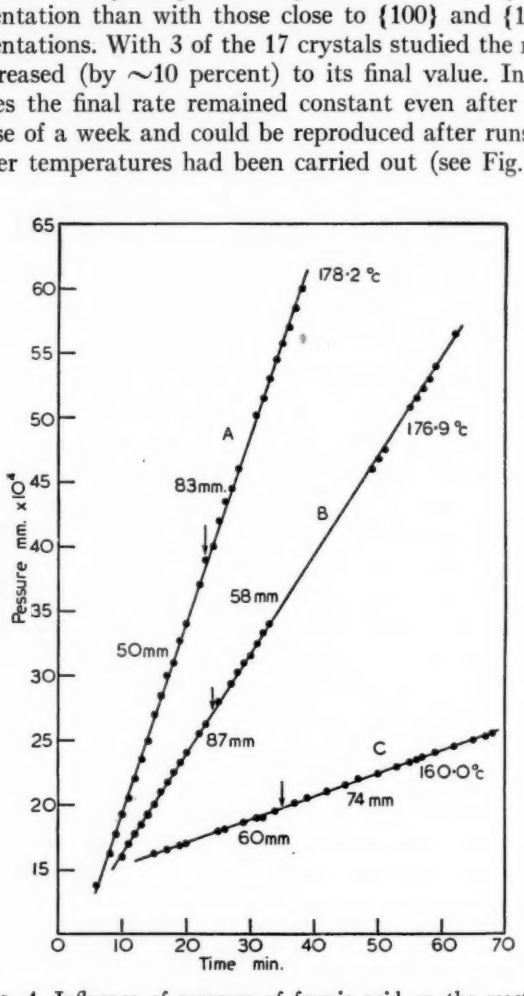

FIG. 4. Influence of pressure of formic acid on the reaction rate. Pressure changed at points indicated by arrows. *A* and *C* obtained with single crystals, *B* with polycrystalline specimen.

However, in a single experiment, a crystal after standing *in vacuo* for 8 weeks at 186°C showed a 40 percent increase in rate.

RESULTS

The results of a typical series of runs are shown in Fig. 3. Reaction rates ρ were obtained from the slopes of such plots after allowing for the decomposition on the walls. At 460°K they were of the order of $10^{-10}-10^{-11}$ mole/sec cm² geometrical area. The influence of the pressure of formic acid vapor on the rate is illustrated in Fig. 4. The pressure was changed during the runs at the points marked by the arrows. The absence of any effect of pressure on the rate shows that

the reaction is of zero order within the range of pressures studied. This was found to be so throughout the temperature range with crystals of different orientations and, as shown in Fig. 4, with the polycrystalline metal. Experiments were normally carried out with a formic acid pressure of 55 to 70 mm.

Experimental activation energies (E) were obtained by plotting $\log\rho$ against $1/T$ and taking the least-square line. No systematic deviation from linearity was detected in any of the Arrhenius plots. Typical examples of such plots are given in Fig. 5. The maximum error in the activation energy is estimated as ± 0.5 kcal/mole.

The activation energies thus found vary strongly with the crystal orientation. The orientations of the

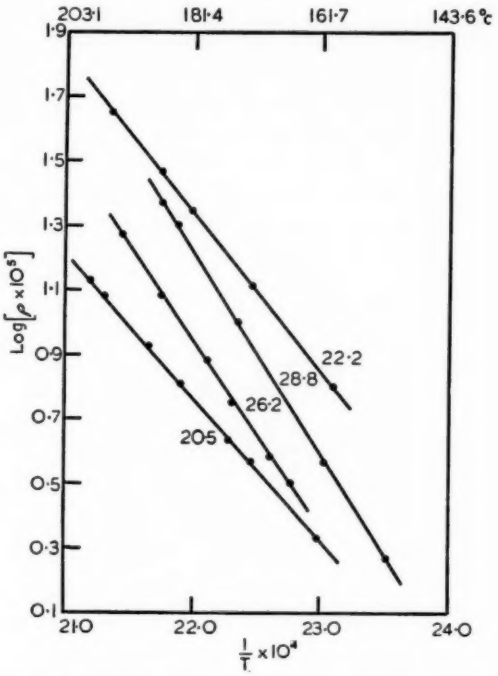

FIG. 5. Typical Arrhenius plots for crystals of different orientations. The activation energies (in kcal/mole) derived from the lines are indicated.

16 crystals used are plotted stereographically in Fig. 6 together with the corresponding values of E. It will be seen that E ranges from 16.0 to 30.4 kcal/mole. The highest values are to be found in the neighborhood of the [110] corner and the lowest mostly in the [111] corner of the stereographic triangle. However, it appears that E is not uniquely determined by the bulk orientation of the crystal, since crystals of similar orientation show differences in E. Examples of this are a crystal with $E=20.5$ kcal/mole which is found close to crystals showing values of $E\sim 27$ kcal/mole and a crystal with $E=23.5$ kcal/mole which is close to others with $E=29.5$ and 25.8 kcal/mole. Those effects are probably due to differences in the detailed nature of the surfaces of crystals of similar bulk orientation (see Discussion).

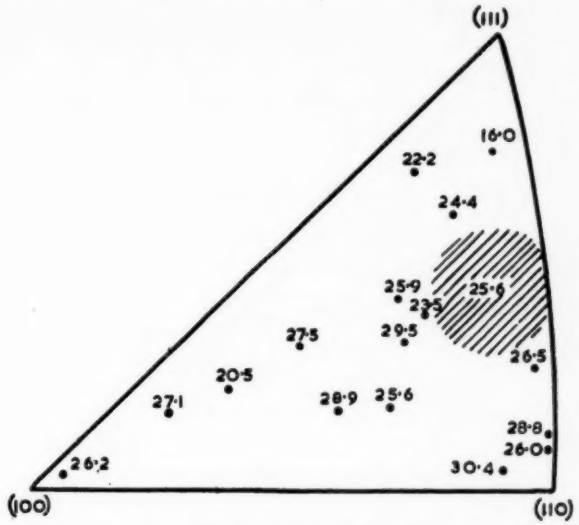

FIG. 6. Standard stereographic projection of cubic crystal. The points indicate the normals of the macroscopic surfaces of the crystals. The experimental activation energies are shown. The shaded area refers to the polycrystalline specimen.

Measurements on a polycrystalline specimen gave a value for E of 25.6 kcal/mole. X-ray examination revealed a marked preferred orientation of the crystals in the specimen, the majority having orientations described by the shaded region in Fig. 6.

Reaction rates varied by less than a factor of 10, in most cases within a factor of 2, over the whole range of crystal orientations. However, no correlation of ρ with orientation is possible since the relative order of reactivity of the crystals changes with the temperature. In any case, such a correlation would be of little value at this stage since it is not known how the true surface area varies with the orientation. However, as is commonly found with other types of physical modification of a catalyst, there is a linear relationship

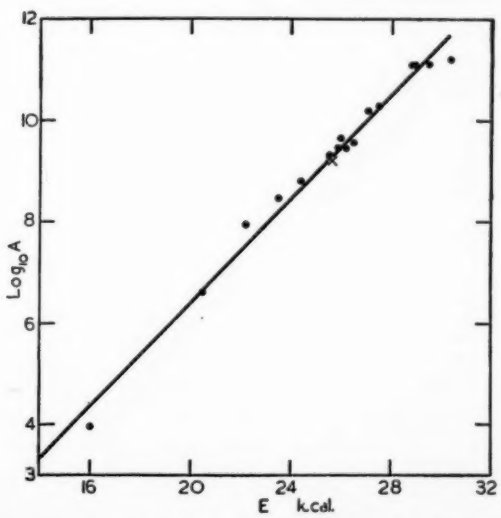

FIG. 7. Plot of $\log A$ (for 20 cm² geometrical area) against E for all crystals investigated. The cross indicates the values of the polycrystalline specimen.

between the Arrhenius constants $\log A$ and E for the various crystals. This is shown in Fig. 7. The effect of the maximum change in E of 14.4 kcal/mole on the rate is largely compensated by a simultaneous change in A by a factor of 10^7.

DISCUSSION

The results show that the orientation of the macroscopically flat surface has a marked effect on the activation energy. The value characteristic of a crystal close to the {110} orientation is about $1\frac{1}{2}$ times that obtained with a crystal close to the {111} orientation and the activation energies for all other crystals lie within these limits. Such a dependence on orientation does not seem to have been demonstrated unequivocally in previous work.

However, it should be emphasized again, that this activation energy E was obtained from the experiments assuming the validity of an Arrhenius equation and that the physical significance of E is not clear. The surfaces of the crystals used are not atomically flat, and probably consist of facets of a crystallographic nature different from that of the macroscopically apparent surface. The occurrence of such facets of the {100}, {110}, {210}, and {311} types on electrolytically etched silver crystals with {100} and {110} planes in the apparent surface has been shown by Pashley.[10] The type of the facets developed and their relative size may depend on factors such as method of growth of the crystals and their pretreatment in the reaction chamber, and this suggestion is supported by the previously noted fact that crystals of similar orientation give different values of E.

[10] D. W. Pashley, Proc. Phys. Soc. (London) **A64**, 1113 (1951).

If the surface of each crystal is made up of facets of more than a single type and each of these types $(1, 2, 3\cdots)$ has a different activation energy $(E_1, E_2\cdots)$ the reaction rate will not be described by a simple Arrhenius equation but by an expression of the form

$$\rho = C_1 A_1 e^{-E_1/RT} + C_2 A_2 e^{-E_2/RT} + \cdots C_n A_n e^{-E_n/RT},$$

where $C_1, C_2\cdots$ are the total areas of types $1, 2\cdots$ and $A_1, A_2\cdots$ the corresponding frequency factors.

If we now assume that two types of facets only are developed and assign to them the extreme values of E (i.e., $E_1 = 16.0$ and $E_2 = 30.4$ kcal/mole), it is indeed possible to choose values of C_1 and C_2 for each crystal so as to reproduce within 2 percent the values of the rates obtained with all crystals and temperatures studied. The values of the total effective areas $(C_1 + C_2)$ vary within a factor of 8.

This means that from the present experiments it cannot be decided whether an individual activation energy has to be ascribed to each crystal according to its macroscopic orientation or whether at least two activation energies, characteristic of the types of facets developed, have to be used; in this case the manner in which the surface is composed of these types of facets changes with orientation and, to a lesser degree, with other factors. In any case, it is clear that the activation energy for the catalytic reaction investigated depends on the crystallographic nature of the actual surface exposed to the reaction.

ACKNOWLEDGMENTS

The author wishes to thank Mr. A. J. White for preparing the crystals, and Dr. G. J. Ogilvie and Mr. E. D. Hondros for determining the pole figure of the polycrystalline specimen.

Thermodynamics of Sorption by Solids under Finite Strain with Particular Reference to Fibers

HOWARD J. WHITE, JR.*
Textile Research Institute, Princeton, New Jersey
(Received November 5, 1954)

Equations have been derived expressing the conditions of equilibrium for a strained solid absorbent in contact with fluid absorbates. The results are more general than any previously derived and are not limited to infinitesimal strains or isotropic absorbents; it is necessary that the principal axes of stress and of strain coincide. The results are applied to a few cases involving various states of strain in fibrous absorbents such as might be encountered in the textile industry.

One result was obtained which was uniquely different from the usual thermodynamic relations involving hydrostatic pressure. Essentially, three different forms of Gibbs free energy appear. These differ in accordance with the way in which the extensive variable for the absorbent was defined.

IN this paper expressions are derived for the thermodynamic functions of a solid which is capable of withstanding shear stresses, and which contains components that can be exchanged with a surrounding liquid or gaseous medium. The expressions are used to determine the conditions of equilibrium for an absorbent fiber in a few different states of strain which are commonly found in textile processing. The analysis will not, in general, be limited to infinitesimal strains or isotropic media since neither limitation holds for fibers which can undergo rather large dimensional changes reversibly and are radially symmetrical at best. All states of strain for which the principal axes of stress coincide with the principal axes of strain can be treated using the expressions derived, and all expressions are strictly thermodynamic in nature.

Various aspects of the thermodynamics of absorption by strained solids have been considered previously. Absorption by solids under infinitesimal strains has been considered by Gibbs,[1] Goranson,[2] Barkas,[3] Gurney,[4] Warburton,[5] and Treloar.[6] Hill[7] has discussed the case of absorption by a fiber under a finite strain from an axial load, and Treloar[8] has dealt with certain specific absorption problems involving finite strain.

EQUILIBRIUM CONDITIONS

To obtain the conditions of equilibrium consider a solid absorbent fastened in a nonabsorbent holder surrounded by absorbable vapors in the usual rigid, impermeable, nonconducting container. Let the vapor and the rest of the system be allowed to exchange heat, volume, and two components. It is readily shown by the methods of Gibbs[1] that the entire system will have two independent intensive variables, that the temperature will be the same throughout the system, and that the partial molal free energy of each diffusible component will be the same throughout. Any complicated system of forces arising from interactions between the solid and the holder or the solid and an adsorbed film must be balanced in such a way that a resultant pressure equal and opposite to the hydrostatic pressure of the vapor exists at every point of contact between the solid and the vapor.

No detailed description of the sorption process has been necessary so that the conditions mentioned so far apply to either adsorption or solution. If, in the case of adsorption, the adsorbent is constrained to remain constant with respect to degree of subdivision, adsorption and solution are indistinguishable on purely thermodynamic grounds. Thus, any relationship expressed in terms appropriate to the one form of sorption can readily be transcribed into terms appropriate to the other. It seems likely at the present time that the terminology used in describing solutions is more suitably applied to absorption by fibers than that used in describing adsorption, and solution terms will be used for the rest of the analysis.

INTERNAL ENERGY OF STRAINED SOLIDS OF CONSTANT COMPOSITION

To proceed with the analysis, it is necessary to consider the internal energy of the strained solid. It is convenient first to consider the energy change as a function of the variables representing the strain with the entropy and composition of the solid kept constant. The behavior of solids under strain at constant entropy (or temperature) and composition belongs in the field of elasticity. Only enough will be given here to obtain the relation between stresses and strains through use of the strain energy. (For a general discussion see Love.[9]) The

* Associate Director of Research, Textile Research Institute, Princeton, New Jersey.
[1] J. W. Gibbs, *The Collected Works of J. Willard Gibbs*, Vol. 1, "Thermodynamics" (Longmans Green, New York, 1931).
[2] R. W. Goranson, *Thermodynamic Relations in Multi-Component Systems* (Carnegie Institute, Washington, 1930).
[3] W. W. Barkas, *Swelling Stresses in Gels* (Her Majesty's Stationery Office, London, 1945); Trans. Faraday Soc. **38**, 194 (1942).
[4] G. Gurney, Proc. Phys. Soc. (London) **59**, 629 (1947).
[5] F. L. Warburton, Proc. Phys. Soc. (London) **58**, 589 (1946).
[6] L. R. G. Treloar, Trans. Faraday Soc. **48**, 567 (1952).
[7] T. L. Hill, J. Chem. Phys. **18**, 791 (1950).
[8] L. R. G. Treloar, Proc. Roy. Soc. (London) **200A**, 176 (1950).
[9] A. E. H. Love, *The Mathematical Theory of Elasticity* (Dover Publications, New York, 1944), fourth edition.

strain energy equations for the case of finite strains have been discussed from various aspects by Rivlin,[10–13] Murnaghan,[14,15] and Mooney.[16]

Consider a solid body at equilibrium under the influence of surface forces but not of body forces. We wish to derive an expression for the change in internal energy which the solid body undergoes by virtue of the strains imposed and a relation between the strains and the applied stresses.

Let $\mathbf{t}_{nl}$ be the average force per unit area on a small area $d\sigma_n$ of the strained body. The subscript l on $\mathbf{t}_{nl}$ refers to the direction of the force, and the subscript n refers to the direction of the outward normal to the surface as well as to the identity of the unit of surface. Let $\delta\mathbf{r}_n$ be a small displacement of a point on $d\sigma_n$. Since $d\sigma$ is assumed small, $\delta\mathbf{r}_n$ is the displacement of the surface to the first order in infinitesimals. Then the work done in the virtual displacement (again to the first order in infinitesimals) can be written:

$$\delta W_n=(\mathbf{t}_{nl}\cdot\delta\mathbf{r}_n)\delta\sigma_n. \tag{1}$$

If this is summed over the entire body and no heat or matter is exchanged with the surroundings, the sum equals the internal energy change of the body occurring during the displacement.

$$\delta E=\int_\sigma(\mathbf{t}_{nl}\cdot\delta\mathbf{r}_n)d\sigma_n, \tag{2}$$

where the integral is a surface integral over the surface of the body in its final state.

If the vectors are resolved in the directions of the coordinate axes and the resulting terms rearranged, Eq. (2) can be written:

$$\begin{aligned}\delta E=\int_\sigma[&(t_{xx}\delta x_n+t_{xy}\delta y_n+t_{xz}\delta z_n)\cos\alpha\\&+(t_{yx}\delta x_n+t_{yy}\delta y_n+t_{yz}\delta z_n)\cos\beta\\&+(t_{zx}\delta x_n+t_{zy}\delta y_n+t_{zz}\delta z_n)\cos\gamma]d\sigma_n,\end{aligned} \tag{3}$$

where t_{ij} is the force in the jth direction acting across the plane perpendicular to the ith axis, $\cos\alpha$, $\cos\beta$, $\cos\gamma$ are the direction cosines of the outward normal to the surface $\delta\sigma_n$, and δx_n, δy_n, δz_n are the components of $\delta\boldsymbol{r}_n$.

Since the t_{ij} and δx_n, δy_n, δz_n are continuous single-valued functions of the coordinates, by using Gauss' theorem and regrouping, Eq. (3) can be converted to:

$$\begin{aligned}\delta E=\int\Big[&\Big(\frac{\partial t_{xx}}{\partial x}+\frac{\partial t_{yx}}{\partial y}+\frac{\partial t_{zx}}{\partial z}\Big)\delta x_n\\&+\Big(\frac{\partial t_{xy}}{\partial x}+\frac{\partial t_{yy}}{\partial y}+\frac{\partial t_{zy}}{\partial z}\Big)\delta y_n\\&+\Big(\frac{\partial t_{xz}}{\partial x}+\frac{\partial t_{yz}}{\partial y}+\frac{\partial t_{zz}}{\partial z}\Big)\delta z_n+t_{xx}\frac{\partial}{\partial x}\delta x_n+t_{yx}\frac{\partial}{\partial y}\delta x_n\\&+t_{zx}\frac{\partial}{\partial z}\delta x_n+t_{xy}\frac{\partial}{\partial x}\delta y_n+t_{yy}\frac{\partial}{\partial y}\delta y_n+t_{zy}\frac{\partial}{\partial z}\delta y_n\\&+t_{xz}\frac{\partial}{\partial x}\delta z_n+t_{yz}\frac{\partial}{\partial y}\delta z_n+t_{zz}\frac{\partial}{\partial z}\delta z_n\Big]dV,\end{aligned} \tag{4}$$

where the integral is to be taken over the volume of the body in its final strained state. Since the virtual displacement is considered small, the change in internal energy will be the same to the first order in infinitesimals if the integration is carried out over the volume of the initial strained configuration.

Since the body is not acted on by body forces and is not in motion, the three terms in parentheses, which constitute the stress equations of equilibrium, are zero at every point in the body, and $t_{yx}=t_{xy}$: $t_{xz}=t_{zx}$: $t_{zy}=t_{yz}$.[17] Thus Eq. (4) reduces to:

$$\begin{aligned}\delta E=\int_V\Big[&\Big(t_{xx}\frac{\partial}{\partial x}+t_{xy}\frac{\partial}{\partial y}+t_{zx}\frac{\partial}{\partial z}\Big)\delta x_n\\&+\Big(t_{xy}\frac{\partial}{\partial x}+t_{yy}\frac{\partial}{\partial y}+t_{yz}\frac{\partial}{\partial z}\Big)\delta y_n\\&+\Big(t_{zx}\frac{\partial}{\partial x}+t_{yz}\frac{\partial}{\partial y}+t_{zz}\frac{\partial}{\partial z}\Big)\delta z_n\Big]dV.\end{aligned} \tag{5}$$

It is now convenient to introduce the displacement vector whose components can be defined in the following way. A portion of the material which is at the point x, y, z in the strained state can be considered to have been at the point ξ, η, ζ, in the unstrained state. The two points can be related by the equations $\xi=x-u(x,y,z)$, $\eta=y-v(x,y,z)$, $\zeta=z-w(x,y,z)$, where the terms u, v, w, represent the transformation occurring during the strain. Here the coordinates of the strained state have been taken as the independent variables. It is equally possible to take the coordinates of the unstrained state as the independent variables, in which case the equations of the transformation would be $x=\xi+u(\xi,\eta,\zeta)$, $y=\eta+v(\xi,\eta,\zeta)$, $z=\zeta+w(\xi,\eta,\zeta)$.

A knowledge of the nine partial derivatives $\partial u/\partial\xi=u_\xi$, u_η, u_ζ, v_ξ, v_η, v_ζ, w_ξ, w_η, w_ζ at a point is enough to give a complete description of the strain around the

[10] R. S. Rivlin, Proc. Roy. Soc. (London) **195A**, 463 (1949).
[11] R. S. Rivlin, Trans. Roy. Soc. **242A**, 173 (1949).
[12] R. S. Rivlin, Trans. Roy. Soc. **241A**, 379 (1948).
[13] R. S. Rivlin, Trans. Roy. Soc. **240A**, 459, 491, 509 (1948).
[14] F. D. Murnaghan, *Finite Deformation of an Elastic Solid* (John Wiley and Sons, Inc., New York, 1951).
[15] F. D. Murnaghan, Am. J. Math. **59**, 235 (1937).
[16] M. Mooney, J. Appl. Phys. **19**, 434 (1948).
[17] See reference 9, Secs. 44 and 54.

point.[18] Therefore, the part of the change in internal energy resulting from the strain is a function of these nine derivatives. In an analogous way the strain can be described in terms of the nine partial derivatives $u_x \cdots w_z$. Thus the internal energy change for a differential volume when the substance undergoes a small deformation, δr, is a function of $\delta u_x \cdots \delta w_z$, or

$$\delta E = \int_V \left[\frac{\partial E_V}{\partial u_x}\delta u_x + \frac{\partial E_V}{\partial u_y}\delta u_y + \frac{\partial E_V}{\partial u_z}\delta u_z + \frac{\partial E_V}{\partial v_x}\delta v_x + \frac{\partial E_V}{\partial v_y}\delta v_y + \frac{\partial E_V}{\partial v_z}\delta v_z + \frac{\partial E_V}{\partial w_x}\delta w_x + \frac{\partial E_V}{\partial w_y}\delta w_y + \frac{\partial E_V}{\partial w_z}\delta w_z \right] dV, \quad (6)$$

where $E_V = \partial E/\partial V$ in the unit of volume being considered.

The interrelationships between the undeformed and the two deformed states considered initially are shown in Fig. 1. The letters on the outside of the triangle refer to the use of the coordinates of the initial deformed state as the independent variables, the letters on the inside, to the use of the coordinates of the undeformed state as independent variables. The arrows show the transformations between states. The relative proportions of the sides of the triangle are meaningless. Actually the two deformed states are considered to differ infinitesimally, whereas the undeformed state may differ more than infinitesimally from the other two. Since no change in the coordinate axes has been used, where the coordinates of one point have two sets of expressions these must be equivalent. Thus

$$\delta x_n = \delta u; \quad \delta y_n = \delta v; \quad \delta z_n = \delta w. \quad (7)$$

Also since u, v, w are single-valued and continuous functions of x, y, z, $(\partial/\partial x)\delta u = \delta u_x$, etc.

Thus substituting Eqs. (7) into (5),

$$\delta E = \int_V \left[t_{xx}\delta u_x + t_{xy}\delta u_y + t_{zx}\delta u_z + t_{xy}\delta v_x + t_{yy}\delta v_y + t_{yz}\delta v_z + t_{zz}\delta w_x + t_{yz}\delta w_y + t_{zz}\delta w_z \right] dV. \quad (8)$$

Differentiating Eqs. (6) and (8) with respect to the volume, and equating coefficients of independent variations,

$$\begin{aligned} \frac{\partial E_V}{\partial u_x} &= t_{xx}; & \frac{\partial E_V}{\partial u_y} &= t_{xy}; & \frac{\partial E_V}{\partial u_z} &= t_{zx}, \\ \frac{\partial E_V}{\partial v_x} &= t_{xy}; & \frac{\partial E_V}{\partial v_y} &= t_{yy}; & \frac{\partial E_V}{\partial v_z} &= t_{yz}, \\ \frac{\partial E_V}{\partial w_x} &= t_{zx}; & \frac{\partial E_V}{\partial w_y} &= t_{yz}; & \frac{\partial E_V}{\partial w_z} &= t_{zz}. \end{aligned} \quad (9)$$

[18] See reference 9, Secs. 24 and 25.

Equations (9) relate the stresses to the various partial derivatives of the displacement vector through the internal energy which is a function (the strain energy) of these derivatives only. The strain coefficients are functions of the same partial derivatives; hence a relation between stress and strain through the internal energy and its derivatives has been effected, and this relation is not limited in applicability by the magnitude of the strain.[19] Until some function is chosen for the strain energy, the nature of the dependence of stress on strain remains unknown.

It is possible to rewrite the stress-strain-internal energy relationships in terms of the coordinates of the unstrained state as the independent variables. If ξ, η, ζ, the coordinates of the point x, y, z, in the undeformed state are now taken as the independent variables,

$$\begin{aligned} \frac{\partial}{\partial \xi}\delta u = \delta u_\xi &= \delta u_x x_\xi + \delta u_y y_\xi + \delta u_z z_\xi \\ \delta u_\eta &= \delta u_x x_\eta + \delta u_y y_\eta + \delta u_z z_\eta \\ \delta u_\zeta &= \delta u_x x_\zeta + \delta u_y y_\zeta + \delta u_z z_\zeta \end{aligned} \quad (10)$$

with similar equations for $\delta v_\xi \cdots \delta w_\zeta$. Defining

$$\tau = \begin{vmatrix} 1+u_\xi & u_\eta & u_\zeta \\ v_\xi & 1+v_\eta & v_\zeta \\ w_\xi & w_\eta & 1+w_\zeta \end{vmatrix} \quad (11)$$

and using the relations $x_\xi = (\partial/\partial\xi)(\xi+u) = 1+u_\xi$, $x_\eta = u_\eta$ etc., Eqs. (10) can be solved for δu_x, δu_y, and δu_z.

Since $dV(x,y,z) = \tau dV_0(\xi,\eta,\zeta)$, Eq. (8) can be rewritten incorporating Eqs. (10), to give

$$\begin{aligned} \delta E = \int_{V_0} \Bigg[& t_{\xi\xi}\left(\delta u_\xi \frac{\partial \tau}{\partial u_\xi} + \delta u_\eta \frac{\partial \tau}{\partial u_\eta} + \delta u_\zeta \frac{\partial \tau}{\partial u_\zeta}\right) \\ & + t_{\xi\eta}\left(\delta u_\xi \frac{\partial \tau}{\partial v_\xi} + \delta u_\eta \frac{\partial \tau}{\partial v_\eta} + \delta u_\zeta \frac{\partial \tau}{\partial v_\zeta}\right) + t_{\zeta\xi}\left(\delta u_\xi \frac{\partial \tau}{\partial w_\xi} \right. \\ & \left. + \delta u_\eta \frac{\partial \tau}{\partial w_\eta} + \delta u_\zeta \frac{\partial \tau}{\partial w_\zeta}\right) + t_{\xi\eta}\left(\delta v_\xi \frac{\partial \tau}{\partial u_\xi} + \delta v_\eta \frac{\partial \tau}{\partial u_\eta} + \delta v_\zeta \frac{\partial \tau}{\partial u_\zeta}\right) \\ & + t_{\eta\eta}\left(\delta v_\xi \frac{\partial \tau}{\partial v_\xi} + \delta v_\eta \frac{\partial \tau}{\partial v_\eta} + \delta v_\zeta \frac{\partial \tau}{\partial v_\zeta}\right) + t_{\eta\zeta}\left(\delta v_\xi \frac{\partial \tau}{\partial w_\xi} \right. \\ & \left. + \delta v_\eta \frac{\partial \tau}{\partial w_\eta} + \delta v_\zeta \frac{\partial \tau}{\partial w_\zeta}\right) + t_{\zeta\xi}\left(\delta w_\xi \frac{\partial \tau}{\partial u_\xi} + \delta w_\eta \frac{\partial \tau}{\partial u_\eta} \right. \\ & \left. + \delta w_\zeta \frac{\partial \tau}{\partial u_\zeta}\right) + t_{\eta\zeta}\left(\delta w_\xi \frac{\partial \tau}{\partial v_\xi} + \delta w_\eta \frac{\partial \tau}{\partial v_\eta} + \delta w_\zeta \frac{\partial \tau}{\partial v_\zeta}\right) \\ & + t_{\zeta\zeta}\left(\delta w_\xi \frac{\partial \tau}{\partial w_\xi} + \delta w_\eta \frac{\partial \tau}{\partial w_\eta} + \delta w_\zeta \frac{\partial \tau}{\partial w_\zeta}\right)\Bigg] dV_0. \end{aligned} \quad (11)$$

[19] This is in agreement with Murnaghan (see reference 15) who states, "The virtual work is obtained by integrating over the medium the scalar product of the stress tensor by the space derivative of the virtual displacement vector." The coordinates of the strained state were considered independent variables by Murnaghan.

Here $l_{\xi\xi}$ has been written for l_{xx}, etc. since the shift from x, y, z as independent variables to ξ, η, ζ does not involve a shift in coordinate axes. An equation entirely similar to Eq. (6) can be written involving u_ξ etc., and differentiating with respect to V_0, the volume of the undeformed material, it is possible to get the set of equations:

$$\begin{aligned}
\frac{\partial Ev_0}{\partial u_\xi} &= t_{\xi\xi}\frac{\partial \tau}{\partial u_\xi} + t_{\xi\eta}\frac{\partial \tau}{\partial v_\xi} + t_{\xi\zeta}\frac{\partial \tau}{\partial w_\xi}, \\
\frac{\partial Ev_0}{\partial u_\eta} &= t_{\xi\xi}\frac{\partial \tau}{\partial u_\eta} + t_{\xi\eta}\frac{\partial \tau}{\partial v_\eta} + t_{\xi\zeta}\frac{\partial \tau}{\partial w_\eta}, \\
\frac{\partial Ev_0}{\partial u_\zeta} &= t_{\xi\xi}\frac{\partial \tau}{\partial u_\zeta} + t_{\xi\eta}\frac{\partial \tau}{\partial v_\zeta} + t_{\xi\zeta}\frac{\partial \tau}{\partial w_\zeta}, \\
\frac{\partial Ev_0}{\partial v_\xi} &= t_{\xi\eta}\frac{\partial \tau}{\partial u_\xi} + t_{\eta\eta}\frac{\partial \tau}{\partial v_\xi} + t_{\eta\zeta}\frac{\partial \tau}{\partial w_\xi},
\end{aligned} \tag{12}$$

etc. These equations have been derived previously by Rivlin.[20]

INTERNAL ENERGY OF SOLIDS OF VARIABLE COMPOSITION UNDERGOING PURE HOMOGENEOUS STRAIN

A homogeneous strain is characterized by the fact that the components u_x, etc. at a point are independent of the positional coordinates of the point. This means that the displacements are linear functions of the coordinates. Many important strain systems are homogeneous and Love[21] shows that, under any strain system, the strain in a small region about any point is homogeneous to a first approximation. Thus bodies under nonhomogeneous systems of strain, in principle, can be broken up into small regions undergoing homogeneous strain.

Any homogeneous strain can be resolved into a rotation such as can be undergone by a rigid body and a homogeneous pure strain.[22] A homogeneous pure strain is characterized by the fact that three orthogonal lines retain their directions and senses during the strain and hence remain orthogonal. It seems entirely reasonable to assume that no change in the internal energy of the body occurs during the rotation. Hence, the problem of the determination of the strain energy change accompanying a general strain is reduced to the determination of the change accompanying a pure homogeneous strain.

In a pure homogeneous strain the three orthogonal lines which retain their directions and senses are the principal axes of the strain and, referred to them, the strain consists of three simple extensions along the principal axes. The stress also has principal axes and, if the principal axes of stress are used as coordinate axes, the stresses are three simple tensions across planes perpendicular to the axes. It is difficult to prove without knowing the form of the strain energy function that the principal axes of stress and of strain coincide; however, in some cases it is evident that they do. For a solid under hydrostatic pressure, any orthogonal axes are principal axes of stress, and hence the principal axes of stress and strain can coincide. In the case of a fiber under uniform radial compression and axial tension, any orthogonal axes including the fiber axis are principal axes of stress, and they can be seen intuitively to be principal axes of strain also.

If the principal axes of stress and strain coincide, using the principal axes, denoted by primes, as the coordinate axes, it is possible to write

$$\begin{aligned}
&x'=\lambda_1\xi', \quad y'=\lambda_2\eta', \quad z'=\lambda_3\zeta', \\
&\text{where } \lambda_1=1+u'_{\xi'}, \quad \lambda_2=1+v'_{\eta'}, \quad \lambda_3=1+w'_{\zeta'}, \\
&\tau=\lambda_1\lambda_2\lambda_3,
\end{aligned} \tag{13}$$

and

$$\frac{\partial Ev_0}{\partial \lambda_1}=t'_{\xi'\xi'}\lambda_2\lambda_3; \quad \frac{\partial Ev_0}{\partial \lambda_2}=t'_{\eta'\eta'}\lambda_1\lambda_3; \quad \frac{\partial Ev_0}{\partial \lambda_3}=t'_{\zeta'\zeta'}\lambda_1\lambda_2, \tag{14}$$

so that

$$dEv_0=t'_{\xi'\xi'}\lambda_2\lambda_3 d\lambda_1+t'_{\eta'\eta'}\lambda_3\lambda_1 d\lambda_2+t'_{\zeta'\zeta'}\lambda_1\lambda_2 d\lambda_3. \tag{15}$$

Since nothing on the right-hand side of Eq. (15) depends on V_0 (the λ's are constants for homogeneous strain) it is possible to integrate over V_0. For convenience set $f_1=t'_{\xi'\xi'}$; $f_2=t'_{\eta'\eta'}$; $f_3=t'_{\zeta'\zeta'}$ and integrate, obtaining

$$dE=l_1l_2l_3(f_1\lambda_2\lambda_3 d\lambda_1+f_2\lambda_3\lambda_1 d\lambda_2+f_3\lambda_1\lambda_2 d\lambda_3), \tag{16}$$

where l_1, l_2, l_3 are the dimensions of the original unstrained sample, taken for convenience to be a cuboid with edges perpendicular to the coordinate axes. So far the energy changes have been restricted to those occurring in a cuboid of fixed initial dimensions without exchange of heat or matter with the surroundings. Altering l_1 with other variables constant causes work $\lambda_1\lambda_2\lambda_3 f_1 l_2 l_3 dl_1$ to be performed by the surroundings with similar terms for l_2 and l_3. The heat and matter exchange terms can be introduced in the usual way giving

$$\begin{aligned}
dE=TdS&+l_1l_2l_3[f_1\lambda_2\lambda_3 d\lambda_1+f_2\lambda_3\lambda_1 d\lambda_2+f_3\lambda_1\lambda_2 d\lambda_3] \\
&+\lambda_1\lambda_2\lambda_3[f_1l_2l_3dl_1+f_2l_3l_1dl_2+f_3l_1l_2dl_3] \\
&+\sum_i \mu_i dN_i.
\end{aligned} \tag{17}$$

Several features of Eq. (17) can be pointed out. In the first place, if $f_1=f_2=f_3=-p$, the mechanical work term reduces to $-pdV$ as is to be expected. In the second place, if the definitions, $\psi_1=f_1\lambda_2\lambda_3$; $\psi_2=f_2\lambda_3\lambda_1$;

[20] R. S. Rivlin, Trans. Roy. Soc. **A240**, 459 (1948).
[21] See reference 9, Sec. 7.
[22] See reference 9, Secs. 33 and 34.

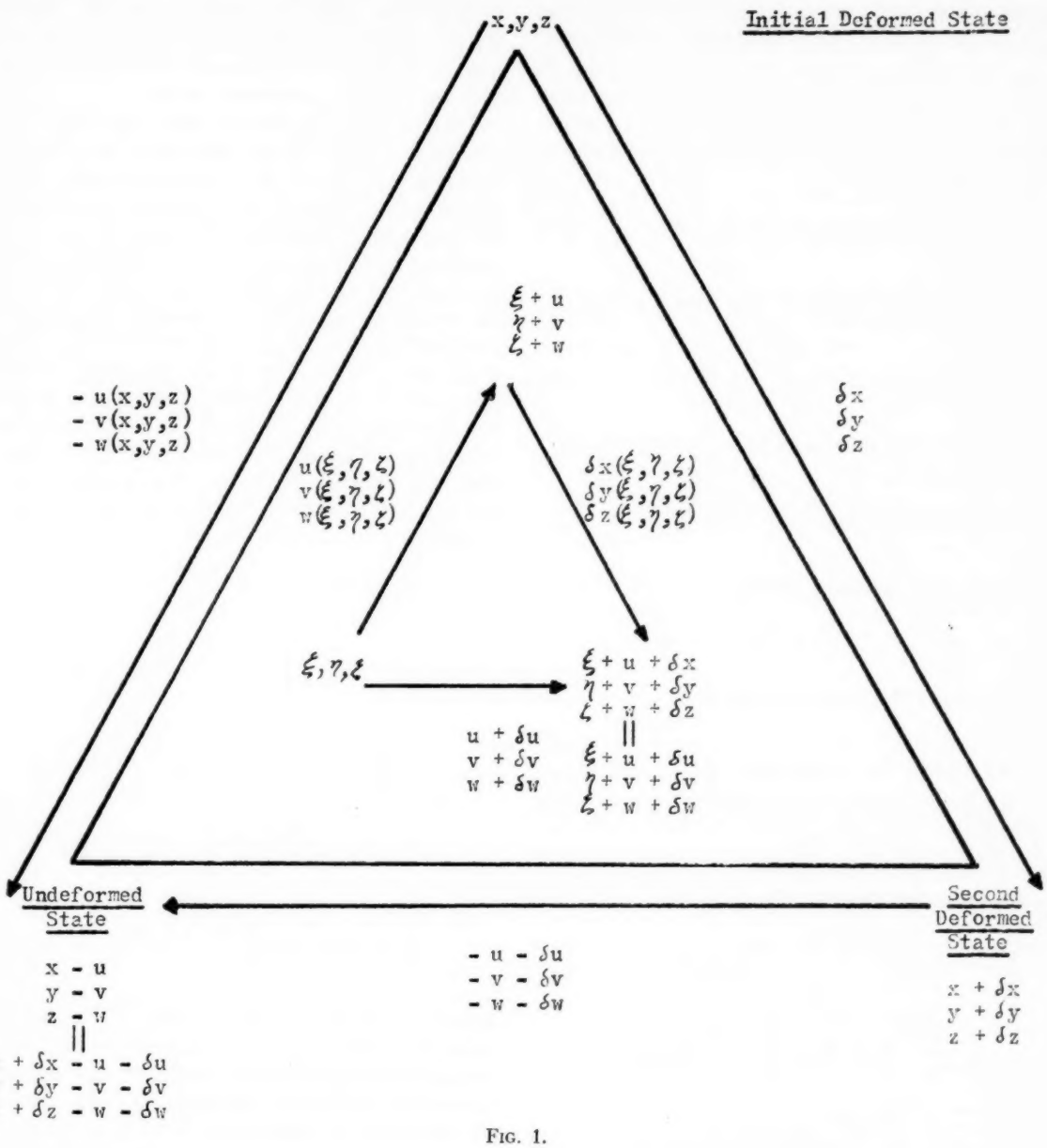

FIG. 1.

$\psi_3 = f_3\lambda_1\lambda_2$, are introduced, Eq. (17) can be written

$$dE = TdS + \psi_1 l_2 l_3 d(\lambda_1 l_1) + \psi_2 l_3 l_1 d(\lambda_2 l_2) + \psi_3 l_1 l_2 d(\lambda_3 l_3) + \sum_i \mu_i dN_i. \quad (18)$$

This form of the equation makes more evident the fact that the mechanical portions of the energy change are force-times-distance terms dimensionally.

For purposes of defining other thermodynamic functions, it is useful to be able to integrate Eqs. (17) or (18). In general, the energy depends on the shape as well as the size of the undeformed starting material and an integration cannot be made. However, there are three ways in which the size of the starting material can be made to depend on one extensive variable in which case the integration can be made. If it is assumed, for simplicity, that the undeformed material is a pure substance, A, which is not present in other phases, i.e., the pure undeformed absorbent, either one, two, or all of the dimensions of the undeformed cuboid can be made linearly dependent on N_A with the others in each case kept constant. These three ways correspond to allowing the length to increase keeping the cross section constant, allowing the area to increase keeping the length and shape of cross section constant, and allowing the sample to increase in size while keeping the shape constant, respectively.[23]

[23] Hill (see reference 7) has discussed the first two ways briefly in connection with a treatment of a fiber under an axial load.

If E, S, and the N_i are considered to be products of N_A and terms involving only intensive variables, Eq. (17) can be integrated from zero to N_A keeping all intensive variables constant using each of the three methods of increasing the size of the sample in turn. If l_1 is linear in N_A and l_2 and l_3 are constant, Eq. (17) can be integrated to give

$$E=TS+\lambda_1\lambda_2\lambda_3 l_1 l_2 l_3 f_1+\sum_i \mu_i N_i. \tag{19}$$

If l_1 is constant and l_2 and l_3 are linear in N_A, the integration gives

$$E=TS+\lambda_1\lambda_2\lambda_3 l_1 l_2 l_3 \frac{f_2+f_3}{2}+\sum_i \mu_i N_i. \tag{20}$$

Finally, if l_1, l_2, and l_3 are each linear functions of N_A, the integration gives

$$E=TS+\lambda_1\lambda_2\lambda_3 l_1 l_2 l_3 \frac{f_1+f_2+f_3}{3}+\sum_i \mu_i N_i. \tag{21}$$

If a function, F, is defined such that

$$F\equiv\sum_i \mu_i N_i, \tag{22}$$

then, from Eq. (19), remembering that l_2 and l_3 are constants,

$$dF=-SdT+l_1 l_2 l_3[(f_2-f_1)\lambda_3\lambda_1 d\lambda_2 + (f_3-f_1)\lambda_1\lambda_2 d\lambda_3-\lambda_1\lambda_2\lambda_3 df_1]+\sum_i \mu_i dN_i. \tag{23}$$

From Eq. (20), remembering that l_1 is constant, and l_2 and l_3 are linear functions of N_A

$$dF=-SdT+l_1 l_2 l_3\left[\left(\frac{2f_1-f_2-f_3}{2}\right)\lambda_2\lambda_3 d\lambda_1 + \left(\frac{f_2-f_3}{2}\right)\lambda_3\lambda_1 d\lambda_2+\left(\frac{f_3-f_2}{2}\right)\lambda_1\lambda_2 d\lambda_3 - \frac{\lambda_1\lambda_2\lambda_3}{2}(df_2+df_3)\right]+\sum_i \mu_i dN_i. \tag{24}$$

Finally from Eq. (21), remembering that l_1, l_2, l_3 are linear functions of N_A,

$$dF=-SdT+l_1 l_2 l_3\left[\left(\frac{2f_1-f_2-f_3}{3}\right)\lambda_2\lambda_3 d\lambda_1 + \left(\frac{2f_2-f_3-f_1}{3}\right)\lambda_3\lambda_1 d\lambda_2 + \left(\frac{2f_3-f_1-f_2}{3}\right)\lambda_1\lambda_2 d\lambda_3 - \frac{\lambda_1\lambda_2\lambda_3}{3}(df_1+df_2+df_3)\right]+\sum_i \mu_i dN_i. \tag{25}$$

In Eqs. (24) and (25), terms in $\partial l_2/\partial T$, $\partial l_3/\partial T$, and $\partial l_1/\partial T$, $\partial l_2/\partial T$, $\partial l_3/\partial T$ have been neglected as small. Alternatively, the temperature of the undeformed reference state can be considered fixed.

Two points in connection with Eqs. (23), (24), (25) are worth noting. In the first place, only three of the variables $\lambda_1, \lambda_2, \lambda_3, f_1, f_2, f_3$ are independent. It has been shown that, at constant entropy and composition, either set can be determined from the other, if the form of the strain energy function is known. By defining a Helmholtz free energy, from Eq. (17) it can readily be shown that the strain energy exists at constant temperature and composition also. Thus only three of the mechanical work terms are independent, the extra terms being functions of the independent terms, the temperature and the composition. Second, the different forms of dF arise from the use of Eq. (22) in defining F. They really refer to different functions. For example, if a new function, F', is defined, under conditions where only l_1 is allowed to vary, by

$$F'=F+\lambda_1\lambda_2\lambda_3 l_1 l_2 l_3\left(\frac{2f_1-f_2-f_3}{2}\right), \tag{26}$$

then

$$dF'=-SdT+l_1 l_2 l_3\left[\left(\frac{2f_1-f_2-f_3}{2}\right)\lambda_2\lambda_3 d\lambda_1 + \left(\frac{f_2-f_3}{2}\right)\lambda_3\lambda_1 d\lambda_2+\left(\frac{f_3-f_2}{2}\right)\lambda_1\lambda_2 d\lambda_3 - \lambda_1\lambda_2\lambda_3\left(\frac{df_2+df_3}{2}\right)\right]+\sum_{j\neq A}\mu_j dN_j + \left[\mu_A+\lambda_1\lambda_2\lambda_3 l_2 l_3\left(\frac{2f_1-f_2-f_3}{2}\right)\frac{\partial l_1}{\partial N_A}\right]dN_A. \tag{27}$$

Equation (27) is equivalent to Eq. (24) except that the value of μ_A differs in the two cases. Thus the same results will be obtained with any of the three equations except where μ_A is concerned. The exact meaning of μ_A depends on the choice of conditions for integrating the energy Eq. (17). Since in most absorption problems the absorbent is not soluble in the surrounding fluid, μ_A is seldom wanted.

By differentiating Eqs. (23), (24), (25) with respect to N_i to obtain the dependence of μ_i on temperature and strain, and adding terms expressing its concentration dependence at constant temperature and strain, the total derivative of μ_i can be written

$$d\mu_i=-\bar{S}_i dT+l_1 l_2 l_3\left[\frac{\partial}{\partial N_i}((f_2-f_1)\lambda_3\lambda_1)d\lambda_2 + \frac{\partial}{\partial N_i}((f_3-f_1)\lambda_1\lambda_2)d\lambda_3-\frac{\partial}{\partial N_i}(\lambda_1\lambda_2\lambda_3)df_1\right] + \sum_j \frac{\partial\mu_i}{\partial\Gamma_j}d\Gamma_j, \tag{28}$$

or

$$d\mu_i=-\bar{S}_i dT+l_1l_2l_3\left[\frac{\partial}{\partial N_i}\left(\frac{2f_1-f_2-f_3}{2}\lambda_2\lambda_3\right)d\lambda_1+\frac{\partial}{\partial N_i}\left(\frac{f_2-f_3}{2}\lambda_3\lambda_1\right)d\lambda_2+\frac{\partial}{\partial N_i}\left(\frac{f_3-f_2}{2}\lambda_1\lambda_2\right)d\lambda_3-\frac{\partial}{\partial N_i}\frac{\lambda_1\lambda_2\lambda_3}{2}(df_2+df_3)\right]+\sum_j\frac{\partial\mu_i}{\partial\Gamma_j}d\Gamma_j, \quad (29)$$

or

$$d\mu_i=-\bar{S}_i dT+l_1l_2l_3\left[\frac{\partial}{\partial N_i}\left(\frac{2f_1-f_2-f_3}{3}\lambda_2\lambda_3\right)d\lambda_1+\frac{\partial}{\partial N_i}\left(\frac{2f_2-f_3-f_1}{3}\lambda_3\lambda_1\right)d\lambda_2+\frac{\partial}{\partial N_i}\left(\frac{2f_3-f_1-f_2}{3}\lambda_1\lambda_2\right)d\lambda_3-\frac{\partial}{\partial N_i}\times\left(\frac{\lambda_1\lambda_2\lambda_3}{3}\right)(df_1+df_2+df_3)\right]+\sum_j\frac{\partial\mu_i}{\partial\Gamma_j}d\Gamma_j, \quad (30)$$

where the $\bar{S}_i$ are second partial derivatives of Eqs. (23), (24), and (25) with respect to T and N_i, and $\Gamma_j=N_j/N_A$; the sum over j includes terms for all i except $i=A$.

It has already been shown that the familiar equilibrium condition, $\mu_i{}^\alpha=\mu_i{}^\beta$, where α and β refer to different phases, holds for diffusible components, so that for a change during which equilibrium is ma intained

$$d\mu_i{}^\alpha=d\mu_i{}^\beta. \quad (31)$$

Equation (31) and either (28), (29), or (30) are equations which can be used to correlate and predict experimentally measurable quantities. They are general enough to cover practically any equilibrium thermodynamic problem, at least in principle.

APPLICATIONS OF THE BASIC EQUILIBRIUM EQUATIONS TO FIBERS IN SOME SIMPLE STATES OF STRAIN

The applications given here will be some of the simpler ones possible and will be selected to bear on certain important fiber absorption problems. Specifically, the effect of certain simple states of strain on the amount absorbed will be discussed. For the sake of simplicity when discussing different states of strain or stress only one diffusible component will be considered. Extensions to more complex cases can be made easily. Superscript α will be used to denote the fiber, β the other phase.

1. Effect of Hydrostatic Pressure on Absorption

If $f_1=f_2=f_3=-p$, Eqs. (28), (29), or (30) reduce to

$$d\mu^\alpha=-\bar{S}^\alpha dT+\bar{V}^\alpha dp+\frac{\partial\mu^\alpha}{\partial\Gamma}d\Gamma \quad (31)$$

and, assuming the surrounding phase to have only two components (one not absorbed),

$$d\mu^\beta=-\bar{S}^\beta dT+\bar{V}^\beta dp+\frac{\partial\mu^\beta}{\partial x}dx, \quad (32)$$

where x is a concentration variable. If T and x are kept constant,

$$\frac{d\Gamma}{dp}=\frac{\bar{V}^\beta-\bar{V}^\alpha}{\partial\mu^\alpha/\partial\Gamma}. \quad (33)$$

Since the denominator on the right-hand side is positive, pressures will increase or decrease absorption according to whether $\bar{V}^\beta>\bar{V}^\alpha$ or $\bar{V}^\beta<\bar{V}^\alpha$.

2. Fiber under an Axial Load

In this case $f_1=-p+f$, $f_2=-p$, $f_3=-p$. Using Eq. (28),

$$d\mu^\alpha=-\bar{S}^\alpha dT-l_1l_2l_3\bar{\lambda}_1{}^\alpha d\psi+\bar{V}^\alpha dp+\frac{\partial\mu^\alpha}{\partial\Gamma}d\Gamma, \quad (34)$$

where $\bar{\lambda}_1{}^\alpha$ is the increase in elongation per unit component absorbed, and $\psi=f\lambda_2\lambda_3$. At constant T, p, and x

$$\frac{d\Gamma}{d\psi}=l_1l_2l_3\frac{\bar{\lambda}_1{}^\alpha}{\partial\mu^\alpha/\partial\Gamma}. \quad (35)$$

Again the sign of $d\Gamma/d\psi$ depends on $\bar{\lambda}_1{}^\alpha$, being positive if absorption causes swelling in the direction 1. It should again be emphasized that modifications of Eq. (29) or (30) could be used to obtain the same result; Eq. (28) was used only because of its easy applicability.

3. Fiber under a Given Extension

In this case $f_2=f_3=-p$, $f_1=f-p$, $\lambda_1=\lambda$, and Eq. (29) can be written

$$d\mu^\alpha=-\bar{S}^\alpha dT+l_1l_2l_3\frac{\partial\psi}{\partial N}d\lambda+\bar{V}^\alpha dp+\frac{\partial\mu^\alpha}{\partial\Gamma}d\Gamma. \quad (36)$$

At constant T, p, and x

$$\frac{d\Gamma}{d\lambda}=-l_1l_2l_3\left(\frac{\partial\psi}{\partial N}\Big/\frac{\partial\mu^\alpha}{\partial\Gamma}\right). \quad (37)$$

Thus, if at a given value of λ an increase in amount absorbed would reduce the force per unit area referred to the undeformed fiber cross section, i.e., the force on the fiber, the amount absorbed would increase as the fiber is extended.

Examples 2 and 3 have been discussed by Hill[7] who gives a complete set of equations governing a fiber under an axial load.

4. Fiber under Lateral Compression

In this case, $f_1=-p$, $f_2=f_3=-f-p$, and Eq. (23) becomes

$$dF^\alpha=-S^\alpha dT+l_1l_2l_3[-f\lambda_3\lambda_1d\lambda_2-f\lambda_1\lambda_2d\lambda_3+\lambda_1\lambda_2\lambda_3dp+\mu dN]+\mu_A dN_A. \quad (38)$$

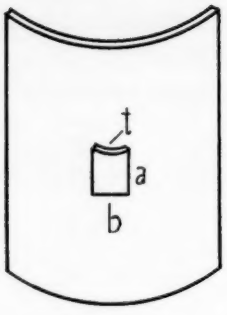

FIG. 2.

Define F' by

$$F'=F+l_1l_2l_3(\psi_2\lambda_2+\psi_3\lambda_3), \tag{39}$$

where

$$\psi_2=f\lambda_3\lambda_1, \quad \psi_3=f\lambda_1\lambda_2.$$

Then

$$dF'=-S^\alpha dT+l_1l_2l_3[\lambda_2 d\psi_2+\lambda_3 d\psi_3+\lambda_1\lambda_2\lambda_3 dp]$$

$$+\mu dN+\left[\mu_A+(\psi_2\lambda_2+\psi_3\lambda_3)\frac{\partial(l_1l_2l_3)}{\partial N_A}\right]dN_A. \tag{40}$$

From (40)

$$d\mu=-\bar{S}^\alpha dT+l_1l_2l_3\left[\bar{\lambda}_2 d\psi_2+\bar{\lambda}_3 d\psi_3+\frac{\partial\lambda_1\lambda_2\lambda_3}{\partial N}dp\right]$$

$$+\frac{\partial\mu^\alpha}{\partial\Gamma}d\Gamma. \tag{41}$$

If T, p, x are constant

$$\frac{\partial\mu^\alpha}{\partial\Gamma}d\Gamma=-l_1l_2l_3\left[\lambda_2\left(\lambda_3\lambda_1+f\lambda_3\frac{\partial\lambda_1}{\partial f}+f\lambda_1\frac{\partial\lambda_3}{\partial f}\right)df\right.$$

$$\left.+\lambda_3\left(\lambda_1\lambda_2+f\lambda_1\frac{\partial\lambda_2}{\partial f}+f\lambda_2\frac{\partial\lambda_1}{\partial f}\right)df\right]. \tag{42}$$

For a radially isotropic fiber the two coefficients of df on the right-hand side of Eq. (42) are identical. If the strain is infinitesimal $\psi_2=\psi_3\cong f$ and

$$\frac{d\Gamma}{df}=\frac{-2l_1l_2l_3\bar{\lambda}\Gamma}{\partial\mu^\alpha/\partial\Gamma}. \tag{43}$$

Thus lateral compressive forces will decrease absorption if the absorption is accompanied by radial swelling. For large strains, a correction term, essentially allowing for the increase in length accompanying radial compression, modifies the effect of the radial swelling term.

The case of lateral compression for infinitesimal strain has been discussed by Treloar,[6] who used an equation equivalent to Eq. (43).

5. Fiber in Torsion

No general equations will be given for a fiber in torsion. Only the case of infinitesimal torsion in an isotropic fiber will be discussed. Love[24] shows that a state of stress $t_{yz}=kx$, $t_{zx}=-ky$, where k is a constant, can be maintained in a fiber of circular cross section with axis parallel to the z-axis by couples about the z-axis applied to the ends of the fiber. The state of strain is given by $u=-lyz$, $v=lzx$, $w=0$, where l is a constant, and corresponds to the turning of any section through an angle proportional to the distance from the fixed end of the fiber, i.e., z. The volume of the fiber is not changed. Since the strain is not homogeneous, the fiber must be considered broken down into small regions in which the strain is homogeneous.

Consider a thin annular section of the fiber and a small cuboidal portion of this section which in the undeformed state has the thickness of the annulus and sides a, parallel to the z-axis, and b, perpendicular to the plane through the z-axis and a radius through the cuboid as shown in Fig. 2. This cuboid is changed by the strain so that the angle between a and b is no longer a right angle. The amount of change of this angle is proportional to the distance of the annulus from the center of the fiber. The strain undergone by the cuboid is a pure shear. Thus, to a first approximation, a fiber in torsion can be considered to be made up of a series of annular layers undergoing pure shear. Since the volume of the cuboid does not change during the pure shear, it is evident that the effects of expansion and contraction resulting from the forces causing the shear are exactly compensated. The effects of pure shear, and hence torsion, on the amount absorbed will be zero to a first approximation.

Treloar[8] has discussed pure shear for amorphous cross-linked rubbers and has shown that infinitesimal strains representable as pure shears do not affect the amount absorbed.

ACKNOWLEDGMENTS

This work was undertaken as part of the Dyeing Research Project of Textile Research Institute. The author appreciates the guidance of the Project's Advisory Committee representing the textile and chemical manufacturing firms who sponsored this work.

[24] See reference 9, Sec. 86d.

Structure and Internal Motion of C_2F_6 and Si_2Cl_6 Vapors

D. A. SWICK AND I. L. KARLE
U. S. Naval Research Laboratory, Washington, D. C.
(Received August 5, 1954)

The molecular structure and internal motion of C_2F_6 vapor and of Si_2Cl_6 vapor have been investigated by means of the sector-microphotometer method of electron diffraction. Both molecules exhibit hindered internal rotation, with equilibrium in the *trans* position. The interdependence of the potential barrier and the modes of vibration other than the torsional is presented graphically. The values for the bonded distances are: C−F=1.32±0.01 A, C−C=1.56±0.03 A with ∠CCF=109½°±1½° and Si−Cl=2.01±0.01 A, Si−Si=2.24±0.06 A with ∠SiSiCl=109½°±1°.

HEXAFLUOROETHANE and hexachlorodisilane are members of a series of ethane-type molecules which is being studied in this laboratory. The results for $C_2H_4Cl_2$[1] and C_2Cl_6[2] have been previously reported. Of particular interest in these molecules is the potential barrier V_0 which hinders the torsional oscillation about the $X-X$ bond. To obtain the potential barrier from spectroscopic data, one would need to know the fundamental frequency of this mode of vibration. However, the torsional mode for X_2Y_6 molecules is inactive in both the Raman and infrared spectra.

Although it may be possible to obtain the fundamental frequency of the torsional mode from combination bands, only the fundamental frequencies for the other eleven modes have been assigned for C_2F_6.[3,4] From a combination of calorimetric data and the known fundamental frequencies, Pace and Aston[5] have evaluated the potential barrier in C_2F_6. They found V_0 to be 4350 cal/mole. Recently this value has been revised to 3920 cal/mole.[6]

Hexachlorodisilane has been previously reported to exhibit free or almost free rotation about the Si−Si bond. Stitt and Yost[7] found some evidence of internal rotation in the Raman spectrum. Brockway and Beach[8] concluded from visual electron diffraction data that there was some freedom of rotation with equilibrium in the *trans* configuration. Yamazaki, Kotera, Tatematsu, and Iwasaki,[9] using more extensive visual electron diffraction data, concluded that the rotation was almost free. Katayama, Simanouti, Morino, and Mizushima,[10] on the basis of their investigation of the Raman spectrum, assigned this molecule to D_{3h} symmetry (free rotation).

In the electron diffraction method, the radial distribution curve represents the sum of the probability distributions of the distances between pairs of atoms in a molecule. From a knowledge of the distributions for the distances which change with internal rotation, it is possible to obtain information concerning the potential barrier hindering rotation. Theoretical functions which facilitate the analysis of electron scattering data from molecules which undergo internal rotation have been developed.[11,12] If a molecule of the X_2Y_6 type is undergoing restricted rotation in addition to the other modes of vibration, the probability distribution for the *trans* distance is approximated quite well by the function[13]

$$\exp[-H(r_0-r-c_2/8r_0b^2)^2], \tag{1}$$

[see Eq. (27) of reference 12] and the probability distribution for the *gauche* distance is approximated quite well by the function[13]

$$\exp[-\{H/(1+3c_2^2H/16r_0^2b^2)\}(r_0-r)^2], \tag{2}$$

[see Eq. (38) ($\phi=120°$) of reference 12] where r_0 is the equilibrium distance, $c_2=(l_2^2-l_1^2)/2$ where l_2 is the *trans* (maximum) distance and l_1 is the *cis* (minimum) distance in the course of a complete rotation; H is related to the average amplitude of vibration,[14,15] and b^2 is related to the potential barrier.[12] A cosine-like potential with three identical minima may be defined,[16]

$$V=\tfrac{1}{2}V_0(1-\cos 3\phi), \tag{3}$$

where V_0 is the barrier height and ϕ the angle of rotation. For this potential function,

$$b^2=(9/4)V_0/kT, \tag{4}$$

when the oscillations are small (k is the Boltzmann constant and T is the absolute temperature). When approximate values of H and b^2 are obtained from

[1] J. Ainsworth and J. Karle, J. Chem. Phys. **20**, 425 (1952).
[2] Swick, Karle, and Karle, J. Chem. Phys. **22**, 1242 (1954).
[3] D. H. Rank and E. L. Pace, J. Chem. Phys. **15**, 39 (1947).
[4] Nielsen, Richards, and McMurry, J. Chem. Phys. **16**, 67 (1948).
[5] E. L. Pace and J. G. Aston, J. Am. Chem. Soc. **70**, 566 (1948).
[6] D. E. Mann and E. K. Plyler, J. Chem. Phys. **21**, 1116 (1953).
[7] F. Stitt and D. M. Yost, J. Chem. Phys. **5**, 90 (1937).
[8] L. O. Brockway and J. Y. Beach, J. Am. Chem. Soc. **60**, 1836 (1938).
[9] Yamazaki, Kotera, Tatematsu, and Iwasaki, J. Chem. Soc. Japan **69**, 104 (1948).
[10] Katayama, Simanouti, Morino, and Mizushima, J. Chem. Phys. **18**, 506 (1950).
[11] J. Karle and H. Hauptman, J. Chem. Phys. **18**, 875 (1950).
[12] J. Karle, J. Chem. Phys. **22**, 1246 (1954).
[13] The range of validity of this approximation in the present application is discussed later.
[14] I. L. Karle and J. Karle, J. Chem. Phys. **17**, 1052 (1949).
[15] J. Karle and I. L. Karle, J. Chem. Phys. **18**, 957 (1950).
[16] A cosine-like potential was assumed to conform with usual practice [see G. Herzberg, *Infrared and Raman Spectra of Polyatomic Molecules* (D. Van Nostrand Company, Inc., New York, 1945), pp. 226, 519].

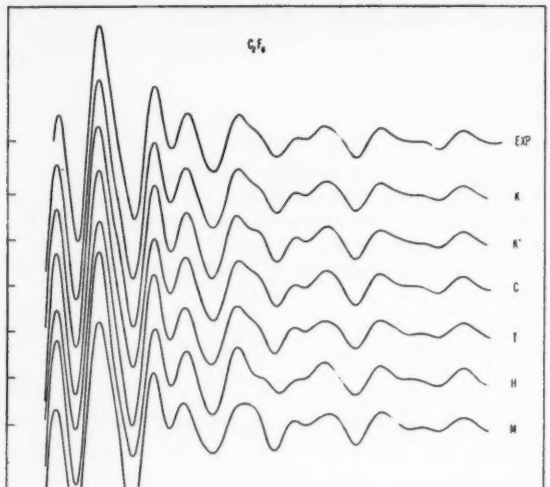

FIG. 1. Experimental and theoretical intensity curves for C_2F_6.

(1) and (2) their validity can be checked by numerically integrating the integral describing the probability distribution [e.g., Eq. (11) of reference 12].

C_2F_6

The sample of C_2F_6 was obtained from the Jackson Laboratory (E. I. DuPont de Nemours and Company) and was used without further purification. Multiple electron diffraction exposures of 0.1 second were taken at room temperature with an electron wavelength $\sim$0.06 A and a camera length $\sim$11 cm. The sector-microphotometer techniques and methods of analysis previously described were used.[14,15,17]

The experimental molecular intensity curve $I(s)$ is illustrated at the top of Fig. 1. The radial distribution curve, computed from the experimental intensity curve $I(s)$ with $a=0.0022$, is shown in Fig. 2. The radial distribution curve was readily decomposed into six Gaussian peaks[18] with the proper areas which are

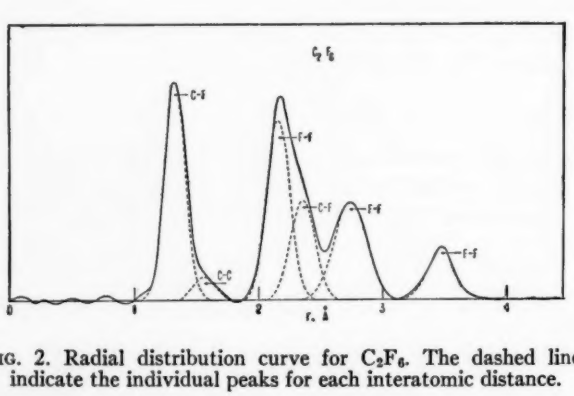

FIG. 2. Radial distribution curve for C_2F_6. The dashed lines indicate the individual peaks for each interatomic distance.

[17] I. L. Karle and J. Karle, J. Chem. Phys. **18**, 963 (1950).

[18] Note that the approximate functions (1) and (2) are Gaussian also.

consistent with the *trans* configuration except that the largest $F-F$ distance was somewhat smaller ($\sim$0.01 $-$0.015 A) than would be required for a molecule with no torsional oscillation. This condition is consistent with Eq. (1); however, the magnitude of the shift is so small that a reliable evaluation of b^2 cannot be made. The width of the *gauche* $F-F$ peak is considerably greater than that of the other peaks. This greater width also indicates torsional oscillation in the molecule. An evaluation of b^2 from this peak will be made later in the paper.

A computed intensity curve using the values for the interatomic distances and average amplitudes of vibration which were derived from the radial distribution curve is illustrated in Fig. 1, model K. It reproduces the features of the experimental curve satisfactorily. The average s/s_0 value for fourteen features is 1.000 with an average deviation of 0.002. Model K' has the same parameters as model K except that the width of the *gauche* peak in the radial distribution curve was assumed to be the same order of magnitude as that for the *trans* peak. This curve is unsatisfactory in that the peak at $s=12$ is too large and that the shapes of the peaks at $s=15$ and 20 do not reproduce the experimental curve. All the distance and amplitude parameters were varied and intensity curves were computed and compared to the experimental curve in order to establish the limits of error. The parameter chart (Fig. 3) illustrates which models were used to compute intensity curves. Curves for models in the diagonal directions B to Q, A to T, and D to S differed very little from each other. On the other hand, curves along the horizontal direction, H to M, for example, differed greatly from each other. The various lines denote when particular features of the intensity curves no longer reproduced those of the experimental curve. Models E, F, J, K, and O are satisfactory whereas models G, L, N, P, and R are borderline. Curves for several of the models which illustrate various unacceptable features are reproduced in Fig. 1.[19] The shapes of some of the unsatisfactory features in the unacceptable curves can be improved by varying the amplitudes of vibration only, however, at the expense of making other features of the curves less acceptable.

The equilibrium distances, the average displacements from equilibrium, and the limits of uncertainty are listed in Table I.[20,21] The C$-$F distance is the same or

[19] The minimum at $s=8$ is too deep in curve T (—·—· line on parameter chart), the maximum at $s=10$ is too low in curve C (···· line on parameter chart), the maximum at $s=12$ is displaced and too low in curve M (—— line on parameter chart), the maximum at $s=15$ is too narrow in curve H and too wide in curve M (– – – – lines on parameter chart) and the two maxima near $s=20$ are not properly shaped in curves H, M, and T (——— line on parameter chart).

[20] The results of two previous investigations of C_2F_6 by the visual method in electron diffraction are listed in Tables of Interatomic Distances [P. W. Allen and L. E. Sutton, Acta Cryst.

nearly the same as that found for CH_2CF_2(1.32),[17] CF_2CF_2(1.31),[17] CF_4(1.32),[22] CF_3X(1.33)[23] and other similar molecules. The C−C distance is nearly the same (within limits of uncertainty) as that found in C_2H_6(1.53),[24] (1.543),[25] and C_2Cl_6(1.57)[2]. The CCF angle is tetrahedral; the uncertainty in the value of this angle is, however, dependent upon the uncertainty in the C−C bond, the angle becoming larger as the C−C value decreases (see Fig. 3). The average amplitudes of vibrations are compared with those computed by Morino *et al.*[26]

The width of the peak in the radial distribution curve for the *gauche* F−F distance is considerably greater than that of all the other peaks (Fig. 2). On applying Eq. (2) to this peak,[27] it is readily seen that unique values cannot be obtained for H and b^2, but that the value of one depends upon the other. The relationship between $\langle l^2\rangle_{Av}^{\frac{1}{2}}[\langle l^2\rangle_{Av}=(1-4aH)/2H]$ and V_0, obtained from b using Eq. (4), is shown in Fig. 4. If there were no torsional oscillation ($V_0=\infty$), then the average amplitude of vibration would be 0.114 A. On the other hand, if the only mode of vibration were the torsional mode, then the potential barrier would be 2.5 kcal/mole. If the assumption is made that the average amplitude of vibration for the *gauche* F−F (excluding the torsional mode) is the same order of magnitude as the *trans* F−F, i.e., about 0.07 A, then $V_0\sim4$ kcal/mole. This value is consistent with the value obtained by Pace and Aston[5] from their entropy calculations using calorimetric and spectroscopic data.

TABLE I. Equilibrium distances and average amplitudes of vibration for C_2F_6.[a]

	r, A	$\langle l^2\rangle_{Av}^{\frac{1}{2}}$, A (exp)	$\langle l^2\rangle_{Av}^{\frac{1}{2}}$, A (calc)[b]
C−F	1.32 ±0.01	0.050±0.007	0.045
C−C	1.56 ±0.03		
F−F	2.155±0.01	0.057±0.01	0.056
C−F	2.355±0.015	0.073±0.01	
F−F	2.74 ±0.015	see Fig. 4	
F−F	3.485±0.015	0.069±0.015	0.061
∠CCF = 109.5°±1.5°			

[a] The interdependency of the uncertainties is included in the ranges of uncertainty reported in this table. As a consequence, not all of the models permitted by this table are in satisfactory agreement with the experimental curve.
[b] See reference 26.

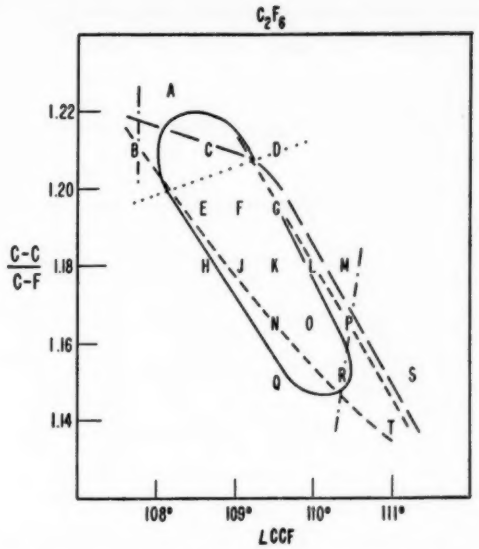

FIG. 3. Parameter chart for C_2F_6. The positions of the letters indicate the parameters of the models for which intensity curves were computed. The various types of lines indicate the borderline of the acceptable region for certain particular features.

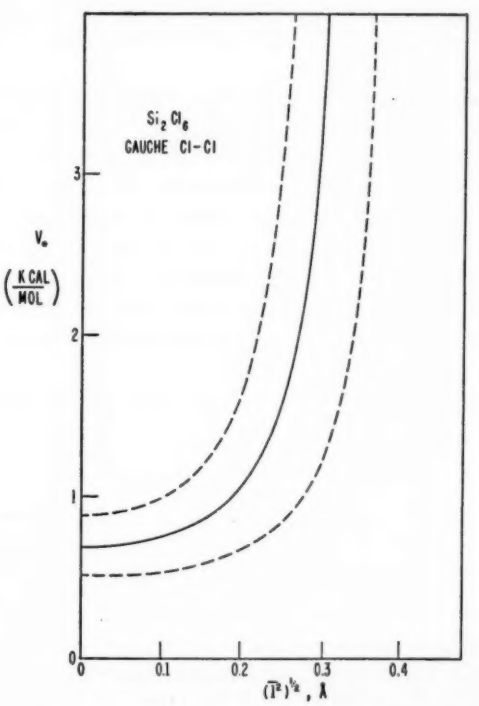

FIG. 4. Graph showing the corresponding values of the potential barrier hindering rotation and the rms projected amplitude from all modes except the torsional mode which would satisfy the experimental data for the *gauche* F−F distance in C_2F_6.

3, 46 (1950)]. The bonded distances differ from the ones obtained here.

[21] Concurrently with this investigation, C_2F_6 was being studied by the visual method at Purdue University. The parameters obtained by J. A. Brandt and R. L. Livingston are C−C = 1.51 ±0.06 A, C−F = 1.33±0.015 A, ∠FCF = 108±1½°, $V_0\sim4$ kcal/mole. [Am. Chem. Soc. Meeting, Sept. 1952; J. Am. Chem. Soc. 76, 2096 (1954).]

[22] C. W. W. Hoffman and R. L. Livingston, J. Chem. Phys. **21**, 565 (1953).

[23] J. Sheridan and W. Gordy, J. Chem. Phys. **20**, 591 (1952).

[24] K. Hedberg and V. Schomaker, J. Am. Chem. Soc. **73**, 1482 (1951).

[25] G. E. Hansen and D. M. Dennison, J. Chem. Phys. **20**, 313 (1952).

[26] Morino, Kutchitsu, Takashi, and Maeda, J. Chem. Phys. **21**, 1927 (1953).

[27] Numerical integration of the integrals describing the probability distribution for the *gauche* and *trans* positions (see reference 12) using the distance parameters and various combinations of H and b^2 obtained in this experiment results in curves which are experimentally indistinguishable from the Gaussians described by Eqs. (1) and (2).

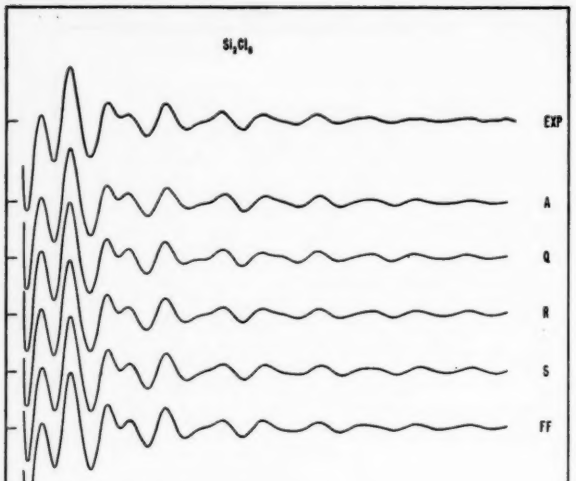

FIG. 5. Experimental and theoretical intensity curves for Si_2Cl_6.

Si_2Cl_6

The sample of Si_2Cl_6 was obtained from Anderson Laboratories, Inc., Adrian, Michigan. The experimental procedures were the same as those previously described.

The experimental molecular scattering curve for Si_2Cl_6 is shown at the top of Fig. 5. A radial distribution curve was computed from the experimental intensity curve with $a=0.0057$. This was decomposed into individual peaks for each interatomic distance, and is shown in Fig. 6.

Molecular scattering curves, computed with extensive variations in the parameters of interatomic distance and vibrational amplitude, were compared with the experimental curve to determine the best values of these parameters and their limits of uncertainty. Some of the curves are shown in Fig. 5. Curve *R* is the one which best fits the experimental data. Its average deviation from the average s/s_{exp} ratio is ± 0.005. The various combinations of the structural parameters for the models tested are shown in Fig. 7, where the various types of lines illustrate the boundaries of acceptable regions for certain particular features.[28] Some of these features are quite sensitive to changes in vibrational amplitudes, but can be improved only at the expense of other features. For each model the set of vibrational amplitudes was chosen which produced an intensity curve best agreeing with the experimental curve. The interdependence between the vibrational amplitudes and interatomic distances was included in the limits of uncertainty.

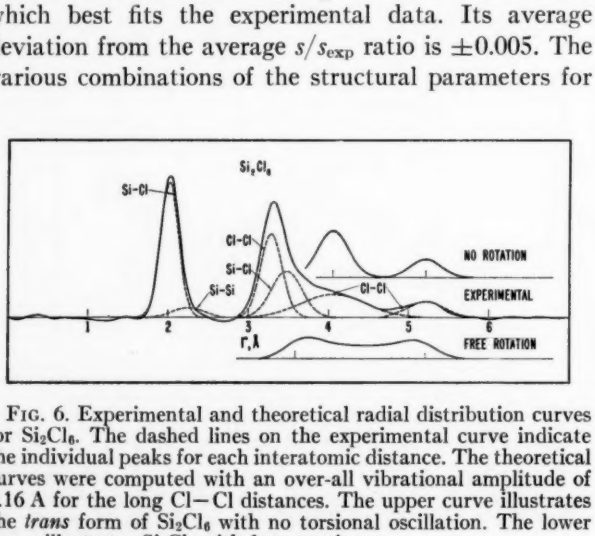

FIG. 6. Experimental and theoretical radial distribution curves for Si_2Cl_6. The dashed lines on the experimental curve indicate the individual peaks for each interatomic distance. The theoretical curves were computed with an over-all vibrational amplitude of 0.16 A for the long Cl—Cl distances. The upper curve illustrates the *trans* form of Si_2Cl_6 with no torsional oscillation. The lower curve illustrates Si_2Cl_6 with free rotation.

The resulting equilibrium interatomic distances and projected rms amplitudes of vibration are listed in Table II. The assigned limits of uncertainty of the interatomic distances determined in this investigation overlap those of the previous investigation.[8,9] Except for a scale factor, the earlier results almost coincide with each other and with model *A* of Fig. 7. The large vibrational amplitude for the unbonded Si—Cl distance should be noted. In the last column are the vibrational amplitudes computed by Morino *et al.*[26]

TABLE II. Equilibrium distances and average amplitudes of vibration for Si_2Cl_6.[a]

	r, A	$\langle l^2\rangle_{Av}^{\frac{1}{2}}$, A (exp)	$\langle l^2\rangle_{Av}^{\frac{1}{2}}$, A (calc)[b]
Si—Cl	2.01±0.01	0.040±0.015	0.044
Si—Si	2.24±0.06		
Cl—Cl	3.28±0.01	0.065±0.020	0.094
Si—Cl	3.47±0.04	0.16±0.03	
Cl—Cl	4.05±0.04	see Fig. 8	
Cl—Cl	5.21±0.03	0.19±0.05	0.119
∠SiSiCl = 109.5°±1.0°			

[a] The interdependency of the uncertainties is included in the ranges of uncertainty reported in this table. As a consequence, not all of the models permitted by this table are in satisfactory agreement with the experimental curve.
[b] See reference 26.

There is disagreement between the amplitudes of vibration for two Cl—Cl distances as obtained from electron diffraction experiment and spectroscopic calculations. At first glance, it may appear that this is due to undetermined errors, arising in the electron diffraction experiment, due to the fact that these Cl—Cl distances appear as part of an initially unresolved peak in the radial distribution curve. Any uncertainty in resolving a complex peak, however, is reflected in the final values of results given in Table II, and is arrived at by the standard method of comparing

[28] The — — — line of Fig. 7 concerns the depth of the minimum at $s=5.3$, relative to the maximum at $s=6.4$. This feature is borderline in *A* and in *S*, and is excessive in *FF*. The shape of the region $10<s<14$ is represented by the – – – – line. On models *A* and *Q*, this minimum is too shallow, relative to adjacent maxima. The shape of the small shelf at $s=12$ is also unsatisfactory in *Q* and in *S*. The solid line of Fig. 7 concerns the shape of the region at $s\sim 18$, which is unsatisfactory in *Q*, *S*, and *FF*. Some features other than those illustrated in Fig. 7 were also used as criteria in rejecting intensity curves, e.g., the maximum at $s=7.7$ is too high in curve *Q*, and the maximum at $s\sim 23$ is unsatisfactory in curves *S* and *FF*. The minimum at $s=8.8$, represented by the — – — – line of Fig. 7, is too deep in model *FF*.

computed and experimental intensity curves.[14,15,17] There have been several previously determined structures in which discrepancies occur between the electron diffraction amplitudes and spectroscopic theory.[1,2,17,29] When there is such a discrepancy, theoretical intensity curves of electron scattering cannot be made to agree with the experimental electron scattering curve when the spectroscopic amplitudes are used. Consequently the discrepancies are real and cannot be ascribed to unrealistic evaluations of the experimental error.

The lack of agreement occurring in many instances is a dilemma. There may be some electron scattering effect which is being overlooked. On the other hand, excellent agreement exists for amplitudes found by electron diffraction experiment and spectroscopic theory for diatomic molecules and carbon dioxide. These are cases in which the fundamental frequency assignments and force models are not open to question. Perhaps the latter are a source of difficulty. Further work will be required to resolve this problem.

The experimental intensity curve for Si_2Cl_6 indicates the existence of considerable intramolecular motion. It does not, however, distinguish between torsional oscillation and other modes of vibration. The major effect of vibration in any mode, including torsion, is to dampen the contribution to the intensity curve of those distances which are changing. As a consequence of internal motion, there is no contribution to the scattering curve for Si_2Cl_6 from the 1, 2 Cl distances beyond $s \sim 10$.

In addition to the experimental radial distribution curve, Fig. 6 shows two theoretical radial distribution curves computed with an over-all vibrational amplitude of 0.16 A for the long Cl—Cl distances. The upper curves illustrates the *trans* form of Si_2Cl_6 with no torsional oscillation and the lower curve illustrates Si_2Cl_6 with free rotation. Comparison of the experimental curve with these computed curves clearly indicates the existence of restricted rotation.

The shift of the *trans* peak, predicted by Eq. (1),[27] is less than the experimental uncertainty of the radial distribution curve, and consequently yields no information about b. By fitting the *gauche* peak with Eq. (2),[27] the relationship between b^2 and the average amplitude of vibration $[\langle l^2\rangle_{Av} = (1-4aH)/2H]$ is obtained. If Eqs. (3) and (4) are assumed, the curve shown in Fig. 8 results. (The dashed lines indicate the limits of uncertainty.)

The probability integral [Eq. (11) of reference 12] was derived on the assumption of small torsional oscillations. Its application to the region of Fig. 8 which relates to a low barrier, i.e., small amplitudes of vibration in the other modes, is not *a priori* valid. To test the validity of the approximations in this region, a comparison was made between a radial distribution

[29] The electron diffraction experiment on C_2F_4 has been repeated in this laboratory and essentially the same results were obtained as in reference 17.

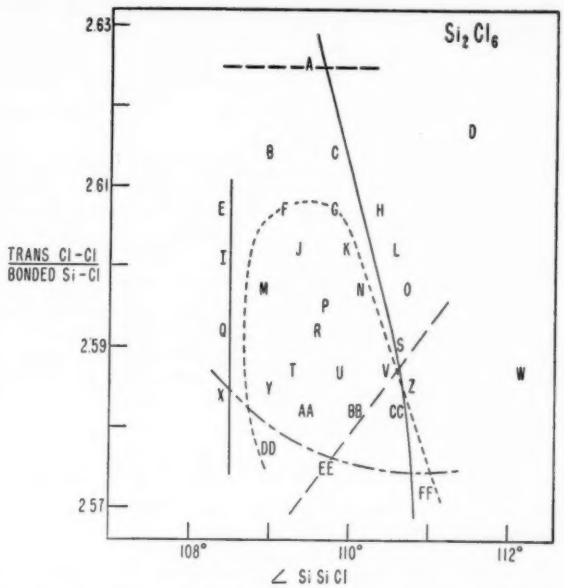

FIG. 7. Parameter chart for Si_2Cl_6. The positions of the letters indicate the parameters of the models for which intensity curves were computed. The various types of lines indicate the borderline of the acceptable region for certain particular features.

curve computed using an exact cosine-like potential function and one computed using the quadratic approximation, with a barrier height of 500 cal/mole. To obtain these curves, molecular scattering curves were first computed by averaging the intensity curves for molecules in all configurations at 10° intervals around the circle of rotation. The averages were weighted

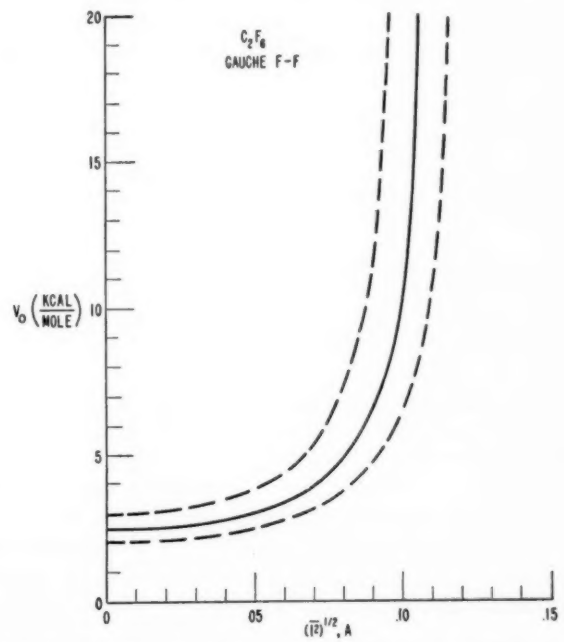

FIG. 8. Graph showing the corresponding values of the potential barrier hindering rotation and the rms projected amplitude from all modes except the torsional mode which would satisfy the experimental data for the *gauche* Cl—Cl distance in Si_2Cl_6.

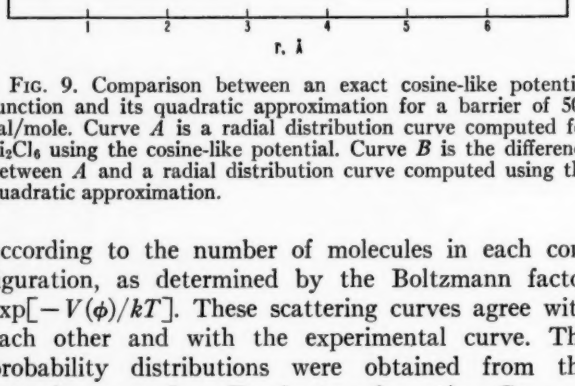

FIG. 9. Comparison between an exact cosine-like potential function and its quadratic approximation for a barrier of 500 cal/mole. Curve *A* is a radial distribution curve computed for Si_2Cl_6 using the cosine-like potential. Curve *B* is the difference between *A* and a radial distribution curve computed using the quadratic approximation.

according to the number of molecules in each configuration, as determined by the Boltzmann factor $\exp[-V(\phi)/kT]$. These scattering curves agree with each other and with the experimental curve. The probability distributions were obtained from the intensity curves by a Fourier transformation. Curve *A* of Fig. 9 is the radial distribution curve computed using the cosine-like potential; curve *B* is the difference between *A* and the radial distribution curve computed using the quadratic potential. Since this difference is less than the uncertainty in the experimental radial distribution, the validity of the probability integral has been demonstrated for Si_2Cl_6 for a barrier as low as 500 cal/mole.

The experimental evidence shows conclusively that the internal rotation in Si_2Cl_6 is not free. If torsional oscillation were the only mode, the barrier would be 700 ± 200 cal/mole. In view of the large vibrational amplitudes found for the unbonded Si—Cl and for the *trans* Cl—Cl, it is unlikely that the barrier is this low. On the other hand, the experimental results can be accounted for by over-all vibration alone ($V_0=\infty$), but only with a vibrational amplitude for the *gauche* Cl—Cl distance of 0.35 ± 0.05 A. If the *gauche* amplitude were about the same as the *trans*, the potential barrier would be approximately 1 kcal/mole.

This result is consistent with that found for disilane in a recent investigation of its infrared spectrum by Gutowsky and Stejskal,[30] who report that internal rotation in Si_2H_6 is not free. Their observation of the relative instability of the Si—Si bond in Si_2Cl_6 is not surprising in view of the large vibrational amplitudes between atoms at opposite ends of the molecule found in this investigation.

ACKNOWLEDGMENTS

We wish to thank R. C. McHarness of the Jackson Laboratory for supplying samples of C_2F_6, P. O'Hara of the National Bureau of Standards for the IBM computations of the radial distribution and intensity functions, and J. Karle for helpful discussions.

[30] H. S. Gutowsky and E. O. Stejskal, J. Chem. Phys. **22**, 939 (1954).

Rates of Isotopic Reactions between Methyl and Hydrogen*

J. C. POLANYI†
Division of Pure Chemistry, National Research Council, Ottawa, Canada
(Received August 10, 1954)

The absolute rate calculations made by Eyring and collaborators on the series of eight isotopic reactions H+H$_2$, etc., fail to provide a real test of their method. Recent data on the eight reactions CH$_3$+H$_2$, +HD, +DH, +D$_2$; CD$_3$+H$_2$, +HD, +DH, +D$_2$, provide the first set of independent observations on a series of simple isotopic exchange reactions. Detailed calculation of the entropies of activation give values for the temperature independent factors $A_{\text{calc}}^{400°\text{K}}$. The energy surface for the reactions is calculated according to the method of Gorin, Kauzmann, Walter, and Eyring in conformity with the H.L.S.P. treatment of methane. The surface obtained, $E=f(\omega,r,s)$, has a single barrier indicating a classical activation energy of ~13 kcal for the forward reaction, in adequate agreement with observed values. The surface described is, therefore, the "best semiempirical surface"; the height of the barrier being regarded as a calibrated, not a predicted, quantity. The surface is accordingly made the basis for a calculation of the total zero-point energies of the eight reactions in their initial states and transition states. Substantial differences in activation energy are predicted. However, rate constants calculated on this basis show no correlation with observation, indicating failure of the method. Using a differently calibrated surface, designed to give the lowest barrier height compatible with a surface free of energy basins, a "symmetrical" surface is obtained for the present series of reactions. Zero-point energies derived from this surface lead to relative rate constants in fair agreement with the eight observed values. This correlation is more properly described as a correlation between A_{calc} and k_{obs}, and is discussed on this basis.

RATES OF ISOTOPIC REACTIONS BETWEEN METHYL AND HYDROGEN

THE "semi-empirical method" has not proved very effective in predicting activation energies; uncertainty in the choice of the constant Coulombic fraction to be used introduces an excessive uncertainty into the value of E obtained. Suppose, however, that a potential energy surface is "calibrated" for a particular reaction by choosing a percentage of Coulombic energy that will give nearly the correct activation energy. The question which arises is: Does the surface obtained in this way correctly represent the energy of intermediate configurations? Hirschfelder, Eyring, and Topley[1] attempted to put this to the test by calculating from the shape of the surface in the region of the transition state the zero point energies for the transition state complex and hence the *changes* in activation energy within the series of 8 isotopic reactions: H+H$_2$ (k_1), H+*H*D (k_2), H+*D*H (k_3), H+D$_2$ (k_4), D+H$_2$ (k_5), D+*H*D (k_6), D+*D*H (k_7), D+D$_2$ (k_8). (Note that in reactions 2, 3, 6, and 7, the italicized atom is the one under attack.) They combined their calculated activation energies with temperature independent factors obtained from absolute theory and compared their rate constants with eight values of Farkas and Farkas.[2]

Unfortunately only two of the values of Farkas and Farkas (reactions 1 and 8) are independent observations. Of the remaining six reactions, two did not occur in their experiments and four took place simultaneously when H$_2$ and D$_2$ were mixed in their reaction vessel (reactions 4, 5, 7, 8). From the rate of formation of HD, making plausible assumptions, it is possible to obtain k_4/k_5 and k_7/k_2. Individual rate constants can be obtained only for reactions 1 and 8. Rough values for the remaining constants were calculated by Farkas and Farkas by applying collision theory in conjunction with an approximate calculation of the changes in zero point energy of the transition state complexes. This necessarily affects six of the eight rate constants listed by Hirschfelder, Eyring, and Topley for comparison with their own calculated values. Therefore it is not possible, at the present time, to make an estimate of the accuracy of the calculated values of Eyring *et al.*

Recently, through the work of Majury and Steacie[3] and Whittle and Steacie,[4] rate constants have been measured for the following eight reactions:

1. $CH_3+H_2 \xrightarrow{k_1} CH_4+H$
2. $CH_3+HD \xrightarrow{k_2} CH_4+D$
3. $CH_3+DH \xrightarrow{k_3} CH_3D+H$
4. $CH_3+D_2 \xrightarrow{k_4} CH_3D+D$
5. $CD_3+H_2 \xrightarrow{k_5} CD_3H+H$
6. $CD_3+HD \xrightarrow{k_6} CD_3H+D$
7. $CD_3+DH \xrightarrow{k_7} CD_4+H$
8. $CD_3+D_2 \xrightarrow{k_8} CD_4+D.$

Each of these eight rate constants constitutes an independent observation (reactions 2 and 3 occur simultaneously, as do 6 and 7, but the products are different for each reaction).

Within the H+H$_2$ series of reactions, the trend of transition-state zero-point energies is found to closely match the trend in initial-state zero-point energies, with the result that predicted changes in activation

* Contribution N.R.C. 3663 from the National Research Council, Ottawa, Canada.
† National Research Laboratories Postdoctorate Research Fellow. Present address: Department of Chemistry, Princeton University, Princeton, New Jersey.
[1] Hirschfelder, Eyring, and Topley, J. Chem. Phys. **4**, 170 (1936).
[2] A. Farkas and L. Farkas, Proc. Roy. Soc. (London) **A152**, 124 (1935); see also Van Meersche, Bull. soc. chim. Belges **60**, 99 (1951).
[3] T. G. Majury and E. W. R. Steacie, Discussions Faraday Soc. **14**, 45 (1953).
[4] E. Whittle and E. W. R. Steacie, J. Chem. Phys. **21**, 993 (1953).

TABLE I. Transition-state standard entropies (eu) at 400°K.

	S_T^*	S_R^*	S_V^*	$S^*_{T,R,V,E}$	$-\Delta S_p^*$	$A^{4000°K}_{\times 10^{-12}}$
1. CH_3-H-H	35.9	15.9	1.94	55.1	26.4	3.28
2. CH_3-H-D	36.1	16.9	2.06	56.5	28.3	1.25
3. CH_3-D-H	36.1	16.2	2.73	56.4	28.4	1.19
4. CH_3-D-D	36.2	17.1	3.01	57.7	27.3	2.09
5. CD_3-H-H	36.4	17.0	1.94	56.7	27.4	1.99
6. CD_3-H-D	36.5	17.9	2.06	57.9	29.5	0.69
7. CD_3-D-H	36.5	17.3	2.73	57.9	29.5	0.69
8. CD_3-D-D	36.7	18.0	3.01	59.1	28.5	1.14

energy are very small. This should no longer be the case for the present series since the transition-state complexes include the comparatively heavy group CH_3 not present in the initial molecule.

For the rate constant of a bimolecular reaction,[5] the absolute theory of reaction rates gives

$$k_r=\kappa\cdot\tau\cdot\left(\frac{kT}{h}\right)\cdot\exp(\Delta S_c^*/R)\cdot\exp(-E_0/RT), \quad (1)$$

where E_0 is the difference in heat content between the transition-state complex and the initial state (if the experimental activation energy, E, is used in place of E_0, then the whole expression must be multiplied by e^2); ΔS_c^* is the difference in entropy between the transition-state complex and the initial state in a standard state of unit concentration; τ is a factor which allows for quantum-mechanical tunneling through the energy barrier; κ is the "transmission coefficient" or fraction of transition-state complexes which reach the final state; k and h are the Boltzmann and Planck constants, kT/h having the dimensions of frequency.

The various unknowns in this equation, as it applies to the isotopic series CH_3+H_2 etc. will be considered in turn.

ENTROPY TERMS

Molar entropies for reactants and transition-state complexes have been calculated in detail in order to obtain values for the entropies of activation, ΔS_c^*. Methods for calculating entropies of translation, rigid rotation, and simple-harmonic vibration are to be found in the textbooks of statistical thermodynamics, and are collected in a review by E. B. Wilson.[6] Entropies for the hydrogen isotopes are listed in a monograph of the National Bureau of Standards.[7]

A planar configuration (symmetry number $\sigma=6$) has been assumed for the methyl and deuterated-methyl radicals (*cf.* A. D. Walsh[8]) though spectroscopic evidence is lacking. A term $R\ln 2$ allows for the electron degeneracy of the radical resulting from the presence of an unpaired electron: the electronic state is $^2A_1$ according to Mulliken.[9] All entropies are "virtual," i.e., nuclear spin contributions are omitted, since they do not change during the reaction. The entropy value obtained for CH_3 agrees with that calculated by Bywater and Roberts[10] and by Trotman-Dickenson.[11]

The transition-state complex is treated as a symmetric top; two of its three moments of inertia are therefore identical. The symmetry number for all the transition-state complexes is 3. The electronic entropy term remains equal to $R\ln 2$ since the complex has presumably still an unpaired electron. However, a new term enters into the expression for total entropy: since there is now a soft bending frequency, entropy of vibration constitutes an appreciable contribution. Stretching vibrations in the initial state and in the transition-state complex are too hard to have appreciable entropy. Standard vibrational entropies (S_V^0), as a function of frequency and temperature, are conveniently listed in the tables of Miller, West, and Bernstein.[12] Entropy contributions to the various transition state complexes are listed in Table I. Table I also lists entropies of activation for the eight reactions referred to unit pressure ($-\Delta S_p^*$); these values are obtained from the standard entropies listed in Tables I and II. In Eq. (1) ΔS_c^* is the same entropy difference referred to unit concentration of 1 mole/cc (ΔS_c^* at 400°K $=\Delta S_p^*+20.6$ eu). From these figures the "temperature-independent factors" at 400°K are calculated [Eq. (1)].

THE POTENTIAL-ENERGY SURFACE FOR CH_5

The same potential-energy surface should be applicable to all eight reactions since the integrals which define the surface are not sensitive to nuclear mass. The surface was the subject of calculation by Gorin, Kauzmann, Walter, and Eyring[13] in connection with their study of the reaction

$$H+CH_4\xrightarrow{k_9}H_2+CH_3$$

which is the reverse of the reaction we wish to study. These workers incorporated into their semiempirical treatment of the three-electron system, H_3C-H-H,

TABLE II. Initial-state standard entropies (eu) at 400°K.

	S_T^0	S_R^0	S_E^0	$S^0_{T,R,E}$
H_2	29.5	3.6	...	33.1
HD	30.8	5.6	...	36.4
D_2	31.6	5.0	...	36.6
CH_3	35.5	11.5	1.4	48.4
CD_3	36.1	13.5	1.4	51.0

[5] Glasstone, Laidler, and Eyring, *The Theory of Rate Processes* (McGraw-Hill Book Company, Inc., 1941).
[6] E. B. Wilson, Chem. Revs. **27**, 17 (1940).
[7] J. Research Natl. Bur. Standards **41**, 379 (1948).
[8] A. D. Walsh, Discussions Faraday Soc. **2**, 18 (1947).
[9] R. S. Mulliken, J. Chem. Phys. **3**, 520 (1935).
[10] S. Bywater and R. Roberts, Can. J. Chem. **30**, 773 (1952).
[11] A. F. Trotman-Dickenson, J. Chem. Phys. **21**, 211 (1953).
[12] Miller, West, and Bernstein, N.R.C. Bull. No. 1 (1951).
[13] Gorin, Kauzmann, Walter, and Eyring, J. Chem. Phys. **7**, 633 (1939).

the Heitler-London-Slater-Pauling treatment of methane due to Van Vleck[14] and Voge.[15] They also solved the nine-electron problem in order to determine whether the potential surface would be appreciably altered by the additional resonance, and obtained a 1- to 2-kcal lowering in the energy of the transition state; this demonstrates the adequacy of the three-electron approximation.

Gorin, Kauzmann, Walter, and Eyring obtained a potential energy surface with a barrier 9.5 kcal high, at an extended H−H distance (this figure is relative to the energy of CH_4+H as zero). This is in satisfactory agreement with experimental values for the activation energy of reaction 9. They did not explore the C−H coordinate in detail but considered that a low barrier probably existed corresponding to the activation energy for reaction 1.

In their calculation Gorin *et al.* use a value for the bond-dissociation energy of C−H in methane which is 8.5 kcal less than the best present-day values. The principal cross sections of their surface have been recalculated for the present work using the higher value for $D(CH_3-H)$. The C−H coordinate has been explored in detail.

The integrals required for the calculation are defined by Gorin *et al.* in terms of four fundamental integrals of methane described by Van Vleck and evaluated by Voge. Numerical values for the CH_5 integrals are listed in Table III, as a function of ω, the angle that the CH_3 umbrella makes with the figure axis of the complex (90° for planar CH_3, 109.5 for tetrahedral configuration). Considered as a three-electron problem, the energy of the complex H_3C-H-H is then expressible as

$$E=Q+(\tfrac{1}{2}\{(\theta-\mu)^2+(\theta-\nu)^2+(\mu-\nu)^2\})^{\frac{1}{2}} +J_{ii}-\tfrac{1}{2}\sum_{ij}J_{ij} \quad (2)$$

where J_{ii} are exchange terms between bonded centers (α) and J_{ij} those between nonbonded centers ($\beta,\eta,\gamma,\epsilon,\phi,\sigma,\delta,\psi$). The integrals, η, λ, γ are H−H integrals and have been calculated from the Morse equation[16] assuming 10 percent Coulombic bonding in conformity with Voge's treatment of methane. By the Morse equation,

$$V(r)=D_e[e^{-2a(r-r_e)}-2e^{-a(r-r_e)}]; \qquad a=1.2\cdot 10^7\omega_e(\mu_A/D_e)^{\frac{1}{2}}, \quad (3)$$

where D_e is the sum of the bond-dissociation energy and the zero-point energy, r_e is the equilibrium separation, ω_e is the fundamental frequency, and μ_A is the reduced mass in atomic weight units. For H_2, $\omega_e=4395$ cm^{-1}, $a=1.94$, $r_e=0.74$ A, and $D_e=109$ kcals/mole.

In addition to being a function of ω, the integrals θ, ν, ϵ, ϕ, are dependent on the C−H separation along the figure axis. They have been assumed to vary in the same way as the C−H binding energy given by the Morse curve with $\omega_e=3030$ cm^{-1}, $a=1.86$, $r_e=1.09$ A, and $D_e=105$ kcal/mole.

TABLE III. Exchange integrals (kcal for C−H=1.12A) as a function of ω.

ω	θ,ν	ϵ,ϕ	α	β	σ	δ	ψ	γ[a]	ΔQ_e[b]
90°	53.0	6.2	87.2	1.2	13.8	18.9	25.6	18.2	7.4
95°	62.7	3.2	87.4	1.4	13.3	18.9	24.7	18.4	6.2
100°	71.5	0	87.6	1.9	11.8	19.1	23.8	19.2	4.4
105°	79.3	−3.2	86.7	3.1	9.2	19.8	22.4	20.5	2.3
109.5°	84.9	−4.4	84.9	4.4	4.4	20.8	20.8	22.0	0

[a] Calculated from Morse function on the assumption of 10 percent Coulombic contribution.
[b] These values for ΔQ_e were taken from the paper by Gorin *et al.* ΔQ_e is the difference in Coulombic energy between the carbon atom with valence angle ω and tetrahedral carbon.

With these assumptions it is possible to obtain the four-dimensional potential-energy function

$$E=f(\omega,r,s), \quad (4)$$

where r is the C−H separation, s the H−H separation along the figure axis of H_3C-H-H, and ω the angle between the CH_3 umbrella and the axis. By minimizing E with respect to ω for every new configuration, r, s, the function can be plotted in three dimensions. The surface obtained has a minimal trough corresponding to the "reaction coordinate." The energy along this coordinate can be represented in two dimensions (Fig. 1), since, except in the region $r\simeq s$, it runs fairly parallel to either the r- or the s-axis.

In agreement with Gorin, Kauzmann, Walter, and Eyring, the surface is seen to have an 8-kcal basin along the C−H axis and a barrier along the H−H axis. The height of this barrier is 8.1 kcal above CH_4+H, in substantial agreement with the 9.5-kcal value of Gorin *et al.* The lowest point of the saddle (the transition-state configuration) is at $r=1.20$ A, $s=1.40$ A, and $\omega=109.5$. This is almost identical with the configuration given by Gorin *et al.*

However, it is evident that there is no barrier along the C−H axis. The barrier that is identified with the activation energy for reaction 9 is, therefore, also the energy barrier for reaction 1. On Gorin *et al.*'s surface this would have implied a classical activation energy (i.e., exclusive of zero-point energy) $E_e=1.9$ kcal; on the present surface it leads to $E_e=13.4$ kcal/mole. This figure when reduced by 1–2 kcal to allow for additional resonance in the nine-electron solution agrees well enough with the mean experimental activation energy for the eight reactions CH_3+H_2 etc. ($\bar{E}=11$ kcal/mole).

Other estimates of the activation energies of reactions within this series have been made as follows. Rebbert and Steacie[17] recently obtained $E=12.7\pm0.5$ kcal/mole for the reaction CH_3+D_2 using mercury dimethyl in place of acetone as a source

[14] J. H. Van Vleck, J. Chem. Phys. **1**, 183 (1933).
[15] H. H. Voge, J. Chem. Phys. **4**, 581 (1936).
[16] P. M. Morse, Phys. Rev. **34**, 57 (1929).
[17] R. E. Rebbert and E. W. R. Steacie, Can. J. Chem. **32**, 113 (1954).

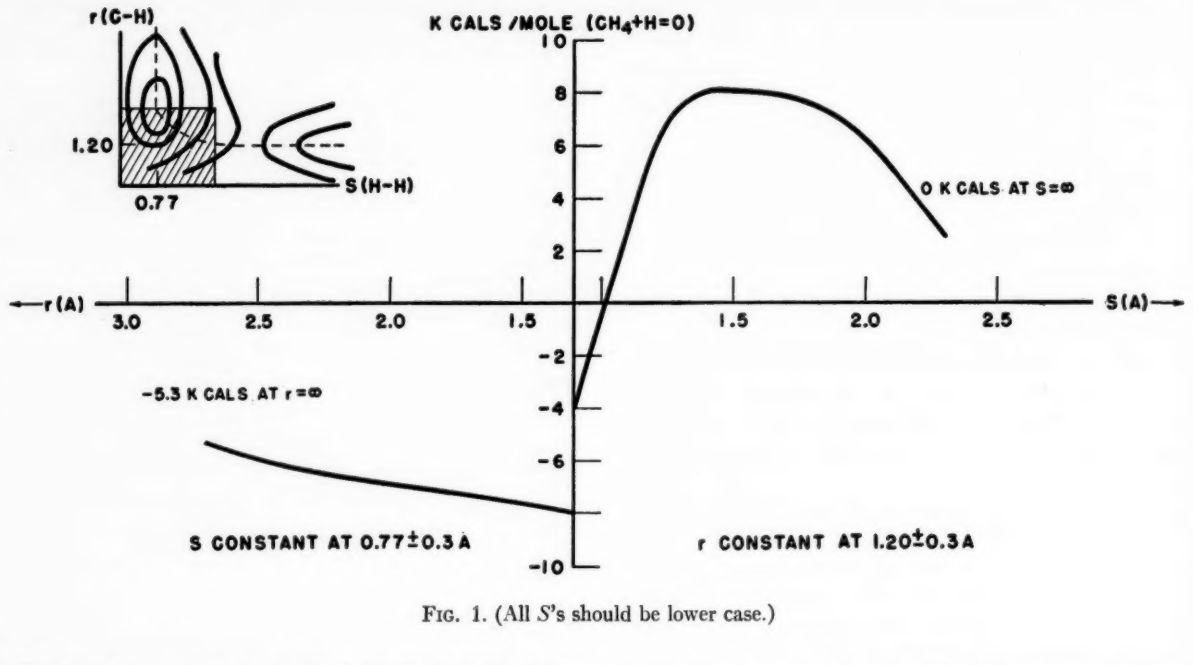

FIG. 1. (All S's should be lower case.)

of CH_3. Davison and Burton[18] obtained $E=13.5$ kcal/mole, $P\simeq10^{-2}$, for the reaction CH_3+H_2. The heat of the reaction is fairly well established as -2 kcal/mole; this makes it possible to derive activation energies for the forward reaction from experimental values for the back reaction. In this way a value $E=8.6$ kcals, with the remarkably low-steric factor $P\simeq10^{-4}$, is obtained for the forward reaction from the experiments of Berlie and LeRoy[19] on the back reaction. This is in contradiction with the work of Darwent and Roberts[20] on the back reaction, which would suggest an activation energy "significantly greater" than 8.8 kcal/mole for the forward reaction.

So far as the evidence goes we can say that this potential-energy surface, with an energy barrier ~12 kcal in the forward direction, and ~10 kcal in the reverse direction, comes close to being the best semi-empirical surface.

ZERO-POINT ENERGIES

In order to calculate the zero-point energies of the various transition-state complexes it is necessary to calculate force constants for stretching and bending. The potential energy for stretching and bending will be assumed to take the simple harmonic form:

$$V=\tfrac{1}{2}f_1(r-1.20)^2+f_{12}(r-1.20)(s-1.40)+\tfrac{1}{2}f_2(s-1.40)^2, \quad (5)$$

$$V_\theta=\tfrac{1}{2}f_\theta\cdot\theta^2, \quad (6)$$

where θ is the angle of bending away from the linear $H_3C—H—H$ configuration. Equation (5) fits the energy profile along the crest of the saddle (Fig. 2) with $f_1=680$, $f_2=-64$, and $f_{12}=-100$ kcal mole^{-1} A^{-2}. Equation (2) applied to slightly bent configurations leads to $f_\theta=8.1$ kcal mole^{-1} rad^{-2}.

The stretching frequencies (ν_+, ν_-) are expressible[21] in terms of f_1, f_2, f_{12} and the masses m_A, m_B, m_C within the complex A–B–C. Following Hirschfelder, Eyring, and Topley we identify ν_+ with the vibration of the complex. Owing to the fact that f_2 is negative, ν_- is an imaginary quantity. In general,

$$\nu_\pm=\frac{1}{2\pi A^{\frac{1}{2}}}\cdot\{\alpha\pm[\alpha^2-2AM(f_1f_2-f_{12})]^{\frac{1}{2}}\}^{\frac{1}{2}}, \quad (7)$$

where

$$\alpha=m_A(m_B+m_C)f_2+m_C(m_A+m_B)f_1-2m_Am_Cf_{12},$$
$$A=2m_Am_Bm_C \quad M=m_A+m_B+m_C.$$

The doubly degenerate bending frequency is given by

$$\nu_\theta=\frac{1}{2\pi}\left\{\frac{f_\theta}{r^2s^2}\left(\frac{s^2}{m_A}+\frac{(r+s)^2}{m_B}+\frac{r^2}{m_C}\right)\right\}^{\frac{1}{2}}.$$

The theoretical activation energy for each reaction will be given by

$$E_0=E_C+\Sigma\epsilon_0^*-\epsilon_0, \quad (8)$$

where E_C is the height of the barrier, and ϵ_0^*, ϵ_0 are zero-point energies for the transition-state complex and the initial state. Values of the last two terms in Eq. (8) are listed in Table IV. The assumption is made that the stretching and bending frequencies within the CH_3 group retain their characteristic values in the transition-state complex. In view of the remarkable invariance of force constants in different molecular environments[22]

[18] S. Davison and M. Burton, J. Am. Chem. Soc. 74, 2307 (1952).
[19] Berlie and D. J. LeRoy, Discussions Faraday Soc. 14, 120 (1953).
[20] B. de B. Darwent and R. Roberts, Discussions Faraday Soc. 14, 121 (1953).
[21] G. Herzberg, *Infrared and Raman Spectra* (D. Van Nostrand Company, Inc., New York, 1945), p. 173. See also reference 5.
[22] Reference 21, p. 192.

TABLE IV. Zero-point energies (kcal/mole) from the asymmetric energy surface.

Reaction	Transition state	$\frac{1}{2}Nh\nu_+$	$Nh\nu_\theta$	$\Sigma\epsilon_0^*$	ϵ_0	$\Sigma\epsilon_0^*-\epsilon_0$	τ
1.	CH_3-H-H	4.52	1.52	6.04	6.28	−0.24	1.36
2.	CH_3-H-D	4.53	1.46	5.99	5.46	0.53	1.19
3.	CH_3-D-H	3.27	1.17	4.44	5.46	−1.02	1.36
4.	CH_3-D-D	3.28	1.08	4.36	4.46	−0.10	1.19

this assumption has some justification. However, the argument that follows would be unaffected if E_0 for all the reactions for which CH_3 is the attacking group, and all those for which CD_3 is the attacking group, contained a similar contribution due to a modification of the CH_3 or CD_3 vibrations on complex formation.

If CH_3 in the transition-state complexes listed in Table IV is replaced by CD_3, the change in mass is too slight to alter the zero-point energies appreciably. Table IV, therefore, also applies to reactions 5, 6, 7, and 8.

Two further factors, κ and τ, enter into Eq. (1). The transmission coefficient, κ, arises[5] from the existence of a metastable complex with a configuration (and consequently an energy) similar to that of the transition-state complex. If such a metastable complex exists there is a finite probability that it will revert to its constituents instead of continuing in the direction of reaction. This corresponds to $\kappa<1$. In the present case the only "basin" in the energy surface lies well away from the transition-state configuration and cannot be the cause of any activated molecules returning to the initial state. We therefore put $\kappa=1$.

The factor τ allows for the possibility of varying amounts of quantum-mechanical tunneling in the various reactions. According to Wigner[23]

$$\tau=1+\tfrac{1}{6}\beta^2\nu_-^2, \qquad (9)$$

where $\beta=h/2kT$, ν_- is a function of the negative force constant across the top of the barrier [Eq. (7)]. The factor τ increases the rate by up to 36 percent (Table IV).

The values for $\Sigma\epsilon_0^*-\epsilon_0$ require $E_C=9-10$ kcal to bring E_0 values within the range of the observed activation energies. Taking $E_C=9.5$ kcal gives E_0 from Eq. (8) varying over the range 9.25 ± 0.8 kcal.[24] As was anticipated, the variation in the calculated value of the activation energy for the present series of reactions is very appreciable, and corresponds to a six-fold variation in rate constant at 400°K. The values of E_0, when combined with the corresponding values for $A_{calc}^{400°}$, give [Eq. (1)] the values for k_{calc} listed in Table V. The predicted over-all variation in rate constant is seen to be 40:1, as compared with the observed range of 7:1. Also, k_3 and k_7 are predicted 20 times larger than k_4 and k_8, instead of being 20 percent smaller in accordance with observation. The absence of any correlation between the trend of values in k_{calc} and the observed rate constants (listed in Table VI) indicates complete failure of the method employed in calculating zero-point energies.

[23] E. Wigner, Z. physik Chem. **B19**, 203 (1932).

[24] It will be observed that the values (Table IV) do not run parallel to those calculated by Hirschfelder, Eyring, and Topley for the $H+H_2$ case. These authors appear to have interchanged f_1 and f_2 in their numerical calculations.

TABLE V. Calculated rate constants (cc $mole^{-1}$ sec^{-1} at 400°K) from the asymmetric surface.

Reaction	1	2	3	4	5	6	7	8
$k_{calc}\times10^{-6}$	38.9	4.93	37.1	1.80	23.5	2.71	21.5	0.99

A "SYMMETRICAL" SURFACE

A curious aspect of both the energy surface for $H+H_2$ (reference 1) and that for CH_3+H_2 (Fig. 2) is the presence of a potential basin a few kilocalories deep, indicating the existence of an H_3 or CH_5 molecule.

In the $H+H_2$ example, this basin may be pictured as arising in the following manner. If the energy surface is constructed using Morse functions to give the three exchange integrals $[\alpha(r_{AB}), \beta(r_{BC}), \gamma(r_{AC})]$, ignoring the Coulombic contribution, an energy surface is obtained[25] with a barrier 32 kcal high relative to $H+H_2$. If now a Coulombic percentage is introduced into the binding, the height of the barrier falls. For 7 percent coulombic energy (i.e., using the absolute values for Coulombic energy calculated by Sugiura[26]) the barrier is ~20 kcal, with a very flat top. For 20 percent Coulombic energy the barrier is ~8 kcal, and a depression several kilocalories deep has appeared with its center on the principal diagonal of the surface (the term principal diagonal is used here to describe the line bisecting the angle between the AB and BC coordinates of the surface; points on this line have $r_{AB}=r_{BC}$). Owing to the presence of the potential-energy basin on the principal diagonal, the highest point of the barrier becomes shifted to the position $r_{AB}\simeq2r_{BC}$ ($r_{AB}=1.35$ A, $r_{BC}=0.75$ A). This is an unexpected transition-state configuration for o.p. hydrogen conversion (a reaction which is completely symmetrical, both as regards energy terms and masses involved).

By restricting the coulombic percentage to 7 percent we obtain an energy surface for $H+H_2$ with no potential-energy basin. The most probable transition-state configuration is then a symmetrical one:

$$H+H-H \rightarrow H-H-H \rightarrow H-H+H.$$

The energy barrier is ~12 kcal higher than the observed activation energy; this we shall take to be a measure of the failure of the equations. The error must be considered in relation to the limits of energy for the system H−H−H, i.e., 12 kcal in 109 kcal≃10 percent. The equations may therefore be sufficiently accurate over

[25] H. Eyring and M. Polanyi, Z. physik Chem. **B12**, 279 (1931).

[26] Y. Sugiura, Z. Physik **45**, 484 (1927).

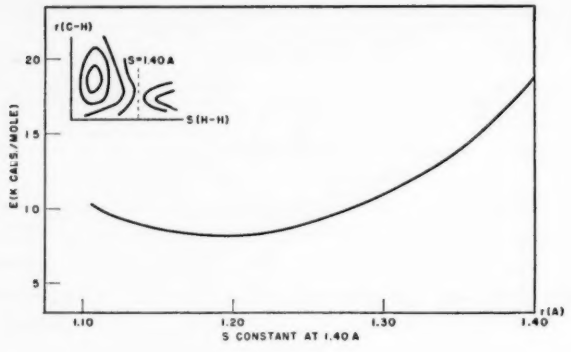

FIG. 2.

small regions to make a calculation of zero-point energy in the neighborhood of the transition state worthwhile.

The stretching frequency of the transition-state complex on the symmetrical surface can be conveniently calculated as follows. At any point on the surface the potential energy is given by

$$V=Q+\{\tfrac{1}{2}[(\alpha-\beta)^2+(\beta-\alpha)^2+(\alpha-\gamma)^2]\}^{\frac{1}{2}}, \tag{10}$$

where $Q=Q_{AB}+Q_{BC}+Q_{AC}$. Along the principal diagonal, $\alpha=\beta$. The potential energy is therefore

$$V_p=Q+(\alpha-\gamma), \tag{11}$$

where $Q=2Q_{AB}+Q_{AC}$. The minimum value for V_p is the predicted activation energy exclusive of zero-point energy (E_c); the value of $r_{AB}(=r_{BC})$ which gives that minimum is the transition-state configuration, and dV_p/dr, in that region, is twice the force constant for symmetrical stretching (motion of a point along the diagonal corresponds to stretching of both bonds). The quantities can be obtained graphically (Fig. 3). Both curves in Fig. 3 are H−H Morse curves plotted against bond extension. The lower curve is plotted on twice the abscissa scale of the upper curve. The difference in height between the curves is therefore equal to $(\alpha-\gamma)+Q_{AB}-Q_{AC}$. To this must be added $Q_{AB}+2Q_{AC}$ (i.e., 7 percent of the lower curve +14 percent of the upper curve)

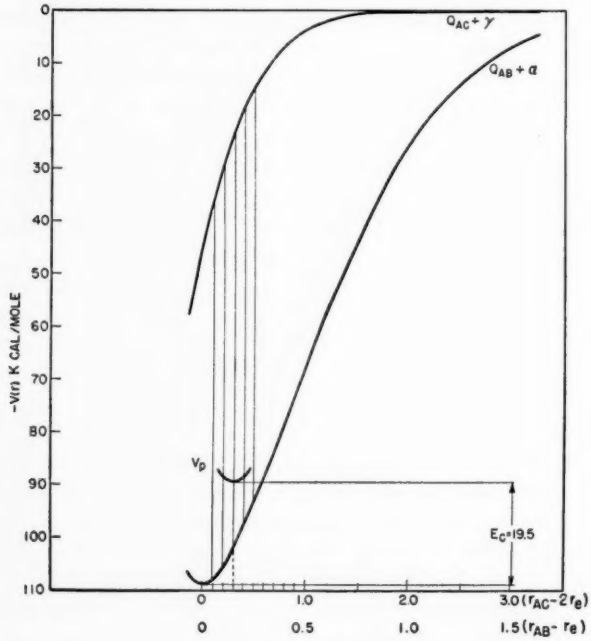

FIG. 3.

in order to obtain V_p. The lowest point of the V_p curve falls at $(r_{AB}-r_e)=1.63$ A, i.e., $r_{AB}(=\frac{1}{2}r_{AC})=0.89$ A. The height of the barrier is seen to be $E_c\cong 20$ kcal. The symmetrical stretching force constant is given by

$$V_p=\tfrac{1}{2}f_2(r_{AB}-0.89)^2+\tfrac{1}{2}f_2(r_{BC}-0.89)^2=f(r_{AB}-0.89)^2 \tag{12}$$

since $f_1=f_2$. In fact V_p is not simple harmonic, but can be fitted by Eq. (12) to ±10 percent for small extensions. The constant $f=388$ kcal mole^{-1} A^{-2} ($2.69\cdot10^{-5}$ dynes mole^{-1} cm^{-1}).

An argument of the same type can be applied to the case of CH_3+H_2. The potential-energy surface (Fig. 1) again contains an energy basin with the lowest level lying close to a symmetrical configuration $(r_{AB}-r_e')=(r_{BC}-r_e)$. Thus, for $r_{AB}=1.25$ A, $r_{BC}=0.84$ A, $\omega=100°$; $V\simeq-8$ kcal. This point corresponds to $(r_{AB}-r_e')=(r_{BC}-r_e)=0.12$ A: the same position as that of the basin in the H+H_2 case. The reason for this is that the two Morse functions which form the basis of the surface are extremely similar in the CH_3+H_2 case to those which are operative in the H+H_2 case. For H_2; $D_e=109$ kcal/mole, and $a=1.94$ [Eq. (3)]. For CH_3-H; $D_e=105$ kcal/mole and $a=1.86$. The corresponding force constants as given by Linnett[27] are $f(H-H)=5.76\cdot10^5$, $f(CH_3-H)=5.4\cdot10^5$ dynes mol^{-1} cm^{-1}. Within the limits of the approximation, Fig. 3 will therefore be taken to apply as well to the reaction CH_3+H_2 as to H+H_2.

For the symmetrical case, $f_1=f_2$, Eq. (7) reduces to

$$\nu_\pm=\frac{1}{2\pi}\left(\frac{f}{A}\right)^{\frac{1}{2}}\{B\pm[b^2-2m_Am_B^2m_C]^{\frac{1}{2}}\}^{\frac{1}{2}}, \tag{13}$$

where

$$B=m_Am_B+2m_Am_C+m_Bm_C,\quad b^2=m_A^2m_B^2+4m_A^2m_C^2+m_B^2m_C^2,$$

and $A=2m_Am_Bm_C$. Of these two frequencies ν_- is the symmetric frequency and ν_+ is an antisymmetric frequency which would lead to reaction. Eyring *et al.*, and also Farkas and Wigner,[28] in their calculations, obtained ν_+ as the only nonimaginary frequency, and therefore took it to be an index of the transition-state zero-point energy. It is not, however, a symmetric vibration, for ν_+ and ν_- are easily identified by writing $m_A=m_C$ (true for H−H−H, D−H−D etc.). Then

$$\nu_+=\frac{1}{2\pi}\left(\frac{f}{m_A}\right)^{\frac{1}{2}}\left\{1+\frac{2m_A}{m_B}\right\}^{\frac{1}{2}}, \tag{14}$$

$$\nu_-=\frac{1}{2\pi}\left(\frac{f}{m_A}\right)^{\frac{1}{2}}. \tag{15}$$

In this simple case ν_- refers to a completely symmetrical vibration with the central atom at rest.

Zero-point energies for the symmetric vibration ν_- are listed in Table VII. It has been assumed that the bending-force constant is not significantly affected by the change to a symmetrical surface (this force constant is found to be insensitive to transition-state configuration). However, the bending frequency has been recalculated using new transition-state dimensions and moment of inertia; ν_0 is found to have increased by 26 percent. There is an equivalent increase in the zero-point energy of bending, and a slight decrease in S_θ^* which necessitates recalculation of the temperature-independent factor. The new temperature-independent factor also takes account of a decrease of 0.55 (±0.1) eu in rotational entropy of the transition-state complex due to the change in transition-state dimensions, and the emergence of a small new entropy term, S_-^*, corre-

[27] J. W. Linnett, Quart. Revs. (London) **1**, 85 (1947).
[28] L. Farkas and E. Wigner, Trans. Faraday Soc. **32**, 708 (1936).

sponding to the fairly slow vibration ν_-. The tunneling factor τ is put equal to unity for the present case since the extensive transition-state plateau effectively rules out the possibility of quantum mechanical tunneling. The values of E_0 in Table VI are based on a classical activation energy of 11.3 kcal/mole.

The values listed as observed in Table VI (k_{obs}) are from the data of Majury and Steacie,[3] and Whittle and Steacie.[4] These authors measured the relative rates of the eight reactions under consideration, by the photolysis of acetone and *d*-acetone in the presence of H_2, HD, and D_2, over the temperature range 403–693°K. To obtain absolute rates it is necessary to multiply their values by $k_B^{\frac{1}{2}}$, where k_B is the rate constant for dimerization of methyl or *d*-methyl. The value used here for k_B is that obtained by Kistiakowsky and Roberts[29] from the photolysis of acetone at 438°K: $k_B = 3.7 \cdot 10^{13}$ cc mole^{-1} sec^{-1}; the same rate for methyl and *d*-methyl. The figure agrees well with that previously obtained by Gomer and Kistiakowsky[30] and (after a pressure correction has been applied) with that obtained by Ingold and Lossing.[31]

DISCUSSION

It is suggested that for two reasons the calculations of Hirschfelder, Eyring, and Topley fail to provide a good test of their method. In the first place their predicted activation energies for the 8 isotopic reactions between atomic and molecular hydrogen do not vary by an appreciable amount; secondly, experimental data against which to check the predictions is lacking. Their method has therefore been applied in the present work in detail to the 8 isotopic reactions between methyl radicals and hydrogen molecules, for which a complete set of experimentally observed rate constants have recently become available. As was anticipated, for this series of reactions the method of Eyring and collaborators predicts an appreciably different trend of zero-point energies for the transition-state complexes from that of the initial state molecules, with correspondingly large variations in activation energy. However, when these calculated energies are combined with calculated temperature independent factors they yield values for the rate constant, k_{calc}, which bear no relation to the observed quantities, k_{obs}. The predicted spread of values (k_{calc}) is 40:1, as compared with the observed 7:1.

An attempt has been made to remedy this by using a potential energy surface with sufficiently low percentage of Coulombic energy to contain no potential-energy basin. The new surface has the correct energy barrier to within 10 percent of the range of interpolation, and can therefore still be regarded as correctly "calibrated." The lowest point on the energy barrier falls close to what previously was the center of the energy basin, i.e., at a configuration which is symmetrical with respect to bond extension (though not with respect to bond length). We therefore refer to this as a "symmetrical" surface. The zero-point energies and hence differences in activation energy for the 8 reactions are easily derived from the symmetrical surface. They are found to increase slightly (0.7 kcal) along the series $E_1 < E_2 (= E_3) < E_4$ and once again along the series $E_5 < E_6 (= E_7) < E_8$. A slight alteration in the calculated temperature independent factor has to be made as a result of the change in transition-state dimensions. The rate constant, k_{calc}, from the symmetrical surface, is found to agree fairly well with k_{obs} (Table VI). Predicted spread of rate constant values is 8:1, as compared with the observed 7:1. The two fastest reactions are correctly predicted as reactions 1 and 5.

It should be noted that though the 8 calculated rate constants are presented for the sake of clarity in two groups, each value has been calculated separately using the appropriate 3-dimensional model for the transition-state complex. Because of the manner in which the classical activation energy (E_c) was chosen, one of the 8 quantities is a calibrated quantity; the remaining 7 are derived.

Calculation of the activation energy on the assumption of 11.3 kcal for the classical activation energy leads to values for E_0 (Table VI) varying over the range 9.3 ± 0.35 kcal. The values obtained by Steacie *et al.* for the 8 reactions vary in a haphazard fashion over the range 10.8 ± 0.9. Our value has been chosen so that the absolute values of k_{calc} fall into the same range as the k_{obs} values; it then becomes possible to compare the trend of rates in each case. The fact that the activation energy required to give this correspondence is so close to the mean experimental figure ($\bar{E}$) indicates that the absolute value of A_{calc} is very close to the experimental

TABLE VI. Calculated and observed rate constants for the eight isotopic reactions methyl+hydrogen.

Reaction	1	2	3	4	5	6	7	8
$A_{calc}^{400°} \times 10^{-12}$	1.86	0.68	0.65	1.13	1.13	0.37	0.37	0.58
E_0 kcal mole^{-1}	8.93	9.25	9.11	9.69	8.91	9.23	9.09	9.67
$k_{calc} \times 10^{-6}$	24.5	6.03	6.78	5.79	15.3	3.38	3.97	3.06
$k_{obs} \times 10^{-6}$ (cc mole^{-1} sec^{-1})	20.1	7.05	3.02	4.19	16.3	6.99	3.98	5.47

TABLE VII. Zero-point energies (kcal/mole) from the "symmetrical" surface.

Reaction	Transition state	$\frac{1}{2}Nh\nu_-$	$Nh\nu_\theta$	$\Sigma\epsilon_0^*$	ϵ_0	$\Sigma\epsilon_0^* - \epsilon_0$
1.	CH_3-H-H	2.00	1.91	3.91	6.28	−2.37
2.	CH_3-H-D	1.56	1.85	3.41	5.46	−2.05
3.	CH_3-D-H	1.79	1.48	3.27	5.46	−2.19
4.	CH_3-D-D	1.49	1.36	2.85	4.46	−1.61

[29] G. B. Kistiakowsky and E. K. Roberts, J. Chem. Phys. **21**, 1637 (1953).
[30] R. Gomer and G. B. Kistiakowsky, J. Chem. Phys. **19**, 85 (1951).
[31] K. U. Ingold and F. P. Lossing, J. Chem. Phys. **21**, 1135 (1953).

FIG. 4. (All K's should be lower case.)

figure. The discrepancy of ~1.5 kcal between E_0 and $\bar{E}$ would be accounted for by a $4x$ error in the absolute value of A_{calc}, or error in the value of k_B used in deriving k_{obs}, or, of course, error in the observed value for $\bar{E}$.

The significance of the change to a symmetric surface rests in the fact that with $f_1 = f_2 (>0)$ a true symmetric vibration takes place in which m_A and m_C contribute equally (per mass unit) to the frequency expression, and m_B makes an insignificant contribution (no contribution at all when $m_A = m_C$). Thus, for example, the theory predicts that the exchange reaction

$$A+B-A \rightarrow A-B+A$$

will have a constant activation energy whatever isotope is put in place of B (A could be H, and B successively H, D, and Tr.). All other effects attendant on the change to a symmetrical surface are minor ones. The energy profile along the crest of the saddle is altered, but only from 680 to 776 kcal mole^{-1} A^{-2}. Also, r_{AB} and r_{BC} are altered, with consequent slight changes in zero-point energy of bending in the transition state, and entropy of rotation and vibration in the transition state. All these effects have been taken into account, but are of minor importance.

A less empirical method for eliminating energy basins from the potential energy surface is that suggested by Hirschfelder.[32] The energy basins cease to exist if the Coulombic energy is made a function of interatomic separation.[33] Hirschfelder obtains this function from experimental data for the forces between nonbonded atoms. Use of this method would not, however, cause any substantial alteration in our conclusions for the present case.

If we discount the slight trend in predicted activation energies since this is likely to lie outside the accuracy of the method employed, we are left with the simple prediction that for reactions in which the Morse function of the molecule being formed is nearly identical with that of the molecule being disrupted (i.e., the only reactions to which a symmetrical surface is likely to apply) the change in activation energy within an isotopic series is negligible. Figure 4 illustrates to what extent this prediction is borne out by the present series of 8 reactions: values of the rate constant calculated (broken line) for a constant E_0, 9 kcal/mole, are plotted alongside the observed values (unbroken line). The divergence between the curves would be accounted for by a steady rise in E_0 along the series, of over-all magnitude 0.7 kcal (in fair agreement with our predicted trend in E_0) but could very well be accounted for in other ways. In this connection, it should be noted that neither Whittle and Steacie nor the workers on the H+H$_2$ series[2] were able to find any systematic trend in the observed activation energies.

It is interesting to consider to what extent the correspondence between the trend of calculated temperature independent factors (i.e., the trend of k_{calc} for constant E_0) and the trend of observed rate constants can be regarded as real. First, as regards the reliability of the experimental data; the fact that the series k_5, k_6, k_7, k_8 reproduces the sequence of values for the independently determined k_1, k_2, k_3, k_4 suggests strongly that the observed changes are real. These changes consist of a large drop in rate from k_1 to k_2 (or k_5 to k_6), a small drop from k_2 to k_3 (or k_6 to k_7) and a rise from k_3 to k_4 (or k_7 to k_8). It is also noteworthy that (despite the small observed differences in activation energy) all these features have been confirmed experimentally at 80° and 160° higher temperature.[4]

The errors in calculating the temperature independent factors are contained in three entropy terms. The translational entropies are subject only to the ideal-gas approximation. For H$_2$ this amounts to 10^{-4} percent. For methyl gas it will be much larger but is still likely to be inappreciable. In calculating the rotational entropy for methyl the only significant uncertainty lies in the choice of configuration. We have used a planar configuration with symmetry $\sigma = 6$. The moment of inertia would be only weakly affected by a change to pyramidal structure. The change to $\sigma = 3$ would give rise to a constant decrease of 1.3 eu in all entropies of activation, leaving the relative values unchanged. In calculating the rotational entropy for the transition-state complexes, it is essential to use a full 3-dimensional model (this point has been made by Bywater and Roberts[10]) and this has been done. The rotational entropy function is surprisingly insensitive to changes in the internuclear separation along the figure axis of the complex. Even the considerable change in the dimensions on going from the asymmetric to the "symmetric" transition-state complex only results in a change of 0.5 eu in the absolute value of S_R^*; the relative values within the series remain unaltered. The third entropy term, vibrational entropy, is made

[32] J. O. Hirschfelder, Ph.D. thesis, Princeton University, 1935.

[33] V. Griffing and J. T. Vanderslice (to be published), in a recent calculation using a molecular orbital approach to the H+H$_2$ reaction obtain a potential energy function free of "energy basins," and a transition-state complex ("ambivalent complex") corresponding to a stretched configuration of high symmetry.

up almost entirely of the contribution from the soft-bending frequency in the transition state. In absolute value this is a small contribution, nevertheless its variations are significant. Uncertainty in this quantity arises out of uncertainty in the value of the bending force constant f_θ. If the bending force constant were doubled then the deviation of the theoretical line from the experimental in Fig. 4 would be reduced by ~30 percent; if the force constant were halved, then the opposite effect would be observed. This probably corresponds to the maximum limits of uncertainty of the bending force constant. Finally, there may be a contribution to the entropy of activation arising from modification of the soft bending frequencies of the methyl group when it enters the transition state complex. It has been assumed that the methyl group will have appreciably the same characteristic frequencies in all the transition-state complexes where it is present as CH_3, and in all those where it is present as CD_3. If this assumption is correct, then it would appear from the foregoing discussion that we are justified in regarding the correlation described in Fig. 4 as being real.

Calculated values of $A^{400°K}$, E_0 (based on the same symmetrical surface but referring the results to, $E_c=7.5$ kcal) and $k_{calc}^{400°K}$, for the eight isotopic reactions between atomic and molecular hydrogen (the reactions are listed at the beginning of this paper) are given in Table VIII.

It should be remarked that the correlation observed arises from the thermodynamic aspects of absolute rate theory, rather than its tenuous links with quantum mechanics through the semiempirical method of Eq. (10). To say that the semiempirical method can predict correctly the near constancy of E_0 within the simplest isotopic series, is not to say that it could ever be used for the quantitative prediction of varying activation energies. Appreciably varying activation energies would be obtained, as has been demonstrated, only from an asymmetric surface; and once the problem becomes sufficiently complex to require an asymmetric surface serious difficulties are encountered. The first of these concerns the definition of the vibrational frequency in the transition-state complex. Even if this difficulty were overcome the further difficulty would arise that the extent of asymmetry is a sensitive function of the percentage of coulombic energy. Finally, it is questionable whether even the "best semiempirical surface," if a way could be found of choosing it, would be capable of making quantitative predictions of the small activation energy differences between isotopic reactions, owing to the approximate nature of the equations which define the surface.

TABLE VIII. Calculated rate constants for the eight isotopic reactions between atomic and molecular hydrogen.

	1	2	3	4	5	6	7	8
$A^{400°K}\times10^{-13}$	6.00	1.32	1.14	2.07	2.33	0.98	0.85	3.09
E_0 kcal mole^{-1}	6.68	6.96	7.04	7.48	6.14	6.40	6.48	6.90
$k_{calc}^{400°K}\times10^{-9}$ cc mole^{-1} sec^{-1}	13.4	2.10	1.61	1.68	10.2	3.10	2.45	5.25

ACKNOWLEDGMENT

The author wishes to thank Dr. E. W. R. Steacie for his advice and encouragement throughout the course of this work.

Solid Mixture Permittivities

WILLIAM FULLER BROWN, JR.
Sun Physical Laboratory, Newtown Square, Pennsylvania

(Received November 10, 1954)

A macroscopically homogeneous aggregate contains two materials A, B, with dielectric constants ϵ_A, ϵ_B, in volume ratio $p:(1-p)$; what is the dielectric constant of the aggregate? By a method used by Yvon and others in molecular theory, this very old problem is formulated rigorously and solved in series form. One form of the solution is $\epsilon/\epsilon'=1+\frac{1}{3}p(1-p)(\delta'/\epsilon')^2+\cdots$, where $\epsilon'=p\epsilon_A+(1-p)\epsilon_B$, $\delta'=\epsilon_A-\epsilon_B$. The cubic and higher terms depend on statistical properties of particle geometry: namely, on such functions as $p^{(3)}{}_{123}$, the probability that three specified points 1, 2, 3 are all in material A. The relation to earlier calculations is discussed.

1. THE PROBLEM

THE following problem has been discussed many times.[1] A solid is macroscopically homogeneous and isotropic. Microscopically it is composed of regions, hereafter called *particles*, of two materials A and B. Each material has a known dielectric constant (or magnetic permeability, or electric conductivity). A fraction p of the volume is occupied by material A, a fraction $q=1-p$ by material B. What is the dielectric constant (or magnetic permeability, or electric conductivity) of the composite material?

A basic question is whether the problem, as stated, is determinate: is the dielectric constant of the mixture completely determined by p and by the dielectric constants of the component materials, or does it depend also on details of the particle geometry?

The method to be used here has not, as far as I know, been applied before to this problem. The problem is first formulated rigorously, for arbitrary particle geometry. A solution is then found in series form. Enough terms are evaluated to demonstrate that particle geometry is important, and to indicate what information about it is needed to make the problem determinate.

2. BASIC CONCEPTS AND DEFINITIONS

The terminology used will be that of the dielectric problem. By trivial changes, the results can be applied to magnetism or conductivity.

Consider a sample of N specimens, all of the same size and shape, and all prepared from the same composite material. Let f be any quantity that has a microscopic value at each point of each specimen. In ordinary measurements, what is observed is not this microscopic value, but an average $[f]_V$ over a macroscopic volume V. Let the external conditions (e.g., applied field) be so arranged that $[f]_V$ is as nearly uniform as is possible over the specimen. Then since the material is macroscopically homogeneous, $[f]_V$ is practically the same for all specimens, if V is large. Now let $\langle f\rangle_N$ be the sample average of f over the N specimens, at a single point $\mathbf{r}$. Then since the material is macroscopically homogeneous, $\langle f\rangle_N$ is practically the same for all points $\mathbf{r}$, if N is large. The phrase "practically the same" means that statistical fluctuations occur but are negligibly small.

Under these conditions, the averages $[f]_V$ and $\langle f\rangle_N$ are practically the same; for each is practically the same as the double average $\langle[f]_V\rangle_N=[\langle f\rangle_N]_V$. This is not a precise statement, but it may be replaced by the following precise one: $[f]_V$ with increasing V and $\langle f\rangle_N$ with increasing N *converge in probability*[2] to the same value. This value is equal to $\langle f\rangle$, the expected value of f (at a fixed point $\mathbf{r}$) for the *infinite population* from which the specimens are considered to be drawn; $\langle f\rangle$ is independent of $\mathbf{r}$.

It is usual to define a macroscopic dielectric constant ϵ^* by $[\mathbf{D}]_V=\epsilon^*[\mathbf{E}]_V$.[3] According to the last paragraph, this definition is practically the same as one in which $[\mathbf{D}]_V$ and $[\mathbf{E}]_V$ are replaced by $\langle\mathbf{D}\rangle_N$ and $\langle\mathbf{E}\rangle_N$. Such unprecise terms as "practically the same" will be avoided here by adopting, instead of either of these definitions, the definition

$$\langle\mathbf{D}\rangle=\epsilon\langle\mathbf{E}\rangle. \tag{2.1}$$

Both $[f]_V$ and $\langle f\rangle_N$ may be regarded as estimates of the population parameter $\langle f\rangle$; ϵ^* may be regarded as an estimate of the population parameter ϵ. Distinct symbols will be used for population parameters (e.g., $\langle f\rangle$, ϵ) and for estimates of these parameters (e.g., $\langle f\rangle_N$, ϵ^*). The former are elements in a theoretical model; the latter are quantities calculable from observations.[4]

Let ϕ be a function of position, equal by definition to 1 in material A and to 0 in material B. Then $p^*=[\phi]_V$ is the fraction of the volume occupied, in a particular specimen, by material A; and $p=\langle\phi\rangle$ is the probability that a definite point $\mathbf{r}$, in a specimen chosen at random, lies in material A. The observable quantity p^* may be regarded as an estimate of the population parameter p.

[1] For bibliographies, see D. A. Bruggeman, Ann. Physik [5] **24**, 636–679 (1935); C. J. F. Böttcher, *Theory of Electric Polarisation* (Elsevier Publishing Company, Houston, Texas, 1952), pp. 415–420; R. E. Burgess, Wireless Engr. **23**, 172–178 (1946); discussion, *ibid.* **23**, 156–157, 231, 291, 313, 315 (1946); **24**, 33–34, 63, 156–157, 187–188, 218–219, 249, 267–270 (1947); J. Ph. Poley, Physica **19**, 298–300 (1953); Hugo Fricke, J. Appl. Phys. **24**, 644–646 (1953).

[2] Harald Cramér, *Mathematical Methods of Statistics* (Princeton University Press, Princeton, New Jersey), pp. 252 ff.

[3] $\mathbf{E}$=field intensity, $\mathbf{D}$=flux density (electric displacement).

[4] Reference 2, Chapters 13 and 26.

The averaging process $\langle\ \rangle$ can be applied also to a function of several position vectors $\mathbf{r}_1, \mathbf{r}_2, \cdots, \mathbf{r}_n$. In particular, let

$$p^{(n)}{}_{12\cdots n}=\langle\phi_1\phi_2\cdots\phi_n\rangle, \tag{2.2}$$

where ϕ_i means $\phi(\mathbf{r}_i)$. Then $p^{(n)}{}_{12\cdots n}$ is the probability that the points $\mathbf{r}_1, \mathbf{r}_2, \cdots, \mathbf{r}_n$, in a specimen chosen at random, all lie in material A. Since the material is macroscopically homogeneous and isotropic, $p^{(n)}{}_{12\cdots n}$ is unchanged by a rigid displacement or rotation of the system of n points within the specimen. Thus $p^{(1)}{}_1=p$ is independent of position, and $p^{(2)}{}_{12}$ is a function only of the distance $r_{12}=|\mathbf{r}_2-\mathbf{r}_1|$. From the definition (2.2), $p^{(2)}{}_{12}\to p$ as $r_{12}\to 0$; but for large r_{12}, we expect $p^{(2)}{}_{12}\doteqdot p^2$. This expectation is based on the assumption that the microscopic structure of the mixture possesses no long-range order; then for large r_{12}, the probability that point 2 is in material A is practically independent of whether point 1 is in material A or in material B.[5] More generally,

$$\lim_{r_{(n-1)n}\to 0} p^{(n)}{}_{12\cdots n}=p^{(n-1)}{}_{12\cdots(n-1)}; \tag{2.3}$$

$$\lim_{r_{(n-1)n}\to \infty} p^{(n)}{}_{12\cdots n}=p^{(n-1)}{}_{12\cdots(n-1)}p. \tag{2.4}$$

3. MATHEMATICAL FORMULATION OF THE PROBLEM

To insure uniform macroscopic polarization, let the specimen be ellipsoidal and the applied field $\mathbf{E}_0$ uniform.[6] Let the dielectric constants of the two materials be ϵ_A and ϵ_B, and let the specimen be embedded in an infinite material C of dielectric constant ϵ_C. By a change of the units of $\mathbf{D}$, the problem can be reduced to one in which a specified one of the three constants ϵ_A, ϵ_B, and ϵ_C is 1. The calculations will be simplified by taking $\epsilon_B=1$, $\epsilon_A=\epsilon_0\neq 1$; and since the external material is not expected to affect the result, ϵ_C will also be taken equal to 1. In the final formulas, generality can be regained by replacing ϵ by ϵ/ϵ_B and ϵ_0 by ϵ_A/ϵ_B.

It is convenient to introduce the Lorentz field intensity[7]

$$\mathbf{F}=\tfrac{2}{3}\mathbf{E}+\tfrac{1}{3}\mathbf{D} \tag{3.1}$$

and the polarization

$$\mathbf{P}=(\mathbf{D}-\mathbf{E})/\gamma. \tag{3.2}$$

The constant γ is 4π in Gaussian units, 1 in Lorentz-Heaviside. The relations $\mathbf{D}=\epsilon_0\mathbf{E}$ and $\langle\mathbf{D}\rangle=\epsilon\langle\mathbf{E}\rangle$, which define ϵ_0 and ϵ, are equivalent to relations

$$\mathbf{P}=\kappa_0\mathbf{F}, \quad \langle\mathbf{P}\rangle=\kappa\langle\mathbf{F}\rangle, \tag{3.3}$$

with

$$\kappa_0=3(\epsilon_0-1)/\gamma(\epsilon_0+2), \quad \kappa=3(\epsilon-1)/\gamma(\epsilon+2). \tag{3.4}$$

The first formula (3.3) holds in material A; in material B, $\mathbf{D}=\mathbf{E}$ and $\mathbf{P}=0$.

In a single specimen, the value of $\mathbf{F}$ at a point $\mathbf{r}_1$ is

$$\mathbf{F}_1=\mathbf{E}_0+\int \mathbf{A}_{12}\cdot\mathbf{P}_2 dV_2, \tag{3.5}$$

where $\mathbf{A}_{12}$ is the dyadic operator

$$\mathbf{A}_{12}=(\gamma/4\pi)(-1+3\mathbf{1}_{12}\mathbf{1}_{12})/r_{12}{}^3; \tag{3.6}$$

$\mathbf{1}_{12}$ is a unit vector along $\mathbf{r}_{12}=\mathbf{r}_2-\mathbf{r}_1$. [See Böttcher, reference 1, p. 9, Eq. (1.28).] The integral is to be extended over the part of the ellipsoid outside a small sphere $r_{12}=$ const. $=r_0$, and then r_0 is to approach 0. This specification is necessary because the integral is only semiconvergent at $r_{12}=0$.[8] The integral also depends on the shape of the ellipsoid.

In the single specimen being considered, the value of $\mathbf{P}$ at a point $\mathbf{r}_1$ is $\kappa_0\mathbf{F}_1$ if $\mathbf{r}_1$ is in material A and is zero if $\mathbf{r}_1$ is in material B; therefore

$$\mathbf{P}_1=\kappa_0\phi_1\mathbf{F}_1. \tag{3.7}$$

Substitution of Eq. (3.5) in Eq. (3.7) gives the following integral equation, which determines $\mathbf{P}$ in a single specimen:

$$\mathbf{P}_1=\kappa_0\phi_1\mathbf{E}_0+\kappa_0\int \phi_1\mathbf{A}_{12}\cdot\mathbf{P}_2 dV_2. \tag{3.8}$$

Averaging of Eq. (3.5) over the population of specimens gives

$$\langle\mathbf{F}\rangle=\mathbf{E}_0+\{\mathbf{A}_{12}dV_2\}\cdot\langle\mathbf{P}\rangle. \tag{3.9}$$

This is the Lorentz field intensity within a uniformly polarized ellipsoid with polarization $\langle\mathbf{P}\rangle$ in an applied field $\mathbf{E}_0$; it has a known uniform value, dependent on the ellipsoid shape.[6]

To solve the problem it is necessary to derive a second relation among $\langle\mathbf{P}\rangle$, $\mathbf{E}_0$, and $\langle\mathbf{F}\rangle$; elimination of $\mathbf{E}_0$ will then give a relation $\mathbf{P}=\text{const}\times\mathbf{F}$, from which κ and ϵ can be deduced by use of Eqs. (3.3) and (3.4).

4. FORMAL SOLUTION

Since $\mathbf{P}$ vanishes when κ_0 vanishes, let us seek a solution of Eq. (3.8) in the form of a power series in κ_0. The solution can be found by successive substitutions of Eq. (3.8) in itself, with advancing of subscripts:

$$\mathbf{P}_1=\kappa_0\phi_1\mathbf{E}_0+\kappa_0{}^2\int \phi_1\phi_2\mathbf{A}_{12}\cdot\mathbf{E}_0 dV_2$$

$$+\kappa_0{}^3\int dV_2\int \phi_1\phi_2\phi_3\mathbf{A}_{12}\cdot\mathbf{A}_{23}\cdot\mathbf{E}_0 dV_3+\cdots. \tag{4.1}$$

[5] The variance of p^* is $\sigma^2{}_{p^*}=V^{-2}\int_V dV_1\int_V(p^{(2)}{}_{12}-p^2)dV_2$. If $p^{(2)}{}_{12}-p^2=O(r_{12}{}^{-\alpha})$, with $\alpha>0$, then $\sigma^2{}_{p^*}\to 0$ as $V\to\infty$, and the convergence in probability of p^* is assured.

[6] Julius Adams Stratton, *Electromagnetic Theory* (McGraw-Hill Book Company, Inc., New York, 1941), pp. 211–213.

[7] H. A. Lorentz, *The Theory of Electrons* (B. G. Teubner, Leipzig, 1909; Dover Publications, New York, 1952), pp. 137–139.

[8] H. Jeffreys and B. S. Jeffreys, *Methods of Mathematical Physics* (Cambridge University Press, Cambridge, England, 1946), pp. 198–199.

Averaging over the population of specimens we get

$$\langle\mathbf{P}\rangle=\kappa_0 p\mathbf{E}_0+\kappa_0^2\int p^{(2)}{}_{12}\mathbf{A}_{12}\cdot\mathbf{E}_0 dV_2$$
$$+\kappa_0^3\int dV_2\int p^{(3)}{}_{123}\mathbf{A}_{12}\cdot\mathbf{A}_{23}\cdot\mathbf{E}_0 dV_3+\cdots. \quad (4.2)$$

The desired relation between $\langle\mathbf{P}\rangle$ and $\langle\mathbf{F}\rangle$ is to be found by eliminating $\mathbf{E}_0$ between Eqs. (4.2) and (3.9).

Equation (4.2) can be solved for $\mathbf{E}_0$ by successive substitutions or by other methods.[9] The result is[10]

$$\mathbf{E}_0=\frac{1}{\kappa_0 p}\langle\mathbf{P}\rangle-\int\frac{p^{(2)}{}_{12}}{p^2}\mathbf{A}_{12}\cdot\langle\mathbf{P}\rangle dV_2$$
$$-\kappa_0\int dV_2\int\left[\frac{p^{(3)}{}_{123}}{p^2}-\frac{p^{(2)}{}_{12}p^{(2)}{}_{23}}{p^3}\right]$$
$$\times\mathbf{A}_{12}\cdot\mathbf{A}_{23}\cdot\langle\mathbf{P}\rangle dV_3+\cdots. \quad (4.3)$$

The first integral is the Lorentz field intensity at point 1 produced by polarization $(p^{(2)}{}_{12}/p^2)\langle\mathbf{P}\rangle$ at points 2. Since the specimen is of macroscopic size, the value of $p^{(2)}{}_{12}/p^2$ for all but microscopically small values of r_{12} differs negligibly from the limiting value 1 at $r_{12}=\infty$. Under these conditions, the Lorentz field intensity is the same as for a uniform polarization $\langle\mathbf{P}\rangle$. If, therefore, the term containing the first integral is transposed to the left in Eq. (4.3), the left member becomes the $\langle\mathbf{F}\rangle$ of Eq. (3.9). Replacement of this left member by $\langle\mathbf{F}\rangle$ eliminates $\mathbf{E}_0$:

$$\langle\mathbf{F}\rangle=\frac{1}{\kappa_0 p}\langle\mathbf{P}\rangle-\kappa_0\int dV_2\int\left[\frac{p^{(3)}{}_{123}}{p^2}\right.$$
$$\left.-\frac{p^{(2)}{}_{12}p^{(2)}{}_{23}}{p^3}\right]\mathbf{A}_{12}\cdot\mathbf{A}_{23}\cdot\langle\mathbf{P}\rangle dV_3+\cdots. \quad (4.4)$$

The shape dependence of the integral has now disappeared, for the expression in parentheses vanishes at $r_{23}=\infty$ and at $r_{12}=\infty$, because of Eq. (2.4), and becomes negligible at macroscopic r_{23} or r_{12}. Furthermore the semiconvergence at zero has also disappeared; for the expression in parentheses vanishes at $r_{23}=0$ and at $r_{12}=0$, because of Eq. (2.3).

If it is tentatively assumed that the operator applied to $\langle\mathbf{P}\rangle$ is equivalent to a scalar, then Eq. (4.4) gives

$$\frac{1}{\kappa}=\frac{1}{p\kappa_0}-\lambda\kappa_0+\cdots, \quad (4.5)$$

with

$$\lambda=\int dV_2\int\left[\frac{p^{(3)}{}_{123}}{p^2}-\frac{p^{(2)}{}_{12}p^{(2)}{}_{23}}{p^3}\right]\mathbf{A}_{12}\cdot\mathbf{A}_{23}dV_3. \quad (4.6)$$

To verify that λ is in fact a scalar, introduce polar coordinates (r_{12},θ_2,ψ_2) for dV_2 and polar coordinates (r_{23},θ_3,ψ_3) for dV_3, with the polar axis for θ_3 and ψ_3 along r_{12}. Then the integrations over ψ_3, ψ_2, and θ_2 can be carried out, with the result

$$\lambda=\left(\frac{\gamma}{4\pi}\right)^2\cdot 2\int dV_2\int\left[\frac{p^{(3)}{}_{123}}{p^2}\right.$$
$$\left.-\frac{p^{(2)}{}_{12}p^{(2)}{}_{23}}{p^3}\right]\frac{P_2(\cos\theta_3)}{r_{12}{}^3r_{23}{}^3}dV_3; \quad (4.7)$$

$P_2(\cos\theta_3)$ is a Legendre polynomial, and $dV_2=4\pi r_{12}{}^2dr_{12}$, $dV_3=2\pi r_{23}{}^2\sin\theta_3 d\theta_3 dr_{23}$.

Equation (4.5) is the desired formula for κ. It shows that κ depends not only on p and on κ_0, but also on certain statistical properties of the particle geometry. These statistical properties are embodied in the functions $p^{(2)}{}_{ij}$, $p^{(3)}{}_{ijk}$, etc.

5. WORKING FORMULAS

For two materials with dielectric constants ϵ_A and ϵ_B, κ_0 in Eq. (4.5) must be replaced by $3(\epsilon_A-\epsilon_B)/\gamma(\epsilon_A+2\epsilon_B)$, and κ by $3(\epsilon-\epsilon_B)/\gamma(\epsilon+2\epsilon_B)$. From the resulting equation, ϵ can be expressed as a series in $\epsilon_A-\epsilon_B$. Let

$$\epsilon'=p\epsilon_A+q\epsilon_B, \quad \delta'=\epsilon_A-\epsilon_B, \quad q=1-p. \quad (5.1)$$

Then the following result can be obtained by solving for ϵ, expressing ϵ_A and ϵ_B in terms of ϵ' and δ', and expanding in powers of δ':

$$\epsilon/\epsilon'=1-\tfrac{1}{3}pq(\delta'/\epsilon')^2+(-\tfrac{1}{3}p^2q+\tfrac{1}{9}pq^2$$
$$+p^2\lambda/\gamma^2)(\delta'/\epsilon')^3+\cdots. \quad (5.2)$$

An alternative formula can be obtained by interchanging the roles of components A and B. This replaces p by q, q by p, δ' by $-\delta'$, and λ by a new quantity μ; μ is defined by a formula similar to Eq. (4.7) except that the probabilities are now probabilities that points 1, 2, etc. will be in material B. Equivalence of Eq. (5.2) and of the alternative formula requires that

$$p^2\lambda+q^2\mu=(2/9)\gamma^2pq. \quad (5.3)$$

This relation can be proved directly, but the proof is tedious and is not needed here. A symmetrical formula can be obtained by taking half the sum of the original and alternative expressions in Eq. (5.2); this gives Eq. (5.7).

[9] Konrad Knopp, *Theory and Applications of Infinite Series*, (Hafner Publishing Company, New York), second English edition, p. 182.

[10] The general term is

$$(-1)^n\kappa_0{}^{n-1}p^{-n-1}\int dV_2\cdots\int q_n\mathbf{A}_{12}\cdot\mathbf{A}_{23}\cdots\mathbf{A}_{n(n+1)}\cdot\langle\mathbf{P}\rangle dV_{n+1},$$

with

$$q_n=\begin{vmatrix} p^{(2)}{}_{12} & p & 0 & \cdots & 0 & 0 \\ p^{(3)}{}_{123} & p^{(2)}{}_{23} & p & \cdots & 0 & 0 \\ \cdots & \cdots & \cdots & \cdots & \cdots & \cdots \\ p^{(n)}{}_{12\ldots n} & p^{(n-1)}{}_{23\ldots n} & p^{(n-2)}{}_{34\ldots n} & \cdots & p^{(2)}{}_{(n-1)n} & p \\ p^{(n+1)}{}_{12\ldots(n+1)} & p^{(n)}{}_{23\ldots(n+1)} & p^{(n-1)}{}_{34\ldots(n+1)} & \cdots & p^{(3)}{}_{(n-1)n(n+1)} & p^{(2)}{}_{n(n+1)} \end{vmatrix}$$

Other formulas can be obtained by using, instead of ϵ' and δ', ϵ'' and δ'', defined by

$$\epsilon''^{-1}=p\epsilon_A^{-1}+q\epsilon_B^{-1}, \quad \delta''=\epsilon_A^{-1}-\epsilon_B^{-1}; \tag{5.4}$$

and by introducing

$$\eta=\ln\epsilon, \quad \eta_A=\ln\epsilon_A, \quad \eta_B=\ln\epsilon_B \tag{5.5}$$

and using η' and δ, defined by

$$\eta'=p\eta_A+q\eta_B, \quad \delta=\eta_A-\eta_B. \tag{5.6}$$

The equations that result from these various choices of variables are

$$\epsilon/\epsilon'=1-\tfrac{1}{3}pq(\delta'/\epsilon')^2+[-(2/9)pq(p-q)+(p^2\lambda-q^2\mu)/2\gamma^2](\delta'/\epsilon')^3+\cdots, \tag{5.7}$$

$$\epsilon/\epsilon''=1+\tfrac{2}{3}pq(\epsilon''\delta'')^2+[(5/9)pq(p-q)-(p^2\lambda-q^2\mu)/2\gamma^2](\epsilon''\delta'')^3+\cdots, \tag{5.8}$$

$$\eta=\eta'+\tfrac{1}{6}pq\delta^2+[-(1/18)pq(p-q)+(p^2\lambda-q^2\mu)/\gamma^2]\delta^3+\cdots. \tag{5.9}$$

All these equations have the following properties.

(a) Omission of all terms after the first gives a simple averaging formula of the form $f(\epsilon)=pf(\epsilon_A)+qf(\epsilon_B)$, with $f(\epsilon)=\epsilon$, $1/\epsilon$, and $\ln\epsilon$ for Eqs. (5.7), (5.8), and (5.9), respectively.

(b) The approximation (a) is correct to the first order in δ', δ'', or δ.

(c) The approximation (a) can be improved by adding a second-order term that depends only on ϵ_A, ϵ_B, and p and not on particle geometry.

(d) If a still better approximation is needed, additional information must be available. This information relates to statistical properties of the particle geometry; it consists in the probabilities $p^{(2)}{}_{12}$, $p^{(3)}{}_{123}$, etc.

Equations (5.7)–(5.9) are presumably not reliable unless $(\epsilon_A-\epsilon_B)/\epsilon'$ is small. They are therefore presumably not reliable if the ratio ϵ_A/ϵ_B is very small or very large. This limits their usefulness in the magnetic case, where high-permeability dust cores are of interest, and in the conduction case, where one of the materials is sometimes a nonconductor. Treatment of these extreme cases requires some other technique for solving the equations of Sec. 3, or at least a thorough study of the convergence of the series.

6. RELATION TO EARLIER CALCULATIONS

The three averaging formulas $f(\epsilon)=pf(\epsilon_A)+qf(\epsilon_B)$, with $f(\epsilon)=\epsilon$, $1/\epsilon$, and $\ln\epsilon$, have all been proposed as approximate solutions of the problem.[1] The first is correct when **E** is uniform and the second when **D** is uniform. These conditions are satisfied in an array of parallel plates with boundaries parallel and perpendicular, respectively, to the field direction; they are not satisfied in an isotropic aggregate. The third averaging formula, the logarithmic, has been proposed both on semitheoretical[11] and on empirical[12] grounds. Equations (5.7)–(5.9) show that each of the averaging formulas is subject to correction, and that the leading term in the correction is independent of particle geometry.

Maxwell[13] derived an approximate solution on the assumption that material A exists as small spheres embedded in material B. Maxwell's formula is equivalent to Eq. (4.5) with the terms $-\lambda\kappa_0+\cdots$ omitted. It is therefore equivalent to Eqs. (5.7)–(5.9) to the second order of small quantities, regardless of whether the particles are spheres. This is one order better than the averaging formulas and is the best that can be done without knowing more than merely p, ϵ_A, and ϵ_B. Maxwell's formula, written in full, is

$$(\epsilon-\epsilon_B)/(\epsilon+2\epsilon_B)=p(\epsilon_A-\epsilon_B)/(\epsilon_A+2\epsilon_B); \tag{6.1}$$

it is essentially the "Clausius-Mossotti" formula of molecular theory.

For spheres, both Bruggeman and Böttcher[1] have attempted to improve on Maxwell's formula. Bruggeman's formula is

$$(\epsilon_A-\epsilon)/(\epsilon_A-\epsilon_B)=q(\epsilon/\epsilon_B)^{\frac{1}{3}}; \tag{6.2}$$

Böttcher's is

$$(\epsilon-\epsilon_B)/3\epsilon=p(\epsilon_A-\epsilon_B)/(\epsilon_A+2\epsilon). \tag{6.3}$$

Both these formulas, when expanded as series, agree with Eq. (5.7) (and therefore with Maxwell's formula) to the second order of small quantities. For agreement to the third order, λ must be assigned the values 0 according to Maxwell, $2q/9$ according to Bruggeman, and $q/9$ according to Böttcher. To decide which of these is the best approximation, it would be necessary to calculate the probabilities $p^{(2)}{}_{ij}$ and $p^{(3)}{}_{ijk}$, and so to evaluate λ as a function of p, for the assumed distribution of spheres.

The calculation presented here was suggested by a calculation in molecular theory.[14] The functions $p^{(n)}$ are analogous in some respects to the distribution functions of the molecular theory. In other respects they are more closely analogous to correlation functions used in the theory of random noise.[15] The Fourier method, which has been fruitful in noise theory, can be used here too. It leads to a verification of the second-order terms in Eqs. (5.7)–(5.9) and to an alternative formula for λ, in terms of coefficients in the three-dimensional Fourier expansion of ϕ.

---

[11] By K. Lichtenecker; see Bruggeman, reference 1.

[12] V. E. Legg and F. J. Given, Bell System Tech. J. **19**, 385–406 (1940).

[13] James Clerk Maxwell, *A Treatise on Electricity and Magnetism*, 3d ed. (The Clarendon Press, Oxford, England, 1904), Vol. 1, p. 440.

[14] J. Yvon, *Actualités Scientifiques et Industrielles*, Nos. 542 and 543 (Hermann et Cie., Paris, France, 1937); John G. Kirkwood, J. Chem. Phys. **4**, 592–601 (1936); William Fuller Brown, Jr., J. Chem. Phys. **18**, 1193–1200 (1950) and **21**, 1121 (1953); H. S. Green, *Molecular Theory of Fluids* (Interscience Publishers, Inc., New York, 1952), pp. 207–211.

[15] S. O. Rice, Bell System Tech. J. **23**, 282–332 (1944) and **25**, 47–156 (1945); Ming Chen Wang and G. E. Uhlenbeck, Revs. Modern Phys. **17**, 323–342 (1945).

Ring Formation and Molecular Weight Distributions in Branched-Chain Polymers. I

FRANK E. HARRIS
General Electric Research Laboratory, Schenectady, New York, and Department of Chemistry, Harvard University, Cambridge, Massachusetts

(Received November 18, 1954)

The theory of molecular weight distributions in branched-chain polymers is extended to include possible intramolecular reaction leading to ring formation. The problem is more complicated than the noncyclic case in that, in addition to the more complex combinatory and algebraic considerations, it is necessary to consider geometric restrictions on the number and relative probability of many configurations. Two approximate models for describing the extent of ring closure are investigated. The first of these, in which it is assumed that spatial restrictions may be ignored, predicts far too many structures for large molecules with many rings, and as a result always predicts gel formation. In the second approximation it is assumed that geometric restrictions limit the number of rings so that the probability of ring closure is independent of molecular weight, but only depends upon the density of available ends. This model predicts that ring closures will shift the gel point to higher extents of reaction, producing at volumes larger than a "critical volume," completely soluble polymers even at complete reaction. The dependence of the molecular weight distribution on the experimental variables is discussed in some detail.

I. INTRODUCTION

THE theory of molecular weight distribution and gel formation in branched-chain polymers has been developed in detail, subject to two major assumptions. (1) All unreacted functional groups are equally reactive and (2) intramolecular reactions, leading to cyclic structures, do not occur.[1–3] In a previous study,[4] we have already examined assumption (1), which produces the same molecular weight distribution as does a polymerization assumed to be governed by a kinetic mechanism, in which all possible reactions are assumed to be bimolecular with the same rate constant. Although the postulate of equal reactivity of all functional groups is attractive, it was shown that the free energy of solution of the mixture of various sized molecules, under nonideal conditions, would serve to alter the apparent reactivity of intrinsically equally reactive functional groups on different sized molecules. However, since the complexity of the resulting equations then determining the equilibrium molecular weight distribution precludes an easily analyzed result, and since, in addition, many polymerizations may proceed by mechanisms such that an original weight distribution, governed primarily by kinetic considerations, is transformed only very slowly into the thermodynamically stable distribution, it does not follow that the postulate of equal reactivity should be completely abandoned.

Irrespective of the fate of the assumption of equal reactivity of all functional groups, it is desirable to know the effect of assumption (2) prohibiting intramolecular condensations. Although it has been found that in some cases the effect of intramolecular reaction is small,[2] contributing only of the order of 5% of the total reaction prior to gelation, it is to be presumed that as the volume is increased, thereby fostering the tendency toward ring closure, intramolecular reactions should become progressively more important. Such a situation would manifest itself in a concentration dependence of the gel point as well as in a change in the distribution of molecular weights of the soluble polymeric species. Moreover, one might also surmise that the extent of intramolecular reaction could vary among different types of polymerizations. The present communication will be concerned with means of extending the theory of branched-chain polymerizations to include the possible formation of rings.

We consider two different models for approximating the behavior of the cyclizing systems. The first model assumes that spatial limitations do not interfere with the probability or number of possible structures, and the number of structures is therefore calculated for that model by a simple combinatorial argument. It is found that the number of structures for the large molecules is greatly overestimated, and that, as a result, gel formation is increasingly favored by including ring formation. A second, and more satisfactory model, assumes that spatial limitations primarily determine the number of opportunities a functional group has for intramolecular condensation, and that therefore the number of ends available to a given end for ring closure depends only on the density of ends in the polymer, rather than upon their total number. This model leads to the intuitively plausible result that the consideration of intramolecular reaction shifts the gel point to higher extents of reaction. The equations necessary to characterize the molecular weight distributions obtained from the second model are exhibited in Sec. VI.

The relation of the molecular weight distribution to the volume and to the extent of reaction exhibit an interesting parallelism to the results of Jacobson and

[1] W. H. Stockmayer, J. Chem. Phys. **11**, 45 (1943).
[2] P. J. Flory, J. Am. Chem. Soc. **63**, 3083, 3091, 3096 (1941).
[3] P. J. Flory, *Principles of Polymer Chemistry* (Cornell University Press, Ithaca, New York, 1953).
[4] F. E. Harris, J. Polymer Sci. (to be published).

Stockmayer[5] for linear polymerizations including rings. Just as Jacobson and Stockmayer found that there is a unique volume such that at larger volumes, complete reaction in their linear systems produces only rings of finite molecular weight, so does the present development indicate that above a certain volume gel is not produced, even at complete reaction, but that the system then consists totally of soluble polymers with all functional groups used up in ring formation. As the volume decreases, the gel point, and the entire weight distribution approaches that originally obtained by Stockmayer for noncyclizing polymerizations.

II. BASIC FORMULATION

The discussion will, throughout the paper, be confined to the simplest system showing all the necessary characteristics, namely a solution mixture containing a total of N identical polymerizable units, each of which possesses f functional groups capable of combining with any other functional group of the system (including those on the same unit).

Consider now the state of the system when polymerization has taken place to such an extent that there is a total of J bonds between functional groups. The fraction of reacted end groups, or extent of reaction, p, is then

$$p=\frac{2J}{fN}. \tag{1}$$

Let m_{nj} be the number of polymers of the system of degree of polymerization n, connected together with j bonds between functional groups. For any given value of n, the permissible values of j will range from $n-1$ to the largest integer smaller than $\frac{1}{2}nf$. The range of n will be from 1 to infinity. The set $\{m_{nj}\}$ indicating the molecular weight and bond distribution must satisfy the relations

$$\begin{aligned}\sum nm_{nj}&=N,\\ \sum jm_{nj}&=J,\end{aligned} \tag{2}$$

where in Eq. (2), and subsequently, except where explicitly otherwise specified, the summations include all permissible values of n and j.

The most probable distribution of molecules of the various types, $\{m_{nj}\}$, may be obtained from the requirement that the free energy of the system be a minimum. The total free energy for a given distribution, $F(\{m_{nj}\})$, will be divided into three terms. The first term, denoted by F_1, shall contain that portion of the free energy arising solely from the multiplicity of ways the N polymerizable units and J bonds can be used to construct a set of polymers $\{m_{nj}\}$. This division of F will be most useful when all the different structures corresponding to a polymer of type (n,j) occur with equal probability, so that F_1 will depend only upon their *number*. Therefore it will be assumed that all structures of type (n,j) may be classified as either permitted or not permitted, and all the permitted structures will be assumed to occur with equal probability. An estimate of the validity of this assumption may be more readily made when criteria for selecting the permissible structures have been adopted, and will be discussed at that time.

The second part of F, F_2, will contain the free energy of bond formation, including the free-energy changes involved in closing rings. By virtue of the dichotomic division already assumed, the contribution to F_2 from each polymeric structure of a given type must be taken as identical, so that F_2 may be computed in terms of average free energies of bond formation and ring closure. It is then reasonable to suppose that each bond of an (n,j) polymer after the $n-1$ bonds necessary to completely connect the structure has associated with its formation a constant average free energy of ring closure, computed for a suitably determined average sized ring.

The remainder of F, F_3, will include the configurational free energy and the free energy of mixing of each polymer in solution. In computing F_3, as for F_2, it is permissible to use average quantities for each type (n,j) of polymer.

The additional assumptions necessary to reduce the problem to the equivalent of a kinetic polymerization include setting F_3=constant, thereby removing the effect of configurational or solution free energy upon the equilibrium distribution. In addition, it is necessary to assume that the free energy of bond formation in F_2 is independent of the size of the molecule in which the bond occurs. Both these assumptions will be carried through the entire development, so that the only factors influencing the molecular weight distributions will be the number of structures and the average free energy of ring closure, which will be denoted by χ and discussed at greater length in a subsequent section.

As indicated in the aforementioned, $F_1(\{m_{nj}\})$ may be written

$$F_1(\{m_{nj}\})=-kT\ \ln\Omega(\{m_{nj}\}) \tag{3}$$

where $\Omega(\{m_{nj}\})$ is the number of ways the N distinguishable units, each with f distinguishable bonds, can be divided into the set $\{m_{nj}\}$, and is therefore

$$\Omega(\{m_{nj}\})=N!\prod_{n,j}\frac{1}{m_{nj}!}\left(\frac{w_{nj}}{n!}\right)^{m_{nj}} \tag{4}$$

where w_{nj} is the number of ways a polymer of type (n,j) can be constructed from n distinguishable units with distinguishable functional groups.

Now, $F_2(\{m_{nj}\})$ may also be written. It will contain, as a constant term, the free energy of forming J bonds, and, in addition, the free energy of closing $j-n+1$ rings in each polymer of type (n,j), summed

[5] H. Jacobson and W. H. Stockmayer, J. Chem. Phys. **18**, 1600 (1950).

over all the polymeric species. Thus,

$$F_2(\{m_{nj}\})=\text{const}+\sum(j-n+1)\chi m_{nj}. \quad (5)$$

The equilibrium set $\{m_{nj}\}$ may now be found by minimizing F, as given by Eqs. (3) to (5), subject to the conditions (2). Applying Stirling's formula to the factorials, and using Lagrange's method of undetermined multipliers, one may find

$$m_{nj}=\frac{w_{nj}}{n!}e^{-\chi/kT}\xi^n\eta^j \quad (6)$$

where quantities ξ and η are determined by requiring Eqs. (2) to be satisfied.

III. RING FORMATION

To evaluate χ, the free energy of ring closure in a system of constant N and J, it is convenient to proceed, as did Stockmayer,[5] by considering the process

$$\begin{aligned}&(\text{chain of } x+y \text{ units})\\ &\quad=(\text{ring of } x \text{ units})+(\text{chain of } y \text{ units}).\end{aligned} \quad (7)$$

As Stockmayer points out, only the entropy change in (7) is important, since the net number of bonds remains unchanged. It should be noticed that the free-energy change of reaction (7) is χ, if the symmetry numbers of all the species involved are taken as unity, for χ is the free-energy change of the reaction to close a particular ring at a particular point, thereby concomitantly increasing by one the total number of molecules. In the present development an overwhelming majority of the rings to be formed will in fact have symmetry number unity, by virtue of the opportunity for branching at each unit of the ring. Continuing with Stockmayer, divide (7) into two steps, first breaking the bond between units x and $x+1$, then closing the ring through reaction between units 1 and x. The entropy change for the first step is $k\ln(V/v_s)$, where v_s is the equivalent volume available to a unit bonded to a stationary neighbor. For the second step, Stockmayer estimates the entropy change to be $k\ln\{(3/2\pi)^{\frac{3}{2}}v_s/h_0^3\}$, where h_0 is the root-mean-square end-to-end distance of a chain of x units. Replacement of h_0^3 by $\langle h_0^3\rangle$, its average over the distribution of ring sizes, will yield a mean value for χ.

From the foregoing, it may be seen that

$$e^{-\chi/kT}=\left(\frac{3}{2\pi}\right)^{\frac{3}{2}}\frac{V}{\langle h_0^3\rangle}\equiv AV \quad (8)$$

where Eq. (8) will be taken as the definition of A.

IV. A MAXIMAL APPROXIMATION TO w_{nj}

The characterization of the molecular weight distribution can now be completed if means are devised for the calculation of w_{nj}. In this and the following section two approximations to w_{nj} are presented and discussed.

For the first approximation to w_{nj}, consider the limiting case where the size and shape of the polymerizable units does not restrict the number of polymers of any given type. The number w_{nj} is given in this limit as just the total number of ways j pairs of functional groups can be selected out of the nf functional groups of n monomer units in such a way that all the monomer units are formed into one connected structure. It is clear that the numbers w_{nj} obtained in this way will be larger than the correct values, because the assumption is implicit in this mode of calculation that the presence of a number of rings does not impart sufficient rigidity to the polymer to preclude the formation of an additional ring between any two remaining ends of the branched chain.

As an aid to the calculation of w_{nj} consider also quantities w_{nj}^0, defined similarly to w_{nj} in that w_{nj}^0 will represent the number of ways j bonds can be made among the functional groups of n units, but different from w_{nj} in that among the structures counted in w_{nj}^0 will be those, not in w_{nj}, in which all n units are not connected into a single polymer. Recognizing that the number of ways one can construct a not necessarily connected structure is expressible in terms of the numbers of ways smaller connected structures can be formed, the w_{nj}^0 can be seen to be related to w_{nj} as follows:

$$w_{nj}^0=\sum_{\substack{\{x_{st}\}\\ \sum sx_{st}=n\\ \sum tx_{st}=j}}\left[n!\prod_{s,t}\frac{1}{x_{st}!}\left(\frac{1}{s!}\right)^{x_{st}}\right]\cdot\left[\prod_{s,t}(w_{st})^{x_{st}}\right]. \quad (9)$$

The first factor of each term of the restricted multiple sum on the right-hand side of (9) is the number of ways a partitioning of (n,j) into the set $\{x_{st}\}$ of polymers of type (s,t), $1\leqslant s\leqslant n$, $s-1\leqslant t\leqslant\frac{1}{2}fs$, can be performed, remembering that the n units are distinguishable but that the j bonds are not. The remaining factor of each term of the sum represents the multiplicity of ways the polymers of the partitioning involved can be formed from the requisite number of distinguishable functional groups. Since it will be possible to write down an expression for w_{nj}^0, Eq. (9) enables one, in principle at least, to obtain the w_{nj}.

Next, operate on Eq. (9) as follows: first, divide through by $n!$; second, multiply by $\xi^n\eta^j$; and finally sum over all compatible values of n and j, plus, in addition $n=j=0$. In this way one may construct a generating function, $\varphi^0(\xi,\eta)$, for the w_{nj}^0. The definition of w_{nj}^0 will be extended by defining $w_{00}^0=1$ so as to simplify subsequent analysis. Thus,

$$1+\varphi^0(\xi,\eta)\equiv\sum_{n,j=0}\frac{w_{nj}^0}{n!}\xi^n\eta^j=\sum_{n,j=0}\sum_{\substack{\{x_{st}\}\\ \sum sx_{st}=n,\\ \sum tx_{st}=j}}\times\xi^n\eta^j\prod_{s,t}\frac{1}{x_{st}!}\left(\frac{w_{st}}{s!}\right)^{x_{st}}. \quad (10)$$

Now, observe that the sums over n and j on the right-hand side of (10) can be incorporated into the sums over the $\{x_{st}\}$ simply by removing the restrictions, and writing $\xi^n\eta^j$ as $\xi^{\Sigma sx_{st}}\eta^{\Sigma tx_{st}}$. With these modifications, the right-hand side of (10) becomes

$$1+\varphi^0(\xi,\eta)=\sum_{\{x_{st}\}}\prod_{s,t}\frac{1}{x_{st}!}\left(\frac{w_{st}\xi^s\eta^t}{s!}\right)^{x_{st}}. \quad (11)$$

Upon interchanging the sum and product on the right-hand side of (11), the summation can be performed and the product expressed as a sum in the exponent, leading to

$$1+\varphi^0(\xi,\eta)=e^{\varphi(\xi,\eta)} \quad (12)$$

where $\varphi(\xi,\eta)$ is defined as

$$\varphi(\xi,\eta)=\sum_{n,j=1}\frac{w_{nj}}{n!}\xi^n\eta^j. \quad (13)$$

Comparison of (13) with (6) and (8) reveals that

$$M\equiv\sum m_{nj}=AV\varphi(\xi,\eta) \quad (14)$$

where M is the total number of polymer molecules, and that Eqs. (2) are equivalent to

$$N=AV\xi\frac{\partial\varphi}{\partial\xi},\qquad J=AV\eta\frac{\partial\varphi}{\partial\eta}. \quad (15)$$

Furthermore, by virtue of (12), Eqs. (14) and (15) can be rewritten in terms of φ^0.

The present development will be complete when an expression is obtained for φ^0. Accordingly, now consider $w_{nj}{}^0$ which is simply the total number of ways nf distinguishable functional groups can be divided into j unnumbered groups of 2 members each, or

$$w_{nj}{}^0=\frac{(nf)!}{2^j j!\,(nf-2j)!}. \quad (16)$$

Therefore,

$$\varphi^0(\xi,\eta)=\sum_{n=1}^{\infty}\sum_{j=n-1}^{\leq nf/2}\frac{(nf)!\,\xi^n\eta^j}{2^j n!\,j!\,(nf-2j)!}. \quad (17)$$

It is now appropriate to consider the significance of the generating function φ yielded by the aforementioned development. By virtue of the physical quantities represented, the region of (ξ,η)-space corresponding to actual polymeric systems must be the region of real, positive ξ and η. It may, in addition, be inferred that the proportion of molecules of large n and j will increase as ξ and η increase, respectively. So long as ξ and η lie within the region of convergence of φ, the proportion of molecules of macroscopic will be negligible, but when the radius of convergence is passed, the proportion of the polymer possessing infinite molecular weight will become appreciable, indicating the presence of gel. To apply the foregoing discussion to the present case, observe that since φ and φ^0 have the same singularities for positive φ^0, it will suffice to determine the radius of convergence of φ^0. For this purpose, turn again to Eq. (17). If the series over j in (17) be replaced by its maximum term (which for all nonzero η can be shown to be, in the limit of large n, a term for which $j=\alpha n$, where α is a constant greater than unity), the resulting series over n diverges for all nonzero ξ. Since replacement of the series over j by its maximum term resulted in a decrease in the value of each term of the series over n, it may be inferred that φ^0 diverges whenever both ξ and η assume positive values.

The divergence of (17) when both ξ and η are positive indicates that the approximation to w_{nj} introduced in this section predicts gel formation at all concentrations at all nonzero extents of reaction. The increased tendency to gel formation as compared with noncyclizing systems is not in accord with the intuitive view that ring formation would remove ends which otherwise would link the material together into larger units. However, because the model of this section does not limit the various interconnections among the ends, the number of different structures increases so rapidly as the size and extent of ring formation increases that formation of large and complex molecules is overwhelmingly favored.

V. A SECOND APPROXIMATION TO w_{nj}

It has been shown in the preceding section that an approximation to w_{nj} which disregards geometric restrictions results in a serious overestimate of w_{nj} for large n. Therefore, consider next an approximation such that the number of ends available for ring closure to a given end depends only on the number of ends per unit weight of the polymer, and therefore does not increase with the size of the polymer. Such a restriction is approximately equivalent to the assumption that spatial restrictions allow an end to be available for reaction only to ends within a fixed distance.

This approximation will be implemented by computing w_{nj} as

$$w_{nj}=C_n\frac{u_{nj}}{v_{nj}}, \quad (18)$$

where C_n is the number of noncyclic branched chains of degree of polymerization n, u_{nj} is the average number of ways a given noncyclic branched chain of degree of polymerization n can be transformed, by $j-n+1$ ring closures without breaking bonds, into different noncyclic polymers which can lead, through ring closures, to the same polymer of type (n,j).

The quantity C_n has been calculated by Stockmayer,[1]

who found

$$C_n=\frac{f^n(fn-n)!}{(fn-2n+2)!}. \tag{19}$$

A rigorous calculation of v_{nj} would require a more accurate analysis of the entire problem than is to be presented here. However, v_{nj} will be approximated by assuming each of the $j-n+1$ independent rings could have been formed by closure at any one of its links so that, if x is the number of links in the average ring, $v_{nj}=x^{j-n+1}$.[6] This approximation is inaccurate because a given bond may be a part of more than one ring, and the number of ways a cyclic structure can be formed depends upon the interrelation of the various rings as well as upon their number.

The quantity u_{nj} can be expressed in the form

$$u_{nj}=\frac{u_{nj}^{(1)}u_{nj}^{(2)}}{u_{nj}^{(3)}} \tag{20}$$

where $u_{nj}^{(1)}$ is the number of ways $j-n+1$ ends can be selected from the $nf-2n+2$ ends of a noncylic polymer of degree of polymerization n, or

$$u_{nj}^{(1)}=\frac{(nf-2n+2)!}{(j-n+1)!\,(nf-j-n+1)!}. \tag{21}$$

The factor $u_{nj}^{(2)}$ is the average number of ways $j-n+1$ chosen ends can be bonded to other ends within range, and $u_{nj}^{(3)}=2^{j-n+1}$ accounts for the fact that each ring closure can occur as a result of either member of a pair of ends being selected first. To evaluate $u_{nj}^{(2)}$, it is necessary to invoke the basic approximation of the present section, namely that each end of the noncyclic chain is assumed to have a constant number, σ, of ends within range for possible closure. The process associated with $u_{nj}^{(2)}$ may be considered stepwise. The first chosen end is assumed to have available to it for closure $\sigma(nf-n-j+1/nf-2n+2)$ ends, where the factor multiplying σ allows for the fact that the $n-j+1$ chosen ends are not eligible for bonding between each other, and may be regarded as evenly distributed throughout the polymer. After $y-1$ rings have been closed, the yth ring closure may be expected to be possible in $\sigma(nf-n-j-y+2/nf-2n+2)$ ways, where account is taken of the fact that $y-1$ additional ends have been excluded from further ring formation. By multiplying together the number of ways the $(j-n+1)$ ring closures can be performed, one obtains

$$u_{nj}^{(2)}=\left(\frac{\sigma}{nf-2n+2}\right)^{j-n+1}\frac{(nf-n-j+1)!}{(nf-2j)!}. \tag{22}$$

[6] "Independent" means that this number of ring closures is required to form a polymer of type (n,j), even though the actual number of rings may be much larger if rings have common bonds. The number of links x, is to be regarded as that effective ring size necessary to make v_{nj} an optimum approximation.

Combination of these factors leads to

$$u_{nj}=\frac{(nf-2n+2)!}{(j-n+1)!\,(nf-2j)!}\times\left(\frac{\sigma}{2(nf-2n+2)}\right)^{j-n+1}. \tag{23}$$

Inserting (19), (20), and (23) into (18), one may then find

$$w_{nj}=\frac{f^n(fn-n)!}{(j-n+1)!\,(nf-2j)!}\times\left(\frac{\sigma}{2x(nf-2n+2)}\right)^{j-n+1}. \tag{24}$$

As in the preceding section, form the generating function $\varphi(\xi,\eta)$, where φ is, as before, defined by Eq. (13), but with w_{nj} now given by expression (24). To facilitate the discussion, make the change of variable $r=j-n+1$. It will be noted that r is the number of independent rings in a polymer of type (n,j). Also, use Stirling's formula to approximate $(2r)!/r!(nf-2n+2)^r$ by $2^{\frac{1}{2}}(4re^{-1}/nf-2n+2)^r$. With these modifications,

$$\frac{M}{AV}=\varphi(\xi,\eta)=\sum_{n=1}^{\infty}\sum_{r=0}^{\leq\frac{1}{2}(nf-2n+2)}\times f^n\xi^n\eta^{r+n-1}\left(\frac{\sigma}{2x}\right)^r\left(\frac{(fn-n)!}{n!\,(fn-2n+2)!}\right)\times\left(\frac{(fn-2n+2)!}{(2r)!\,(fn-2n+2-2r)!}\right)\left(\frac{4e^{-1}r}{nf-2n+2}\right)^r. \tag{25}$$

Furthermore, N/AV and J/AV are given by expressions similar to (25) except for an additional factor in each summand, of n, and $r+n-1$, respectively.

VI. EVALUATION OF THE SUMS

Further progress requires the evaluation of the sums for M, N, and J. While the author has not succeeded in an exact summation of the series (25), it is nevertheless possible to obtain an asymptotic form for (25), valid in the limiting region where most of the important contribution to the sum over n arises from large n. Since in typical polymerizations, and for all polymer solutions near the gel point, the most important contribution is from n large relative to unity, such an asymptotic form will closely represent the behavior of $\varphi(\xi,\eta)$ in the region of primary physical interest.

By approximate methods discussed in detail in

Appendix 1, one may show that in the limit of large t,

$$\sum_{r=0}^{t/2} r^i y^r \frac{t!}{(2r)!\,(t-2r)!}\binom{r}{t}^r \sim \left(\frac{\bar{u}t}{2}\right)^i \frac{1}{2(1+\bar{u})^{\frac{1}{2}}}\left[\frac{e^{-\bar{u}/2}}{1-\bar{u}}\right]^t \quad (26)$$

where $\bar{u}$ and y are related by

$$y=\frac{2\bar{u}}{e(\bar{u}-1)^2}. \quad (27)$$

Applying the asymptotic form (26) with $i=0$ to the summation over r in Eq. (25), and using this result for each value of n, it may be seen that

$$\varphi(\xi,\eta)\sim g\sum_{n=1}^{\infty}\frac{(fn-n)!}{n!(fn-2n+2)!}\left\{f\xi\eta\left(\frac{e^{-\bar{u}/2}}{1-\bar{u}}\right)^{f-2}\right\}^n \quad (28)$$

where $y=(2\sigma/ex)\eta$ and

$$g=\frac{e^{-\bar{u}}}{2\eta(1+\bar{u})^{\frac{1}{2}}(1-\bar{u})^2}. \quad (29)$$

The summation in (28) is identical to a sum S_0 already evaluated by Stockmayer.[1] Inserting his result,

$$\varphi(\xi,\eta)\sim g\frac{\alpha\left(1-\frac{\alpha f}{2}\right)}{(1-\alpha)^2 f}, \quad (30)$$

where α is related to ξ, η by

$$\alpha(1-\alpha)^{f-2}=f\xi\eta\left(\frac{e^{-\bar{u}/2}}{1-\bar{u}}\right)^{f-2}. \quad (31)$$

It is now more convenient to regard α and $\bar{u}$ as the independent variables. Substituting Eq. (27) in (29), and using the relation between y and η, one may obtain a form for g involving $\bar{u}$ alone:

$$g=\left(\frac{\sigma}{2^{\frac{1}{2}}xe}\right)\frac{e^{1-\bar{u}}\cdot 2^{\frac{1}{2}}}{\bar{u}(1+\bar{u})^{\frac{1}{2}}}=\left(\frac{\sigma}{2^{\frac{1}{2}}xe}\right)g^*(\bar{u}). \quad (32)$$

Equation (25) then assumes the form

$$M=A'Vg^*(\bar{u})\frac{\alpha\left(1-\frac{\alpha f}{2}\right)}{(1-\alpha)^2 f} \quad (33)$$

where M is the total number of polymer molecules in the solution, and $A'=A(\sigma/2^{\frac{1}{2}}xe)$.

The series for N analogous to Eq. (25) may be treated in precisely the same manner, the only difference being that the sum corresponding to that of Eq. (28) contains an extra factor n, and is the sum S_1 of Stockmayer's paper.[1] The result is

$$N=A'Vg^*(\bar{u})\frac{\alpha}{(1-\alpha)^2 f}. \quad (34)$$

Finally, an expression for J is desired. Recalling that the sum analogous to (25) defining J contains an extra factor $n+r-1$, we are able to separate J into three sums, the first and third of which we have already evaluated. The second sum is performed in the same way, using this time Eq. (26) for $i=1$. The result is

$$J=A'Vg^*(\bar{u})\frac{\alpha}{2(1-\alpha)^2}[\alpha+\bar{u}(1-\alpha)]. \quad (35)$$

Equations (33) to (35) may be combined with Eq. (1) to give p, the extent of reaction. Thus,

$$p=\alpha+\bar{u}(1-\alpha). \quad (36)$$

By simultaneous solution of Eqs. (36) and (34), it may now be seen that specification of the extent of reaction and volume per molecule suffice to determine α and $\bar{u}$, with but one parameter A' describing ring formation.

VII. DISCUSSION

Let us first consider the various average degrees of polymerization and the criterion for gel formation. The number average, Z_n, is simply N/M or

$$Z_n=\frac{1}{1-\frac{\alpha f}{2}}. \quad (37)$$

while the weight average Z_w is

$$Z_w=\frac{A'V}{N}\sum_{n=1}^{\infty}\frac{n^2(fn-n)!}{n!(fn-2n+2)!}\left\{f\xi\eta\left(\frac{e^{-\bar{u}/2}}{1-\bar{u}}\right)^{f-2}\right\}^n, \quad (38)$$

which, by use of Stockmayer's sum S_2, can be reduced to

$$Z_w=\frac{1+\alpha}{1-(f-1)\alpha}. \quad (39)$$

Stockmayer showed that the sums S_0, S_1, and S_2 have a radius of convergence

$$\alpha_c=\frac{1}{f-1}, \quad (40)$$

and that S_0 and S_1 converge at $\alpha=\alpha_c$, but that S_2 does not.[1] Accordingly, when α approaches α_c, the weight average molecular weight becomes infinite while the number average does not, signifying the presence of infinite molecular weight material which is identified as gel.

Since the gel condition is independent of $\bar{u}$, the region of completely soluble polymer is that for which $\alpha<\alpha_c$, $0\leqslant\bar{u}\leqslant 1$, the latter condition, according to (27), covering the entire range $\eta\geqslant 0$.

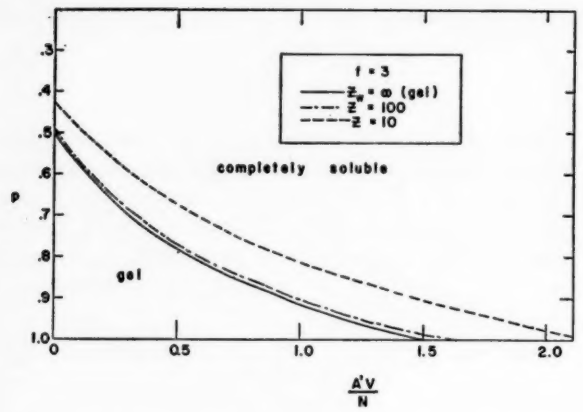

FIG. 1. Gelation as a function of extent of reaction, p, and volume, $A'V/N$. The broken curves indicate conditions for various weight average molecular weights.

It is apparent from the preceding two paragraphs that while α may not be indentified with p, as it is in the treatment of noncyclic polymers, it plays a role which might be characterized as an "effective p" in that α indicates the p which would be necessary in a noncyclizing system to reproduce the molecular weight distribution of the cyclizing system.

To ascertain the region of p and V which corresponds to gel, let us first consider conditions of complete reaction, $p=1$. Then by (36), $\bar{u}=1$, and since $g^*(1)=1$,

$$\frac{A'V}{N}=\frac{(1-\alpha)^2 f}{\alpha}, \quad (p=1), \tag{41}$$

an expression which shows that $A'V/N$ decreases from infinity to a critical value $A'V_c/N$ as α increases from 0 to α_c. Substituting from Eq. (40),

$$\frac{A'V_c}{N}=\frac{(f-2)^2 f}{f-1}. \tag{42}$$

Therefore, at volumes larger than V_c, it is possible to have soluble polymer of finite molecular weight, even at complete reaction, but at volumes of V_c or less, complete reaction will be accompanied by gelation. The parallelism should be noticed between the "critical volume" predicted by this approximate theory and the "condensation point" found by Jacobson and Stockmayer[5] in the treatment of linear systems with possible ring formation. Jacobson and Stockmayer's calculations showed that, at complete reaction, there was a volume such that at larger volumes the system consisted only of rings of finite size, but that at smaller volumes the system was not entirely made up of rings, but included a fraction composed of chains of infinite length.[7]

[7] Although Jacobson and Stockmayer only discussed calculations in detail for a system more complex than the analog of the system of this study, the behavior they describe is also shown by their calculations for the exactly analogous polymerization with $f=2$.

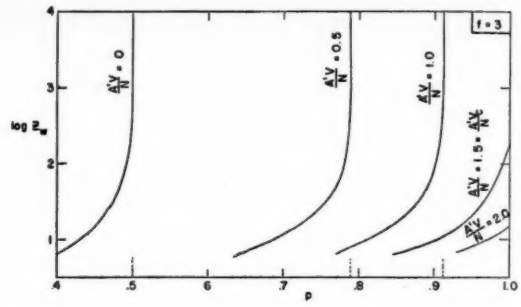

FIG. 2. Weight average molecular weight as a function of extent of reaction, p, at various volumes, $A'V/N$.

These infinite length chains are the linear analog of the gel observed below the volume V_c in the present theory.

It may be noticed that the equations of the present study do not reduce to Jacobson and Stockmayer's result for $f=2$, but rather predict the "critical volume" to be $V=0$. This discrepancy is primarily a result of the asymptotic formulation of the problem, which is not valid for $f=2$, because the series over r, rather than going to large values of r for large n, assumes only the values $r=0$, $r=1$, independently of n. In addition, the presence of symmetry numbers other than unity, which we neglect here, assumes importance in the linear systems.

Next, consider the limiting behavior at small V or small A'. This limit corresponds to the prohibition of ring formation and thus reduces to a type of polymerization already studied by Stockmayer. The limit may be achieved from the present formulation by allowing $A'V$ and $\bar{u}$ to simultaneously approach zero in such a way that the product $A'Vg^*(\bar{u})$ approaches a finite nonzero limit. Then p is simply equal to α, and gel formation occurs at

$$p=\alpha_c=\frac{1}{f-1}. \quad (A'V=0) \tag{43}$$

It is also possible to show that the distribution of molecular sizes reduces in this limit to a result identical to that of Stockmayer.

In intermediate cases where neither $p=1$ nor $V=0$, the system will contain or not contain a gel depending upon whether the value of α necessary to simultaneously satisfy (34) and (36) is greater than, or less than, α_c. Values of p and $A'V/N$ for various $\bar{u}$ when $\alpha=\alpha_c$ have been plotted, and a typical resulting curve for $f=3$ showing the regions where gelation should take place is exhibited in Fig. 1. Also shown in Fig. 1 are the values of p and $A'V/N$ corresponding to various Z_w in order to indicate the variation in weight average degree of polymerization with the experimental parameters.

Since it may be useful to know how rapidly the average degree of polymerization changes with extent

of reaction, curves have also been plotted in Fig. 2 for $f=3$ showing the relation between Z_w and p at various values of $A'V/N$. Note that for $V \leqslant V_c$, a definite Z_w is approached in the limit $p=1$. Just as in linear polymerizations, a choice of V only slightly larger than V_c is optimum for synthesizing large molecules, while smaller Z_w can be produced at complete reaction in more dilute solution.

VIII. ACKNOWLEDGMENTS

The author gratefully acknowledges indebtedness to Dr. H. Poritsky, for a valuable discussion on convergence questions, and to Dr. B. H. Zimm and Dr. J. H. Gibbs for suggestions and criticism.

APPENDIX I

This appendix is concerned with the asymptotic evaluation, for large t, of the sum given in Eq. (26) of the main text. Replacing the factorials of the sum on the left side of (26) by Stirling's formula, and replacing the sum by an equivalent integral with the aid of the leading term of the Euler-Maclaurin formula, it is possible to show that

$$B_i = \sum_{r=0}^{t/2} r^i y^r \frac{t!}{(2r)!(t-2r)!}\binom{r}{t}^r \sim \int_0^{t/2} dr r^i y^r \frac{t^{t+\frac{1}{2}}(r/i)^r}{(2\pi)^{\frac{1}{2}}(2r)^{2r+\frac{1}{2}}(t-2r)^{t-2r+\frac{1}{2}}} \quad \text{(A-1)}$$

where $i=0$ or 1.

Making the change of variable $2r/t=u$, the sum becomes, after some simplification,

$$B_i \sim \frac{(t/2)^{1+i}}{(2\pi t)^{\frac{1}{2}}} \int_0^1 \frac{du u^i}{u^{\frac{1}{2}}(1-u)^{\frac{1}{2}}} \left\{ \left(\frac{y}{2u}\right)^{u/2} (1-u)^{u-1} \right\}^t. \quad \text{(A-2)}$$

The integral of (A-2) is a form whose asymptotic expansion may be most conveniently evaluated by the method of steepest descents.[8] By suitable rearrangement, one may write

$$B_i \sim \frac{(t/2)^{1+i}}{(2\pi t)^{\frac{1}{2}}} 2\left[\left(\frac{y}{2\bar{u}}\right)^{\bar{u}/2}(1-\bar{u})^{\bar{u}-1}\right]^t \times \int_0^\infty df e^{-ft}\left(\frac{du}{df}\right)\frac{[u(f)]^{i-\frac{1}{2}}}{[1-u(f)]^{\frac{1}{2}}}, \quad \text{(A-3)}$$

where $\bar{u}$ is the value of u such that the expression in curly brackets in (A-2) is a maximum, and f and $u(f)$ are related by

$$e^{-f} = \frac{\left(\frac{y}{2u}\right)^{u/2}(1-u)^{u-1}}{\left(\frac{y}{2\bar{u}}\right)^{\bar{u}/2}(1-\bar{u})^{\bar{u}-1}}. \quad \text{(A-4)}$$

The approximation of the method of steepest descents consists of extending the limits of f to ∞ rather than only to the values of f when $u=1$ or 0. By suitable manipulation of (A-4), it is possible to express u as a power series in f whose leading terms are

$$u = \bar{u} + \left(\left[\frac{d^2 f}{du^2}\right]_{u=\bar{u}}\right)^{-\frac{1}{2}} f^{\frac{1}{2}} + \cdots. \quad \text{(A-5)}$$

Taking the derivative du/df from (A-5), and introducing (A-5) into (A-3), the desired asymptotic expansion may be found by term by term integration of (A-3). The validity of such a procedure has been demonstrated.[9] Upon substituting the value of d^2f/du^2 from (A-4), one may arrive at the result

$$B_i \sim \left(\frac{\bar{u}t}{2}\right)^i \frac{1}{2(1+\bar{u})^{\frac{1}{2}}}\left[\left(\frac{y}{2\bar{u}}\right)^{\bar{u}/2}(1-\bar{u})^{\bar{u}-1}\right]^t. \quad \text{(A-6)}$$

To complete the characterization of B_i, it remains to find $\bar{u}$. By direct differentiation of the expression in curly brackets of (A-2), one may obtain Eq. (27). Simplification of (A-6) may then be made by eliminating y with the aid of (27). The resulting expression is the right-hand side of Eq. (26).

[8] See, for example, E. T. Copson, *Theory of Functions of a Complex Variable* (Oxford University Press, New York, 1935), p. 330.

[9] G. N. Watson, Proc. London Math. Soc. (2), **17**, 133 (1918).

Non-Newtonian Viscosity of Solutions of Ellipsoidal Particles*

HAROLD A. SCHERAGA
Department of Chemistry, Cornell University, Ithaca, New York
(Received November 3, 1954)

The specific viscosity, and its dependence on velocity gradient, plays an important role in studies of the structure of macromolecules in dilute solution. A satisfactory theoretical interpretation of the non-Newtonian viscosity of solutions of ellipsoidal particles has been given by Kuhn and Kuhn, and also by Saito, who made use of Peterlin's distribution function for the orientation of particle axes in the streaming liquid and calculated the energy dissipation due to both the hydrodynamic orientation and the Brownian motion. Also, a theory for the non-Newtonian viscosity of solutions of rod-like particles has been developed by Kirkwood. These theories involve extensive computations which have been carried out here with the aid of a computing machine by expressing Saito's results in terms of Legendre coefficients previously evaluated in the related problem of double refraction of flow. As a result, data are available for the dependence of the viscosity factor ν on axial ratio and on the parameter α, where $\alpha=G/\Theta$, G being the velocity gradient in $\sec^{-1}$ and Θ being the rotary diffusion constant in $\sec^{-1}$. With these data it will be possible to determine the rotary diffusion constants of ellipsoidal particles from the non-Newtonian viscosity of their solutions, and also to correct viscosity measurements to zero velocity gradient in order to obtain the intrinsic viscosity. Data are also included for the evaluation of Θ from the dependence of ν at $\alpha=0$ on the frequency of periodic shear waves.

INTRODUCTION

THE interpretation of the hydrodynamic properties of solutions of macromolecules has usually been based upon a knowledge of the behavior of reasonable models under the same experimental conditions. If the macromolecule does not possess too much flexibility, as seems to be the case for proteins, the rigid ellipsoid of revolution appears to be a good model. Measurements of two independent quantities permit one to compute the size and shape of a rigid ellipsoid which has the same hydrodynamic properties as the protein.[1] One of these quantities is the intrinsic viscosity, obtainable from the specific viscosity which, in general, depends on the velocity gradient in the flowing solution. The dependence of the viscosity of solutions on the size and shape of the dissolved ellipsoidal particles and on the velocity gradient has been treated by several investigators.[2–8] The dependence on the velocity gradient involves computational problems which have been resolved in the present work with the aid of a computing machine.[9] For this purpose the theory of Saito,[7] making use of the hydrodynamic treatment of Jeffery[2] and the distribution function of Peterlin,[3] is easiest[10] to put into convenient form for computation. The calculation is very similar to that previously carried out for the related problem of double refraction of flow[11] with the aid of the Mark I computer of the Harvard Computation Laboratory, and makes use of some of the results of the previous computations. As a result, data are available for the dependence of the viscosity factor on axial ratio and on velocity gradient. With these data it will be possible to correct experimental measurements to zero velocity gradient to obtain the intrinsic viscosity which is easily related to the particle size and shape, and also to determine the rotary diffusion constants of asymmetrical particles from the dependence of the viscosity on velocity gradient. Thus, such viscosity experiments will provide two hydrodynamic quantities useful in studies of the configurations of proteins in dilute solution.[1]

EXPERIMENTAL OBSERVATION

If a viscous liquid is maintained between two parallel planes of area A, one of which moves relative to the other with a velocity V, the velocity gradient in the liquid will be $G=dV/dr$ in $\sec^{-1}$, where r is taken in a direction normal to the two planes. The viscosity coefficient η_0 of the liquid is a measure of the internal friction which determines the value of the tangential force $\mathfrak{F}$ required to maintain the velocity gradient G between the planes. According to Newton,

$$\mathfrak{F}=\eta_0 GA. \tag{1}$$

This situation is most easily realized experimentally if the liquid is placed in the annular gap between two concentric cylinders of a Couette-type apparatus, and one of the cylinders rotated. If the gap is large G

* This work was supported by the Office of Naval Research and by the National Science Foundation.

[1] H. A. Scheraga and L. Mandelkern, J. Am. Chem. Soc. **75**, 179 (1953).
[2] G. B. Jeffery, Proc. Roy. Soc. (London), **A102**, 161 (1922–23).
[3] A. Peterlin, Z. Physik **111**, 232 (1938).
[4] R. Simha, J. Phys. Chem. **44**, 25 (1940).
[5] W. Kuhn and H. Kuhn, Helv. Chim. Acta **28**, 97 (1945).
[6] J. G. Kirkwood, Rec. trav. Chim. **68**, 649 (1949); J. G. Kirkwood and P. L. Auer, J. Chem. Phys. **19**, 281 (1951).
[7] N. Saito, J. Phys. Soc. Japan **6**, 297 (1951).
[8] B. H. Zimm (private communication) has obtained an asymptotic solution for ellipsoidal particles at very high velocity gradients, and Kirkwood (private communication) has obtained a solution for thin rods as a function of velocity gradient.
[9] These calculations were carried out at the Cornell Computing Center with the aid of an IBM card-programmed calculator under the direction of R. Lesser.
[10] Kuhn and Kuhn (see reference 5) have also given a complete treatment for the dependence of viscosity on velocity gradient for dilute solutions of ellipsoidal particles. See their Eqs. (73) and (74). The equivalence of their treatment and that of Saito (see reference 7) and Kirkwood (see reference 6) has been demonstrated by Saito and Sugita [J. Phys. Soc. Japan **7**, 554 (1952)].
[11] Scheraga, Edsall, and Gadd, J. Chem. Phys. **19**, 1101 (1951); Annals of the Computation Laboratory of Harvard University, **26**, 219 (1951).

varies with r, but if it is small compared with the cylinder radius, the behavior of G approaches that for the ideal case of two parallel planes of infinite extent, where it is constant. The determination of η_0 in the Couette apparatus is carried out by rotating the outer cylinder (the inner one being suspended freely by a torsion wire) and measuring the torque transmitted by the liquid from the outer to the inner cylinder.[12]

If η_0 is independent of G the liquid is said to be Newtonian in its viscous behavior; if η_0 depends on G it is said to be non-Newtonian. If G exceeds a certain critical value in a given experiment the flow becomes turbulent; we are concerned here only with values of G below this critical region so that the flow is laminar. Most pure liquids in laminar flow exhibit Newtonian behavior whereas many solutions of macromolecules are non-Newtonian. Dilute solutions of relatively small and symmetrical molecules like serum albumin approach Newtonian behavior whereas dilute solutions of large asymmetrical molecules like tobacco mosaic virus are non-Newtonian.

The viscosity coefficient defined in Eq. (1) is also a measure of the dissipation of energy in the flowing liquid, the amount of work done in overcoming frictional resistance per unit time per unit volume being $G^2\eta_0$. When large particles are suspended in a flowing liquid made up of small molecules, there is an increased energy dissipation which depends on the size and shape of the dissolved particles.[13] The total energy dissipation per unit time per unit volume[14] in the *solution* is $G^2\eta$.

$$G^2\eta = G^2\eta_0 + n\left\langle \frac{dW}{dt} \right\rangle_{Av}, \tag{2}$$

where η is the viscosity coefficient of the solution, η_0 is that for the pure solvent, n is the number of particles per unit volume, and $\langle dW/dt \rangle_{Av}$ is the average increment in rate of energy dissipation per unit volume due to the presence of a single dissolved particle; $G^2\eta_0$ is that part of the energy dissipation due to the solvent when present alone and is assumed to be the same even when the particles are dissolved in the solvent. As a result, η will be greater than η_0. If each ellipsoidal particle has a volume of $v = 4\pi ab^2/3$ where a is the semiaxis of revolution and b is the equatorial radius then[14]

$$\left\langle \frac{dW}{dt} \right\rangle_{Av} = G^2\eta_0 v\nu, \tag{3}$$

where ν is a factor dependent on the shape of the particle. Inserting Eq. (3) in Eq. (2) we obtain[13]

$$\lim_{nv \to 0} \frac{\eta - \eta_0}{nv\eta_0} = \nu, \tag{4}$$

where nv is the volume concentration of the particles in the solution. If, in turn, the data are extrapolated to zero velocity gradient, then $\nu = [\eta]_v$ where $[\eta]_v$ is the intrinsic viscosity for volume concentration. Since concentration is usually expressed as c in g/100 cc and the quantity computed for a protein of molecular weight M is the equivalent hydrodynamic volume V_e, the working form of Eq. (4) will be

$$[\eta] = \lim_{\substack{c \to 0 \\ G \to 0}} \frac{\eta - \eta_0}{\eta_0 c} = \left(\frac{N}{100}\right)\left(\frac{V_e}{M}\right)\nu, \tag{5}$$

where N is Avogadro's number and $[\eta]$ is the intrinsic viscosity for concentration in g/100 cc. Since the treatment here is confined to the rigid ellipsoid of revolution model, we are concerned only with the quantity ν for an ellipsoid of volume v. In the special case where the ellipsoid becomes a sphere, ν takes on the Einstein value of 2.5 and is independent of G; such a solution exhibits Newtonian viscous behavior. If the dissolved particles are asymmetrical, then the solution will exhibit non-Newtonian viscosity wherein ν will be larger than 2.5 at zero G and will decrease with increasing G, i.e., $\langle dW/dt \rangle_{Av}$ decreases as the velocity gradient is increased due to increasing orientation of the asymmetrical particles in the streaming liquid. For any velocity gradient the average increment in rate of energy dissipation per unit volume, due to the presence of the particles, is given by Eq. (3) where ν depends on G and on the axial ratio[14] $p = a/b$. Therefore the factor ν is determinable from a knowledge of $\langle dW/dt \rangle_{Av}$ as a function of G for particles of a given size and shape in a solvent of viscosity coefficient η_0.

THEORY

The evaluation of the increment in energy dissipation is based on the theory that a solution of ellipsoidal particles in laminar flow is in an equilibrium steady state dependent upon the magnitude of two opposing forces, one arising from the velocity gradient which tends to orient the particles in the direction of the stream lines, the other due to the Brownian motion which tends to produce a random orientation. The Brownian motion may be characterized by a rotary diffusion constant Θ (in $\sec^{-1}$) which depends on the volume and shape of the ellipsoid.[15] To evaluate ν the distribution function $F(\vartheta, \varphi, t)$ for the orientation of the major axes of the

[12] For experimental details and results of viscosity measurements see A. E. Alexander and P. Johnson, *Colloid Science* (Oxford University Press, New York, 1949), Chap. XIII.

[13] In the treatment presented here it is assumed that there is no interaction between dissolved particles and, therefore, no increment in energy dissipation due to such interactions. This situation is realized experimentally by making viscosity measurements at various concentrations and extrapolating to infinite dilution.

[14] It should be pointed out that the notation for p differs among various authors. For example, several authors (see references 1 and 15) have defined p as b/a where a and b have the same meaning as used here.

[15] F. Perrin, J. phys. radium **5**, 497 (1934).

particles at any time at a given value of G must first be computed.[16] This has been carried out by Peterlin[3] using Jeffery's[2] hydrodynamic treatment. Once the distribution function is known then $\langle dW/dt\rangle_{Av}$ may be evaluated for any distribution according to Saito's theory.[7,10] We shall thus outline the Jeffery-Peterlin-Saito treatment wherein the quantities required for the evaluation of ν have been obtained by means of a computing machine.

The distribution function for ellipsoidal particles suspended in a continuous liquid medium under the condition of laminar flow obeys the general diffusion equation

$$\frac{\partial F}{\partial t}=\Theta\Delta F-\mathrm{div}(F\omega) \tag{6}$$

where Δ is the Laplacian operator and ω is the angular velocity of the rotating ellipsoid due to the hydrodynamic forces and has been computed by Jeffery as a function of G and R, where

$$R=\frac{p^2-1}{p^2+1}. \tag{7}$$

For a prolate ellipsoid $a>b$, whereas for an oblate one $a<b$. Therefore, $R=1$ for an infinitesimally thin rod, 0 for a sphere, and -1 for an infinitesimally flat disk.

If the particles are relatively small (no dimension greater than 10 000 A), then within a very short time after initiation of the rotation of the cylinder a steady state is reached in which $\partial F/\partial t=0$. For the steady state Peterlin,[3] making use of Jeffery's results for ω, expressed the solution of the diffusion equation in terms of slowly converging series of spherical harmonics.

$$F=\sum_{j=0}^{\infty}R^j\Big[\frac{1}{2}\sum_{n=0}^{j}a_{n0,\,j}P_{2n}+\sum_{n=1}^{j}\sum_{m=1}^{n}(a_{nm,\,j}\cos 2m\varphi+b_{nm,\,j}\sin 2m\varphi)P_{2n}{}^{2m}\Big]. \tag{8}$$

The Legendre coefficients $a_{nm,\,j}$ and $b_{nm,\,j}$ are functions of the parameter $\alpha=G/\Theta$. P_{2n} are spherical functions of $\cos\vartheta$ and $P_{2n}{}^{2m}$ are their derivatives of order $2m$. Recurrence relations are available[3,11] for computation of these Legendre coefficients. Evaluation of these coefficients gives F as a function of α and R. This distribution function has been used previously for flow birefringence calculations[11] based on the theory of Peterlin and Stuart.[17]

Using this distribution function for the particle orientation as a function of α, Peterlin[3] computed ν by taking into account the energy dissipation due only to the rotation of the particle in the hydrodynamic field. His results were at variance with those of Simha[4] who took into account the energy dissipation arising also from the Brownian motion. Simha's treatment was applied only to the limiting case of $\alpha=0$ where the particles have random orientation due to the Brownian motion and can be considered as rotating with uniform angular velocity. A complete theory for ν as a function of α was finally obtained by Kirkwood and Auer[6] for rods, and by Kuhn and Kuhn,[5] and also by Saito,[7] for ellipsoids.[18] These theories consider that Peterlin's distribution function F correctly describes the orientation of ellipsoidal particles, and that the increment in energy dissipation, $\langle dW/dt\rangle_{Av}$, contains contributions not only from the hydrodynamic orientation but also from the Brownian motion.[19] The result obtained by Saito[7] is

$$\nu=(J+K-L)\int F\sin^4\vartheta\sin^2 2\varphi d\Omega+L\int F\sin^2\vartheta d\Omega+M\int F\cos^2\vartheta d\Omega+\frac{N}{\alpha}\int F\sin^2\vartheta\sin 2\varphi d\Omega \tag{9}$$

where the coefficients J, K, L, M, N depend *only* on the axial ratio p of the ellipsoid[20] and are defined as follows:

$$J=\frac{1}{ab^2}\frac{\alpha_0''}{2b^2\alpha_0'\beta_0''},\qquad K=\frac{1}{ab^2}\frac{1}{2b^2\alpha_0'},$$
$$L=\frac{1}{ab^2}\frac{2}{\beta_0'(a^2+b^2)},\qquad M=\frac{1}{ab^2}\frac{1}{b^2\alpha_0'},$$
$$N=\frac{6}{ab^2}\frac{a^2-b^2}{a^2\alpha_0+b^2\beta_0}. \tag{10}$$

[16] See reference 11 for the definition of the coordinate system in the Couette cylinder apparatus.

[17] A. Peterlin and H. A. Stuart, Z. Physik **112**, 1 (1939).

[18] This problem was discussed extensively at the International Rheological Congress, Scheveningen (Holland), 1948, the Proceedings of which have been published.

[19] For further justification that there is a contribution to the energy dissipation from the Brownian motion see Kuhn and Kuhn (reference 5) and also Saito and Sugita (reference 10). An apparent disagreement over the effect of the rotary Brownian motion on the viscosity of solutions of rod-like macromolecules was reported in the discussion following Kirkwood's paper [J. Polymer Sci. **12**, 1 (1954)] which was presented at the Uppsala Symposium on Macromolecules. This disagreement has been resolved by Saito [J. Polymer Sci. **14**, 212 (1954)].

[20] While Eqs. (10) appear to be functions of a and b, rather than of p, the substitution of Eqs. (12) into Eqs. (10) leads to a dependence on only the *ratio* a/b.

The quantities α_0, α_0', α_0'', β_0, β_0', β_0'' are functions of a and b defined by Jeffery.[2]

$$\alpha_0=\int_0^\infty \frac{dx}{(a^2+x)^{\frac{1}{2}}(b^2+x)},$$

$$\beta_0=\int_0^\infty \frac{dx}{(a^2+x)^{\frac{1}{2}}(b^2+x)^2},$$

$$\alpha_0'=\int_0^\infty \frac{dx}{(a^2+x)^{\frac{1}{2}}(b^2+x)^3},$$

$$\beta_0'=\int_0^\infty \frac{dx}{(a^2+x)^{\frac{1}{2}}(b^2+x)^2},$$

$$\alpha_0''=\int_0^\infty \frac{xdx}{(a^2+x)^{\frac{1}{2}}(b^2+x)^3},$$

$$\beta_0''=\int_0^\infty \frac{xdx}{(a^2+x)^{\frac{1}{2}}(b^2+x)^2}. \tag{11}$$

Evaluation of these integrals gives

$$\alpha_0=\frac{1}{b^3(p^2-1)}\left\{-\frac{2}{p}-A\right\},$$

$$\beta_0=\frac{1}{b^3(p^2-1)}\left\{p+\frac{A}{2}\right\},$$

$$\alpha_0'=\frac{p^4}{4a^3b^2(p^2-1)^2}\left\{(2p^2-5)-\frac{3A}{2p}\right\},$$

$$\beta_0'=\frac{2p^2}{a^3b^2(p^2-1)^2}\left\{1+\frac{p^2}{2}+\frac{3pA}{4}\right\}, \tag{12}$$

$$\alpha_0''=\frac{2p^2}{ab^2(p^2-1)^2}\left\{\frac{p^2}{4}+\frac{1}{8}+\frac{(4p^2-1)}{16p}A\right\},$$

$$\beta_0''=\frac{2p^2}{ab^2(p^2-1)^2}\left\{-\frac{3}{2}-\frac{(2p^2+1)}{4p}A\right\},$$

where

$$A=\frac{1}{(p^2-1)^{\frac{1}{2}}}\ln\frac{p-(p^2-1)^{\frac{1}{2}}}{p+(p^2-1)^{\frac{1}{2}}} \quad \text{for prolate ellipsoids } (p>1)$$

$$=\frac{-2\arccos p}{(1-p^2)^{\frac{1}{2}}} \quad \text{for oblate ellipsoids } (p<1).$$

The integrals in Eq. (9) represent mean values of the given trigonometric functions which may be expressed in terms of spherical harmonics and evaluated after F is known.

$$\langle\sin^4\vartheta\sin^2 2\varphi\rangle_{Av}$$

$$=\int F\left[\frac{4}{15}P_0-\frac{8}{21}P_2+\frac{4}{35}P_4-\frac{\cos 4\varphi}{210}P_4^4\right]d\Omega$$

$$=\frac{4}{15}\left[1+4\pi\sum_{j=1}^{\infty}R^j\left(-\frac{a_{10,j}}{7}+\frac{a_{20,j}}{42}-40a_{22,j}\right)\right]. \tag{13}$$

$$\langle\cos^2\vartheta\rangle_{Av}$$

$$=\int F[\tfrac{1}{3}P_0+\tfrac{2}{3}P_2]d\Omega$$

$$=\frac{1}{3}\left[1+\frac{4\pi}{5}\sum_{j=1}^{\infty}R^j a_{10,j}\right]. \tag{14}$$

$$\langle\sin^2\vartheta\rangle_{Av}$$

$$=1-\langle\cos^2\vartheta\rangle_{Av}. \tag{15}$$

$$\langle\sin^2\vartheta\sin 2\varphi\rangle_{Av}$$

$$=\int F\left[\frac{\sin 2\varphi}{3}P_2^2\right]d\Omega$$

$$=\frac{16\pi}{5}\sum_{j=1}^{\infty}R^j b_{11,j}. \tag{16}$$

Whereas a complete set of Legendre coefficients $a_{nm,j}$ and $b_{nm,j}$ would be required to determine the distribution function F, it can be seen from Eqs. (13) to (16) that, after integration, the only ones which are required for the evaluation of ν are $a_{10,j}$, $a_{20,j}$, $a_{22,j}$, $b_{11,j}$.

RESULTS AND DISCUSSION

As α approaches zero Eq. (9) reduces to the form

$$\nu=r-s\alpha^2\cdots \tag{17}$$

where r and s are constants; i.e., ν shows a quadratic dependence on α with a horizontal tangent at $\alpha=0$.[5,7] As α increases, the complete solution for ν as a function of α in Eq. (9) is obtainable by evaluation of the coefficients $a_{10,j}$, $a_{20,j}$, $a_{22,j}$, $b_{11,j}$ of Eqs. (13) to (16). These coefficients have all been previously computed[11] for values of α up to 200 in connection with the related problem of double refraction of flow. As reported previously,[11] a sufficient number of j-values required to attain the limiting values of the summations appearing in Eqs. (13) to (16) was obtained for $\alpha\leqq 60$. However, for $\alpha>60$, the additional j-values required could not be obtained because of the limited internal storage capacity of the Mark I computer. Therefore, no results are reported here for $\alpha>60$. For $\alpha\leqq 60$ the values obtained are probably accurate to well within 1%.[21]

[21] See the Appendix and also reference 11 for some discussion of the convergence of these series.

TABLE I. Prolate ellipsoids; ν as a function of α for various axial ratios, p.

α \ p	1	2	3	4	5	6	7	8	9	10	12	14	16	18	20	25	50	100	300
0.00	2.500	2.908	3.685	4.663	5.806	7.099	8.533	10.10	11.80	13.63	17.67	22.19	27.18	32.63	38.53	55.19	176.8	593.7	4279
0.25	2.500	2.907	3.683	4.661	5.802	7.094	8.526	10.09	11.79	13.62	17.65	22.17	27.15	32.60	38.49	55.13	176.6	593.0	4274
0.50	2.500	2.906	3.679	4.653	5.791	7.078	8.506	10.07	11.76	13.59	17.60	22.10	27.07	32.50	38.37	54.96	176.0	591.0	4260
0.75	2.500	2.903	3.672	4.641	5.773	7.053	8.474	10.03	11.71	13.53	17.52	22.00	26.94	32.34	38.18	54.68	175.1	587.7	4235
1.00	2.500	2.899	3.663	4.624	5.748	7.019	8.429	9.973	11.65	13.45	17.41	21.85	26.76	32.12	37.91	54.29	173.8	583.2	4202
1.25	2.500	2.895	3.651	4.604	5.717	6.977	8.374	9.904	11.56	13.34	17.28	21.68	26.54	31.84	37.59	53.81	172.1	577.6	4161
1.50	2.500	2.890	3.637	4.579	5.681	6.927	8.310	9.823	11.46	13.23	17.11	21.47	26.28	31.53	37.21	53.25	170.3	571.1	4113
1.75	2.500	2.884	3.621	4.552	5.640	6.872	8.237	9.732	11.35	13.09	16.94	21.24	25.98	31.17	36.78	52.62	168.1	563.8	4059
2.00	2.500	2.877	3.604	4.522	5.596	6.811	8.158	9.633	11.23	12.95	16.74	20.98	25.66	30.78	36.31	51.93	165.8	555.8	4000
2.25	2.500	2.871	3.586	4.490	5.548	6.746	8.074	9.528	11.10	12.80	16.53	20.71	25.32	30.36	35.81	51.20	163.4	547.4	3938
2.50	2.500	2.863	3.566	4.457	5.499	6.678	7.986	9.418	10.97	12.64	16.31	20.43	24.97	29.93	35.29	50.44	160.8	538.5	3873
3.00	2.500	2.848	3.526	4.387	5.396	6.537	7.804	9.190	10.69	12.31	15.86	19.84	24.24	29.03	34.22	48.86	155.5	520.3	3738
3.50	2.500	2.832	3.485	4.316	5.291	6.395	7.619	8.958	10.41	11.97	15.41	19.25	23.49	28.12	33.13	47.26	150.1	501.8	3602
4.00	2.500	2.816	3.444	4.246	5.188	6.254	7.437	8.731	10.13	11.64	14.96	18.67	22.77	27.24	32.07	45.70	144.9	483.8	3470
4.50	2.500	2.801	3.405	4.179	5.089	6.119	7.263	8.514	9.868	11.32	14.53	18.12	22.07	26.38	31.05	44.21	139.9	466.6	3343
5.00	2.500	2.787	3.367	4.115	4.995	5.991	7.097	8.307	9.617	11.03	14.12	17.59	21.41	25.58	30.09	42.80	135.2	450.3	3223
6.00	2.500	2.760	3.299	3.999	4.824	5.759	6.797	7.933	9.162	10.48	13.39	16.64	20.22	24.12	28.35	40.24	126.6	421.0	3007
7.00	2.500	2.738	3.240	3.897	4.675	5.558	6.537	7.608	8.768	10.01	12.75	15.82	19.19	22.87	26.84	38.04	119.2	395.7	2822
8.00	2.500	2.718	3.189	3.810	4.547	5.383	6.312	7.328	8.427	9.608	12.21	15.11	18.30	21.78	25.55	36.14	112.9	374.0	2663
9.00	2.500	2.702	3.145	3.734	4.435	5.232	6.117	7.085	8.132	9.257	11.73	14.49	17.53	20.85	24.42	34.50	107.5	355.3	2527
10.00	2.500	2.688	3.107	3.668	4.338	5.100	5.947	6.872	7.874	8.950	11.32	13.96	16.86	20.03	23.45	33.07	102.7	339.1	2408
12.50	2.500	2.661	3.031	3.536	4.143	4.834	5.603	6.444	7.355	8.332	10.48	12.88	15.51	18.38	21.48	30.21	93.19	306.7	2171
15.00	2.500	2.642	2.975	3.435	3.989	4.623	5.329	6.101	6.936	7.833	9.804	12.00	14.42	17.05	19.90	27.89	85.54	280.7	1983
17.50	2.500	2.629	2.934	3.361	3.880	4.476	5.139	5.866	6.652	7.496	9.350	11.42	13.69	16.17	18.84	26.34	80.43	263.3	1856
20.00	2.500	2.619	2.900	3.300	3.788	4.349	4.974	5.660	6.402	7.199	8.949	10.90	13.05	15.38	17.90	24.98	75.93	248.0	1746
22.50	2.500	2.611	2.874	3.250	3.712	4.245	4.839	5.491	6.198	6.956	8.621	10.48	12.52	14.74	17.13	23.86	72.28	235.7	1657
25.00	2.500	2.605	2.852	3.208	3.647	4.155	4.723	5.346	6.021	6.745	8.337	10.11	12.06	14.18	16.47	22.90	69.12	225.0	1580
30.00	2.500	2.597	2.819	3.142	3.545	4.012	4.536	5.112	5.736	6.406	7.878	9.520	11.32	13.29	15.40	21.35	64.05	207.9	1457
35.00	2.500	2.591	2.795	3.092	3.465	3.900	4.389	4.927	5.511	6.138	7.517	9.054	10.74	12.58	14.56	20.12	60.39	194.5	1361
40.00	2.500	2.587	2.777	3.053	3.401	3.809	4.269	4.776	5.327	5.918	7.220	8.671	10.27	12.00	13.87	19.12	56.80	183.6	1283
45.00	2.500	2.584	2.763	3.021	3.348	3.733	4.167	4.646	5.167	5.728	6.960	8.336	9.847	11.49	13.26	18.24	53.94	174.0	1214
50.00	2.500	2.582	2.752	2.995	3.303	3.667	4.078	4.533	5.028	5.560	6.732	8.039	9.477	11.04	12.73	17.46	51.40	165.5	1154
60.00	2.500	2.579	2.736	2.955	3.232	3.560	3.933	4.345	4.794	5.278	6.344	7.535	8.845	10.27	11.81	16.12	47.04	151.0	1050

From Eq. (7) it can be seen that $R(p)=-R(1/p)$. This transformation from prolate to oblate does not affect the summations in Eqs. (13) to (15) since these a-coefficients have nonzero values only for even powers of j. However, the b-coefficient in Eq. (16) has nonzero values only for odd powers of j. Therefore, the contribution of this term to ν in Eq. (9) is of opposite sign for prolate and oblate ellipsoids (as far as the effect of R^j

TABLE II. Oblate ellipsoids; ν as a function of α for various axial ratios, p.

α \ $1/p$	1	2	3	4	5	6	7	8	9	10	12	14	16	18	20	25	50	100	300
0.00	2.500	2.854	3.431	4.059	4.708	5.367	6.032	6.700	7.371	8.043	9.391	10.74	12.10	13.45	14.80	18.19	35.16	69.10	204.9
0.25	2.500	2.854	3.430	4.058	4.706	5.365	6.029	6.697	7.367	8.039	9.386	10.73	12.09	13.44	14.79	18.18	35.13	69.06	204.8
0.50	2.500	2.853	3.427	4.053	4.700	5.357	6.019	6.686	7.354	8.025	9.369	10.72	12.07	13.42	14.77	18.15	35.06	68.91	204.3
0.75	2.500	2.850	3.422	4.045	4.689	5.344	6.004	6.668	7.334	8.002	9.341	10.68	12.03	13.37	14.72	18.09	34.95	68.68	203.6
1.00	2.500	2.847	3.415	4.034	4.675	5.326	5.983	6.643	7.306	7.971	9.304	10.64	11.98	13.32	14.66	18.01	34.79	68.36	202.7
1.25	2.500	2.844	3.406	4.021	4.657	5.304	5.956	6.613	7.272	7.933	9.257	10.59	11.92	13.25	14.58	17.91	34.59	67.97	201.5
1.50	2.500	2.839	3.396	4.005	4.636	5.278	5.926	6.577	7.231	7.887	9.203	10.52	11.84	13.16	14.49	17.80	34.36	67.51	200.1
1.75	2.500	2.834	3.384	3.988	4.613	5.249	5.891	6.537	7.186	7.837	9.141	10.45	11.76	13.07	14.38	17.67	34.10	66.99	198.6
2.00	2.500	2.829	3.371	3.968	4.587	5.217	5.853	6.493	7.136	7.781	9.074	10.37	11.67	12.97	14.27	17.52	33.82	66.42	196.9
2.25	2.500	2.823	3.358	3.948	4.560	5.183	5.813	6.447	7.083	7.722	9.003	10.29	11.57	12.86	14.15	17.37	33.51	65.82	195.0
2.50	2.500	2.817	3.344	3.926	4.531	5.147	5.770	6.398	7.028	7.660	8.928	10.20	11.47	12.75	14.02	17.22	33.20	65.18	193.1
3.00	2.500	2.804	3.314	3.881	4.471	5.073	5.682	6.296	6.912	7.531	8.772	10.02	11.26	12.51	13.76	16.89	32.54	63.87	189.2
3.50	2.500	2.790	3.283	3.834	4.410	4.997	5.592	6.192	6.795	7.399	8.613	9.830	11.05	12.27	13.49	16.55	31.87	62.53	185.2
4.00	2.500	2.777	3.253	3.788	4.349	4.922	5.503	6.089	6.678	7.269	8.456	9.647	10.84	12.03	13.23	16.22	31.21	61.20	181.2
4.50	2.500	2.764	3.224	3.744	4.290	4.850	5.417	5.990	6.566	7.144	8.304	9.469	10.64	11.80	12.97	15.90	30.57	59.92	177.4
5.00	2.500	2.751	3.196	3.701	4.234	4.781	5.335	5.895	6.458	7.024	8.159	9.299	10.44	11.59	12.73	15.60	29.96	58.70	173.7
6.00	2.500	2.729	3.144	3.623	4.131	4.653	5.184	5.720	6.260	6.803	7.893	8.987	10.08	11.18	12.28	15.04	28.84	56.46	167.0
7.00	2.500	2.709	3.099	3.555	4.040	4.541	5.050	5.566	6.086	6.608	7.657	8.712	9.769	10.83	11.89	14.54	27.85	54.48	161.0
8.00	2.500	2.692	3.060	3.494	3.960	4.442	4.933	5.430	5.932	6.436	7.450	8.469	9.490	10.51	11.54	14.11	26.97	52.73	155.8
9.00	2.500	2.678	3.026	3.442	3.890	4.354	4.829	5.310	5.796	6.284	7.266	8.254	9.244	10.24	11.23	13.72	26.20	51.19	151.2
10.00	2.500	2.666	2.996	3.395	3.827	4.277	4.737	5.204	5.675	6.149	7.103	8.062	9.025	9.990	10.96	13.38	25.51	49.82	147.1
12.50	2.500	2.642	2.936	3.300	3.699	4.117	4.546	4.983	5.424	5.868	6.764	7.665	8.570	9.477	10.39	12.66	24.08	46.96	138.5
15.00	2.500	2.626	2.891	3.225	3.597	3.988	4.390	4.801	5.217	5.636	6.482	7.334	8.190	9.049	9.909	12.07	22.89	44.57	131.3
17.50	2.500	2.614	2.856	3.169	3.520	3.892	4.276	4.669	5.066	5.468	6.279	7.096	7.918	8.742	9.568	11.64	22.03	42.86	126.2
20.00	2.500	2.605	2.829	3.123	3.455	3.809	4.176	4.552	4.933	5.319	6.097	6.883	7.674	8.467	9.262	11.26	21.27	41.33	121.6
22.50	2.500	2.598	2.807	3.084	3.400	3.739	4.091	4.453	4.820	5.192	5.944	6.703	7.467	8.234	9.002	10.93	20.62	40.03	117.7
25.00	2.500	2.593	2.789	3.051	3.352	3.677	4.017	4.365	4.720	5.079	5.806	6.541	7.281	8.023	8.768	10.64	20.03	38.86	114.2
30.00	2.500	2.585	2.760	2.998	3.275	3.577	3.894	4.221	4.554	4.893	5.579	6.273	6.973	7.676	8.381	10.15	19.06	36.91	108.4
35.00	2.500	2.580	2.740	2.957	3.215	3.497	3.795	4.104	4.420	4.741	5.393	6.054	6.721	7.391	8.064	9.753	18.24	35.32	103.60
40.00	2.500	2.577	2.724	2.925	3.165	3.431	3.712	4.005	4.306	4.612	5.235	5.867	6.505	7.147	7.792	9.411	17.57	33.94	99.50
45.00	2.500	2.574	2.712	2.899	3.124	3.375	3.643	3.922	4.209	4.501	5.098	5.705	6.318	6.935	7.555	9.114	16.97	32.75	95.92
50.00	2.500	2.572	2.703	2.878	3.090	3.327	3.581	3.848	4.122	4.403	4.975	5.559	6.149	6.743	7.341	8.844	16.43	31.66	92.65
60.00	2.500	2.570	2.690	2.846	3.036	3.251	3.483	3.727	3.980	4.240	4.772	5.316	5.867	6.423	6.982	8.391	15.51	29.82	87.15

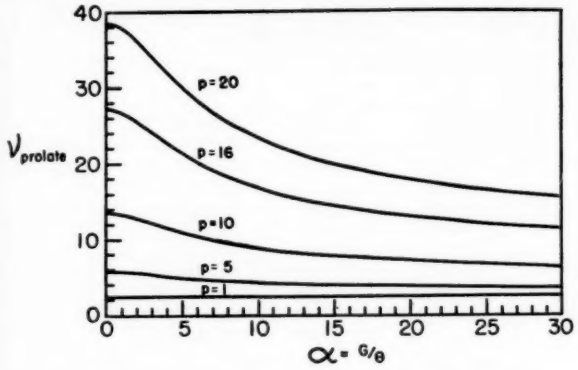

FIG. 1. Dependence of ν on α for prolate ellipsoids of various axial ratios.

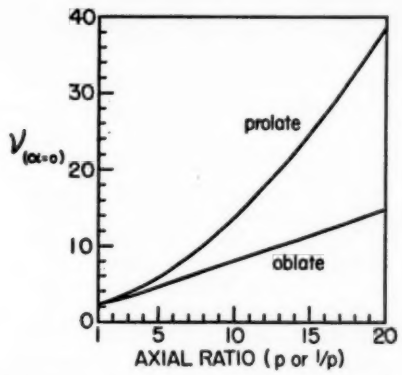

FIG. 3. Dependence of ν at $\alpha=0$ on axial ratio for prolate and oblate ellipsoids.

is concerned). However, the quantity N is positive for prolate and negative for oblate ellipsoids so that this term always increases the value of ν. As α increases, the last term of Eq. (9) (arising from the energy dissipation due to the Brownian motion, and neglected by Peterlin) becomes negligible. The values of J, K, L, M, N of Eqs. (10) are different for prolate and oblate ellipsoids. Therefore, the numerical values of ν as a function of α will differ for prolate and oblate ellipsoids. The results of the computations of ν as a function of α for various axial ratios p are given in Table I for prolate and in Table II for oblate ellipsoids. Some of these results are also shown in Figs. 1 and 2 which are qualitatively similar to those of Kuhn and Kuhn[5] and Saito.[7]

The special case where $\alpha=0$ is of interest. Taking the limiting forms of the summations in Eqs. (13) to (16) for $\alpha=0$, and substituting in Eq. (9), the following result is obtained

$$\nu=\frac{4}{15}(J+K-L)+\frac{2}{3}L+\frac{1}{3}M+\frac{RN}{15}. \qquad (18)$$

This equation is identical with that obtained previously by Simha[4] for the case of complete Brownian motion. Computations of ν as a function of p, for $\alpha=0$, have been reported by Mehl, Oncley, and Simha.[22] An expanded form of their results was obtained during the course of the present computations and is reported in Table III and Fig. 3.

It has been pointed out by Zimm[8] that the frequency dependence of ν at $\alpha=0$ provides an alternative method to that of non-Newtonian viscosity for the determination of rotary diffusion constants. If one uses periodic shear waves of frequency ω [not the same ω as used in Eq. (6)], then the frequency dependence is expressible by a modified form of Eq. (18) in terms of a complex

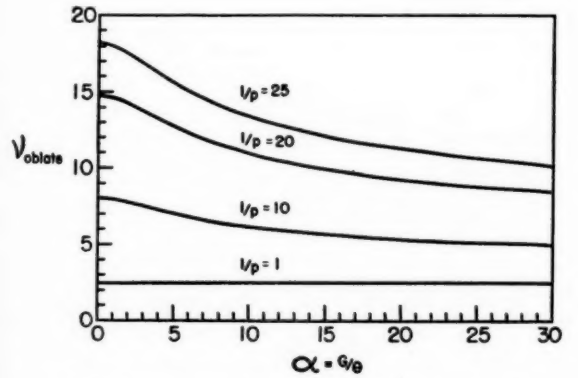

FIG. 2. Dependence of ν on α for oblate ellipsoids of various axial ratios.

TABLE III. Dependence of viscosity factors ν, ν_A, and ν_B on axial ratio for prolate and oblate ellipsoids at $\alpha=0$ and $\omega=0$.

	Prolate				Oblate		
$p=a/b$	ν_A	ν_B	ν	$1/p=b/a$	ν_A	ν_B	ν
1.0	2.500	0.000	2.500	1.0	2.500	0.000	2.500
1.2	2.504	0.021	2.525	1.2	2.505	0.019	2.524
1.4	2.516	0.072	2.588	1.4	2.520	0.063	2.583
1.6	2.533	0.144	2.677	1.6	2.542	0.119	2.661
1.8	2.555	0.229	2.784	1.8	2.573	0.180	2.753
2.0	2.583	0.325	2.908	2.0	2.610	0.244	2.854
2.25	2.623	0.455	3.078	2.25	2.664	0.325	2.989
2.50	2.671	0.595	3.266	2.50	2.727	0.405	3.132
2.75	2.726	0.743	3.469	2.75	2.795	0.485	3.280
3.0	2.786	0.899	3.685	3.0	2.868	0.562	3.430
3.5	2.922	1.230	4.152	3.5	3.027	0.714	3.741
4.0	3.077	1.586	4.663	4.0	3.198	0.861	4.059
4.5	3.248	1.967	5.215	4.5	3.378	1.004	4.382
5.0	3.434	2.372	5.806	5.0	3.563	1.145	4.708
6.0	3.844	3.254	7.098	6.0	3.947	1.420	5.367
7	4.302	4.230	8.532	7	4.342	1.690	6.032
8	4.804	5.299	10.103	8	4.744	1.956	6.700
9	5.346	6.458	11.804	9	5.151	2.220	7.371
10	5.928	7.706	13.634	10	5.562	2.481	8.043
12	7.203	10.466	17.669	12	6.390	3.001	9.391
14	8.622	13.567	22.19	14	7.224	3.519	10.74
16	10.179	17.002	27.18	16	8.061	4.034	12.10
18	11.868	20.762	32.63	18	8.901	4.548	13.45
20	13.688	24.842	38.53	20	9.743	5.061	14.80
25	18.787	36.406	55.19	25	11.853	6.340	18.19
30	24.65	49.86	74.51	30	13.966	7.618	21.58
35	31.24	65.15	96.39	35	16.083	8.894	24.98
40	38.53	82.23	120.76	40	18.200	10.170	28.37
50	55.20	121.61	176.81	50	22.438	12.720	35.16
60	74.54	167.74	242.28	60	26.678	15.268	41.95
70	96.45	220.46	316.9	70	30.92	17.82	48.74
80	120.88	279.60	400.5	80	35.16	20.36	55.52
90	147.77	345.03	492.8	90	39.40	22.91	62.31
100	177.06	416.65	593.7	100	43.64	25.46	69.10
150	358.44	864.74	1223.2	150	64.86	38.19	103.05
200	595.6	1457.3	2052.9	200	86.08	50.93	137.01
300	1226.9	3052.5	4279.4	300	128.52	76.39	204.91

[22] Mehl, Oncley, and Simha, Science **92**, 132 (1940).

viscosity factor whose real part is given by[23]

$$\nu=\nu_A+\frac{\nu_B}{1+\omega^2/36\Theta^2} \tag{19}$$

where

$$\nu_A=\frac{4}{15}(J+K-L)+\frac{2}{3}L+\frac{1}{3}M,$$

and

$$\nu_B=RN/15.$$

For zero frequency Eq. (19) reduces to Eq. (18); at high frequency ν approaches ν_A. As indicated by Cerf,[23] Θ is determinable from the slope of the curve of ν *vs* ω at the inflection point. For this purpose values of ν_A and ν_B as a function of p are also included in Table III.

Now that data are available for ν_A and ν_B as a function of p at $\alpha=0$, and for ν as a function of α and p, it will be very desirable to have extensive experimental tests to check the validity of the theory. Some preliminary results on non-Newtonian viscosity have already been obtained.[24]

APPENDIX

In connection with the convergence problem[24] it is of interest to examine the values of the summations of Eqs. (13) to (16) for increasing j-values for the case $R=1$. Such data are shown in Table IV for $\alpha=25$, 40, and 60, where each entry is the cumulative value of the summation as j increases. It can be seen that enough terms have been computed to obtain the limiting values of the summations within the precision of the data reported in Tables I and II.

TABLE IV. Values of summations as a function of j for several values of α.

α	$-\Sigma a_{10,j}$	$\Sigma a_{20,j}$	$\Sigma a_{22,j}$	$\Sigma b_{11,j}$
25	0.06449	0.01935	0.0005235	0.009029
	0.09624	0.03951	0.0006101	0.015774
	0.10956	0.05068	0.0005530	0.019813
	0.11145	0.05478	0.0004914	0.021399
	0.10923	0.05492	0.0004622	0.021545
	0.10742	0.05390	0.0004568	0.021256
	0.10670	0.05317	0.0004600	0.021017
	0.10658	0.05292	0.0004636	0.020918
	0.10669	0.05292	0.0004653	0.020908
	0.10678	0.05297	0.0004657	0.020923
	0.10681	0.05301	0.0004656	0.020934
				0.020939
40	0.06671	0.02001	0.0006295	0.005837
	0.10338	0.04490	0.0008667	0.010806
	0.12504	0.06255	0.0009241	0.014767
	0.13611	0.07356	0.0009037	0.017518
	0.13917	0.07915	0.0008639	0.019029
	0.13857	0.08093	0.0008301	0.019628
	0.13720	0.08075	0.0008093	0.019723
	0.13603	0.07999	0.0007998	0.019616
	0.13533	0.07934	0.0007971	0.019482
	0.13496	0.07894	0.0007974	0.019383
	0.13481	0.07874	0.0007984	0.019328
				0.019303
60	0.06753	0.02026	0.0006731	0.003939
	0.10599	0.04769	0.0009891	0.007460
	0.13104	0.06925	0.0011394	0.010583
	0.14748	0.08494	0.0011965	0.013208
	0.15578	0.09505	0.0012054	0.015137
	0.15917	0.10117	0.0011934	0.016389
	0.16021	0.10429	0.0011754	0.017107
	0.16023	0.10543	0.0011590	0.017461
	0.15983	0.10564	0.0011471	0.017597
	0.15933	0.10547	0.0011397	0.017620
	0.15889	0.10519	0.0011356	0.017595
				0.017563

[23] R. Cerf, Compt. rend. **234**, 1549 (1952).
[24] E. Wada, J. Sci. Research Inst. (Tokyo) **47**, 168 (1953); J. Polymer Sci. **14**, 305 (1954).

Mechanism of Potential Inversion of the Joshi Effect

S. R. MOHANTY
Physico-Chemical Laboratories, Banaras Hindu University, India
(Received November 12, 1954)

The positive Joshi effect $+\Delta i$ (i.e., the photoincrease of the current i) increases initially with the exciting ac potential $V(<V_m$ the "threshold potential") to a maximum at V_m, decreases precipitously and changes sign (to the negative *effect* $-\Delta i$, i.e., photosuppression of i) at an inversion potential V_i^{I}. Beyond V_i^{I}, $-\Delta i$ first increases rapidly and diminishes slowly thereafter. A second inversion, $-\Delta i \rightarrow +\Delta i$, obtains, in certain systems, at V_i^{II} in the region of high V. Oscillographic studies reveal simultaneous occurrence, at $V>V_m$, of intrinsic $(+\Delta i)$ and intrinsic $(-\Delta i)$; the integrating current indicator shows the balance.

The initial $+\Delta i$ at $V<V_m$, and its enhancement with V, results from photoelectron emission from the (momentary) cathode of field diminished work function. At V_m, consequent to the continuous discharge and an electron residuum from the antecedent half-cycle, largely enhanced emission and space accumulation of negative ions (from attachment of the electrons) lead to incipience of $(-\Delta i)$ due to inhibition of γ and $\eta\theta g$ processes. Electrons able to cross the barrier cause $(+\Delta i)$. The observed co-occurrence of $(+\Delta i)$ and $(-\Delta i)$ follows. Beyond V_m, increase in emission due to field reduction of surface work function enhances space charge density and therefore $(-\Delta i)$. Observed diminution in $+\Delta i$ follows from the above, and the reduction in the number of photoelectrons able to cross the barrier. At V_i^{I}, $(+\Delta i)=(-\Delta i)$ and therefore, $\pm\Delta i=0$. Increase of $-\Delta i$ above V_i^{I} also follows from the above considerations. The decrease in attachment probability $P=f(p/F)$, where p is the gas pressure and F the field, leads to subsequent diminution of $(-\Delta i)$ at large V. Increase in the associated $(+\Delta i)$ is a contributory factor, and above V_i^{II} causes the observed positive *effect*.

POTENTIAL INVERSION OF THE JOSHI EFFECT

THE Joshi effect,[1,2] *viz.*, the instantaneous and reversible photovariation (enhancement $+\Delta i$ and diminution $-\Delta i$) of the current i under discharge, has been observed in a number of gases and vapors,[3] elemental and compound, over a wide range of the operative conditions, e.g., the applied potential[4–8] V, the gas pressure[4–6] p, etc. The net *effect* is given by $\pm\Delta i=i_L-i_D$, where i_L and i_D are the values of i under light and in dark respectively, and the relative *effect*, expressed as a percentage, by $\pm$ percent $\Delta i=(\pm\Delta i/i_D)\times 10^2$.

The dependence of $\pm\Delta i$, at constant light intensity (I) and frequency ν, on V is shown graphically in Fig. 1. The positive *effect*[1,7,9] $+\Delta i$ is small at low V and increases initially with V to a maximum at V_m the "threshold potential"[2,10,11] of the self-maintained discharge. Above V_m, $+\Delta i$ decreases rapidly and changes sign (to the negative *effect* $-\Delta i$) at an inversion potential V_i^{I}. Beyond V_i^{I}, $-\Delta i$ first increases rapidly, and diminishes slowly thereafter. A second inversion,[12] $-\Delta i \rightarrow +\Delta i$, obtains, in certain systems, at V_i^{II} in the region of high V; this part of the curve is shown discontinuous in Fig. 1. The $\pm$ percent $\Delta i-V$ curve is essentially similar. The changes $+\Delta i \rightleftarrows -\Delta i$ and $-\Delta i \rightleftarrows +\Delta i$ are potential reversible.[7,13] Furthermore, studied oscillographically, the observed *effect* is found, depending upon the conditions, to be made up of simultaneously occurring intrinsic $(+\Delta i)$ and intrinsic $(-\Delta i)$ represented respectively by an increase (in number and/or amplitude) of certain current pulses and decrease of others (Fig. 2); the current indicator, e.g., the thermocouple-galvanometer system, is an integrating device, and therefore, shows the balance.[14–16]

THE JOSHI THEORY

For the occurrence of $\pm\Delta i$, Joshi[13,14,17] postulates that (a) an adsorption-like electrode layer consisting of excited particles, ions, and electrons is formed under discharge; (b) light releases electrons from this layer; (c) negative ion formation due to capture of the photoelectrons by excited neutral particles reduces i to give $-\Delta i$, mainly as a space charge effect; and (d) uncaptured photoelectrons, and their secondaries produced under the applied fields, cause $+\Delta i$.

The observed influence on $\pm\Delta i$ of "aging"[18,19] under discharge and electrode films[20] supports the postulate (a); furthermore, the marked increase of

[1] S. S. Joshi, Proc. Indian Sci. Congr., Chemistry Section, Presidential Address, 70 (1943).
[2] S. S. Joshi, Proc. Indian Acad. Sci. **A22**, 389 (1945).
[3] See H. J. Arnikar, J. Chem. Phys. **20**, 917 (1952).
[4] S. R. Mohanty and G. S. Kamath, J. Indian Chem. Soc. **25**, 405 (1948).
[5] S. R. Mohanty, J. Indian Chem. Soc. **26**, 553 (1949).
[6] Mohanty, Rao, and Ramaiah, J. Indian Chem. Soc. **31**, 539 (1954).
[7] Mohanty, Jayaraman, and Krishna Rao, J. Phys. Soc. Japan **9**, 576 (1954).
[8] B. N. Prasad and T. C. Jain, Proc. Indian Acad. Sci. **A25**, 515 (1947).
[9] H. J. Arnikar, Indian J. Phys. **25**, 353 (1951).
[10] S. S. Joshi, Current Sci. **8**, 548 (1939); **15**, 281 (1946).
[11] S. R. Mohanty, J. Sci. Ind. Research (India) **B13**, 145 (1954); Mohanty, Jayaraman, and Rao, J. Sci. Ind. Research (India) **B13**, 526 (1954).
[12] B. M. Shukla, J. Phys. & Colloid Chem. **53**, 1239 (1949).
[13] S. S. Joshi, Current Sci. **16**, 19 (1947).
[14] S. S. Joshi, Proc. Indian Sci. Congr., Phys. Sec., Part III, Abstract 25 (1947).
[15] D. P. Jatar, J. Sci. Ind. Research (India) **B9**, 283 (1950).
[16] S. R. Mohanty, J. Indian Chem. Soc. **30**, 9 (1953).
[17] S. S. Joshi, Proc. Indian Sci. Congr., Phys. Sec., Part III, Abstract 26 (1946).
[18] P. G. Deo, Proc. Indian Acad. Sci. **A21**, 76 (1945).
[19] S. R. Mohanty, J. Indian Chem. Soc. **28**, 487 (1951).
[20] S. R. Mohanty, J. Phys. Chem. **58**, 178 (1954).

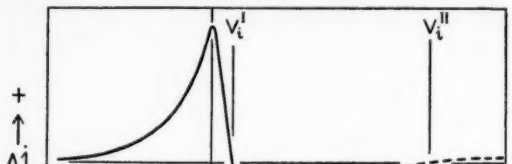

FIG. 1. Potential inversion of the Joshi effect.

$\pm\Delta i$ with such films of photosensitive substances[21,22] follows from (b). A direct consequence of (c) is that the magnitude of $-\Delta i$ depends upon the electron affinity of the excited media.[4,13]

THE MECHANISM OF INVERSION

In the production of $\pm\Delta i$, the photoelectric emission from the (momentary) cathode surface takes place under fields F due to the applied V. The surface work function ϕ is therefore lowered,[23,24] as a Schottky consequence, to ϕ' given by the equation

$$\phi' = \phi - \sqrt{F}, \tag{1}$$

the validity of which has been demonstrated by Lawrence and Linford.[25] As the applied V on the discharge tube is progressively increased, emission occurs when, depending upon the nature of the photoactive surface and ϕ, the applied F is such that ϕ' is equal to or less than the energy $h\nu$ of the incident light. The electrons are ejected with Maxwellian distribution of velocities[26] spread over zero and a maximum v_{max} calculable from the Einstein equation

$$\tfrac{1}{2}mv_{max}^2 = h\nu - \phi'. \tag{2}$$

A certain fraction of the released photoelectrons is attached by the neutral gas (vapor) particles to form negative ions; this attachment is governed by a probability[27,28] P which is an inverse function of the electron energy and hence F/p. The negative ions, on account of their low mobility, do not contribute to the current (by themselves, or by electron multiplication), but tend to accumulate in space in the immediate neighborhood of the photoactive surface. Initially, well below V_m, the photoemission is small. The meagre space charge due to the small number of negative ions formed does not sensibly alter the potential distribution. The enhancement of i under light, i.e., $+\Delta i$, is caused by the photoelectrons which escape attachment.

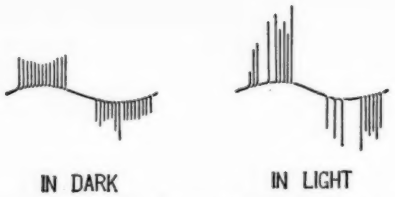

FIG. 2. Simultaneous occurrence of intrinsic positive and intrinsic negative Joshi effect.

With further increase in V (and F), $1/\phi'$ and the emission, and therefore $+\Delta i$, increase. If the value of ϕ' obtained from (1) is substituted in the Richardson equation

$$I = AT^2 \exp(-e\phi'/kT), \tag{3}$$

there results

$$I = I_0 \exp(e\sqrt{F}/kT), \tag{4}$$

where I_0 is the current for zero external field. Experimental evidence for relationship (4) has been adduced by Pforte[29] and by de Bruyne.[30] Below V_m, i_D is chiefly capacitative; $+\Delta i$ is thus the conductivity due to the photoelectrons released under F. Hence, considering (justifiably, since V is small) gas amplification due to impact ionization to be of less importance,

$$+\Delta i = (+\Delta i)_0 \exp(e\sqrt{F}/kT), \tag{5}$$

where $(+\Delta i)_0$ is the hypothetical $+\Delta i$ due to the primary photoelectron emission with zero external field. Since, for a given arrangement of electrodes, F is directly proportional to V, it follows from (5) that the plots of $\log(+\Delta i)$ against $\sqrt{V}$ should lie on a straight line. The fact that this anticipation is realized experimentally[7,9] for the potential enhancement of $+\Delta i$ is in accord with the above deductions.

At (and above) V_m, on account of the continuous discharge, the interelectrode space consists of a fair concentration of electrons and positive ions which move toward the oppositely charged electrodes. While the electrons reaching the (momentary) anode during a major part of the half-cycle are neutralized, those arriving immediately before the electrode changes sign are deposited as such on the glass walls. These loosely bound electrons impart to the (momentary) cathode surface, during the subsequent half-cycle, a markedly low ϕ, and a high photoelectron activity. There is thus a copious release of electrons under irradiation, even with the red and the near infrared. The negative space charge resulting from attachment of these electrons (together with that due to the electrons emitted, also with the Maxwellian distribution of velocities, by the γ and $\eta\theta g$ processes)[28] is therefore large, and, as such, constitutes a retarding barrier and appreciably alters the potential distribution. In consequence, the further

[21] B. M. Shukla, Proc. Indian Sci. Congr., Chem. Sec., Part III, Abstract 34 (1949).
[22] Shukla, Tikkoo, and Khare, Proc. Indian Sci. Congr., Phys. Sec., Part III, Abstract 19 (1952).
[23] W. Schottky, Z. Physik **14**, 63 (1923).
[24] I. Langmuir and K. T. Compton, Revs. Modern Phys. **2**, 124 (1930).
[25] E. O. Lawrence and L. B. Linford, Phys. Rev. **36**, 482 (1930).
[26] A. L. Hughes and L. A. DuBridge, *Photoelectric Phenomena* (McGraw-Hill Book Company, Inc., New York, 1932).
[27] H. S. W. Massey, *Negative Ions* (The University Press, Cambridge, 1938).
[28] L. B. Loeb, *Fundamental Processes of Electrical Discharge in Gases* (John Wiley and Sons, Inc., New York, 1939).
[29] W. S. Pforte, Z. Physik **49**, 46 (1928).
[30] N. A. de Bruyne, Proc. Roy. Soc. (London) **A120**, 423 (1928).

emission of electrons, especially of low energy, by the external light and the γ and $\eta\theta g$ processes, is inhibited; this constitutes the incipience of the intrinsic negative *effect* $(-\Delta i)$. Electrons with large enough energies are, however, able to shoot through the barrier, and, together with their secondaries,[28,31–33] are responsible for the intrinsic positive *effect* $(+\Delta i)$. This accounts for the co-occurrence, observed oscillographically, of $(+\Delta i)$ and $(-\Delta i)$ (see above). The former predominates, so that the resultant *effect* is positive. With increase (in dark) in V (and therefore in F), both ϕ and the attachment probability P diminish. For a small increase in F, diminution in $P=f(p/F)$ is, however, not appreciable at the fairly large p (of the order of a few hundreds of mm Hg) usually employed in studies of the phenomenon. Consequently, for such a change in V, effects due to diminution in ϕ preponderate. The emission, the space charge density, and therefore the intrinsic $(-\Delta i)$, increase. The negative space charge, formed under light, diminishes the field (existing prior to irradiation) near the emitting surface. The probability P in this region is therefore enhanced, after a suitable space charge is formed; this constitutes a contributory factor. Furthermore, the number of electrons overcoming the barrier, and the intrinsic $(+\Delta i)$, are smaller. The observed resultant $+\Delta i$ consequently diminishes. At V_i^{I}, $i_D=i_L$ and $(+\Delta i)=(-\Delta i)$; the inhibitory influence of the space charge is exactly counterbalanced by the electrons which escape the barrier. Beyond V_i^{I}, the increase in the observed $-\Delta i$, over a narrow V range, to a maximum, also follows from the above considerations. With further rise in V, the diminution in P becomes appreciable. The space charge density $(-\Delta i)$, and therefore the observed $-\Delta i$, diminish. Simultaneously, the number of electrons crossing the enfeebled barrier, and the associated $(+\Delta i)$, increase, and beyond V_i^{II}, predominate over the inhibitive influence of the space barrier and $(-\Delta i)$, so that the resultant *effect* is positive.

[31] J. J. Thomson and G. P. Thomson, *Conduction of Electricity through Gases* (The University Press, Cambridge, 1933).
[32] J. S. E. Townsend, *Electrons in Gases* (Hutchinson's Scientific and Technical Publications, London, 1947).
[33] J. M. Meek and J. D. Craggs, *Electrical Breakdown of Gases* (The Clarendon Press, Oxford, 1953).

THE JOURNAL OF CHEMICAL PHYSICS VOLUME 23, NUMBER 8 AUGUST, 1955

Semiempirical Study of the H_2Cl Transition Complex through the Use of Hydrogen Isotope Effects*

JACOB BIGELEISEN AND MAX WOLFSBERG
Chemistry Department, Brookhaven National Laboratory, Upton, Long Island, New York
(Received November 3, 1955)

Linear and triangular structures for the H_2Cl transition complex have been analyzed in terms of normal vibration theory and by an evaluation of the experimental data on the effect of hydrogen isotope substitution on the rate of reaction of hydrogen molecules and chlorine atoms. The frequencies of the bending vibrations are probably sufficiently small that their contribution to the relative rates can be expressed in terms of a small quantum correction of the order of $(hc/kT)^2(\omega_H^2-\omega_{D,T}^2/24)$. The near classical behavior of the bending frequencies for both linear and triangular structures of the H_2Cl complex serves to reduce the ratio of the frequency factors, $A_H/A_{D,T}$, in the Arrhenius equation from that expected from structural considerations alone. Quantitative agreement is found between the calculated and experimentally determined frequency factor ratios for the triangular complex. The "symmetrical" stretching frequencies, for both linear and triangular complexes respectively, have been evaluated from the relative rates of reaction of H_2 and HT with chlorine atoms at 0°C and the known properties of the isotopic hydrogen molecules. This empirically evaluated parameter, together with thermodynamic data, and an estimate of the tunnel correction, suffice to calculate the relative rates of reaction of the isotopic hydrogen molecules with chlorine atoms as a function of temperature. Good agreement is found between the calculated rates for both linear and triangular structures and the available experimental data on HD, D_2, and HT.

INTRODUCTION

STUDIES of the gaseous reactions of atomic and molecular hydrogen, in their various isotopic and *ortho*- and *para*-modifications, have a foremost position in the development and elucidation of the statistical mechanical theory of chemical rate processes. This is a consequence of several important aspects of such reactions, namely: (1) reactions involving a total of two or three atoms can be studied, (2) the structures of the hydrogen atom and molecule are well understood, and (3) it is feasible to carry out *a priori* quantum-mechanical calculations, which although rough still are of some significance with respect to the structure of the transition state complex.

Some typical elementary reactions, which have been studied in more or less detail,[1] are the reactions of hydrogen atoms with hydrogen molecules, the homo-

* Research carried out under the auspices of the U. S. Atomic Energy Commission.

[1] See Glasstone, Laidler, and Eyring, *The Theory of Rate Processes* (McGraw-Hill Book Company, Inc., New York, 1941), Chap. V.

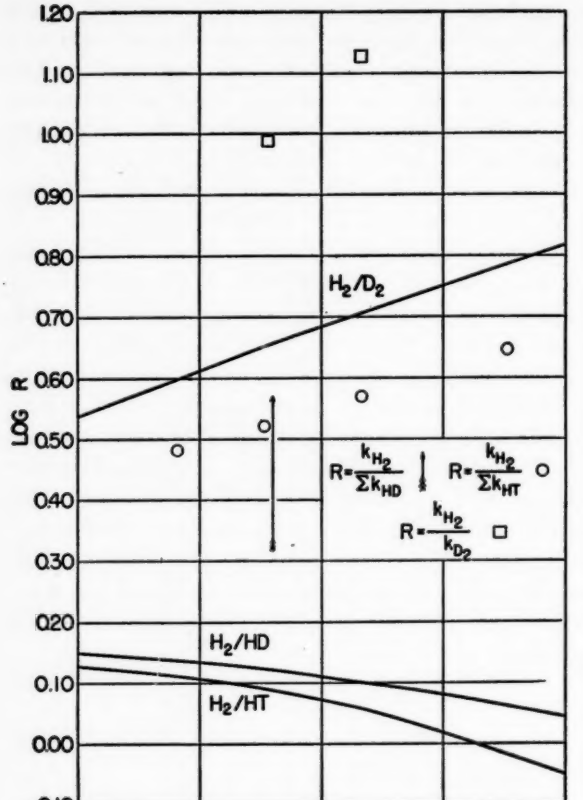

FIG. 1. Relative rates of reaction of the isotopic hydrogen molecules with chlorine atoms as a function of temperature. Solid lines calculated from the Wheeler, Topley, and Eyring potential for H_2Cl.

geneous recombination of hydrogen atoms, the reactions of hydrogen molecules with the hydrogen molecule ion, and the reactions of hydrogen molecules with halogen atoms. The greatest body of experimental data exists for the reactions of hydrogen molecules with hydrogen and halogen atoms. In the former case theoretical calculations show reasonable agreement with the experimental data of Farkas and Farkas[2] and Van Meersche.[3] However, recent, although incomplete, experiments by Careri and co-workers[4] show that the true rates of these reactions are probably slower than what has been previously reported and that the corresponding activation energies may be in error by one or two kilocalories. It may be concluded from Careri's results that the classical activation energy as well as some of the frequencies of the H_3 complex may have to be revised somewhat from those calculated *a priori* by Hirschfelder, Eyring, and Topley[5] and the similar ones evaluated by Farkas and Wigner[6] from experimental data. Jones[7] has summarized the lack of agreement between theory and experiment in the case of reactions between the isotopic hydrogen molecules and chlorine atoms.

At present it seems doubtful that significant improvements in the computation of the energy surfaces of the transition state can be made conveniently. A semiempirical approach in which the parameters of the transition state are in part calculated and in part evaluated from experimental data offers the next best approach to the study of the molecular structure and the forces between atoms in the activated complex. In the use of this method it is naturally desirable to have more independent experimental measurements than parameters which require evaluation.

The experimental data by Jones on the relative rates of H_2 and HT with chlorine atoms are sufficient for such a semiempirical study. The relative rates have been studied as a function of temperature. In addition there are some measurements on the ratio of the rates of H_2 and D_2[8] and H_2, HD and D_2 mixtures.[9] A comparison of the experimental data with calculations from the Wheeler, Topley, and Eyring potential[10] is given in Fig. 1. The discrepancy in the ratio of the rate constants for isotopic molecules approaches a factor 5, and in the case of the H_2-HT pair the calculated difference in activation energies is of the wrong sign.

OUTLINE OF THE METHOD

We shall start with the usual transition-state equation, which neglects quantum corrections for motion across the potential barrier, but will include the Wigner correction for tunneling through the barrier. Application of the latter correction to Eq. (4) given by Bigeleisen and Wolfsberg[11] leads to

$$k_1/k_2=(K_1/K_2)(\nu_{1i}/\nu_{2i})(f/f_{N^{\neq}}) \times\left(1+\frac{1}{24}|u_{1i}|^2\right)\Big/\left(1+\frac{1}{24}|u_{2i}|^2\right) \quad (1)$$

for the ratio of rate constants for a pair of isotopic molecules. The terms in Eq. (1) have been defined previously.[11,12] We take (K_1/K_2), the ratio of transmission coefficients, as equal to unity. The partition function ratio, f, for the isotopic hydrogen molecules is known. The rotational correction can be approximated by an exponential[13] and the excitation of the vibrations of the hydrogen molecules is negligible below 350°K, the maximum temperature of interest in this study. This reduces f to the relation

$$f=(s'\omega/s\omega')e^{[3\Delta u_0+2(\sigma-\sigma')]/6}. \quad (2)$$

In treating the partition function ratio for the transi-

[2] A. Farkas and L. Farkas, Proc. Roy. Soc. (London) **A152**, 124 (1935).
[3] M. Van Meersche, Bull. soc. chim. Belges **60**, 99 (1951).
[4] Boato, Careri, Cimino, Molinari, and Volpi, XIIIth International Congress of Pure and Applied Chemistry, Stockholm, Sweden, July, 1953.
[5] Hirschfelder, Eyring, and Topley, J. Chem. Phys. **4**, 107 (1936).
[6] L. Farkas and E. Wigner, Trans. Faraday Soc. **32**, 708 (1936).
[7] W. M. Jones, J. Chem. Phys. **19**, 78 (1951).
[8] G. K. Rollefson, J. Chem. Phys. **2**, 144 (1934).
[9] L. Farkas and A. Farkas, Naturwiss. **22**, 218 (1934).
[10] Wheeler, Topley, and Eyring, J. Chem. Phys. **4**, 178 (1936).
[11] J. Bigeleisen and M. Wolfsberg, J. Chem. Phys. **21**, 1972 (1953).
[12] J. Bigeleisen, J. Chem. Phys. **17**, 675 (1949).
[13] Perlman, Bigeleisen, and Elliott, J. Chem. Phys. **21**, 70 (1953).

tion state, it is convenient to work with a quantity $f_{Np}^{\neq}$ which is defined as

$$f_{Np}^{\neq} = \nu_{2i} f_N^{\neq} / \nu_{1i} \tag{3}$$

$$= (s_1^{\neq}/s_2^{\neq}) \prod^{3n-6} \frac{\omega_2^{\neq}{}_j}{\omega_1^{\neq}{}_j} \prod^{3n-7} \times \exp(\Delta u_j^{\neq}/2) \frac{[1-\exp(-u_1^{\neq}{}_j)]}{[1-\exp(-u_2^{\neq}{}_j)]}. \tag{4}$$

The quantity $f_{Np}^{\neq}$ will be evaluated for two models, a linear one and an isosceles triangle. For the asymmetric linear H_2Cl complex, the symmetry number ratio $s_1^{\neq}/s_2^{\neq}$ is unity; for the isosceles triangle this ratio is 2 when only one protium atom is isotopically substituted. The latter complex has two different but equally probable methods of decomposing. The rate of each partial reaction is obtained by dividing $f_N^{\neq}{}_p$ by 2, which amounts to cancelling $s_1^{\neq}/s_2^{\neq}$. The quantity $\prod^{3n-6} \omega_2^{\neq}{}_j/\omega_1^{\neq}{}_j$ is just the product rule ratio for a pair of isotopic molecules and can be calculated from the masses and moments of inertia. This ratio is quite insensitive to considerable variations in the H—H and H—Cl distances in the complex and to the H—H—Cl angle. The bond distances and angles are, therefore, relatively unimportant in considering various structures for the activated complex. In Eq. (4) two frequencies, one of which is a bending one, contribute to the zero point energy and excitation terms for a triangular H_2Cl complex, while three frequencies, one of which is a doubly degenerate bending one, contribute to this term for a linear model. The potential function of Wheeler, Topley, and Eyring,[10] which leads to frequencies for the transition state which are too high, gives 491 cm^{-1} for the bending frequency. The contribution of such a frequency to $f_N^{\neq}{}_p$ at 300°K can be approximated by the $u^2/24$ law within about one-tenth of 1%. The symmetrical stretching frequency is anticipated to be sufficiently large that the term involving its excitation, $[1-\exp(-u_1^{\neq}{}_{H_2})]/[1-\exp(-u_1^{\neq}{}_{D,T})]$, can be neglected. These observations serve to reduce $f_N^{\neq}{}_p$ to the following:

$$f_N^{\neq}{}_p = (\omega_1^{\neq}\omega_i^{\neq})_{D,T}/(\omega_1^{\neq}\omega_i^{\neq})_{H_2} \times \exp[(hc/2kT)\Delta\omega_1^{\neq}]\left(1+\frac{\Delta u_b^{\neq 2}}{24}\right)^{g_n} \tag{5}$$

where $\omega_1^{\neq}$ is the symmetrical stretching frequency, $\omega_i^{\neq}$ is the asymmetric stretching frequency and is imaginary, $u_b^{\neq}$ is (hc/kT) times the bending frequency, g_n is the degeneracy of the bending frequency, the subscript D,T refers to isotopes of hydrogen other than protium, and H_2 refers to the H_2Cl complex. The temperature independent factor $(\omega_1^{\neq}\omega_i^{\neq}{}_{D,T}/\omega_1^{\neq}\omega_i{}_{H_2})$ can be calculated from the theory of small vibrations. The correction for the bending frequencies can be estimated by an educated guess, which need not be accurate at all. The correction for the tunneling in Eq. (1) can be similarly approximated. By intercomparison of Eqs. (1), (4), and (5) with the experimental data on HT at 273°K, $\omega_1^{\neq}{}_{H_2Cl}$ can be evaluated. The method outlined is, therefore, similar in most respects to that adopted by Farkas and Wigner[6] for the H+H_2 reaction.

EVALUATION OF $\omega_1^{\neq}$ FOR LINEAR AND TRIANGULAR MODELS

In conformity with other studies of the photochemical reaction of hydrogen and chlorine, we assume that the slow step in the reaction is that between hydrogen molecules and chlorine atoms. In the experimental investigation of the relative rates of H_2 and HT with Cl atoms, there is the complication resulting from the fact that there are two reactions involving HT, one to give HCl and the other to give TCl. Experimentally one measures R, which is defined by the following relations[7]:

$$H_2+Cl \xrightarrow{k_1} HCl+H, \tag{6}$$

$$HT+Cl \xrightarrow{k_{2a}} TCl+H, \tag{7}$$

$$HT+Cl \xrightarrow{k_{2b}} HCl+T, \tag{8}$$

$$R = k_1/(k_{2a}+k_{2b}). \tag{9}$$

Reactions (7) and (8) correspond to the following structures for the activated complexes for linear and triangular models:

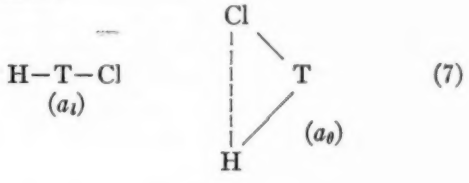

(7)

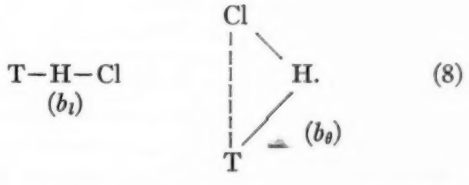

(8)

The principal differences in these structures, insofar as they affect the quantities k_1/k_{2a}, k_1/k_{2b}, and R, are the following. The difference in the degeneracy of the bending frequency will make a difference in all three quantities by at most 10% and is, therefore, relatively insignificant. In considering the contributions of the entropy terms to the ratio k_1/k_{2a}, one finds, from Lechner's[14] formulas for the vibrations of a bent XYZ molecule, that the ratio $(\omega_1^{\neq}\omega_i^{\neq})_{HTCl}/(\omega_1^{\neq}\omega_i^{\neq})_{H_2Cl}$ is rather insensitive to large variations in the H—T—Cl angle. Furthermore, the ratio $\omega 1^{\neq}{}_{HTCl}/\omega 1^{\neq}{}_{H_2Cl}$ is close to $1/\sqrt{3}$, while the ratio $\omega_i^{\neq}{}_{HTCl}/\omega_i^{\neq}{}_{H_2Cl}$ is close to unity. The symmetrical stretching frequency, $\omega 1^{\neq}{}_{H_2Cl}$, is also rather insensitive to the H—T—Cl angle, except insofar as the force constants may vary with the angle. The calculations of Magee[15] are insufficient to give a definitive answer to this problem. These considerations show that the value of $\omega 1^{\neq}{}_{H_2Cl}$ evaluated from a given value

[14] F. Lechner, Sitz. Akad. Wiss. Wien **141a**, 291 (1932).
[15] J. L. Magee, J. Chem. Phys. **8**, 677 (1940).

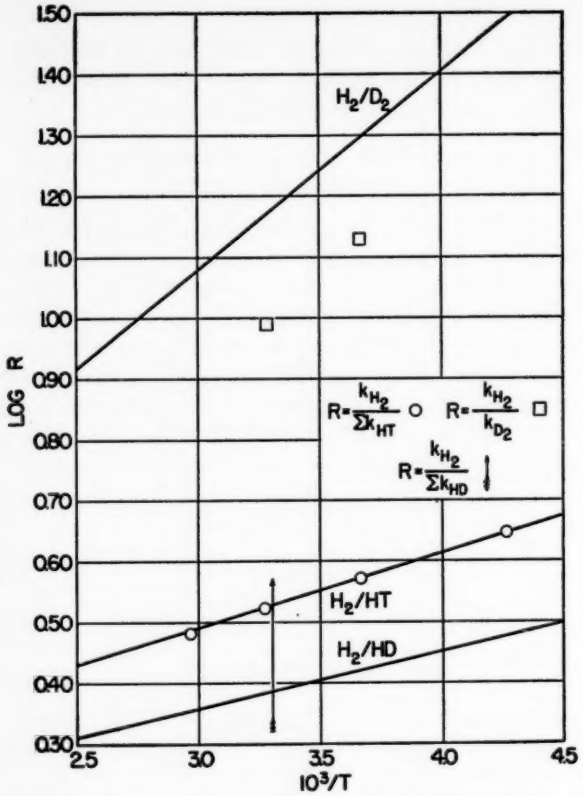

FIG. 2. Relative rates of reaction of the isotopic hydrogen molecules with chlorine atoms as a function of temperature. Solid lines calculated for an isosceles triangular H_2Cl complex, $\omega_1^{\neq}=1002$ cm^{-1}.

of k_1/k_{2a} will not differ significantly for either a linear or triangular model.

On the other hand significant differences in the ratio k_1/k_{2b} can be obtained for linear and triangular models. In the structure $8b_l$ the symmetric frequency is unchanged from that in H_2Cl, while $\omega i^{\neq}{}_{HTCl}/\omega i^{\neq}{}_{H_2Cl}$ is close to $1/\sqrt{3}$. Since $\omega_i^{\neq}$ does not contribute to the zero-point energy term, k_{2b} will be smaller than k_{2al} by a factor of $\exp(-0.30\omega_1^{\neq}/T)$, where $\omega_1^{\neq}$ is expressed in cm^{-1}, for the linear model. On the other hand for an isosceles triangular model with Cl at the apex, k_{2a} is equal to k_{2b}. Therefore, the difference in the values of $\omega 1^{\neq}{}_{H_2Cl}$ evaluated from R for linear and triangular models will depend on the contribution of k_{2b}/k_{2a} to R. The range of variation of k_{2b}/k_{2a} is from 1 for the isosceles triangle to $\exp(-0.30\omega_1^{\neq}/T)$ for the linear model.

We shall evaluate $\omega 1^{\neq}{}_{H_2Cl}$ for two models, a linear one and an isosceles triangle, i.e., $k_{2a}=k_{2b}$. For either a linear or triangular model, the ratios $\omega 1^{\neq}{}_{HTCl}/\omega 1^{\neq}{}_{H_2Cl}$ and $\omega i^{\neq}{}_{HTCl}/\omega i^{\neq}{}_{H_2Cl}$ are rather insensitive to large variations in the H−H and H−Cl force constants. For the linear model the frequency *ratios* will be calculated

TABLE I. Frequency ratios for H_2Cl complexes.

	Linear HTCl/H_2Cl	Linear THCl/H_2Cl	Triangular HTCl/H_2Cl
$\omega_1^{\neq}$	0.597	0.998	0.6183
$\omega_2^{\neq}$	0.680	0.938	0.8313
$\omega_i^{\neq}$	0.993	0.595	0.9863

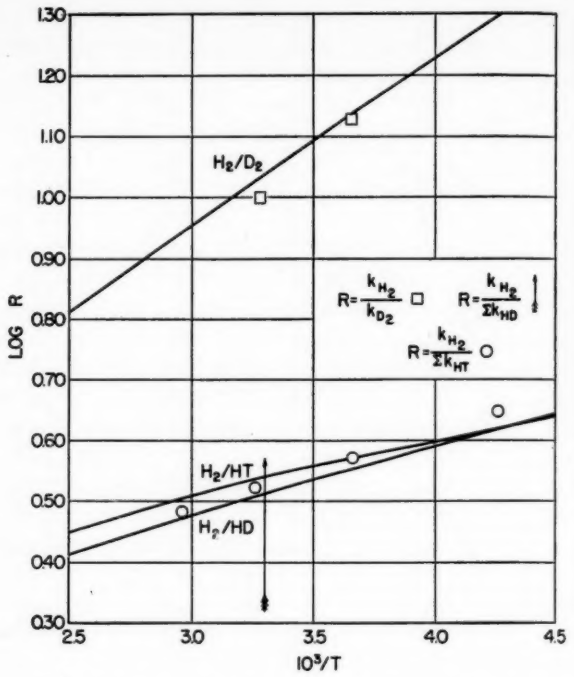

FIG. 3. Relative rates of reaction of the isotopic hydrogen molecules with chlorine atoms as a function of temperature. Solid lines calculated for a linear H_2Cl complex, $\omega_1^{\neq}=1460$ cm^{-1}.

from the WTE potential.[10] For the triangular model the only uncertain frequency ratio is the bending one. This could be calculated from the product rule and the ratios for $\omega_1^{\neq}$ and $\omega_i^{\neq}$. Inasmuch as the product rule value for HTO and H_2O comes within the range of a number of triangular complexes and since the $\omega_1^{\neq}$ and $\omega_i^{\neq}$ ratios of HTCl and H_2Cl are practically the same as those for the water molecules, as a matter of convenience, all the frequency ratios will be taken as those in the water molecules. Since the bending frequency plays the role of a small correction only, this assumption does not imply that the isosceles triangular H_2Cl complex has the H_2O structural parameters. The frequency ratios used are given in Table I.

It was recognized by Wheeler, Topley, and Eyring[10] that their potential function led to frequencies for the transition state which were too large. They calculated $\omega_1^{\neq}$ and $\omega_2^{\neq}$ to be 2489 and 491 cm^{-1} respectively. We shall arbitrarily take $\omega_2^{\neq}$ to be 200 cm^{-1} for the two H_2Cl complexes. As we have pointed out previously, this choice need not be accurate at all. This large difference in the value of the bending frequencies makes but a 10% change in the value of $\omega_1^{\neq}$ calculated from the experimental data. Since the absolute value of the imaginary frequency enters only into the tunnel correction, its value will be taken as $720i$ in accord with the WTE potential.

TABLE II. Frequency assignment for triangular H_2Cl complex.

$\omega_1^{\neq}$	1002 cm^{-1} calculated from HT experimental data at 273.16°K
$\omega_2^{\neq}$	200 cm^{-1} approximated
$\omega_i^{\neq}$	$720i$ cm^{-1} calculated by WTE for a linear model

Jones'[17] experimental data give for $R\equiv k_1/(k_{2a}+k_{2b})=1.35e^{278/T}$. Therefore, for the isosceles triangular model

$$(k_1/k_{2a})_{\text{exp}}=2.70e^{278/T}. \quad (9)$$

The ratio of partition functions for the hydrogen molecules, f_{HT/H_2}, can be written[16]

$$f=(2)(0.8167)e^{556.3/T}. \quad (10)$$

These lead to the following relation for $\omega_1^{\neq}{}_{\text{H}_2\text{Cl}}$

$$2.70e^{278/T}=\left(\frac{(2)(0.8167)}{(0.6183)(0.9863)}\right)\times\left(1-0.086216\frac{(200^2-166^2)}{T^2}\right)\times\frac{\left(1+0.086216\left(\frac{720}{T}\right)^2\right)}{\left(1+0.086216\left(\frac{710}{T}\right)^2\right)}\times\exp\left(556.3-\left(\frac{1.438}{2}\right)\times(0.3817\omega_1^{\neq}{}_{\text{H}_2\text{Cl}})\right)\Big/T. \quad (11)$$

It is interesting to note that the temperature independent factor in k_1/k_{2a}, which is equal to

$$(2)(\omega_{\text{HT}}/\omega_{\text{H}_2})/(\omega_1^{\neq}\omega_i^{\neq})_{\text{HTCl}}/(\omega_1^{\neq}\omega_i^{\neq})_{\text{H}_2\text{Cl}},$$

is calculated to be 2.68. This is in excellent agreement with the experimental value of $2(1.35\pm0.03)$. The calculated value is based entirely on Eq. (1), the treatment of the bending frequencies as a quantum correction, and a set of frequency ratios for the transition state which are practically invariant with respect to the structural parameters for the transition state. Furthermore, $\omega_1^{\neq}{}_{\text{H}_2\text{Cl}}$ is evaluated by choosing $T=273.16°\text{K}$ and is found to be 1002 cm^{-1}. A plot of $R\equiv k_{\text{H}_2}/2k_{2a}$, calculated from Eq. (11) as a function of temperature is given in Fig. 2. The results are in excellent agreement with the experimental data at the three other temperatures.

The ratio of the rate constants, $R\equiv k_{\text{H}_2}/k_{\text{D}_2}$, $R\equiv k_{\text{H}_2}/\Sigma k_{\text{HD}}$, for the analogous deuterium reactions can be calculated from the frequency assignment given in Table II and the appropriate frequency ratios. The latter ratios can again be taken from those of the appropriate H_2O molecules. The fit with the experimental data shown in Fig. 2 is probably within the limits of error of the deuterium data.

A value for $\omega_1^{\neq}{}_{\text{H}_2\text{Cl}}$ can similarly be calculated for the linear model, except that in this case $k_{2a}\neq k_{2b}$. At 273.16°K we find from the experimental data

$$\frac{1}{R}=0.2688=\frac{k_{2a}}{k_1}+\frac{k_{2b}}{k_1} \quad (12)$$

[16] J. Bigeleisen, J. Chem. Phys. **18**, 481 (1950).

TABLE III. Frequency assignment for a linear H_2Cl complex.

$\omega_1^{\neq}$	1460 cm^{-1} calculated from HT experimental data at 273.16°K
$\omega_2^{\neq}$	200 cm^{-1} approximated
$\omega_i^{\neq}$	$720i$ cm^{-1} calculated by WTE

and theoretically

$$\frac{k_{2a}}{k_1}=\frac{(0.597)(0.993)}{(2)(0.8167)}\frac{(1+0.0224u_b^2)^2}{(1+616/T^2)}\times\exp[(0.2899\omega_1^{\neq}-556.3)/T], \quad (13)$$

$$\frac{k_{2b}}{k_1}=\frac{(0.595)(0.998)}{(2)(0.8167)}\frac{\left(1+0.086216\left(\frac{428}{T}\right)^2\right)}{\left(1+0.086216\left(\frac{720}{T}\right)^2\right)}\times(1+0.0050u_b^2)^2\exp(-556.3/T). \quad (14)$$

Solution of Eqs. (12), (13), and (14) gives 1460 cm^{-1} for $\omega_1^{\neq}{}_{\text{H}_2\text{Cl}}$. In Fig. 3 we intercompare $\log R_{\text{calc}}$ with the experimental data as a function of $1/T$. It is obvious that the HT data at other temperatures do not agree as well with the linear as with the isosceles triangular model. For the linear model the deviations between R_{calc} and R_{obs} approach 5%. It does not appear that the agreement can be significantly improved by a different choice of $\omega_2^{\neq}{}_{\text{H}_2\text{Cl}}$ or $\omega_i^{\neq}{}_{\text{H}_2\text{Cl}}$. On the other hand, the linear model, with the frequency assignment given in Table III and the frequency ratios calculated from the WTE potential,[10] gives excellent agreement with the data of Rollefson[8] on the relative rates of reaction of H_2 and D_2. It should be pointed out that the temperature coefficient of Rollefson's relative rate constants is probably too high, since it is practically equal to the zero-point energy difference between H_2 and D_2. A fit of $(R_{\text{HT}})_{\text{calc}}$ to an equation of the form $R=Ae^{B/T}$ leads to values of A and B which are respectively high and low compared with the experimental data.

Both the triangular and the linear models give fairly satisfactory fit with the experimental data. They remove many of the questions and uncertainties raised by the poor agreement with experiment shown by the WTE potential. The inadequacy of the latter is not at all surprising. It is known from exchange equilibria involving the isotopes of hydrogen that the entropy changes are readily calculable, but a calculation of the enthalpy change requires a potential function which is correct even with respect to the anharmonic corrections.[13,17–19] Figures 2 and 3 suggest the importance of additional experimental data on isotopic species other than HT as further confirmation for either the linear or isosceles triangular model or one in between.

[17] R. E. Weston, Jr. and J. Bigeleisen, J. Chem. Phys. **20**, 1400 (1952).
[18] J. Bigeleisen and A. Kant, J. Am. Chem. Soc. **76**, 5957 (1954).
[19] W. F. Libby, J. Chem. Phys. **11**, 101 (1943).

Letters to the Editor

THIS section will accept reports of new work, provided these are terse and contain few figures, and especially few half-tone cuts. The Editorial Board will not hold itself responsible for opinions expressed by the correspondents. Contributions to this section should not exceed 600 words in length and must reach the office of the Editor not later than the 15th of the second month preceding that of the issue in which the Letter is to appear. No proof will be sent to the authors. A publication charge of $10.00 per Letter is made which, when honored, will entitle the Institution to 100 free reprints.

Nuclear Hyperfine Structure in the Paramagnetic Resonance Absorption of Triarylaminium Perchlorates*

O. R. GILLIAM, *Department of Physics*, AND ROBERT I. WALTER, *Department of Chemistry, University of Connecticut Storrs, Connecticut*
AND
V. W. COHEN, *Brookhaven National Laboratory, Upton, New York*
(Received June 15, 1955)

WE have observed hyperfine splitting in the microwave paramagnetic resonances of dilute liquid solutions of a series of free radical triarylaminium perchlorates.[1]

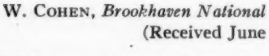

The compounds studied have the three substituents $G=CH_3O-$, C_6H_5-, and CH_3OCO-. Each compound exhibits a single resonance line when observed as a polycrystalline solid.[2] In dilute solution this line separates into three equally spaced peaks. We attribute this splitting to interaction of the unpaired electron moment with the N^{14} nuclear magnetic moment, which has three possible orientations in the applied magnetic field. The separation between peaks for the strong field case[3] is a measure of the interaction constant for these magnetic moments. For the trianisyl- and tribiphenylylaminium radicals in 0.001 M tetrachloroethane solution this separation is 10 ± 1 gauss. Within these limits we have been unable to detect a difference in the interaction constants for the two compounds. The tris(*p*-carbomethoxyphenyl) aminium salt decomposed too rapidly in solution to permit similar measurement. The partially resolved hyperfine structure at a concentration of 0.006 M is shown in Fig. 1 for the tribiphenylylaminium salt.

The apparatus used by Kikuchi and Cohen[4] was modified for this research as follows. A 2K50 klystron oscillator was stabilized at a frequency of 24 300 Mc/sec for the rf source. For the line separation measurements the crystal detector output signal was fed to a 30-cps selective amplifier with a phase-sensitive detector, and the amplified signal was traced by a recorder. The 30-cps magnetic field modulation was about four gauss peak-to-peak. Thin-walled quartz tubes drawn to 1.0–1.3 mm inside diameter held a 1-cm column of sample solution in the cavity. Larger amounts of sample were less effective due to dielectric losses of the solvents required for these free radicals.

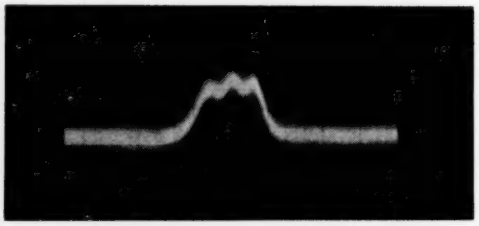

FIG. 1. Oscilloscope picture of partially resolved hyperfine structure for tribiphenylylaminium perchlorate in 0.006 M tetrachloroethane solution, at a frequency of 24 300 Mc/sec.

Weissman[5] has shown that observation of nuclear hyperfine structure in the paramagnetic resonance absorption of polyatomic free radicals in liquid solution is possible only if the orbital part of the odd electron wave function be nonvanishing at the nucleus. We conclude from this that the wave function of the unpaired electron in the aminium salts has partial *s* character at the central nitrogen nucleus. Consequently, the three bonds to this nitrogen (and to the central carbon in C^{13} triphenylmethyl[6]) cannot be pure sp^2 hybrids, and may not be coplanar. They have generally been assumed to be coplanar since the papers of Hückel[7] and of Pauling and Wheland[8] on the stability of aromatic free radicals. Conclusive experimental evidence bearing on the stereochemistry is lacking, but the available data suggest that such molecules can assume a pyramidal configuration[9] (two of these are possible, related as object and mirror image), but cannot retain a given configuration in solution.[10] The hyperfine structure reported here reinforces the previous evidence for a pyramidal configuration in these radicals.

We wish to thank Mr. Max Weiss and Dr. D. S. Gilbert of Bookhaven National Laboratory for their interest and cooperation during the course of this work.

* Work performed at the Brookhaven National Laboratory under contract with the U. S. Atomic Energy Commission.
[1] R. I. Walter, J. Am. Chem. Soc. (to be published).
[2] Walter, Codrington, D'Adamo, and Torrey (to be published).
[3] Norman Ramsey in *Experimental Nuclear Physics, Vol. I* (John Wiley and Sons, Inc., New York, 1953), edited by E. Segrè, p. 371.
[4] C. Kikuchi and V. W. Cohen, Phys. Rev. **93**, 394 (1954).
[5] S. I. Weissman, J. Chem. Phys. **22**, 1378 (1954).
[6] S. I. Weissman and J. C. Snowden, J. Am. Chem. Soc. **75**, 503 (1953).
[7] E. Hückel, Z. Physik **83**, 632 (1933).
[8] L. Pauling and G. W. Wheland, J. Chem. Phys. **1**, 362 (1933).
[9] S. I. Weissman, J. Chem. Phys. **22**, 155 (1954). Described solid solutions of triphenylmethyl in triphenylamine, which is known to be pyramidal. G. Karagunis and G. Drikos, Z. physik Chem. **B26**, 428 (1934). Demonstrated preferential halogenation of one of the pyramidal configurations of a solution of a triarylmethyl exposed to circularly polarized light.
[10] E. S. Wallis and F. H. Adams, J. Am. Chem. Soc. **55**, 3838 (1933). Showed that triarylmethyls fail to retain optical activity when prepared in solution from optically active starting materials.

Photoionization Efficiencies and Cross Sections in NH_3†

W. C. WALKER AND G. L. WEISSLER
Department of Physics, University of Southern California, Los Angeles 7, California
(Received May 27, 1955)

ALTHOUGH absorption spectra,[1] absorption coefficients,[2] and photoionization cross sections[3] of the NH_3 molecule have been reported for the region above 1000 A, at shorter wavelengths there appear to be no published data. In this letter recent measurements of the absorption cross sections, ionization efficiencies, and ionization cross sections of NH_3 from the onset of the ionization continuum to 687 A are presented. The equipment and experimental method have been reported previously.[4]

In Fig. 1(a) are shown the efficiencies of NH_3 in percent or ion pairs per 100 absorbed quanta. Ionization began at 1231 ± 5 A, corresponding to 10.07 ± 0.05 ev. This is in agreement with the first ionization potential of 10.25 ± 0.1 ev obtained by Watanabe[3] and the electron impact value of 10.5 ± 0.1 ev by Mann, Hustrulid, and Tate.[5] The absorption and ionization cross sections are presented in Fig. 1(b). An estimate of the accuracy of these data indicated a probable error of 5 to 10% for the absorption cross sections and 15 to 20% for the ionization cross sections, depending on the intensity of the source lines. The contour of the ionization continuum below 1000 A is shown by the solid line. Due to insufficient light intensity, no ionization data were obtained between 991 A and 1216 A. This region has been, however, carefully investigated by Watanabe,[3] whose data are shown in the figure by the dotted line. His curve is in agreement with that extrapolated from the present data on the basis of the trend of the absorption cross sections.

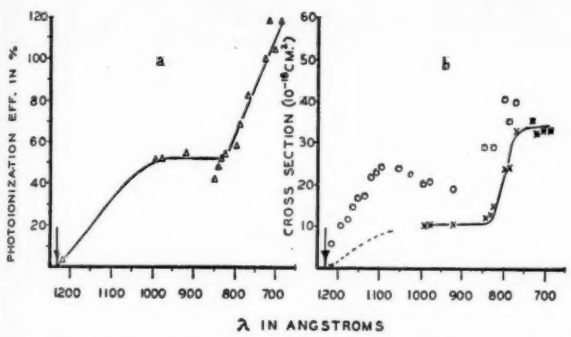

FIG. 1. (a) Photoionization efficiencies of NH_3. (b) Absorption and ionization cross sections of NH_3. ○ Absorption cross sections. × Ionization cross sections. The ionization onset at 1231 ±5 A is marked by an arrow. All data were taken with 3 cm ionization chambers and a 5 A resolution (see reference 4). The dotted line represents Watanabe's (see reference 3) ionization measurements.

The continuum for wavelengths longer than 825 A appears to be due to the direct ionization of the most weakly bound electron of the NH_3 molecule. Near the onset, however, there may be preionized bands present.[3] At 824 A both the ionization efficiency and cross section were found to rise steeply, which may be caused by the onset of a second continuum at about 15 ev as proposed by Sun and Weissler.[2] In this regard, however, electron impact work[5] has shown that the dissociative ionization process

$$NH_3 \rightarrow NH_2^+ + H + e^-$$

has an appearance potential of 15.7 ev with a probability comparable to that of the direct ionization process. It is therefore possible that this process also contributes to the increase in cross section at short wavelengths.

† The aid of the Office of Naval Research is gratefully acknowledged.

[1] A. B. F. Duncan, Phys. Rev. **47**, 822 (1933).
[2] H. Sun and G. L. Weissler, J. Chem. Phys. (to be published).
[3] K. Watanabe, J. Chem. Phys. **22**, 1564 (1954).
[4] Wainfan, Walker, and Weissler, Phys. Rev. (to be published).
[5] Mann, Hustrulid, and Tate, Phys. Rev. **58**, 340 (1940).

On the Fluorescence of Self-Activated Zinc Sulfide

ARRIGO ADDAMIANO
Advanced Lamp Development Laboratory, Lamp Division, General Electric Company, Nela Park, Cleveland, Ohio
(Received May 31, 1955)

THE mechanism of "self-activation" of zinc sulfide has been discussed in a number of recent papers by Bube[1–3] who found that pure zinc sulfide fired, without addition of halides, at 950°–1350°, shows the characteristic blue fluorescence due to "self-activation." According to Bube, a cation vacancy is responsible for the blue band.

Such an interpretation is favored by Kröger and Vink[4,5] who suggest that the luminescent center in self-activated ZnS be a cation vacancy whose nearest surroundings have lost one electron (V_c^+). In support of such a model, Kröger points out that "at low firing temperatures the appearance of the blue fluorescence of self-activated ZnS depends upon the presence of 'promotor ions' (monovalent anions or trivalent cations)."

It seemed interesting, in view of this interpretation, to see what is the minimum firing temperature at which self-activation of pure zinc-sulfide takes place. As the firing times used by Bube were extremely short,* some 10 minutes, it was possible that self-activation at lower temperatures could be detected if due time was allowed.

I have fired luminescent grade ZnS in an atmosphere of nitrogen at 800, 750, 700, 650, and 600°C for times varying from one hour to 48 hours. For all the samples fired at any of the above-mentioned temperatures, except 600°C, I could observe self-activation, that is the characteristic blue-band peaking at about 4700 A as found by Bube for cubic ZnS (λ_{exc} 3650 A). Higher brightness was obtained if higher firing temperatures and longer firing times were used—as it should be expected. In agreement with Bube the brightness of the samples fired without additions was much lower than that of analogous samples fired with addition of halides for the same length of time at the same temperature.

It should be noted that, according to experiments of Tiede and Weiss,[6] the diffusion of CdS in ZnS, with formation of solid solution, can be detected at temperatures as low as 650°. This fact, together with the observation by Bube, that an increase in temperature is equivalent to an addition of halides, and the result of my experiments, seems to indicate that self-activation is due to some kind of lattice disorder.

[1] R. H. Bube, Phys. Rev. **80**, 655 (1950).
[2] R. H. Bube, J. Chem. Phys. **20**, 708 (1952).
[3] R. H. Bube, J. Phys. Chem. **57**, 785 (1953).
[4] F. A. Kröger and H. J. Vink, J. Chem. Phys. **22**, 250 (1954).
[5] F. A. Kröger, Brit. J. Appl. Phys. Suppl. No. 4, 58 (1955).
* Bube fired the ZnS in air to avoid oxidation.
[6] E. Tiede and E. Weiss, Chem. Ber. **65**, 364 (1932).

Intramolecular O−H−O Hydrogen Bonds in Bis-(Dimethylglyoximato)-Cobalt (III)-Complexes

JUNNOSUKE FUJITA, AKITSUGU NAKAHARA, AND RYUTARO TSUCHIDA
Department of Chemistry, Faculty of Science, Osaka University, Nakanoshima, Osaka, Japan
(Received May 17, 1955)

RECENTLY Rundle *et al.*[1–3] have shown by x-ray and infrared examinations that the complex molecule of bis-(dimethylglyoximato)-nickel(II) is planar and contains four five-membered rings as shown in Fig. 1. Of special interest was the

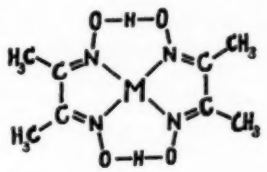

FIG. 1.

very short O−H−O hydrogen bond, 2.44 A, shorter than any O−H−O hydrogen bond heretofore reported. Furthermore, it was also noteworthy that the O−H stretching frequency for this hydrogen bond is only 1775 cm^{-1}, and that spectroscopic arguments have been presented indicating that the hydrogen lies symmetrically between the two oxygens in this case. The above structure is, however, not always expected in sexa-coördinate complexes, since there are two possible types of configurations concerning the way of coördination of two dimethylglyoximate ions about a cobalt atom, i.e., the one is planar and the other is nonplanar coördination. We have measured infrared absorption spectra of hydrogen dichloro-bis-(dimethylglyoximato)-cobaltate(III)[4,5] preparing with both normal and deuterated dimethylglyoxime and several other bis-(dimethylglyoximato)-cobalt(III)-complexes.[6] The spectra were obtained with a Perkin-Elmer Model 21 spectrophotometer using sodium-chloride prisms and Nujol suspensions of the compounds in question.

TABLE I.

Complex[a]	O−H stretching freq. in cm^{-1}
$H[Co(DH)_2Cl_2]$	1725
$H[Co(DH)_2Br_2]$	1685
$Na[Co(DH)_2(NO_2)_2]$	1740
$[Co(OH_2)(DH)_2(NO_2)]$	1770

[a] (DH = dimethylglyoximate ion, $H_3CC(NO)C(NOH)CH_3$.

As is seen in Table I, all the curves of bis-(dimethylglyoximato)-cobalt(III)-derivatives show a similar O—H stretching band as that assigned by Rundle on the curve of bis-(dimethylglyoximato)-nickel(II) in their respective region, 1680 to 1770 cm^{-1}. On the other hand, the absorption band at 1725 cm^{-1} on the curve of hydrogen dichloro-bis-(dimethylglyoximato)-cobaltate(III) disappeared on substitution of D for H. Moreover, there could not be found any absorption band on the curve of tris-(dimethylglyoximato)-cobalt(III)[7] in the corresponding region. Namely, the above-mentioned absorption bands found in the region of 1680 to 1770 cm^{-1} are characteristic of bis-(dimethylglyoximato)-cobalt(III)-derivatives. Since the strong hydrogen bond of such kind as presented in the case of bis-(dimethylglyoximato)-nickel(II) will be expected only with the planar coördination of two dimethylglyoximate ions, *the present O—H stretching bands are the first direct evidence for the planar coördination of two dimethylglyoximate ions in bis-(dimethylglyoximato)-cobalt(III)-complexes.*

As is clear from Table I, however, O—H stretching frequencies in the cobalt(III) complexes are somewhat lower than that in the nickel(II) complex, although they vary with the sorts of two other ligands. But many examples of very short O—H—O hydrogen bond are expected in the series of bis-(dimethylglyoximato)-cobalt(III)-derivatives.

The authors are indebted to Mr. Naofumi Ooi of the Sumitomo Chemical Company for obtaining most of the spectra and to Dr. M. Kobayashi and Dr. S. Seki for their helpful discussions.

[1] Godycki, Rundle, Voter, and Banks, J. Chem. Phys. **19**, 1205 (1951).
[2] R. E. Rundle and M. Parasol, J. Chem. Phys. **20**, 1487 (1952).
[3] L. E. Godycki and R. E. Rundle, Acta Cryst. **6**, 487 (1953).
[4] F. Feigl and H. Rubinstein, Ann. **433**, 183 (1923).
[5] L. Cambi and C. Coriselli, Gazz. chim. ital. **66**, 81 (1933).
[6] A. Nakahara, Bull. Chem. Soc. Japan (to be published).
[7] A. Nakahara and R. Tsuchida, J. Am. Chem. Soc. **76**, 3103 (1954); A. Nakahara, Bull. Chem. Soc. Japan **27**, 560 (1954).

Second Virial Coefficient for Ellipsoids with Imbedded Dipoles*

CHARLES MUCKENFUSS AND C. F. CURTISS *Department of Chemistry,*
AND
R. B. BIRD, *Department of Chemical Engineering, University of Wisconsin, Madison, Wisconsin*

(Received June 8, 1955)

ACCORDING to statistical mechanics, the second virial coefficient for cylindrically symmetric molecules is[1]

$$B(T)=(N/4)\int_0^\infty\int_0^{2\pi}\int_0^\pi\int_0^\pi(1-e^{-\varphi/kT})r^2 \times\sin\theta_1\,\sin\theta_2 d\theta_1 d\theta_2 d\phi dr, \quad (1)$$

where $\varphi(r,\theta_1,\theta_2,\phi)$ is the intermolecular potential. As shown in Fig. 1, r is the distance between centers of interacting molecules,

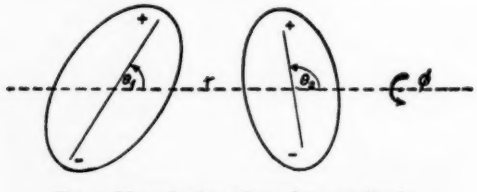

FIG. 1. Mutual orientations of two molecules.

and θ_1, θ_2, and ϕ describe the orientations of the interacting molecules.

Equation (1) has been used to calculate $B(T)$ for a number of molecular models involving either shape effects or the interaction of multipole moments. As a first attempt to include both shape and polar characteristics of the molecules, we have calculated $B(T)$ for rigid ellipsoids of revolution with point dipoles imbedded along the axis of revolution. The ellipsoids (all identical)

TABLE I. Values of the B_{mn}.

m \ n	0	2	4	6
0	+1	−1	$+\frac{1}{15}$	0
2	$-\frac{1}{3}$	$-\frac{4}{15}$	$-\frac{26}{105}$	$-\frac{76}{315}$
4	$-\frac{1}{75}$	$-\frac{17}{525}$	$-\frac{151}{3675}$	$-\frac{15\,707}{175\,175}$
6	$-\frac{29}{55\,125}$	$-\frac{2}{1575}$	$-\frac{2932}{1\,091\,475}$	$-\frac{535\,993}{42\,567\,525}$

are characterized by two parameters: σ, the length of the axis about which the generating ellipse is rotated; and ϵ, the eccentricity, which is defined by $\epsilon=[1-(\tau/\sigma)^2]^{\frac{1}{2}}$, where τ is the length of the other axis of the generating ellipse. For prolate ellipsoids ϵ is real, for both oblate ellipsoids ϵ is imaginary. For this model the intermolecular potential is

$$\begin{aligned}\varphi(r,\theta_1,\theta_2,\phi)&=\infty && r<r_c\\ \varphi(r,\theta_1,\theta_2,\phi)&=-(\mu^2/r^3)g(\theta_1,\theta_2,\phi) && r>r_c\end{aligned} \quad (2)$$

where

$$g(\theta_1,\theta_2,\phi)=2\cos\theta_1\cos\theta_2-\sin\theta_1\sin\theta_2\cos\phi,$$

μ is the dipole moment, and r_c is the distance between the centers of the ellipsoids when they are in contact (a function of θ_1, θ_2, ϕ and, parametrically, σ and ϵ).

The integral expression for $B(T)$ in Eq. (1) may be written as the sum of two integrals over r: the first from 0 to r_c and the second from r_c to ∞. When $\exp(-\varphi/kT)$ in the second integral is expanded in a series, Eq. (1) becomes

$$B(T)=(N/4)\int_0^{2\pi}\int_0^\pi\int_0^\pi\left[\int_0^{r_c}r^2dr\right]\sin\theta_1\,\sin\theta_2 d\theta_1 d\theta_2 d\phi$$
$$-(N/4)\sum_{j=1}^\infty\frac{1}{j!}\left(\frac{\mu^2}{kT}\right)\int_0^{2\pi}\int_0^\pi\int_0^\pi g^j\left[\int_{r_c}^\infty r^{2-3j}dr\right]$$
$$\times\sin\theta_1\,\sin\theta_2 d\theta_1 d\theta_2 d\phi. \quad (3)$$

The integration over r presents no difficulty; in order to perform the integrations over the angles one needs an expression for r_c in terms of σ, ϵ, and the angles representing the orientations of the molecules. For both prolate and oblate ellipsoids r_c may be expressed[2] as a power series in ϵ:

$$\begin{aligned}(\sigma/r_c)^2=1&+\epsilon^2[1-\tfrac{1}{2}(c_1^2+c_2^2)]\\ &+\epsilon^4[1-\tfrac{3}{4}(c_1^2+c_2^2)+\tfrac{1}{16}(c_1^2-c_2^2)^2\\ &\qquad+\tfrac{1}{2}(c_1^2c_2^2+s_1s_2c_1c_2c)]\\ &+\epsilon^6[1-\tfrac{7}{8}(c_1^2+c_2^2)+\tfrac{1}{16}(c_1^2-c_2^2)^2\\ &\quad+(c_1^2c_2^2+s_1s_2c_1c_2c)+\tfrac{1}{32}(c_1^2+c_2^2)(c_1^2-c_2^2)^2\\ &\qquad-\tfrac{1}{8}(c_1^2+c_2^2)(c_1c_2+s_1s_2c)^2]+\cdots,\end{aligned} \quad (4)$$

where $s_1=\sin\theta_1$, $c_i=\cos\theta_i$, and $c=\cos\phi$.

After integrating Eq. (3) one obtains $B(T)$ as a double-power series in (μ^2/σ^3kT) and ϵ:

$$B(T)=(2/3)\pi N\sigma^3\sum_{m=0}^\infty\sum_{n=0}^\infty B_{mn}(\mu^2/\sigma^3kT)^m\epsilon^n, \quad (5)$$

where the B_{mn} are

$$B_{mn}=[8(m-1)(m!)]^{-1}\int_0^{2\pi}\int_0^\pi\int_0^\pi g^m f_{mn}(\theta_1,\theta_2,\phi) \times\sin\theta_1\,\sin\theta_2 d\theta_1 d\theta_2 d\phi$$

for $m\geqslant 2$. The $f_{mn}(\theta_1,\theta_2,\phi)$ are the coefficients of ϵ^n in the expansion of $(r_c/\sigma)^{3(1-m)}$. For $m=0$ the coefficients are calculated from the first integral in Eq. (3). For m or n an odd integer, the B_{mn} are zero.

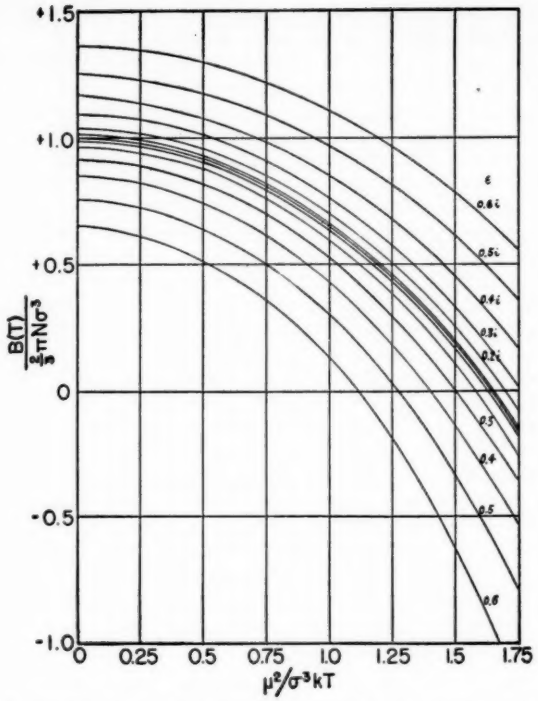

FIG. 2. The reduced second virial coefficient $B(T)/\frac{2}{3}\pi N\sigma^3$ as calculated from Eq. (5) as a function of the reduced dipole moment for $|\epsilon| \leq 0.6$.

The B_{mn} are given in Table I and the reduced second virial coefficient $B(T)/\frac{2}{3}\pi N\sigma^3$ is plotted in Fig. 2 as a function of ϵ and $(\mu^2/\sigma^3 kT)$. From these results it is clear that shape effects are of considerable importance in the second virial coefficient of elongated or flattened polar molecules.

* This research was supported by National Science Foundation Grant No. G-994, Department of Chemistry (CM and CFC), and National Science Foundation Grant No. NSF G-356, Department of Chemical Engineering (RBB).

[1] Hirschfelder, Curtiss, and Bird, *Molecular Theory of Gases and Liquids* (John Wiley and Sons, Inc., New York, 1954), Sec. 3.4.

[2] Muckenfuss, Curtiss, and Bird, The Second Virial Coefficient for Ellipsoids with Imbedded Dipoles, University of Wisconsin Naval Research Laboratory Report WIS-NSF-2 (April 29, 1955).

State of Nitrogen Adsorbed on Tungsten

GERT EHRLICH
General Electric Research Laboratory, Schenectady, New York
(Received June 13, 1955)

THE work of Roberts[1] and of Beeck[2] established that the adsorption of diatomic gases such as H_2, N_2, and O_2 on metal surfaces occurred rapidly and with an initially high liberation of heat (40 to 160 kcal per mole of gas for tungsten) provided adequate precautions were taken to obtain and maintain system and specimen clean. However, the first *detailed* measurements of the kinetics of chemisorption on a metal surface have only recently been reported by Becker and Hartman,[3] who investigated the adsorption of nitrogen on tungsten using the flash filament technique. For this system the rate of chemisorption decreases with increasing temperature, and from this unexpected temperature dependence it has been concluded that chemisorption occurs through the intermediary of physically adsorbed molecules, held to the surface by the van der Waals forces.[4]

It has now been observed in this laboratory that, upon rapidly heating a tungsten filament kept in a dilute atmosphere of nitrogen ($\sim 10^{-7}$ mm Hg), the adsorbed gas is given off in two distinct temperature ranges; evolution of the first component (designated as α) is complete at a temperature below 800°K, that of the second component (β) below 2000°K. A somewhat similar dependence of gas evolution upon filament temperature has been reported by Hagstrum[5] for the residual gases in a high vacuum line. The fine structure of the burst is apparent from Fig. 1, in which is plotted the pressure variation in our system, as traced by an ion gauge during a typical run; Fig. 2 gives the dependence of the rate of impingement of gas on the sample (ν), as well as of the number of molecules adsorbed in state α and β, upon the duration of the time interval during which adsorption occurred on the tungsten. It is interesting that although the number of molecules adsorbed in the β component, $n_{2\beta}$, increases monotonically with time, the population of state α, $n_{2\alpha}$, passes through a maximum.

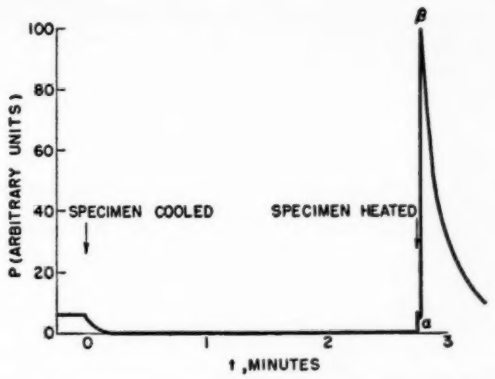

FIG. 1. Pressure variation in flash filament cell. Initial nitrogen pressure $=8.5\cdot10^{-8}$ mm Hg; $t=25$°C.

Adsorption of gases other than nitrogen does not appear to be responsible for the α peak—the residual pressure in the system and the impurity content of the gas admitted were kept at a level too low to account for the rate of increase of $n_{2\alpha}$. Neither can the α component of the burst be due to positively charged ions from the adsorption sample, inasmuch as these would not be recorded by the gauge. The α peak *may* indicate a surface complex in which a nitrogen "molecule" is bonded to the tungsten substrate through its π electrons, with only the σ orbital bonding two nitrogen atoms. Such a species could in catalytic reactions play the role envisaged by Rideal for molecules in deep lying van der Waals levels.[6]

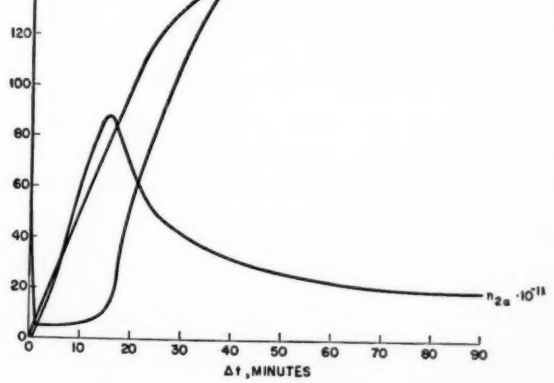

FIG. 2. Time dependence of nitrogen adsorption on tungsten at 25°C. ν = No. of molecules striking filament per minute. $n_{2\alpha}$ = No. of molecules adsorbed in α component. $n_{2\beta}$ = No. of molecules adsorbed in β component. Filament area = 0.97 cm². Initial nitrogen pressure $=8.5\cdot10^{-8}$ mm Hg.

Although the nature of the α component is not established, it has been possible to show that it does *not* constitute the precursor for the irreversibly bound nitrogen, previously postulated.[4] The quantity

$$\frac{1}{n_{2\alpha}}\left(\frac{dn_{2\beta}}{dt}\right)$$

which, at a fixed $n_{2\beta}$ must be invariant with pressure if the α component constitutes the precursor to chemisorption, has been found to *increase* with increasing pressure. Moreover, removal of species α from the surface, by subjecting the filament to a short low, temperature flash, does not affect the rate $dn_{2\beta}/dt$. The number of α species, however, depends upon the rate $dn_{2\beta}/dt$ and decreases from its maximum value with a rate proportional to the rate of increase of $n_{2\beta}$. Though the precursor state to chemisorption has not been isolated, it appears from these studies, details of which will be published in the future, that at least three distinct levels of interaction are involved in the absorption of nitrogen on a sparsely covered tungsten surface.

[1] A. R. Miller, *Adsorption of Gases on Solids* (Cambridge University Press, Cambridge, England, 1949).
[2] A. Wheeler, *Structure and Properties of Solid Surfaces* (University of Chicago Press, Chicago, 1953), p. 449.
[3] J. A. Becker and C. D. Hartman, J. Phys. Chem. **57**, 157 (1953).
[4] G. Ehrlich, J. Phys. Chem. **59**, 473 (1955).
[5] H. D. Hagstrum, Rev. Sci. Instr. **24**, 1122 (1953).
[6] E. K. Rideal, Proc. Cambridge Phil. Soc. **35**, 130 (1939).

Determination of the Equilibrium Constant of the Reaction between BF_3 and BCl_3†

T. H. S. Higgins, E. C. Leisegang, C. J. G. Raw, and A. J. Rossouw
Department of Chemistry and Chemical Technology, University of Natal, Pietermaritzburg, South Africa
(Received May 24, 1955)

Nightingale and Crawford[1] have recently reported a preliminary study of the kinetics of the reaction

$$BF_3+BCl_3=BFCl_2+BF_2Cl$$

and Professor Crawford has kindly supplied us with details of his work on this reaction. As Gamble, Gilmont, and Stiff[2] did not observe any reaction between BF_3 and BCl_3, it was decided to investigate the extent to which the reaction takes place. This was done by using a single-beam infrared spectrometer constructed in these laboratories,[3] as the only available data on the hitherto unreported mixed halides were their unpublished vibrational spectral assignments, for which the authors are indebted to Professor M. K. Wilson of Harvard University.

The course of the reaction was followed by measuring the intensity of the absorption band at 955 cm^{-1}, due to $^{11}BCl_3$.[4] This band is not affected by any of the other components which are present in the reaction. The relationship between the concentration of the absorbing medium and the intensity of the transmitted radiation is expressed by the Beer-Lambert law in the following form:

$$\log I_0/I=E'\cdot c, \qquad (1)$$

where $E'=E\cdot l$, I_0 is the intensity of the incident radiation, I the intensity of the transmitted radiation, E the extinction coefficient for unit concentration, l the length of the absorption cell, and c the concentration of the absorbing medium.

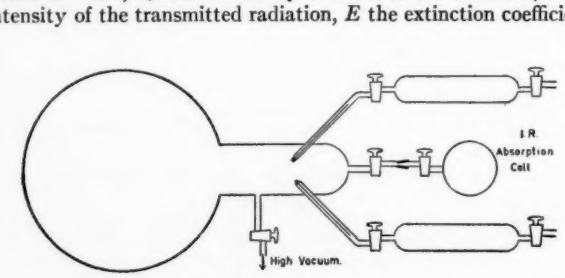

Fig. 1. Diagram of reaction vessel.

Because of the strength of the band, the initial pressure of the BCl_3 and BF_3 had to be of the order of 2 mm, using a 10-cm gas cell. Accurate measurement of the pressures was obtained by first introducing the gas in question at a pressure of 25 to 35 cm to a bulb of small but known volume (±6 cc) attached to the reaction vessel (Fig. 1). The gas was then expanded into the reaction vessel and the infrared absorption cell, the total volume of which was known (±1290 cc). The pressure of the gas in the cell could then be calculated.

The constant E' [Eq. (1)] was obtained by measuring the ratio I_0/I for varying concentrations of BCl_3 and was found to be independent of concentration, within the limits of experimental error, for the range of concentrations used. The value obtained, with a 95% confidence interval, was $E'=3.69\pm0.08$ when the concentrations of the gases were measured in terms of their pressures. To determine the equilibrium constant the two bulbs were filled with the respective gases at known pressures and the taps leading to the reaction vessel were opened simultaneously. Adequate mixing was ensured by the two capillary jets (Fig. 1), and as an added precaution the cell was left connected to the reaction vessel for 15 minutes before being placed in the spectrometer. It was found that the reaction came to equilibrium after a time of about 30 minutes. The equilibrium concentration of BCl_3 was calculated from the resulting spectra, which were obtained at temperatures of between 27°C and 29°C.

The equilibrium constant of the reaction is given by

$$\frac{[BFCl_2]\cdot[BF_2Cl]}{[BF_3]\cdot[BCl_3]}=K_c. \qquad (2)$$

The mean of a number of determinations of K_c was found to be 0.53 ± 0.04. The uncertainty in this result lies within the estimated limits of error of the method. Therefore, in an equimolecular mixture of BF_3 and BCl_3 approximately 42% of these gases will be converted into the mixed halides. As has been pointed out in the case of the BBr_3-BCl_3 reaction,[5] it is not possible to isolate the mixed halides by fractional distillation. This fact probably explains why the reaction was not reported earlier.

† The authors received financial support for this research from the South African C.S.I.R. and one of us (A.J.R.) also from the South African Maize Industry Control Board.
[1] R. E. Nightingale and B. Crawford, Jr., J. Chem. Phys. **22**, 1468 (1954).
[2] Gamble, Gilmont, and Stiff, J. Am. Chem. Soc **62**, 1257 (1940).
[3] Leisegang and Rossouw, J. Sci. Inst. (to be published).
[4] Scruby, Lacher, and Park, J. Chem. Phys. **19**, 386 (1951).
[5] Long and Dollimore, J. Chem. Soc. 4457 (1954).

Light Scattering by Water*

J. Kraut and W. B. Dandliker
Department of Biochemistry, School of Medicine, University of Washington, Seattle, Washington
(Received May 31, 1955)

Two recent communications[1,2] have been concerned with the light-scattering properties of water, though neither reported direct measurements of the transverse scattering of clean water. Goring and Napier[1] assumed that clean water would exhibit Rayleigh scattering and on this basis extrapolated from high values of θ to obtain the scattering to be expected at 90° in the absence of foreign particles. They found $R_u(90)=1.05\times10^{-6}$ cm^{-1} at a wavelength of 5461 A. Fessenden and Stein[2] measured the 90° scattering of dilute salt solutions, since these were more readily freed of particulate contamination than pure water, and extrapolated to zero salt concentration. This procedure resulted in a value of $R_u(90)=0.97\times10^{-6}$ cm^{-1} at 5461 A.

In the course of a recent investigation of solution-cleaning procedures in light scattering[3] we have constructed a cell exhibiting extremely small stray-light effects down to $\theta=25°$. The apparatus is similar to that employed by Zimm.[4] Stray-light characteristics, however, are considerably improved by the introduction of an

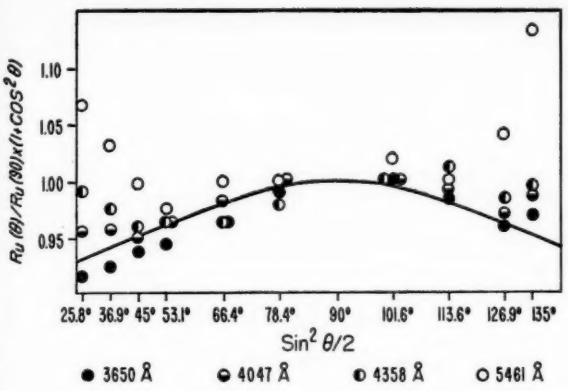

FIG. 1. Angular dependence of scattering by water.

entrance window at the end of a blackened tube extending about 5 cm from the outer container, and a Rayleigh horn light trap instead of an exit window. With this apparatus we have found it possible to determine directly the scattering envelope of water over the range $\theta=25°$ to $\theta=135°$. In order to insure cleanliness of the sample, we have followed the classical procedure[5] of employing a sealed evacuated U-shaped vessel, one arm of which connects to a conical inner cell and the other arm to a "boiler" filled with multiply distilled water. By slowly condensing water from the boiler into the conical cell and rinsing back several times, a perfectly clean sample could be obtained.

The results of scattering measurements on clean water in this apparatus are shown in Fig. 1, in which are plotted the ratios of scattering intensities at various values of θ to the intensity at 90°, multiplied by $F/(1+\cos^2\theta)$, where F is the experimentally determined "fluorescein" factor (approximately $\sin\theta$). Measurements were made with unpolarized incident light at the four mercury-arc wavelengths indicated. That F is independent of wavelength was verified by comparison of angular measurments of the fluorescence of fluorescein and sodium salicylate. The former shows a yellow-green fluorescence while the latter fluoresces violet.

It is evident from the distribution of points representing the shorter wavelengths (where stray light is increasingly negligible with respect to the scattering by water) that the scattering envelope deviates slightly from the Rayleigh law. The solid curve was calculated from an expression given by Stockmayer[6] for the angular dependence of scattering by anisotropic particles irradiated by unpolarized light:

$$\frac{[I(\theta)]_u}{[I_0]_u}=\beta_0^2\left[\left(\frac{6-3\rho_u}{6-7\rho_u}\right)\left(\frac{1+\cos^2\theta}{2}\right)+\left(\frac{3\rho_u}{6-7\rho_u}\right)\left(\frac{3-\cos^2\theta}{2}\right)\right].$$

The depolarization, ρ_u, was taken as 8.3%, the value determined experimentally at 4358 A. It may be concluded that water is *almost* a Rayleigh scatterer, deviating slightly from the $1+\cos^2\theta$ law as a result of molecular anisotropy.

Values for $R_u(90)$ were obtained by "Ludox" calibration. The inner cell was filled with colloidal silica solutions and light-scattering instrument readings at $\theta=90°$ were recorded. Spectrophotometric turbidities were then obtained for the same silica solutions, and the ratios of 90° readings to turbidities were extrapolated to zero turbidity, giving the instrument calibration factor. Values for $R_u(90)$ of water are shown in Table I. Our result for $R_u(90)$ at 5461 A by direct measurement is in excellent agreement with those obtained indirectly by other investigators.

TABLE I. Rayleigh's ratio for water at several wavelengths; unpolarized incident light.

λ, A	$R_u(90)$ of water, cm^{-1}
3650	6.80×10^{-6}
4047	4.05×10^{-6}
4358	2.89×10^{-6}
5461	1.05×10^{-6}

* This investigation has been supported in part by a grant from Initiative 171 of the State of Washington and also by grant H-1111 from the U. S. Public Health Service.

[1] D. A. I. Goring and P. G. Napier, J. Chem. Phys. **22**, 147 (1954).
[2] R. W. Fessenden and R. S. Stein, J. Chem. Phys. **22**, 1778 (1954).
[3] W. B. Dandliker and J. Kraut (to be published).
[4] B. H. Zimm, J. Chem. Phys. **16**, 1099 (1948).
[5] S. Bhagavantam, *Scattering of Light and the Raman Effect* (Chemical Publishing Company, Brooklyn, New York, 1942).
[6] W. H. Stockmayer, personal communication to W. B. Dandliker.

Note on Singular Integral Equations of the Kirkwood-Riseman Type

PETER L. AUER, *General Electric Research Laboratory, The Knolls, Schenectady, New York*

AND

CLIFFORD S. GARDNER,* *General Electric Advanced Electronic Center, Ithaca, New York*

(Received May 26, 1955)

THE use of Oseen's formula to describe hydrodynamic interaction between elements of a polymer chain in solution leads to singular integral equations of the form[1]

$$\phi(x)=f(x)-\lambda\int_{-1}^{+1}\frac{\phi(t)dt}{|x-t|^{\alpha}}. \tag{1}$$

The purpose of this note is to point out that if $0<\alpha<1$, then the kernel of the integral equation has a convenient diagonal representation in terms of certain polynomials related to Legendre polynomials; they are usually termed Gegenbauer[2] polynomials.

We have employed the following definition for the Gegenbauer polynomials defined for $-1\leqslant x\leqslant 1$,

$$P_n^{(\nu)}(x)=\frac{(-1)^n\Gamma(\nu+1)}{2^n\Gamma(n+\nu+1)}(1-x^2)^{-\nu}\frac{d^n}{dx^n}(1-x^2)^{n+\nu}. \tag{2}$$

The polynomials satisfy the differential equation

$$(1-x^2)\frac{d^2}{dx^2}P_n^{(\nu)}(x)-2(\nu+1)x\frac{d}{dx}P_n^{(\nu)}(x)+n(n+2\nu+1)P_n^{(\nu)}(x)=0; \tag{3}$$

and are normalized according to the formula

$$\int_{-1}^{+1}(1-x^2)^{\nu}P_m^{(\nu)}(x)P_n^{(\nu)}(x)dx=\delta_{mn}N_n^{(\nu)}=\delta_{mn}\frac{2^{(1+2\nu)}[\Gamma(1+\nu)]^2\Gamma(n+1)}{(2n+2\nu+1)\Gamma(n+2\nu+1)}.$$

It will be shown below that the kernel appearing in the integral equation may be represented as

$$|x-t|^{-\alpha}=\sum_0^{\infty}a_n(\nu)P_n^{(\nu)}(x)P_n^{(\nu)}(t) \qquad \nu=\tfrac{1}{2}(\alpha-1) \qquad 0<\alpha<1. \tag{5}$$

With the above definition of the quantity ν, the differential equation given by (3) may be recognized as the separated form of Laplace's equation in $2+\alpha$ dimensions with cylindrical symmetry about the x axis. It may also be recognized that the kernel of the integral equation bears a simple relation to the fundamental solution of Laplace's equation for the same geometry.

The expansion coefficients $a_n(\nu)$ may be evaluated in the following manner. It is necessary to evaluate the integral

$$I(\nu,x)=\int_{-1}^{+1}(1-t^2)^{\nu}\frac{P_n^{(\nu)}(t)dt}{|x-t|^{\alpha}}=\delta_{nm}a_m(\nu)N_m^{(\nu)}P_m^{(\nu)}(x). \tag{6}$$

Upon transforming variables, the integral becomes

$$I(\nu,x)=\frac{2^{\alpha}}{(1-x)^{\alpha}}\int_0^{\infty}\frac{u^{\nu}P_n^{(\nu)}\left(\frac{u-1}{u+1}\right)du}{(u+1)\left|\frac{1+x}{1-x}-u\right|^{\alpha}}. \tag{7}$$

The above integral may be evaluated conveniently in terms of a contour integral having branch cuts along the entire positive half of the real axis. The contour is taken along one sheet of the associated Riemann surface and the only contribution to the contour integral arises from the residue of the isolated singularity at -1 on the negative real axis. In this fashion we find

$$I(\nu,x)=2^{(1-\alpha)}\,\pi\ (\text{residue of } F(Z) \text{ at } 0) \tag{8}$$

$$F(Z)=\frac{(1-Z)^{\nu}}{Z\left(1-\left[\frac{1-x}{2}\right]Z\right)^{\alpha}}P_n^{(\nu)}(1-2/Z);$$

after some calculation this becomes

$$I(\nu,x)=\frac{-\pi}{\sin(\nu\pi)}\,\frac{\Gamma(n+2\nu+1)}{\Gamma(2\nu+1)\Gamma(n+1)}P_n^{(\nu)}(x). \tag{9}$$

Collecting the results of Eqs. (6) to (9) and (4), we obtain

$$a_n(\nu)\frac{-\pi}{2^{(1+2\nu)}}\sin(\nu\pi)\left[\frac{\Gamma(n+2\nu+1)}{\Gamma(1+\nu)\Gamma(n+1)}\right]^2\frac{(2n+2\nu+1)}{\Gamma(2\nu+1)}$$

The solution of the integral equation given by (1) may now be reduced to a matrix inversion problem by conventional steps. The question of convergence has to be investigated for each individual case, since (5) does not necessarily converge in the usual sense throughout the fundamental interval. Equation (6) is, nevertheless, always valid and presents the basis for our treatment.

When a Gaussian model is used to describe the statistics of the polymer chain, α assumes the value of $\frac{1}{2}$ and Eq. (1) becomes identical in form with the original Kirkwood-Riseman integral equation.[1] It is to be expected that use of statistics other than Gaussian will lead to values of α lying somewhere between zero and unity. It is hoped the exposition given above will aid in the investigation of the non-Gaussian models.

* Present address: University of California Radiation Laboratory, Livermore, California.

[1] J. G. Kirkwood and J. Riseman, J. Chem. Phys. **16**, 565 (1948).

[2] Whittaker and Watson, *Modern Analysis* (Cambridge University Press, London, 1947), p. 329.

Solution of the Kirkwood-Riseman Integral Equation in the Asymptotic Limit

PETER L. AUER, *General Electric Research Laboratory, The Knolls, Schenectady, New York*

AND

CLIFFORD S. GARDNER,* *General Electric Advanced Electronic Center, Ithaca, New York*

(Received May 26, 1955)

WE specialize the discussion contained in the previous note to the particular case of $\alpha=\frac{1}{2}$, $\nu=-\frac{1}{4}$. The Gegenbauer polynomials $P_n^{(-\frac{1}{4})}(x)$ appropriate in this instance will be denoted simply $P_n(x)$ in what follows and all reference to the superscript notation ν will be suppressed in order to simplify notation.

The pertinent information concerning the required polynomial is contained in the previous note.

In the limit of large molecular weight, the Kirkwood-Riseman integral equation given by Eq. (1) of the previous note is approximated asymptotically by an integral equation of the first kind. The solution of integral equations of the first kind may be accomplished in a relatively simple manner using the Gegenbauer polynominal expansion since the problem of matrix inversion can be avoided entirely.

The prototypes of the equations to be considered is given below together with the formal solution. We include an auxiliary variable which appears in the Kirkwood-Riseman formulation.[1]

$$f(x;y)=\int_{-1}^{+1}\frac{\phi(t;y)}{|x-t|^{\frac{1}{2}}}\,dt \tag{1}$$

$$T=\int_{-1}^{+1}\phi(x;x)dx;$$

$$\phi(x;y)=\sum_0^{\infty}N_m^{-1}b_m(y)P_m(x)/(1-x^2)^{\frac{1}{2}}. \tag{2}$$

Substitution of (2) into (1) and use of the kernel expansion given above yields

$$f(x;y)=\sum_0^{\infty}a_mb_m(y)P_m(x); \tag{3}$$

and upon multiplying both sides of (3) by $P_n(x)/(1-x^2)^{\frac{1}{2}}$ and integrating, we obtain

$$\int_{-1}^{+1}\frac{f(x;y)}{(1-x^2)^{\frac{1}{2}}}P_n(x)dx=\delta_{nm}a_mN_mb_m(y)=c_m(y). \tag{4}$$

Introduction of (4) into (2) yields after terms have been combined

$$\phi(x;y)=A\sum_0^{\infty}(m+\tfrac{1}{4})c_m(y)\,\frac{P_n(x)}{(1-x^2)^{\frac{1}{2}}} \tag{5}$$

$$A=\{\pi^{\frac{1}{2}}[\Gamma(3/4)]^2\}^{-1}.$$

The trace defined by (1) now has the value

$$T=A\sum_0^{\infty}(m+\tfrac{1}{4})\tau_{mm} \tag{6}$$

$$\tau_{mm}=\int_{-1}^{+1}\frac{c_m(x)P_m(x)}{(1-x^2)^{\frac{1}{2}}}dx.$$

We shall now present the solution of (1) for two particular cases

(A) $$f(x;y)=\tfrac{3}{8}(x^2+y^2)+\tfrac{1}{4}$$

(B) $$f(x;y)=|x-y|.$$

The solution for (A) can be written down immediately,

$$\phi_A(x;y)=(x^2+\tfrac{3}{8}y^2)/\pi\sqrt{2}(1-x^2)^{\frac{1}{2}} \tag{7}$$

$$T_A=\left(\frac{11}{8}\right)\left(\frac{N_1^2}{\pi\sqrt{2}}\right)=0.300.$$

The quantity T_A represents contributions of even terms to the viscosity function given below.

The solution of (B) is obtained in the form of an infinite series. The expression for T_B, however, can be summed directly. The calculation of this trace proceeds in the following manner:

$$\tau_{nn}=2\int_{-1}^{+1}dx\frac{P_n(x)}{(1-x^2)^{\frac{1}{2}}}\int_x^{+1}\frac{sP_n(s)}{(1-s^2)^{\frac{1}{2}}}ds$$

$$-2\int_{-1}^{+1}dx\frac{xP_n(x)}{(1-x^2)^{\frac{1}{2}}}\int_x^{+1}\frac{P_n(s)ds}{(1-s^2)^{\frac{1}{2}}} \tag{8}$$

$$=-4\int_{-1}^{+1}dx\frac{xP_n(x)}{(1-x^2)^{\frac{1}{2}}}\int_x^{+1}\frac{P_n(s)ds}{(1-s^2)^{\frac{1}{2}}};\quad n>0.$$

The quantity in the second line of (8) may be evaluated with the aid of the differential equation satisfied by the $P_n(x)$. Following an integration by parts we obtain

$$\tau_{nn}=-\frac{4}{n(2n+1)}\int_{-1}^{+1}(2x^2-1)\frac{P_n(x)P_n(x)}{(1-x^2)^{\frac{1}{2}}}dx;\quad n>0. \tag{9}$$

The above integral is evaluated with the aid of the definition of $P_n(x)$ given by (2) of the previous note. The value of τ_{00} is obtained from an expression similar to (8). The result is given in the form

$$\tau_{nn}=-\frac{4\pi^{\frac{1}{2}}}{3}\left[\frac{1}{(n+1)(2n-1)}\right]\frac{\Gamma(n+\frac{1}{2})}{\Gamma(n+1)};\quad n\geq 0. \tag{10}$$

Substitution of the above expression into (6) and performing the required summation yields

$$T_B=-\tfrac{2}{3}\pi^{\frac{1}{2}}[\Gamma(3/4)]^{-2}. \tag{11}$$

We can now compute the viscosity function denoted $F(x)$ by Kirkwood and Riseman[1]

$$\sqrt{2}[T_A - \tfrac{3}{4}T_B] = 1.259 = \lim_{x\to\infty}\{xF(x)\}. \quad (12)$$

The original value[1] given for this quantity was 1.588 and the revised value[2] reported was 1.48. Using a model in which averages are referred to the center of frictional force instead of the center of mass, Zimm[3] obtains a value of 1.243 for the corresponding quantity.

Professor Kirkwood confirms our value for the asymptotic limit. He states that his recently revised value is too large because of slow convergence of his method of calculation.

* Present address: University of California Radiation Laboratory, Livermore, California.
[1] J. G. Kirkwood and J. Riseman, J. Chem. Phys. **16**, 565 (1948).
[2] Kirkwood, Zwanzig, and Plock, J. Chem. Phys. **23**, 213 (1955).
[3] Bruno Zimm (private communication).

Heats of Absorption on a Prepared Uniform Surface*

W. A. Steele and J. G. Aston
College of Chemistry and Physics, The Pennsylvania State University, University Park, Pennsylvania
(Received June 13, 1955)

In a recent paper,[1] the adsorption of rare gases on titanium dioxide was discussed in terms of a simple model of surface heterogeneity. It was postulated that high-energy sites for adsorption were due to topographical heterogeneity; that is, cracks and surface roughnesses occur at which an adsorbate atom can realize two or more times the adsorption energy expected for a planar adsorbent surface. Measurements of the heat of adsorption of helium on titanium dioxide covered with one half layer of argon strongly support the assumptions of reference 1. Figure 1 shows the heats of adsorption of helium on the two systems: bare titanium dioxide and titanium dioxide plus one half layer of preadsorbed argon. The temperature of measurement in these determinations was 14.5°K. Some heats for helium on the bare surface measured by Tykodi and Aston[2] are included for comparison. The sample of titanium dioxide used by them was identical to that used in the present work; however, the temperature of measurement in the earlier experiments was 17.1°K. The units of coverage (cc $-$STP/m^2) are based on an area for the bare surface as determined by a BET plot of the nitrogen adsorption data. By this convention, equal V_a values give equal number of atoms adsorbed; thus, the intercomparison of the various surfaces is facilitated. The actual amount of argon preadsorbed was 0.136 cc $-$STP/m^2 in run 1 and 0.134 in run 2.

The accuracy of the heats for helium on the bare surface at low coverages ($V_a<0.05$) is estimated to be $\pm$30–40 cal/mole; at higher coverages, the accuracy is considerably improved, and is $\pm$15–20 cal/mole. The reason for this is that the time required to reach temperature equilibrium at low coverage is quite long (due to poor thermal conduction in the sample—the pressure of the helium over the adsorbent is still negligible in this region, insofar as heat conduction is concerned). However, as the coverage increases, the equilibration time improves somewhat, and the points have less scatter. In the runs with the preadsorbed argon, the equilibration times were quite short at all coverages, and the accuracy of the points is estimated to be $\pm$10–15 cal/mole (presumably, the argon fills in the cracks and voids, thus making better thermal contact between the particles of powder).

In the simple model of reference 1, it was assumed that $\sim$40% of the sites were of energy higher than the planar surface (the energy of adsorption on the planar surface was estimated to be 180 cal/mole). Even at $V_a=0.14$ ($\theta\sim0.6$), the high-energy sites of the bare surface are still filling in slowly; however, at the lowest coverages, the surface with one half layer of argon shows little

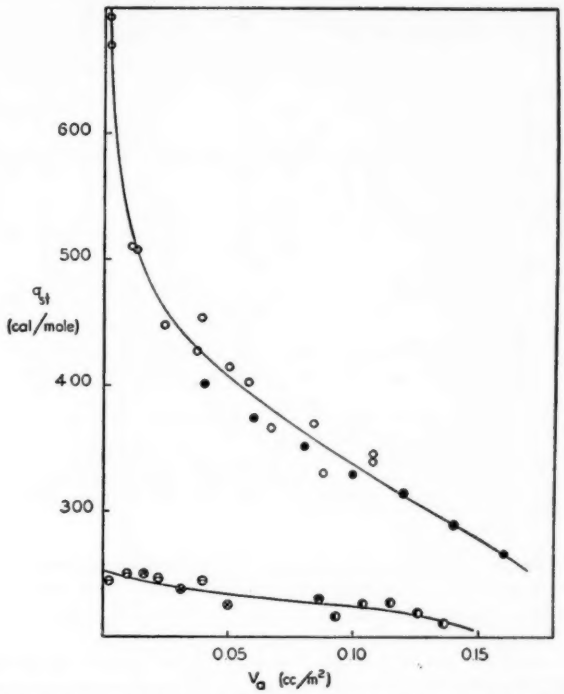

FIG. 1. Heats of adsorption of helium on titanium dioxide surfaces. ⊖: Calorimetric heats at 14.5°K on titanium dioxide plus one half-layer of preadsorbed argon. Run 1. ⊗: Calorimetric heats on titanium dioxide plus one-half layer of argon. Run 2. ◐: Isosteric heats at 14.5°K calculated from isotherms. Titanium dioxide plus one-half layer of argon. ○: Calorimetric heats at 14.5°K on bare titanium dioxide. This work. ●: Isosteric heats at 17.1°K calculated from isotherms of Tykodi and Aston on the bare surface.

evidence of the strong heterogeneity of the bare surface. These results show that the preadsorbed argon is quite effective in smoothing out surface roughnesses and in filling in the cracks.

Further experiments are now under way to determine heats at argon coverages higher and lower than one half layer in order to determine the degree of homogeneity at lower coverages, and to ascertain whether the A$-$TiO$_2$ mixed surface is a stronger adsorber than the TiO$_2$ alone.

* This research was carried out under Contract DA-36-061-ORD-403 of the Office of Ordnance Research.
[1] Aston, Tykodi, and Steele (to be published).
[2] R. J. Tykodi and J. G. Aston (to be published).

Preliminary Data on Photoionization Efficiencies and Cross Sections in C_2H_4 and C_2H_2†

W. C. Walker and G. L. Weissler
Department of Physics, University of Southern California, Los Angeles 7, California
(Received May 27, 1955)

THE total absorption cross sections, photoionization efficiencies, and ionization cross sections of C_2H_4 and C_2H_2 for radiation in the region from the onset of the ionization continuum to 687 A have been obtained using the equipment and techniques previously described.[1] For wavelengths longer than about 1000 A both the absorption spectra[2,3] and absorption coefficients[4,5] of these gases have been reported; however, for shorter wavelengths within the ionization continuum there appear to be no published data.

In the present investigation, the onset of ionization for C_2H_4 was found at 1185$\pm$5 A, corresponding to 10.46$\pm$0.05 ev. This value is in agreement with the 10.52$\pm$0.01 ev obtained by Watanabe,[6] the 10.45$\pm$0.04 ev from Rydberg series by Price and Tutle,[2] and the 10.6$\pm$0.1 ev of Lossing, Tickner, and Bryce[7]

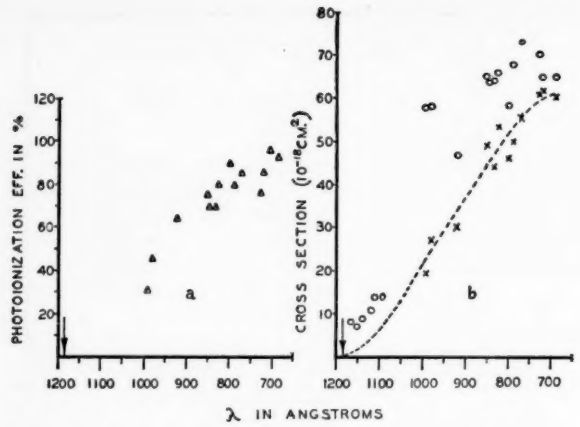

FIG. 1. (a) Photoionization efficiencies of C_2H_4. (b) Absorption and photoionization cross sections of C_2H_4. O Absorption cross sections. × Ionization cross sections. All data were taken with 3-cm ionization chambers and a 5 A resolution (see reference 1). The first ionization potential of 10.46±0.05 ev is shown by the arrow.

from electron impact measurements. The ionization efficiencies of C_2H_4 in percent or ion pairs per 100 absorbed quanta are shown in Fig. 1(a). From these efficiencies and the measured absorption coefficients, the ionization cross sections were calculated. In Fig. 1(b) both the absorption and ionization cross sections are presented. The error in the absorption cross sections was estimated to be within ±10 percent, while that for the ionization cross sections was ±20 percent. It should be noted that the absorption for wavelengths shorter than 850 A was large, corresponding to absorption coefficients of the order of 1500 cm^{-1}. The dotted line indicates the contour of the ionization continuum established by these data. Although no ionization cross sections were obtained for wavelengths longer than 991 A, the extension of the curve to the ionization limit seemed justified by the trend of the total absorption cross sections.

In the case of C_2H_2 the onset of ionization occurred at 1100±5 A corresponding to 11.25±0.05 ev, again in agreement with the electron impact value of 11.4±0.1 ev by Lossing, Tickner, and Bryce[7] and the spectroscopic value of 11.35±0.01 ev obtained by Price.[8] Since the most likely impurity in the tank C_2H_2 used was acetone, with an ionization onset at 1279 A,[6] the existence of a sharp onset at 1100 A indicated that the gas sample was free from this impurity. The possibility of the presence of small amounts of other impurities cannot be entirely ruled out, although it was felt that their effects in this investigation were small. The ionization efficiencies of C_2H_2 are shown in Fig. 2(a) and the corresponding absorption and ionization cross sections in Fig. 2(b). A dotted line again has been used to indicate the contour of the continuum. It was observed that a distinct break in this curve occurred at about 827 A. This increase in the ionization cross section may be due to a second ionization continuum beginning at about 15 ev. There appears to be no published information concerning the existence of this second continuum. Price[8] reported, on the basis of absorption spectra, that continuous absorption in C_2H_2 began at about 1050 A and decreased toward shorter wavelengths becoming very weak between 800 A and 150 A. This is not substantiated by these results, since relatively large cross sections were observed near 800 A. The present data show, however, that the absorption does decrease rapidly for wavelengths shorter than 750 A.

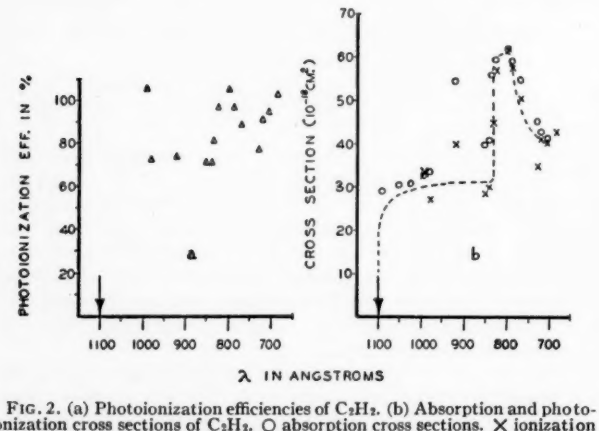

FIG. 2. (a) Photoionization efficiencies of C_2H_2. (b) Absorption and photoionization cross sections of C_2H_2. O absorption cross sections. × ionization cross sections. All data were taken with 3-cm ionization chambers and a 5 A resolution (see reference 1). The first ionization potential of 11.25±0.05 ev is shown by the arrow.

† The aid of the Office of Naval Research is gratefully acknowledged.

[1] Wainfan, Walker, and Weissler, Phys. Rev. (to be published).
[2] W. C. Price and W. T. Tutle, Proc. Roy. Soc. (London) **A174**, 207 (1940).
[3] W. C. Price and A. D. Walsh, Trans. Faraday Soc. **41**, 381 (1945).
[4] M. Zelikoff and K. Watanabe, J. Opt. Soc. Am. **43**, 756 (1953).
[5] G. Moe and A. B. F. Duncan, J. Am. Chem. Soc. **74**, 3136 (1952).
[6] K. Watanabe, J. Chem. Phys. **22**, 1564 (1954).
[7] Lossing, Tickner, and Bryce, J. Chem. Phys. **19**, 1254 (1951).
[8] W. C. Price, Phys. Rev. **47**, 444 (1935).

Free-Electron Treatment of Diels-Alder's Reaction

SADHAN BASU
Department of Chemistry, University of Calcutta, 92 Upper Circular Road, Calcutta 9, India
(Received May 2, 1955)

MOLECULAR orbital calculations have been successful in predicting the reactivities of a number of complicated organic molecules; especially the theoretical calculations of Brown[1] have agreed well, at least qualitatively, with the experimental results of a large number of Diels-Alder's reactions. Of late, free electron wave functions[2,3] have been used in predicting the spectral transition in the case of a number of conjugated compounds and the calculated frequencies have been found to agree with the experimental values better than those of MO method in some cases. It has been shown by Basu[4] that the free electron model can be used effectively in explaining the orientation of substituents in aromatic molecules. The object of the present investigation is to show that free-electron model can also be used effectively in explaining Diels-Alder's reactions.

The formation of maleic anhydride addition product consists in localizing two π electrons of the conjugated system with the formation of two σC−C bonds. The fundamental assumption of Brown[1] is that, the ease of formation of an addition product at a pair of carbon atoms of the conjugated system depends on the energy required to localize two of the π electrons upon atoms, say m and n, provided they are suitably oriented. In the case of aromatic hydrocarbons the latter provisions mean that m and n must be para to each other. This energy quantity is termed para localization energy, P, and is given by

$$P=2\alpha+E_r-E, \tag{1}$$

where E is the total π-electron energy of the original conjugated system, 2α the energy of two isolated π electrons and E_r the total π-electron energy of one or more conjugated systems left after two π electrons are localized in two suitably oriented atoms. The total π-electron energy of the parent and residual molecules were calculated by Brown by MO method. These quantities may be calculated by the free electron network model.[5,6] For these purposes the conjugated system is divided into a number of segments; the free-electron wave function in each segment is then expressed in the form

$$a\cos\omega x+b\sin\omega x \tag{2}$$

where x is expressed in unit of l, the C−C bond length, and ω

TABLE I. Para localization energies.[a]

Compound	Positions	P	$P'(-\gamma)$	k_a
Benzene	1:4	$2\alpha+3.560$ K	2.67	*ca* 10^{-15}
Naphthalene	1:4	$2\alpha+1.604$	2.40	*ca* 10^{-8}
Anthracene	1:4	$2\alpha+1.599$	2.34	*ca* 10^{-7}
	9:10	$2\alpha-0.353$	2.07	1
Naphthacene	1:4	$2\alpha+1.601$	2.33	···
	5:12	$2\alpha-0.357$	2.01	30
Pentacene	1:4	$2\alpha+1.595$	2.33	···
	5:14	$2\alpha-0.361$	1.99	90
	6:13	$2\alpha-0.368$	1.94	1600
Phenanthrene	1:4	$2\alpha+1.615$	2.47	···
Triphenylene	1:4	$2\alpha+0.205$	···	···
Perylene	1:12	$2\alpha+2.388$	2.60	···

[a] K stands for $h^2/8ml^2$ and k_a, the rate constant, is expressed relative to 9:10 addition to anthracene.

in terms of π. At each junction point of the segments we apply the continuity and conservation condition, and get a number of secular equations which may be solved for ω. The energy is given by

$$E\frac{l^2\omega^2}{8ml^2\pi^2}. \tag{3}$$

Starting from the lowest state, π electrons are distributed among these energy states, two for each state, and the total π-electron energies are calculated. The π-electron energy of the residual molecule is also calculated similarly; for example, 1:4 addition to anthracene leaves the residual molecules of naphthalene and ethylene, while 9:10 addition leaves two phenyl nuclei.

The para localization energies P calculated for a number of aromatic hydrocarbons are given in Table I along with those calculated by Brown (P') (corrected for overlap) by the MO method.

It may be observed that the calculated values are in the right sequence with the experimental results. As per calculation, benzene and napthalene do not add maleic anhydride, anthracene undergoes 9:10 addition and naphthacene and pentacene add maleic anhydride at central "meso-position" with increasing ease. The angular ring systems do not undergo maleic anhydride addition at all. Another point that emerges out of the present calculation is that maleic anhydride addition is possible only when the para localization energy is less than the energy (2α) of the two isolated π electrons.

[1] Brown, J. Chem. Soc. **1950**, 691.
[2] Bayliss, J. Chem. Phys. **16**, 287 (1948).
[3] Kuhn, Helv. chim. Acta. **31**, 1441 (1948).
[4] Basu, J. Chem. Phys. **22**, 1952 (1955).
[5] Rudenberg and Scherr, J. Chem. Phys. **21**, 1565 (1953).
[6] Griffith, Trans. Faraday Soc. **49**, 345 (1953).

Simultaneous Transitions in Liquids. A New Kind of Molecular Spectrum

J. A. A. KETELAAR AND F. N. HOOGE
Laboratory for General and Inorganic Chemistry of the University of Amsterdam, Amsterdam, Holland
(Received June 10, 1955)

SIMULTANEOUS vibrational transitions have recently been observed in mixtures of compressed gases (CO_2) with H_2, O_2, and N_2,[1] HCl with H_2[2] and in liquid mixtures (CS_2 with Br_2 and I_2[3]). Simultaneous vibrational transitions in liquid mixtures are by no means rare as we have observed them in mixtures of CS_2 with such substances as S_2Cl_2, PCl_3, PBr_3, $SOCl_2$, $PSCl_3$, and CCl_3SCl.

The infrared absorption spectra of these mixtures may be said to furnish examples of a new class of molecular spectra besides Raman spectra and ordinary infrared absorption spectra. The system of bands due to simultaneous transitions with some frequencies forms a complete molecular spectrum, analogous to the Raman spectrum, but shifted to higher frequencies by 1515 cm^{-1} of the ν_3 CS_2 band (liquid state). Only the observable range is restricted by the transparency region of CS_2 between 1500 and 2100 cm^{-1} to molecular frequencies between about 160 and 500 cm^{-1}.

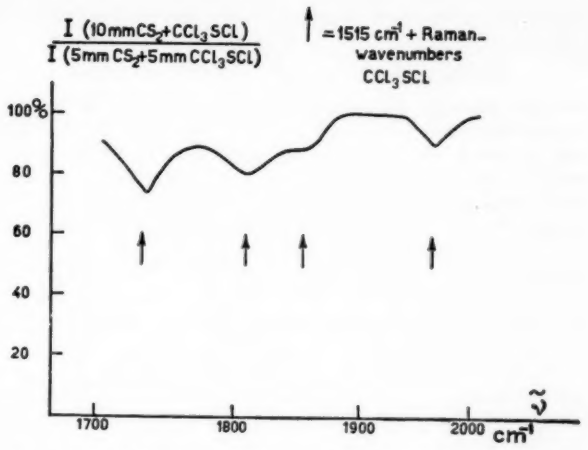

FIG. 1. Simultaneous transition spectrum of CCl_3SCl (perchloromercaptane) with CS_2. The arrows indicate the positions of Raman lines shifted by 1515 cm^{-1} (ν_3 of CS_2 in liquid state).

Absorption spectra were recorded for a 10-mm optical path length of mixtures of equal volumes of CS_2 and the second component. The spectra obtained with two superimposed cells of 5 mm thickness, each filled with one of the pure components served as the reference (Fig. 1). Results are given in Table I. The frequencies found are in excellent agreement with the values found from the Raman spectra. Also, the relative intensities are in good agreement with those observed in the Raman spectra as expected from the theoretical treatment. However, differences might be expected for frequencies of groups which are situated in different parts of larger molecules.

Assuming electrostatic interaction the intensity of the simultaneous transitions is determined by the presence of terms in the

TABLE I.

Substance	Simultaneous transition-spectrum with CS_2	Raman spectrum
S_2Cl_2	202	203[a]
	~250 Shoulder	242
	447	445
PCl_3	181	190[a]
	258	258
	505	484, 511
PBr_3	158	162[a]
	376	380, 400
$SOCl_2$	201	192[a]
	293	283
	348	343
	435 Shoulder	443
	488	488
$PSCl_3$	168	168[a,b]
	249	244
	430	429
CCl_3SCl	217	216[c]
	292	293
	337	336
	450	451

[a] Average values according to Landolt-Börnstein, *Zahlenwerte und Funktionen, Atom- und Molekularphysik* (Springer Verlag, Berlin, 1951), Part 2.
[b] The very weak band at 382 cm^{-1} is omitted; see H. Gerding and R. Westrik, Rec. trav. chim. **61**, 842 (1942).
[c] J. Duchesne, Bull. Soc. Roy. Sci. Liège **1**, 61 (1942).

expansion of the dipole moment of the pair of molecules $A \cdot B$ such as[4]

$$(d\alpha/dq_i)_A \cdot (d\mu/dq_k)_B \quad \text{and} \quad (d\mu/dq_l)_A \cdot (d\alpha/dq_m)_B$$

with the q's being the normal coordinates for all possible vibrations of the molecules A and B and with α and μ the polarizabilities and the dipole moments of both molecules. This new kind of molecular spectrum can only be observed in those cases where both components are sufficiently transparent in relative thick layers. However, in those cases this method of investigation permits the observation in absorption in the rock salt or LiF region of low frequencies which are difficult to investigate with the ordinary infrared absorption technique. In comparison with the Raman effect it permits observations on colored or photochemically unstable substances in small quantities.

This work is part of the research program of the Foundation for Fundamental Research of Matter (F.O.M.) and was made possible by financial support from the Netherlands Organization for Pure Research (Z.W.O.). One of us (F.N.H.) acknowledges the financial support from N. V. Philips Nederland.

[1] J. Fahrenfort and J. A. A. Ketelaar, J. Chem. Phys. **22**, 1631 (1954).
[2] Coulon, Rosin, and Vodar, Compt. rend. **240**, 956 (1955).
[3] J. A. A. Ketelaar and F. N. Hooge, J. Chem. Phys. **23**, 749 (1955).
[4] J. Fahrenfort, thesis, University of Amsterdam, 1955; J. A. A. Ketelaar, Rec. trav. chim. (to be published).

Mobility and Quantum Yield of Charge Carriers in Crystal Violet*

R. C. Nelson
The Ohio State University, Columbus, Ohio
(Received May 16, 1955)

WHEN a small portion of an extensive crystal violet film well removed from one or both electrodes is illuminated, the observed increase of conductance is only a few percent of that expected if the same energy were uniformly distributed over the whole surface. Since the material is a good insulator and the mobility in the dark part of the film is low due to the large number of traps, the secondary effect of illumination of a small area is to cause the field across it to be greatly reduced by space-charge effects, and little change in conductance is seen.

This phenomenon is illustrated by the changes observed while a spot of light is being moved continuously across a cell as shown in Fig. 1A. The rise of conductance is slow until the spot approaches the far electrode and the resistance of the portion remaining unilluminated becomes comparable to that of the part already illuminated; then the voltage drop across the latter begins to rise sharply and there is apparently a burst of conduction.

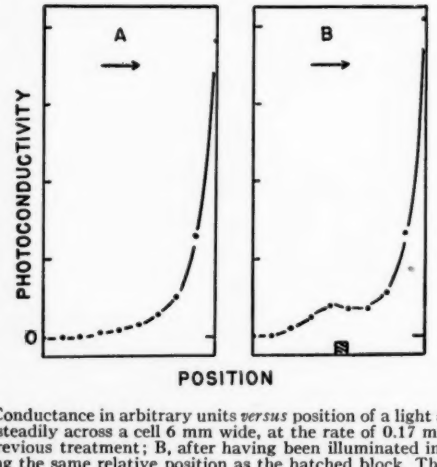

FIG. 1. Conductance in arbitrary units *versus* position of a light spot being traversed steadily across a cell 6 mm wide, at the rate of 0.17 mm/sec: A, without previous treatment; B, after having been illuminated in a narrow strip having the same relative position as the hatched block. The nominal field is 30 volts/cm.

Since the traversal required 35 seconds, the mobility of carriers in the dark region must be extremely low. This pattern is observed independently of the direction of traversal with respect to electrode polarity, the small asymmetry in detailed shape being consistent with the previous finding that electron conduction predominates.[1]

In the experiment of Fig. 1B a narrow transverse zone parallel to the electrodes was illuminated for 30 seconds. Then a spot of light was traversed as before. The same pattern is seen except for a hump on one side of the illuminated area and a flattening at it. The flattening can be attributed to space-charge effects as before, but the hump is most probably due to optical re-excitation of carriers formed during the stationary illumination and trapped in the dark part of the film. The invoking of such a process is not inconsistent with earlier kinetic data for the early stages of illumination, although there is no evidence that they are important when the film is in the steady state in light.

In an earlier note[2] the writer estimated the quantum yield of charge carriers in pure crystal violet films to be ~ 0.1 based on measurements of the initial rate of rise of conductance in illumination, assuming the carriers to be in thermal equilibrium with the trapping levels, so that only the fraction $\exp(-0.38 \text{ ev}/kT)$ was free. This assumption is strongly suspect not only because of the evidence for optical re-excitation of trapped carriers, but also because studies on impure films having traps of various depths show rather constant initial rise rates. The preferred interpretation of the experiment seems rather to be that during its course a substantial fraction of the carriers was mobile, and that in consequence the quantum yield is more probably of approximate order $\exp(-0.38 \text{ ev}/kT)$ or about 10^{-6}.

This agrees with the conclusion reached for the very similar dye basic fuchsin, that the quantum yield was temperature dependent quite apart from considerations of mobility, with an activation energy of 0.38 ev.[1]

* This work was supported by the Charles F. Kettering Foundation.
[1] R. C. Nelson, J. Chem. Phys. **22**, 885, 890, 892 (1954).
[2] R. C. Nelson J. Chem. Phys. **19**, 798 (1951).

Space-Time Yield and Reaction Rate

George J. Janz and Samuel C. Wait, Jr.
Department of Chemistry, Rensselaer Polytechnic Institute, Troy, New York
(Received May 27, 1955)

SPACE–TIME–YIELD, defined as quantity of product per unit volume per unit time, was recommended by Haber and Greenwood[1] and Rideal and Taylor[2] as a useful concept in the study of gaseous reactions in continuous flow systems. Recent applications of this concept for calculations of yields,[3,4] catalyst activity evaluations,[5,6] and correlation of relative reactivity of a molecular species with structural modifications[4,7] within the molecule imply a direct proportionality to the rates of reaction. The present communication examines this concept in the light of the rate equations in flow systems. It is shown that space-time yield is a convenient criterion for estimating reaction order, and relative activities of chemical reactants or catalyst surfaces providing certain experimental requirements are fulfilled.

Good treatments of the problems relating to the establishment of rate equations in flow systems are found in the more recent works of Denbigh,[8] Hulburt,[9] and Harris.[10] There are three main differences between static and flow systems as far as kinetic treatments are concerned. Reactions in flow systems generally take place under conditions of constant pressure. A volume effect, arising when there is a continuous change in the number of moles of reacting mixture must be considered in the definition of concentration terms. If lateral diffusion of the reactant molecules occurs, the concentration terms must also take this effect into account. In practice the diffusion effect can be made negligible by use of large flow rates, small reactor cross section, moderate temperatures and pressures. For the case of negligible lateral

diffusion, the integrated rate expressions[10] for a first-order reaction are

$$k_1=\frac{V_0}{V_r}\left[n\ln\left(\frac{N_A}{NA_0-\frac{1}{n}N_c}\right)-\frac{n-1}{n}\left(\frac{N_c}{NA_0}\right)\right] \quad (1)$$

where V_0 is the velocity of flow of entering mixture, V_r the reactor volume, n the moles of product per mole of reactant undergoing change, N_A, N_c the moles of reactant (A) and product (C) leaving the reaction zone, and NA_0 the moles of reactant entering per second. If there is no volume change (i.e., $n=1$), and the conversion per pass is small (<10%), this expression simplifies to

$$k_1=\frac{V_0}{V_r}\left(\frac{N_c}{NA_0}\right) \quad (2)$$

where it is readily seen that the concept of space-time-yield (moles product/unit time/unit reaction volume) is realized in the ratio (N_c/V_r). Thus it follows that if the experiments are effected under conditions of constant input, contact time, temperature, and pressure, the space-time-yield (S.T.Y.) may be expressed in terms of the rate constant by

$$\text{S.T.Y.}=k_1(Q) \quad (3)$$

where $Q=(V_0/NA_0)$, a constant for the given set of conditions. A direct proportionality thus exists between the space-time yield and the rate constant in the region where the conversions are a measure of the initial rate. From a consideration of the integrated rate expressions[8,10] for the second-order reactions, an expression quite similar to (3) can be derived, where Q again is a parameter dependent only on the moles of reactants and velocity of flow entering the reaction zone.

A comparison of the space-time yields under comparable conditions in the region of small conversions for two similar processes is thus a direct comparison of the rate constants for the two reactions. Providing the operating conditions are comparable, and the processes are similar, the concept of space-time yield offers a ready means for estimating the order of reaction and comparing activities of catalyst surfaces or chemical reactants.

[1] F. Haber and F. C. Greenwood, Z. Elektrochem. **21**, 251 (1915).
[2] E. K. Rideal and H. S. Taylor, *Catalysis in Theory and Practice* (MacMillan and Company Ltd. London, 1919), p. 66.
[3] H. H. Storch, *Advances in Catalysis* (Academic Press, Inc., New York, 1948), Volume II, pp. 132, 147.
[4] G. J. Janz and R. E. Myers, J. Am. Chem. Soc. **75**, 1510 (1953).
[5] Janz, Timpane, and McCulloch, Ind. Eng. Chem. **45**, 1343 (1953).
[6] G. J. Janz and W. J. G. McCulloch, J. Am. Chem. Soc. (to be published).
[7] G. J. Janz and S. C. Wait, Jr., J. Am. Chem. Soc. **76**, 6377 (1954).
[8] G. Denbigh, Trans. Faraday Soc. **40**, 352 (1944).
[9] H. M. Hulburt, Ind. Eng. Chem. **36**, 1012 (1944); **37**, 1063 (1945).
[10] G. M. Harris, J. Phys. & Colloid Chem. **51**, 505 (1947).

Thermodynamic Properties of the System Methane-Carbon Monoxide at 90.67°K

V. Mathot,* L. A. K. Staveley, J. A. Young, and N. G. Parsonage
Inorganic Chemistry Laboratory, Oxford, England
(Received June 13, 1955)

THE cell theory applied to solutions[1] predicts a *positive* excess free energy together with a volume *contraction* on mixing if the molecules are spherical and of equal radius, and if, moreover, ε_{12}^* is the geometric mean of ε_{11}^* and ε_{12}^*, where ε_{ij}^* is the maximum intermolecular potential energy of a pair ij. We report here briefly the results of experiments designed to test this prediction. These were carried out on the system methane-carbon monoxide since this both fulfils the theoretical requirements and also lends itself to accurate measurement.

The following properties of the condensed system have been measured: (1) the total vapor pressure; (2) the condensation pressure; (3) the volume change on mixing; (4) the virial coefficients of the gases.

All measurements were made at 90.67°K, the triple-point of methane, at which the vapor pressure of methane is 87.85 mm and that of carbon monoxide 1895.9 mm. The essential results are shown graphically in Fig. 1, in which the excess free energy and the excess volume are plotted as a function of mole fraction. Not only are the predictions of the cell theory qualitatively confirmed, but the quantitative agreement between the observed values (solid curves) and calculated values (dotted curves) of these two excess functions is very satisfactory.

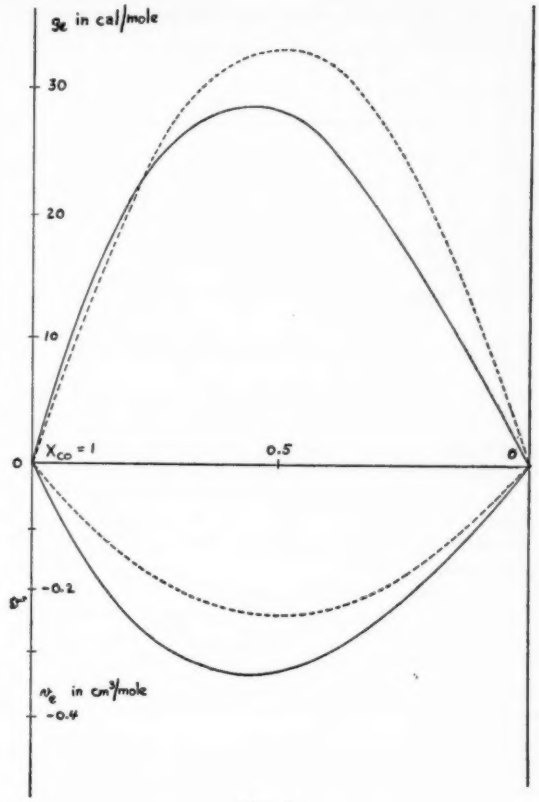

FIG. 1.

A detailed account of this work will be submitted for publication in the Transactions of the Faraday Society.

One of us (V.M.) is much indebted to Professor Sir Cyril Hinshelwood for the hospitality and facilities accorded to him in this laboratory. We also wish to thank Imperial Chemical Industries, Ltd., and the Centre national belge d'Etude scientifique du Froid for financial assistance.

* Associé au Fonds National de la Recherche Scientifique Belge.
[1] I. Prigogine and V. Mathot, J. Chem. Phys. **20**, 49 (1952); Prigogine, Bellemans, and Englert-Chwoles, J. Chem. Phys. (to be published).

Note on the Potential of the α-Pd/H_2 Electrode

Sigmund Schuldiner and James P. Hoare
Naval Research Laboratory, Washington, D. C.
(Received June 16, 1955)

RECENT work of the authors[1] has shown that the open circuit potential difference of an α-Pd/H_2 electrode against a hydrogen (Pt/H_2) electrode both in the same sulfuric acid solution was about +0.050 v. Similar results were obtained by Hitzler and Knorr[2] and Stout.[3] However, Aten and Zieren[4] and Frumkin and Aladjalova[5] obtained for the same apparent electrode system a zero potential difference. The following experiments were conducted at this laboratory which render these divergent results compatible.

In the first experiment, a palladium plate was plated with palladium black (from a $PdCl_2$ solution containing 1% lead

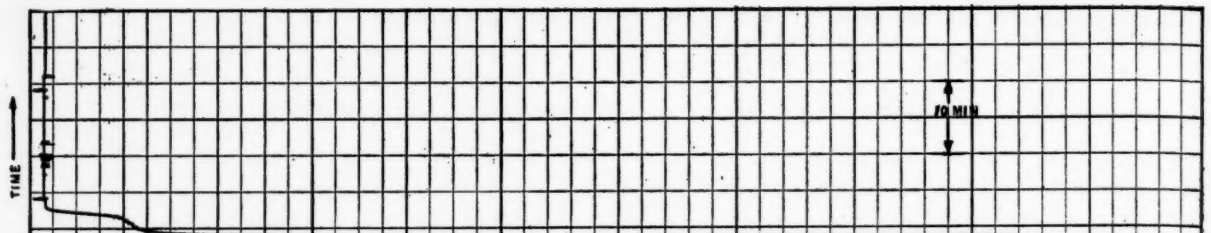

FIG. 1. A section of the recorder chart showing the open circuit potential of an anodically polarized, palladized platinum electrode as a function of time.

acetate). The electrode was thoroughly cleaned and placed in a Teflon cell containing 2*N* sulfuric acid solution stirred with purified hydrogen. The solution was purified by pre-electrolysis and the palladium electrode was cleaned by anodic polarization. After this was done, the current was disconnected and the palladium electrode was allowed to reach a steady potential compared to Pt/H_2 electrode in the same solution. This potential difference was $+0.048\pm0.001$ v.

In the second experiment a platinum plate was plated with palladium black. The same purification procedure was used. The steady-state potential compared to the Pt/H_2 electrode was zero volts. Figure 1 shows the change in potential with time for this electrode when the anodizing circuit was broken. The break in the curve at about +0.060 v shows the influence of the palladium black coating.

The work of Hitzler and Knorr, Stout, and the authors was all done with pure palladium electrodes. However, Aten and Zieren used platinum wire electrodes either plated with smooth palladium or palladium black. Frumkin and Aladjalova used a pure palladium electrode which was welded to a platinum ring which was sealed in glass. The part of the platinum ring which was exposed to the solution was plated with smooth palladium.

The experiments involving possible solution contact with platinum (through pores in the palladium coat) gave a zero potential because of the local cell action between the exposed platinum and the palladium. This local cell action caused the palladium to be charged with hydrogen until there was a zero potential difference between it and the Pt/H_2 electrode. Work by the authors[1] showed that at this potential the palladium-hydrogen system is in the beta phase.

Gillespie and Hall, Bruning and Sieverts, Gillespie and Galstaun, and Owen and Jones[6] showed that in the gas phase the β-palladium-hydrogen system is stable with respect to the alpha phase at room temperature and an ambient hydrogen partial pressure of one atmosphere or greater. The work of the authors[1] showed that in the solution phase under the same conditions of temperature and partial pressure of hydrogen that the alpha phase is stable with respect to beta. In order to confirm these findings, a third experiment was performed. In this experiment a small clean palladium bead lightly coated with palladium black was suspended in a hydrogen atmosphere (atmospheric pressure) overnight. The electrode was then plunged into a purified 2*N* sulfuric acid solution stirred with purified hydrogen. The potential change of this electrode compared with a Pt/H_2 electrode gave the results shown in Fig. 2. These results show that in the gas phase the palladium was charged to the β-palladium-hydrogen system. When the electrode was plunged into the acid solution, the initial potential was zero volts; in time, however, the potential very slowly increased, so that, at the end of nine days, its value was +0.030 v. In order to convert the electrode entirely to the α phase, it was anodized and allowed to come to equilibrium in the hydrogen stirred solution. This steady (sixteen hours) potential was +0.050 v. This experiment indicates that on contact with solution the β palladium was converted to the alpha form.

Further work is being done on this problem which shall be reported soon.

[1] J. P. Hoare and S. Schuldiner, J. Electrochem. Soc. (to be published). S. Schuldiner and J. P. Hoare, submitted to J. Electrochem. Soc.; J. P. Hoare and S. Schuldiner, submitted to J. Electrochem. Soc.
[2] M. Hitzler and C. A. Knorr, Z. Elektrochem. **53**, 233 (1949).
[3] H. P. Stout, Discussions Faraday Soc. **1**, 107 (1947).
[4] A. H. W. Aten and M. Zieren, Trans. Am. Electrochem. Soc. **58**, 153 (1930).
[5] A. Frumkin and N. Aladjalova, Acta Physiocochim. U.R.S.S. **19**, 1 (1944).
[6] L. J. Gillespie and F. P. Hall, J. Am. Chem. Soc. **48**, 1207 (1926); H. Brüning and A. Sieverts, Z. physik. Chem. **A163**, 409 (1932); L. J. Gillespie and L. S. Galstaun, J. Am. Chem. Soc. **58**, 2565 (1936); E. A. Owens and J. I. Jones, Proc. Phys. Soc. (London) **49**, 587, 603 (1937).

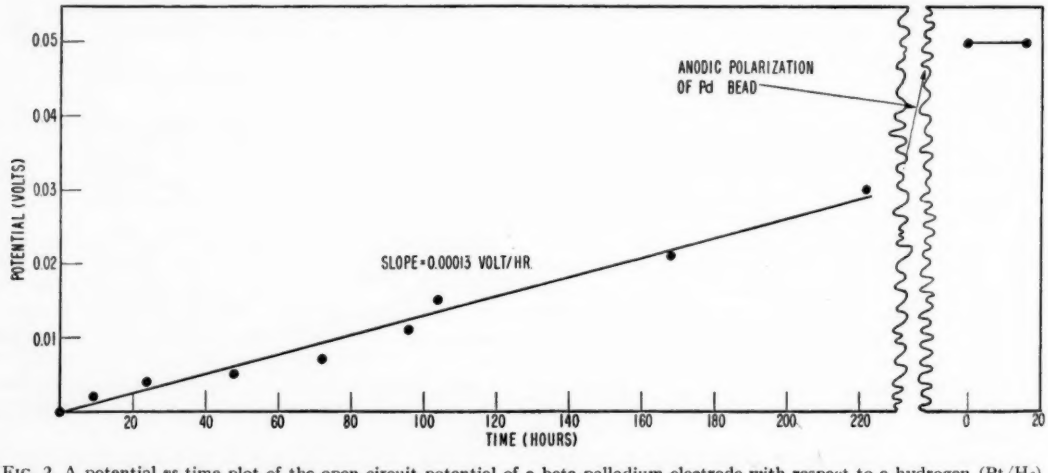

FIG. 2. A potential *vs* time plot of the open circuit potential of a beta-palladium electrode with respect to a hydrogen (Pt/H_2) electrode in the same solution ($2N\ H_2SO_4$) showing the conversion from beta palladium to alpha palladium.

Thermoluminescence Measurements on ZnS Phosphors *in Vacuo*

G. NEUMARK, J. FAJANS,* AND D. R. FRANKL
Sylvania Electric Products Inc., Bayside, New York
(Received May 4, 1955)

SINCE thermoluminescence results from the release of trapped electrons,[1] it provides a convenient tool for studying traps in phosphors. In view of some recent experiments[2–4] indicating surface traps due to adsorbed gases on CdS and ZnS crystals, we believe it to be of interest that we have observed no evidence of such traps in the thermoluminescence of ZnS powders. The thermoluminescence was the same in air as in vacuum, SO_2, or H_2O. However, in order to obtain correct results in vacuum, it is essential to minimize radiative heating of the phosphor.

The phosphor samples were settled at the bottom of a cylindrical chamber having a quartz or Pyrex window on top for excitation and observation. The lower part of the chamber was cooled, usually by liquid nitrogen to about 77°K, and the phosphor then excited by 3650 A radiation.

With a Pyrex or quartz chamber, the thermoluminescence of samples of both ZnS(Cu) and ZnS(Ag) did not differ significantly at pressures of 10^{-8} to 10^{-9} mm Hg from that at a few mm Hg.

Similarly, a sample of ZnS(Cu,Co) gave the same thermoluminescence in air, SO_2 vapor, and H_2O vapor, all at about 0.1 to 0.5 mm Hg. Here, the chamber was cooled to only about 230°K, due to the low vapor pressure of H_2O and SO_2 at lower temperatures.

However, with a Dural or copper chamber, the thermoluminescence at pressures below about 10^{-3} to 10^{-4} mm Hg frequently was considerably different from that at pressures above about 10^{-1} mm Hg, the major difference being a sharp reduction in intensity. An example is shown in Fig. 1. This effect is due not to adsorbed gas, but to a higher phosphor temperature at the lower pressures, resulting in the trapping of fewer electrons during the excitation. The cause of the higher temperature in vacuum is that the thermal conduction through the powder is insufficient to remove the energy absorbed from incident room temperature radiation. At the higher pressures, the atmosphere provides the necessary conduction. This problem has recently been discussed by Bube and Shrader.[5]

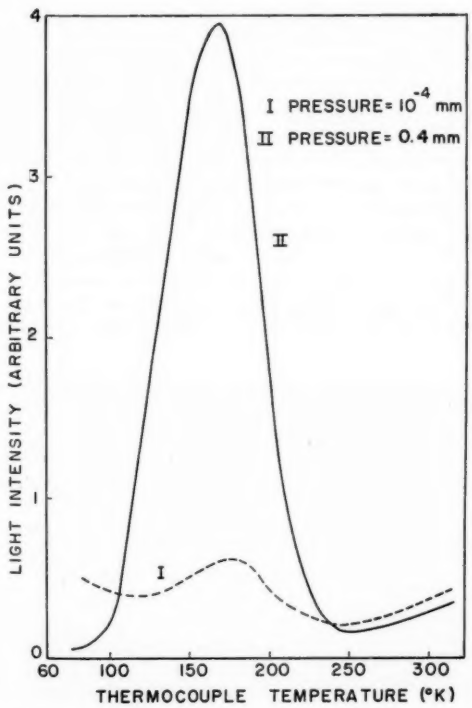

FIG. 1. Thermoluminescence of ZnS(Cu,Co) with the sample in a copper cup.

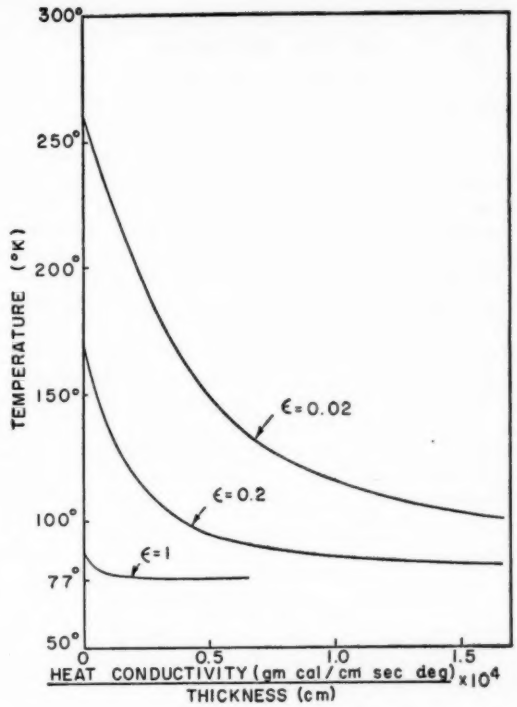

FIG. 2. Calculated temperature of the phosphor surface as a function of the ratio of the phosphor's heat conductivity to its thickness for various chamber emissivities (ϵ) and with a chamber temperature of 77°K; see text for the assumptions of the calculation.

We have calculated the phosphor surface temperature assuming the phosphor to be located at the bottom of a cylindrical chamber at 77°K, with a window at 300°K at the top. The chamber height was taken as nine times its diameter; such a ratio is convenient experimentally while still resulting in a fairly small solid angle of room temperature radiation. It was assumed that the average absorptivities for the incident radiation are equal to the average emissivities for the emitted radiation, and that the phosphor and the window are blackbodies (i.e., emissivity=1). Figure 2 shows the resultant temperature as a function of the ratio of the powder's heat conductivity to its thickness for various chamber emissivities. It can be seen that for chambers of high emissivities the phosphor temperature is nearly equal to the chamber temperature even in the absence of any conduction; this is presumably the situation in a quartz or Pyrex chamber. However, metals generally have low emissivities, that of copper for example being 0.03 at room temperature.[6] In this case most of the radiation entering the system is not absorbed by the chamber, but is reflected onto the phosphor, so that thermal conduction is needed for the phosphor temperature to approach the chamber temperature. The results with the copper and Dural systems indicate that the powder conductivity is insufficient for this purpose.

We are indebted to Professor J. J. Dropkin for many helpful discussions and some phosphor samples, and to Mr. W. S. Romito for assistance in the experimentation.

* Present address: Stevens Institute of Technology, Hoboken, New Jersey.

[1] J. T. Randall and M. H. F. Wilkins, Proc. Roy. Soc. (London) **A184**, 366 (1945); F. Urbach, Wiener Ber. (IIA) **139**, 363 (1930).
[2] R. H. Bube, Phys. Rev. **83**, 393 (1951).
[3] R. H. Bube, J. Chem. Phys. **21**, 1409 (1953).
[4] S. H. Liebson, J. Electrochem. Soc. **101**, 359 (1954).
[5] R. H. Bube and R. E. Shrader, Rev. Sci. Instr. **25**, 921 (1954).
[6] J. H. Perry, *Chemical Engineers Handbook* (McGraw-Hill Book Company, Inc., New York, 1950).

Some Remarks on the Structure of NH_3 and PH_3 Molecules

WŁODZIMIERZ KOŁOS
Institute of Physics, Polish Academy of Sciences, Warsaw, Poland
(Received June 6, 1955)

THE problem of bond angles has been treated recently by various authors.[1-4] From the results of Pople[1] and Mellish and Linnett[2] it may be concluded that the valences in molecules with lone pair electrons are to be regarded as being approximately tetrahedral, the effect of lone pairs being such that the bond angles are reduced below the tetrahedral value. However Artmann[3] using the valence-bond method, and assuming the bond eigenfunctions in XH_2 molecules to be formed from the pure p orbitals of the central atom was able to calculate the bond angles in agreement with experiment. Taking into account the effect of hybridization of atomic orbitals[4] the agreement was improved.

Using the method of equivalent orbitals in the two-centers approximation for bond orbitals[1] we have calculated the variation with bond angle of the total energy of the NH_3 and PH_3 molecules. The energy was calculated from the well-known formula[5]

$$E=2\sum_n H_{nn}+\sum_m\sum_n\{2(mn|G|mn)-(mn|G|nm)\}+\sum_{\alpha\neq\beta}Z_\alpha Z_\beta/r_{\alpha\beta}. \quad (1)$$

Following Pople[1] we have neglected the exchange energy terms, however, the "local energy" has been calculated. For the atomic orbitals Slater's[6] approximation was used.

The relations between the hybridization parameters (ϵ_b and ϵ_l for bond and lone pair orbitals respectively) and the angle α between the bonds or β between the lone pair and a bond were obtained from the orthogonality conditions for the orbitals

$$\lambda^2(\cos^2\epsilon_b+\sin^2\epsilon_b\cos\alpha)+2\lambda\mu(S_s\cos\epsilon_b+S_p\sin\epsilon_b\cos\alpha)+\mu^2S_H=0 \quad (2)$$

$$\lambda(\cos\epsilon_b\cos\epsilon_l+\sin\epsilon_b\sin\epsilon_l\cos\beta)+\mu(S_s\cos\epsilon_l+S_p\sin\epsilon_l\cos\beta)=0. \quad (3)$$

The directions of the p functions of the central atom are assumed to coincide with the directions of the bonds.

Using the relations (2), (3) with a plausible assumption of the value of the bond polarity parameter λ/μ no minimum of the energy could be obtained. This has been found to be partly due to over-emphasizing of the overlap between the hydrogen orbitals. Assuming in the orthogonality conditions for the "screening constant" Z_H in the hydrogen $1s$ function various values larger than unity the energy has been found to have a minimum. Some results of the calculations are given in Table I. It may be seen that the orthogonality conditions for the orbitals, determining the hybridization of atomic orbitals, play an essential part in determining the structure of molecules. It follows from the calculations that neither the orthogonality conditions for atomic orbitals of the central atom nor the conditions for the localized molecular orbitals give a satisfactory relation between the hybridization parameters and bond angles. A more detailed analysis of the results shows that the theory in this approximation over-emphasizes the part played by the lone pairs in determining the molecular structure.

TABLE I.

Molecule	Bond angle exper.	Bond angle theoretical c	d	e
NH_3	106°47′[a]	107°		110°
PH_3	93°50′[b]	101°	94°	106°

[a] G. Herzberg, *Infrared and Raman Spectra of Polyatomic Molecules* (D. Van Nostrand Company, Inc., New York, 1945), p. 439.
[b] V. M. McConaghie and H. H. Nielsen, J. Chem. Phys. **21**, 1836 (1953).
[c] $Z_H=2.5$ in the orthogonality conditions for localized molecular orbitals (2), (3).
[d] $Z_H=5.3$ in the orthogonality conditions for localized molecular orbitals (2), (3).
[e] $\mu=0$ in the orthogonality condition for the localized bond orbital (2) (see reference 1).

It seems therefore, in connection with the results of Artmann[3,4] that although the hybridization is an important factor in determining the molecular structure, in the simple approximation it is more justified to regard the bond angles in XH_n molecules as deviating rather from 90° than from the tetrahedral angle.

A more detailed paper on the subject will be published in Acta Physica Polonica.

[1] J. A. Pople, Proc. Roy. Soc. (London) **A202**, 323 (1950).
[2] C. E. Mellish and J. W. Linnett, Trans. Faraday Soc. **50**, 657 (1954).
[3] K. Artmann, Z. Physik **137**, 137 (1954).
[4] K. Artmann, Z. Physik **138**, 640 (1954).
[5] J. Lennard-Jones and J. A. Pople, Proc. Roy. Soc. (London) **A202**, 166 (1950).
[6] J. C. Slater, Phys. Rev. **36**, 57 (1930).

Hindered Rotation of Water Molecules of Hydration in $Mg(H_2O)_6Cl_2$ and $Mg(H_2O)_6Br_2$

TUNAHIKO SIDEI AND SYUKURO YANO
Faculty of Engineering, Kyoto University, Kyoto, Japan
(Received June 2, 1955)

IN a series of experiments on proton magnetic resonance absorption in several hexahydrated crystals at a magnetic field of 3100 gauss, narrow curves with two peaks were found in powdered magnesium hexahydrate and corresponding bromide at room temperature.

A record obtained in $Mg(H_2O)_6Cl_2$ at room temperature is shown in Fig. 1. The typical line shapes measured at −30°C and 110°C are reproduced in Fig. 2. Figure 3 shows the second moments and peak separations obtained from experimental curves as a function of temperature. Second moment transition occurs in the range −20–0°C and 100–110°C.

For the interpretations of these experimental results, the following two cases can be taken into consideration: 1. It is assumed that water molecules are rigid to the higher temperature transition, and the transition at lower temperature originates in a phase change of the crystal. 2. The line shapes and second moments in room temperature region correspond to the rotational motion of the water molecules of hydration.

The first assumption is less adequate than the second one, because the proton pair distance calculated from the second moment[1] of 6.0±0.5 gauss[2] gives a value of 1.98±0.2 A, even when this experimental value is regarded as resulting only from the intra-water molecule interaction, and it becomes longer when other interaction is added, and such a long proton-proton distance cannot be responsible for ordinary water molecules of hydration. Moreover, smaller second moments have been found in other hydrated crystals and it will be reported elsewhere.[2] According to the second explanation the following treatment will be more plausible. The rigid lattice second moment of 26.0±2.0 gauss[2] measured at about −30°C may be divided into two parts: (I)

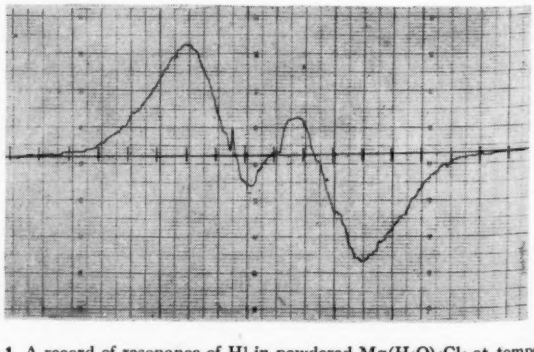

FIG. 1. A record of resonance of H^1 in powdered $Mg(H_2O)_6Cl_2$ at temperature of 24°C. Vertical bars indicate the scales of each gauss.

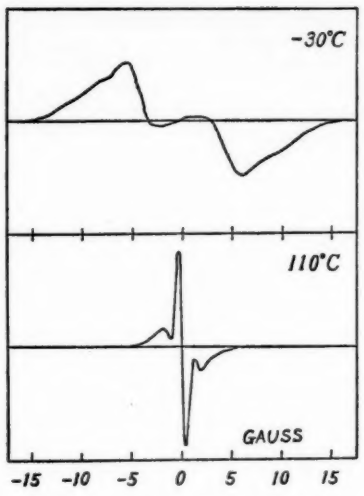

FIG. 2. Derivative curves of proton signals in $Mg(H_2O)_6Cl_2$ at 30°C (above) and 110°C (below).

ΔH_1^2, the dipole pair interaction in a given water molecule, (II) ΔH_2^2, inter-molecule interaction with protons in other water molecules and with all other magnetic nuclei. To separate each contribution from the total observed value, we have calculated numerically the theoretical line shapes for a two-spin system of this kind for several cases of parameter σ which is equal to $3\alpha/(2)^{\frac{1}{2}}\beta$, where we denote $\Delta H_1^2=(2/5)\alpha^2$ and $\Delta H_2^2=\beta^2$. Then σ is determined by comparing experimental curves with these theoretical ones. Thus we could choose a reasonable value of $\Delta H_1^2=20$ gauss^2, $\Delta H_2^2=6.0$ gauss^2 for the low-temperature data and $\Delta H_1^2=4.5$ gauss^2, $\Delta H_2^2=1.5$ gauss^2 for the room temperature data. This result shows that the ΔH_1^2 value for room temperature reduces approximately to the one-fourth value of ΔH_1^2 for a rigid case.

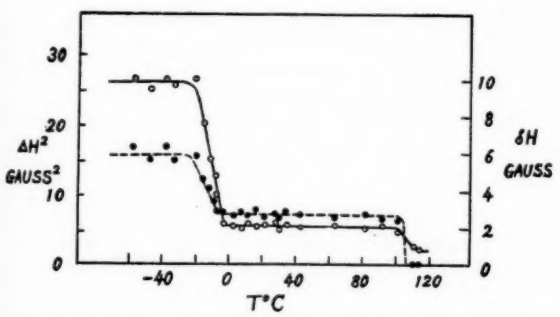

FIG. 3. Doublet separation (broken line) and second moment (solid line) *vs* temperature curves for $Mg(H_2O)_6Cl_2$.

It will be reasonable to conclude that this narrowing is due to a certain type of hindered rotational motion[3] of water molecules having the similar form of ordinary crystal water with a proton-proton distance of about 1.6 A. The transition about 100°C perhaps corresponds to the early state of decomposition of H_2O into HCl by chemical reaction at 116.7°C.

Powdered $Mg(H_2O)_6Br_2$ showed a quite similar absorption curve with a doublet separation of 2.8±0.2 gauss and second moment of 5.9±0.5 gauss^2 at room temperature.

A single crystal of $Mg(H_2O)_6Cl_2$ was grown from aqueous solution and a preliminary investigation has been carried out. The absorption curves of the crystal showed a much more distinct doublet structure depending on orientation of the *a* axis against the static magnetic field. In a certain direction two peaks were almost completely separated from each other, and in another direction both lines completely overlapped.

It is in progress to repeat the experiment to check this conclusion upon a single crystal of available size.

[1] J. H. Van Vleck, Phys. Rev. **74**, 1168 (1948).
[2] Results on other hydrated crystals will be published in J. Phys. Soc. Japan.
[3] H. S. Gutowsky and G. E. Pake, J. Chem. Phys. **18**, 162 (1950).

Active Nitrogen in the Rare Gases and Its Excitation of Metal Vapors

CARL KENTY
Lamp Division of the General Electric Company, Advanced Lamp Development Laboratory, Nela Park, Cleveland, Ohio
(Received June 13, 1955)

IF a low current (1–10 ma) is passed through a mixture of 100–300 mm argon and 0.1–0.3 mm N_2, an orange glow[1] is obtained. With current cutoff, the glow remains spectrally unchanged and decays in about 5 seconds. The spectrum is therefore produced secondarily by action of an energy carrier, *C*, present in both discharge and afterglow.

The spectrum is a selection of N_2 first positive bands ($A^3\Sigma_u^+-B^3\pi_g$), where $v=8$ and 4 of $B^3\pi_g$ (about 8.8 and 8.1 v) are emphasized. Also present are the second positive bands ($B^3\pi_g-C^3\pi_u$). Collisions involving energy carriers and N_2 molecules, A atoms, or slow electrons[2] may result in the production of $N_2(B^3\pi_g)$ and $N_2(C^3\pi_u)$. Conductivity measurements indicate ion concentrations of 10^8-10^9 cm^{-3} in the afterglow, probably produced by collisions of pairs[3] of carriers. The fast electrons appear mainly to produce the carriers.[4]

If a metal vapor such as Li, Na, Tl, Mg, Ga, In, Pb, Ca, Zn, Cd, etc. is added from a warmed source near the tube bottom, a flamelike afterglow ("fountain flame") appears, rising all the way to the tube top and flowing down the sides. With Tl this flame is green and is of striking beauty. It lasts about 10 seconds.

This experiment indicates that two carriers are present, *C* and *X*, of lower energy and longer life than *C* which excites Tl, etc. but not $N_2(B^3\pi_g)$.

If Ba is used a 5- to 8-second violet flame is produced. This is due to 4934.1 and 4554.0 of Ba II. To ionize Ba and excite the ion to the $6^2P_{\frac{1}{2}}$ level (4554.0) requires 5.19+2.71=7.9 v. This indicates that *X* has an energy >7.9 v. If Na is also present, a Na flame appears after the Ba II flame, indicating a third carrier of energy <7.9 v, possibly vibrating normal N_2 molecules.[5]

With Sr, a bright deep violet flame appears after the current is shut off, which decays along with the orange afterglow. This is followed by an 8- to 10-sec blue-green flame. The violet flame is due to 4215.5 and 4077.7 of Sr II. The second line requires 5.67+3.03 =8.7 v for its excitation from Ba. The decay of the violet flame along with the orange afterglow suggests that both are excited by carrier *C*. The blue-green flame consists of Sr I lines of only a few volts energy and is presumably excited by *X* and possibly a third carrier.

The afterglow contains, with He, Ne, and A, the first and second positive bands; with Kr, the first positive and (weakly) the first negative bands and the Kr continua; with Xe, only the whitish continuum of Xe together with a violet fluorescence of the glass revealing the vacuum uv continuum[6] of Xe. Long persisting after-flames of Tl, etc. and Ba II are obtained with Xe, quite as strong as with A. It is concluded that *C* quickly loses its energy to Xe (lowest excited state, $1s_5$=8.28 v), while some levels of *X* slowly excite Xe producing the Xe continua in the afterglow. It is also concluded that *X* does not excite $B^3\pi_g$, that $v=0$ of *C* lies above 8.28 v, and $v=0$ of *X* lies below 8.28 v. The results suggest that *C* and *X* are the N_2 metastables *w* and *a'* ($^1\Sigma_u^-$). The energies of these states are ~0.5 v apart,[6] but are otherwise unknown. However, Gaydon[6] has placed them tentatively at about 8.5 and 8 v. The present results indicate that *w* lies between 8.28 and 8.78 v and *a'* between 7.78 and 8.28 v, thus confirming Gaydon's placements within these limits.

The discharge is too mild to produce N atoms directly. $N_2(A^3\Sigma_u^+)$ and $a^1\pi$ are neglected as probably being too short-lived to account for the fountain flame. The Vegard-Kaplan bands are not observed; the energy of $N_2(A^3\Sigma_u^+)$ may be transferred through collisions to $v \geqq 24$ of $N_2(X^1\Sigma_g^+)$.

[1] C. Kenty, Phys. Rev. **98**, 563 (1955); **93**, 651 (1954); **89**, 336 (1953). R. W. Nicholls, J. Chem. Phys. **21**, 568 (1953); Nature **179**, 496 (1954). Jenkins, Bowtell, and Strong, Nature **163**, 401 (1949). R. S. Mackay, Am. J. Phys. **18**, 319 (1950). N. D. Sayers and K. G. Emeleus, Proc. Phys. Soc. (London) **A65**, 219 (1952).
[2] R. W. Nicholls, J. Chem. Phys. **20**, 1040 (1952).
[3] M. A. Biondi, Phys. Rev. **88**, 660 (1953). L. S. Frost and A. V. Phelps, Phys. Rev. **98**, 559 (1955).
[4] R. W. Nicholls, J. Chem. Phys. **21**, 568 (1953).
[5] R. W. Nicholls, Nature **179**, 496 (1954).
[6] A. G. Gaydon, *Dissociation Energies* (Dover Publications, New York, 1950), p. 155.

X-Ray Diffraction Patterns of $TiCl_2$ and $TiCl_3$†

MILTON FARBER, A. J. DARNELL, AND FRANK BROWN*
Jet Propulsion Laboratory, California Institute of Technology, Pasadena 3, California
(Received June 6, 1955)

X-RAY diffraction patterns have been obtained of powdered samples of solid $TiCl_2$ and $TiCl_3$. The method used for the preparation of anhydrous $TiCl_3$ has been described previously[1] and consists essentially in the reduction of $TiCl_4(g)$ with H_2 in a hot tube and the collection of the resulting $TiCl_3(s)$ on a cold finger located in the hot zone. The $TiCl_4$ of high purity was obtained from the National Bureau of Standards. $TiCl_2$ was prepared by the thermal decomposition of $TiCl_3(s)$ at 475°C under a high vacuum. At this temperature, the reaction is essentially the disproportionation of $TiCl_3$ as

$$2TiCl_3(s) = TiCl_2(s) + TiCl_4(g).$$

At a temperature of 475°C, the $TiCl_3$ is completely disproportionated to $TiCl_2$ and $TiCl_4(g)$, which is collected in a liquid N_2 trap, in approximately 100 hours with no formation of Ti metal. Higher temperatures should be avoided as the disproportionation of $TiCl_2$ into Ti metal and $TiCl_4(g)$ begins to occur when the $TiCl_3(s)$ has been used up.

Due to the high reactivity of the titanium halides with oxygen and moisture, it was necessary to load the samples inside a dry box under prepurified helium. The powder samples of $TiCl_2$ and $TiCl_3$ were loaded and sealed into glass capillary tubes 0.7 mm i.d. inside the dry box. The capillary tubes were placed in a General Electric XRD-3 x-ray unit and photographs of the diffraction patterns were taken with a General Electric powder camera of 14.7 in. in diameter. A copper target ($K\alpha$ radiation) and nickel foil filter were used for the radiation. The prominent diffraction lines for solid $TiCl_2$ and $TiCl_3$ are listed in Table I. The film spacings were corrected for shrinkage during development. The structures of the two compounds were not identifiable from information on the films, due to the weakness of the back reflection lines. The intensities of the lines in Table I are relative and based on a scale of 100. The $TiCl_3$ lines are in good agreement with those of Klemm and Krose[2] who determined the structure of $TiCl_3$ as hexagonal-rhomboid. Baenziger and Rundle[3] determined the crystal structure of $TiCl_2$ (which was prepared by H_2 reduction of $TiCl_4$) as a hexagonal unit cell but did not report the diffraction lines.

TABLE I. Prominent x-ray diffraction lines of $TiCl_2$ and $TiCl_3$.

Time exposure: 2.5 hr
Target: Cu $K\alpha_1$, 1.540 A
$K\alpha_2$, 1.544 A

$TiCl_2$		$TiCl_3$	
dA	Relative intensity	dA	Relative intensity
6.09	80	5.69	80
5.20	20	3.33	10
2.68	100	2.99	10
2.51	20	2.89	20
2.38	20	2.80	10
2.27	20	2.70	60
2.14	60	2.47	100
2.03	10	2.10	60
1.95	40	1.79	10
1.86	40	1.77	10
1.72	50	1.75	60
1.68	40	1.71	10
1.66	20	1.64	50
1.53	40	1.48	10
1.44	40	1.46	20
1.14	40	1.41	10
1.11	40	1.36	10
		1.24	10
		1.20	10
		1.17	10
		1.14	10
		1.13	50
		1.11	50
		1.09	10
		1.08	10
		1.03	10
		1.02	10
		0.999	40
		0.932	20
		0.789	20
		0.786	10

† This paper presents the results of one phase of research carried out at the Jet Propulsion Laboratory, California Institute of Technology, sponsored by the Department of Army, Ordnance Corps, and the Department of Navy, Office of Naval Research, under Contract No. DA-04-495-ORD 18.
* Present address: North American Aviation Company, Propulsion Center, Los Angeles, California.
[1] M. Farber and A. J. Darnell, J. Phys. Chem. **59**, 156 (1955).
[2] W. Klemm and W. Krose, Z. anorg. u. allgem. Chem. **253**, 218 (1947).
[3] N. C. Baenziger, and R. E. Rundle, Acta Cryst. **1**, 274 (1948).

Streamer and Brush Flames Excited by Active Nitrogen in the Rare Gases

CARL KENTY
Lamp Division of the General Electric Company, Advanced Lamp Development Laboratory, Nela Park, Cleveland, Ohio
(Received June 13, 1955)

IF a Tesla spark passes between W electrodes, one flat and one pointed, separated ~2 mm, in 100–600 mm pure A+0.1–0.3 mm N_2, a striking blue flame[1] streams away from the flat electrode. The spectrum is a selection of W arc lines mostly of <3.8 v excitation energy. There is no orange afterglow (from $N_2B^3\pi_g$). Atoms of W, sputtered from the electrodes, are excited by a long-lived (~5 sec) nitrogen carrier (or carriers) of energy.

Also (strongly) present are the N_2 second positive bands. These decay somewhat faster than the W lines. If Ta electrodes are used, a weak flame is produced, in which much the strongest line is 5212.8. This line has an excitation energy[2] of 2.37 v, which is very close to the energy of the metastable N atom ^2D (2.38 v), suggesting the presence of N^2D atoms (undisturbed life ~1 hour).

In the case of Mo, a weak flame is produced in which an accentuated line, 5506.5 (3.57 v) suggests the presence of N^2P metastables, also of 3.57 v energy, and life ~4 seconds.

The observed second positive bands, of energy 11–11.5 v, could be produced from a union of, for example, a metastable $N(^2D)$ atom and a normal N atom in the presence of a third body.

If Na, Tl, or Hg are introduced in the flame the D lines (2.1 v), Tl 5350.5 (3.27 v) weakly, or Hg 2536.6 (4.86 v), respectively, are excited in the flame. The presence of a metastable carrier of energy $\geqq$4.86 v is thus indicated, possibly $N_2(a')$. $N_2(A^3\Sigma_u^+)$ would be a possibility, but its life (~10^{-3} sec) is considered too short. Strongly vibrating normal N_2 molecules may be a possibility.[3]

Measurements of the rate of loss of tungsten, the speed (150 cm sec^{-1}), cross section, and brightness of the streamer, indicate a concentration of W atoms of ~2×10^{11} cm^{-3}, and a concentration of energy carriers >10^{12} cm^{-3}. Conductivity measurements indicate an ion concentration of ~10^9 cm^{-3}. The velocity appears to be imparted to the flame by partial rebound[4] of neutralized ions from the flat cathode.

Weaker flames are obtained with Kr as main gas (the N_2 second positive bands being absent), and much weaker ones with Xe.

If a condensed spark is passed[1] between electrodes separated 1-2 mm in 100–600 mm A plus 5–20 mm N_2, a brush-like flame is produced which is more erratic than the streamer flame, more intense, and of shorter duration. Whereas the streamer flame is obtained with only a few metals. W being outstanding, the "brush" flame can be produced with any of the metals so far tried,[1] about 30. The hard metals, however, give the best brush flames.

Brush flames can be produced with little spectral change with He, Ne, A, Kr, and Xe (weakly) as main gas.

Spectrograms show the presence of many more lines in the brush flame than in the streamer flame; also many of the lines are of higher energy. Yet lines which are strong in the streamer are also strong in the brush. Some yellow afterglow accompanies the brush, but no second positive bands. Many types of nitrogen energy carrier, and free electrons are doubtless present. The brush flames are mostly violet or magenta, but V produces an outstanding red, Cb a yellow, and Pd a green.

In addition to their bearing on active nitrogen these flames provide new spectral sources and may be of use in studies of the reactions of ions at surfaces and sputtering.

[1] C. Kenty, Phys. Rev. **98**, 563 (1955); **93**, 651 (1954); **89**, 336 (1953).
[2] Excitation potentials of lines are taken mostly from *A Multiplet Table of Astrophysical Interest*, Part I, by Charlotte E. Moore.
[3] R. W. Nicholls, Nature **179**, 496 (1954).
[4] K. T. Compton and C. C. Van Voorhis, Phys. Rev. **35**, 1438 (1930).

Microwave Spectrum of Cyclopropyl Chloride*

JAMES P. FRIEND, ROBERT F. SCHNEIDER, AND B. P. DAILEY
Department of Chemistry, Columbia University, New York 27, New York
(Received May 18, 1955)

THE problem of the structure and the nature of the bonding orbitals in cyclopropane and its derivatives is one of considerable interest and importance because of its bearing on the theory of "strain" in small ring systems. Cyclopropyl chloride was selected as a suitable cyclopropane derivative for microwave study because it has the necessary permanent electric dipole moment, is a nearly symmetric rotor, and because Dr. John D. Roberts was kind enough to supply us with a sample of this material. In addition it might be possible to obtain information about the bonding orbitals from a study of the nuclear quadrupole hyperfine structure.

The $J=2\rightarrow3$ and $J=3\rightarrow4$ transitions for both $C_3H_5Cl^{35}$ and $C_3H_5Cl^{37}$, involving the component of the dipole moment along the A axis, have been observed. The lines were identified by means of a study of their frequency distribution, Stark effect patterns, and quadrupole hyperfine structure.

Table I lists the "undisplaced" frequencies for each observed transition calculated from the quadrupole hyperfine patterns. In Table II are given the observed rotational constants together with those calculated from the following structural model which gave the best fit to the experimental constants of any so far tried:

TABLE I. "Undisplaced" frequencies for cyclopropyl chloride.

Transition	$C_3H_5Cl^{35}$	$C_3H_5Cl^{37}$
$2_{02}\rightarrow3_{03}$		
$2_{12}\rightarrow3_{13}$	22 156.5	21 646.7
$2_{11}\rightarrow3_{12}$	23 005.7	22 455.2
$2_{21}\rightarrow3_{22}$	22 587.8	22 060.6
$2_{21}\rightarrow3_{21}$	22 602.4	22 073.0
$3_{03}\rightarrow4_{04}$	30 076.6	
$3_{13}\rightarrow4_{14}$	29 536.3	28 856.2
$3_{12}\rightarrow4_{13}$	30 668.6	29 935.1
$3_{21}\rightarrow4_{22}$	30 154.7	29 443.1
$3_{22}\rightarrow4_{23}$	30 112.2	29 403.8
$3_{30}\rightarrow4_{31}$	30 119.4	
$3_{31}\rightarrow4_{32}$	30 119.4	

TABLE II. Observed *vs* calculated rotational constants for cyclopropyl chloride.

	Observed	Calculated
$C_3H_5Cl^{35}$	$B=3905.4$ Mc $C=3622.4$	$B=3902.7$ Mc $C=3626.9$
$C_3H_5Cl^{37}$	$B=3810.0$ $C=3540.5$	$B=3807.2$ $C=3544.5$

C–H 1.09 A°, C–C 1.47 A°, C–Cl 1.755 A°, H–C–H angle 109°, H–C–Cl angle 109°.

Unfortunately, it has not proved possible to obtain additional rotational constants either through observing new rotational transitions or through the use of isotopically substituted molecules. However, the spectral data obtained, while not sufficient to determine the entire structure, especially the C–H bond length and the bond angles, does restrict the C–C and C–Cl bond distances to fairly narrow limits. The C–C bond appears to be appreciably shorter than the usual single bond value (1.551 observed for ethyl chloride.[1]). This may be the result of the formation of "bent" bonds in which the bonding orbitals are no longer directed along the C–C axis. Coulson and Moffitt[2] predict a value of the H–C–H angle larger than 109° for cyclopropane but the present experiments are insufficient to determine this parameter accurately.

Analysis of the quadrupole coupling hyperfine structure gives the following values $eQqzz=-55.76$ Mc, $\eta=0.1242$ for $C_3H_5Cl^{35}$. For the structural model assumed this corresponds to a value of eQq of -68.70 Mc along the C–Cl bond. This would appear to correspond to the expected small increase in ionic character in going from ethyl chloride ($eqQ=-69.1$ Mc) to cyclopropyl chloride. The decrease in eqQ is slightly less than that observed by Livingston[3] for solid ethyl chloride as compared to solid isopropyl chloride. It seems unlikely that the apparent difference in the electronegativity of carbon in the cyclopropyl and isopropyl groups is really significant.

* Work assisted in part by a contract with the Signal Corps and a grant from the Research Corporation.
[1] Roselin S. Wagner and B. P. Dailey, J. Chem. Phys. **22**, 1459 (1954).
[2] C. A. Coulson and W. E. Moffitt, Phil. Mag. **40**, 1, 1949.
[3] R. Livingston, J. Chem. Phys. **20**, 1170 (1952).

Determination of Adsorption Energy Heterogeneity of Solid Surfaces

J. M. HONIG
Department of Chemistry, Purdue University, Lafayette, Indiana
(Received May 23, 1955)

IN a paper with the same title, Honig and Hill[1] postulated that the function $F(\eta)$, characterizing the distribution of adsorption energies among surface sites, should be independent of the temperature T. Using this postulate, together with an extension of the procedure employed by Sips[2] for inversion of the integral equation relating θ and F, the authors were led to the system of equations

$$F(\eta)=[1/kT+(\partial \ln j_s/\partial\eta)_T]\phi(\eta,T) \quad (1)$$

$$\left(\frac{1}{kT}+\frac{\partial \ln j_s}{\partial\eta}\right)\frac{\partial\phi}{\partial T}+\left(\frac{\partial \ln j_s}{\partial\eta\partial T}-\frac{1}{kT^2}\right)\phi=0 \quad (2)$$

in the notation of reference 1.

In this note the general solution to these equations is provided. It may be verified by direct substitution that (2) is solved by

$$\partial \ln j_s/\partial\eta=C(\eta)/\phi(\eta,T)-1/kT \quad (3)$$

where $C(\eta)$ is an arbitrary function of the variable η.

If (3) is now substituted in (1), it emerges that $C(\eta)=F(\eta)$, and hence that (3) and (1) are identical. As a result, one of the statements in reference 1 requires modification. It is not possible to obtain $j_s(\eta,T)$ and $F(\eta)$ separately from a given set of adsorp-

tion isotherms, since Eqs. (1) and (2) are not independent; however, if one function is known, the other can then be evaluated. In practice one would normally determine j_s from theoretical estimates and then calculate F from (1).

Equation (2) is a direct consequence of the requirement that F be independent of T. Now ϕ is related by Eq. (16) of reference 1 to the function $\theta(p,T)$, which represents the isotherm data at a series of temperatures. Therefore, the isotherm functions to be used in the inversion process must not only meet the requirements listed by Sips[2] but will also have to satisfy Eq. (2). That is, they must yield functions ϕ of the form:

$$\phi=\psi(\eta)\Big/\left[-\frac{1}{kT}+\frac{\partial \ln j_s}{\partial \eta}\right]. \quad (4)$$

It should be pointed out that if one considers the adsorption of atoms on surfaces in the limit of low temperatures, $\partial \ln j_s/\partial\eta$ becomes small compared to $1/kT$, as is seen from Eq. (20) of reference 1. In such a case, Eq. (4) reduces to the form $\phi=kT\psi(\eta)$.

The writer is indebted to Professor R. Kikuchi for helpful discussions.

[1] J. M. Honig and E. L. Hill, J. Chem. Phys. **22**, 851 (1954).
[2] R. Sips, J. Chem. Phys. **18**, 1024 (1950).

Effect of Turbulence on Free Flame Growth

W. R. Mickelsen and N. E. Ernstein
Lewis Flight Propulsion Laboratory, National Advisory Committee for Aeronautics, Cleveland, Ohio
(Received May 19, 1955)

THE effect of turbulence on the propagation of a free flame has recently been investigated at this laboratory.[1] The free flames were spark-ignited in a flowing, turbulent stream of combustible gas. The propagation rate of the free flame globule was observed photographically and with ionization gaps which defined the cone swept out by the globule as it was carried along by the stream. The growth rates were observed over times of the same order, but less than, the characteristic diffusion time of the turbulence as defined by Taylor.[2]

The growth rates of the turbulent free flame was found to be a statistical variable which had random distributions about mean values. For all turbulence and fuel-air conditions investigated, the lower portion of the distribution curves fell below the laminar flame speed value. This result is in agreement with the observations of Olsen and Gayhart[3] which were made over times less than those of the present experiment. Botha and Spalding[4] have reported the effect of flame temperature on laminar flame speed and found that laminar flame speed was greatly reduced in the lean and rich fuel-air regions by relatively small decreases in flame temperature. The free flame propagation rates showed a similar trend with fuel-air ratio, and in addition, showed an effect of turbulence scale on the proportion of sublaminar propagation rates. Data taken with the smallest of the three turbulence generating grids had the greatest proportion of sublaminar flame speeds. These two trends are interpreted as indicating a diffusive effect of the turbulence which lowered the flame temperature and, hence, the propagation rate.

[1] Mickelsen and Ernstein, NACA Technical Note 3456 (1955).
[2] Taylor, Proc. London Math. Soc. **20**, 196 (1921).
[3] Olsen and Gayhart, J. Chem. Phys. **23**, 402 (1955).
[4] Botha and Spalding, Proc. Roy. Soc. (London) **A225**, 71 (1954).

Tritium-Carbon Monoxide Reaction

David L. Douglas
Knolls Atomic Power Laboratory, Schenectady, New York*
(Received May 31, 1955)

A BRIEF investigation of the radiation induced reaction between tritium and carbon monoxide has been carried out in this laboratory. The photochemical behavior of the system is reviewed by Noyes and Leighton.[1] That hydrogen and carbon monoxide will combine to formaldehyde in an electrical discharge has been reported.[2] Lind[3] studied the a-particle induced reaction and reported the formation of an unidentified white solid, while hydrogen and carbon monoxide disappeared at a rate of approximately three molecules ($CO+H_2$) per ion pair. Caress and Rideal[4] investigated the reaction taking place under electron impact.

Tritium, hydrogen, and carbon monoxide were introduced into a 100-ml Pyrex bulb. Amounts of each of the gases were determined from the pressures as measured with a mercury manometer attached to the bulb. Tritium and hydrogen were purified as described by Dorfman and Hemmer.[5] The initial gas mixtures were analyzed on a General Electric analytic mass spectrometer and the compositions are given in Table I.

TABLE I. Composition of initial gas mixtures.

Experiment No.	Pressure in mm				
	H_2[a]	T_2[a]	H_2O	CO	CO_2
1	88.1	53.5	...	114	1.2
2	244.3	106.3	0.2	97.4	0.1

[a] The HT has been converted back to H_2 and T_2.

Evidence of reaction was twofold: (1) a white solid appeared on the walls of the bulb; and (2) the pressure decreased several millimeters after two or three days. Initial rates were determined graphically and converted to the number of molecules disappearing per second. Since polymerized formaldehyde was the principal reaction product (see below) the molecular rates are expressed as molecules of formaldehyde formed per second. A computation, based on the work of Dorfman,[6] shows that greater than 99% of the total beta particle energy is expended in the gas. Table II gives the pertinent experimental data and results. Experimental errors totaled less than 5%. Assuming 35 ev required to form an ion pair the ion pair yields for the two experiments are 0.86 and 2.25, respectively. These are of the same order as those found by Lind (multiply by two to convert to his units). The difference in the G-values for the two experiments is probably accounted for by the much more efficient removal of the H_2CO from the vapor phase at the lower temperature. In fact, in the room temperature run, unless the removal of formaldehyde by polymerization proceeds at a greater rate than the formation of the monomer the yield calculated from the pressure decrease can be interpreted only as a lower limit.

The condensable reaction products were frozen out at −195°C and the gases pumped off, a sample being analyzed on the mass spectrometer. Warming to 80°C vaporized all the condensed substances and these vapors were analyzed on the mass spectrometer. The noncondensable fraction contained only the original constituents. The absence of methane is in agreement with Lind. Formaldehyde was the principal reaction product in the condensed material. Water, carbon dioxide, acetaldehyde, glycol, and glyoxal were also found. The observed relative peak heights of the various aldehyde species are tabulated in Table III.

No conclusions as to the reaction kinetics are drawn from the limited data. However, the results are in general accord with those of previous workers.

TABLE II. Reaction between tritium and carbon monoxide. Bulb volume = 100 cc; bulb diameter = 2.2 cm.

Expt. no.	Total pressure (mm at 26°C)	Temperature of expt.	$\Delta P/\Delta T$ (mm/sec) ($\times 10^5$)	Molecules H_2CO/sec ($\times 10^{10}$)	G (Molecules per 100 ev)
1	257	26±1°C	5.35	1.42	0.025
2	448	−195°C	7.10	7.35	0.064

TABLE III. Reaction between tritium and carbon monoxide. Mass spectrometer analysis of solid product.

Expt. no.	Relative peak heights[a]									
	H_2CO	HTCO	T_2CO	CH_3CHO	CH_3TCO	CH_2T_2CO	CHT_3CO	CT_4CO	$(CH_2OH)_2$	$(CH_2O)_2$
1	9.8	3.7	1	4.4	1.7	0.8	0.5	0.5	...	...
2	91.1	20	1	9.0	12.2	6.9	1.5	0.3	1.3	0.2

[a] Corrections have been applied from the known cracking patterns of formaldehyde, acetaldehyde, and glycol.

Certain preparative applications of the reaction suggest themselves. Using pure T_2 and CO the pure isotopic CT_2CO could be prepared for infrared and other spectroscopic work. Also, this would seem to be a useful method for preparing tritium labeled aldehydes and ketones.

The author is indebted to Mr. C. F. Pachucki of the Metallurgical and Chemical Analysis Activity for the mass spectrometric analyses and to Dr. L. M. Dorfman, of the General Electric Research Laboratory, for many helpful suggestions in frequent discussions.

* Operated by the General Electric Company for the U. S. Atomic Energy Commission.

[1] W. A. Noyes, Jr., and P. A. Leighton, *The Photochemistry of Gases* (Rheinhold Publishing Corporation, New York, 1941) pp. 222 and 254.
[2] G. Glockler and S. C. Lind, *The Electrochemistry of Gases and Other Dielectrics* (John Wiley and Sons, Inc., New York, 1939), pp. 140 and 141, 192–195.
[3] D. C. Bardwell and S. C. Lind, J. Am. Chem. Soc. **47**, 2675 (1925).
[4] A. Caress and F. K. Rideal, Proc. Roy. Soc. (London) **A120**, 370 (1928).
[5] L. M. Dorfman and B. A. Hemmer, J. Chem. Phys. **22**, 1555 (1954).
[6] L. M. Dorfman, Phys. Rev. **95**, 393 (1954).

Effect of Interfacial Conductivity on Dielectric Properties

C. T. O'KONSKI*
Department of Chemistry and Chemical Engineering, University of California, Berkeley, California
(Received May 23, 1955)

THE importance of electric polarization phenomena associated with boundary layers has been widely recognized qualitatively,[1] but present theories of the dielectric properties of disperse systems do not include explicitly the effects of a two-dimensional surface conductivity. Such a conductivity may be assigned to systems in which the mobilities of charge carriers are large along a surface, but small normal to it, and to systems like charged colloids or rigid macromolecules, under conditions such that a relatively high ion concentration (ion atmosphere) is confined to a thin layer at the interface. While the consequences of the surface conductivity are being explored in a more general manner,[2] the result of the solution of a special problem will serve to illustrate the nature of the effects which occur.

Consider a random suspension of spheres of radius **R** and dielectric constant ϵ_2 immersed in a medium of dielectric constant ϵ_1, with an interface characterized by the surface conductivity λ. Assume that the currents produced by the volume conductivities are small compared to the displacement currents within the two regions. At sufficiently low angular frequencies ω, or high λ, the semiconducting surface will transmit charge carriers, giving rise to a distribution of charge density and an induced polarization like that of a conducting sphere, and the dielectric constant of the suspension will exceed ϵ_1. At very high ω, or low λ, the surface charge transfer will become negligible. Then the dielectric constant will approach some lower value, depending upon the ratio ϵ_1/ϵ_2, and the volume concentration. In the intermediate region the out-of-phase surface current will give rise to dielectric losses. The transition region can be characterized by a relaxation time τ. A transient treatment[2] of the decay of surface charge density upon removal of a polarizing field for the case of an isolated sphere leads to

$$\tau = R(\epsilon_2 + 2\epsilon_1)/8\pi\lambda, \qquad (1)$$

in electrostatic units, cgs. From this it can be seen that a dilute suspension of the above properties will exhibit a Debye-type dispersion.

It is of particular interest that τ is proportional to R/λ. This suggests that λ can be determined quite accurately from dielectric dispersion studies on uniform suspensions. Evidently a distribution of particle sizes will give rise to a distribution of relaxation times. For nonspherical particles there will be more than one relaxation time, depending upon the direction of the polarizing field with respect to the particle axes.

Since the interfacial polarization influences the electric field within the sphere, this effect is of importance in the evaluation of dipole moments of the charged macromolecules from dielectric properties of their solutions. Experiments on the Kerr electro-optic effect in macromolecular solutions suggested the importance of ion atmosphere polarization.[3] Recent additional work[4] supports this suggestion, and revealed the existence (in aqueous solutions of tobacco mosaic virus) of a dispersion of the Kerr effect in a frequency region far removed from the critical frequency corresponding to molecular reorientation. This may have its origin in ion atmosphere polarization effects.

An idea of the order of magnitude of the values of λ to be attributed to electrical double layers at surfaces in contact with water may be obtained by reference to calculated and measured values for glass,[5] which are in the range 5×10^{-10} to 5×10^{-8} ohm^{-1}, with more recent results nearer the lower value. From the foregoing equation, one then obtains $\tau = 1.4\times10^{-2}\ R$ to $1.4\times10^{-4}\ R$ for materials of low dielectric constant in water. This suggests that of the ion atmosphere polarization dispersion may be the phenomenon observed in protein solutions, rather than dipolar dispersion as was formerly supposed.[6]

* Guggenheim Fellow at the University of Leiden, Holland, February to August, 1955.

[1] For reviews, see C. J. F. Böttcher, *Theory of Electric Polarization*, (Elsevier Publishing Company, Amsterdam, 1952), Chapter 10, and J. Th. G. Overbeek, Chapter 5, Vol. I, H. R. Kruyt, *Colloid Science* (Elsevier Publishing Company, Amsterdam, 1952).
[2] It is hoped that a more complete treatment, based on similar models but including volume conduction currents in the media, will be possible. This is being undertaken in collaboration with Professor J. J. Hermans of the University of Leiden, Holland.
[3] C. T. O'Konski and B. H. Zimm, Science **111**, 113 (1950).
[4] A. J. Haltner, Ph.D. thesis, University of California, January, 1955.
[5] White, Monaghan, and Urban, J. Phys. Chem. **40**, 207 (1936); Urban, White, and Strassner, *ibid.* **39**, 311 (1935); J. W. McBain and J. F. Foster, *ibid.* **39**, 331 (1935); A. J. Rutgers and M. de Smet, Trans. Faraday Soc. **43**, 102 (1947).
[6] J. L. Oncley in E. J. Cohn and J. T. Edsall, *Proteins, Amino Acids, and Peptides*, (Reinhold Publishing Corporation, New York, 1943), Chapter 22; J. G. Kirkwood, *ibid.*, Chapter 12.

Errata: Pressure Broadening of Linear Molecules. II. Theory

[J. Chem. Phys. **23**, 389 (1955)]

WILLIAM V. SMITH, H. A. LACKNER, AND A. B. VOLKOV
University of Delaware, Department of Physics, Newark, Delaware

THE numerical factors of Eqs. (21) and (22) are incorrect. The fraction 11/180 should be replaced by 7/45. The final numerical factor of Eq. (22) is then 2.53 instead of 1.86. These corrections change the quadrupole moment values on page 396. For BrCN the calculated quadrupole moment is $Q/e = 4.2\times10^{-16}$ cm^2 instead of 5.7×10^{-16} cm^2. For OCS the calculated quadrupole moment is $Q/e = 1.8\times10^{-16}$ cm^2 instead of 2.4×10^{-16} cm^2.

A factor of 3 is missing in Eq. (15d).

On the Application of the Kinetic Theory of Liquids of Born and Green to the Problem of the Calculation of the Volume Viscosity

R. E. NETTLETON*
Department of Physics, Brown University, Providence 12, Rhode Island
(Received June 15, 1955)

BORN and Green[1] have proposed to apply the superposition approximation of Kirkwood[2] to the second in the hierarchy of recurrence relations originally obtained by Yvon[3] for the configuration-velocity distribution functions in a fluid to yield a closed equation for the pair distribution function for two molecules in the twelve-dimensional space of pairs. Following the method suggested by Born and Green, a solution to this equation was assumed in the form of an expansion in the gradients of temperature and fluid velocity. On substitution of this solution into the integro-differential equation for the pair distribution function, equations are obtained for the coefficients in the assumed solution. From these coefficients, if they could be calculated, one could obtain the contribution of collisional transfer to the transport coefficients in a liquid.

Unfortunately, the equations for the coefficients in the assumed expansion for the pair distribution function are found to be homogeneous, in agreement with Klein and Prigogine,[4] so that while approximate solutions can be obtained by a Fourier transform method similar to that of Born and Green, they are undetermined to the extent of an arbitrary multiplicative constant. There appears to be lacking a principle of irreversibility.

An attempt was made to estimate the bulk viscosity in a gas by going out to the next order in the calculation and comparing coefficients of second-order space derivatives of temperature in the expression obtained after substitution of the assumed expansion into the equation for the pair distribution function. On the neglect of terms which should be of the order of the contributions of triple collisions, a formula was obtained yielding the value of 4 micropoises for the bulk viscosity of gaseous argon, zero for nitrogen, both at 0°C, 1 atmos. The formula has the form:

$$\eta_0=\frac{2\lambda m}{3P\alpha_v k}\left(\frac{3P}{T}-P\alpha_v-\frac{2\rho k}{m}\right)+\frac{5}{3}\eta_c.$$

Here η_0=bulk viscosity, λ=thermal conductivity, P=pressure, k=Boltzmann's constant, $\alpha_v=1/P(\partial P/\partial T)_v$, T=absolute temperature, m=molecular mass, ρ=mass density, and η_c=contribution of collisional transfer to the shear viscosity. The latter quantity was estimated by subtracting from the measured value of shear viscosity a value for the kinetic component calculated from a formula of Lennard-Jones.[5] The estimate for argon is probably too high because of inaccuracies in the available data. It is, however, still too small to show up in the acoustic absorption and streaming experiments which have been made.[6]

* Corrinna Borden Keen Research Fellow, Brown University, 1954–1955.
[1] Born and Green, Proc. Roy. Soc. (London) **A190**, 455 (1947).
[2] J. G. Kirkwood, and E. M. Boggs, J. Chem. Phys. **10**, 394 (1942).
[3] J. Yvon, Actualités Scientifiques et Industrielles, No. 203 (1935).
[4] Klein and Prigogine, Physica **19**, 89 (1953).
[5] S. Chapman and T. G. Cowling, *The Mathematical Theory of Non-uniform Gases* (Cambridge University Press, London, 1952), Chapter 12.
[6] See, e.g., H. Medwin, J. Acoust. Soc. Am. **26**, 332 (1954).

Reply to Tietz' Letter: "Approximate Analytic Solution of the Thomas-Fermi Equation for Atoms"

H. C. BRINKMAN
Central Laboratory T.N.O., Delft, Netherlands
(Received April 21, 1955)

IN a recent letter to the editor, Tietz[1] gives a modification of my method of solving the Thomas-Fermi equation[2] applied to atoms. The following remarks may serve to compare the relative positions of Tietz' modification and my original method for atoms:

	Exact	Approximations: Brinkman	Approximations: Tietz
Equation	$d^2\varphi/d\chi^2=\chi^{-\frac{1}{2}}\varphi^{\frac{1}{2}}$	$d^2\varphi/d\chi^2=(\chi\varphi)^{\frac{1}{2}}\frac{\varphi}{\chi}$	$d^2\varphi/d\chi^2=\frac{\varphi^2}{(\chi\varphi)^{\frac{1}{2}}}$
		$(\chi\varphi)^{\frac{1}{2}}=c_1=0.64$	$(\chi\varphi)^{\frac{1}{2}}=c_2=0.576$
Solution	numerical	$\varphi=c\chi^{\frac{1}{2}}k_1(2c_1^{\frac{1}{2}}\chi^{\frac{1}{4}})$	$\varphi=\frac{6c_2}{[\chi+(6c_2)^{\frac{1}{2}}]^2}$
Asymptotic behavior	$\chi\to\infty$, $\varphi\to144/\chi^3$	exponential	$\varphi\to6c_2/\chi^2$

The approximate solutions do not differ much numerically for intermediate values of χ, while Tietz' solution has a simpler form. For $\chi\to\infty$ my solution decreases too fast and Tietz' solution too slowly.

However, the essential difference lies in the fact that my equation is linear, while Tietz' equation is not. Linearity greatly facilitates the application of the method to molecules, as was shown in my treatment of the H_2O molecule.[3] On the other hand, the extension of Tietz' method to molecules seems to be hardly possible.

[1] T. Tietz, J. Chem. Phys. **22**, 2094 (1954).
[2] H. C. Brinkman, Physica **20**, 44 (1954).
[3] H C. Brinkman and B. Peperzak, Physica **21**, 48 (1955).

Reply to Brinkman's Letter: Concerning My Letter "Approximate Analytic Solution of the Thomas-Fermi Equation for Atoms"

T. TIETZ
Department of Theoretical Physics, University of Łódź, Łódź, Poland
(Received May 19, 1955)

MY approximate[1] analytic solution of the Thomas-Fermi equation for a free neutral atom

$$\Phi=\frac{b^2}{(b+x)^2}=\frac{1}{(1+ax)^2};\quad \frac{1}{a}\equiv b \tag{1}$$

is the next homolog of the simplest form given by Kerner[2] $1/1+cx$. The general homolog $1/(1+ax)^\alpha$ has not only sufficient foundation in the modification of Brinkman's method[3] given by me, but also has foundation through the following variational integral:

$$I[\Phi]\equiv\int_0^\infty[(\Phi')^2+\tfrac{4}{5}\Phi^{5/2}/x^{\frac{1}{2}}]dx. \tag{2}$$

For the measure of the approximate degree of the approximate solution of the Thomas-Fermi equation for a free neutral atom, Umeda[4] proposes to employ the numerical value of the variational integral evaluated by putting the given approximate solution in place of Φ. Since the minimization of I is equivalent to the integration of the Thomas-Fermi equation, the better approximate solution being the convergence limits. For Miranda's[5] exact solution, direct numerical quadrature of (2) gives the value

$$I=1.3625$$

which should be, of course, the limiting minimum value of I. The general homolog is now being studied on the basis of the approximation degree mentioned above. For the Sommerfeld approximation, Umeda[4] has found for I the best value $I=1.3670$. According to Table I, we see that the general homolog seems to be capable of extensive application by virtue of its simplicity and higher degree of approximation. The simplicity is of essential interest for the approximate solutions. The linearity of nonlinearity of the equation in different problems of this field has no great importance, because the simplicity of the approximate solution is of essential interest. The application of Brinkman's method to the following problems: free positive ion, compressed neutral atom, the solution of the Schrödinger equation for an approximate

TABLE I. The functional dependence of I and a of the general homolog for α.

	$\alpha=1.0$	$\alpha=1.2$	$\alpha_{\text{minimum}}=1.3939$[a]	$\alpha=7/5=1.4$	$\alpha=3/2=1.5$	$\alpha=8/5=1.6$	$\alpha=9/5=1.8$	$\alpha=2$
I	1.3679	1.3653	1.3635	1.3636	1.3637	1.3640	1.3650	1.3663
a	1.3679	1.1565	0.88608	0.881206	0.80812	0.74566	0.64599	0.56927

[a] The values of this column were privately communicated to the author by Professor K. Umeda for which I am very grateful.

atomic field and so on, we see to be complicated or hardly possible. My method[6] seems to have an application to these problems. Brinkman's solution has two constants whose values we find by trial. For $x\to\infty$, my solution decreases too slowly, Brinkman's solution too fast. But for $x>20$, my solution is more accurate than Brinkman's solution as we see in the following:

x	Fermi	Sommerfeld	Brinkman	Tietz[7]
20	0.0058	0.0056	0.0027	0.0065

Brinkman's solution has exponential behavior and my solution has the following behavior:

$$\Phi\to\frac{1}{(ax)^2} \quad \text{for} \quad x\to\infty.$$

The application to Brinkman's[8] method to molecules is much simpler than my method, which seems to be hardly possible.

[1] T. Tietz, J. Chem. Phys. **22**, 2094 (1954).
[2] E. H. Kerner, Phys. Rev. **83**, 71 (1951).
[3] H. C. Brinkman, Physica **20**, 42 (1954).
[4] K. Umeda, J. Phys. Soc. Japan **9**, 290 (1954).
[5] C. Miranda, Mem. R. Acad. d'Italia **5**, 285 (1934).
[6] T. Tietz, Nuovo cimento (to be published).
[7] The value for a in Eq. (1) is given in Table I.
[8] H. C. Brinkman and B. Peprzak, Physica **21**, 48 (1955).

r-Centroids for Diatomic Molecules*

R. W. NICHOLLS AND W. R. JARMAIN
Department of Physics, University of Western Ontario, London, Canada
(Received June 6, 1955)

THE fairly general conditions under which it is possible to use a quantity $\bar{r}_{v'v''}$ associated with the $v'\to v''$ molecular band, where

$$\bar{r}_{v'v''}=\frac{\int\psi_{v'}r\psi_{v''}dr}{\int\psi_{v'}\psi_{v''}dr} \tag{1}$$

and also under which it is possible to write

$$\int\psi_{v'}f(r)\psi_{v''}dr=f(\bar{r}_{v'v''})\int\psi_{v'}\psi_{v''}dr \tag{2}$$

have been discussed elsewhere by Fraser.[1] $\psi_{v'}$ and $\psi_{v''}$ are molecular vibrational wave functions and r is the internuclear separation. Because of Eq. (1), the name *r-centroid* is ascribed to $\bar{r}_{v'v''}$ which is evidently an "average" internuclear separation with respect to the weighting factor $\psi_{v'}\psi_{v''}$, associated with the $v'\to v''$ transition. An array of r-centroids for a band system is a set of discrete values which lie across the range experienced by the molecules in all levels of both electronic states of the transition. $\bar{r}_{v'v''}$ lies within or close to the range of r which is common to the regions between the classical turning points of motion in the upper (v') and lower (v'') levels, respectively.

The use to which r-centroids have so far been put is, through Eq. (2), to determine how the electronic transition moment—$f(r)$ in this case—varies with internuclear separation,[1-4] and it is to be expected that similar uses may be found to determine other r-dependent quantities. A number of methods by which arrays of r-centroids may be evaluated for band systems have been developed and will be published shortly. Arrays of r-centroids are available for some band systems.[5]

A further interpretation or $\bar{r}_{v'v''}$ may be seen in the following:

By definition, the average or expectation value of r experienced by the molecule in the level v' is

$$\bar{r}_{v'}=\int\psi_{v'}{}^2rdr. \tag{3}$$

Now

$$\psi_{v'}=\sum_{v''}(v',v'')\psi_{v''} \tag{4}$$

where

$$(v',v'')=\int\psi_{v'}\psi_{v''}dr.$$

The Franck-Condon factor of the transition is

$$q_{v'v''}=(v',v'')^2. \tag{5}$$

It strongly influences the relative probability that the transition occurs.

From Eqs. (1), (3), (4), and (5)

$$\bar{r}_{v'}=\sum_{v''}q_{v'v''}\bar{r}_{v'v''}. \tag{6}$$

Similarly

$$\bar{r}_{v''}=\sum_{v'}q_{v'v''}\bar{r}_{v'v''}. \tag{7}$$

It may thus be observed from Eqs. (6) and (7) that the expectation values $\bar{r}_{v'}$ and $\bar{r}_{v''}$ may be considered as weighted averages of r-centroids with respect to the Franck-Condon factors and that $q_{v'v''}\bar{r}_{v'v''}$ is the contribution to each from the $v'\to v''$ transition.

Finally it may be remarked that a smooth variation has been observed, and established analytically, between $\bar{r}_{v'v''}$ and the band wavelength $\lambda_{v'v''}$. If r_e' and r_e'' are the equilibrium internuclear separations of the upper and lower states of the transition, $\bar{r}_{v'v''}$ is an increasing function of $\lambda_{v'v''}$ when $r_e'>r_e''$ and is a decreasing function of $\lambda_{v'v''}$ when $r_e'<r_e''$.

* This work has been made possible by the Air Force Cambridge Research Center through Contract AF 19(122)-470.
[1] P. A. Fraser, Can. J. Phys. **32**, 515 (1954).
[2] R. G. Turner and R. W. Nicholls, Can. J. Phys. **32**, 468-474 (1954).
[3] R. G. Turner and R. W. Nicholls, Can. J. Phys. **32**, 475-479 (1954).
[4] L. V. Wallace and R. W. Nicholls, J. Atm. and Terrest. Phys. (to be published).
[5] W. R. Jarmain and R. W. Nicholls, Scientific Report No. 20, Contract AF 19(122)-470, Department of Physics, University of Western Ontario, April, 1955.

Lattice Energies of the Alkaline Earth Imides and the Heat of Formation of NH^{-2}

AUBREY P. ALTSHULLER
2715 East 116th Street, Cleveland 20, Ohio
(Received June 13, 1955)

THE lattice constants of the alkaline earth imides, CaNH, SrNH, and BaNH, have been determined.[1,2] They are found to have the NaCl type lattice as do the alkaline earth oxides and sulfides.[2] The lattice energies of CaNH, SrNH, and BaNH can be calculated by the Born equation.[3] A more detailed calculation is unjustified since the compressibilities of the alkaline earth imides and the polarizability and "main frequency" energy[4] of NH^{-2} are unavailable. The minimum cation-anion distances for CaNH, SrNH, and BaNH are 2.58, 2.72$_5$, and 2.92 A, respectively.[1,2] The repulsion constants n used here for CaNH, SrNH, and BaNH, 8, 8.5, and 9.5, are the same as those used formerly for the corresponding alkaline earth oxides.[3] The lattice energies calculated for CaNH, SrNH, and BaNH are 787, 752, and 711

kcal/mole, respectively. Since the repulsion function is approximate[3] and the Van der Waals energy contribution is not included[5] (the effect of the small N−H dipole is also neglected), these lattice energies are uncertain to at least ±10 kcal/mole.

The heat of formation of BaNH is −53.8 kcal/mole.[6] Since the lattice energy of BaNH and $\Delta H_f^0(Ba^{+2},g)$[6] are now available, the the heat of formation of $NH^{-2}(g)$ can be calculated from the reaction

$$BaNH(s) \rightarrow Ba^{+2}(g) + NH^{-2}(g)$$

as +261 kcal/mole. For comparison, the heat of formation of O^{-2} and S^{-2} are 215 and 145 kcal/mole.[7]

Reversing the type of calculation discussed above leads to heats of formation for CaNH(*s*) and SrNH(*s*) of −62 and −63 kcal/mole.

The double electron affinity of $NH[NH(g)+2e^- \rightarrow NH^{-2}(g)]$ is −184 kcal/mole [ΔH_f^0(NH,g) equals 77 kcal/mole[8]]. In comparison, the double electron affinities of $0(0+2e^- \rightarrow O^{-2})$ and $S(S+2e^- \rightarrow S^{-2})$ are −156 and −80 kcal/mole.[7]

The heat of protonation of $NH^{-2}(g)$ to $NH_2^{-1}(g)$[7] also can be calculated to be −613 kcal/mole. The heat of protonation of $NH_2^{-1}(g)$ to $NH_3(g)$ is −393 kcal/mole, while the heat of protonation of $NH_3(g)$ to $NH_4^+(g)$ is −202 kcal/mole.[9]

[1] Hartman, Fröhlich, and Ebert, Z. anorg. u. allgem. Chem. **218**, 181 (1934).
[2] Landolt-Börnstein, *Numerical Values of Functions from Physics, Chemistry, Astronomy, Geophysics and Technology, Atomic and Molecular Physics, Part IV. Crystals* (Springer-Verlag, Berlin, 1955).
[3] J. Sherman, Chem. Revs. **11**, 93 (1932).
[4] J. Mayer, J. Chem. Phys. **1**, 270 (1933).
[5] Mayer and McC. Maltie [J. E. Mayer and M. McC. Maltie, Z. Physik **73**, 748 (1932)] have calculated approximate Van der Waals energies for the alkaline earth oxides and sulfides of only 2 to 4 kcal/mole. However, in view of the fact that for the alkali metal halides these earlier calculations were 50% too low, the Van der Waals contributions to the lattice energies of the alkaline earth oxides and sulfides and perhaps imides probably amount to 5 to 10 kcal/mole.
[6] F. D. Rossini *et al.*, "Selected Values of Chemical Thermodynamic Properties," NBS Circular 500 (1952).
[7] H. O. Pritchard, Chem. Revs. **52**, 529 (1953).
[8] A. P. Altshuller, J. Chem. Phys. **22**, 1947 (1954).
[9] A. P. Altshuller, J. Am. Chem. Soc. (to be published).

Method of Extrapolating Equation-of-State Data to Higher Temperatures

ROGER A. STREHLOW
Ballistic Research Laboratories, Aberdeen Proving Ground, Maryland
(Received May 31, 1955)

VERY high-pressure high-temperature equation-of-state data are difficult to obtain experimentally and there is as yet no adequate theory to cover this region. For calculations on a proposed high-pressure shock tube we needed equation-of-state data to pressures of 2500 atmospheres and temperatures of 2000°K. Data for quite a number of pure gases have been taken in this pressure range but the upper experimental temperature limit is usually 150°C.[1] (A recent determination on CO_2 has been made to 1000°C.[2])

Extrapolations of these data to higher temperatures were made in the following manner: the values of $Z=PV/RT$ were calcuated and plotted against $1/T$°K at constant pressure. These curves were then extrapolated to infinite temperature where Z is equal to one. The slope of the line in the region of infinite temperature was determined by calculating the value of Z using the virial equation of state $PV/RT=1+B/V+C/V^2=Z$. The values of the virial coefficients were determined from the Lennard-Jones 6–12 potential model using the calculations of Hirschfelder, Curtis, and Bird,[3] and the appropriate molecular constants. This extrapolation procedure assumes that there is no dissociation or ionization at any temperature. While this is a presumably valid assumption for the purpose of extrapolation, the results are not valid above the temperature when dissociation becomes appreciable.

The procedure was checked with argon, nitrogen, and carbon dioxide. In all cases the low pressure (50 atmos and lower) data agreed well with the calculated virial equation curves. In the case of argon and nitrogen, the high-pressure extrapolation was very smooth from the infinite temperature theoretical slope to the low-temperature experimental values. However, carbon dioxide data did not extrapolate well at the higher pressures. For this gas the Z values predicted by the theory fell well above the experimental values. A possible explanation of this behavior is that while argon and nitrogen act as spherical molecules at the high pressure, carbon dioxide does not pack in the same fashion at the two pressure levels. The lower experimental Z values indicate that the molecules pack closer at high pressures than the spherical Lennard-Jones theory predicts for the low-pressure behavior.

For argon and nitrogen, the maximum estimated extrapolation error, assuming that the theory is correct near infinite temperature, is about 1% in the value of Z. The errors involved in assuming the validity of the Lennard-Jones potential at infinite temperature could not be evaluated; the results indicate, however, that the assumption is satisfactory for monatomic or diatomic nonpolar molecules.

The author wishes to thank Mrs. Marjory Watermeier for performing some of the calculations used in the extrapolations.

[1] Michels, Lunbeck, and Wolkers, Appl. Sci. Res. **A.2**, 345 (1950); also Physica **17**, 801 (1951).
[2] Kennedy, Am. J. Sci. **252**, 225–241 (April, 1954).
[3] Hirschfelder, Curtis, and Bird, *Molecular Theory of Gases* (John Wiley and Sons, Inc., New York, 1954).

Barrier Height and Thermodynamic Functions of Gaseous HNO_3 and DNO_3†

ANN PALM AND MARTIN KILPATRICK
Department of Chemistry, Illinois Institute of Technology, Chicago 16, Illinois
(Received June 1, 1955)

VALUES for the entropy, free energy, and heat content of gaseous HNO_3 previously calculated[1] were based on an incomplete Raman spectrum of 100% liquid nitric acid.[2] The recent measurements of the vibrational spectra of gaseous HNO_3 and DNO_3[3] permitted more accurate computations of these functions. Although there may be disagreement[4] with the assignment of some of the vibrational bands,[3] it appears adequate for use in the statistical-mechanical calculations.

The thermodynamic properties, heat content, free energy, entropy, and heat capacity for the ideal gaseous state at one atmosphere pressure were evaluated to a rigid rotator harmonic oscillator approximation with one independent internal rotation. The contributions of the translations, over-all rotations, and vibrations were computed in the usual manner, while the torsional contributions were estimated from the tables of Pitzer and Gwinn[5] by linear interpolations. For this purpose a knowledge of the potential restricting the internal rotation was essential. This has been determined by three methods. Throughout, the potential function was assumed to be a twofold barrier of the form $V=\frac{1}{2}V_0(1-\cos 2\phi)$. (1) The procedure for obtaining V_0 by the entropy difference between the third law value[1] and the calcu-

TABLE I. The fundamentals of gaseous nitric acid.

HNO_3				DNO_3			
3560[a,b]	a'	765	a'	2627	a'	764	a'
1710	a'	583	a'	1685	a'	543	a'
1335	a'	680[c]	a''	1313	a'	670[c]	a''
1320	a'	465	a''	1014	a'	365[d]	a''
886	a'			888	a'		

[a] The units are cm^{-1}.
[b] The degeneracy is 1 throughout.
[c] This value was determined from the Raman spectrum of the liquid.
[d] This value was estimated from a combination band.

TABLE II. Structure parameters for gaseous HNO_3 and DNO_3.

N=O	1.22 A	I_{xx} 39.30 awu A²	I_{xx} 39.32 awu A²
N–O	1.41 A	I_{yy} 81.47 awu A²	I_{yy} 84.00 awu A²
O–H	0.96 A	I_{zz} 42.16 awu A²	I_{zz} 44.69 awu A²
	130°	I_r 0.9041 awu A²	I_r 1.757 awu A²
	115°	$V_0=74.55\theta$ cm^{-1}	$V_0=38.36\theta$ cm^{-1}
	90°	$W_r=18.64(a_r+2\theta)$ cm^{-1}	$W_r=9.59(a_r+2\theta)$ cm^{-1}

lated quantity could be used for HNO_3 only at 298°K since no other experimental data are available for HNO_3 or DNO_3. (2) From the spectroscopically observed torsional modes, 465 cm^{-1} for HNO_3 and 365 cm^{-1} for DNO_3, V_0 for both isotopic molecules was evaluated by the harmonic oscillator approximation. (3) In turn these values were initially used in the quantum-mechanical

TABLE III.

Method	HNO_3 V_0[a]	ν[b]	DNO_3 V_0	ν
S(third law)-S(trans. rot. vib.)	9.77	...	...	...
Harmonic oscillator	8.29	465	9.93	365
Torsional oscillator-rotator	8.98	465	10.5	364
Average V_0	9.74	486	9.74	350

[a] The units are kcal/mole.
[b] The wave numbers are in cm^{-1}.

torsional oscillator-rotator treatment which affords a closer estimate of the actual barrier height. With the resulting Mathieu equation and tables relating to these functions[6] a new set of V_0 values was determined.

The fundamental vibrational frequencies which were used here are given in Table I. The structure parameters[7] as well as the numerical values expressing the barrier height and the torsional energy levels in terms of θ and the eigenvalues a_r contained in the Mathieu function are summarized in Table II. The reduced moments of inertia were derived according to Pitzer's method for

TABLE IV. Thermodynamic functions of nitric acid for the ideal gaseous state at one atmosphere pressure.[a]

	$-(F^0-H_0^0)/T$		$(H^0-H_0^0)/T$		S^0		C_p^0	
T°K	A	B	A	B	A	B	A	B
				HNO_3				
298.16	53.99	54.22	8.92	9.46	62.90	63.68	11.42	12.80
300	54.05	54.28	8.93	9.48	62.97	63.75	11.46	12.86
325	54.77	55.05	9.15	9.77	63.91	64.81	12.01	13.49
350	55.45	55.78	9.37	10.05	64.82	65.83	12.53	14.09
375	56.11	56.48	9.60	10.34	65.71	66.82	13.04	14.67
400	56.73	57.16	9.83	10.63	66.56	67.79	13.52	15.21
425	57.34	57.82	10.06	10.92	67.39	68.73	13.98	15.74
450	57.92	58.45	10.29	11.20	68.21	69.65	14.42	16.22
475	58.48	59.06	10.52	11.48	68.99	70.53	14.83	16.66
500	59.03	59.66	10.74	11.74	69.77	71.40	15.22	17.10
				DNO_3				
298.16	54.17	54.57	9.03	9.79	63.20	64.36	11.77	13.39
300	54.22	54.62	9.05	9.82	63.27	64.44	11.81	13.43
325	54.96	55.42	9.28	10.11	64.24	65.53	12.39	14.08
350	55.66	56.17	9.52	10.42	65.17	66.57	12.94	14.68
375	56.33	56.89	9.77	10.75	66.09	67.64	13.47	15.28
400	56.96	57.58	10.02	11.04	66.98	68.61	13.98	15.85
425	57.57	58.23	10.26	11.32	67.84	69.57	14.45	16.35
450	58.17	58.89	10.51	11.60	68.67	70.47	14.90	16.82
475	58.74	59.50	10.75	11.89	69.49	71.39	15.32	17.27
500	59.30	60.10	10.99	12.16	70.29	72.25	15.71	17.70

[a] The units are cal mole^{-1} deg^{-1}.

asymmetric tops attached to a rigid frame.[8] The computed values for V_0 of the two isotopic molecules shown in Table III differ considerably. An average V_0 reproduces the observed torsional modes to approximately 4% for HNO_3 and DNO_3. Deviations in the barrier height are expected since these calculations constitute merely a first approximation to the problem. A hindering potential to the internal rotation of the order of 9–10 kcal/mole is not surprising for this type of molecule considering the polarity of the bond.

The results for the thermodynamic properties of HNO_3 and DNO_3 for the ideal gaseous state at one atmosphere pressure are presented in Table IV. Column A gives the contributions of the translations, over-all rotations, and vibrations, and column B includes the contributions of the internal rotation. This separation was made in order to permit a convenient revision of the torsional contributions should a more accurate value for V_0 be derived. The previously computed functions[1] and the present ones differ by less than 1 cal, whereas the heat capacities evaluated by means of the expression given by Egan[9] disagree considerably.

† Supported by the U. S. Navy, Office of Naval Research under Contract N7onr-32913, Project NR 051 056.

[1] W. R. Forsythe and W. F. Giauque, J. Am. Chem. Soc. **64**, 48 (1942).
[2] A. Dadieu and K. W. F. Kohlrausch, Naturwiss. **19**, 690 (1931).
[3] Cohn, Ingold, and Poole, J. Chem. Soc. 4272 (1952); C. Fréjacques, Compt. rend. **234**, 1769 (1952).
[4] R. Ryason and M. K. Wilson, J. Chem. Phys. **22**, 2000 (1954).
[5] K. S. Pitzer and W. D. Gwinn, J. Chem. Phys. **10**, 428 (1942).
[6] Eyring, Walter, and Kimball, *Quantum Chemistry* (John Wiley and Sons, Inc., New York, 1949), p. 358; S. Goldstein, Trans. Cambridge Phil. Soc. **23**, 303 (1927).
[7] L. R. Maxwell and V. M. Mosley, J. Chem. Phys. **8**, 738 (1940).
[8] K. S. Pitzer, J. Chem. Phys. **14**, 239 (1946).
[9] E. P. Egan, Jr., Ind. Eng. Chem. **37**, 303 (1945).

Bending Force Constant of the Carbon Tetrafluoride Molecule

EIKO AIHARA
Physics Department, Tokyo Institute of Technology, Oh-okayama, Tokyo, Japan
(Received June 10, 1955)

THE carbon tetrafluoride molecule possesses four fundamental modes of vibration and in one of these (ν_2) the C–F distances do not alter. The change δE in the total energy of the molecule in this special type of displacement is given by

$$\delta E=8\pi^2 m_F r_0^2 \nu_2^2 \theta^2,$$

where ν_2 is the frequency of the vibration, m_F the mass of the F atom, r_0 the C–F distance and 2θ a small change in the F–C–F angle.

We have calculated δE under the following assumptions: (1) The total energy of the electron system can be calculated by the valence bond method, in which, for the ionic structure, only the type such as $C^+F^-F_3$ is taken into account.

If Ψ_0 and Ψ_i represent the normalized wave functions for the covalent and ionic structures, respectively, the complete molecular wave function is

$$\Psi=\Psi_0+\lambda\Psi_i,$$

where λ is a parameter giving the degree of ionic character. (2) The K-shell electrons of each atom are replaced by a point charge $-2e$ at the position of the nucleus. (3) The valence orbitals of the C atom are the sp^3 tetrahedral hybrids which remain unchanged during the vibrations. (4) The electronic configuration of each F atom is given by $(2s)^2(2p\pi)^2(2p\pi')^2(2p\sigma)^1$, where $2p\sigma$ is the $2p$-type atomic orbital possessing axial symmetry around the F–C line. (5) We adopt the Slater function for the analytical form of each atomic orbital, but assume that each orbital satisfies the Hartree equation for separated atom and its eigenvalue can be taken from the empirical value of the ionization energy estimated by Mulliken.[1] (6) Nonorthogonality between the paired orbitals is completely taken into account, but more than three powers of the overlap integrals between the unpaired valence orbitals of C

TABLE I. The numerical values of the energy matrix element and their second derivatives with respect to θ (in atomic unit).[a]

H_{00}	H_{0i}	H_{ii}	S_{0i}
$0.512+Q$	$-0.115+Q$	$0.430+Q$	0.7172
$\left(\frac{\partial^2 H_{00}}{\partial\theta^2}\right)_{\theta=0}$	$\left(\frac{\partial^2 H_{0i}}{\partial\theta^2}\right)_{\theta=0}$	$\left(\frac{\partial^2 H_{ii}}{\partial\theta^2}\right)_{\theta=0}$	$\left(\frac{\partial^2 S_{0i}}{\partial\theta^2}\right)_{\theta=0}$
2.078	2.278	2.614	−0.268

[a] The sum of all Coulomb integrals in the covalent structure and the atomic energy of the C and F atoms, is represented by Q.

and F atoms and more than two powers of the other type of overlap integrals can be neglected.

Then, the molecular energy E is given by

$$E=\int\Psi\mathcal{H}\Psi d\tau\Big/\int\Psi^2 d\tau=(H_{00}+2\lambda S_{0i}H_{0i}+\lambda^2 H_{ii})/(1+2\lambda S_{0i}+\lambda^2),$$

where $\mathcal{H}$ is the total Hamiltonian,

$$H_{\alpha\beta}=\int\Psi_\alpha\mathcal{H}\Psi_\beta d\tau\Big/\int\Psi_\alpha\Psi_\beta d\tau\quad(\alpha,\beta=0\text{ or }i)$$

and

$$S_{0i}=\int\Psi_0\Psi_i d\tau.$$

Then, we can write

$$\left(\frac{\partial^2 E}{\partial\theta^2}\right)_{\theta=0}=\left(\frac{\partial^2 H_{00}}{\partial\theta^2}\right)_{\theta=0}+\Omega(\lambda),$$

where

$$\Omega(\lambda)=\left[\frac{\partial^2}{\partial\theta^2}\left\{\frac{2S_{0i}\lambda(H_{0i}-H_{00})+\lambda^2(H_{ii}-H_{00})}{1+2S_{0i}\lambda+\lambda^2}\right\}\right]_{\theta=0}.$$

Table I shows the result of the calculation, in which the numerical values of the two center homonuclear integrals are taken from the table by Kotani, Ishiguro, and Hijikata.[2] For the heteronuclear and the three-center integrals, Mulligan's[3,4] and Mulliken's[5] approximation are employed, respectively.

It can be shown that the value of $\frac{1}{2}(\partial^2 E/\partial\theta^2)_{\theta=0}$ is not sensitive to the value of λ, which is assumed to be unity in our calculation. Then, the final result is

$$\frac{1}{2}\left(\frac{\partial^2 E}{\partial\theta^2}\right)_{\theta=0}=37\text{ ev},$$

which is in good agreement with the observed value 49.3 ev. When the squares of the all overlap integrals between the unpaired orbitals and the possibility of the hybridization of the $2p\sigma$ and $2s$ orbitals of the F atoms are taken into account, the result would be improved further.

The author wishes to thank Dr. K. Niira and Dr. K. O-ohata for their helpful discussion with this problem.

[1] J. F. Mulliken, J. Chem. Phys. **2**, 782 (1934).
[2] Kotani, Ishiguro, and Hijikata, J. Phys. Soc. Japan **8**, 553 (1954).
[3] J. F. Mulligan, J. Chem. Phys. **19**, 347 (1951).
[4] R. O. Brennan and J. F. Mulligan, J. Chem. Phys. **20**, 1635 (1952).
[5] R. S. Barker and H. Eyring, J. Chem. Phys. **22**, 2072 (1954).

Infrared Study of the Adsorption on Silica Gel

TSUNEO YOSHINO
Tokyo Institute of Technology, Oh-okayama, Meguro-ku, Tokyo, Japan
(Received June 7, 1955)

RECENTLY some infrared studies of adsorbed D_2O,[1] NH_3,[2] CO,[3] and phenol, etc.[4] have been reported.

The author measured the infrared absorption bands of 1,2-dichloroethane and acetyl acetone adsorbed on silica gel. These compounds have a rotational or a keto-enol isomerism, and the abundance ratios between isomers have been measured for the various other states and their relations with the mediums have been discussed.[5,6]

The amyl alcohol paste of the silica gel powder was dried at 300°C on an NaCl plate, leaving a thin film of about 1 mg/cm². The particle diameter of the silica gel was 0.7∼0.9 micron. The surface area was found to be 700 m²/g by the nitrogen adsorption at −195.8°C. The vapor of the compound was adsorbed on the film adsorbent by an amount less than that necessary to form a monolayer. The film was kept dry in a small measuring glass cell with NaCl windows.

Spectral data were obtained by a Perkin-Elmer Model 112 spectrometer with CaF_2 and LiF prisms. The 1430 cm^{-1} band of *gauche*-form and the 1450 cm^{-1} band of *trans*-form were measured for the 10% chloroform solution, the pure liquid, and the adsorbed one. The frequencies of these bands do not change appreciably. From the peak intensities of these bands, relative values of the abundance ratios were obtained and listed in Table I. Even if the errors in measuring the ratios are taken into consideration, the *gauche/trans* ratio for the adsorbed state is not smaller than that for the liquid.

TABLE I. Relative values of *gauche/trans* ratio of dichloroethane in various states.

Chloroform solution	1
Pure liquid	1.4
Adsorbed	1.9

The absorption bands of acetyl acetone were measured for the 1.5% chloroform solution, the pure liquid, the liquid saturated with water, and the adsorbed one. In all these measurements, only three bands at 1600, 1700, and 1730 cm^{-1} were observed in the region above 1400 cm^{-1}. The absence of OH stretching band in the ordinary OH region conceivably shows that the enol molecule always forms an intramolecular hydrogen bond. When the compound is adsorbed, the frequency of the 1600 cm^{-1} band of enol form decreases by about 25 cm^{-1} while those of the other bands of keto form do not change appreciably. From the peak intensities of 1600 and 1700 cm^{-1} bands, the relative values of the abundance ratios were obtained and listed in Table II together with the values by bromine titration quoted from Richter's book.[6]

TABLE II. Relative values of keto/enol ratios of acetyl acetone in various states.

	Present measurement	Bromine titration[a]
Chloroform solution	1	1
Pure liquid	2.4	1.2
Liquid saturated with water	2.4	...
Adsorbed	8.6	...
Water solution	...	16

[a] See reference 6.

As the values of the abundance ratios of the adsorbed compounds were found to be close to those of the compounds dissolved in highly polar solvents, the surroundings of the adsorbed molecules may be similar to those of the molecules in these solvents, as to their effects on the surrounded molecules. The infrared absorptions of the adsorbed water at 1650 and 3400 cm^{-1} were found to be very little for the film adsorbent. In consideration of the high absorption coefficient of liquid water, which was found in the present study, and that of the adsorbed heavy water in the literature,[1] the amount of the water adsorbed on the film may at the most be 1% of the silica gel. Therefore, polar character of the surroundings of the adsorbed molecules may be attributed to the silica gel.

The frequency of the enol-form band and the keto/enol ratio of the adsorbed acetyl acetone are much different from those of the liquid. The adsorbed molecules may be unimolecularly spread over the surface, being directly affected by the silica gel.

The author would like to express his appreciation to Professor K. Kozima for his encouragement and to Professor N. Hara and Dr. K. Mita for the measurement of the area of silica gel.

[1] Pimentel, Garland, and Jura, J. Am. Chem. Soc. **75**, 803 (1953).
[2] J. E. Mapes and R. P. Eischens, J. Phys. Chem. **58**, 1059 (1954).
[3] Eischens, Plinskin, and Francis, J. Chem. Phys. **22**, 1786 (1954).
[4] N. G. Yoloslavskiĭ and A. N. Terenin, Doklady Akad. Nauk S.S.S.R. **66**, 885 (1949).
[5] S. Mizushima, *Structure of Molecules and Internal Rotation* (Academic Press, Inc., New York, 1954), p. 38.
[6] E. N. Allot, *Richter's Organic Chemistry* (Nordemann Publishing Company, Inc., New York, 1934), p. 50; K. H. Meyer, Ber. deut. chem. Ges. **45**, 2843 (1912).

Natural Spin Orbitals for Helium

HARRISON SHULL* AND PER-OLOV LÖWDIN
Institute of Mechanics and Mathematical Physics, Uppsala University, Uppsala, Sweden
(Received June 6, 1955)

WE have attacked the problem of the Coulomb correlation in two-electron systems from the viewpoint of avoiding the direct introduction of the r_{12} term into the wave function. In his treatment of the ground state of He, Hylleraas[1] was surprisingly successful in obtaining a considerable amount of spatial correlation by changing the closed-shell form, $(1s)$,[2] to an open-shell form, $(1s,1s')$, in which the two electrons are permitted to occupy different orbitals.[2]

In order to try to improve these results, we have investigated the ground state of He by the method of superposition of configurations, using as (ns) orbitals the Laguerre functions, $L^2_{n+1}(2Zr)\exp(-Zr)$, which form a complete orthogonal set. From the three orbitals $1s$, $2s$, $3s$, we can form six symmetrized and normalized configurations, and by means of the variation principle, we found the following best spatial wave function for $Z=2$:

$$\Psi(1,2)=0.963175(1s)^2-0.250366(1s,2s)-0.032613(2s^2)+0.092211(1s,3s)-0.000310(2s,3s)-0.006692(3s)^2 \quad (1)$$

having the energy -2.878116 a.u.[3] The results were then analyzed in terms of natural spin orbitals (NSO).[4] By diagonalizing the generalized first-order density matrix, we obtained the following three NSO's:

NSO	Occupation No.	Normalized NSO
X_1	0.995660	$0.983545(1s)-0.168992(2s)+0.063880(3s)$
X_2	0.004265	$0.178369(1s)+0.964488(2s)-0.194800(3s)$
X_3	0.000075	$-0.028690(1s)+0.202991(2s)+0.978760(3s)$.

Introduction of these NSO's into (1) gives

$$\Psi(1,2)=\sqrt{n_1}(X_1)^2-\sqrt{n_2}(X_2)^2-\sqrt{n_3}(X_3)^2 \quad (2)$$

in which the coefficients are the square roots of the occupation numbers. The occurrence of the minus sign in the second term can be shown to be connected with the Coulomb correlation; see below.

Comparison of (1) and (2) shows the optimum convergency property of the NSO's. In general a wave function $\Psi(1,2)$ for a two-electron system which is built up from n basic orbitals contains $n(n+1)/2$ terms, but by introducing the "natural expansion" corresponding to (2), the wave function may be reduced to contain a maximum of only n "diagonal" configurations.[5]

We have also investigated which functions of the $(s)^2$ and (s,s') forms, respectively have the smallest quadratic deviation from the exact function $\Psi(1,2)$ by using a principle of maximum overlap. It can be shown that $(X_1)^2$ is the best $(s)^2$ form and X_1 is therefore in the limit $n\to\infty$ closely related to the Hartree SCF function for He, but obtained by a linear process. In fact, the energy of $(X_1)^2$ in our case is found to be -2.861335 as compared to the SCF energy reported by Wilson of -2.861_5. The normalized radial function differs from the SCF function reported by Wilson and Lindsay by no more than 0.005 in any part of space.[6] We note, however, that X_1 can never be identical with the SCF orbital since the latter gives the optimum energy and is defined by a nonlinear process.

Correspondingly, the normalized form of the superposition $(X_1)^2-\alpha^2(X_2)^2$ with $\alpha=(n_2/n_1)^{\frac{1}{2}}$, which is equivalent[7] to $(X_1-\alpha X_2, X_1+\alpha X_2)$, is the "best" wave function of the open-shell type (s,s') having the smallest quadratic deviation from (1). The energy found, -2.877236, is a considerable improvement on the Hylleraas-Eckart simple exponential result of -2.87566. A rather large part of the correlation is therefore taken into account as a result of the tendency of the two electrons with antiparallel spins to avoid each other by occupying spatially different orbitals.[8] The inner orbital, $(X_1-\alpha X_2)$, is very closely exponential, whereas the outer one, $(X_1+\alpha X_2)$, is somewhat more contracted than an exponential orbital. We note that the occurrence of two different real orbitals depends on the minus sign in the second term of (2).

The work on helium is now being extended to include angular functions. Similar computations are also in progress for the H_2 molecule. We are greatly indebted to Fil. Kand. Klaus Appel for his valuable assistance in carrying out the numerical work.

* Guggenheim Fellow 1954–1955, on leave from Chemistry Department and Institute for Atomic Research, Iowa State College, Ames, Iowa. Address after September, 1955: Chemistry Department, Indiana University, Bloomington, Indiana.

[1] E. A. Hylleraas, Z. Physik **54**, 347 (1929). The same kind of wave function was introduced independently by Eckart, Phys. Rev. **36**, 878 (1930).
[2] The terminology used here was introduced by Mulliken in connection with the Shelter Island Conference in 1951. See R. S. Mulliken, Proc. Natl. Acad. Sci. **38**, 160 (1952).
[3] For the energy, we have used the modified atomic unit: 1 a.u. $=2hcR_{y_{He}}$.
[4] P.-O. Löwdin, Phys. Rev. **97**, 1474 (1955).
[5] G. Koster, Quarterly Progress Reports of Solid-State and Molecular Theory Group, M.I.T., October 15, 1954, p. 36, who investigated the case $n=2$, obtained a somewhat misleading result since he never introduced the "natural expansion."
[6] W. S. Wilson, Phys. Rev. **48**, 536 (1935). W. S. Wilson and R. B. Lindsay, Phys. Rev. **47**, 681 (1935).
[7] Compare also Coulson and Fischer, Phil. Mag. **40**, 386 (1949) and Mulliken, reference 2.
[8] P.-O. Löwdin, Phys. Rev. **97**, 1509 (1955).

Note on the Atom Form Factor Calculated from the Thomas-Fermi Model

T. TIETZ
Department of Theoretical Physics, University of Łódź, Łódź, Poland
(Received June 2, 1955)

USING my approximate formula[1] for the Thomas-Fermi function, the dependence of the atom form factor of the Thomas-Fermi atom on atomic number Z as well as on $(\sin\theta)/\lambda$ was expressed in closed form. The atom form factor F of the Thomas-Fermi atom of atomic number Z is[2]

$$F(Z,K)=\int_0^\infty \frac{\sin 4\pi Kr}{4\pi Kr}\rho 4\pi r^2 dr \quad (1)$$

$$=Z\left[1-4\pi K\mu\int_0^\infty \sin 4\pi K\mu x\cdot\varphi(x)dx\right] \quad (2)$$

where $\varphi(x)$ is the Thomas-Fermi function, $K=(\sin\theta)/\lambda$ (λ in 10^{-8} cm), and μ ($a_0=0.52920/10^8$) is the Thomas-Fermi unit. The integral (2) was carried out by Bragg and West[3] in such a way that exact values are taken for $\varphi(x)$ and the integral is approximated by sum. The results can be given naturally only in tabular form, so that its dependence on Z as well as on K is at first sight not clear. The similarity rule, however, of the F curve for an atom Z_0 is transformed so as to be suitable for any other atom Z, by multiplying F and K by Z/Z_0 and $(Z/Z_0)^{\frac{1}{2}}$, respectively. Moreover, owing to the oscillating nature of sine, it is necessary to take the summation in as small steps as possible. Umeda,[4] using Rozental's[5] approximate formula for $\varphi(x)$ in 2 and 3 terms, has found in first case for F following approximate formula:

$$F=Z\left[1-K^2\left(\frac{0.7345}{K^2+0.009112Z^{\frac{4}{3}}}+\frac{0.2655}{K^2+0.3319Z^{\frac{4}{3}}}\right)\right]. \quad (3)$$

TABLE I. Values of the atom form factor for Cs ($Z=55$) by Eqs. (3) and (5) and the standard values given by Bragg and West.

$(\sin\theta)/\lambda A^{-1}$	0.1	0.2	0.3	0.4	0.6	0.8	1.0	1.2	1.4	1.6	1.3
Bragg-West	50.7	43.8	37.6	32.4	25.8	20.8	17.0	14.5	12.3	10.4	9.2
Eq. (3)	52.1	45.5	38.3	32.4	24.4	19.8	16.8	14.6	12.9	11.5	10.3
Eq. (5)	50.6	44.6	39.8	34.2	26.9	21.0	17.4	14.3	12.0	9.9	9.5

In our case, for

$$\Phi=\frac{a^\alpha}{(a+x)^\alpha}=\frac{1}{(1+bx)^\alpha}a=\frac{1}{b}; \tag{4}$$

in particular case, for $\alpha=2$ and $a=1.75661$, we find

$$F(Z,K)=Z[1+16\pi^2K^2\mu^2a^2(\cos4\pi K\mu a\ \mathrm{ci}4\pi K\mu a + \sin4\pi K\mu a\ \mathrm{si}4\pi K\mu a)] \tag{5}$$

where si and ci are sine and cosine integrals. In Table I the values of Eqs. (3) and (5) are compared to the standard values given by Bragg and West. We see that our approximate formula (4) for $\alpha=2$ gives a sensible value for the atom form factor. For $\alpha=7/5$, $b=0.88126$ and $\alpha=\frac{3}{2}$, $b=0.80812$ we obtain more accurate values for F. The formula (4) gives us sensible value in the case of the atom form factor F for the atom at rest. In conclusion, the author wishes to express his sincere thanks to Professor Kwai Umeda for his kindness in sending him the numerical tables of his results.

[1] T. Tietz, J. Chem. Phys. **22**, 2094 (1954); Ann Physik **15**, 186 (1955).
[2] The leading review, P. Gombas, *Die statistische Theorie des Atoms und ihre Anwendungen* (Springer-Verlag, Wien, 1949).
[3] W. L. Bragg and J. West, Z. Krist. **69**, 118 (1929).
[4] K. Umeda, J. Fac. Sci. Hokkaido Univ. Ser. **IV**, 1 (1951).
[5] S. Rozental, Z. Physik **98**, 742 (1935).

Modified Bond-Eigenfunction Method of Calculating Potential Energy Surfaces and its Application to the Reaction $H+H_2\rightarrow H_2+H$

IWAO YASUMORI
Laboratory of Physical Chemistry, Tokyo Institute of Technology, Ookayama, Meguro-ku, Tokyo, Japan
(Received June 9, 1955)

IN order to evaluate the chemical reaction rates theoretically, it is necessary to know the detailed feature of the interaction potential between the reacting species, i.e., the potential energy surfaces of the reaction. At present, however, we have no available method for constructing the surface except the semiempirical one devised by Eyring *et al.*[1] because of mathematical difficulty. Here the author presents another method which gives a basis for some approximate procedure to plot the surface. Let us consider, as an example, the reaction system $A+BC\rightarrow AB+C$, consisted of three atoms A, B, and C. Taking several combinations of stable molecules and atoms $A+BC$ or $B+CA$ or $C+AB$ as the initial or the final states, their electronic states are expressed by the product functions $\psi_A\cdot\psi_{BC}$ or $\psi_B\cdot\psi_{CA}$ or $\psi_C\cdot\psi_{AB}$, where ψ_A and ψ_{BC} are assumed to be the exact wave functions for the definite electronic states of atom A and molecule BC, respectively. From these "composite wave functions," the approximate wave function of the whole system is constructed as follows:

$$\Psi=\sum_m c_m\mathfrak{A}\psi_m=c_1\mathfrak{A}\psi_A\cdot\psi_{BC}+c_2\mathfrak{A}\psi_B\cdot\psi_{CA}+\cdots\cdots, \tag{1}$$

where $\mathfrak{A}$ is the antisymmetrizer[2] which makes the composite wave functions totally antisymmetrical for the exchange between any pair of electrons in the system. Then the electronic energies of the system, i.e., the potential energy surfaces of the reaction are obtained by solving the usual secular determinant

$$\text{Det.}\ |H_{mn}-ES_{mn}|=0, \tag{2}$$

where

$$H_{mn}=\int\mathfrak{A}\psi_m{}^*H\mathfrak{A}\psi_n d\tau \quad\text{and}\quad S_{mn}=\int\mathfrak{A}\psi_m{}^*\cdot\mathfrak{A}\psi_n d\tau. \tag{2}$$

Dividing the total Hamiltonian H into the partial Hamiltonian H_n for the composite state n and the interaction operator H_n' and noting $H_n\psi_n=E_n\psi_n$, Eq. (2) is also written as follows:

$$\text{Det.}\ |(E_n-E)S_{mn}+H_{mn}'|=0, \tag{3}$$

where

$$H_{mn}'=\int\mathfrak{A}\psi_m{}^*H_n'\mathfrak{A}\psi_n d\tau.$$

Since E_n represents the energy for the state n, we can utilize its observed value, if it is known. Unknown quantities S_{mn} and H_{mn}' may be evaluated approximately by giving the appropriate analytical forms of the composite functions. As a simple example calculated by this method, the results of the hydrogen atom-molecule reaction of linear configuration are shown in Table I.

TABLE I. Calculated energy values for the reaction $H+H_2\rightarrow H_2+H$ of linear configuration.

Type of used molecular function[a]	Heitler-London	H. L. plus ionic term	Wang	Wang plus ionic term
Energy of act. state E_{H_3}. (kcal/mole)	−76.8 (−53.11)[b]	−75.0 (−60.39)	−84.2 (−56.16)	−83.7 (−67.09)
Energy of ini. state E_{H_2}. (kcal/mole)	−109.5 (−72.18)	−109.5 (−74.02)	−109.5 (−86.94)	−109.5 (−92.24)
Activation energy E_a. (kcal/mole)	32.7 (19.07)	34.5 (13.63)	25.3 (30.78)	25.8 (25.15)
Nuclear distance r_a. (a.u.)	1.87 (2.00)	1.88 (2.00)	1.72 (1.89)	1.75 (1.84)

[a] Explicit forms of all molecular wave functions and Morse function for H_2 were taken from the work of J. O. Hirschfelder and J. W. Linnett, J. Chem. Phys. **18**, 130 (1950).
[b] Values in parenthesis are those obtained by Hirschfelder, Rosen, and Eyring, J. Chem. Phys. **4**, 121 (1936).

In the calculation, the ground state of hydrogen molecule $^1\Sigma_g^+$ and those of atom ^2S were only taken as the composite states. The improvements from the previous work[3] of energy values at the activated state of linear symmetric configuration are remarkable. Also it is to be noted that, in the calculation with Wang type function, the energy value decreases as the effective nuclear charge z increases and attains to about −103 kcal/mole, the observed value, when $z=1.45$. The above result will be further improved by a treatment including the higher states of composite species. However, it is more desirable to determine semiempirically S_{mn} and H_{mn}', without complicated calculations, for practical purposes. Detailed discussion will be published later.

[1] Glasstone, Laidler, and Eyring, *The Theory of Rate Processes* (McGraw-Hill Book Company, Inc., New York, 1941), p. 91.
[2] W. Moffitt, Proc. Roy. Soc. (London) **A210**, 245 (1951).
[3] Herschfeldelder, Rosen, and Eyring, J, Chem. Phys. **4**. 121 (1936).

CONTENTS—*Continued*

Letters to the Editor:

Nuclear Hyperfine Structure in the Paramagnetic Resonance Absorption of Triarylaminium Perchlorates . . . . . O. R. Gilliam, Robert I. Walter, and V. W. Cohen 1540

Photoionization Efficiencies and Cross Sections in NH_3 . . W. C. Walker and G. L. Weissler 1540

On the Fluorescence of Self-Activated Zinc-Sulfide . . . . . Arrigo Addamiano 1541

Intramolecular O—H—O Hydrogen Bonds in Bis-(Dimethylglyoximato)-Cobalt (III)-Complexes . . . . . Junnosuke Fujita, Akitsugu Nakahara, and Ryutaro Tsuchida 1541

Second Virial Coefficient for Ellipsoids with Imbedded Dipoles . . . . . Charles Muckenfuss, C. F. Curtiss, and R. B. Bird 1542

State of Nitrogen Adsorbed on Tungsten . . . . . Gert Ehrlich 1543

Determination of the Equilibrium Constant of the Reaction between BF_3 and BCl_3 . . . . . T. H. S. Higgins, E. C. Leisegang, C. J. G. Raw, and A. J. Rossouw 1544

Light Scattering by Water . . . . . J. Kraut and V. B. Dandliker 1544

Note on Singular Integral Equations of the Kirkwood-Riseman Type . . . . . Peter L. Auer and Clifford S. Gardner 1545

Solution of the Kirkwood-Riseman Integral Equation in the Asymptotic Limit . . . . . Peter L. Auer and Clifford S. Gardner 1546

Heats of Absorption on a Prepared Uniform Surface . . . . W. A. Steele and J. G. Aston 1547

Preliminary Data on Photoionization Efficiencies and Cross Sections in C_2H_4 and C_2H_2 . . . . . W. C. Walker and G. L. Weissler 1547

Free-Electron Treatment of Diels-Alder's Reaction . . . . . Sadhan Basu 1548

Simultaneous Transitions in Liquids. A New Kind of Molecular Spectrum . . . . . J. A. A. Ketelaar and F. N. Hooge 1549

Mobility and Quantum Yield of Charge Carriers in Crystal Violet . . . . . R. C. Nelson 1550

Space-Time Yield and Reaction Rate . . . . . George J. Janz and Samuel C. Wait, Jr. 1550

Thermodynamic Properties of the System Methane-Carbon Monoxide at 90.67°K . . . . . V. Mathot, L. A. K. Staveley, J. A. Young, and N. G. Parsonage 1551

Note on the Potential of the α-P/dH_2 Electrode . Sigmund Schuldiner and James P. Hoare 1551

Thermoluminescence Measurements on ZnS Phosphors *in Vacuo* . . . . . G. Neumark, J. Fajans, and D. R. Frankl 1553

Some Remarks on the Structure of NH_3 and PH_3 Molecules . . . . . Włodzimierz Kołos 1554

Hindered Rotation of Water Molecules of Hydration in $Mg(H_2O)_6Cl_2$ and $Mg(H_2O)_6Br_2$ . . . . . Tunahiko Sidei and Syukuro Yano 1554

Active Nitrogen in the Rare Gases and Its Excitation of Metal Vapors . . . . . Carl Kenty 1555

X-Ray Diffraction Patterns of $TiCl_3$ and $TiCl_4$ . . . . . Milton Farber, A. J. Darnell, and Frank Brown 1556

Streamer and Brush Flames Excited by Active Nitrogen in the Rare Gases . . . Carl Kenty 1556

Microwave Spectrum of Cyclopropyl Chloride . . . . . James P. Friend, Robert F. Schneider, and B. P. Dailey 1557

Determination of Adsorption Energy Heterogeneity of Solid Surfaces . . . . J. M. Honig 1557

Effect of Turbulence on Free Flame Growth . . . . . W. R. Mickelsen and N. E. Ernstein 1558

Tritium-Carbon Monoxide Reaction . . . . . David L. Douglas 1558

Effect of Interfacial Conductivity on Dielectric Properties . . . . . C. T. O'Konski 1559

Errata: Pressure Broadening of Linear Molecules. II. Theory . . . . . William V. Smith, H. A. Lackner, and A. B. Volkov 1559

On the Application of the Kinetic Theory of Liquids of Born and Green to the Problem of the Calculation of the Volume Viscosity . . . . . R. E. Nettleton 1560

Reply to Tietz' Letter: "Approximate Analytic Solution of the Thomas-Fermi Equation for Atoms" . . . . . H. C. Brinkman 1560

Reply to Brinkman's Letter: Concerning My Letter "Approximate Analytic Solution of the Thomas-Fermi Equation for Atoms" . . . . . T. Tietz 1560

r-Centroids for Diatomic Molecules . . . . . R. W. Nicholls and W. R. Jarmain 1561

Lattice Energies of the Alkaline Earth Imides and the Heat of Formation of NH^{-2} . . . . . Aubrey P. Altshuller 1561

Method of Extrapolating Equation-of-State Data to Higher Temperatures . . . . . Roger A. Strehlow 1562

Barrier Height and Thermodynamic Functions of Gaseous HNO_3 and DNO_3 . . . . . Ann Palm and Martin Kilpatrick 1562

Bending Force Constant of the Carbon Tetrafluoride Molecule . . . . . Eiko Aihara 1563

Infrared Study of the Adsorption on Silica Gel . . . . . Tsuneo Yoshino 1564

Natural Spin Orbitals for Helium . . . . . Harrison Shull and Per-Olov Löwdin 1565

Note on the Atom Form Factor Calculated from the Thomas-Fermi Model . . . . . T. Tietz 1565

Modified Bond-Eigenfunction Method of Calculating Potential Energy Surfaces and its Application to the Reaction $H+H_2 \rightarrow H_2+H$ . . . . . Iwao Yasumori 1566